Asymptotische Theorie wandgebundener und abgelöster turbulenter Scherströmungen

Habilitationsschrift

eingereicht an der

Technischen Universität Wien,
Fakultät für Maschinenwesen und Betriebswissenschaften,

zur Erlangung der Lehrbefugnis (Venia Legendi) im Fachgebiet

Strömungsmechanik

Dipl.-Ing. Dr.techn. Bernhard Scheichl

Wien, 29. November 2010

Asymptotic theory of wall-bounded and separated turbulent shear flows

Habilitation thesis

submitted at the

Vienna University of Technology,
Faculty of Mechanical and Industrial Engineering,

to achieve the Venia Legendi in

Fluid mechanics

Dipl.-Ing. Dr.techn. Bernhard Scheichl

Vienna, 29 November 2010

Contents

1 Acknowledgements

Special thanks go to my mentor, Professor Alfred Kluwick, for the conceptual formulation of the challenging subjects considered here and originating from the theme of my PhD thesis, many essential ideas, and other inputs and hints he brought in during our collaboration. These reflect his long-standing experience and excellent international reputation in the field of theoretical fluid mechanics. Without doubt, the prosperity of this long-term cooperation has been represented by the successful treatment of the demanding theoretical questions tackled.

Sincere thanks are expressed to all my colleagues at the Institute of Fluid Mechanics and Heat Transfer at the Vienna University of Technology for numerous fruitful scientific discussions in the past decade. In particular, here the expertise of Stefan Braun, Herbert Steinrück, and my brother Stefan Scheichl shall be emphasised.

I also express my thanks to my co-author Professor Frank T. Smith (Department of Mathematics, University College London) for clues that proved helpful for the elegant treatment of some very difficult analytical problems and, not least, for linguistic improvements of the manuscript underlying a joint paper contributing to this thesis. Furthermore, Michael Alletto's substantial contribution as a co-author of a further paper brought forward in terms of the numerical solution of the boundary layer equations is gratefully appreciated. This is also part of his master thesis finished in 2008, supervised by Professor Alfred Kluwick and co-supervised by me. Finally, thanks are due Jon Paton (TotalSim Ltd, Brackley, UK) for carrying out the Detached Eddy Simulation mentioned in the survey on current and future research presented.

2 Preface

The present habilitation thesis covers the essence of the scientific progress the candidate has achieved in the years 2002–2010 as a postdoctoral research fellow at the Institute of Fluid Mechanics and Heat Transfer at the Vienna University of Technology.

2.1 Outline

The work concerns the advances in a comprehensive rigorous description of initially firmly attached turbulent boundary layers that separate further downstream, either marginally or massively. The methods involved include matched asymptotic expansions and appropriate numerical techniques for solving the equations that govern the crucial physical processes as they are derived from the ensemble-averaged Navier–Stokes equations in a rational manner.

It is noted that the knowledge gained by the candidate's PhD thesis (*Asymptotic theory of marginal turbulent separation*, Vienna University of Technology (2001), supervision by Professor Alfred Kluwick) provided a basis insofar as the proposed asymptotic two-parameter description of turbulent boundary layers allowed for a first insight into the process of internal separation. However, the knowledge gained subsequently is, most importantly, tied in with the development of novel strategies in the treatment of locally strong interaction between the boundary layer and the circumjacent flow regions. These aspects have proven crucial for a self-consistent hierarchical flow description of both marginally and massively separated flows as comprised by the present thesis.

2.2 Organisation of the thesis

This is the principal part of the cumulative thesis, which comprises ten selected published contributions. An introductory overview (chapter 3) subsumes the essential aspects of the new theories established put forward in the original papers (chapter 4). The thesis is concluded by a brief survey on recent results and further perspectives concerning the massive-separation case which are topic of the current and planned research (chapter 5). The individual published contributions are enumerated as follows:

[1] A. Kluwick, B. Scheichl: *High-Reynolds-Number Asymptotics of Turbulent Boundary Layers: From Fully Attached to Marginally Separated Flows*, in: "BAIL 2008 – Boundary and Interior Layers. Proceedings of the International Conference on Boundary and Interior Layers – Computational and Asymptotic Methods, Limerick, July 2008", M. Stynes, A. Hegarty (eds.), Springer, Lecture Notes in Computational

Science and Engineering, **69**, Berlin, Heidelberg (2009), ISBN: 978-3-642-00604-3 / ISSN: 1439-7358, pp. 3–22 (invited Keynote Lecture);

[2] B. Scheichl, A. Kluwick: *Non-unique Self-similar Turbulent Boundary Layers in the Limit of Large Reynolds Numbers*, in: "Progress in Turbulence", J. Peinke, A. Kittel, S. Barth, M. Oberlack (eds.), Springer, Springer Proceedings in Physics, **101**, Berlin, Heidelberg, New York (2005), ISBN: 3-540-23216-8, pp. 111–114.

[3] B. Scheichl, A. Kluwick: *Non-Unique Quasi-Equilibrium Turbulent Boundary Layers*, in: "ICTAM04 Abstracts Book and CD-ROM Proceedings", W. Gutkowski, T. A. Kowalewski (eds.), Ippt Pan, Warsaw (2004), ISBN: 83-89687-01-1, Paper ID: FM2L_11083, 2 pages;

[4] B. Scheichl, A. Kluwick: *Singular solutions of the boundary layer equations in the case of marginal separation as Re tends to infinity*, in: "Advances in Turbulence IX. Proceedings of the Ninth European Turbulence Conference", I. P. Castro, P. E. Hancock (eds.), CIMNE, Barcelona (2002), ISBN: 84-95999-07-2, pp. 829–832;

[5] B. Scheichl, A. Kluwick: *Turbulent Marginal Separation and the Turbulent Goldstein Problem*, AIAA Journal, **45** (2007), 1, 20–36 (DOI: 10.2514/1.23518);

[6] B. Scheichl, A. Kluwick: *On turbulent marginal boundary layer separation: how the half-power law supersedes the logarithmic law of the wall*, International Journal of Computing Science and Mathematics (IJCSM), **1** (2007), 2/3/4, 343–359;

[7] B. Scheichl, A. Kluwick: *Asymptotic theory of bluff-body separation: a novel shear-layer scaling deduced from an investigation of the unsteady motion*, Journal of Fluids and Structures, **24** (2008), 8, 1326–1338;

[8] B. Scheichl, A. Kluwick, M. Alletto: *"How turbulent" is the boundary layer separating from a bluff body for arbitrarily large Reynolds numbers?*, Acta Mechanica, **201** (2008), 1/2/3/4, 131–151;

[9] B. Scheichl, A. Kluwick: *Level of Turbulence Intensity Associated with Bluff-Body Separation for Large Values of the Reynolds Number*, AIAA Meeting Paper 2008–4348 (2008);

[10] B. Scheichl, A. Kluwick, F. T. Smith: *Break-away separation for high turbulence intensity and large Reynolds number*, Journal of Fluid Mechanics, in print (2010, DOI: 10.1017/S0022112010005306).

Paper [1] represents a survey on the description of attached and marginally separated boundary layers. With the exception of paper [4], all contributions are listed in chronological order of their (initial) submission, which thus reflects the deepening of the understanding gained. All papers are attached in their original form, apart from paper [10] where the accepted manuscript submitted for typesetting (September 2010) is provided. The specific topics covered by each of the contributed papers are summarised subsequently.

All papers refer to peer-reviewed conference or represent peer-reviewed journal contributions, respectively.

The Addendum to this main part refers to other research work in fluid mechanics and heat transfer carried out by the candidate. It aims at demonstrating his diversified knowledge in these fields.

3 Brief overview in view of the papers

The discussion of the individual papers is commenced by a terse review on the problem of separation of an initially firmly attached turbulent boundary layer.

3.1 Turbulent separation: a long-standing challenge

Asymptotic methods have undeniably proven very successful in the treatment of turbulent shear flows in the limit of large Reynolds numbers. In particular, for both incompressible and compressible internal flows as pipes flows, open-channel flows, and wall-bounded flows driven by essentially inviscid external flows self-consistent theories have been established, which are based on merely a few assumptions that are intrinsically tied in with the loss of information about the nature of turbulence due to the time- or Reynolds-averaging process. Here seminal work associated with great names as, just to name some most important representatives (in alphabetical order), Afzal, Bush, Deriat, Fendell, Gersten, Guiraud, Mellor, Sykes, Walker, and Yajnik have to be acknowledged. Their work is referenced in paper [1]. However, despite their pioneering and promising contributions to the last category of flows all subsequent attempts to cope with turbulent separation have remained incomplete. As found out in the course of the research presented here, the classical boundary-layer scaling applies to firmly attached flows only, which in turn reveals a major source for the intractability of this extremely demanding but nevertheless fundamental and important problem in fluid mechanics in the past.

The discussion of turbulent boundary layers can be classified in terms of the three sections 3.2–3.4. It is initiated by a study of the asymptotic structure of the initially wall-bounded flow, which in turn indicates two distinctly different types of boundary layers: namely those having a relatively small and a large streamwise velocity deficit across their fully turbulent main region with respect to the imposed external flow. The first type includes boundary layers of a so-called moderately large (but still small) defect, which remain attached. Their appealing properties which a link between the two flow families. The first type is found to have a proclivity to massive, the second to marginal separation. In turn, they are associated with different routes to separation, depending on the specific flow configuration: here the flow past a bluff obstacle and internal flow (like that in a volute chamber) serve as typical representatives referring to the first and the second kind, respectively.

It is stressed that the analysis presented is restricted to nominally steady and two-dimensional flow, which is initially attached to a impervious rigid surface.

3.2 Wall-bounded and internally separating turbulent shear layers: hypotheses and asymptotic concepts

Papers [1]–[3] serve as an overview on the theoretical concepts underlying the description of both attached and separating flows.

- **Paper [1]** provides a concise synopsis of the asymptotic description of turbulent boundary layers in general. More specifically, it includes the aspects of non-uniqueness for quasi-equilibrium flows with a moderately large velocity deficit and marginal (i.e. internal) separation. It starts with a precise formulation of the hypotheses that underly a rigorous theory: here the question how the time-mean scaling of turbulent boundary layers can be traced back to a minimum of assumptions motivated by physical insight serves as the principal guidance. It is shown subsequently how a systematic extension of the classical theory of firmly attached boundary layers eventually leads to flow description that covers the aforementioned phenomena. The essential results of the marginal-separation analysis are summarised: papers [4]–[6]. Finally, first considerations regarding the distinct differences to a flow structure consistent with the occurrence of massive or gross separation are put forward: papers [7]–[10].

- **Paper [2]** is on an interesting engineering application of the non-uniqueness addressed in paper [1]: a diffusor shaped in form of a plane curved duct such that the turbulent boundary at its inner wall assumes the corresponding self-similar form allows the flow to withstand the maximum pressure rise possible *without* undergoing separation. Furthermore, it is demonstrated how early experimental data back the description of non-unique flows.

- **Paper [3]** is on the formulation and solution strategy of the problem resulting from the boundary layer approximation already mentioned in paper [2] that confirms the rigorous prediction of double-valued self-preserving flow. It shall be noted that this remarkable property of flows having a moderately large velocity deficit is envisaged in more detail in the current investigations.

3.3 Marginal separation

Papers [4]–[6] represent a detailed discussion of "thick" (large-defect) boundary layers undergoing marginal separation:

- **Paper [4]** summarises the local analysis of the solutions of the non-interactive boundary layer equations near their breakdown associated with the onset of separation. The asymptotic scaling of the flow is argued in paper [1] and introduced in more depth and breath in paper [5]. Particular emphasis is placed on the local structures of both the marginal-separation and the Goldstein singularity. Hence, these preliminary investigation serves as a pilot study to paper [5].

- **Paper [5]** elucidates the multi-layer structure of a turbulent boundary layer that is sensitive to marginal separation: this is established on the basis of the mixing-length concept, where commonly accepted scaling arguments are adopted. In turn, our concern is with a relatively "thick" boundary layer having a large streamwise velocity defect rather than an asymptotically small one as known from the classical scaling. Moreover, the scaling of the outer two-tiered wake-type flow region that comprises most of the boundary layer is found to be essentially independent of the Reynolds number, which may take on arbitrarily large values. As an important consequence of this non-classical flow description, the outermost wake layer plays a crucial role in the analysis of internal separation. To a large extent, it can be treated separately from the flow regions more close to the wall as the conditions of matching provide sufficient information which is needed to devise the novel triple-deck theory. This finally describes the recirculating flow in the formal limit of infinite Reynolds number.

- **Paper [6]** includes complementary material to the marginal-separation case as it focusses on the behaviour of both the inner wake layer and the near-wall flow. Here the so-called viscous wall layer adjacent to the surface and the drastic modification of the classical law of the wall as separation is encountered requires specific attention. Thus this analysis completes the description of attached and marginally separating "thick" turbulent boundary layers as it allows for perturbations of the limit considered in paper [4] due to high but finite values of the Reynolds number.

3.4 Massive separation

Papers [7]–[10] deal with boundary layers on bluff bodies, i.e. solid obstacles in uniform stream at very high Reynolds numbers. Here the strongly viscosity-affected flow originates close to the front stagnation point, is found to undergo laminar–turbulent transition within an encompassing boundary-layer region of asymptotically small streamwise extent, and forms a turbulent boundary layer further downstream. Finally, this is subject to gross separation a finite distance from the leading edge. The analysis discards the possibility of flow detachment close to a rear stagnation point associated with a fully attached external potential flow. Therefore, any possible candidate of the separation point lies within a certain section of the body surface, so that the corresponding external flow is sought in the class of irrotational flows that exhibit a free streamline which departs tangentially but with infinite curvature from the wall. This characteristic of the inviscid flow leads to a new interaction strategy governing the local separation process. Most importantly, it predicts a delay of transition to fully developed turbulent flow as long as the boundary layer remains attached. The development of the theory is reproduced by the chronological order of the four contributions:

- **Paper [7]** is devoted to the possible structures of both the imposed external and the attached boundary layer flow. To this end, related previous studies are reinvestigated. In turn, the analytical findings point to an external flow of Helmholtz–

Kirchhoff type and the possibility of a "thick" boundary layer as it has proven successful in the description of marginal separation. Here numerical results that simulate the singular terminal behaviour of the solutions of the boundary layer equations when separation is approached seem encouraging. Finally, a short but nevertheless promising attempt is made to underpin the flow scaling on the basis of a multiple-scales analysis applied to the unsteady Navier–Stokes equations. Future efforts in this direction are expected to reduce the number of hypotheses underlying the flow structure as formulated in the papers [1], [5] and [6].

- **Paper [8]** highlights the finding that this type of boundary layer is inconsistent with the scenario of laminar–turbulent transition of the flow that must take place sufficiently far upstream of separation. More precisely, a remarkable consequence can be drawn at this stage of knowledge: a self-consistent description of bluff-body separation that accounts for the structure of the global flow (rather than just the embedded boundary layer as studied in preceding work) requires the turbulent boundary layer to be of classical two-tiered small-defect type – provided the flow is assumed to exhibit fully developed turbulence. This is a consequence of the analysis of the time-averaged transition process near the leading edge. On the other hand, matching the transitional with the developed turbulent flow further downstream provides a first hint that this flow picture has presumably be relaxed insofar as there the level of turbulence intensity remains indeed below its theoretical limit associated with the traditional boundary layer scaling. Furthermore, a new method devised for an efficient numerical treatment of the external Kirchhoff flow is introduced briefly. It allows for a systematic numerical investigation of the boundary layer flow for various turbulence intensity levels and different positions of separation. To this end, the Reynolds shear stress gradient is included in the Prandtl-type boundary layer equations. However, yet no final judgement can be made at this stage of the research, neither of the effective scaling of the boundary layer nor the associated flow structure near separation.

- **Paper [9]** corroborates these findings as wind tunnel experiments carried out much earlier seem to support the existence of underdeveloped turbulence in the boundary layer flow past blunt bodies. This new and rather surprising interpretation of published and unpublished data motivates a careful analysis of the boundary layer equations parametrised by the level of turbulence intensity and (tentatively) dealt with numerically in paper [8]. Their detailed asymptotic analysis for sufficiently high turbulence intensity levels reveals/confirms the internal two-layer structure as already proposed there. The outer small-defect region is found to terminate in a weak singular behaviour at the position of inviscid separation, where the flow structure remains essentially unaltered. Hence, the evolution of the viscous wall layer from stagnation towards separation is under focus, which undergoes a pronounced change to subsequent breakdowns of the identified flow regions that govern its streamwise development. As an important result, under rather general conditions the solution of the boundary layer equations are found terminate in form

of a Goldstein singularity: its strength increases above all bounds with increasing turbulence intensity; simultaneously,its position asymptotically approaches that of inviscid flow detachment.

- **Paper [10]** first integrates the results gained so far and puts it in the context of the ultimate goal to obtain a self-consistent description of the entire flow field: the attached boundary layer exhibits underdeveloped turbulence and an asymptotically small velocity deficit in its outer tier. On the one hand, this situation is traced back to the structure of the transitional flow near the leading edge. On the other (and even more importantly), it satisfies the requirement of a viscous–inviscid interaction mechanism that locally describes the separation process in a rigorous manner. The latter rationale exploits the necessity that the thickness of the wall layer varies essentially algebraically with that of the outer tier, rather than exponentially as in the classical scaling valid for fully developed turbulent flow. Both the external inviscid and the boundary layer flow encounter a singular behaviour near separation. Its regularisation finally yields a new interacting-flow problem, studied in detail. This comprises two interaction mechanisms having a rather complex interplay: an "inner" one that points to a close resemblance with the triple-deck structure known from laminar separation, whereas the "outer" one describes an inviscid vortex flow induced in the just separating small-defect region. Remarkably, matching both mechanisms is expected to determine of the effective position of separation and thus fix the structure of the flow on the obstacle scale. A thorough investigation of this demanding problem is part of the current research activities. In the conclusions the different pathways to separation and their impact on open questions are elucidated: here the present knowledge of the asymptotic structure of turbulent boundary layers shows great promise for a comprehensive treatment of hitherto unsolved or partially solved related turbulent-flow problems having engineering relevance. Examples are, amongst others, the flow past cusp- and wedge-shaped trailing edges of airfoils and flat plates, both aligned and under an angle of attack, and shock/boundary layer interaction. In the appendix two issues regarding the potential-flow problem are scrutinised: the detailed structure of the singularity and the method enabling its convenient numerical solution (addressed concisely in paper [8]).

Chapter 5 reviews the description of massive separation. The intention of this synopsis is to condense the current status quo of of understanding covered by the papers [7]–[10] and address open points.

4 Selected papers

The papers are enclosed subsequently in the order of the list given in section 2.2. Each contribution represents a section of this chapter.

High-Reynolds-Number Asymptotics of Turbulent Boundary Layers: from Fully Attached to Marginally Separated Flows

Dedicated to Professor Klaus Gersten on the occasion of his 80th birthday

Alfred Kluwick and Bernhard Scheichl

Institute of Fluid Mechanics and Heat Transfer, Vienna University of Technology, Resselgasse 3/E322, A-1040 Vienna, Austria
alfred.kluwick@tuwien.ac.at, bernhard.scheichl@tuwien.ac.at

Summary. This paper reports on recent efforts with the ultimate goal to obtain a fully self-consistent picture of turbulent boundary layer separation. To this end, it is shown first how the classical theory of turbulent small-defect boundary layers can be generalised rigorously to boundary layers with a slightly larger, i.e. moderately large, velocity defect and, finally, to situations where the velocity defect is of $O(1)$. In the latter case, the formation of short recirculation zones describing marginally separated flows is found possible, as described in a rational manner.

Key words: marginal separation; perturbation methods; turbulent boundary layers
PACS: 40.10.A; 47.27.eb; 47.27.Jv; 47.27.nb; 47.32.Ff

1 Introduction

Despite the rapid increase of computer power in the recent past, the calculation of turbulent wall-bounded flows still represents an extremely challenging and sometimes insolvable task. Direct-Numerical-Simulation computations based on the full Navier–Stokes equations are feasible for moderately large Reynolds numbers only. Flows characterised by much higher Reynolds numbers can be investigated if one resorts to turbulence models for the small scales, as accomplished by the method of Large Eddy Simulation, or for all scales, as in computer codes designed to solve the Reynolds-averaged Navier–Stokes equations. Even then, however, the numerical efforts rapidly increase with increasing Reynolds number. This strongly contrasts the use of asymptotic theories, the performance of which improves as the values of the Reynolds number become larger and, therefore, may be considered to complement purely numerically based work.

With a few exceptions (e.g. [7,21]), studies dealing with the high-Reynolds-number properties of turbulent boundary layers start from the Reynolds-averaged equations. By defining non-dimensional variables in terms of a representative length $\tilde{L}$ and flow speed $\tilde{U}$ and assuming incompressible nominally steady two-dimensional flow they take on the form

$$\frac{\partial u}{\partial x}+\frac{\partial v}{\partial y}=0\ , \tag{1a}$$

$$u\frac{\partial u}{\partial x}+v\frac{\partial u}{\partial y}=-\frac{\partial p}{\partial x}+\frac{1}{Re}\nabla^2 u-\frac{\partial\overline{u'^2}}{\partial x}-\frac{\partial\overline{u'v'}}{\partial y}\ , \tag{1b}$$

$$u\frac{\partial v}{\partial x}+v\frac{\partial v}{\partial y}=-\frac{\partial p}{\partial y}+\frac{1}{Re}\nabla^2 v-\frac{\partial\overline{u'v'}}{\partial x}-\frac{\partial\overline{v'^2}}{\partial y}\ . \tag{1c}$$

Herein $\nabla^2=\partial^2/\partial x^2+\partial^2/\partial y^2$, and (x,y), (u,v), $(u'v')$, $\overline{u'^2}$, $\overline{u'v'}$, $\overline{v'^2}$, and p are Cartesian coordinates measuring the distance along and perpendicular to the wall, the corresponding time mean velocity components, the corresponding velocity fluctuations, the components of the Reynolds stress tensor, and the pressure, respectively. The Reynolds number is defined by $Re:=\tilde{U}\tilde{L}/\tilde{\nu}$, where $\tilde{\nu}$ is the (constant) kinematic viscosity. Equations (1) describe flows past flat walls. Effects of wall curvature can be incorporated without difficulty but are beyond the scope of the present analysis.

When it comes down to the solution of the simplified version of these equations provided by asymptotic theory in the limit $Re\to\infty$, one is, of course, again faced with the closure problem. The point, however, is that these equations and the underlying structure represent closure independent basic physical mechanisms characterising various flow regions identified by asymptotic reasoning. This has been shown first in the outstanding papers [5, 8, 10, 31], and more recently and in considerable more depth and breath, in [24,30] for the case of small-defect boundary layers, which will be considered in Sect. 2. Boundary layers exhibiting a slightly larger, i.e. a moderately large, velocity defect are treated in Sect. 3. Finally, Sect. 4 deals with situations where the velocity defect is of $O(1)$ rather than small.

2 Classical Theory of Turbulent Small-Defect Turbulent Boundary Layers

We first outline the basic ideas underlying an asymptotic description of turbulent boundary layers.

2.1 Preliminaries

Based on dimensional reasoning put forward by L. Prandtl and Th. v. Kármán, a self-consistent time-mean description of firmly attached fully developed turbulent boundary layers holding in the limit of large Reynolds numbers Re, i.e.

for $Re \to \infty$, has been proposed first in the aforementioned studies [5,8,10,31]. One of the main goals of the present investigation is to show that this rational formulation can be derived from a minimum of assumptions:

(a) all the velocity fluctuations are of the same order of magnitude in the limit $Re \to \infty$, so that all Reynolds stress components are equally scaled by a single velocity scale $u_{\rm ref}$, non-dimensional with a global reference velocity (hypothesis of locally isotropic turbulence);
(b) the pressure gradient does not enter the flow description of the viscous wall layer to leading order (assumption of firmly attached flow);
(c) the results for the outer predominantly inviscid flow region can be matched directly with those obtained for the viscous wall layer (assumption of "simplest possible" flow structure).

In the seminal studies [5, 8, 10, 31], $u_{\rm ref}$ is taken to be of the same order of magnitude in the fully turbulent main portion of the boundary layer and in the viscous wall layer and, hence, equal to the skin friction velocity

$$u_\tau := \left[Re^{-1}(\partial u/\partial y)_{y=0}\right]^{1/2} \ . \tag{2}$$

This in turn leads to the classical picture, according to which (i) the streamwise velocity defect with respect to the external impressed flow is small and of $O(u_\tau)$ across most of the boundary layer, while (ii) the streamwise velocity is itself small and of $O(u_\tau)$ inside the (exponentially thin) wall layer, and (iii) $u_\tau/U_e = O(1/\ln Re)$. Furthermore, then (iv) the celebrated universal logarithmic velocity distribution

$$u/u_\tau \sim \kappa^{-1} \ln y^+ + C^+ \ , \quad y^+ := y\, u_\tau Re \to \infty \ . \tag{3}$$

is found to hold in the overlap of the outer (small-defect) and inner (viscous wall) layer. Here κ denotes the v. Kármán constant; in this connection we note the currently accepted empirical values $\kappa \approx 0.384$, $C^+ \approx 4.1$, which refer to the case of a perfectly smooth surface, see [16] and have been obtained for a zero pressure gradient.

This might be considered to yield a stringent derivation of the logarithmic law of the wall (3), anticipating the existence of an asymptotic state and universality of the wall layer flow as $Re \to \infty$; a view which, however, has been increasingly challenged in more recent publications (e.g. [2–4]). It thus appears that – as expressed by Walker, see [30] – "although many arguments have been put forward over the years to justify the logarithmic behaviour, non are entirely satisfactory as a proof, ...". As a result, one has to accept that matching (of inner and outer expansions), while ensuring self-consistency, is not sufficient to uniquely determine (3). In the following, from the viewpoint of the time-averaged flow description the logarithmic behaviour (3), therefore, will be taken to represent an experimentally rather than strictly theoretically based result holding in situations where the assumption (b) applies. The description of the boundary layer in the limit $Re \to \infty$ can then

readily be formalised. In passing, we mention that in the classical derivations, see [5,8,10,31], the assumption (b) is not adopted and (3) results from matching, rather than in the present study where it is imposed.

2.2 Leading-Order Approximation

Inside the wall layer where $y^+ = y\,u_\tau Re = O(1)$ the streamwise velocity component u, the Reynolds shear stress $\tau = -\overline{u'v'}$ and the pressure p are expanded in the form

$$u \sim u_\tau(x;Re)\,u^+(y^+) + \cdots\ , \tag{4a}$$

$$\tau \sim u_\tau^2(x;Re)\,t^+(y^+) + \cdots\ , \tag{4b}$$

$$p \sim p_0(x) + \cdots\ , \tag{4c}$$

where u^+ exhibits the limiting behaviour implied by (3):

$$u^+(y^+) \sim \kappa^{-1}\ln y^+ + C^+\ , \quad y^+ \to \infty\ . \tag{5}$$

Assumption (c), quoted in Subsect. 2.1, then uniquely determines the asymptotic expansions of, respectively, u, τ, and p further away from the wall where the Reynolds stress τ is predominant. Let $\delta_\mathrm{o}(x;Re)$ characterise the thickness of this outer main layer, i.e. of the overall boundary layer. In turn, one obtains

$$u \sim U_e(x) - u_\tau(x;Re)\,F_1'(x,\eta) + \cdots\ , \tag{6a}$$

$$\tau \sim u_\tau^2(x;Re)\,T_1(x,\eta) + \cdots\ , \tag{6b}$$

$$p \sim p_e(x) + \cdots\ , \tag{6c}$$

where $\eta := y/\delta_\mathrm{o}$. Here and in the following primes denote differentiation with respect to η. Furthermore, U_e and p_e stand for the velocity and the pressure, respectively, at the outer edge $\eta = 1$ of the boundary layer (here taken as a sharp line with sufficient asymptotic accuracy) imposed by the external irrotational flow.

Matching of the expansions (4) and (6) by taking into account (5) forces a logarithmic behaviour of F_1',

$$F_1' \sim -\kappa^{-1}\ln\eta + C_0(x)\ , \quad \eta \to 0\ , \tag{7}$$

yields $p_0(x) = p_e(x)$, and is achieved provided $\gamma := u_\tau/U_e$ satisfies the skin friction relationship

$$\kappa/\gamma \sim \ln(Re\gamma\delta_\mathrm{o}U_e) + C^+ + C_0 + O(\gamma)\ . \tag{8}$$

From substituting (4) into the x-component (1b) of the Reynolds equations (1) one obtains the well-known result that the total stress inside the wall layer is constant to leading order,

$$\mathrm{d}u^+/\mathrm{d}y^+ + t^+ = 1\ . \tag{9}$$

Moreover, the expansions (6) lead to a linearisation of the convective terms in the outer layer, so that there Bernoulli's law holds to leading order,

$$\mathrm{d}p_e/\mathrm{d}x = -U_e\,\mathrm{d}U_e/\mathrm{d}x\ . \tag{10}$$

The necessary balance with the gradient of the Reynolds shear stress then determines the magnitude of the thickness of the outer layer, i.e. $\delta_\mathrm{o} = O(u_\tau)$. As a consequence, the expansions (6) are supplemented with

$$\delta_\mathrm{o} \sim \gamma\,\Delta_1(x) + \cdots\ , \tag{11}$$

which in turn gives rise to the leading-order outer-layer streamwise momentum equation. After integration with respect to η and and employing the matching condition $T_1(x,0) = 1$, the latter is conveniently written as

$$(E + 2\beta_0)\eta F_1' - EF_1 - \Delta_1 F_{1,e}\,F_{1x} = F_{1,e}(T_1 - 1)\ , \tag{12a}$$

$$F_{1,e} := F_1(x,1)\ , \quad E := 1 - \Delta_1\frac{\mathrm{d}F_{1,e}}{\mathrm{d}x}\ , \quad \beta_0 := -\Delta_1 F_{1,e}\frac{U_{ex}}{U_e}\ . \tag{12b}$$

From here on, the subscript x means differentiation with respect to x. The boundary layer equation (12a) is unclosed, and in order to complete the flow description, turbulence models for t^+ and T_1 have to be adopted. Integration of (12) then provides the velocity distribution in the outer layer and determines the yet unknown function $C_0(x)$ entering (7) and the skin friction relationship (8), which completes the leading-order analysis.

As a main result, inversion of (8) with the aid of (11) yields

$$\gamma \sim \kappa\sigma[1 - 2\sigma\ln\sigma + O(\sigma)], \quad \sigma := 1/\ln Re\ , \quad \partial\gamma/\partial x = O(\gamma^2)\ . \tag{13}$$

The skin friction law (13) implies the scaling law (iii), already mentioned in Subsect. 2.1, which is characteristic of classical small-defect flows.

2.3 Second-Order Outer Problem

Similar to the description of the leading-order boundary layer behaviour, the investigation of higher-order effects is started by considering the wall layer first. Substitution of (4a), (4b), (8) into (1b) yields upon integration (cf. [30]),

$$\frac{1}{Re}\frac{\partial u}{\partial y} + \tau \sim \gamma^2 U_e^2 - \frac{U_e U_{ex}}{\gamma Re}\,y^+ + \frac{\gamma U_e U_{ex}}{Re}\int_0^{y^+} {u^+}^2\,\mathrm{d}y^+ + \cdots\ . \tag{14}$$

Here the second and third terms on the right-hand side account, respectively, for the effects of the (imposed) pressure gradient, c.f. (10), and convective terms, which have been neglected so far. By using (5) and (12), the asymptotic behaviour of τ as $y^+ \to \infty$ can easily be obtained (e.g. [30]). Rewritten in terms of the outer-layer variable η, it is found to be described by

$$\frac{\tau}{U_e^2} \sim \gamma^2\left[1 + 2\frac{\Delta_0 U_{ex}}{\kappa U_e}\eta\ln\eta + \cdots\right] + \gamma^3\left[\frac{\Delta_0 U_{ex}}{\kappa^2 U_e}\eta(\ln\eta)^2 + \cdots\right] + \cdots\ , \tag{15}$$

as $\eta \to 0$, which immediately suggests the appropriate generalisation of the small-defect expansions (6a), (6b), (11):

$$u/U_e \sim 1 - \gamma F_1' - \gamma^2 F_2' + \cdots \,, \tag{16a}$$

$$\tau/U_e^2 \sim \gamma^2 T_1 + \gamma^3 T_2 + \cdots \,, \tag{16b}$$

$$\delta_o \sim \gamma\, \Delta_1(x) + \gamma^2 \Delta_2(x) + \cdots \,. \tag{16c}$$

Here matching with the wall layer is achieved if

$$F_1' \sim -\kappa^{-1} \ln \eta + C_0(x) \,, \quad F_2' \sim C_1(x) \,, \tag{17a}$$

$$T_1 \sim 1 + 2\frac{\Delta_0 U_{ex}}{\kappa U_e}\eta \ln \eta \,, \quad T_2 \sim \frac{\Delta_0 U_{ex}}{\kappa^2 U_e}\eta (\ln \eta)^2 \,, \tag{17b}$$

as $\eta \to 0$, provided that the skin friction relationship (8) is modified to explicitly include an additional term of $O(\gamma)$,

$$\kappa/\gamma \sim \ln(Re\gamma\delta_o U_e) + C^+ + C_0 + \gamma C_1 + \cdots \,. \tag{18}$$

Similar to $C_0(x)$, the function $C_1(x)$ depends on the specific turbulence model adopted, as well as the upstream history of the boundary layer.

2.4 Can Classical Small-Defect Theory Describe Boundary Layer Separation?

An estimate of the thickness δ_w of the viscous wall layer is readily obtained from the definition of y^+, see (3), and the (inverted) skin friction relationship (13): $\delta_w = O[\gamma^{-1} \exp(-\kappa/\gamma)]$. In the limit $Re \to \infty$, therefore, the low-momentum region close to the wall is exponentially thin as compared to the outer layer, where Reynolds stresses cause a small $O(\gamma)$ reduction of the fluid velocity with respect to the mainstream velocity $U_e(x)$. This theoretical picture of a fully attached turbulent small-defect boundary layer has been confirmed by numerous comparisons with experimental data for flows of this type (e.g. [1, 14, 30]). However, it also indicates that attempts based on this picture to describe the phenomenon of boundary layer separation, frequently encountered in engineering applications, will encounter serious difficulties. Since the momentum flux in the outer layer, which comprises most of the boundary layer, differs only slightly from that in the external flow region, an $O(1)$-pressure rise almost large enough to cause flow reversal even there appears to be required to generate negative wall shear, which hardly can be considered as flow separation. This crude estimate is confirmed by a more detailed analysis dealing with the response of a turbulent small-defect boundary layer to a surface-mounted obstacle, carried out, among others, in [28]. Moreover, to date no self-consistent theory of flow separation compatible with the classical concept of a turbulent small-defect boundary layer has been formulated.

The above considerations strikingly contrast the case of laminar boundary layer separation, where the velocity defect is of $O(1)$ across the whole boundary layer and the associated pressure increase tends to zero as $Re \to \infty$. It,

however, also indicates that a turbulent boundary layer may become more prone to separation by increasing the velocity defect. That this is indeed a realistic scenario can be inferred by seeking self-preserving solutions of (12), i.e. by investigating equilibrium boundary layers. Such solutions, where the functions F_1, T_1, characterising the velocity deficit and the Reynolds shear stress in the outer layer, respectively, solely depend on η, exist if the parameter β_0 in the outer-layer momentum equation (12a) is constant, i.e. independent of x. Equation (12a) then assumes the form

$$(1+2\beta_0)\eta F_1' - F_1 = F_{1,e}(T_1-1)\ , \tag{19}$$

where

$$U_e \propto (x-x_\mathrm{v})^m\ , \quad m=-\beta_0/(1+3\beta_0)\ , \quad \Delta_1 F_{1,e} = (1+3\beta_0)(x-x_\mathrm{v})\ . \tag{20}$$

Herein $x=x_\mathrm{v}$ denotes the virtual origin of the boundary layer flow. In the present context flows associated with large values of β_0 are of most interest. By introducing suitably (re)scaled quantities in the form $F_1=\beta_0^{1/2}\hat{F}(\hat{\eta})$, $T_1=\beta_0\hat{T}(\hat{\eta})$, $\eta=\beta_0^{1/2}\hat{\eta}$, the momentum equation (19) reduces to

$$2\hat{\eta}\hat{F}' = \hat{F}_e\hat{T}\ , \quad F_e := \hat{F}(1) \tag{21}$$

in the limit $\beta_0\to\infty$. Solutions of (21) describing turbulent boundary layers having a velocity deficit measured by $u_\mathrm{ref}:=\beta_0^{1/2}u_\tau \gg u_\tau$ have been obtained first in [11]. Unfortunately, however, it was not realised that this increase of the velocity defect no longer allows for a direct match of the flow quantities in the outer and inner layer, which has significant consequences, to be elucidated below.

We note that in general $\beta_0(x)$ can be regarded as the leading-order contribution to the so-called Rotta–Clauser pressure-gradient parameter (e.g. [24]),

$$\beta := -U_eU_{ex}\delta^*/u_\tau^2\ , \quad \delta^* := \delta_\mathrm{o}\int_0^\infty (1-u/U_e)\,\mathrm{d}\eta\ . \tag{22}$$

As already mentioned in [11], this quantity allows for the appealing physical interpretation that u_ref is independent of the wall shear stress u_τ^2 for $\beta_0\gg 1$.

3 Moderately Large Velocity Defect

Following the considerations summarised in the preceding section, we now seek solutions of (1) describing a relative velocity defect of $O(\varepsilon)$, where the newly introduced perturbation parameter ε is large compared to γ but still small compared to one: $\gamma\ll\varepsilon\ll 1$. From assumption (a), see Subsect. 2.1, we then have $-\overline{u'v'}\sim\varepsilon^2$, and the linearised x-momentum equation immediately yields the estimate $\delta_\mathrm{o}=\varepsilon\Delta$, where $\Delta=O(1)$, for the boundary layer

thickness. However, since $-\overline{u'v'} \sim \varepsilon^2 \gg u_\tau^2$, the solution describing the flow behaviour in the outer velocity defect region no longer matches with the solution for the universal wall layer as in the classical case. As a consequence, the leading-order approximation to the Reynolds shear stress must vanish in the limit $\eta = y/\delta_\mathrm{o} \to 0$. This indicates that the flow having a velocity defect of $O(\varepsilon)$ in the outer main part of the boundary layer exhibits a wake-type behaviour, leading to a finite wall slip velocity at its base and, therefore, forces the emergence of a sublayer, termed intermediate layer, where the magnitude of $-\overline{u'v'}$ reduces to $O(u_\tau^2)$, being compatible with the wall layer scaling.

3.1 Intermediate Layer

Here the streamwise velocity component u is expanded about its value at the base $\eta = 0$ of the outer defect region: $u/U_e \sim 1 - \varepsilon W - \gamma U_\mathrm{i} + \cdots$, so that the quantities W, U_i, assumed to be of $O(1)$, account, respectively, for the wall slip velocity, given by $u = U_e(1 - \varepsilon W)$ with $W > 0$, and the dominant contribution to u that varies with distance y from the wall. Integration of the x-momentum balance then shows that the Reynolds shear stress increases linearly with distance y for $y/\delta_\mathrm{o} \ll 1$:

$$\tau \sim \tau_w - \varepsilon (U_e^2 W)_x y \;, \quad y/\delta_\mathrm{i} = O(1) \;. \tag{23}$$

Herein δ_i denotes the thickness of the intermediate layer and τ assumes its near-wall value τ_w as $y/\delta_\mathrm{i} \to 0$. Matching with the wall layer then requires that $\tau_w \sim u_\tau^2$, which, by taking into account (22), yields the estimate $\delta_\mathrm{i}/\delta_\mathrm{o} = O(\beta^{-1})$. Also, since $\tau_w \sim u_\tau^2$, we infer that $\delta_\mathrm{i} = O(u_\tau^2/\varepsilon)$ and, in turn, recover the relationship $\varepsilon \sim u_\tau \beta^{1/2}$, already suggested by the final considerations of Subsect. 2.4. Formal expansions of u and $-\overline{u'v'}$ in the intermediate layer, therefore, are written as

$$u/U_e \sim 1 - \varepsilon W(x;\varepsilon,\gamma) - \gamma U_\mathrm{i}(x,\zeta) \;, \tag{24a}$$

$$-\overline{u'v'}/(\gamma U_e)^2 \sim T_\mathrm{i}(x,\zeta;\varepsilon,\gamma) \sim 1 + \lambda\zeta \;, \tag{24b}$$

where $\zeta := y/\delta_\mathrm{i} = y\varepsilon/(\Delta\gamma^2)$ and $\lambda := -\Delta (U_e^2 W)_x / U_e^2$.

To close the problem for U_i, we adopt the common mixing length concept,

$$-\overline{u'v'} := \ell^2 \frac{\partial u}{\partial y} \left| \frac{\partial u}{\partial y} \right| \;, \tag{25}$$

by assuming that the mixing length ℓ behaves as $\ell \sim \kappa y$ for $y = O(\delta_\mathrm{i})$, which is the simplest form allowing for a match with the adjacent layers. Integration of (24b) then yields

$$\kappa U_\mathrm{i} = -\ln\zeta + 2\ln\left[(1+\lambda\zeta)^{1/2} + 1\right] - 2(1+\lambda\zeta)^{1/2} \;, \tag{26}$$

from which the limiting forms

$$\kappa U_{\rm i} \sim -2(\lambda\zeta)^{1/2} + (\lambda\zeta)^{-1/2} + O(\zeta^{-3/2}) \;, \quad \zeta \to \infty \;, \tag{27a}$$

$$\kappa U_{\rm i} \sim -\ln(\lambda\zeta/4) - 2 - \lambda\zeta/2 + O(\zeta^2) \;, \qquad \zeta \to 0 \;, \tag{27b}$$

can readily be inferred. The behaviour (27a) holding at the base of the outer defect layer is recognised as the square-root law deduced first by Townsend in his study [29] of turbulent boundary layers exhibiting vanishingly small wall shear stress; the outermost layer so to speak "anticipates" the approach to separation as the velocity defect increases to a level larger than u_τ. We remark that Townsend in [29] identified the intermediate region as the so-called "equilibrium layer", where convective terms in (1b) are (erroneously within the framework of asymptotic high-Reynolds-number theory) considered to be negligibly small. Equation (27b) provides the logarithmic variation of $U_{\rm i}$ as $\zeta \to 0$, required by the match with the wall layer, which gives rise to the generalised skin friction relationship

$$\frac{\kappa}{\gamma} \sim \ln\!\left(\frac{Re\gamma^2 U_e^3}{\beta_0^{1/2}}\right) + \beta_0\kappa W + O(\gamma\beta_0) \sim (1+\varepsilon W)\ln Re \;. \tag{28}$$

Note that (28) reduces to (8) when $\beta_0 = O(1)$.

Having demonstrated that classical theory of turbulent boundary layers in the limit of large Reynolds number can – in a self-consistent manner – be extended to situations where the velocity defect is asymptotically large as compared to u_τ but still $o(1)$, we now consider the flow behaviour in the outer wake-type region in more detail.

3.2 Outer Defect Region

Following the arguments put forward at the beginning of Sect. 3, we write, by making use of the stream function ψ, the flow quantities in the outer layer in the form

$$p \sim p_e(x) + \varepsilon^2 P(x,\eta;\varepsilon,\gamma) \;, \tag{29a}$$

$$\psi/U_e \sim y - \varepsilon\delta_o F(x,\eta;\varepsilon,\gamma) \;, \tag{29b}$$

$$-\left[\overline{u'^2}, \overline{v'^2}, \overline{u'v'}\right] \sim U_e^2\varepsilon^2 [R,S,T](x,\eta;\varepsilon,\gamma) \;. \tag{29c}$$

As before, here $\eta = y/\delta_{\rm o}$ and we accordingly expand

$$Q \sim Q_1 + \varepsilon\, Q_2 + \cdots \;, \quad Q := F,P,R,S,T,W \;, \tag{30a}$$

$$\delta \sim \varepsilon\Delta_1 + \varepsilon^2\Delta_2 + \cdots \;, \tag{30b}$$

$$\beta/\beta_{\rm v} \sim B_0(x) + \varepsilon B_1(x) + \cdots \;, \quad \beta_{\rm v} \to \infty \;, \tag{30c}$$

where we require (without any loss of generality) that $\beta_{\rm v}$ equals β_0 at $x = x_{\rm v}$, so that $\beta_0 = \beta_{\rm v} B_0$ and $B_0(x_{\rm v}) = 1$, $B_i(x_{\rm v}) = 0$, $i = 1, 2, \ldots$. In analogy to (12), the first-order problem then reads

$$\frac{1}{U_e}\frac{\mathrm{d}(U_e\Delta_1)}{\mathrm{d}x}\eta F_1' - \frac{1}{U_e^3}\frac{\partial(U_e^3\Delta_1 F_1)}{\partial x} = T_1 \ , \tag{31a}$$

$$F_1(x,0) = F_1'(x,1) = F_1''(x,1) = T_1(x,1) = 0 \ , \tag{31b}$$

$$\eta \to 0: \quad T \sim (\kappa\eta F_1'')^2 \ , \quad F_1' \sim W_1(x) - (2/\kappa)(\lambda\eta)^{1/2} \ . \tag{31c}$$

In the following we concentrate on solutions which are self-similar up to second order, i.e. $\partial F_1/\partial x \equiv \partial T_1/\partial x \equiv 0$ and $\partial F_2/\partial x \equiv \partial T_2/\partial x \equiv 0$. By again adopting the notations $U_e = \hat{U}(x)$, $F_1 = \hat{F}(\eta)$, $T_1 = \hat{T}(\eta)$, $\Delta_1 = \hat{\Delta}(x)$, we recover the requirements (20), (21) for self-similarity at first order resulting from classical small-defect theory in the limit of large values of β_v, in agreement with (30b) and the definition of β provided by (22):

$$B_0 \equiv 1 \ , \quad \hat{\Delta}\hat{F}_e = 3(x - x_\mathrm{v}) \ , \quad \hat{U} = (C/3)^{1/3}(x - x_\mathrm{v})^{-1/3} \ , \tag{32}$$

with a constant C, and

$$2\eta\hat{F}' = \hat{F}_e\hat{T} \ , \quad \hat{F}(0) = \hat{T}(0) = \hat{F}'(1) = \hat{F}''(1) = \hat{T}(1) = 0 \ . \tag{33}$$

If, as in the discussion of the flow behaviour in the intermediate layer, a mixing length model $\hat{T} = [\ell(\eta)\hat{F}''(\eta)]^2$ in accordance with (25) is chosen to close the problem, integration of (33) yields the analytical expressions

$$\hat{F}'(\eta) = \frac{1}{2\hat{F}_e}\left[\int_\eta^1 \frac{z^{1/2}}{\ell(z)}\,\mathrm{d}z\right]^2 \ , \quad \hat{F}_e = \left\{\frac{1}{2}\int_0^1 \left[\int_\eta^1 \frac{z^{1/2}}{\ell(z)}\,\mathrm{d}z\right]^2 \mathrm{d}\eta\right\}^{1/2} \ . \tag{34}$$

Equations (34) have been evaluated numerically by using a slightly generalised version of the mixing length closure originally suggested in [13],

$$\ell = c_\ell I(\eta)^{1/2}\tanh(\kappa\eta/c_\ell) \ , \quad I = 1/(1 + 5.5\eta^6) \ , \quad c_\ell = 0.085 \ . \tag{35}$$

Herein $I(\eta)$ represents the well-known Klebanoff's intermittency factor proposed in [9]. One then obtains $W_1 = \hat{F}'(0) \doteq 13.868$, $\hat{F}_e \doteq 5.682$, and $\mathrm{d}\hat{\Delta}/\mathrm{d}x \doteq 0.528$, cf. (32). As seen in Fig. 1a, both $\hat{F}'$ and $\hat{T}$ vanish quadratically as $\eta \to 1$ as a result of the boundary conditions $\hat{T}(1) = \hat{T}'(1) = 0$, cf. (33). Also, note that $\hat{F}'$ exhibits the square-root behaviour required from the match with the intermediate layer as $\eta \to 0$.

Turning now to the second-order problem, we consider the most general case that the wall shear enters the description of the flow in the outer layer at this level of approximation (principle of least degeneracy). Therefore, we require $\varepsilon^3 T_2(0) \sim \gamma^2$, which finally determines the yet unknown magnitude of ε relative to γ, namely that $\varepsilon \sim \gamma^{2/3}$. Since, as pointed out before, $\varepsilon \sim \gamma\beta_0^{1/2}$, this implies that $\varepsilon\beta_0 = \Gamma = O(1)$. Inspection of the resulting second-order problem indicates that self similar solutions exist only if the external velocity distribution (32) predicted by classical theory is slightly modified in the form

$$\hat{U}(x) = (C/3)^{1/3}(x - x_\mathrm{v})^{-1/3+\mu}, \quad \mu \sim \gamma^{2/3}\mu_1 + \cdots \ , \tag{36}$$

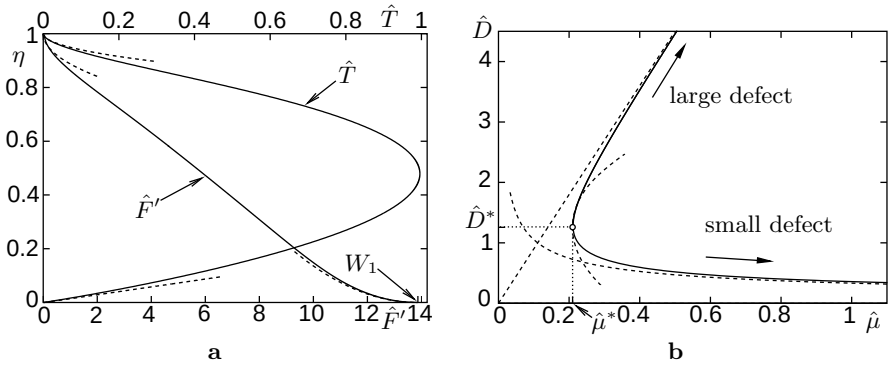

Fig. 1. Quasi-equilibrium flows: **a** $\hat{F}'(\eta)$, $\hat{T}(\eta)$, *dashed*: asymptotes found from (31b), (31c); **b** canonical representation (37), *dashed*: asymptotes (see last paragraph of Sect. 3) and parabola approximating the curve in the apex to leading order

where the $O(1)$-parameter μ_1 satisfies a solvability condition that represents the integral momentum balance obtained from integrating the second-order x-momentum equation from $\eta = 0$ to $\eta = 1$. It can be cast into the canonical form

$$9\hat{D}^2\hat{\mu} = 1 + \hat{D}^3 \; . \tag{37}$$

Herein $\hat{D} = r^{1/3}\Gamma^{1/3}$, $\hat{\mu} = r^{-2/3}\mu_1$, and

$$r = \hat{F}_e^{-1} \int_0^1 (\hat{F}'^2 - \hat{R} + \hat{S})\, \mathrm{d}\eta \; . \tag{38}$$

A graph of the relationship (37) which represents the key result of the analysis dealing with quasi-equilibrium boundary layer having a moderately large velocity defect is shown in Fig. 1b. Most interesting, it is found that solutions describing flows of this type exist for $\hat{\mu} \geq \hat{\mu}^* = 2^{1/3}/6$ only and form two branches, associated with non-uniqueness of the quantity $\hat{D}$, which serves as a measure of velocity defect, for a specific value of the pressure gradient. Along the lower branch, $\hat{D} \leq \hat{D}^* = 2^{1/3}$ and decreases with increasing values of $\hat{\mu}$, so that classical small defect theory is recovered in the limit $\hat{\mu} \to \infty$, where $\hat{D} \sim (9\hat{\mu})^{-1/2}$. In contrast, this limit leads to an unbounded growth of values $\hat{D} \geq \hat{D}^*$ associated with the upper branch: $\hat{D} \sim 9\hat{\mu}$ as $\hat{\mu} \to \infty$. This immediately raises the question if it is possible to formulate a general necessarily nonlinear theory which describes turbulent boundary layers having a finite velocity defect in the limit of infinite Reynolds number. We also note that the early experimental observations made by Clauser, see [6], seem to strongly point to this type of non-uniqueness.

4 Large Velocity Deficit

As in the cases of small and moderately small velocity defect we require the boundary layer to be slender. However, in contrast to the considerations of Sects. 2 and 3, the validity of this requirement can no longer be inferred from assumption (a) and the balance between convective and Reynolds stress gradient terms in the outer predominately inviscid region of the boundary layer which now yields $\partial\tau/\partial y = O(1)$, rather than $\partial\tau/\partial y \ll 1$ as earlier. A hint how this difficulty can be overcome is provided by the observation that the transition from a small to a moderately small velocity defect is accompanied with the emergence of a wake type flow in this outer layer. One expects that this effect will become more pronounced as the velocity defect increases further, suggesting in turn that the outer part of the boundary layer, having a velocity defect of $O(1)$, essentially behaves as a turbulent free shear layer. An attractive strategy then is to combine the asymptotic treatment of such flows (e.g. [25]) in which the experimentally observed slenderness is enforced through the introduction of a Reynolds-number-independent parameter $\alpha \ll 1$ with the asymptotic theory of turbulent wall bounded flows.

4.1 Outer Wake Region

Let the parameter $\alpha \ll 1$ measure the lateral extent of the outer wake region, so that $\bar{y} := y/\alpha = O(1)$. Appropriate expansions of the various field quantities then are

$$p \sim p_e(x) + O(\alpha) \,, \tag{39a}$$

$$q \sim \alpha\, q_0(x,\bar{y}) + o(\alpha) \,, \tag{39b}$$

where q stands for Δ, ψ, $\tau = -\overline{u'v'}$, $\sigma_{(x)} = -\overline{u'^2}$, $\sigma_{(y)} = -\overline{v'^2}$. From substitution into (1b–1c) the leading order outer wake problem is found to be

$$\frac{\partial\psi_0}{\partial\bar{y}}\frac{\partial^2\psi_0}{\partial\bar{y}\partial x} - \frac{\partial\psi_0}{\partial x}\frac{\partial^2\psi_0}{\partial\bar{y}^2} = -U_eU_{ex} + \frac{\partial\tau_0}{\partial\bar{y}} \,, \tag{40a}$$

$$\bar{y} = 0: \quad \psi_0 = \tau_0 = 0 \,, \tag{40b}$$

$$\bar{y} = \Delta_0(x): \quad \partial\psi_0/\partial\bar{y} = U_e \,, \quad \tau_0 = 0 \,. \tag{40c}$$

As in the case of a moderately large velocity defect, we expect a finite wall slip $U_s(x) := \partial\psi_0/\partial\bar{y}$ at the base $\bar{y} = 0$ of this outer layer, which yields the limiting behaviour

$$\partial\psi_0/\partial\bar{y} \sim U_s(x) + O(\bar{y}^{3/2}) \,, \quad \tau_0 \sim \Lambda_0\bar{y} + O(\bar{y}^{3/2}) \,, \tag{41}$$

with $\Lambda_0 := U_sU_{sx} - U_eU_{ex} > 0$.

It is easily verified that the various layers introduced so far in the description of turbulent boundary layers share the property that their lateral extent is of the order of the mixing length ℓ characteristic for the respective

layer. In contrast, the scalings given by (39) imply that ℓ is much smaller than the thickness of the outer wake region: $\ell \sim \alpha^{3/2} \ll \alpha$. This is a characteristic feature of free shear layers, of course, but also indicates that the outer wake region "starts to feel" the presence of the confining wall at distances $y \sim \alpha^{3/2}$, which in turn causes the emergence of an inner wake region.

4.2 Inner Wake Region

Introducing the stretched wall distance $Y = y/\alpha^{3/2} = O(1)$ inspection of (41) suggests the expansions

$$\psi \sim \alpha^{3/2} U_s(x) + \alpha^{9/4} \bar{\psi}(x, Y) + \cdots \,, \tag{42a}$$

$$\tau \sim \alpha^{3/2} \bar{T}(x, Y) + \cdots \,, \quad \ell \sim \alpha^{3/2} \bar{L}(x, Y) + \cdots \,, \tag{42b}$$

which leads to

$$\bar{T} = \Lambda_0 Y \,. \tag{43}$$

Furthermore, $\bar{T}$ and $\bar{\psi}$ are subject to the boundary conditions

$$T(x, 0) = \bar{\psi}(x, 0) = 0 \,, \tag{44a}$$

$$\bar{\psi}_Y \sim \frac{2}{3} \frac{\Lambda_0^{1/2}}{\bar{L}_0} Y^{3/2} \,, \quad Y \to \infty \,, \quad \bar{L}_0 = \lim_{Y \to \infty} \bar{L} \,. \tag{44b}$$

The solution of the inner wake problem posed by (43), (44) can be obtained in closed form. It exhibits the expected square-root behaviour of $\bar{\psi}_Y$,

$$\bar{\psi}_Y \sim \bar{U}_s(x) + 2 \frac{(\Lambda_0 Y)^{1/2}}{\chi(x)}, \quad \bar{L} \sim \chi(x) \bar{Y} \,, \quad Y \to 0 \,. \tag{45}$$

Here $\bar{U}_s(x)$ denotes the correction of the slip velocity $U_s(x)$ caused by the inner wake region,

$$u_s \sim U_s(x) + \alpha^{3/4} \bar{U}_s(x) + \cdots \,, \tag{46a}$$

$$\bar{U}_s(x) = - \int_0^\infty \left(\frac{1}{\bar{L}} - \frac{1}{\bar{L}_0} \right) (\Lambda_0 Y)^{1/2} \, \mathrm{d}Y \,. \tag{46b}$$

At this point it is important to recall the basic assumption made at the beginning of this section, namely, that the slenderness parameter α is independent of Re, or more generally, asymptotes to a small but finite value as $Re \to \infty$. As a consequence, the outer and inner wake regions provide a complete description of the boundary layer flow in the formal limit $Re^{-1} = 0$. If, however, $0 < 1/Re \ll 1$ an additional sublayer forms at the base of the inner wake region. This sublayer plays a similar role as the intermediate layer discussed in Subsect. 3.1: there the magnitude of the Reynolds shear stress, still varying linearly with distance from the wall, is reduced to $O(u_\tau^2)$, which is necessary to provide the square-root behaviour expressed in (45) and, finally, to allow for the match with the universal wall layer, see [19].

4.3 Numerical Solution of the Leading-Order Outer-Wake Problem

As earlier, a slightly modified version of the mixing length model proposed by [13] will be adopted to close the outer wake problem posed by (40). Numerical calculations were carried out for a family of retarded external flows controlled by two parameters m_s, k, with $m_s < 0$, $0 \le k < 1$:

$$U_e(x; m_s, k) = (1+x)^{m(x;m_s,k)} \,, \tag{47a}$$

$$\frac{m}{m_s} = 1 + \frac{k}{1-k}\,\Theta(2-x)\big[1-(1-x)^2\big]^3 \,. \tag{47b}$$

Herein Θ denotes the Heaviside step function. Self-similar solutions of the form $\psi_0 = \Delta_0 F(\xi)$, $\xi := Y/\Delta_0$, $\Delta_0 = b(1+x)$, where $b = \text{const}$ and the position $x = -1$ defines the virtual origin of the flow, exist for $k = 0$ if $m_s > -1/3$ and are used to provide initial conditions at $x = 0$ for the downstream integration of (40) with U_e given by (47). As a specific example, we consider the case $F'(0) = 0.95$ of a relatively small velocity defect, imposed at $x = 0$, for which the requirement of self-similarity for $-1 < x < 0$ yields $b \doteq 0.3656$ and $m_s \doteq -0.3292$. The key results which are representative for the responding boundary layer and, most important, indicate that the present theory is capable of describing the approach to separation are displayed in Fig. 2. If k is sufficiently small, the distribution of the wall slip velocity U_s is smooth and $U_s > 0$ throughout. However, when k reaches a critical value $k_M \doteq 0.84258$, the slip velocity U_s is found to vanish at a single location $x = x_M$, but is positive elsewhere. A further increase of k provokes a breakdown of the calculations, accompanied with the formation of a weak singularity slightly upstream of x_M at $x = x_G$. A similar behaviour is observed for the boundary layer thickness Δ_0, which is smooth in the subcritical case $k < k_M$, exhibits a rather sharp peak $\Delta_{0,M}$ for $k = k_M$ at $x = x_M$, and approaches a finite limit $\Delta_{0,G}$ in an apparently singular manner in the supercritical case $k > k_M$.

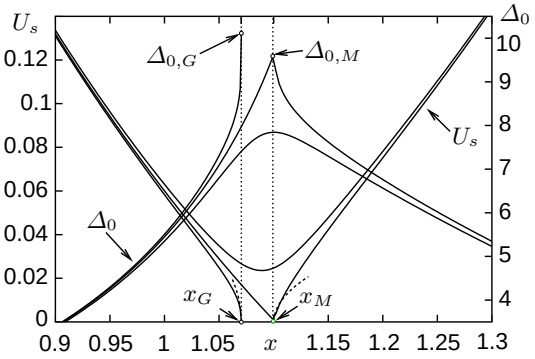

Fig. 2. Solutions of (40) for $|x - x_M| \ll 1$, $|k - k_M| \ll 1$, *dashed*: asymptotes expressed by (48b), (49)

Following the qualitatively similar behaviour of the wall shear stress that replaces U_s in the case of laminar boundary layers, see [17, 18, 27], the critical solution with $k = k_M$ is termed a marginally separating boundary layer solution. However, in vivid contrast to its laminar counterpart, is is clearly seen to be locally asymmetric with respect to $x = x_M$ where it is singular. This numerical finding is supported by a local analysis of the flow behaviour near $x = x_M$, carried out in [20]: it indicates that U_s decreases linearly with x upstream of $x = x_M$ but exhibits a square-root singularity as $x - x_M \to 0_+$,

$$U_s/P_{00}^{1/2} \sim -B(x - x_M) \,, \quad x - x_M \to 0_- \,, \tag{48a}$$

$$U_s/P_{00}^{1/2} \sim U_+(x - x_M)^{1/2} \,, \quad x - x_M \to 0_+ \,, \tag{48b}$$

where $P_{00} = (\mathrm{d}p_e/\mathrm{d}x)(x_M)$. It is found that $U_+ \doteq 1.1835$, whereas the constant B remains arbitrary in the local investigation and has to be determined by comparison with the numerical results for $x \leq x_M$.

This local analysis also shows that a square-root singularity forms at a position $x = x_G < x_M$ for $k > k_M$,

$$U_s/P_{00}^{1/2} \sim U_-(x_G - x)^{1/2} \,, \quad x - x_G \to 0_- \,, \tag{49}$$

with some U_- to be determined numerically, and that the solution cannot be extended further downstream. This behaviour, which has been described first in [12], is reminiscent of the Goldstein singularity well-known from the theory of laminar boundary layers and, therefore, will be termed the turbulent Goldstein singularity. As shown in the next section, the bifurcating behaviour of the solutions for $k - k_M \to 0$ is associated with the occurrence of marginally separating flow.

4.4 Marginal Separation

According to the original boundary layer concept, pressure disturbances caused by the displacement of the external inviscid flow due to the momentum deficit, which is associated with the reduced velocities close to the wall, represent a higher order effect. Accordingly, higher-order corrections to the leading-oder approximation of the flow quantities inside and outside the boundary layer can be calculated in subsequent steps. However, as found first for laminar flows, this so-called hierarchical structure of the perturbation scheme breaks down in regions where the displacement thickness changes so rapidly that the resulting pressure response is large enough to affect the lowest-order boundary layer approximation (e.g. [26]). A similar situation is encountered for the type of turbulent flows discussed in the preceding section. Indeed, the slope discontinuity of Δ_0 and, in turn, of the displacement thickness forces a singularity in the response pressure, indicating a breakdown of the hierarchical approach to boundary layer theory. As for laminar flows, see [17, 18, 27], this deficiency can be overcome by adopting a local interaction strategy, so

that the induced pressure disturbances enter the description of the flow in leading rather than higher order.

Again, similar to laminar flows, three layers (decks) characterising regions of different flow behaviour have to be distinguished inside the local interaction region, see Fig. 3. Effects of Reynolds stresses are found to be confined to the lower deck region (LD), having a streamwise and lateral extent of $O(\alpha^{3/5})$ and $O(\alpha^{6/5})$, respectively. Here the flow is governed by equations of the form (40). The majority of the boundary layer, i.e. the main deck (MD) behaves passively in the sense that it transfers displacement effects caused by the lower deck region unchanged to the external flow region taking part in the interaction process, the so-called upper deck (UD) and transfers the resulting pressure response unchanged to the lower deck. Solutions to the leading order main and upper deck problems can be obtained in closed form which finally leads to the fundamental lower deck problem. By using suitably stretched variables, it can be written in terms of a stream function $\hat{\psi}(\hat{X},\hat{Y})$ as (see [20])

$$\frac{\partial\hat{\psi}}{\partial\hat{Y}}\frac{\partial^2\hat{\psi}}{\partial\hat{Y}\partial\hat{X}}-\frac{\partial\hat{\psi}}{\partial\hat{X}}\frac{\partial^2\hat{\psi}}{\partial\hat{Y}^2}=-1-\Lambda(\Gamma)\,\hat{P}'(\hat{X})+\frac{\partial\hat{T}}{\partial\hat{Y}}\,, \tag{50a}$$

$$\hat{T}=\frac{\partial^2\hat{\psi}}{\partial\hat{Y}^2}\left|\frac{\partial^2\hat{\psi}}{\partial\hat{Y}^2}\right|\,, \tag{50b}$$

$$\hat{P}(\hat{X})=\frac{1}{\pi}\,{\Xint-}_{-\infty}^{\infty}\frac{\hat{A}'(\hat{S})}{\hat{X}-\hat{S}}\,\mathrm{d}\hat{S} \tag{50c}$$

$$\hat{Y}=0:\quad \hat{\psi}=\hat{T}=0\,, \tag{50d}$$

$$\hat{Y}\to\infty:\quad \hat{T}-\hat{Y}\to\hat{A}(\hat{X})\,, \tag{50e}$$

$$\hat{X}\to-\infty:\quad \hat{\psi}\to(4/15)\hat{Y}^{5/2}+\Gamma\hat{Y}\,,\quad 0\le\Gamma\le1\,, \tag{50f}$$

$$\hat{X}\to\infty:\quad \hat{\psi}\to\hat{X}^{5/6}F_+(\hat{\eta})\,,\quad \hat{\eta}:=\hat{Y}/\hat{X}^{1/3}\,. \tag{50g}$$

The first and second term on the right-hand side of (50a) account for the imposed and induced pressure, respectively. The latter is given by the Hilbert integral (50c), where $\hat{A}$ characterises the displacement effect exerted by the lower deck region. The far-field condition (50e) expresses the passive character of the main deck mentioned before, whereas the conditions (50f), (50g) follow from the match with regions LD_-, LD_+ immediately upstream and downstream of the local interaction zone. The analysis of region LD_+ determines the function $F_+(\hat{\eta})$. Finally, the parameter Γ measures the intensity of the interaction process as the monotonically increasing but otherwise arbitrary function $\Lambda(\Gamma)$ expresses the magnitude of the induced pressure gradient.

As a representative example of flows encountering separation, the distributions of $\hat{A}$, $\hat{P}$, and the wall slip $\hat{U}_s:=(\partial\hat{\psi}/\partial\hat{Y})(\hat{X},\hat{Y}=0)$, obtained by numerical solution of the triple-deck problem (50) for $\Gamma=0.019$, $\Lambda=3$ are depicted in Fig. 4a. Here the dot-and-dash lines indicate the upstream and downstream asymptotes, obtained from the analysis of the flow behaviour in the pre- and post-interaction regions, while $\hat{X}_D$ and $\hat{X}_R$ denote the positions

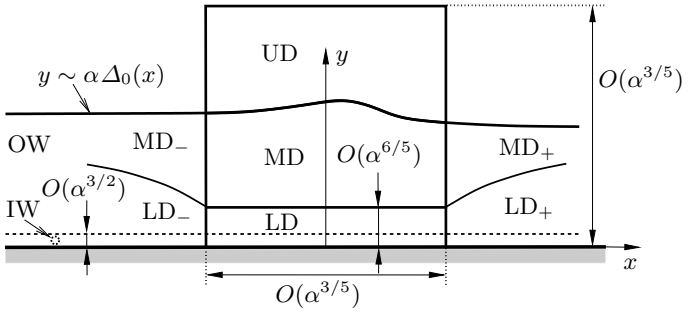

Fig. 3. Triple-deck structure, for captions see text, subscripts "−" and "+" refer to the continuation of flow regions up- and downstream of the local interaction zone, *dashed* line indicates inner wake

of, respectively, detachment and reattachment. It is interesting to note that the passage of $\hat{U}_s$ into the reverse-flow region where $\hat{U}_s < 0$ causes the interaction pressure $\hat{P}$ to drop initially before it rises sharply, overshoots and finally tends to zero in the limit $\hat{X} \to \infty$. This is in striking contrast to laminar flows, where flow separation always is triggered by an initial pressure rise, and reflects the fact that – in the case of turbulent flows considered here – the streamwise velocity component at the base $\hat{Y} = 0$ of the lower deck region is allowed to take on finite values, whereas the no-slip condition is enforced in its laminar counterpart.

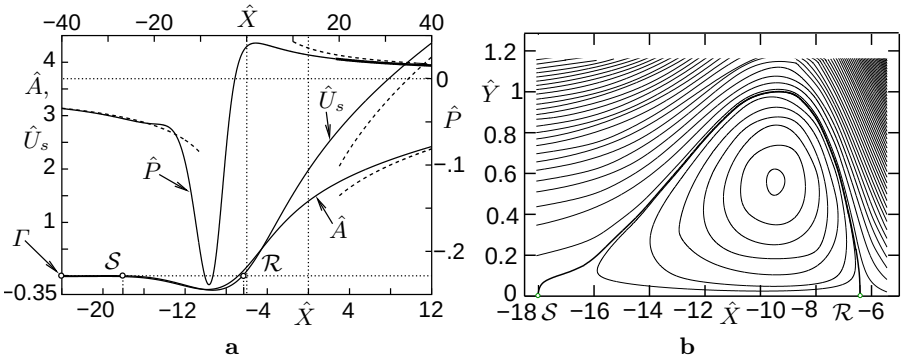

Fig. 4. Solution of (50), separation in $\mathcal{S}$, reattachment in $\mathcal{R}$: **a** key quantities, *dashed*: asymptotes found analytically; **b** streamlines

Streamlines inside the lower-deck region are displayed in Fig. 4b which clearly shows the formation of a recirculating eddy. Also, we draw attention to the increasing density of streamlines further away from the wall and downstream of reattachment associated with the strong acceleration of the fluid there as evident from the rapid increase of $\hat{U}_s$.

The interaction process outlined so far describes the behaviour or marginally separated turbulent flows in the limit $1/Re = 0$. As in the case of conventional, i.e. hierarchical, boundary layers having a velocity of defect of $O(1)$, additional sublayers form closer to the wall if $1/Re \ll 1$ but finite. Their analysis, outlined in [19], provides the skin friction relationship in generalised form to include the effects of vanishing and negative wall shear – treated first in a systematic way in [24] – but also shows that these layers behave passively insofar as the lower deck problem (50) remains intact.

5 Conclusions and Outlook

In this study an attempt has been made to derive the classical two layer structure of a turbulent small-defect boundary layer from a minimum of assumptions. As in [30], but in contrast to earlier investigations (e.g. [10]), the law of the wall is taken basically as an empirical observation rather than a consequence of matching inner and outer layers, as the latter is not felt rich enough to provide a stringent foundation of this important relationship reflecting the dynamics of the flow close to the wall, which is not understood in full at present. Probably the first successful model that describes essential aspects of this dynamics is provided by Prandtl's mixing length concept, proposed more than 50 years before the advent of asymptotic theories in fluid mechanics. Significant progress has been achieved in more recent years and, in particular, by the pioneering work of Walker (e.g. [30]), whose untimely death ended a line of thought which certainly ought to be taken up again.

Following the brief outline of the classical small-defect theory, it is shown how a description of turbulent boundary layers having a slightly larger (i.e. moderately large) velocity defect, where the outer predominately inviscid layer starts to develop a wake-type behaviour, can be formulated. Further increase of the velocity defect to values of $O(1)$ causes the wake region to become even more pronounced and is seen to allow for the occurrence of reverse-flow regions close to the wall, resulting in what we believe to be the first fully self-consistent theory of marginally separated turbulent flows.

Unfortunately, however, this success seemingly does not shed light on the phenomenon of global or gross separation associated with flows past (more-or-less) blunt bodies or, to put it more precisely, flows which start at a stagnation point rather than a sharp leading edge. Indeed, a recent careful numerical investigation for the canonical case of a circular cylinder, presented, among others, in [22,23], undoubtedly indicates that the boundary layer approaching separation exhibits a small rather than a large velocity defect, leading in turn to the dilemma addressed in Subsect. 2.4. Accompanying asymptotic analysis based on the turbulence intensity gauge model introduced in [15], however, strongly suggests that a boundary layer forming on a body of finite extent and originating in a front stagnation point does not reach a fully development turbulent state, even in the limit $Re \to \infty$. Specifically, it is found that the

boundary layer thickness and the Reynolds shear stress are slightly smaller than predicted by classical small-defect theory, while, most important, the thickness of the wall layer is slightly larger. As a consequence, the outer large-momentum region does not penetrate to distances from the wall which are transcendentally small. In turn, this situation opens the possibility to formulate a local interaction mechanism that describes the detachment of the boundary layer from the solid wall within the framework of free-streamline theory at pressure levels which are compatible with experimental observation. This is a topic of intense current investigation.

References

1. N. Afzal. Scaling of Power Law Velocity Profile in Wall-Bounded Turbulent Shear Flows. Meeting paper 2005-109, AIAA, 2005.
2. G. I. Barenblatt and A. J. Chorin. A note on the intermediate region in turbulent boundary layers. *Phys. Fluids*, 12(9):2159–2161, 2000. Letter.
3. G. I. Barenblatt, A. J. Chorin, and V. M. Prototoskin. Self-similar intermediate structures in turbulent boundary layers at large Reynolds numbers. *J. Fluid Mech.*, 410:263–283.
4. G. I. Barenblatt and N. Goldenfeld. Does fully developed turbulence exist? Reynolds number independence versus asymptotic covariance. *Phys. Fluids*, 7(12):3078–3082, 1995.
5. W. B. Bush and F. E. Fendell. Asymptotic analysis of turbulent channel and boundary-layer flow. *J. Fluid Mech.*, 56(4):657–681, 1972.
6. F. H. Clauser. The Turbulent Boundary Layer. In H. Dryden and Th. v. Kármán, editors, *Advances in Applied Mechanics*, volume 4, pages 1–51. Academic Press, New York, 1956.
7. E. Deriat and J.-P. Guiraud. On the asymptotic description of turbulent boundary layers. *J. Theor. Appl. Mech.*, 109–140, 1986. Special issue on Asymptotic Modelling of Fluid Flows. Original French article in *J. Méc. Théor. Appl.*
8. F. E. Fendell. Singular Perturbation and Turbulent Shear Flow near Walls. *J. Astronaut. Sci.*, 20(11):129–165, 1972.
9. P. S. Klebanoff. Characteristics of turbulence in a boundary layer with zero pressure gradient. NACA Report 1247, NASA – Langley Research Center, Hampton, VA, 1955. See also NACA Technical Note 3178, 1954.
10. G. L. Mellor. The Large Reynolds Number, Asymptotic Theory of Turbulent Boundary Layers. *Int. J. Engng Sci.*, 10(10):851–873, 1972.
11. G. L. Mellor and D. M. Gibson. Equilibrium turbulent boundary layers. *J. Fluid Mech.*, 24(2):225–253, 1966.
12. R. E. Melnik. An Asymptotic Theory of Turbulent Separation. *Computers & Fluids*, 17(1):165–184, 1989.
13. R. Michel, C. Quémard, and R. Durant. Hypothesis on the mixing length and application to the calculation of the turbulent boundary layers. In S. J. Kline, M. V. Morkovin, G. Sovran, and D. J. Cockrell, editors, *Proceedings of Computation of Turbulent Boundary Layers – 1968 AFOSR-IFP-Stanford Conference*, volume 1, pages 195–207, Stanford, CA, 1969. Stanford University.
14. P. A. Monkewitz, K. A. Chauhan, and H. M. Nagib. Self-consistent high-Reynolds-number asymptotics for zero-pressure-gradient turbulent boundary layers. *Phys. Fluids*, 19(11):115101-1–115101-12, 2007.

15. A. Neish and F. T. Smith. On turbulent separation in the flow past a bluff body. *J. Fluid Mech.*, 241:443–467, August 1992.
16. J. M. Österlund, A. V. Johansson, H. M. Nagib, and M. Hites. A note on the overlap region in turbulent boundary layers. *Phys. Fluids*, 12(1):1–4, 2000. Letter.
17. A. I. Ruban. Singular Solutions of the Boundary Layer Equations Which Can Be Extended Continuously Through the Point of Zero Surface Friction. *Fluid Dyn.*, 16(6):835–843, 1981. Original Russian article in *Izvestiya Akademii Nauk SSSR, Mekhanika Zhidkosti i Gaza* (6), 42–52, 1981.
18. A. I. Ruban. Asymptotic Theory of Short Separation Regions on the Leading Edge of a Slender Airfoil. *Fluid Dyn.*, 17(1):33–41, 1982. Original Russian article in *Izvestiya Akademii Nauk SSSR, Mekhanika Zhidkosti i Gaza* (1), 42–51, 1982.
19. B. Scheichl and A. Kluwick. On turbulent marginal boundary layer separation: how the half-power law supersedes the logarithmic law of the wall. *Int. J. Computing Science and Mathematics (IJCSM)*, 1(2/3/4):343–359, 2007. Special Issue on Problems Exhibiting Boundary and Interior Layers.
20. B. Scheichl and A. Kluwick. Turbulent Marginal Separation and the Turbulent Goldstein Problem. *AIAA J.*, 45(1):20–36, 2007. See also *AIAA paper 2005-4936*.
21. B. Scheichl and A. Kluwick. Asymptotic theory of bluff-body separation: a novel shear-layer scaling deduced from an investigation of the unsteady motion. *J. Fluids Struct.*, 24(8), December 2008. Special issue on the IUTAM Symposium on Separated Flows and their Control, accepted for publication.
22. B. Scheichl, A. Kluwick, and M. Alletto. "How turbulent" is the boundary layer separating from a bluff body for arbitrarily large Reynolds numbers? *Acta Mech.*, 2008. Special issue dedicated to Professor Wilhelm Schneider on the occasion of his 70th birthday, accepted for publication.
23. B. Scheichl and A. Kluwick. Level of Turbulence Intensities Associated with Bluff-Body Separation for Large Values of the Reynold number. Meeting paper 2008-4348, AIAA, 2008.
24. H. Schlichting and K. Gersten. *Boundary-Layer Theory*. Springer-Verlag, Berlin, Heidelberg, New York, 8th edition, 2000.
25. W. Schneider. Boundary-layer theory of free turbulent shear flows. *Z. Flugwiss. Weltraumforsch. (J. Flight Sci. Space Res.)*, 15(3):143–158, 1991.
26. K. Stewartson. Multistructured Boundary Layers on Flat Plates and Related Bodies. In Y. Chia-Sun, editor, *Advances in Applied Mechanics*, volume 14, pages 145–239. Academic Press, New York, San Francisco, London, 1974.
27. K. Stewartson, F. T. Smith, and K. Kaups. Marginal separation. *Studies in Applied Mathematics*, 67(1):45–61, 1982.
28. R. I. Sykes. An asymptotic theory of incompressible turbulent boundary-layer flow over a small hump. *J. Fluid Mech.*, 101(3):631–646, 1980.
29. A. A. Townsend. Equilibrium layers and wall turbulence. *J. Fluid Mech.*, 11(1):97–120, 1961.
30. J. D. A. Walker. Turbulent Boundary Layers II: Further Developments. In A. Kluwick, editor, *Recent Advances in Boundary Layer Theory*, volume 390 of CISM Courses and Lectures, pages 145–230. Springer-Verlag, Vienna, New York, 1998.
31. K. S. Yajnik. Asymptotic theory of turbulent shear flows. *J. Fluid Mech.*, 42(2):411–427, 1970.

Non-Unique Self-Similar Turbulent Boundary Layers in the Limit of Large Reynolds Number

B Scheichl and A Kluwick

Institute of Fluid Mechanics and Heat Transfer, Vienna University of Technology, Resselgasse 3/E322, A-1040 Vienna, Austria bernhard.scheichl@tuwien.ac.at

A rigorous asymptotic analysis concerning the phenomenon of non-uniqueness of quasi-equilibrium turbulent boundary layers in the large Reynolds number limit has recently been carried out in [2]. The approach contains the classical asymptotic theory of wall-bounded turbulent shear flows, cf. [3], as a limiting case. Compared to the latter, the novel theory allows for a moderately large but still asymptotically small velocity defect with respect to the external inviscid flow. Therefore, it applies to attached flow only which, however, exhibits some properties known from separating turbulent boundary layers. Here a first comparison of the theoretical results with numerical and experimental data is presented. As a special aspect, the impact of the equilibrium conditions on the associated external potential flow field is elucidated.

1 Fundamentals and basic concepts

Near-equilibrium nominally two-dimensional incompressible turbulent boundary layers play an important role in many internal flow situations. An example is provided by diffuser flows where the boundary layer has to sustain a (preferably) large pressure rise, exerted by the outer irrotational bulk flow. In order to prevent separation it is then advisable to control the pressure gradient such that the boundary layer globally is in an almost self-preserving state, or, equivalently, remains close to equilibrium.

1.1 Classical small-defect theory

Let Re denote a suitably defined global Reynolds number. Classical analysis on the basis of the Reynolds equations in the limit $Re \to \infty$, cf. [3], then shows that the main boundary layer characteristics may be expressed as

$$\begin{gathered} 1 - u/U_e = \varkappa(s) + \epsilon F_1'(\eta) + O(\epsilon^2), \quad \eta = y/\delta(s,\epsilon), \\ \delta \propto \epsilon s + O(\epsilon^2), \quad U_e(s) \propto s^m, \quad s = x - x_v. \end{gathered} \tag{1}$$

Here u denotes the streamwise velocity component and U_e its value imposed at the boundary layer edge by the external irrotational free-stream flow. The principal perturbation parameter $\epsilon = O\big((\ln Re)^{-1}\big)$ characterises the magnitude of the boundary layer thickness δ as well as the velocity defect $1 - u/U_e$ in the fully turbulent outer main layer. Furthermore, F_1 is the stream function, and x, y are curvilinear coordinates along and normal to the surface considered, respectively, and x_v denotes the virtual origin. The local curvature of the surface contour is denoted by $\varkappa$. All quantities in (1) are non-dimensional with respect to a suitable global length and velocity scale, respectively.

Furthermore, we note that classical theory establishes the well-known condition necessary for self-similarity in leading order that the inviscid surface slip velocity U_e must vary as a power m of the streamwise coordinate x. Most important, it is argued in [2] by employing first principles that $m > -1/3$ whereas the classical boundary layer structure applies only when $\mu \equiv m + 1/3 = O(1)$.

1.2 New theory: distinguished limit $\mu^{3/2} \ln Re = O(1)$

As pointed out in [2], the breakdown of classical theory associated with the limit $\mu \to 0_+$ is prevented by considering a wake-type flow indicating a state of incipient separation. Then (1) still holds but ϵ is seen to be of $O\big((\ln Re)^{-2/3}\big)$. However, the wall shear remains of $O\big((\ln Re)^{-2}\big)$ as in the classical case, thus entering the analysis in second order only. Assuming quasi-equilibrium implies

$$m + 1/3 \propto \epsilon\hat{\mu}(s) + O(\epsilon^2) \quad \text{and} \quad \varkappa = k(s) + O(\epsilon), \;\; k(s) = \Lambda/s. \tag{2}$$

Herein Λ denotes a free constant with the values $\Lambda = 0$, $\Lambda < 0$, and $\Lambda > 0$ for a plain, concave, and convex surface, respectively. The condition (2) states the remarkable result that the exponent m slightly depends on Re.

Restricting the investigation to flows having $\mathrm{d}\hat{\mu}/\mathrm{d}s \equiv 0$ agrees with the requirement that the boundary layer is in equilibrium up to second order. The necessary condition derived from the second-order integral momentum balance without employing any turbulence closure represents one of the main results of the analysis. Written in the canonical form (dashed curve in Fig. 1 *a*)

$$9\hat{D}^2\hat{\mu} = 1 + \hat{D}^3 \tag{3}$$

it provides a relationship between $\hat{\mu}$, the rescaled measure of the velocity defect $\hat{D} = O(1)$, and the wall shear stress which is scaled to 1. In the case $\Lambda = 0$ the quantity $\hat{D}^3$ is directly proportional to the shape factor G, see [3], if the contributions of Reynolds normal stresses are neglected. Most interestingly, (3) gives a theoretical explanation for the early experimental observations of non-unique near-equilibrium flows for a given value of m, [1]. The solid curves in Fig. 1 (*a*) refer to numerical solutions of the boundary layer equations for finite values of Re having adopted a simple mixing-length shear stress closure, see [2]. Due to the logarithmic dependence of ϵ on Re convergence for $Re \to \infty$ to the limit given by (3) is rather slow. In Fig. 1 (*b*) these results are compared with measurements of a flow approaching separation where m varies slowly.

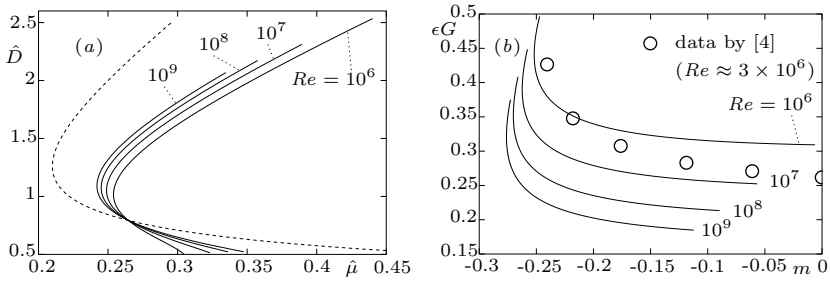

Fig. 1. (a) Canonical defect measure $\hat{D}$, (b) data for G by [4] taken from [3]

2 Effect of surface curvature on external bulk flow

Outside the boundary layer the flow is inviscid and irrotational to the order considered here. The latter property is expressed by the Laplace equation, satisfied by the stream function $\psi(x, y)$. If, as before, the flow is taken to be in equilibrium, the slip velocity U_e at the solid surface is given by (1). Hence,

$$\begin{gathered} \partial_s(h^{-1}\,\partial_s\psi) + \partial_y(h\,\partial_y\psi) = 0, \\ h = 1 + \varkappa(s)\,y, \quad y = 0\colon \;\; \psi = 0, \;\; \partial_y\psi = U_e(s) \propto s^m. \end{gathered} \tag{4}$$

Supplementing (4) with appropriate inflow and outflow as well as boundary (symmetry) conditions prescribed at the opposite wall (the centerline) of a duct, for example, then defines a well-posed elliptic problem determining ψ. In general, one expects also the wall curvature $\varkappa(s)$ to be part of the solution.

In contrast, equilibrium in the limit $m + 1/3 \to 0_+$ considered here imposes the additional condition for $\varkappa(s, Re)$ provided by (2). Note that by definition $\varkappa \equiv \mathrm{d}\phi/\mathrm{d}s$, see Fig. 2 ($b$). Let X, Y denote Cartesian global coordinates such that, without any loss of generality of the analysis, $s = 1$ and $\phi = 0$ at the origin $X = 0$, $Y = 0$. By integration of the second relation in (2) one then obtains a representation $X = X_c(s; \Lambda)$, $Y = Y_c(s; \Lambda)$ of the surface,

$$\begin{gathered} X_c = \big(s(\Lambda\sin\phi + \cos\phi) - 1\big)/\lambda, \quad Y_c = \big(s(\Lambda\cos\phi - \sin\phi) - \Lambda\big)/\lambda, \\ \phi = \Lambda\ln s, \quad \lambda = 1 + \Lambda^2. \end{gathered} \tag{5}$$

For $\Lambda \neq 0$ the spiral-type curves defined by (5) have their center in the singular point S of the flow field where $s = x - x_v = 0$ and $y = 0$, see Fig. 2 (b). In this case, therefore, the equilibrium flows associated with these contours given by (5) are assumed to take place sufficiently far downstream of $s = 0$.

Combining the specific similarity structure of the boundary layer, see (1), and the condition in (2) for the wall curvature for any value of m suggests the existence of self-similar solutions of (4) of the form $\psi \propto s^{m+1} g(\zeta; \Lambda)$, $\zeta = y/s$. Indeed, inserting this ansatz into (4) yields an ordinary initial value problem for g. In the inviscid limit $m = -1/3$ the problem (4) is then rewritten as

$$\begin{gathered} h(h^2 + \zeta^2)g'' + \big(\Lambda(h^2 - \zeta^2) + 2\zeta h/3\big)g' + (4\Lambda\zeta/9 - 2/9)g = 0, \\ h = 1 + \Lambda\,\zeta, \quad \zeta = 0\colon \;\; g = 0, \;\; g' = 1. \end{gathered} \tag{6}$$

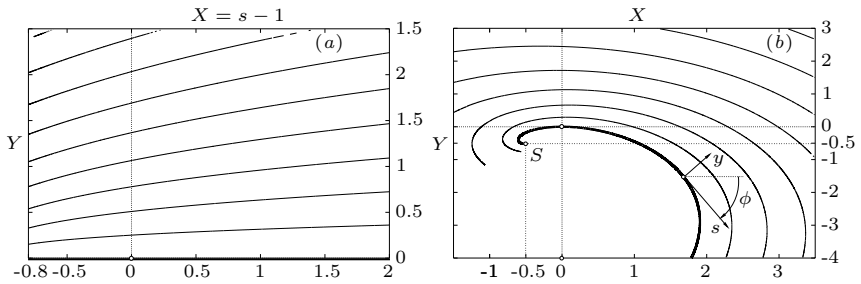

Fig. 2. Streamlines $\psi = 0, 0.25, 0.5, \ldots$ and wall contour (bold): (a) $\Lambda = 0$, (b) $\Lambda = 1$

Here primes denote derivatives with respect to ζ. The problem (6) admits the closed-form solution $g = 3/2\,(1+\zeta^2)^{1/3}\sin(2/3\,\arctan\zeta)$ which describes the potential flow past a flat wall, i.e. $\Lambda = 0$, but has to be solved numerically in general. Two representative results are depicted in Fig. 2 after applying the transformation $X = X_c + y\sin\phi$, $Y = Y_c + y\cos\phi$.

3 Conclusions and further outlook

An asymptotic analysis of turbulent equilibrium flows in the double limit $Re \to \infty$, $m + 1/3 \to 0_+$ has been presented. The results obtained appear to be supported by existing experimental evidence. It has to be noted, however, that experimental data which satisfy the theoretical requirements in a strict sense appear not to be available at present, so that a more rigorous test of the theoretical predictions has to wait for further experimental and/or numerical efforts. In this connection we add that the potential flow solution for a flat wall, i.e. $\Lambda = 0$, fixes a suction rate given by $-\partial_x\psi$ at an opposite wall $Y = const$ to be used in an experimental setup or in order to perform LES/DNS.

We also note that the solutions of (6) in the case $\Lambda > 0$ may be of engineering relevance. For example, consider a spiral diffuser duct formed by contours which collapse onto the convex curve $y = 0$ and a further potential flow streamline where $y > 0$, respectively. The boundary layer adjacent to its convex inner wall withstands the maximum pressure rise possible for a given Reynolds number. Although the opposite boundary layer on the concave outer wall is clearly not in equilibrium it is exposed to a weaker pressure gradient (although over a longer distance) and thus has a smaller velocity defect. Hence, it is supposed to be less sensitive to separation, but this remains to be shown.

References

1. Clauser FH (1954) J Aeronaut Sci 21:91–108
2. Scheichl B, Kluwick A (2004) J Fluid Mech, submitted
3. Schlichting H, Gersten K (2000) Boundary-layer theory. Springer, Berlin
4. Simpson RL, Chew Y-T, Shivaprasad BG (1981) J Fluid Mech 113:23–51

4.3 Extended Abstract for XXI ICTAM (2004)

NON-UNIQUE QUASI-EQUILIBRIUM TURBULENT BOUNDARY LAYERS

Bernhard Scheichl, Alfred Kluwick
Institute of Fluid Mechanics and Heat Transfer, Vienna University of Technology, Resselgasse 3/E322, A-1040 Vienna, Austria

Summary An asymptotic investigation of turbulent boundary layers having a moderately large velocity defect is presented. It extends the classical small-defect theory insofar as the defect is measured by a second perturbation parameter besides the sufficiently large global Reynolds number. Most remarkably, the theory is capable of describing non-uniqueness of quasi-equilibrium flows, a property which has been discussed intensively in the literature.

MOTIVATION AND PROBLEM FORMULATION

Near-equilibrium turbulent boundary layers play an important role in internal flow situations. In particular, here diffuser flows serve as a typical engineering application. In such a flow configuration the boundary layer has to sustain a preferably large pressure rise, exerted by the external irrotational bulk flow, whereas the flow shall remain strictly attached. In order to prevent separation it is advisable to control the pressure gradient such that the boundary layer globally admits a self-preserving state, or, equivalently, remains close to equilibrium. As a well-established condition necessary for self-similarity, the streamwise velocity component at the boundary layer edge must vary as a power m of the streamwise coordinate. Moreover, it has been commonly argued on a partially empirical basis that $m > -1/3$, cf. [4].
On the other hand, it is known from experiments that $m \approx -0.22$ characterises a boundary layer exhibiting identically vanishing wall shear ([3]). As a consequence, this suggests that (at least) double-valued solutions are possible as the associated exponent m measuring the strength of the pressure gradient may fall below that critical value but is greater than $-1/3$. Indeed, in the past several studies indicated the non-uniqueness of turbulent near-equilibrium boundary layers ([3], [4]). An early hint is given by Clauser in his pioneering experimental work [1]. Most notably, an explicit clue is found in [5]: In that study the impact on diffuser design of boundary layer flow that withstands a pressure increase much larger than one provoking separation was investigated numerically using an integral method.
However, this striking feature of near-equilibrium flow has not been investigated so far by a strict rational approach based on first principles. It is, among others, the primary objective of our presentation to elucidate this particular flow structure by means of an asymptotic analysis of the Reynolds-averaged Navier–Stokes equations in the limit of a large global Reynolds number *Re*. To this end, first the few basic assumptions underlying the 'classical' theory of self-preserving boundary layers for $Re \to \infty$ have to be summarised briefly.

ASYMPTOTIC THEORY OF SELF-SIMILAR BOUNDARY LAYERS

The 'classical' limit

A rational asymptotic description of high Reynolds number wall-bounded turbulent shear flows has been formulated first in the early 1970ies, see e.g. the seminal paper of Mellor [2]. It can be shown that this self-consistent theory effectively exploits well-known dimensional arguments which determine the scaling of the viscous sublayer adjacent to the wall and is based on a two-layer structure. Inside the viscous wall layer the streamwise velocity component is of $O(1/\ln Re)$. Matching with the results holding in the fully turbulent main layer yields the celebrated universal logarithmic law of the wall. Moreover, it requires that the velocity defect with respect to the imposed external streamwise velocity U_e as well as the boundary layer thickness δ, non-dimensional with a global length scale, are asymptotically small and also of that magnitude. As a result, the theory does not cover separating flows which apparently exhibit a velocity defect of $O(1)$.
It is demonstrated in [3] on basis of this classical approach that equilibrium flows are characterised by a Rotta–Clauser parameter which varies only slowly in streamwise direction x. Let y denote the distance normal to the wall, it is given by

$$\beta(x) = -\frac{\delta^* U_e \,\mathrm{d}U_e/\mathrm{d}x}{\tau_w} = O(1), \quad \text{with} \quad \delta^* = \int_0^\delta (1 - u/U_e)\,\mathrm{d}y. \tag{1}$$

Furthermore, one infers from the leading-order integral momentum balance that $\beta \sim -m/(1+3m)$. Consequently, the classical theory ceases to be valid as $m \to -1/3_+$ since it predicts an unbounded growth of both the velocity defect and the boundary layer thickness. In present literature this failure is commonly attributed to incipient separation ([3]). In contrast to this suggestion it is shown here that this failure can be avoided by a generalized small-defect theory which is based on a three- rather than a two-layer structure. While the velocity defect is still small, it is, however, asymptotically large compared to the one assumed in the classical case.

Distinguished limit $\beta^{3/2}/\ln Re = O(1)$

In the new theory the double limit $\beta \to \infty$, $Re \to \infty$ considered is found to implicate a wake-type flow in the outermost layer which in fact closely resembles a separating flow. Here the defect is measured by a second small parameter besides $1/\ln Re$ which, among others, characterises the slenderness of the boundary layer. In contrast to the classical analysis,

the new one accounts for weakly nonlinear effects due the inertia terms in the equations of motion. Introduction of the coupling parameter $\Gamma \propto \beta^{3/2}/\ln Re = O(1)$ leads to a new distinguished limit where the still finite wall shear enters the flow description in second order. There the solution is shown to satisfy a solvability condition derived from the integral momentum balance. Assuming strict equilibrium up to second order, the resulting algebraic relationship can – without adopting any turbulence closure – be cast into canonical form,

$$9\hat{D}^2\hat{\mu} = 1 + \hat{D}^3, \quad \text{with} \quad \hat{D} \propto \Gamma^{1/3}, \tag{2}$$

which clearly reveals a double-valued flow structure, see the dashed curve in figure 1 (a). Here $\hat{D}$, and $\hat{\mu}$ measure the velocity defect and the small deviation of the exponent m, characteristic of the external flow, from $-1/3$, respectively. From (2) the fundamental conclusion can be drawn that for high but finite values of Re the effects caused by nonlinearities indeed imply a restriction $m > -1/3$, where $m + 1/3 \propto \hat{\mu}/(\ln Re)^{2/3}$.

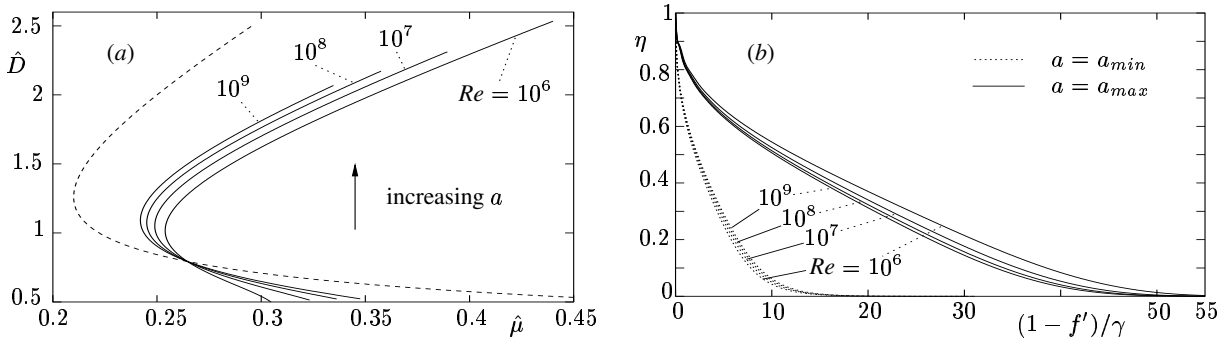

Figure 1. (a) Defect measure $\hat{D}$ (canonical scaling), (b) defect profiles (classical scaling) for different values of Re, $a_{min} \le a \le a_{max}$.

Comparison with numerical results for finite values of *Re*

In order to support the asymptotic results a numerical study was performed by solving the nonlinear boundary layer equations assuming strict equilibrium in the fully turbulent flow regime. By introduction of a suitably defined stream function $f(\eta)$ and by applying an appropriate similarity transformation, they become

$$\begin{gathered} m(f'^2 - 1) - (1+m)ff'' = \tau'/a, \quad \eta = y/\delta, \;\; a = \mathrm{d}\delta/\mathrm{d}x = const; \\ \eta \to 0: \;\; f' \sim (\gamma/\kappa)\ln(\eta\, a\gamma Re), \;\; \tau \sim \gamma^2, \;\; f \sim \eta f', \quad \eta = 1: \;\; f' = 1, \;\; \tau = 0. \end{gathered} \tag{3}$$

Here $\kappa \approx 0.42$ denotes the v. Kármán constant. The boundary conditions for $\eta \to 0$ reflect the behaviour of the flow in the overlap regime between the outer region and the viscous wall layer. To solve the resulting problem (3), it is supplemented with an (asymptotically correct) algebraic closure for the Reynolds shear stress τ. Prescribing a (sufficiently large) Reynolds number, a properly chosen (sufficiently small) linear increase of δ denoted by a as well as a minimum value of η, the exponent m is regarded as an eigenvalue and is thus part of the solution. This procedure allows to calculate the expected double-valued velocity distributions, plotted in figure 1 (b), for a given pressure gradient.

From a rigorous rational point of view (3) represents an *ad hoc* approximation of the full set of Reynolds equations. The Reynolds number enters the solution solely via the logarithmic near-wall portion of the flow. As a consequence, the asymptotic error is inherently of $O(\gamma)$. Therefore, extending the domain of the calculations to the boundary $\eta = 0$ by adopting a wall layer model would not improve the quality of the numerical solution in the limit $Re \to \infty$.

By integration of (3) from $\eta = 0$ to $\eta = 1$ one recovers the well-known v. Kármán's integral momentum balance, specified for equilibrium boundary layers. Introducing a canonical equilibrium shape factor $\hat{G} = O(1)$, it is written as

$$\beta(1+3m) = -m + (1+2m)\hat{D}^3, \quad \text{with} \quad \hat{D}^3 = \gamma\beta^{3/2}\,\hat{G}, \tag{4}$$

where the Rotta-Clauser parameter defined by (1) has to be calculated numerically. The solid curves in figure 1 (a) represent the associated solutions for $\hat{D}$ which show qualitatively good agreement with the predictions of the asymptotic analysis. There the Reynolds number enters in the form $1/\ln Re$, hence the collapse of the numerical results for finite values of Re onto the dashed line holding in the limit $Re \to \infty$ is rather slow. Finally, we note that the lower branches in figure 1 (a) reveal the classical results for $\hat{\mu} \to \infty$. In contrast, the upper branches indicate the existence of a fully nonlinear theory predicting a velocity defect of $O(1)$ and, in turn, even separated flows. This issue is a topic of current research.

References

[1] Clauser F.H.: Turbulent Boundary Layers in Adverse Pressure Gradients. *J. Aeron. Sci.* **21**:91–108, 1954.
[2] Mellor G.L.: The large Reynolds number, asymptotic theory of turbulent boundary layers. *Int. J. Engng Sci.* **10**:851–873, 1972.
[3] Schlichting H., Gersten K.: Boundary-layer theory. Springer, Berlin Heidelberg NY 2000.
[4] Schofield W.H.: Equilibrium boundary layers in moderate to strong adverse pressure gradients. *J. Fluid Mech.* **113**:91–122, 1981.
[5] Winter K.G., East L.F.: The Design of Optimum Diffusers for Incompressible Flow. In *Recent Contributions to Fluid Mechanics* (ed. W. Haase), 312–320, Springer, Berlin Heidelberg NY 1982.

[id:213,1]

Advances in Turbulence IX
Proceedings of the Ninth European Turbulence Conference
I.P. Castro, P.E. Hancock & T.G.Thomas (Eds.)
©CIMNE, Barcelona 2002

Singular solutions of the turbulent boundary layer equations in the case of marginal separation as $Re \to \infty$

B. Scheichl[1] and A. Kluwick[1]

[1]Institute of Fluid Dynamics and Heat Transfer, Vienna University of Technology, Resselgasse 3, 1040 Vienna, Austria (www.fluid.tuwien.ac.at).

We consider a nominally steady and two-dimensional turbulent boundary layer (BL) of uniform density along a flat surface under the action of an adverse pressure gradient. Classical analysis of the flow in the limit of large Reynolds number, $Re \to \infty$, (a survey is found e.g. in [2]) predicts the well-known asymptotically small velocity defect holding within most of a strictly attached BL. However, as demonstrated in [1], a more general asymptotic approach accounting for a large velocity deficit and, in turn, the possibility of separation apparently requires the existence of a second perturbation parameter, denoted by α. The latter is (i) essentially independent of Re, (ii) serves as a measure for the BL slenderness and is (iii) in fact provided by the empirical constants entering any commonly employed Reynolds shear stress closure.

Including $\alpha \ll 1$ in the theoretical considerations as first put forward by Melnik (1989), referred to in [1], has the important consequence that the BL thickness remains finite and of $O(\alpha)$ in the limit $Re^{-1} = 0$, which will be considered here. To this end, let x, y, ψ, δ and ℓ denote Cartesian coordinates parallel and normal to the wall, the stream function, the BL thickness and the mixing length, non-dimensional with global reference quantities, respectively. As shown in [1], appropriately scaled variables in the outer part of the BL are $Y = y/\alpha$, $\Psi = \psi/\alpha$, $L = \ell/\alpha^{3/2}$, $\Delta = \delta/\alpha$ which upon substitution into the set of Reynolds-averaged Navier–Stokes equations yield the leading-order problem

$$\left.\begin{array}{r} \Psi_Y \Psi_{Yx} - \Psi_x \Psi_{YY} = -p_x + T_Y\,, \quad p_x = -U_e U_{ex}\,, \quad T = L^2\,\Psi_{YY}|\Psi_{YY}|\,; \\ Y = 0:\ \Psi = T = 0\,, \quad Y = \Delta(x):\ \Psi_Y = U_e(x,\beta),\ T = 0\,, \end{array}\right\} \quad (1)$$

where we require that $L \to L_0(x) = O(1)$ for $Y \to 0$, implying $\Psi_Y = U_s + O\left(Y^{3/2}\right)$. The resulting wall slip $U_s(x,\beta)$ reflects the absence of viscous forces and is assumed to depend on the controlling parameter β used to characterize the potential flow velocity $U_e(x,\beta)$ imposed at the BL edge. Additional sublayers allowing among others to satisfy the no-slip conditions at the wall emerge if the expansions are carried on to higher orders in α and Re^{-1}. Note, however, that

the solution in the outer region which comprises most of the BL is completely determined by (1). Here we are interested primarily in the case that U_s vanishes locally, indicating the onset of separation.

In this connection numerical solutions of (1) have been obtained for retarded flows specified by

$$U_e(x,\beta) = (x+1)^m \left[\beta\left(\exp(-5x^2)-1\right)+1\right]\ ; \quad L = I\left(Y/\Delta(x)\right)^{1/2}\Delta(x)\,. \quad (2)$$

Klebanoff's intermittency factor $I(Y/\Delta)$ was implemented to improve the prediction of the flow near the BL edge. It is expected, however, that other choices of $U_e(x,\beta)$ will not affect the flow behaviour near $U_s = 0$ significantly. Also note that problem (1) admits (in addition to the trivial result $\Psi_Y \equiv U_e$) self-similar solutions $\Psi = \Delta U_e F(Y/\Delta)$, $\Delta \propto x$, for external flows of the form $U_e \propto x^m$, where the exponent m is a function on $F'(0)$ and $-1/3 < m < 0$, leading to a wall slip $U_s \propto x^m F'(0)$, $F'(0) < 1$; c.f. [1]. These solutions were used to provide initial conditions at $x = 0$ for the numerical calculations with $U_e(x,\beta)$ given by (2) which were carried out for a range of values of β; see Figure 1: If β is sufficiently small the distribution of U_s is smooth, and $U_s > 0$ throughout. However, if the parameter β exceeds a critical value β_{crit}, $U_s(x,\beta_{crit})$ is found to vanish at a single location $x = x_{crit}$ but is positive elsewhere. A further increase of β will cause a breakdown of the calculations accompanied by the occurrence of a weak singularity slightly upstream at $x = x^*$.

A qualitatively similar behaviour of the wall shear in laminar BLs was observed originally by Ruban (1981), see e.g. [2], and is now commonly referred to as marginal separation. This notion is used also here although the mechanism leading to separation is vastly different from the laminar counterpart.

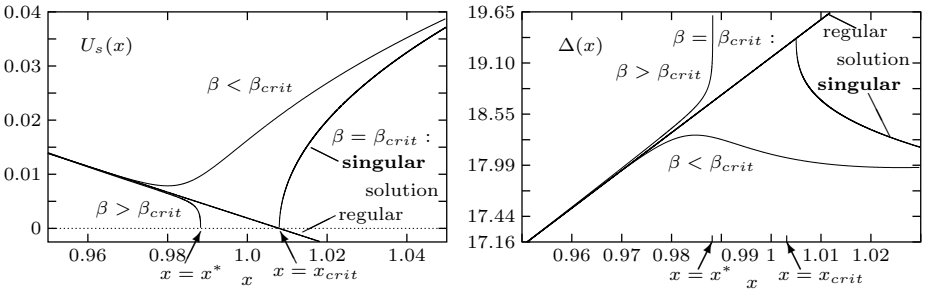

Figure 1: Distributions of U_s and Δ near $x = x_{crit}$.

To study the local flow behaviour near $x = x_{crit}$ the pressure gradient is expanded as $p_x = P_0 + \epsilon + P_1 s + \ldots$ for $s \to 0_\mp$ where $s = x - x_{crit}$, $\epsilon = \beta - \beta_{crit} \ll 1$. We first focus on the case $\epsilon = 0$. Since Δ assumes a finite value Δ_0 at $x = x_{crit}$ one infers that $L_0 \to L_{00}$ as $s \to 0$. The balance (1) is retained in flow regimes II$\mp$, see Figure 2. There the appropriately rescaled local quantities $\eta = y/\left({L_{00}}^{2/3}(\mp s)^{1/3}\right)$, $f = \Psi/\left({L_{00}}^{2/3}{P_0}^{1/2}(\mp s)^{5/6}\right)$ suggest the expansions

$$f = f_0(\eta) + (\mp s)^\lambda \ln^\nu(\mp s)\, f_{1\mp}(\eta) + \ldots\ ; \quad \mp 1/2\, {f_0'}^2 \pm 5/6\, f_0 f_0'' = -1 + \left({f_0''}^2\right)'\,. \quad (3)$$

The solutions of the resulting differential equations for f_0, f_{1-}, f_{1+}, ..., supplemented with boundary conditions following from (1) are sought subject to the requirement of sub-exponential growth for $\eta \to \infty$, in order to provide a match to the solution in the regimes I$\mp$. In case of the upper sign, i.e. $x < x_{crit}$, a numerical treatment indicates that the only acceptable solution of the nonlinear leading-order equation for f_0 is given by $f_0 = 4/15\,\eta^{5/2}$. It expresses the balance between pressure and Reynolds shear stress gradient at the surface for regularly vanishing U_s as $s \to 0_-$. In contrast, numerical calculations for the lower sign, i.e. $x > x_{crit}$, indicate the existence of a further solution having $f_0'(0) \doteq 1.1835$ and $f_0 = 4/15\eta^{5/2} + O\big(\eta^{3/2}\big)$ as $\eta \to \infty$. As a result, the flow exhibits a non-zero wall slip $U_s \sim f_0'(0)(P_0 s)^{1/2}$, which is singular at $s = 0_-$. Hence, the convective term in (1) evaluated at $Y = 0$ jumps from 0 to $U_s U_{sx} \sim P_0 f_0'(0)^2/2$ at $x = x_{crit}$. However, for $s < 0$, the behaviour of U_s is fixed by the homogeneous solution f_{1-} of a linear problem implying the well-known Kummer's equation, together with the inhomogeneous problem arising due to terms of $O\big(\nu(-s)^\lambda \ln^{\nu-1}(-s)\big)$; c.f. (3). Non-exponential growth as $\eta \to \infty$ is provided if $\lambda = 1/2, 3/2, \ldots$ and $\nu = 0$. In turn, the expected linear behaviour $U_s \sim -c\,s$, with $c > 0$, is revealed.

Finally, in regimes I$\mp$ where $Y = O(1)$ expansions $\Psi = \Psi_0(Y) + (\mp s)^{r_\mp}\Psi_1(Y) + \ldots$, $r_- = 1$, $r_+ = 1/3$, hold. In turn, $\Delta \sim \Delta_0 + O\big((-s)^{r_\mp}\big)$; c.f. Figures 1, 2.

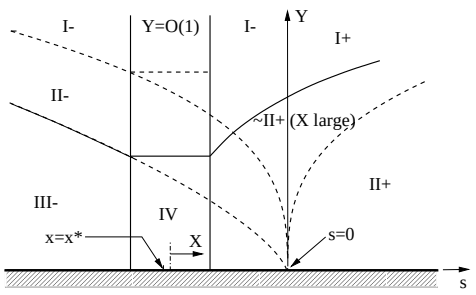

Figure 2: Asymptotic splitting near $x = x_{crit}$ as $\epsilon \to 0$; broken lines: $\epsilon = 0$.

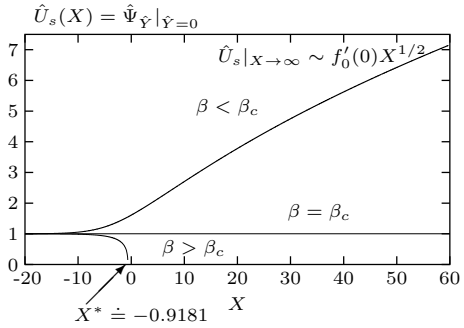

Figure 3: Bifurcating distributions of $\hat{U}_s$, determined by solving (6).

Note that regular terms reflecting the smooth behaviour of p_x have been disregarded since Ψ is near $x = x_{crit}$ mainly governed by local eigensolutions as discussed so far. Therefore, in the case $\epsilon \neq 0$, the above structure for $s < 0$ is perturbed solely due to regular terms, associated with $\lambda = -1/2$ in (3), which cannot explain the excitation of the singular downstream solution as the regular one is obviously suppressed, see Figure 1. However, inspection of the results for $x < x_{crit}$ indicate that the contributions resulting from f_0 and f_1 become of the same size if $\eta \sim (-c^2 s)^{1/3}$, c.f. (3), forcing the formation of a new sublayer III$-$ (see Figure 2), where singular eigensolutions may arise. Introducing the scaled quantities $\hat{\eta} = \eta/(-c^2 s)^{1/3}$, $\hat{f} = f/(-c^2 s)^{5/6}$, it follows that

$$\hat{f} = \hat{f}_0(\hat{\eta}) + O(-s) + \epsilon(-s)^\mu d \exp[-\chi/(c^2 s)]g(\hat{\eta}) + \ldots,\ \hat{f}_0 = 4/15\,\hat{\eta}^{5/2} + \hat{\eta}\,; \quad (4)$$

$$\chi\big[(1+2/3\,\hat\eta^{3/2})g'-\hat\eta^{1/2}g''\big]=2\big(\hat\eta^{1/2}g\big)'\,,\;\; g'(0)=1,\; g(0)=g''(0)=0\,. \quad (5)$$

Thus, the unknown constant $d>0$ measures the perturbation of U_s. A numerical investigation shows that problem (5) allows for an eigensolution g exhibiting non-exponential growth as $\hat\eta\to\infty$ solely if $\chi=1/3$. Only in that case the solution is found analytically. It reads $g=2/3\,\hat\eta\exp(-z)+(2/9)^{1/3}\hat f_0'(\hat\eta)\int_0^z t^{-1/3}\exp(-t)\,\mathrm{d}t$ where $z=2/9\,\hat\eta^{3/2}$. An analogue study of the inhomogeneous higher-order problem for the contribution of $O\big((-s)^{\mu-1}\exp(-\chi/s)\big)$ to the expansion (4) gives the single value $\mu=-9/5$. In turn, the perturbation g provokes exponentially small disturbances $\propto\epsilon f_0'$ and $\propto\epsilon\Psi_0'$ in the flow regimes II− and I−, respectively.

Expansion (4) ceases to be valid within region IV, Figure 2. Here we define appropriate variables X, $\hat Y=Y/(L_{00}\,\hat\epsilon)^{2/3}$ and $\hat\Psi=\Psi/({P_0}^{1/2}{L_{00}}^{2/3}\hat\epsilon^{5/3})$ where

$$-c\,s=\hat\epsilon-\hat\epsilon^2 c\,X\,,\quad c\,\hat\epsilon=-\chi\big(1-\mu\ln(-c^2\ln|d\epsilon|/\chi)/\ln|d\epsilon|\big)/\ln|d\epsilon|\,.$$

Substitution into (1) yields to leading order the reduced problem

$$\left.\begin{aligned}&\hat\Psi_{\hat Y}\hat\Psi_{\hat Y X}-\hat\Psi_X\hat\Psi_{\hat Y\hat Y}=-1+\hat T_{\hat Y}\,,\;\hat T=(\hat\Psi_{\hat Y\hat Y})^2\,;\;\; \hat\Psi|_{\hat Y=0}=\hat\Psi_{\hat Y\hat Y}=0\,,\\ &\hat T|_{\hat Y\to\infty}\sim\hat Y\,;\;\; \hat\Psi|_{X\to-\infty}\sim\hat f_0(\hat Y)+j\,g(\hat Y)\exp(\chi X)\,,\; j=\pm1,0\,,\end{aligned}\right\} \quad (6)$$

which has to be solved numerically. The distributions of the rescaled wall slip $\hat U_s=\hat\Psi_{\hat Y}|_{\hat Y=0}$ are depicted in Figure 3. In the subcritical case $\epsilon<0$, i.e. $j=+1$, the solution of (6) asymptotes to the non-trivial downstream solution $\Psi\sim{L_{00}}^{2/3}{P_0}^{1/2}f_0(\eta)$, holding in region II+, for $X\to\infty$, c.f. Figures 2, 3. Likewise, analysis of the flow regime I+ reveals that $\Delta-\Delta_0=O(X^{1/3})$ as $X\to\infty$ there. For $j=0$ the solution of (6) is $\hat\Psi=\hat f_0(\hat Y)$, which corresponds to the critical case $\epsilon=0$. In the supercritical case $\epsilon>0$, that is $j=-1$, the solution breaks down at a distinct location $X=X^*$, i.e. $x^*<x_{crit}$ in the original scaling.

Again, this behaviour is examined by means of a local analysis: Introducing appropriate local variables $S=X-X^*\to0_-$, $\zeta=\hat Y/(-S)^{1/3}$, $\hat F=\hat\Psi/(-S)^{5/6}$:

$$\hat F=\hat F_0(\zeta)+(-S)^\sigma\hat F_1(\zeta)+\ldots\,;\;\; -1/2\,\hat F_0'^2+5/6\,\hat F_0\hat F_0''=-1+\big(\hat F_0''^2\big)'\,.$$

Here the leading-order term $\hat F_0=2^{1/2}\zeta$ gives rise to a GOLDSTEIN-type singularity, i.e. $U_s\sim(-2P_{00}\,s)^{1/2}$ (c.f. [2]). As the existing limiting profile, $\hat\Psi(X^*,\hat Y)$, of the solution in regime IV cannot be matched to the solution in the region $\zeta=O(1)$, a transition layer is introduced where $\hat Y=O\big((-S)^{1/6}\big)$ and inertia terms balance the imposed pressure gradient to leading order. The matching procedure, which concludes the present analysis, then shows that $\sigma=1/4$, $\hat F_1\propto\zeta^{5/2}$, and $\Delta=\Delta_0+O\big(\gamma,(-S)^{1/6}\big)$ (see the singular branch in Figure 1).

The effect of small finite values of the slenderness parameter α on that singular behaviour is the topic of the current research.

References

[1] B. Scheichl. Asymptotic theory of marginal turbulent separation. Doctoral thesis, Vienna University of Technology, 2001.

[2] H. Schlichting and K. Gersten. Boundary-layer theory. Springer, 2000.

AIAA JOURNAL
Vol. 45, No. 1, January 2007

Turbulent Marginal Separation and the Turbulent Goldstein Problem

Bernhard Scheichl* and Alfred Kluwick†
Vienna University of Technology, 1040 Vienna, Austria

DOI: 10.2514/1.23518

A new rational theory of incompressible turbulent boundary-layer flows having a large velocity defect is presented on basis of the Reynolds-averaged Navier–Stokes equations in the limit of infinite Reynolds number. This wake-type formulation allows for, among others, the prediction of singular solutions of the boundary-layer equations under the action of a suitably controlled adverse pressure gradient, which are associated with the onset of marginally separated flows. Increasing the pressure gradient locally then transforms the marginal-separation singularity into a weak Goldstein-type singularity occurring in the slip velocity at the base of the outer wake layer. Interestingly, this behavior is seen to be closely related to (but differing in detail from) the counterpart of laminar marginal separation, in which the skin friction replaces the surface slip velocity. Most important, adopting the concept of locally interacting boundary layers results in a closure-free and uniformly valid asymptotic description of boundary layers that exhibit small, closed reverse-flow regimes. Numerical solutions of the underlying triple-deck problem are discussed.

Nomenclature

A = displacement function (boundary-layer theory)
$\hat{A}$ = displacement function (triple-deck theory)
$A_{+,-}$ = numerical constants in $F_+(\eta)$ and $F_-(\eta)$
B = upstream slope of U_s
$\hat{B}$ = slope of $\hat{U}_s$ near separation (triple-deck theory)
$\hat{B}_1$ = leading-order coefficient in expansion of $\hat{B}$ about $\hat{L} = \chi - \chi^* = 0$
b = constant slope $\mathrm{d}\Delta/\mathrm{d}x$ (self-preserving boundary-layer solution)
C_+ = numerical constant in $G_+(\eta)$
c_ℓ = constant in mixing length closure, $c_\ell = \alpha^{1/2}$
D = strength of perturbation of B
F = stream function (self-preserving boundary-layer solution)
$F_{+,-}$ = leading-order stream functions (locally expanded boundary-layer solutions)
$f, \bar{f}$ = stream functions (locally expanded boundary-layer solutions)
G = stream function perturbation (locally expanded boundary-layer solutions)
$g, \breve{g}$ = stream function perturbations (locally expanded boundary-layer solutions)
H = auxiliary function
h = surface metric coefficient
I = intermittency factor by Klebanoff
k = surface curvature
$\hat{L}$ = bubble length
$\tilde{L}, \tilde{U}$ = reference length, reference velocity
l = local sublayer thickness
ℓ = mixing length
m = external flow exponent
m_s = external flow exponent (self-preserving boundary layer)
$\hat{P}$ = induced pressure
p = pressure
q = notation to represent a collection of quantities
$\langle q \rangle$ = Reynolds averaging of any quantity represented by q
r = exponent
Re = Reynolds number (globally defined)
$S, \hat{S}$ = local streamwise lower-deck coordinates
s = local streamwise coordinate
$\hat{s}, \hat{x}$ = shifted local streamwise coordinates
T = Reynolds shear stress (boundary-layer solution)
t, z = auxiliary variables
U, P = local representations of u_e, $\mathrm{d}p/\mathrm{d}x$
U_s = surface slip velocity (boundary-layer solution)
$\bar{U}_s$ = lower-deck representation (boundary-layer theory) of U_s
$\hat{U}_s$ = lower-deck representation (triple-deck theory) of U_s
U_+ = numerical constant in $F_+(\eta)$
u, v = velocity components in x and y direction
u_e = surface slip velocity (external potential flow)
u_s = surface slip velocity
u', v' = velocity fluctuations in x and y direction
$X, \bar{Y}$ = lower-deck coordinates (boundary-layer theory)
$\hat{X}, \hat{Y}$ = lower-deck coordinates (triple-deck theory)
$\mathcal{X}, \mathcal{Y}$ = transformed lower-deck coordinates (triple-deck theory)
x, y = natural coordinates
Y = boundary-layer coordinate
$\hat{y}$ = vertical upper-deck coordinate
$\hat{Z}$ = shifted vertical lower-deck coordinate (triple-deck theory)
α = slenderness parameter
β = control parameter
Γ = Gamma function
Γ = upstream limit of $\hat{U}_s$, similarity parameter
γ = bifurcation parameter
Δ = boundary-layer thickness (boundary-layer solution)
δ = boundary-layer thickness
ε = notion for gauge function
ϵ = bifurcation parameter (redefined)
ζ = auxiliary variable
$\eta, \hat{\eta}$ = local similarity variables based on s and $\hat{s}$
$\bar{\eta}, \breve{\eta}, \breve{\eta}$ = local similarity variables
θ = Heaviside step function

Presented as Paper 4936 at the 4th AIAA Theoretical Fluid Mechanics Meeting, Toronto Ontario Canada, 6–9 June 2005; received 27 February 2006; revision received 31 July 2006; accepted for publication 31 July 2006. Copyright © 2006 by the American Institute of Aeronautics and Astronautics, Inc. All rights reserved. Copies of this paper may be made for personal or internal use, on condition that the copier pay the $10.00 per-copy fee to the Copyright Clearance Center, Inc., 222 Rosewood Drive, Danvers, MA 01923; include the code $10.00 in correspondence with the CCC.

*Postdoctoral Research Fellow, Institute of Fluid Mechanics and Heat Transfer, Resselgasse 3/E322; b.scheichl@tuwien.ac.at.

†Full Professor, Institute of Fluid Mechanics and Heat Transfer, Resselgasse 3/E322; a.kluwick@tuwien.ac.at. Senior member AIAA.

κ = von Kármán constant
Λ = strength of induced pressure
λ, μ = invariance parameters
$\tilde{\nu}$ = kinematic viscosity
Ξ, Φ = coefficients in asymptotic series
ξ = boundary-layer coordinate Y related to Δ
ρ, ϑ = polar coordinates
$\hat{\rho}$, ϑ = polar coordinates (upper deck)
σ = triple-deck length scale
τ = surface shear stress
Υ = shear stress gradient evaluated at surface
ϕ = local scaling function
χ = coupling parameter
χ_b = upper bound of χ
Ψ = stream function (boundary-layer solution)
$\hat{\Psi}$, $\hat{T}$ = lower-deck representations (triple-deck theory) of Ψ and T
$\bar{\Psi}$, $\bar{T}$ = lower-deck representations (boundary-layer theory) of Ψ and T
ψ = stream function
$\hat{\psi}$, $\hat{p}$ = upper-deck perturbations of ψ and p
Ω = eigenvalue
ω = exponent
$1a$, $1b$ = oncoming near-surface flow regimes (boundary-layer theory)
2 = downstream and upstream evolving main flow regimes (boundary-layer theory)
$\star$ = dependences on unknown quantities

Subscripts

D, R = detachment, reattachment
G, M = Goldstein-type singularity, marginal-separation singularity
i = ith member in asymptotic series
ij = jth member of ith member in asymptotic series
ijk = kth member of jth member of ith member in asymptotic series
$+$, $-$ = downstream and upstream (of $s = 0$ or $\hat{s} = 0$) evolving forms

Superscript

$*$ = onset of separation

I. Introduction

THE method of matched asymptotic expansions has undoubtedly proven very successful not only in gaining a profound understanding of laminar high-Reynolds-number flows in many aspects, but also in providing a rational framework for a methodical and comprehensive treatment of turbulent shear layers. It is to Professor David Walker's credit (see the Acknowledgments) that he was one of the first to have elucidated the modern and fruitful asymptotic formulation of the classical two-dimensional two-tiered turbulent boundary-layer structure, which is essentially based on the assumption of an asymptotically small streamwise velocity defect with respect to the external freestream flow; see the extensive contribution [1]. For an extension to the three-dimensional case, the reader is referred to [2,3], and a summary is also given in [1]. In contrast to earlier treatments of wall-bounded turbulent shear flows put forward in the pioneering papers by, among others, Yajnik [4], Bush and Fendell [5], Fendell [6], and Mellor [7], in his thorough analysis the local (and not a characteristic) value of the skin friction velocity serves as the principal perturbation parameter. That is, leading and higher-order contributions to the well-established logarithmic law of the wall are effectively summed up to a single leading-order expression, whereas higher-order corrections are free of purely logarithmic terms. In turn, the logarithmic law of the wall appears as the limit far from the surface of the leading-order streamwise velocity distribution inside the viscous wall layer. Hence, the whole information needed for the further analysis of the outer velocity defect layer is subsumed in a single term in an elegant manner. We note that this formulation was also adopted by Gersten [8,9] and, more recently, in the further developments by the present authors [10–12]. Also, a more recent strong experimental support of that classical scaling is found in [13].

Moreover, it must be emphasized that David Walker was substantially involved in providing the initial steps toward a systematic insight into the very complex turbulent near-wall dynamics, by investigating the unsteady Navier–Stokes equations in the high-Reynolds-number limit [1,14–17].

Despite the undeniable progress, much of which must be attributed to David Walker, asymptotic methods have contributed toward an understanding of the fundamental physics of wall-bounded turbulent shear flows, a fully self-consistent theory describing turbulent boundary-layer separation in the limit of high Reynolds number is not available at the moment. In particular, the literature lacks a rational description of the, from an engineering point of view, very important case of separation from a smooth surface that is caused by a smooth adverse pressure gradient, imposed by the external flow. In laminar boundary-layer theory, this type of separation is commonly referred to as *marginal* separation, as the boundary layer may exhibit a closed reverse-flow regime at its base if the pressure gradient is properly chosen. This theory was developed independently by Ruban [18,19] and by Stewartson et al. [20]; also cf. [21]. However, a systematic approach to its turbulent counterpart has been hampered severely by the fact that, generally spoken, turbulent boundary layers are known to be less prone to separate than the corresponding laminar ones, owing to the enhanced wall shear stress. More specifically, the classical small-defect formulation is seen to withstand a smooth adverse pressure gradient, as the wall shear stress remains almost constant in the high-Reynolds-number limit. Furthermore, the velocity defect solution in the outer main layer is characterized by linearized convective terms in leading order, which indicates that it does not terminate in a singularity during downstream evolution. As a matter of fact, this property is demonstrated numerically in the preliminary work provided by [10,22] for the present investigation. Additionally, the study of turbulent separation past a blunt body by Neish and Smith [23] serves as a further strong hint that the classical description of a turbulent boundary layer exposed to a smooth adverse pressure gradient predicts firmly attached flows that do not separate at all (apart from the inevitable flow detachment close to the rear stagnation point, as is the case in the situation considered in [23]) in the limit of high Reynolds number.

The first systematic approach, however, to tackle the challenging problem of pressure-induced turbulent separation from an asymptotic viewpoint was carried out by Melnik [24,25]. He proposed a primary expansion of the flow quantities in terms of a small parameter, denoted by α, which measures the slenderness of the boundary layer and is contained in all commonly employed shear stress closures and/or fixed by experiments. For example, in the case of the algebraic mixing length model by Michel et al. [8] (see also Schlichting and Gersten [26]) it is identified with the square of the constant $c_\ell \approx 0.085$. Most important, its value appears to be essentially independent of the Reynolds number, as the latter may take on arbitrarily large values. Specifically, Melnik adopted Clauser's [27] early idea of adopting the laminarlike well-known algebraic eddy-viscosity closure for the Reynolds shear stress. We note that Clauser already concluded on semi-empirical grounds in his seminal investigation [27] that, in definite contrast to the laminar case, for turbulent boundary-layer flows, the thereby defined Reynolds number given by $1/\alpha$ remarkably takes on a fixed value. By assuming a (nondimensional) velocity defect of $\mathcal{O}(1)$ in the main body of the boundary layer, that strategy is seen to provide a powerful tool for constructing a rational novel description of turbulent boundary layers, which predicts wake-type wall-bounded flows in the limit of infinite Reynolds number and even allows for the treatment of marginal separation.

Among others, a cornerstone of Melnik's analysis is the prediction of a square-root singularity encountered by the slip velocity at the base of the outermost wake region of the boundary layer, as

separation is approached due to the occurrence of an Eulerian flow stage close to the surface. This result may be regarded as the turbulent counterpart to the celebrated Goldstein singularity [28,29] in laminar boundary-layer theory, in which the slip velocity is replaced by the wall shear stress. As a rather remarkable characteristic of the flow, however, it has recently been shown [12,22] that the pressure gradient can be controlled in a way such that the Goldstein-type singularity eventually disappears; then the slip velocity decreases regularly, vanishes in a single point but increases rapidly immediately further downstream, giving rise to an abrupt acceleration of the flow near the surface. In turn, this situation is associated with *turbulent marginal* separation.

Unfortunately, Melnik's theory [24,25] is not only incomplete, as it does not give a hint how to surmount that separation singularity within the framework of the Reynolds-averaged Navier–Stokes equations, but remains conceptually unsatisfactory, also for a number of additional reasons:

1) In definite contrast to the primary premise of α being independent of the globally defined Reynolds number as $Re \to \infty$, the approach implies that $\alpha^{1/2}\,\ell n\, Re = \mathcal{O}(1)$ in order to account for the well-known logarithmic near-wall portion of the streamwise velocity holding upstream of separation.

2) The formation of a square-root singularity in the slip velocity, which also includes the effects due to the Reynolds shear gradient, must be taken into account, in principle. Therefore, if the Eulerian limit indeed holds (independent of a specific closure), the theory lacks an explanation why such a more general form of a singularity does not occur.

3) It remains unclear how far the asymptotic flow structure and the main results depend on Melnik's choice of the algebraic eddy-viscosity-based closure for the Reynolds shear stress in the outer wake regime.

The novel theory to be presented here is based on Melnik's formulation of turbulent boundary layers having a large velocity defect, strikingly contrasting the classical asymptotic theory. Most important, however, it also copes with the issues 1–3. In the subsequent analysis, we concentrate on the case $\alpha \ll 1$ at infinite Reynolds number, formally written as $Re^{-1} = 0$.

The paper is organized as follows: In Sec. II the essential basic assumptions underlying the theory and their implications are presented. In Sec. III we give a short survey of the numerical study of a boundary layer driven by a controlled pressure gradient toward marginal separation and the local analysis of the flow near the point of vanishing slip velocity. A particular form is assumed for the external flow velocity in terms of a single control parameter, such that the local adverse pressure gradient increases as this parameter increases. For a critical value of the parameter, a singularity appears at a certain location, indicating the first appearance of separation. As the parameter is increased slightly, the singularity is shifted a short distance upstream. The singular behavior of the flow near this point of vanishing slip velocity is summarized. Such an investigation has already been presented in [22] and will also be outlined, more extensively, in a separate investigation. The key results of the work are provided by Sec. IV, in which we focus on the local interaction of the marginally separating boundary layer with the induced external irrotational flow. The local flow is seen to have a three-layer, or *triple-deck*, structure; the appropriate limiting forms of the basic equations are presented for the different flow regions. As a highlight, akin to the laminar case [19,20], a fundamental equation governing turbulent marginal separation, which is independent of a specific shear stress closure, is derived and its solutions are discussed. Representative numerical results are shown, demonstrating the extent of the asymptotically short and flat separation bubble.

II. Motivation and Problem Formulation

A. Governing Equations

We consider a nominally steady and two-dimensional fully developed turbulent boundary layer driven by an incompressible and otherwise nonturbulent external bulk flow along a smooth and impermeable solid surface, being, for example, part of a diffuser duct

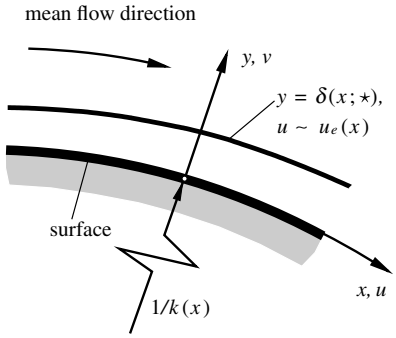

Fig. 1 Flow configuration, shown here for $k(x) > 0$.

(see Fig. 1). Let x, y, u, v, u', v', and p denote plane natural coordinates, respectively, along and perpendicular to the surface given by $y = 0$, the time-mean velocity components in the x and y directions, the corresponding turbulent velocity fluctuations, and the time-mean fluid pressure. These quantities are nondimensional, with a reference length $\tilde{L}$ characteristic for the mean velocity variation of the bulk flow along the surface (and the surface geometry), a reference value $\tilde{U}$ of the surface slip velocity due to the prescribed inviscid and irrotational external freestream flow, and the uniform fluid density. The (constant) kinematic fluid viscosity $\tilde{\nu}$ with $\tilde{L}$ and $\tilde{U}$ then define a suitable global Reynolds number, which is taken to be large:

$$Re = \tilde{U}\tilde{L}/\tilde{\nu} \to \infty \tag{1}$$

We furthermore introduce a stream function ψ by

$$\partial\psi/\partial y = u, \qquad \partial\psi/\partial x = -hv, \qquad h = 1 + k(x)y \tag{2}$$

Here, $k(x) = \mathcal{O}(1)$ is the nondimensional surface curvature, where the cases $k < 0$, $k = 0$, and $k > 0$ refer to a concave, plane, and convex surface, respectively; cf. Fig. 1. Adopting the usual notation for the turbulent stresses, the dimensionless time- or, equivalently, Reynolds-averaged Navier–Stokes equations then read (cf. [8], p. 81)

$$h\left(\frac{\partial\psi}{\partial y}\frac{\partial}{\partial x} - \frac{\partial\psi}{\partial x}\frac{\partial}{\partial y}\right)\frac{\partial\psi}{\partial y} - k\frac{\partial\psi}{\partial x}\frac{\partial\psi}{\partial y} = -h\frac{\partial p}{\partial x} - h\frac{\partial\langle u'^2\rangle}{\partial x} - \frac{\partial(h^2\langle u'v'\rangle)}{\partial y} + \mathcal{O}(Re^{-1}) \tag{3}$$

$$\left(\frac{\partial\psi}{\partial x}\frac{\partial}{\partial y} - \frac{\partial\psi}{\partial y}\frac{\partial}{\partial x}\right)\left(\frac{1}{h}\frac{\partial\psi}{\partial x}\right) - k\left(\frac{\partial\psi}{\partial y}\right)^2 = -h\frac{\partial p}{\partial y} - \frac{\partial(h\langle v'^2\rangle)}{\partial y} - \frac{\partial\langle u'v'\rangle}{\partial x} + k\langle u'^2\rangle + \mathcal{O}(Re^{-1}) \tag{4}$$

Herein, the terms of $\mathcal{O}(Re^{-1})$ refer to the divergence of the viscous stresses, which are presumed to be negligibly small compared with the Reynolds stresses throughout the boundary layer, with the exception of a viscous sublayer adjacent to the surface.

B. Novel Wake-Like Limit of Wall-Bounded Turbulent Shear Flows

A new approach to turbulent boundary layers has been developed to provide an appropriate asymptotic concept for a description of marginally separated flows. This theory is essentially founded on three key assumptions (which, although seeming plausible, nevertheless have to be validated empirically):

1) Both the velocity fluctuations u' and v' are of the same order of magnitude in the limit $Re \to \infty$, so that all Reynolds stress components are scaled equally in the whole flowfield. This requirement for local isotropy in the limit (1) is invoked quite frequently in the further analysis, but will not be addressed again then.

2) As the basic property of the flow, and already mentioned in the introduction, the streamwise velocity deficit in the main part of the

boundary layer, in which Reynolds shear predominates over molecular shear, is a quantity of $\mathcal{O}(1)$.

3) The distance $y = \delta(x; \star)$ (here, and in the following discussion, the asterisk shall indicate any further dependences) from the surface defines the time-mean outer edge of the boundary layer, as sketched in Fig. 1. This is in agreement with the observation of a rather sharp fluctuating outer edge of the time-dependent fluid motion.

1. Leading-Order Boundary-Layer Problem

As a first consequence of items 1–3 in the preceding paragraph, inspection of the equations of motion (3) and (4) suggests a shear layer approximation, for which the slenderness of the associated boundary layer is measured by a small positive parameter, denoted by $\alpha \ll 1$, such that $\delta = \mathcal{O}(\alpha)$. We, therefore, anticipate inner expansions

$$y = \alpha Y \tag{5}$$

$$\{\psi, -\langle u'v'\rangle, \delta\} = \alpha\{\Psi(x, Y), T(x, Y), \Delta(x)\} + \mathcal{O}(\alpha^2) \tag{6}$$

$$p - p_0(x) = \mathcal{O}(\alpha) \quad \text{where } \mathrm{d}p_0/\mathrm{d}x = -u_e \mathrm{d}u_e/\mathrm{d}x = \mathcal{O}(1) \tag{7}$$

Herein, $u_e(x)$ denotes the surface velocity imposed by the external potential bulk flow. Then, the main flow regime of the boundary layer is governed by the boundary-layer equations:

$$\frac{\partial\Psi}{\partial Y}\frac{\partial^2\Psi}{\partial Y\partial x} - \frac{\partial\Psi}{\partial x}\frac{\partial^2\Psi}{\partial Y^2} = u_e\frac{\mathrm{d}u_e}{\mathrm{d}x} + \frac{\partial T}{\partial Y}, \qquad T = \ell^2\frac{\partial^2\Psi}{\partial Y^2}\left|\frac{\partial^2\Psi}{\partial Y^2}\right| \tag{8}$$

where the latter relationship defines the mixing length. Equation (8) is subject to the wake-type boundary conditions:

$$\begin{gathered}\Psi(x,0) = T(x,0) = 0\\ \frac{\partial\Psi}{\partial Y}[x, \Delta(x)] - u_e(x) = T[x, \Delta(x)] = 0\end{gathered} \tag{9}$$

The requirements to be satisfied at the boundary-layer edge given by $y = \delta(x; \alpha, \star)$ [cf. Fig. 1] or, equivalently, $Y \sim \Delta(x)$ reflect the patch with the irrotational external flow, and the conditions holding at the base of the outer wake arise from the match with the α-dependent and Reynolds-number-dependent sublayers. These are not considered here in detail but are discussed in, respectively, [11,12] (and, in a more comprehensive manner, in a separate study) and outlined briefly in Sec. II.B.2.

Note that the solution in the outer wake region comprising most of the boundary layer is completely determined by Eqs. (8) and (9). As an important consequence arising from the boundary conditions (9), a solution of Eq. (8) gives rise to a (in general) nonvanishing slip velocity

$$U_s = \frac{\partial\Psi}{\partial Y}(X, 0) \tag{10}$$

in agreement with the boundary-layer concept already proposed by Clauser [27]. We expect nontrivial solutions of Eqs. (8) and (9), that is, wake-type solutions having $U_s \not\equiv u_e$ and $T \not\equiv 0$. In other words, inside the boundary layer the simple irrotational Eulerian, that is, nonturbulent, time-mean limit of the Navier–Stokes equations, which implies $\partial u/\partial Y \equiv 0$ and, consequently, $u = \partial\Psi/\partial Y \equiv u_e(x)$, is disregarded.

2. Does the Boundary-Layer Thickness Depend on the Reynolds Number?

Highly remarkably, dimensional reasoning and order-of-magnitude analysis suggests that the last of the boundary conditions (9) is fully equivalent to a negation of this question as far as the limit $Re \to \infty$ is concerned. As expressed by the last statement in the foregoing paragraph, the assumed streamwise velocity deficit of $\mathcal{O}(1)$ implicates that the Reynolds equations (3) and (4) admit a further limit apart from the pure Eulerian one, such that the slenderness parameter α remains indeed finite even in the formal limit $Re^{-1} = 0$.

The rationale can be subsumed as follows [8,10–12]: Dimensional and scaling arguments strongly indicate that the mixing length satisfies the well-known von Kármán near-wall law. Using the present notation, it is written as

$$\ell \sim \kappa Y/\alpha^{1/2}, \qquad Y/\alpha^{1/2} \to 0 \tag{11}$$

The relationship (11) holds in the overlap conjoining the fully turbulent part of the boundary layer and the viscous sublayer, in which the molecular shear stress has the same magnitude as its turbulent counterpart [8,10–12]. The celebrated logarithmic law of the wall is fully equivalent to the behavior of the mixing length given by Eq. (11). However, because it clearly prevents matching the flow quantities in the main part of the boundary layer and the viscous sublayer, at least one additional intermediate layer has to be introduced that provides the linear decay of the mixing length predicted by Eq. (11) at its base. Regarding the main layer, the assumed velocity defect of $\mathcal{O}(1)$, together with the resulting homogeneous boundary conditions holding for $Y \to 0$ [see Eq. (9)], then strongly suggest the absence of a viscosity-affected turbulent velocity scale in the outer main layer (as will be outlined in greater detail in a separate publication dealing with finite-Reynolds-number effects; see also [11,12]). That is, the stream function there and, as the most important consequence, the boundary-layer thickness are unaffected by the surface friction and, thus, by the strongly Reynolds-number-affected flow close to the surface, at the least to leading order. Therefore, the scaling parameter α is seen to be independent of the Reynolds number as $Re \to \infty$, and the shear stress tends to zero as $Y \to 0$.

Furthermore, we note that the mixing length ℓ is supposed to admit a finite limit in the overlap with an inner wake layer in which the scaled wall distance $Y/\alpha^{1/2}$ is of $\mathcal{O}(1)$. In turn, ℓ is a quantity of $\mathcal{O}(1)$ in both the main and the intermediate layer. There, the convective terms are linearized, because $u \sim U_s(x)$, as the turbulent velocity scale, which also measures the velocity perturbations about the slip velocity U_s, appears to be of $\mathcal{O}(\alpha^{3/4})$. We emphasize that the here-proposed behavior of ℓ is corroborated by any commonly applied mixing length closure; see the rather simple algebraic model by Michel et al. [8], for instance (see also [26]). Then, the balance between convection and the Reynolds shear stress, which is included in Eq. (8), requires that the width of the latter region is of $\mathcal{O}(\alpha^{3/2})$. As α does not depend on the Reynolds number, the Reynolds shear stress in that layer still does not match the asymptotically constant shear stress in the viscous near-wall region. Consequently, this indicates that both flow regimes are not influenced by viscous effects in leading order and are, therefore, identified as an outer and inner wake layer, respectively; see Fig. 2. It is interesting to note that the resulting asymptotic structure of the boundary layer then closely resembles that of a turbulent free shear flow, which was investigated by Schneider [30]. One major difference is the surface effect expressed by Eq. (11), giving rise to a square-root behavior of u [8,10,11] at the base of the inner wake regime, as sketched in Fig. 2, which has originally been established to hold on top of the viscous sublayer in case of a separating boundary layer; see, for example [8]. Hence, for finite values of the Reynolds number, a further layer

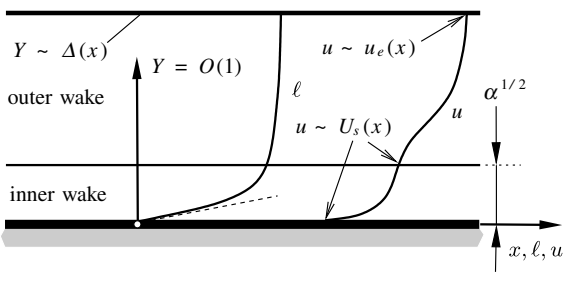

Fig. 2 Two-tiered asymptotic splitting of the boundary layer and schematic distribution of the streamwise velocity u and the mixing length ℓ in the formal limit $Re^{-1} = 0$. The dashed asymptote refers to Eq. (11).

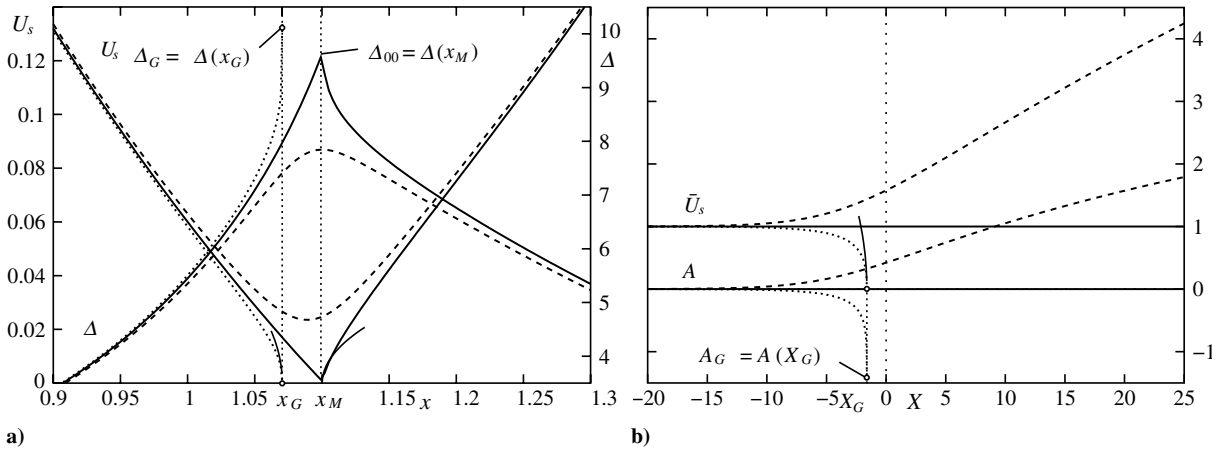

a) b)

Fig. 3 Critical (solid), sub- (dashed), and supercritical (dotted) boundary-layer solutions: a) $\beta \approx \beta_M \doteq 0.84258$ (solid), $\beta = 0.8422$ (dashed), $\beta = 0.8428$ (dotted), b) canonical representation.

emerges between the viscous sublayer and the inner wake region. Therein, the Reynolds shear stress matches the wall shear stress but varies linearly with distance from the surface [10–12]. In view of the subsequent analysis, however, it is sufficient to consider the outer wake layer only. As mentioned before, here, the analysis of the remaining flow regimes is relegated to [11,12] (as well as a more detailed separate publication).

III. Singular Solutions of the Boundary-Layer Equations

Because it provides the motivation of the present analysis, it is useful to present a brief survey of [22]. In this connection we stress that we are interested primarily in particular solutions of Eqs. (8) and (9), where $U_s(x)$ vanishes locally, indicating the onset of separation.

A. Weakly Singular Numerical Solutions

To complete the turbulent boundary-layer problem, Eqs. (8) and (9) are supplemented with the simple mixing length model:

$$\ell = I(\xi)\Delta(x), \qquad I(\xi) = 1/(1 + 5.5\xi^6), \qquad \xi = Y/\Delta(x) \quad (12)$$

where the well-known intermittency factor $I(\xi)$ by Klebanoff [31] accounts for the decrease of the mixing length (and thus for an improved flow prediction) near the boundary-layer edge; cf. the experimental data presented in [32]. In fact, calculations employing the classical almost constant mixing length distribution in the outermost region [8], recovered for $I \equiv 1$, yield a slightly slower decay of the streamwise velocity near $y = \Delta(x)$ and appear to overestimate the boundary-layer thickness function $\Delta(x)$. Note that the proportionality between ℓ and the boundary-layer thickness, as predicted by the model given in Eq. (12), provides the asymptotic representation for the outer wake layer of any well-known algebraic mixing length closure. As an example, for the case $I \equiv 1$, the relationship (12) is easily obtained from the model by Michel et al. [8] (see also [26]) by formally taking the limit $c_\ell \to 0$. As already stated in Sec. I, here, α is taken to be c_ℓ^2.

Numerical solutions of the problem posed by Eqs. (8), (9), and (12) were obtained for retarded external flows that are assumed to be controlled by two parameters m_s and β, which, for example, characterize the diffuser shape, by specifying distributions of u_e of the form

$$u_e(x; m_s, \beta) = (1 + x)^{m(x;m_s,\beta)}$$

$$\frac{m}{m_s} = 1 + \frac{\beta}{1-\beta}\theta(2 - x)[1 - (1 - x)^2]^3, \qquad m_s < 0 \quad (13)$$

$$0 \le \beta < 1$$

Here, $\theta(t)$ denotes the Heaviside step function, where $\theta = 0$ for $t < 0$ and $\theta = 1$ for $t \ge 0$. It is expected, however, that other choices neither of $u_e(x)$ nor of the mixing length closure (12) will significantly affect the behavior of the solution near the location where $U_s = 0$. We also note with respect to the imposed velocity distribution (13) that in the case $\beta = 0$ (i.e., for $m \equiv m_s$), the boundary-layer equations (8) and (9) admit self-similar solutions $\Psi = \Delta F(\xi)$, $\Delta = b(1 + x)$, where $b = \text{const}$ and the position $x = -1$ defines the virtual origin of the flow, if $m_s > -1/3$. Then both the linear growth b of the boundary-layer thickness and the exponent m_s are functions of $F'(0)$, leading to a slip velocity $U_s \propto (1 + x)^m F'(0)$ [8–10,22]. These solutions were used to provide initial conditions at $x = 0$ for the downstream integration of Eqs. (8), (9), and (12), with u_e given by Eq. (13). The calculations were started by prescribing a rather small velocity defect characterized by $F'(0) = 0.95$ at $x = 0$, which, in turn, yields $b \doteq 0.3656$ and $m_s \doteq -0.3292$. Computations were then carried out for a number of positive values of β. Inspection of Eq. (13) shows that m then varies within the range $0 < x < 2$ and thus causes an additional deceleration of u_e there. The key results that are representative for the responding boundary layer are displayed in Fig. 3a.

If β is sufficiently small, the distribution of U_s is smooth, and $U_s > 0$ throughout. However, if β reaches a critical value $\beta_M \doteq 0.84258$, the surface slip velocity U_s is found to vanish at a single location $x = x_M$, but is positive elsewhere. A further increase of β provokes a breakdown of the calculations, accompanied with the formation of a weak singularity slightly upstream at $x = x_G$. An analogous behavior is observed for the boundary-layer thickness Δ, which is smooth in the subcritical case $\beta < \beta_M$, exhibits a rather sharp peak for $\beta = \beta_M$ at $x = x_M$, and approaches a finite limit Δ_G in an apparently singular manner in the supercritical case $\beta > \beta_M$.

Following the qualitatively similar behavior of the wall shear stress that replaces the slip velocity in the case of laminar boundary layers [18], here, the critical solution is termed a *marginally* separating boundary-layer solution. However, in vivid contrast to its laminar counterpart [18], it is clearly seen to be locally asymmetric with respect to the critical location $x = x_M$, where it is singular. Moreover, the turbulent solutions appear to be highly sensitive numerically to very small deviations from $\beta = \beta_M$ as $x - x_M \to 0_-$. As will turn out in the following, these closely related properties reflect the basic mechanism governing the flow in the limits $x \to x_M$ and $\beta \to \beta_M$, which is vastly different from the laminar case.

B. Marginal-Separation Singularity

To study the local flow behavior near $x = x_M$, both the outer-edge velocity u_e and the pressure gradient $\mathrm{d}p_0/\mathrm{d}x$ given by Eq. (7) are Taylor-expanded as

$$u_e = U_{00} + sU_{01} + \gamma U_{10} + \cdots$$

$$\mathrm{d}p_0/\mathrm{d}x = P_{00} + \gamma P_{10} + \cdots \quad (14)$$

$$P_{00} = -U_{00}U_{01}, \qquad P_{10} = -U_{10}U_{01}$$

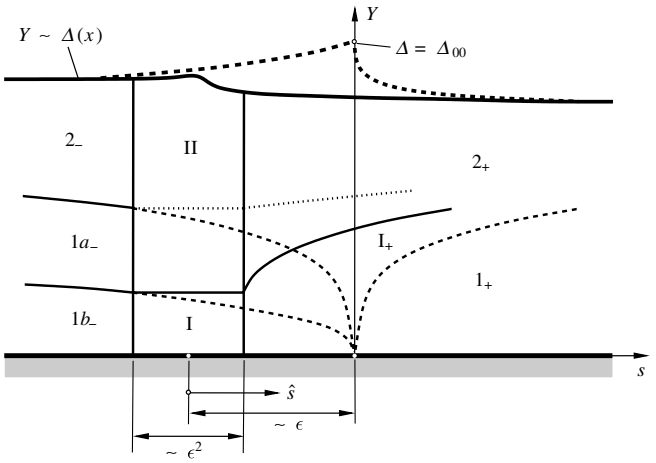

Fig. 4 Asymptotic splitting of the oncoming (subscripts −) and downstream evolving (subscripts +) boundary-layer flow in the formal limit $Re^{-1} = 0$, double-deck structure (lower deck I, main deck II). The case $\gamma \neq 0$ is sketched using solid lines, whereas the limiting structure for $\gamma = 0$ characterizing marginal separation is drawn using dashed lines partly. The flow regimes (the extent of which are marked by dotted lines) are seen to behave passively and are thus not considered in the text.

where the perturbation parameters s and γ are defined by

$$s = x - x_M \to 0, \qquad \gamma = \beta - \beta_M \to 0 \tag{15}$$

At first we focus on the critical case $\gamma = 0$. Then both the quantities Ψ and Δ are seen to assume a finite limit

$$\Psi(x, Y) \to \Psi_{00}(Y), \qquad \Delta(x) \to \Delta_{00} \quad \text{as} \quad s \to 0 \tag{16}$$

(see Figs. 3a and 4) and, in agreement with the considerations pointed out in Sec. II.B.2, inspection of Eq. (12) indicates the important relationships:

$$\ell(x, Y) \to \ell_0(Y) \quad \text{as} \quad s \to 0, \qquad \ell_0 \to \ell_{00} = \mathcal{O}(1) \quad \text{as} \quad Y \to 0 \tag{17}$$

Equation (17) provides the only empirical parameter ℓ_{00} entering the local analysis. Note that, in particular, the latter relationship in Eq. (17) is not only merely a consequence of the specific closure adopted; cf. Eq. (12). Rather, it is a consequence of the behavior of the mixing length, which, related to the two-tiered splitting of the wake regime of the boundary layer as sketched in Fig. 2, characterizes the outer wake layer.

We furthermore mention that, as a result of the limits assumed in Eqs. (16) and (17), in both the main regions 2_- and 2_+, where $Y = \mathcal{O}(1)$ (see Fig. 4), their perturbations for small values of s are governed by the convective operator in Eq. (8) only. Because of the singular behavior of the boundary-layer solution as $s \to 0$, one has to expect the occurrence of disturbances in the expansion of Ψ about its finite limit $\Psi_{00}(Y)$, which vanish as $s \to 0$ and are proportional to $\Psi'_{00}(Y)$. These perturbations represent local eigensolutions of the linear operator obtained from the corresponding linearization of Eq. (8), where $\ell = \ell_0(Y)$. However, as they do not satisfy the boundary conditions at $Y = 0$, expressed by Eq. (9), they singularly perturb that limiting value Ψ_{00}, such that for sufficiently small values of Y at least one sublayer has to be considered. There, the Reynolds stress term comes into play in leading order, as it contains the highest derivative of Ψ with respect to Y. But that means that there exists a region of a local thickness [say, $l(s)$] in which in leading order, a balance between the nonlinear convective terms and the Reynolds shear stress gradient, as provided by Eq. (8), is maintained. Then the stream function there is locally expanded as

$$\Psi = l(s)\varepsilon(s) f_0(\eta) + \cdots, \qquad \mathrm{d}\ell_n\, \varepsilon/\mathrm{d}s \sim l^{-3} \quad \text{as} \quad \varepsilon, l \to 0, \qquad s \to 0 \tag{18}$$

The boundary conditions (8) require $f_0(0) = f_0''(0) = 0$. A careful investigation (to be presented in a separate study) of the resulting boundary-value problem determining $f_0(\eta)$ in the case $s \to 0_-$ shows that, in order to provide a match with the expansion of Ψ about $\Psi_{00}(Y)$ in the main region 2_-, also the pressure gradient has to enter the aforementioned leading-order balance expressed by the second relationship in Eq. (18). The gauge function ε for the streamwise velocity component then is taken proportional to $(-s)^{1/2}$, giving $l \propto (-s)^{1/3}$. As a result, the momentum balance (8) is fully retained in the regions $1a_-$ and 1_+ (see Fig. 4), where the wall coordinate

$$\eta = Y/\left(\ell_{00}^{2/3}|s|^{1/3}\right) \tag{19}$$

is a quantity of $\mathcal{O}(1)$. In these flow regimes, then, the following expansions hold in, respectively, the upstream and the downstream case:

$$s \to 0_-: \ \frac{\Psi}{\ell_{00}^{2/3} P_{00}^{1/2}} = (-s)^{5/6} f_{0-}(\eta) + (-s)^{4/3} f_{1-}(\eta) + \cdots \tag{20}$$

$$s \to 0_+: \ \frac{\Psi}{\ell_{00}^{2/3} P_{00}^{1/2}} = s^{5/6} f_{0+}(\eta) + \cdots \tag{21}$$

and the resulting boundary value problem for $f_{0\mp}(\eta)$ reads

$$\begin{aligned} 1/2\, f_{0\mp}'^2 - 5/6\, f_{0\mp} f_{0\mp}'' &= \pm 1 \mp (f_{0\mp}'')' \\ \eta = 0\text{: } f_{0\mp} = f_{0\mp}'' = 0, \qquad \eta \to \infty\text{: } f_{0\mp} &= O(\eta^{5/2}) \end{aligned} \tag{22}$$

where the upper and lower signs refer to the cases $s \to 0_-$ and $s \to 0_+$, respectively. The conditions at $\eta = 0$ follow from the wake-type boundary conditions (9), and the requirement for $\eta \to \infty$ reflects the match with the flow regimes 2_- and 2_+ (see Fig. 4), in which the relations (16) and (17) hold. It can be shown (as will be demonstrated in a separate paper) that in the upstream case, the problem (22) has only the obvious solution:

$$f_{0-} = F_-(\eta) = 4/15\eta^{5/2} \tag{23}$$

which expresses a balance between the Reynolds shear gradient and the adverse pressure gradient at the surface for vanishing convective terms. In turn, the match with the marginally separating profile $\Psi_{00}(Y)$ of the stream function implies

$$\Psi_{00} \sim \frac{4}{15} \frac{P_{00}^{1/2}}{\ell_{00}} Y^{5/2}, \qquad Y \to 0 \tag{24}$$

and $f_{0+} \sim F_-(\eta)$ as $\eta \to \infty$. However, in the case $s \to 0_+$, a combined analytical and numerical investigation reveals a single (strictly positive) nontrivial solution, denoted by $F_+(\eta)$, that has to be calculated numerically [22]:

$$f_{0+} = F_+(\eta), \qquad \eta \to \infty\text{: } F_+ = 4/15(\eta + A_+)^{5/2} + \mathrm{TST} \tag{25}$$

Here, and in the following discussions, TST means transcendentally small terms. It is found that

$$A_+ \doteq 1.0386, \qquad U_+ = F'_+(0) \doteq 1.1835 \tag{26}$$

As a result of the leading-order analysis, turbulent marginal separation is seen to be associated with a purely regular behavior of the flow upstream of $s = 0$, as expressed by the higher-order term in the expansion (20). Substitution into Eq. (8) yields

$$f_{1-} = B\left(\eta + \frac{\eta^4}{180}\right), \qquad B > 0 \tag{27}$$

where the constant B characterizing the slope $\mathrm{d}U_s/\mathrm{d}s \sim -BP_{00}^{1/2}$ of the linearly decreasing slip velocity in the limit $s \to 0_-$ must be determined numerically from the oncoming flow; cf. the upstream distribution of U_s in Fig. 3a. That is, the flow is locally governed by the eigensolutions $f_{0-}(\eta)$, $f_{1-}(\eta)$, and $f_{0+}(\eta)$, so that

$$s \to 0_-: \ U_s/P_{00}^{1/2} = -Bs + \cdots \tag{28}$$

$$s \to 0_+ \colon\ U_s/P_{00}^{1/2} = U_+ s^{1/2} + \cdots \tag{29}$$

Hence, the existence of the nontrivial downstream solution turns out to be responsible for the (infinitely) strong acceleration of the flow immediately downstream of the location $s = 0$ due to the irregular behavior of U_s; see Eq. (29). In turn, the convective part in Eq. (8) evaluated at $Y = 0$, given by $U_s\,\mathrm{d}U_s/\,\mathrm{d}x$, exhibits a jump at $s = 0$ from 0 to the value $P_{00}U_+^2/2$ in leading order. By adopting the numerical value $P_{00} \doteq 0.02272$, the downstream asymptote (29) is plotted as a thin solid line in Fig. 3a.

The fact that convection does not vanish necessarily at the surface $Y = 0$ not only causes the inherently nonlinear downstream behavior, governed by Eq. (22), in contrast to the theory of laminar marginal separation [18,19], but also gives rise to a fundamentally different analysis of the perturbed case $\gamma \neq 0$.

C. Bifurcating Flow for $\gamma \neq 0$

1. *Exponentially Growing Eigensolutions*

The contributions given by Eqs. (23) and (27) to the expansion (20) become of the same order of magnitude at distances s, where the new variable

$$\bar\eta = \eta/(-B^2 s)^{1/3} \tag{30}$$

is a quantity of $\mathcal{O}(1)$. This situation forces a further sublayer $1b_-$ (see Fig. 4), in which the gradients of the Reynolds shear stress and the pressure dominate over convection. Furthermore, the most rapidly downstream growing perturbations possible are assumed to originate in this layer, as their s derivatives may become asymptotically larger than the disturbances itself there, such that convection comes into play again very close to the surface. This thereby-anticipated balancing of the perturbed convective and Reynolds stress terms is required by the boundary conditions holding for $\bar\eta \to 0$. These considerations and inspection of the boundary-layer equations (8) and (9) then imply that the strongest perturbations are proportional to $\varepsilon(s)g(\bar\eta)$, where the gauge function $\varepsilon(s)$ satisfies the estimate $s^2\mathrm{d}\varepsilon/\mathrm{d}s = \mathcal{O}(\varepsilon)$ and $g(\bar\eta)$ denotes a shape function. Also, these perturbations must be due to the terms proportional to γ in Eq. (14). In turn, this suggests the following expansion in the region $1b_-$:

$$\begin{gathered}\Psi/[\ell_{00}^{2/3}P_{00}^{1/2}(-Bs)^{5/3}] = F_-(\bar\eta) + \bar\eta + \cdots + \varepsilon(s)g(\bar\eta) + \cdots \\ \varepsilon(s) = -\gamma\exp\omega(s) \\ \omega(s) = \Omega/(-B^2 s) + o(1/s), \quad \Omega > 0\end{gathered} \tag{31}$$

The higher-order contributions to the exponent $\omega(s)$ then must be determined by analyzing the higher-order terms in the expansion (31) by means of the common Fredholm alternative, in order to investigate the consecutive inhomogeneous problems (this is a topic of current research; see also [22]). The eigenvalue Ω, however, is fixed by the solution of the leading-order eigenvalue problem for the eigensolution $g(\bar\eta)$, found by linearization of Eqs. (8) and (9):

$$\begin{gathered}\Omega[(2/3\,\bar\eta^{3/2} + 1)g' - \bar\eta^{1/2}g] = 2(\bar\eta^{1/2}g'')' \\ g(0) = g''(0) = 0, \qquad g'(0) = D > 0\end{gathered} \tag{32}$$

Here, the unknown constant D is assumed to be fixed by the oncoming flow, such that the expansion (28) is perturbed according to

$$U_s/P_{00}^{1/2} = -Bs[1 - \gamma D\exp\omega(s)] + \cdots \tag{33}$$

A numerical study shows that problem (32) allows for a solution $g(\bar\eta)$ having subexponential growth for $\bar\eta \to \infty$ solely in the case $\Omega = 1/3$. Moreover, only in that case has the solution of problem (32) been found analytically. It reads

$$\begin{gathered}\frac{g(\bar\eta)}{D} = \frac{2}{3}\bar\eta\exp(-\bar z) + \left(\frac{2}{9}\right)^{1/3}\left(\frac{2}{3}\bar\eta^{3/2} + 1\right)\int_0^{\bar z} t^{-1/3}\exp(-t)\,\mathrm{d}t \\ \bar z = \frac{2}{9}\bar\eta^{3/2}\end{gathered} \tag{34}$$

In turn, the associated perturbation in expansion (31) provokes also exponentially small disturbances in the flow regimes $1a_-$ and $1b_-$, respectively, and in the distribution of the boundary-layer thickness $\Delta(x)$.

The question arises if there exist further perturbations if $\gamma \neq 0$ in the region $1b_-$, which locally grow faster than that considered previously and are, therefore, responsible for a breakdown of the asymptotic flow structure holding in the limit $\gamma = 0$. Consequently, we complete the analysis of the class of eigensolutions that exhibit exponential growth as $s \to 0_-$ by scrutinizing the possibility of the generation of disturbances proportional to γ that originate in a region located even closer to the surface than is the flow regime $1b_-$; see Fig. 4. This is accomplished by the introduction of the new local variables

$$\check\eta = \bar\eta/\phi(-s), \qquad \check g(\check\eta) = g(\bar\eta) \tag{35}$$

which are assumed to be quantities of $\mathcal{O}(1)$. The latter relationship in Eq. (35) expresses the match of the (for the present analysis here unknown) shape function $g(\bar\eta)$ of the respective perturbation in region $1b_-$ with that considered here, denoted by $\check g(\check\eta)$. Independent of the specific choice of the (positive) function $\phi(-s)$, substitution of the coordinate-stretching (35) into the boundary-layer equations (8) and (9) is seen to be consistent with the generalized form

$$\begin{gathered}\frac{\Psi}{\ell_{00}^{2/3}P_{00}^{1/2}(-Bs)^{5/3}\phi} = \check\eta + \phi^3 F_-(3\check\eta) + \cdots - \gamma\exp\omega(s)\check g(\check\eta) + \cdots \\ \frac{1}{\omega(s)} \to 0_+ \quad \text{as} \quad s \to 0_-\end{gathered} \tag{36}$$

of the expansion (31). In the limit

$$\phi(-s) \to 0_+ \quad \text{as} \quad s \to 0_- \tag{37}$$

under consideration, the balance between the perturbations of $\mathcal{O}(\gamma)$ of the convective terms and the Reynolds shear stress gradient requires to write

$$\omega = \omega_0(s) + o(\omega_0) \quad \text{as} \quad s \to 0_- \tag{38}$$

where ϕ can always be scaled such that

$$\omega_0'(s) = (Bs)^{-2}\phi(-s)^{-3} \quad \text{as} \quad s \to 0_- \tag{39}$$

Then the associated disturbances having a growth rate $\omega'(s)$ given by Eqs. (38) and (39), which is stronger than that implied by the expansion (31), are found to be governed by a reduced form of the problem (32). Integrated once, it reads

$$\check g = 2\check\eta^{1/2}\check g'', \qquad \check g(0) = \check g''(0) = 0, \qquad \check g'(0) > 0 \tag{40}$$

However, the solution of problem (40) exhibits exponential growth for $\check\eta \to \infty$. Consequently, no further eigensolutions with a growth rate stronger than that given by Eq. (31) are generated.

2. *Canonical Boundary-Layer Solutions*

The expansion (31) ceases to be valid within region I, the so-called lower deck (see Fig. 4), where the gauge function ε has become a quantity of $\mathcal{O}(1)$. As a consequence of its exponential growth, that region of nonuniformity takes place an asymptotically small extent upstream of $s = 0$, where $-B^2 s \sim \Omega/\ln(1/\gamma)$. With respect to the further analysis, this behavior then is conveniently expressed by introducing the coordinate shift

$$\hat s = s + \epsilon/B, \qquad \hat x = x + \epsilon/B \tag{41}$$

(see Fig. 4), and considering the limit

$$\epsilon = \Omega/(B\,\ell_n\,|D/\gamma|) \to 0, \qquad \Omega = 1/3 \tag{42}$$

Substitution of the variables

$$X = \frac{\hat{s}}{\epsilon^2}, \qquad \bar{Y} = \frac{Y}{(\ell_{00}\epsilon)^{2/3}}, \qquad \bar{\Psi}(X,\bar{Y}) = \frac{\Psi}{\ell_{00}^{2/3}P_{00}^{1/2}\epsilon^{5/3}} \tag{43}$$

which are quantities of $\mathcal{O}(1)$ in the flow regime I, into Eqs. (8) and (9) yields to leading order the reduced, that is, canonical, equations

$$\frac{\partial\bar{\Psi}}{\partial\bar{Y}}\frac{\partial^2\bar{\Psi}}{\partial\bar{Y}\partial X} - \frac{\partial\bar{\Psi}}{\partial X}\frac{\partial^2\bar{\Psi}}{\partial\bar{Y}^2} = -1 + \frac{\partial 2\bar{T}}{\partial\bar{Y}}, \qquad \bar{T} = \frac{\partial^2\bar{\Psi}}{\partial\bar{Y}^2}\left|\frac{\partial^2\bar{\Psi}}{\partial\bar{Y}^2}\right| \tag{44}$$

subject to the boundary conditions

$$\bar{Y} = 0\text{: } \bar{\Psi} = \bar{T} = 0 \tag{45}$$

$$\bar{Y} \to \infty\text{: } \partial\bar{T}/\partial\bar{Y} - 1 \to 0 \tag{46}$$

$$X \to -\infty\text{: } \bar{\Psi} \to F_-(\bar{Y}) + \bar{Y} - \mathrm{sgn}(\gamma)\exp(X/3)g(\bar{Y}) \tag{47}$$

It is furthermore useful to define the rescaled slip velocity

$$\bar{U}_s = \frac{\partial\bar{\Psi}}{\partial\bar{Y}}(X,0) \tag{48}$$

which serves to expand U_s in the form

$$U_s(X) = \epsilon P_{00}^{1/2}\bar{U}_s(x) + \cdots \tag{49}$$

and the displacement function

$$A(X) = \lim_{\bar{Y}\to\infty}(\bar{T} - \bar{Y}) \tag{50}$$

By matching with the flow in the main deck II (see Fig. 4), one obtains

$$\Psi = \Psi_{00}(Y) + \epsilon^{2/3}\ell_{00}^{2/3}A(X)\Psi_{00}'(Y) + \cdots + (\epsilon - \epsilon^2 B\hat{X})\Psi_{01}(Y) + \cdots \tag{51}$$

In turn, applying the boundary conditions given by Eq. (9), which hold for $Y = \Delta(x)$, to the expansion (51) shows that the function $A(X)$ accounts for the variation of the boundary-layer thickness in the form

$$\Delta = \Delta_{00} - \epsilon^{2/3}\ell_{00}^{2/3}A(X) + \cdots \tag{52}$$

In the critical case of vanishing γ, the resulting problem consisting of Eqs. (44–47) has the "trivial" solution $\bar{\Psi} \equiv F_-(\bar{Y})$, giving $A \equiv 0$. However, for $\gamma \neq 0$ it has to be solved numerically. The corresponding solutions are plotted in Fig. 3b. Exponential branching for $X \to -\infty$ is found as a consequence of Eq. (47), which reflects a match with the oncoming flow, as expressed by Eqs. (31) and (33), for both the quantities $\bar{U}_s(X)$ and $A(X)$. In the subcritical case $\gamma < 0$, the solution admits the nontrivial downstream state

$$X \to \infty, \qquad \bar{Y} \to \infty\text{: } \bar{\Psi}X^{-5/6} \to F_+(\eta), \qquad \eta = \bar{Y}/X^{1/3} = \mathcal{O}(1) \tag{53}$$

which implies

$$X \to \infty\text{: } A(X) \sim A_+X^{1/3}, \qquad \bar{U}_s(X) \sim U_+X^{1/2} \tag{54}$$

Equations (53) and (54) formally provide a match with the expansions (21), supplemented with Eqs. (25) and (29) if s is replaced by $\hat{s}$ there. In the latter representation, these expansions are valid in the flow regime I_+, where $0 > s = \mathcal{O}(\epsilon)$; see Fig. 4.

It is important to note that the existence of perturbations of the nontrivial solution can be demonstrated that are due to linearization and, indeed, vanish in the limit $X \to \infty$. This suggests that this specific solution effectively provides a final downstream state of the flow rather than an isolated local solution. However, as the asymptotic analysis turns out to be rather lengthy in its details, that issue will be addressed separately in a subsequent paper.

D. Goldstein-Type Singularity

For supercritical conditions $\gamma > 0$, the solution breaks down at a distinct location $X = X_G$, that is, $x = x_G$ in the original scaling; see Fig. 3. Again, this behavior is studied by means of a local similarity analysis, in which a more detailed description of the associated multilayered asymptotic structure of the local flow is presented in [22] (and will be presented in a future paper).

Introducing appropriate local variables

$$S = X - X_G, \qquad \breve{\eta} = \bar{Y}/(-S)^{1/3}, \qquad \bar{f} = \bar{\Psi}/(-S)^{5/6} \tag{55}$$

the stream function is expanded according to

$$\bar{f} = \bar{f}_0(\breve{\eta}) + (-S)^r\bar{f}_1(\breve{\eta}) + (-S)^{2r}\bar{f}_2(\breve{\eta}) + \cdots, \qquad r > 0, \quad S \to 0_- \tag{56}$$

where

$$1/2\,\bar{f}_0'^2 - 5/6\,\bar{f}_0\bar{f}_0'' = 1 - (\bar{f}_0'^2)', \qquad \breve{\eta} = 0\text{: } \bar{f}_0 = \bar{f}_0'' = 0 \tag{57}$$

cf. Eq. (22). On condition that $\bar{f}_0$ has to exhibit subexponential growth as $\breve{\eta} \to \infty$, an analytical investigation of Eq. (57) shows that this problem has two solutions, namely, $\bar{f}_0 = F_-(\breve{\eta})$ and

$$\bar{f}_0 = \sqrt{2}\,\breve{\eta} \tag{58}$$

However, only the latter solution provides a singular behavior as $S \to 0_-$. It predicts an Eulerian flow state, because the Reynolds shear stress vanishes in leading order. As a consequence,

$$\bar{U}_s \sim \sqrt{-2S}, \qquad U_s \sim \sqrt{P_{00}(x_G - x)}, \qquad x - x_G \to 0_- \tag{59}$$

The local variations of, respectively, U_s and $\bar{U}_s$ are displayed in Fig. 3 as thin solid lines.

Because Eqs. (56) and (58) cannot be matched to the profile $\bar{\Psi}(X_G,\bar{Y})$ in region II (see Fig. 4), a transitional flow regime has to be taken into account, in which the pressure gradient balances the inertia terms and $\bar{Y}/(-S)^{1/6} = \mathcal{O}(1)$. As a consequence, this further region, which is not encountered in the analysis of the marginal-separation singularity outlined in Sec. III.B, then is found to include the sublayer for which $\breve{\eta} = \mathcal{O}(1)$, considered here [22]. A further sublayer accounting for a higher-order breakdown of the expansion [Eq. (56)] emerges where $\bar{Y}/(-S)^{1/2} = \mathcal{O}(1)$. Matching with the near-wall flow there gives $r = 1/4$ and, in turn, $\bar{f}_1 \propto \breve{\eta}^{5/2}$. Likewise, the matching procedure with respect to the flow regime II in the limit $S \to 0_-$ shows that

$$A - A_G = \mathcal{O}[(-S)^{1/6}], \qquad \Delta - \Delta_G = \mathcal{O}[(x_G - x)^{1/6}] \quad \text{as} \quad x - x_G \to 0_- \tag{60}$$

as indicated by the numerical solutions presented in Fig. 3.

Solution (58) and the associated square-root behavior given by Eq. (59) has already been found by Melnik [24,25], but not in the context of marginally separated flow. It provides the analogon to the famous Goldstein singularity in laminar boundary-layer theory [18,28,29].

We note that a Goldstein-type singularity appears quite naturally by evaluating Eqs. (8) and (9) at $Y = 0$, which gives

$$U_s\mathrm{d}U_s/\mathrm{d}x \sim -P_{00} + \partial T/\partial Y, \qquad Y = 0 \quad \text{as} \quad x - x_G \to 0_- \tag{61}$$

In turn, a local square-root behavior of U_s in $x - x_G$ is suggested in general, whereas the marginal singularity characterized by the behavior (28) is seen to be a special case [25]. These results are essentially based upon the observation that Ψ and, thus, both T and

$\partial T/\partial Y$ approach finite limits as $s \to 0$ and $S \to 0_-$, respectively. However, the rather surprising fact that, in the case of the square-root singularity, $\partial T/\partial Y$ does not come into play at $S = Y = 0$ follows from the analysis of the locally self-similar behavior as expressed by Eq. (57).

IV. Local Interaction Theory for Marginally Separated Flows

In the following section, it is demonstrated how, by taking into account the locally strong interaction process between the boundary layer and the external bulk flow, the weak Goldstein-type singularity is eliminated and a uniformly valid description of the flow with respect to the Reynolds equations (3) and (4) is achieved. More precisely, it is pointed out that the locally induced pressure gradient, which is not given in advance, but rather to be determined simultaneously with the flow inside the boundary layer, must enter the analysis if $\epsilon = \mathcal{O}(\alpha^{3/10})$ or smaller. Because nonlinear convective effects cannot be neglected even near the surface, this procedure results in a triple-deck problem that, therefore, clearly differs from the formulation of laminar marginal separation [19,20], but is closely related to laminar short-scale boundary-layer interaction theory [21,33].

Note that the elliptic nature of the equations determining the induced potential flow requires the existence of a boundary-layer solution that does not terminate in a Goldstein-type singularity. Consequently, we at first assume that $\gamma \leq 0$. However, the resulting interaction theory is a posteriori readily seen to apply to flows having $\gamma > 0$ also.

We furthermore stress that inspection of the equations of motion (3) and (4) indicates that the pressure gradient normal to the surface, as well as the Reynolds normal stresses, are negligibly small in any of the flow regimes considered in the subsequent investigation and will, therefore, be disregarded.

A. Induced Potential Flow

We now consider the boundary-layer solutions, assuming that $\epsilon \ll 1$, from the viewpoint of the external freestream flow, which is considered to be irrotational at least up to $\mathcal{O}(\alpha)$, because the Reynolds stresses are of $o(\alpha)$ there. That is, in the double limit $\epsilon \to 0$ and $\alpha \to 0$, the stream function and the pressure are expanded in the form

$$q = q_{00}(\hat{s}, y) + \epsilon q_{01}(\hat{s}, y) + \cdots + \alpha[q_{10}(\hat{s}, y) + \epsilon q_{11}(\hat{s}, y) + \cdots] + \mathcal{O}(\alpha^2), \quad q = \psi, p \tag{62}$$

according to the expansions (14) and (31). The coordinate shift provided by Eq. (41) ensures that the subexpansion in terms of powers of ϵ of the expansion (62) only accounts for the Taylor expansion of u_e around $\hat{s} = 0$. The terms of $\mathcal{O}(\alpha)$ reflect the streamline displacement caused by the boundary layer. Then the stream functions ψ_{00} and ψ_{10} satisfy Laplace's equation

$$\frac{\partial}{\partial \hat{s}}\left(\frac{1}{h}\frac{\partial \psi_{1i}}{\partial \hat{s}}\right) + \frac{\partial}{\partial y}\left(h\frac{\partial \psi_{1i}}{\partial y}\right) = 0, \qquad i = 0, 1 \tag{63}$$

subject to the boundary conditions

$$\psi_{00}(\hat{s}, 0) = 0, \qquad \psi_{10}(\hat{s}, 0) = \Psi_0[\hat{x}, \Delta_0(\hat{x})] - \Delta_0(\hat{x})U_0(\hat{x}) \tag{64}$$

Equation (64) follows from patching the stream function at the boundary-layer edge up to $\mathcal{O}(\alpha)$ by means of a Taylor expansion about $y = 0$, taking into account Eq. (41), and the relationship

$$u_e(x) = U_0(\hat{x}) = \frac{\partial \psi_{00}}{\partial y}(\hat{s}, 0) \tag{65}$$

Hence, ψ_{10} is seen to be determined uniquely in a certain domain $y \geq 0$ and can, in principle, be calculated by adopting standard methods. In turn, the induced pressure disturbance p_{10} follows from evaluating the linearized Bernoulli's law:

$$p_{10} = \frac{1}{h^2}\frac{\partial \psi_{00}}{\partial \hat{s}}\frac{\partial \psi_{10}}{\partial \hat{s}} - \frac{\partial \psi_{00}}{\partial y}\frac{\partial \psi_{10}}{\partial y} \tag{66}$$

We note that, without any loss of generality, in Eq. (66) any remaining pressure perturbation for vanishing velocity variations is discarded.

It is evident from inspection of Eq. (64) and the foregoing analysis of the marginally separating boundary-layer solution given by Ψ_0, Δ_0 that ψ_{10} and p_{10} behave regularly except for the location $\hat{s} = y = 0$. By defining the limiting value

$$\psi_{100} = \psi_{10}(0, 0) = \Psi_{00}(\Delta_{00}) - \Delta_{00}U_{00} \tag{67}$$

which is a quantity of $\mathcal{O}(1)$, a regular upstream but singular downstream behavior of ψ_{10} in the limit $y = 0$ and $\hat{s} \to 0$ is found. That is,

$$\hat{s} \to 0_-: \ \psi_{10}(\hat{s}, 0) - \psi_{100} = \mathcal{O}(\hat{s}) \tag{68}$$

$$\hat{s} \to 0_+: \ \frac{\psi_{10}(\hat{s}, 0) - \psi_{100}}{\ell_{00}^{2/3}U_{00}} \sim A_+\hat{s}^{1/3} \tag{69}$$

These conditions are rich enough to contain the associated singular local behavior of the pressure perturbation p_{10}. A local analysis of Eq. (63) supplemented with Eqs. (64) and (65) shows that

$$\psi_{00}/U_0(\hat{x}) = y - k(\hat{x})y^2/2 + \mathcal{O}(y^3) \quad \text{as} \quad y \to 0_+ \tag{70}$$

and

$$\frac{\psi_{10} - \psi_{100}}{\ell_{00}^{2/3}U_{00}} \sim A_+\rho^{1/3}g(\vartheta), \qquad \vartheta = \arctan(y/\hat{s})$$
$$\pi \geq \vartheta \geq 0 \quad \text{as} \quad \rho = \sqrt{\hat{s}^2 + y^2} \to 0 \tag{71}$$

where

$$g'' + g/9 = 0, \qquad g(\pi) = 0, \qquad g(0) = 1 \tag{72}$$

The solution of this problem is given by

$$g(\vartheta) = \cos(\vartheta/3) - \sin(\vartheta/3)/\sqrt{3} \tag{73}$$

Substituting Eq. (70) evaluated for $\hat{s} \to 0$, Eqs. (71) and (73) into Eq. (66) then yields

$$\frac{p_{10}}{\ell_{00}^{2/3}U_{00}^2} \sim A_+\rho^{-2/3}\left[\frac{\cos(2\vartheta/3)}{3\sqrt{3}} - \frac{\sin(2\vartheta/3)}{3}\right] \tag{74}$$

Finally, one obtains

$$\hat{s} \to 0_-: \ \frac{p_{10}(\hat{s}, 0)}{\ell_{00}^{2/3}U_{00}^2} \sim -\frac{2A_+}{3\sqrt{3}}\hat{s}^{-2/3} \tag{75}$$

$$\hat{s} \to 0_+: \ \frac{p_{10}(\hat{s}, 0)}{\ell_{00}^{2/3}U_{00}^2} \sim \frac{A_+}{3\sqrt{3}}\hat{s}^{-2/3} \tag{76}$$

Again, Eqs. (68), (69), (75), and (76) agree exactly with the behavior of the irrotational flow near the trailing edge of a flat plate that is induced by both the laminar Blasius boundary layer and the near wake. The close relationship between these two different flow configurations arising from the similarity structure of the shear layer downstream of the singular point will also be evident in the resulting interaction problem to be derived subsequently [21,34,35].

The local singularity in the induced potential flow given by Eqs. (71) and (74) indicates a breakdown of the expansions (62) for $\rho \to 0_+$, as one expects from the strong streamwise variations on a length scale of $\mathcal{O}(\epsilon^2)$ of the flow inside the boundary layer, discussed in Sec. III. As already mentioned, the higher-order contributions $q_{11}, \ldots$ to the expansions (62) do not behave more singularly. Therefore, the singularity in p_{10}, represented by Eqs. (75) and (76), and the associated response of the boundary-layer flow suffice to

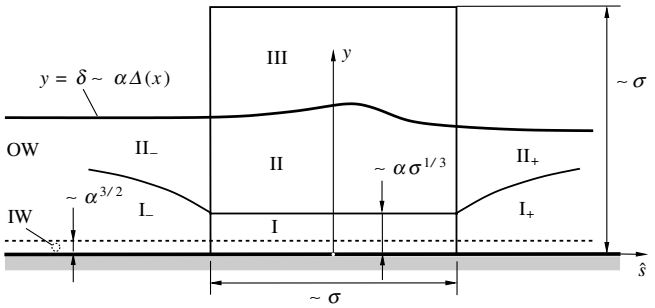

Fig. 5 Asymptotic splitting of the flow in the formal limit $Re^{-1} = 0$ due to the interaction process of the oncoming (subscripts −) and downstream evolving (subscripts +) boundary layer [outer wake (OW) and inner wake (IW); see Sec. II.B.2], triple-deck structure (lower deck I, main deck II, and upper deck III).

determine the scalings of the adjustment regions that will account for a uniformly valid flow description.

B. Triple-Deck Problem for Turbulent Boundary Layers

Because the following analysis also, necessarily, takes into account the effect of the induced pressure on the boundary layer, this section provides a revision of Sec. III.C.2. Therefore, the expansions of the quantities differ in the corresponding details. That is, here, an asymptotically correct analysis of the problem is carried out in line with the set of the full Reynolds equations (3) and (4) rather than their boundary-layer approximation given by Eqs. (8) and (9). By dealing with second-order boundary-layer theory, however, the local perturbations in the boundary layer triggered by the behavior of the induced pressure p_{10} given by Eqs. (74–76) are considered first.

In the limit $\hat{s} \to 0$, the stream function in the boundary-layer where $Y = \mathcal{O}(1)$ is given by $\psi \sim \alpha\Psi_{00}(Y)$; see Eqs. (16) and (51). We now seek the perturbations there owing to the induced pressure p_{10} upstream and downstream of $\hat{s} = 0$. Inspection of the momentum Eq. (3) in combination with the near-wall behavior given by Eq. (24) then shows that the disturbances caused by the pressure gradient $\partial p_{10}/\partial\hat{s}$ of both the Reynolds shear stress gradient and the inertia terms balance in, respectively, the regions I$_-$ and I$_+$ (see Fig. 5), in which the wall coordinate

$$\hat{\eta} = Y/(\ell_{00}^{2/3}|\hat{s}|^{1/3}) \tag{77}$$

is a quantity of $\mathcal{O}(1)$. There, the following expansions are suggested in the triple limit $\epsilon \to 0$, $\alpha \to 0$, and $\hat{s} \to 0$ both for

$$\begin{aligned}\hat{s}\to 0_-:\ &\frac{\psi}{\ell_{00}^{2/3}P_{00}^{1/2}}\\ &=\alpha\Big[(-\hat{s})^{5/6}F_-(\hat{\eta})+(-\hat{s})^{1/3}(\epsilon-B\hat{s})\hat{\eta}+(-\hat{s})^{4/3}\frac{B}{180}\hat{\eta}^4\\ &\quad+\cdots\Big]+\alpha^2(-\hat{s})^{-5/6}\frac{\ell_{00}^{2/3}U_{00}^2}{P_{00}}G_-(\hat{\eta})+\cdots\\ &\frac{p-p_0(x_0)}{P_{00}}=\hat{s}+\cdots-\alpha(-\hat{s})^{-2/3}\frac{2A_+}{3\sqrt{3}}\frac{\ell_{00}^{2/3}U_{00}^2}{P_{00}}+\cdots\end{aligned} \tag{78}$$

and for

$$\begin{aligned}\hat{s}\to 0_+:\ &\frac{\psi}{\ell_{00}^{2/3}P_{00}^{1/2}}=\alpha\hat{s}^{5/6}F_+(\hat{\eta})+\cdots+\alpha^2\hat{s}^{-5/6}\frac{\ell_{00}^{2/3}U_{00}^2}{P_{00}}G_+(\hat{\eta})+\cdots,\\ &\frac{p-p_0(x_0)}{P_{00}}=\hat{s}+\cdots+\alpha\hat{s}^{-2/3}\frac{A_+}{3\sqrt{3}}\frac{\ell_{00}^{2/3}U_{00}^2}{P_{00}}+\cdots\end{aligned} \tag{79}$$

In the expansions (78) and (79), the exponentially growing terms considered in Sec. III.C, which cause a breakdown when $\hat{s} = \mathcal{O}(\epsilon^2)$, are represented by dots. This is sufficient, as we now rather focus on the perturbations proportional to α that are responsible for the onset of the interaction process of the flow upstream and downstream of the interaction region; cf. Fig. 5.

Inserting expansions (78) and (79) into Eq. (3) and rearranging terms up to $\mathcal{O}(\alpha|2\hat{s}|^{-5/3})$ gives rise to a linear inhomogeneous third-order problem for $G_\mp(\hat{\eta})$:

$$\begin{aligned}\pm 2\Big(F_\mp''G_\mp''\Big)'-\frac{5}{6}F_\mp G_\mp'''-\frac{2}{3}F_\mp'G_\mp'+\frac{5}{6}F_\mp''G_\mp=(-1\mp 3)\frac{A_+}{9\sqrt{3}}\\ G_\mp(0)=G_\mp''(0)=0\end{aligned} \tag{80}$$

where the upper and the lower signs correspond to the upstream and the downstream case, respectively.

1. *Upstream Onset of the Interaction Process*

In the upstream case, the problem (80) assumes the form

$$\begin{aligned}(\hat{\eta}^{1/2}G_-'')'-\frac{1}{9}\hat{\eta}^{5/2}G_-''-\frac{2}{9}\hat{\eta}^{3/2}G_-'+\frac{5}{12}\hat{\eta}^{1/2}G_-=-\frac{2A_+}{9\sqrt{3}}\\ G_-(0)=G_-''(0)=0\end{aligned} \tag{81}$$

By applying the transformation

$$G_-(\hat{\eta})=F_-'(\hat{\eta})\Big[\int_0^{\hat{\eta}}\frac{H(z)-H(0)}{\zeta^{3/2}}\,\mathrm{d}\zeta-2\frac{H(0)}{\hat{\eta}^{1/2}}\Big],\qquad z=\frac{\zeta^3}{27} \tag{82}$$

Equation (81) is conveniently cast into an inhomogeneous Kummer's equation [36] for $H(z)$:

$$zH''+(4/3-z)H'-7/6\,H=-A_+/9\,z^{-1/2} \tag{83}$$

where the boundary conditions in Eq. (81) require H to be bounded for $z \to 0$. In addition, the third boundary condition for G_-, missing in Eq. (81), follows from the requirement that H clearly must not grow exponentially for $z \to \infty$. The solution of Eq. (83) is found in terms of a hypergeometric series that, by using the integral representation of the Beta function [36], can be expressed in closed form as an integral. After some manipulations, we obtain

$$H(z)=\frac{A_+}{9}\frac{\pi}{2^{2/3}\Gamma(1/6)\Gamma(4/3)}\int_0^1\frac{t^{1/6}\,\exp(zt)\,\mathrm{erfc}(\sqrt{zt})}{(1-t)^{5/6}}\,\mathrm{d}t \tag{84}$$

Inserting Eq. (84) into Eq. (82) then yields the limiting behavior of $G_-(\hat{\eta})$:

$$G_-'(0)=-A_+\frac{\sqrt{\pi}}{3\sqrt{3}} \tag{85}$$

and

$$G_-=A_-F_-'(\hat{\eta})[1+\mathcal{O}(\hat{\eta}^{-2})]\quad\text{as}\quad\hat{\eta}\to\infty \tag{86}$$

where

$$A_-=\int_0^\infty\frac{H(z)-H(0)}{3^{3/2}z^{7/6}}\,\mathrm{d}z=-A_+\frac{2^{7/3}\Gamma(5/6)\sqrt{\pi}}{27} \tag{87}$$

We now consider the effect of the induced pressure on the surface slip velocity u_s, which is defined by

$$u_s=\partial\psi/\partial y\quad\text{at}\quad y=0 \tag{88}$$

For distances $\hat{s} = \mathcal{O}(1)$, the surface slip is primarily given by the boundary-layer solution, that is,

$$u_s=U_s(x)+\cdots \tag{89}$$

Here, the dots denote higher-order terms due to finite values of ϵ and α. In the triple limit $\alpha \to 0$, $\epsilon \to 0$, and $\hat{s} \to 0_-$ evaluation of Eq. (78) gives

$$\frac{u_s}{P_{00}^{1/2}} = \epsilon - B\hat{s} + \cdots + \alpha(-\hat{s})^{-7/3}\frac{\ell_{00}^{2/3}U_{00}^2}{P_{00}}G'_-(0) + \cdots \tag{90}$$

where the first terms on the right-hand side represent the expansion of $U_s(x)$ about $x = x_0$, using Eq. (41). Equation (90) allows for an appealing physical interpretation: as indicated by Eqs. (78) and (85), the negative (favorable) induced pressure gradient upstream of $\hat{s} = 0$ causes a deceleration of the flow close to the surface. This rather surprising phenomenon has not been observed yet in laminar boundary-layer flows. Here, however, it originates from the fact that convection does not vanish at the surface.

Finally, matching of the expansions (78) and (79) with the flow in the boundary-layer main regimes II_- and II_+ (Fig. 5), where $Y = \mathcal{O}(1)$ demonstrates, by noticing Eq. (86), that the expansions of the stream function there take on the form

$$\hat{s} \to 0_-\colon \psi = \alpha[\Psi_{00}(Y) + (\epsilon - B\hat{s})\Psi_{01}(Y) + \cdots] + \alpha^2(-\hat{s})^{-4/3}\frac{\ell_{00}^{4/3}U_{00}^2}{P_{00}}A_-\Psi'_{00}(Y) + \cdots \tag{91}$$

$$\hat{s} \to 0_+\colon \psi = \alpha[\Psi_{00}(Y) + \hat{s}^{1/3}\ell_{00}^{2/3}A_+\Psi'_{00}(Y) + \cdots] + \alpha^2\hat{s}^{-4/3}\frac{\ell_{00}^{4/3}U_{00}^2}{P_{00}}C_+\Psi'_{00}(Y) + \cdots \tag{92}$$

It is anticipated in Eq. (92) that, in analogy to Eq. (86), the function G_+ behaves as $G_+(\hat{\eta}) \sim C_+F'_+(\hat{\eta} + A_+)$, $\hat{\eta} \to \infty$, with some constant C_+. For this mathematical detail, the reader is again referred to a future publication.

2. Main Deck

A breakdown of the asymptotic structure considered so far occurs due to both the exponentially growing eigensolutions when $\hat{s} = \mathcal{O}(\epsilon^2)$ [see the expansion (31) and Eq. (41)], and the singular induced pressure gradient $\partial p_{10}/\partial\hat{s}$ when $\hat{s} = \mathcal{O}(\alpha^{3/5})$; cf. the preceding expansions (91) and (92). To take into account both causes of nonuniformness, we consider a distinguished limit by introducing the coupling parameter

$$\chi = \frac{\epsilon^{10/3}}{\alpha}\frac{P_{00}}{\ell_{00}^{2/3}U_{00}^2} \tag{93}$$

which is required to be of $\mathcal{O}(1)$ in the double limit $\epsilon \to 0$ and $\alpha \to 0$. Then the streamwise distance, for which the expansions (91) and (92) cease to be valid, is found to be measured by

$$\hat{s} = \sigma\hat{X}, \qquad \sigma = (\epsilon/\Gamma)^2 \quad \text{with} \quad 0 \le \Gamma \le 1 \tag{94}$$

which, in turn, redefines the streamwise extent of the main deck (region II in Fig. 5). Here, the parameter Γ is introduced to provide a bijective function $\chi(\Gamma)$ having the properties

$$\chi'(\Gamma) > 0, \qquad \chi_b = \chi(1) \le \infty, \qquad \chi = \mathcal{O}(\Gamma^{10/3}) \quad \text{as} \quad \Gamma \to 0 \tag{95}$$

where the upper bound χ_b of the coupling parameter may be chosen arbitrarily. It is convenient with respect to the subsequent analysis to specify the relationship between Γ and χ by the definition of a further function $\Lambda(\Gamma)$ in the form

$$\chi(\Gamma) = \Gamma^{10/3}/\Lambda(\Gamma), \qquad \Lambda'(\Gamma) \le 0 \tag{96}$$

Then Λ is seen to be bounded, and

$$\Lambda(0) > \Lambda(1) = 1/\chi_b \tag{97}$$

From Eqs. (93), (94), and (96), one then readily concludes that

$$\epsilon = \sigma^{1/2}\Gamma, \qquad \alpha = \sigma^{5/3}\Lambda\frac{P_{00}}{\ell_{00}^{2/3}U_{00}^2} \tag{98}$$

The meaning of Eqs. (93–98) is as follows. The case $\chi_b = \infty$ or, equivalently, $\Lambda(1) = 0$, recovers the pure boundary-layer limit, that is, $\alpha = 0$ for finite values of ϵ, already discussed in Sec. III.C.2, for which the induced pressure gradient does not come into play at all. On the other hand, the limit $\chi = 0$ refers to the case $\gamma = \epsilon = 0$, where $\sigma = \mathcal{O}(\alpha^{3/5})$. These considerations imply that the regions I, II, and III, as sketched in Fig. 5, are located a distance of $\mathcal{O}(\epsilon)$ upstream of the position of the marginal singularity given by $s = 0$ [cf. Eq. (41)], where the lower and upper limits of the magnitude of their streamwise extent are given by $\mathcal{O}(\alpha^{3/5})$ and $\mathcal{O}(\epsilon^2)$, respectively.

Inspection of Eqs. (91) and (92) indicates that, in the main-deck region, the expansions (51) and (52) now take on the asymptotically correct forms

$$\psi/\alpha = \Psi_{00}(Y) + \sigma^{1/3}\ell_{00}^{2/3}\hat{A}(\hat{X})\Psi'_{00}(Y) + \cdots + (\sigma^{1/2}\Gamma - \sigma B\hat{X})\Psi_{01}(Y) + \cdots \tag{99}$$

and

$$\delta/\alpha = \Delta_{00} - \sigma^{1/3}\ell_{00}^{2/3}\hat{A}(\hat{X}) + \cdots \tag{100}$$

in the limit $\sigma \to 0$. Here, and in the following, the substitutions given by Eq. (98) have been applied. Moreover, the expansions (78) and (79) imply that the pressure in the main deck can be written as

$$p = p_0(x_0) + \sigma P_{00}[\hat{X} + \Lambda\hat{P}(\hat{X})] + \cdots \tag{101}$$

Both the displacement function $\hat{A}(\hat{X})$ and the pressure function $\hat{P}(\hat{X})$ are quantities of $\mathcal{O}(1)$ and are unknown at this stage of the analysis. However, matching with the regions II_- and II_+ reveals the following asymptotes:

$$\hat{X} \to -\infty\colon \hat{A}(\hat{X}) \sim \Lambda A_-\hat{X}^{-4/3} \tag{102}$$

$$\hat{P}(\hat{X}) \sim -\frac{2A_+}{3\sqrt{3}}\hat{X}^{-2/3} \tag{103}$$

$$\hat{X} \to +\infty\colon \hat{A}(\hat{X}) \sim A_+\hat{X}^{1/3} \tag{104}$$

$$\hat{P}(\hat{X}) \sim \frac{A_+}{3\sqrt{3}}\hat{X}^{-2/3} \tag{105}$$

3. Upper Deck

The preceding considerations suggest that the expansion (62) of the flow in the external regime, where both $\hat{s}$ and y are quantities of $\mathcal{O}(1)$, fails in the upper deck (region III in Fig. 5). There, appropriately rescaled variables are given by the scalings (94) and

$$y = \sigma\hat{y}, \qquad \hat{y} = \mathcal{O}(1) \tag{106}$$

The singular behavior of the stream function and the pressure expressed by Eqs. (69), (75), and (76) then gives rise to the expansions

$$\psi = \sigma U_{00}\hat{y} + \cdots + \Lambda\frac{P_{00}}{U_{00}}\left[\sigma^{5/3}\frac{\Psi_{100}}{\ell_{00}^{2/3}U_{00}} + \sigma^2\hat{\psi}(\hat{X},\hat{y}) + \cdots\right] \tag{107}$$

$$p = p_0(x_0) + \sigma P_{00}[\hat{X} + \Lambda\hat{p}(\hat{X},\hat{y})] + \cdots \tag{108}$$

Here, terms proportional to Λ represent the potential flow induced locally by the boundary-layer displacement.

The pressure $\hat{p}$ is calculated from Bernoulli's law [cf. Eq. (66)], which, by balancing terms up to $\mathcal{O}(\sigma^2)$, reduces to

$$\hat{p} = -\frac{\partial \hat{\psi}}{\partial \hat{y}} \tag{109}$$

and the stream function $\hat{\psi}$ is seen to satisfy the Cauchy problem:

$$\begin{gathered} \frac{\partial^2 \hat{\psi}}{\partial \hat{X}^2} + \frac{\partial^2 \hat{\psi}}{\partial \hat{y}^2} = 0, \qquad \hat{\psi}(\hat{X}, 0) = \hat{A}(\hat{X}) \\ \hat{\psi} \sim A_+ \hat{\rho}^{1/3} g(\vartheta) \quad \text{as} \quad \hat{\rho} = \sqrt{\hat{X}^2 + \hat{y}^2} \to \infty \end{gathered} \tag{110}$$

Herein, ϑ is given by Eq. (71), where the ratio $y/\hat{s}$ is to be replaced by $\hat{y}/\hat{X}$ according to the local scaling provided by Eqs. (94) and (106). The boundary conditions in Eq. (110) follow from patching the stream function at the boundary-layer edge by using Eqs. (99) and (100) and from a match of $\hat{\psi}$ with the singular behavior of ψ_{10} given by Eq. (71), respectively. In turn, $\hat{p}$ matches the asymptotic behavior of p_{10} as expressed by Eqs. (74–76). Additionally, comparing Eq. (108) with Eq. (101) and taking into account Eq. (109) yields the relationship

$$\frac{\partial \hat{\psi}}{\partial \hat{y}}(\hat{X}, 0) = -\hat{P}(\hat{X}) \tag{111}$$

where $\hat{P}(\hat{X})$ is seen to be the induced surface pressure. Consequently, and as a well-known result from potential flow theory [33], $\hat{P}(\hat{X})$ and $-\hat{A}'(3\hat{X})$ form a Hilbert pair, that is,

$$\{\hat{P}(\hat{X}), -\hat{A}'(\hat{X})\} = \frac{1}{\pi} \oint_{-\infty}^{\infty} \frac{\{\hat{A}'(\hat{S}), \hat{P}(\hat{S})\}}{\hat{X} - \hat{S}} \mathrm{d}\hat{S} \tag{112}$$

4. Lower Deck

The analysis is finalized by considering the flow in the lower deck (region I in Fig. 5) in the limit $\sigma \to 0$. Hence, we introduce rescaled local variables $\hat{Y}$ and $\hat{\Psi}$ of $\mathcal{O}(1)$ according to

$$\frac{Y}{\ell_{00}^{2/3}} = \sigma^{1/3} \hat{Y}, \qquad \frac{\psi}{\ell_{00}^{2/3} P_{00}^{1/2}} \sim \alpha \sigma^{5/6} \hat{\Psi}(\hat{X}, \hat{Y}) \tag{113}$$

Moreover, the pressure is given by Eq. (101). The leading-order problem governing the flow in the lower deck is found by inserting these quantities into the equations of motion (3) and (4) or, equivalently, by applying the transformation

$$\hat{X} = \Gamma^2 X, \qquad \hat{Y} = \Gamma^{2/3} \bar{Y}, \qquad \hat{\Psi} = \Gamma^{5/3} \bar{\Psi} \tag{114}$$

to Eq. (43). As a result, the inclusion of the induced pressure gradient in Eq. (44) is seen to be sufficient to generate an asymptotically correct description of the flow near the surface. The lower-deck equations then read

$$\begin{gathered} \frac{\partial \hat{\Psi}}{\partial \hat{Y}} \frac{\partial^2 \hat{\Psi}}{\partial \hat{Y} \partial \hat{X}} - \frac{\partial \hat{\Psi}}{\partial \hat{X}} \frac{\partial^2 \hat{\Psi}}{\partial \hat{Y}^2} = -1 - \Lambda(\Gamma) \hat{P}'(\hat{X}) + \frac{\partial \hat{T}}{\partial \hat{Y}} \\ \hat{T} = \frac{\partial^2 \hat{\Psi}}{\partial \hat{Y}^2} \left| \frac{\partial^2 \hat{\Psi}}{\partial \hat{Y}^2} \right| \end{gathered} \tag{115}$$

They are subject to the boundary conditions

$$\hat{Y} = 0\text{: } \hat{\Psi} = \hat{T} = 0 \tag{116}$$

$$\hat{Y} \to \infty\text{: } \hat{T} - \hat{Y} \to \hat{A}(\hat{X}) \tag{117}$$

$$\hat{X} \to -\infty\text{: } \hat{\Psi} \to F_-(\hat{Y}) + \Gamma \hat{Y}, \qquad 0 \le \Gamma \le 1 \tag{118}$$

$$\hat{X} \to \infty, \hat{Y} \to \infty\text{: } \hat{\Psi} \hat{X}^{-5/6} \to F_+(\hat{\eta}), \qquad \hat{\eta} = \hat{Y}/\hat{X}^{1/3} = \mathcal{O}(1) \tag{119}$$

The conditions (117–119) follow from a match with the expansions (78), (79), and (99), respectively, which clearly cease to be valid in the lower-deck flow regime. The asymptotic behavior expressed by relationship (117), however, can be shown to be determined by the upstream initial condition (118) rather than provide an additional boundary condition to be imposed. Most important, because both the functions $\hat{P}(\hat{X})$ and $\hat{A}(\hat{X})$ are seen to be part of the solution, Eqs. (115–119) have to be supplemented with one of the relationships given by Eq. (112) in order to complete the triple-deck problem.

This fundamental problem that governs turbulent marginal separation associated with the triple-deck scheme outlined previously has the following important properties:

1) As a highly remarkable characteristic not known in laminar triple-deck theory at present (apart from a laminar supersonic triple-deck flow model proposed by Lipatov [37]), the lower-deck equations (115) include both the (locally constant) imposed and the induced streamwise pressure gradient given by $\Lambda \hat{P}'(\hat{X})$.

2) A property also not observed in subsonic laminar interacting boundary layers so far is that turbulent marginal separation is linked to the existence of eigensolutions of the underlying triple-deck problem. In this connection we note that Eqs. (112) and (115–119) allow for the trivial solution $\hat{\Psi} = F_-(\hat{Y}) + \Gamma \hat{Y}$, $\hat{A}(\hat{X}) = \hat{P}(\hat{X}) = 0$. However, a nontrivial solution is conveniently enforced by prescribing the downstream condition (119). Therefore, the ellipticity of the triple-deck problem is not only due to the imposed pressure gradient [cf. Eq. (112)], but also arises from the nontrivial downstream state as expressed by Eq. (119) and in agreement with Eq. (53).

3) It is inferred from Eq. (96) that the triple-deck solutions depend on χ solely, independent of the specific choice of the function $\Lambda(\Gamma)$. This is also expressed by the invariance properties

$$\begin{gathered} \hat{\Psi}(\hat{X}, \hat{Y}) = \lambda^{-5/6} \hat{\Psi}(\mathcal{X}, \mathcal{Y}), \qquad \hat{A}(\hat{X}) = \lambda^{-1/3} \hat{A}(\mathcal{X}) \\ \hat{P}(\hat{X}) = \lambda^{2/3} \hat{P}(\mathcal{X}), \qquad \mathcal{X} = \lambda(\hat{X} - \mu), \qquad \mathcal{Y} = \lambda^{1/3} \hat{Y} \end{gathered} \tag{120}$$

satisfied by the solution $\hat{\Psi}$, $\hat{A}$, $\hat{P}$ for a given value of χ. Here, $\hat{X}$ is stretched by an arbitrary factor $\lambda > 0$. The real parameter μ corresponds to an origin shift in $\hat{X}$ of the solution. However, the ambiguity of the solution expressed by that translation invariance has to be eliminated by the exponentially decreasing eigensolutions occurring upstream, giving

$$\begin{aligned} \hat{\Psi} = {} & F_-(\hat{Y}) + \Gamma \hat{Y} + \cdots - \operatorname{sgn}(\gamma) \Gamma^{5/3} f(\hat{Y}/\Gamma^{2/3}) \\ & \times \exp[\hat{X}/(3\Gamma^2)] + \cdots, \qquad \hat{X} \to -\infty \end{aligned} \tag{121}$$

This expansion follows directly from Eq. (47) by taking into account Eq. (114). Equation (121) states that, in definite contrast to the noninteractive case that is expressed by $\Gamma = 1$ and $\Lambda = 0$ or, equivalently, Eq. (44), the interaction process is insensitive to the sign of γ. The latter rather enters the triple-deck solution only via exponentially small terms. Their strength is fixed by the requirement of a match with the oncoming flow, which, in turn, eliminates the translation invariance of the solution by means of an adequate choice of the group parameter μ.

It is useful to introduce the rescaled surface slip velocity

$$\hat{U}_s = \frac{\partial \hat{\Psi}}{\partial \hat{Y}}(\hat{X}, 0) \tag{122}$$

A comparison with Eq. (90) gives

$$u_s \sim \sigma^{1/2} P_{00}^{1/2} \hat{U}_s \quad \text{as} \quad \hat{X} = \mathcal{O}(1) \tag{123}$$

and by matching of Eq. (122) with Eq. (78) or, equivalently, Eq. (90), and Eq. (79), one recovers the expansions holding upstream and downstream, respectively,

$$\hat{X} \to -\infty\colon\ \hat{U}_s \sim \Gamma - \Lambda G'_-(0)\hat{X}^{-7/6} \tag{124}$$

$$\hat{X} \to +\infty\colon\ \hat{U}_s \sim U_+\hat{X}^{1/2} \tag{125}$$

The latter of these relationships reflects the match with the nontrivial self-similar solution expressed by $F_+(\hat{\eta})$. The asymptotic behavior [Eq. (124)] is seen to be valid for all admissible values of Γ and Λ and demonstrates the effects of both the exponentially decaying eigensolutions and of the induced pressure gradient on the triple-deck solution. The first determines the magnitude of the control parameter ϵ and, in turn, Γ, which fixes the upstream limit of the surface slip. The upstream deceleration of the flow, however, is primarily caused by the induced pressure gradient, the strength of which is measured by Λ.

As a consequence of Eqs. (115) and (116), and by noting the definition of $\hat{U}_s$ [Eq. (122)], one obtains the near-wall asymptotes:

$$\begin{aligned} \hat{\Psi} &= \hat{U}_s(\hat{X})\hat{Y} + 4/15\mathrm{sgn}(\Upsilon)|\Upsilon|^{1/2}\hat{Y}^{5/2} + \mathcal{O}(\hat{Y}^4) \\ \hat{T} &= \Upsilon\hat{Y} + \mathcal{O}(\Upsilon\hat{Y}^{5/2}, \hat{Y}^4) \\ \Upsilon(\hat{X}) &= \hat{U}_s(\hat{X})\hat{U}'_s(\hat{X}) + 1 + \Lambda\hat{P}'(\hat{X}), \qquad \hat{Y} \to 0 \end{aligned} \tag{126}$$

Furthermore, as already indicated by the asymptotic behavior [Eq. (25)] of the downstream similarity solution, for large values of $\hat{Y}$, the solution is seen to be invariant with respect to a shift in $\hat{Y}$ of the amount $\hat{A}(\hat{X})$. In other words, a nonvanishing value of A_+ enforces the nontrivial eigensolution of the triple-deck problem having $\hat{A} \not\equiv 0$. On the other hand, one draws the conclusion that the possible shift is an immediate consequence of the hyperbolic convective operator giving rise to the predominating convective terms, far from the surface, on the left-hand side of the momentum balance in Eq. (115). By taking into account the upstream asymptotes given by Eq. (118) together with $\hat{P}(-\infty) = 0$, the analysis then yields

$$\begin{aligned} \hat{\Psi} &= F_-(\hat{Z}) + 3/4\,\Lambda\hat{P}\hat{Z}^{-1/2} - 9/56\,\Gamma\Lambda\hat{P}\hat{Z}^{-2} \\ &\quad + \hat{Z}^{-7/2}\sum_{n=0}^{\infty}\Phi_n\hat{Z}^{-3n/2} + \mathrm{TST} \\ \hat{T} &= \hat{Z} + 9/8\,\Lambda\hat{P}\hat{Z}^{-2} - 27/14\,\Gamma\Lambda\hat{P}\hat{Z}^{-7/2} \\ &\quad + \hat{Z}^{-5}\sum_{n=0}^{\infty}\Xi_n\hat{Z}^{-3n/2} + \mathrm{TST}, \quad \hat{Z} = \hat{Y} + \hat{A} \to \infty \end{aligned} \tag{127}$$

We note that the algebraic terms following the leading-order contributions in these asymptotic expansions vanish if, and only if, $\Lambda = 0$. To be more precise, both the leading-order coefficients Φ_0 and Ξ_0 in the remainder series are quantities of $\mathcal{O}(\Lambda, \Lambda^2, \Lambda\Gamma^2)$. One also easily verifies the match of Eq. (127) with the higher-order contribution determined by $G_-(\hat{\eta})$ to the expansion (78), which characterizes the oncoming flow, in the limit $\hat{\eta} \to \infty$; see Eqs. (86), (87), and (102).

C. Numerical Results

1. Method

For the numerical treatment of the triple-deck problem posed by Eqs. (112) and (115–119), a carefully devised variable transform that maps the interval $-\infty < \hat{X} < \infty$ onto the range $[-1, 1]$ was performed to handle the singular upstream and downstream behavior at infinity in an efficient manner. In addition, a coordinate stretching in $\hat{Y}$ direction was introduced that, among others, accounts for the far-field relationships given by Eq. (127), in which only the terms larger than the remainder sums were regarded. Most important, however, it regularizes the half-power behavior $\hat{\Psi} = \hat{U}_s(\hat{X})\hat{Y} + \mathcal{O}(\hat{Y}^{5/2})$ for $\hat{Y} \to 0$ [see Eq. (126)] and thus allows for a higher resolution of the flow close to the surface. These ideas were put forward in its original form by Smith and Merkin [38]; see also [39,40]. The thereby-transformed equations were discretized on a uniformly spaced mesh by approximating all derivatives using central finite differences with second-order accuracy. Therefore, the elliptic character of the problem is fully retained. The stream function and the pressure served as the only dependent variables. The resulting system of nonlinear algebraic equations was solved directly by adopting a modification of the Powell hybrid method [41] in which the Jacobians are calculated numerically in principle but, whenever feasible, updated by means of a secant approximation during the Newton iteration. In each Newton step, the resulting linear system of equations are solved by advantageously exploiting the sparsity pattern of the Jacobian. Under reasonable conditions, this algorithm guarantees a fast rate of global convergence. We note that, typically, a grid of 300 points in $\hat{X}$ direction and 150 points in $\hat{Y}$ direction was employed, for which the principal limit of resolution depends on the hardware memory available. The stopping criterion for the iteration process was provided by the machine-dependent optimal accuracy of the solution. It should be stressed that the indeterminacy of the solutions with respect to a shift of the origin, expressed by Eq. (120) and discussed in the preceding item 3, is eliminated numerically as a consequence of the discretization process. A more detailed description of the numerical procedure, however, is postponed to a separate publication. In addition, the authors annotate that, if applied to a broader class of problems arising in the field of interacting boundary layers, the technique presented here is even supposed to prove superior to miscellaneous well-established numerical schemes that are purpose-built for tackling such problems. Nevertheless, this is a topic that is yet under investigation.

2. Exemplary Flow Configurations

Numerical solutions have been obtained for several values of Λ, whereas Γ varied in the whole range $0 \le \Gamma \le 1$. Owing to the limitation of space, only the case $\Lambda = 3$ will be discussed in detail. It then follows from Eq. (96) that $\chi = \Gamma^{10/3}/3$ and $0 \le \chi \le \chi_b$ with $\chi_b = 1/3$. Separation is associated with negative values of $\hat{U}_s$. As an important result, such local flow reversal is observed for $0 \le \Gamma \le \Gamma^*$, where $\Gamma^* \doteq 0.205$, that means within the (rather small) range $0 \le \chi \le \chi^*$ with $\chi^* \doteq 1.69 \times 10^{-3}$. We furthermore emphasize that the shear stress gradient at the surface, given by $\Upsilon = (\partial\hat{T}/\partial\hat{Y})(\hat{X}, 0)$ as expressed in Eq. (126), and, in turn, both the Reynolds stress $\hat{T}$ and the streamwise velocity gradient $\partial^2\hat{\Psi}/\partial\hat{Y}^2$ are seen to be positive for all admissible values of $\hat{X}$, $\hat{Y}$, and χ.

Representative numerical results are plotted in Fig. 6, in which consecutive data points are connected using smooth cubic spline interpolation. In Figs. 6a and 6b the positions at the surface $\hat{Y} = 0$ of flow detachment $\hat{X} = \hat{X}_D$ (dashed curves), flow reattachment $\hat{X} = \hat{X}_R$ (dotted curves), and their difference, that is, the length

$$\hat{L} = \hat{X}_R - \hat{X}_D \tag{128}$$

of the recirculation region (solid curves) are presented in the range $0 \le \Gamma \le 0.016$ and $0.017 \le \Gamma \le 0.205 \doteq \Gamma^*$, respectively. Note that the location of detachment tends to $-\infty$ for $\Gamma \to 0$; cf. Eq. (124). In turn, a rather flat separation bubble emerges for values of Γ within the range $0 < \Gamma < 0.017$. For larger values of Γ, that is, for $\Gamma \ge 0.016\ldots$, up to $\Gamma = 0.019\ldots$ the interesting phenomenon of intermediate reattachment followed by a second flow detachment immediately further downstream is noticed. The corresponding values of $\hat{X}_D$, $\hat{X}_R$, and $\hat{L}$ characterizing that first separated flow regime (which, however, appears to be very small and, therefore, difficult to resolve numerically) are shown in Fig. 6c. Exemplarily, in Fig. 6d, the distributions of $\hat{A}(\hat{X})$, $\hat{P}(\hat{X})$, and $\hat{U}_s(\hat{X})$ are displayed for the case $\Gamma = 0.019$, together with the upstream and downstream asymptotes (dashed-dotted lines) given by Eqs. (103–105) and (125). Note the rather flat passage of the quantities $\hat{A}$ and $\hat{U}_s$ to negative values compared with their pronounced rise downstream of reattachment. As a matter of fact, the indicated splitting of the separation bubble is hardly visible and, therefore, rather a conjecture at the present stage of the numerical analysis. Thus, its validation is

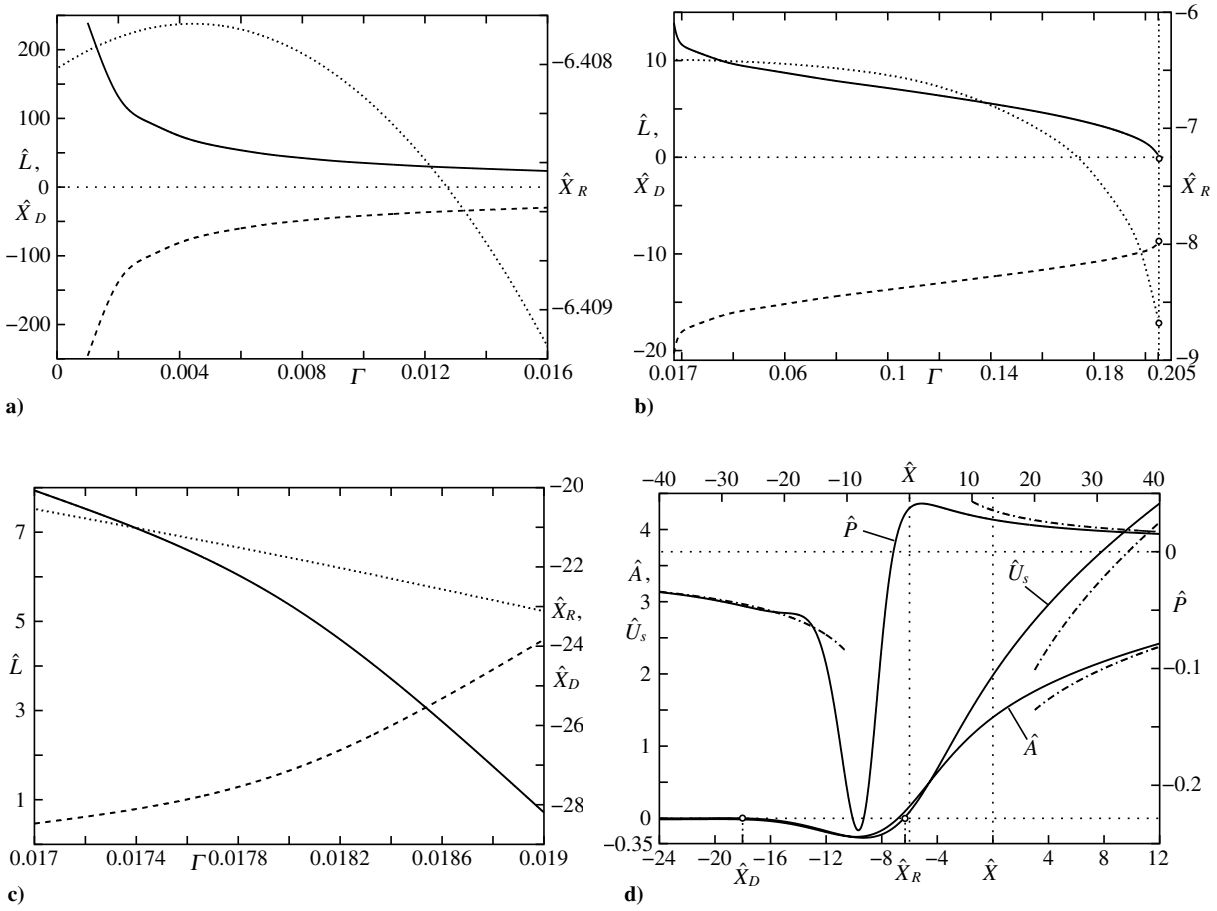

Fig. 6 Numerical solutions of the fundamental interaction problem [Eqs. (112) and (115–119)]: a)–c) locations of detachment $\hat{X} = \hat{X}_D$, reattachment $\hat{X} = \hat{X}_R$, and bubble length $\hat{L} = \hat{X}_R - \hat{X}_D$ in dependence of Γ, where c) applies to the first-separating flow regime, and d) solutions for $\Gamma = 0.019$. Here, $\hat{X}_D \doteq -18.01$ and $\hat{X}_R \doteq -6.40$. The abscissa at the bottom refers to $\hat{A}$ and $\hat{U}_s$; the one at the top refers to $\hat{P}$.

effectively a topic of further numerical effort as it requires the use of an adequately refined mesh.

In addition, both the streamline pattern and the corresponding distributions of $\hat{\Psi}$ for various $\hat{X}$ locations for the reverse-flow regime of the identical flow configuration are depicted in Fig. 7. Note the increasing density of the streamlines further away from the surface and downstream of reattachment, the latter reflecting the strong acceleration there as represented by the correspondingly rapid rise of $\hat{U}_s$. The behavior of the streamlines in the vicinity of $\hat{X} = \hat{X}_D$ and $\hat{X}_R$, respectively, is discussed in Sec. IV.C.3, next. The graphs shown in Fig. 7b agree well with the local analytical representation of $\hat{\Psi}$ given in Eq. (126).

It is noteworthy that the rather rapid acceleration of the near-wall portion of the streamwise velocity immediately downstream of reattachment indicates an intense vortex motion there. This observation is in remarkable agreement with the findings of Perry and Fairlie [42], based on their heuristic inviscid flow model. However, here, the steep rise of $\hat{U}_s$ owes to the specific internal structure of the flow ensuing from a nontrivial eigensolution of the triple-deck problem defined by Eqs. (112) and (115–119). This, in turn, owes to the strongly Reynolds-stress-affected downstream state of the solution enforced by the latter relationship.

3. *Analysis of Small Backflow Regions*

Let $\hat{X} = \hat{X}_0$ denote the point of flow detachment or reattachment. Then the slip velocity and the induced pressure gradient behave as

$$\hat{U}_s = \hat{B}(\chi)\hat{S} + \mathcal{O}(\hat{S}^2), \qquad \hat{P}' = \hat{P}_0(\chi) + \mathcal{O}(\hat{S}) \\ \hat{S} = \hat{X} - \hat{X}_0 \to 0 \tag{129}$$

where $\hat{B} < 0$, $\hat{S} < 0$ and $\hat{B} > 0$, $\hat{S} > 0$ in, respectively, the detaching and the reattaching case. Therefore, it is readily found from substituting the expression for $\hat{U}_s$ in Eq. (129) into the first of the relationships (126), that the branching streamline having $\hat{\Psi} = 0$ is locally given by

$$\hat{Y}|_{\hat{\Psi}=0} \sim \frac{(15\hat{B})^{2/3}}{[16(1 + \Lambda\hat{P}_0)]^{1/3}}\,\hat{S}^{2/3} \tag{130}$$

cf. Fig. 7a. The term in parentheses in the denominator of Eq. (130) represents the Reynolds stress gradient at the surface given by Υ, which is seen to be positive for all values of $\hat{X}$ [cf. Eqs. (115) and (126)], here evaluated for vanishing convection (that is, for $\hat{X} = \hat{X}_0$, it reduces to the overall pressure gradient $1 + \Lambda\hat{P}'$). In connection with the infinite streamline curvature at $\hat{S} = 0$ predicted by Eq. (130) it is interesting to note that there is experimental evidence [43] that the streamline angle to the surface is not small even in the case of mild flow separation, despite the fact that the wall is flat. In this context, the authors also refer to the statements given in [23] in respect of turbulent massive separation.

The points $\hat{X} = \hat{X}_D$ and $\hat{X} = \hat{X}_R$ denoting separation and reattachment, respectively, collapse onto the single point $\hat{X} = \hat{X}^*$ for $\chi = \chi^*$, so that $\hat{B}(\chi^*) = \hat{L} = 0$. Consequently, the emergence of a small, closed reverse-flow regime is described by the relationships

$$\hat{U}_s = \hat{B}_1(\hat{S}^2 - \hat{L}^2/4) + \mathcal{O}(\hat{L}^3), \qquad \hat{P}' = \hat{P}_0(\chi^*) + \mathcal{O}(\hat{L}) \\ \hat{X}_D = \hat{X}^* - \hat{L}/2, \qquad \hat{X}_R = \hat{X}^* + \hat{L}/2 \\ \hat{S} = \hat{X} - \hat{X}^* = \mathcal{O}(\hat{L}), \qquad \hat{L} \to 0_+ \tag{131}$$

where a match with the expression for U_s in Eq. (129) requires

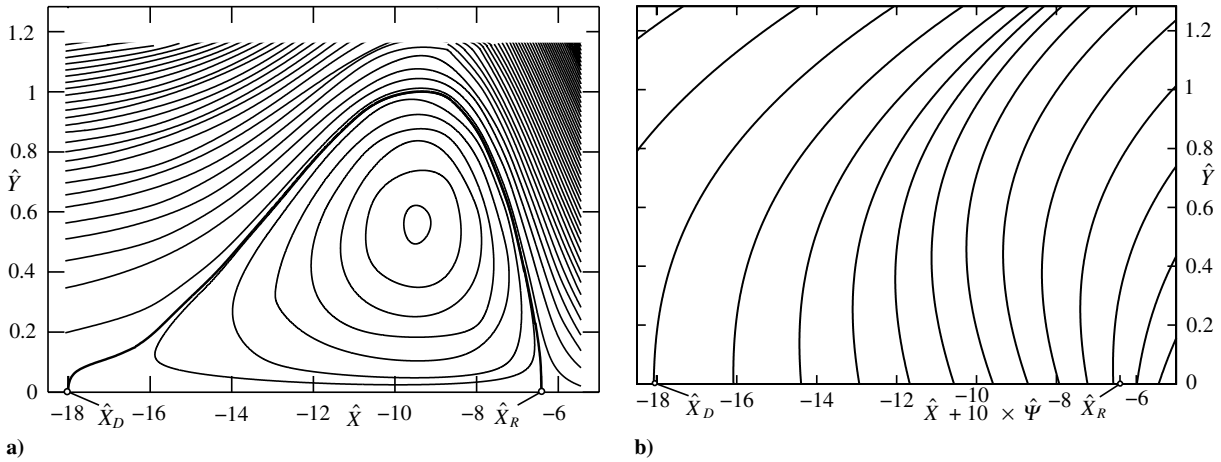

Fig. 7 Separation for the case $\Gamma = 0.019$: a) streamlines $\hat{\Psi} = \text{const}$ in the range $-0.085 \le \hat{\Psi} \le 1.01$, for which Bezier spline interpolation was applied such that the values of $\hat{\Psi}$ for neighboring curves differ by 0.015; in addition, the dividing streamline (bold) is approximated by $\hat{\Psi} = 10^{-10}$ and is rather adjacent to the one for which $\hat{\Psi} = -0.001$, which is also plotted, and b) several profiles of the stream function $\hat{\Psi}$ for the same $\hat{X}$ and $\hat{Y}$ range as in Fig. 7a, magnified by a factor of 10.

$$\hat{B} = \mp \hat{B}_1 \hat{L} + \mathcal{O}(\hat{L}^2), \qquad \hat{B}_1 > 0 \tag{132}$$

Here, the upper and the lower signs refer to, respectively, the position of separation and reattachment in Eq. (129). As the slip velocity $\hat{U}_s$ varies with χ in a regular manner, the relations (131) state that $\hat{L}$ depends on $\chi^* - \chi$ in the form

$$\hat{L} = \mathcal{O}(\sqrt{\chi^* - \chi}), \qquad \chi^* - \chi \to 0_+ \tag{133}$$

This property is captured by the behavior of the numerical results near the endpoints of the curves, indicated by circles, for which $\Gamma = \Gamma^*$ in Fig. 6b. In addition, one readily finds that the streamlines $\hat{\Psi} = \text{const}$ in the vicinity of a very mild separation bubble of length $\hat{L} \ll 1$ are given by

$$\hat{B}_1 \left(\hat{S}^2 - \frac{\hat{L}^2}{4} \right) \hat{Y} + \frac{4}{15} \sqrt{1 + \Lambda \hat{P}_0(\chi^*)}\, \hat{Y}^{5/2} \sim \hat{\Psi}$$
$$\hat{S} = \mathcal{O}(\hat{L}), \qquad \hat{Y} = \mathcal{O}(\hat{L}^{4/3}) \tag{134}$$

Finally, it should be mentioned that, from a computational point of view, the triple-deck formulation presented here is related to the original numerical treatment of transient marginal separation past the leading edge of an airfoil by Briley and McDonald [44]. They employed an advanced mixing-length-based one-equation closure and adopted a time-dependent iterative scheme that reflects the interaction process, albeit in a nonasymptotic sense. This technique allowed for avoiding the occurrence of the Goldstein singularity in the skin friction in the boundary-layer sweeps and the prediction of closed separation bubbles.

V. Conclusions

An asymptotic theory of turbulent marginal separation has been presented that depends on a single similarity parameter $\chi \ge 0$ containing the essential upstream information. Numerical solutions of the fundamental triple-deck problem have been found for a wide range of χ. Open questions include, among others, the effect of the exponentially decaying eigensolutions as $\hat{X} \to -\infty$ that dominate over the algebraically varying terms for $\Gamma = 1$ in the noninteractive case $\Lambda \to 0$ or, equivalently, $\chi \to \infty$ as predicted by Eq. (124). Then only the strictly attached solutions have been found at present, which are related to the subcritical upstream condition $\gamma < 0$. Its supercritical counterpart $\gamma > 0$, however, causing the boundary-layer solution to terminate in the Goldstein-type singularity, is likely associated with a very large recirculation region if the induced pressure is taken into account in an appropriate manner. That is, the triple-deck problem has to be investigated in order to explore the according substructure that emerges for $\Lambda \to 0$ and predicts separation on a correspondingly larger streamwise length scale. Interestingly, the assumption of an almost inviscid but strongly rotational flow inside the separation region proposed much earlier by Perry and Fairlie [42] is possibly pointed to the inviscid character of the boundary-layer solution slightly upstream of the position of breakdown; see Sec. III.D. This observation may therefore become relevant to the study of large-scale separation.

Furthermore, the effects of the inner wake as well as the Reynolds-number-dependent flow regimes adjacent to the surface have to be studied. However, the inner wake layer, not considered here, is seen to behave only passively, as it is characterized by convective terms linearized about the slip velocity imposed by the outer wake. Because $\alpha \ll 1$ even in the limiting case $Re^{-1} = 0$, the perturbations in the wake regime reflecting viscous effects, which primarily arise from the surface shear stress denoted by τ, are of minor (physical) relevance. On the other hand, most important, matching of the logarithmically varying u components of the velocities in the overlap domain of the viscosity-affected near-wall flow regimes gives rise to a relationship determining the surface friction τ in the limit $Re \to \infty$:

$$\frac{\sqrt{\tau}}{u_s} \sim \frac{\kappa}{\ell_n Re}, \qquad \tau = \frac{1}{Re} \frac{\partial u}{\partial y} \quad \text{at} \quad y = 0 \tag{135}$$

That skin friction law is clearly rendered invalid if the surface slip velocity u_s at the base of the wake tends to zero, which is the case as separation is approached. Therefore, the investigation of a flow on the verge of separation, for which the reverse-flow regime is governed by Eq. (134), is expected to give a first hint how to continue the skin friction law (135) asymptotically correctly into the regions in which the flow separates but immediately recovers. It can be shown [11,12] that both $\sqrt{\tau}$ and u_s become quantities of $\mathcal{O}(1)$, provided that u_s has dropped sufficiently. Then the logarithmic law of the wall is superseded by the half-power behavior of u, well known from a boundary layer on the verge of separation, as the viscous wall layer coincides with the flow regime on top of it (see the outline in Sec. II.B.2), and the relationship (135) ceases to be valid. Because the flow inside the viscous wall layer then plays a fundamental role in order to predict the surface friction, a study of the time-dependent motions in that region is presumably necessary. The basis for such a research is provided by the extensive work of Walker et al. [14], Walker and Herzog [15], and Brinckman and Walker [16] (see also [1]), which, however, applies to a firmly attached turbulent boundary layer.

With respect to those aspects, which are presently under investigation, we add that results obtained by means of direct numerical simulation (DNS) [45] indicate that small changes in the

pressure distribution due to an external flow that triggers the occurrence of a mild separation bubble have a relatively great impact on the skin friction distribution. Here, we stress that this observation is corroborated by the theory presented, as the slip velocity is related to the skin friction through Eq. (135). A qualitative comparison of the theory outlined here with the DNS study of marginal separation by Na and Moin [46], as well as the large-eddy simulation by Cabot [47], for the identical flow configuration is also a topic of current research. Unfortunately, a validation of the theoretical results with experimental data, although highly desirable, appears to be presently impossible on the basis of the existing material.

Acknowledgments

This work was supported by the Austrian Science Fund (FWF) under grant no. P16555-N12. Also, the authors would like to thank the referees for several helpful suggestions and advice that aided to enhance the quality of the paper. The authors also wish to acknowledge David Walker for his outstanding work on turbulent boundary layers (see also [48]).

References

[1] Walker, J. D. A., "Turbulent Boundary Layers 2: Further Developments," *Recent Advances in Boundary Layer Theory*, edited by A. Kluwick, Vol. 390, CISM Courses and Lectures, Springer, New York, 1998, pp. 145–230.

[2] Degani, A. T., Smith, F. T., and Walker, J. D. A., "The Structure of a Three-Dimensional Turbulent Boundary Layer," *Journal of Fluid Mechanics*, Vol. 250, 1993, pp. 43–68.

[3] Degani, A. T., Smith, F. T., and Walker, J. D. A., "The Three-Dimensional Turbulent Boundary Layer Near a Plane of Symmetry," *Journal of Fluid Mechanics*, Vol. 234, 1992, pp. 329–360.

[4] Yajnik, K. S., "Asymptotic Theory of Turbulent Shear Flows," *Journal of Fluid Mechanics*, Vol. 42, No. 2, 1970, pp. 411–427.

[5] Bush, W. B., and Fendell, F. E., "Asymptotic Analysis of Turbulent Channel and Boundary-Layer Flow," *Journal of Fluid Mechanics*, Vol. 56, No. 4, 1972, pp. 657–681.

[6] Fendell, F. E., "Singular Perturbation and Turbulent Shear Flow Near Walls," *Journal of the Astronautical Sciences*, Vol. 20, No. 11, 1972, pp. 129–165.

[7] Mellor, G. L., "The Large Reynolds Number, Asymptotic Theory of Turbulent Boundary Layers," *International Journal of Engineering Science*, Vol. 10, No. 10, 1972, pp. 851–873.

[8] Schlichting, H., and Gersten, K., *Boundary-Layer Theory*, 8th ed., Springer, Berlin, 2000.

[9] Gersten, K., "Turbulent Boundary Layers 1: Fundamentals," *Recent Advances in Boundary Layer Theory*, edited by A. Kluwick, Vol. 390, CISM Courses and Lectures, Springer, Vienna, 1998, pp. 107–144.

[10] Scheichl, B. F., Asymptotic Theory of Marginal Turbulent Separation, Ph.D. Thesis, Vienna Univ.of Technology, Vienna, Austria, June 2001.

[11] Scheichl, B., and Kluwick, A., "On Turbulent Marginal Separation: How the Logarithmic Law of the Wall is Superseded by the Half-Power Law," *Proceedings of the International Conference on Boundary and Interior Layers (BAIL 2006)*, edited by G. Lube and G. Rapin, [CD-ROM], Georg-August Univ. of Göttingen, Göttingen, Germany, 2006; also available at http://www.num.math.uni-goettingen.de/bail/.

[12] Scheichl, B., and Kluwick, A., "Turbulent Marginal Separation: A Novel Triple-Deck Problem for Turbulent Flows," *Progress in Turbulence 2*, edited by J. Peinke, A. Kittel, S. Barth, and M. Oberlack, Proceedings in Physics, Springer, Berlin (to be published).

[13] Nagib, H. M., and Chauhan, K. A., "Scaling of High Reynolds Number Turbulent Boundary Layers Revisited," AIAA Paper 2005-4810, 2005.

[14] Walker, J. D. A., Abbott, D. E., Scharnhorst, R. K., and Weigand, G. G., "Wall-Layer Model for the Velocity Profile in Turbulent Flows," *AIAA Journal*, Vol. 27, No. 2, 1989, pp. 140–149.

[15] Walker, J. D. A., and Herzog, S., "Eruption Mechanisms for Turbulent Flows Near Walls," *Transport Phenomena in Turbulent Flows: Theory, Experiment, and Numerical Simulation*, edited by M. Hirata and N. Kasagi, Hemisphere, New York, 1988, pp. 145–156.

[16] Brinckman, K. W., and Walker, J. D. A., "Instability in a Viscous Flow Driven by Streamwise Vortices," *Journal of Fluid Mechanics*, Vol. 432, 2001, pp. 127–166.

[17] Smith, C. R., and Walker, J. D. A., "Chapter 6: Turbulent Wall-Layer Vortices," *Fluid Vortices*, edited by S. I. Green, Vol. 30, of Fluid Mechanics and its Applications, Kluwer Academic, Dordrecht, 1995, pp. 135–290.

[18] Ruban, A. I., "Singular Solutions of the Boundary Layer Equations Which Can Be Extended Continuously Through the Point of Zero Surface Friction," *Fluid Dynamics*, Vol. 16, No. 6, 1981, pp. 835–843 [English]; also *Izvestiya Akademii Nauk SSSR, Mekhanika Zhidkosti i Gaza*, No. 6, 1981, pp. 42–52 [Russian].

[19] Ruban, A. I., "Asymptotic Theory of Short Separation Regions on the Leading Edge of a Slender Airfoil," *Fluid Dynamics*, Vol. 17, No. 1, 1982, pp. 33–41 [English]; also *Izvestiya Akademii Nauk SSSR, Mekhanika Zhidkosti i Gaza*, No. 1, 1982, pp. 42–51 [Russian].

[20] Stewartson, K., Smith, F. T., and Kaups, K., "Marginal Separation," *Studies in Applied Mathematics*, Vol. 67, No. 1, 1982, pp. 45–61.

[21] Sychev, V. V., Ruban, A. I., Sychev, V. V., and Korolev, G. L., *Asymptotic Theory of Separated Flows*, Cambridge Univ. Press, Cambridge, England, U.K., 1998.

[22] Scheichl, B., and Kluwick, A., "Singular Solutions of the Turbulent Boundary Layer Equations in the Case of Marginal Separation as $Re \to \infty$," *Advances in Turbulence 9: Proceedings of the Ninth European Turbulence Conference*, edited by I. P. Castro, P. E. Hancock, and T. G. Thomas, International Center for Numerical Methods in Engineering (CIMNE), Barcelona, 2002, pp. 829–832.

[23] Neish, A., and Smith, F. T., "On Turbulent Separation in the Flow Past a Bluff Body," *Journal of Fluid Mechanics*, Vol. 241, 1992, pp. 443–467.

[24] Melnik, R. E., "A New Asymptotic Theory of Turbulent Boundary Layers and the Turbulent Goldstein Problem," *Boundary-Layer Separation. Proceedings of the IUTAM Symposium*, edited by F. T. Smith and S. N. Brown, Springer, New York, 1987, pp. 217–234.

[25] Melnik, R. E., "An Asymptotic Theory of Turbulent Separation," *Computers & Fluids*, Vol. 17, No. 1, 1989, pp. 165–184.

[26] Michel, R., Quémard, C., and Durant, R., "Hypothesis on the Mixing Length and Application to the Calculation of the Turbulent Boundary Layers," *Computations of Turbulent Boundary Layers: 1968 AFOSR-IFP-Stanford Conference Proceedings*, edited by S. J. Kline, M. V. Morkovin, G. Sovran, and D. J. Cockrell, Vol. 1, Stanford Univ., Stanford, CA, 1969, pp. 195–207.

[27] Clauser, F. H., "The Turbulent Boundary Layer," *Advances in Applied Mechanics*, edited by H. Dryden and T. von Kármán, Vol. 4, Academic, New York, 1956, pp. 1–51.

[28] Goldstein, S., "On Laminar Boundary Layer Flow Near a Position of Separation," *Quarterly Journal of Mechanics and Applied Mathematics*, Vol. 1, No. 1, 1948, pp. 43–69.

[29] Stewartson, K., "Is the Singularity at Separation Removable?," *Journal of Fluid Mechanics*, Vol. 44, No. 2, 1970, pp. 347–364.

[30] Schneider, W., "Boundary-Layer Theory of Free Turbulent Shear Flows," *Zeitschrift für Flugwissenschaften und Weltraumforschung (Journal of Flight Sciences and Space Research)*, Vol. 15, No. 3, 1991, pp. 143–158.

[31] Klebanoff, P. B., "Characteristics of Turbulence in a Boundary Layer with Zero Pressure Gradient," NACA TR 1247, 1955; also NACA TN 3178, 1954.

[32] Skåre, P. E., and Krogstadt, Å. -P., "A Turbulent Equilibrium Boundary Layer Near Separation," *Journal of Fluid Mechanics*, Vol. 272, 1994, pp. 319–348.

[33] Rothmayer, A. P., and Smith, F. T., "High Reynolds Number Asymptotic Theories," *The Handbook of Fluid Dynamics*, Part 3, edited by R. W. Johnson, CRC Press, Boca Raton, FL, and Springer, Heidelberg, Germany, 1998, pp. 23.1–25.26.

[34] Messiter, A. F., "Boundary-Layer Flow Near the Trailing Edge of a Flat Plate," *SIAM Journal on Applied Mathematics*, Vol. 18, No. 1, 1970, pp. 241–257.

[35] Stewartson, K., "On the Flow Near the Trailing Edge of a Flat Plate II," *Mathematika*, Vol. 16, No. 1, 1969, pp. 106–121.

[36] Abramowitz, M., and Stegun, I. A., *Handbook of Mathematical Functions*, 9th ed., Dover, New York, 1972.

[37] Lipatov, I. I., "On the Theory of Separation of a Laminar Boundary Layer in a Supersonic Flow," *Fluid Dynamics*, Vol. 19, No. 4, 1984, pp. 555–560 [English]; also *Izvestiya Akademii Nauk SSSR, Mekhanika Zhidkosti i Gaza*, No. 4, 1984, pp. 51–56 [Russian].

[38] Smith, F. T., and Merkin, J. H., "Triple-Deck Solutions for Subsonic Flows Past Humps, Steps, Concave or Convex Corners and Wedged Trailing Edges," *Computers & Fluids*, Vol. 10, No. 1, 1982, pp. 7–25.

[39] Cassel, K. W., Ruban, A. I., and Walker, J. D. A., "An Instability in Supersonic Boundary-Layer Flow Over a Compression Ramp," *Journal of Fluid Mechanics*, Vol. 300, 1995, pp. 265–285.

[40] Gajjar, J. S. B., and Türkyılmazoğlu, M., "On the Absolute Instability of the Triple-Deck Flow Over Humps and Near Wedged Trailing Edges," *Philosophical Transactions of the Royal Society of London*, Series A: Mathematical, Physical and Engineering Sciences, Vol. 358, No. 1777, 2000, pp. 3113–3128.

[41] Powell, M. J. D., "A Hybrid Method for Nonlinear Algebraic Equations," *Numerical Methods for Nonlinear Algebraic Equations*, edited by P. Rabinowitz, Gordon and Breach, London, 1970, Chap. 6, pp. 87–114.

[42] Perry, A. E., and Fairlie, B. D., "A Study of Turbulent Boundary-Layer Separation," *Journal of Fluid Mechanics*, Vol. 69, No. 4, 1975, pp. 657–672.

[43] Cutler, A. D., and Johnston, J. P., "Adverse Pressure Gradient and Separating Turbulent Boundary Flows: The Effect of Disequilibrium in Initial Conditions," Stanford Univ. Thermosciences Div., Mechanical Engineering Dept., Rept. MD-46, Stanford, CA, 1984.

[44] Briley, W. R., and McDonald, H., "Numerical Prediction of Incompressible Separation Bubbles," *Journal of Fluid Mechanics*, Vol. 69, No. 4, 1975, pp. 631–656.

[45] Skote, M., and Henningson, D. S., "Direct Numerical Simulation of a Separated Turbulent Boundary Layer," *Journal of Fluid Mechanics*, Vol. 471, 2002, pp. 107–136.

[46] Na, Y., and Moin, P., "Direct Numerical Simulation of a Separated Turbulent Boundary Layer," *Journal of Fluid Mechanics*, Vol. 374, 1998, pp. 379–405.

[47] Cabot, W., "Large-Eddy Simulation of a Separated Boundary Layer," *Annual Research Briefs - 1998 (Center for Turbulence Research)*, NASA Ames Research Center and Stanford Univ., Stanford, CA, 1998, pp. 279–287.

[48] Scheichl, B., and Kluwick, A., "Turbulent Marginal Separation and the Turbulent Goldstein Problem," AIAA Paper 2005-4936, 2005.

A. Tumin
Associate Editor

*4.6 IJCSM, **1** (2007), 2/3/4, 343–359*

Int. J. Computing Science and Mathematics, Vol. 1, Nos. 2/3/4, 2007 343

On turbulent marginal boundary layer separation: how the half-power law supersedes the logarithmic law of the wall

B. Scheichl* and A. Kluwick

Institute of Fluid Mechanics and Heat Transfer,
Vienna University of Technology,
Resselgasse 3/E322, A-1040 Vienna, Austria
E-mail: bernhard.scheichl@tuwien.ac.at
E-mail: alfred.kluwick@tuwien.ac.at
*Corresponding author

Abstract: As the authors have demonstrated recently, application of the method of matched asymptotic expansions allows for a self-consistent description of a Turbulent Boundary Layer (TBL) under the action of an adverse pressure gradient, where the latter is controlled such that it may undergo marginal separation. In that new theory, the basic limit process considered is provided by the experimentally observed slenderness of a turbulent shear layer, hence giving rise to an intrinsic perturbation parameter, say α, aside from the sufficiently high global Reynolds number *Re*. Physically motivated reasoning, supported by experimental evidence and the existing turbulence closures, then strongly suggests that α is indeed independent of *Re* as $Re \to \infty$. Here, we show how the inclusion of effects due to high but finite values of *Re* clarifies a long-standing important question in hydrodynamics, namely, the gradual transformation of the asymptotic behaviour of the so-called wall functions, which characterises the flow in the overlap regime of its fully turbulent part and the viscous sublayer (and, consequently, its scaling in the whole shear layer), as separation is approached.

Keywords: interacting boundary layers; marginal separation; matched asymptotic expansions; triple-deck theory; turbulence; turbulent shear flows; wall functions.

Reference to this paper should be made as follows: Scheichl, B. and Kluwick, A. (2007) 'On turbulent marginal boundary layer separation: how the half-power law supersedes the logarithmic law of the wall', *Int. J. Computing Science and Mathematics*, Vol. 1, Nos. 2/3/4, pp.343–359.

Biographical notes: Bernhard Scheichl holds a Postdoc position at the Institute of Fluid Mechanics and Heat Transfer at the Vienna University of Technology, Vienna, Austria. He completed his PhD under the supervision of A. Kluwick from that University in 2001. Since 1997, he has been researching in the asymptotic theory of turbulent shear flows.

Alfred Kluwick holds a Full Professor position at the same Institute. His long-standing research interests include, amongst others, the asymptotic description of high-Reynolds-number flows, with particular emphasis on interacting boundary layers.

Copyright © 2007 Inderscience Enterprises Ltd.

1 Introduction and motivation

A novel rational theory of the incompressible nominally steady and two-dimensional Turbulent Boundary Layer (TBL) exposed to an adverse pressure gradient, which is impressed by the prescribed external potential bulk flow, has been developed recently by the authors, see Scheichl and Kluwick (2007A), for the sake of brevity, in the following referred to as SK07A. This asymptotic flow description exploits the Reynolds-averaged Navier–Stokes equations by taking the limit

$$Re = \tilde{U}\tilde{L}/\tilde{\nu} \to \infty \tag{1}$$

where the Reynolds number *Re* is formed by the global length and velocity scales $\tilde{L}$ and $\tilde{U}$, respectively, which are characteristic for the external inviscid and irrotational bulk flow, as well as the (constant) kinematic viscosity $\tilde{\nu}$. As the most important preliminary result of the approach presented by SK07A, in the limit equation (1), the slenderness of the boundary layer is seen to be independent of *Re* in the formal limit $Re^{-1} = 0$. The rationale underlying this essential property can be cast in the following:

> ***Hypothesis (A):*** *Let all velocities be non-dimensional with the global reference value* $\tilde{U}$. *Furthermore, assume that in the limit equation (1), there exists a small non-dimensional local turbulent velocity scale* U_t *such that the vortical time-mean velocity variations are of* $O(U_t)$. *Then (and only then) all components of the non-dimensional Reynolds stress tensor are quantities of* $O(U_t^2)$.

That is, the time-mean flow is presumed to be governed locally by a single velocity scale if the latter is sufficiently small when compared with the free-stream velocity. Although this supposition is strongly suggested by physical intuition (and corroborated by an asymptotic analysis of any commonly used turbulence closures, see Scheichl and Kluwick (2007A) and Scheichl (2001), and the asymptotic analysis of closures given in Schlichting and Gersten (2000), for example), however, a rigorous justification will have to be based on an adequate investigation of the unsteady Navier–Stokes equations in the limit expressed by equation (1) – a challenging problem the authors intend to tackle yet. As a matter of course, the thereby expected affirmation of the Hypothesis (A) must be regarded to be of fundamental impact on an asymptotic theory of turbulence.

The so-called classical theory, see for instance the pioneering paper by Mellor (1972), is capable of describing a strictly attached TBL only as it relies on the assumption of an asymptotically small streamwise velocity defect with respect to the external flow in the fully turbulent main part of the TBL. As is demonstrated by Scheichl and Kluwick (2007B) (in the following abbreviated by SK07B), it can be derived solely by adopting Hypothesis (A) as the simplest example for an asymptotic description of a TBL, if in the main region U_t is identified with the skin-friction velocity u_τ where u_τ^2 denotes the (non-dimensional) wall shear stress, in the following termed τ_w. Moreover, it has also been elucidated by SK07B that the method of matched (composite) asymptotic expansions allows for an extension of the classical approach, which is capable of predicting flows having a velocity defect of $O(U_t)$ where U_t is still considered to be small but does not necessarily depend on *Re*. In a final step, by taking a streamwise velocity deficit of $O(1)$, which is a necessary characteristic of flows that may even undergo marginal separation, no asymptotically small turbulent velocity scale representative of the

outer main flow region is present there. The reason is that the convective terms and, thus, the balanced Reynolds shear stress gradient normal to the surface in the streamwise momentum equation must be quantities of $O(1)$ in this flow region. However, in order to maintain a shear layer approximation then, the (non-dimensional) Reynolds shear stress and the (non-dimensional) boundary layer thickness must be of comparable magnitude. Therefore, the Reynolds stresses are seen to be governed by a novel turbulent velocity scale, which is small when compared with the streamwise velocity of $O(1)$. One then faces the remarkable consequence of Hypothesis (A), namely, that both the Reynolds shear stress and the slenderness of the boundary layer must be measured by an additional small parameter, in the following denoted by α, which is essentially independent of *Re* as $Re \to \infty$ and, in the current stage of development, to be determined experimentally. Note that the aforementioned reference velocity of the Reynolds stresses then is of $O(\alpha^{1/2})$. In the formal limit

$$\alpha \to 0, \quad Re^{-1} = 0 \tag{2}$$

then to be considered, the Reynolds shear stress must vanish at the surface. For large but finite values of *Re*, on the other hand, in an initially firmly attached TBL the shear stress in the flow region that is located on top of the viscous wall layer adjacent to the surface assumes the value of τ_w in the overlap with that wall layer in leading order, in agreement with Hypothesis (A) as outlined by Scheichl (2001) and Scheichl and Kluwick (2007B), respectively. Therefore, in the former region, in the so-called intermediate layer, U_t is set equal to u_τ and, in turn, seen to be of $O(1/\ln Re)$. The balance between convection, which is of $O(1)$ there and due to the surface slip velocity impressed by the outer main layer, and the Reynolds shear stress gradient requires the thickness of that intermediate layer to be of $O(U_t^2)$. But then, the two-parameter expansion subject to equation (2) does not allow for a match of the velocity gradient normal to the surface with that holding in the outer main region having a thickness of $O(\alpha)$, cf. SK07A. As a consequence, at the base of the latter, a further layer has to be introduced, the scaling of which is also seen to be independent of *Re*. That is, in the limit equation (2), the boundary layer comprises two layers, a so-called outer and inner wake layer and, remarkably, is seen to closely resemble a turbulent free shear layer, which was investigated asymptotically by Schneider (1991).

The description of the outer main layer has been addressed by SK07A. Most important, it is demonstrated there analytically and numerically by adopting a local viscous/inviscid interaction strategy that in the primary limit, given by equation (2), marginal separation is associated with the occurrence of closed reverse-flow regions where the surface slip velocity, which turns out to be a quantity of $O(1)$ in general, assumes negative values along a streamwise distance of $O(\alpha^{3/5})$. By taking into account the inner wake layer also, it is the objective of this paper to demonstrate how the two near-wall flow regions emerging for high but finite values of *Re* then singularly perturb the two-tiered wake flow referring to the limit expressed by equation (2). Particular emphasis is placed on the rather drastic variation of the universal flow behaviour in the overlap region conjoining the viscous wall and the intermediate layer close to the locations of, respectively, separation and reattachment.

We emphasise that the basic principle underlying the present investigation is to deduce as much information about the turbulent flow as possible from the

Reynolds-averaged equations of motion, but independently of the choice of a specific turbulence closure. Within the framework of asymptotic analysis, this is achieved by deriving a fully self-consistent flow description, essentially based on the Hypothesis (A). However, as will turn out in the course of development, the matching principle requires some further weak assumptions regarding the behaviour of the Reynolds shear stress in the overlap domains of the respective layers.

2 Weakly interacting flow for $Re^{-1} = 0$

2.1 Problem formulation

We consider a nominally steady and two-dimensional fully developed TBL, which is driven by the prescribed incompressible and non-turbulent free-stream flow along a smooth and impermeable solid surface, being e.g., part of a diffuser duct. Let x, y, u, v, u', v', and p denote natural coordinates, respectively, along and perpendicular to the surface under consideration given by $y = 0$, the time-mean velocity components in x- and y-direction, the corresponding turbulent velocity fluctuations, and the time-mean fluid pressure. These quantities are non-dimensional with the reference values $\tilde{L}$ and $\tilde{U}$, respectively, introduced above, see equation (1), and the uniform fluid density. We furthermore define a stream function ψ by

$$\partial\psi/\partial y = u, \quad \partial\psi/\partial x = -hv, \quad h = 1 + k(x)y. \tag{3a}$$

Herein $k(x) = O(1)$ is the accordingly non-dimensional surface curvature of the solid wall, which is defined as positive for a convex surface and assumed to be a quantity of $O(1)$. By adopting the usual notation for the turbulent stresses, the dimensionless time or, equivalently, Reynolds-averaged Navier–Stokes equations then read (cf. Schlichting and Gersten, 2000, p.81)

$$\begin{aligned} &h\left(\frac{\partial\psi}{\partial y}\frac{\partial}{\partial x} - \frac{\partial\psi}{\partial x}\frac{\partial}{\partial y}\right)\frac{\partial\psi}{\partial y} - k\frac{\partial\psi}{\partial x}\frac{\partial\psi}{\partial y} = \\ &\quad -h\frac{\partial p}{\partial x} - h\frac{\partial\left\langle u'^2\right\rangle}{\partial x} - \frac{\partial h^2\left\langle u'v'\right\rangle}{\partial y} + \frac{h^2}{Re}\frac{\partial\nabla^2\psi}{\partial y}, \end{aligned} \tag{3b}$$

$$\begin{aligned} &\left(\frac{\partial\psi}{\partial x}\frac{\partial}{\partial y} - \frac{\partial\psi}{\partial y}\frac{\partial}{\partial x}\right)\left(\frac{1}{h}\frac{\partial\psi}{\partial x}\right) - k\left(\frac{\partial\psi}{\partial y}\right)^2 \\ &\quad = -h\frac{\partial p}{\partial y} - \frac{\partial h\left\langle v'^2\right\rangle}{\partial y} - \frac{\partial\left\langle u'v'\right\rangle}{\partial x} + k\left\langle u'^2\right\rangle - \frac{1}{Re}\frac{\partial\nabla^2\psi}{\partial x}, \end{aligned} \tag{3c}$$

where $\nabla^2 = h^{-1}[\partial/\partial x(h^{-1}\partial/\partial x) + \partial/\partial y(h\,\partial/\partial y)]$ is the Laplacian. The governing equations (3) are supplemented with the usual no-slip condition holding at the surface, i.e.,

$$\psi = u = u' = v' = 0 \quad \text{at} \quad y = 0. \tag{4}$$

Although the results of the subsequent asymptotic investigation of the basic equations (3), subject to equation (4), are seen to be independent of the surface curvature

$k(x)$, here the equations of motion, equation (3), are quoted in their most general form for the sake of completeness. Note that effects due to the surface curvature play an important role in the higher-order analysis of a TBL layer having an asymptotically small velocity defect; here the reader is referred to SK07B.

Since we exclude the presence of free-stream turbulence, the turbulent flow is essentially confined to the relatively thin boundary layer along the surface. As outlined in Section 1, its thickness is measured by the quantity α, which is regarded as the primary perturbation parameter. For what follows, it is sufficient to represent the relatively distinct time-mean boundary layer edge by the sharp line $y = \delta(x;\alpha,Re) = O(\alpha)$. It is, furthermore, useful to express the Reynolds shear stress $-\langle u'v' \rangle$ by introducing the (positive) mixing length ℓ in the form

$$-\langle u'v' \rangle = \ell^2 \frac{\partial u}{\partial y}\left|\frac{\partial u}{\partial y}\right|. \tag{5}$$

In addition, let $p_e(x;\beta)$, $u_e(x;\beta)$, and $u_s(x;\beta,\alpha)$ denote the pressure and the (streamwise) velocity component *u*, respectively, of the external potential main flow, evaluated at the surface $y = 0$, as well as the slip velocity, which denotes the, as will be seen later, non-vanishing value of *u* at the surface in the limit equation (2). Here, the control parameter $\beta = O(1)$ shall account for systematic variations in the external irrotational flow. For simplicity in the notation, however, the explicit dependences on β will be omitted in the following.

2.2 Outer wake layer

By considering the outer main layer first, inspection of equation (3) then suggests the following expansions there,

$$\begin{aligned} &\{\psi, -\langle u'v' \rangle, \delta\} = \alpha\{\Psi(x,Y), T(x,Y), \Delta(x)\} + O(\alpha^2), \\ &\ell \sim \alpha^{3/2} L(x,Y) + \cdots, \quad p = p_e(x) + O(\alpha). \end{aligned} \tag{6}$$

Herein $Y = y/\alpha$, and the second-order terms represented by the Landau symbols account for, amongst others, the feedback of the induced external flow. In turn, the resulting leading-order shear layer approximation, allowing for a streamwise velocity deficit with respect to the imposed external flow of $O(1)$, reads

$$\begin{aligned} &\frac{\partial \Psi}{\partial Y}\frac{\partial^2 \Psi}{\partial Y \partial x} - \frac{\partial \Psi}{\partial x}\frac{\partial^2 \Psi}{\partial Y^2} = -\frac{\mathrm{d}p_e}{\mathrm{d}x} + \frac{\partial T}{\partial Y}, \\ &-\frac{\mathrm{d}p_e}{\mathrm{d}x} = u_e \frac{\mathrm{d}u_e}{\mathrm{d}x}, \quad T = L^2 \frac{\partial^2 \Psi}{\partial Y^2}\left|\frac{\partial^2 \Psi}{\partial Y^2}\right|. \end{aligned} \tag{7a}$$

These equations are subject to the wake-type boundary conditions

$$\Psi(x,0) = T(x,0) = 0, \tag{7b}$$

$$(\partial \Psi / \partial Y)(x,\Delta(x)) - u_e(x) = T(x,\Delta(x)) = 0. \tag{7c}$$

The first relationships, equation (7b), provide a match of the flow quantities with those in the inner wake region, and equation (7c) expresses the approximate restriction of vortex motion to the boundary layer.

A reasonable physical interpretation of the mathematical need of the inner wake layer (as outlined in Section 3.2) is obtained from a consideration of a certain domain where surface effects play a dominant role and which remains finite even in the limit expressed by equation (2). One may then infer that in the limit considered here, effects on the mixing length, which arise from the presence of the wall, are restricted to that inner wake layer. As a finding substantiated by an asymptotic analysis of any commonly employed mixing length closures, for an elaborate discussion of those we refer to, e.g., Schlichting and Gersten (2000), this basic idea implies that the rescaled mixing length L exhibits a finite value at the base of the outer main layer, say,

$$L(x,0) = L_0(x) = O(1), \tag{8}$$

see SK07A. Most important, there it is also demonstrated numerically by adopting a specific closure for the Reynolds shear stress T satisfying the requirement equation (8) and an (adverse) pressure distribution $p_e(x)$, that the boundary layer problem equation (7) indeed admits a 'rotational' solution, i.e., one having $\partial^2\Psi/\partial Y^2 \not\equiv 0$ and $T \not\equiv 0$, in addition to the 'trivial', i.e., irrotational Eulerian, one given by $\partial\Psi/\partial Y - u_e(x) \equiv 0, T \equiv 0$ (and then for arbitrary distributions $\Delta(x)$). Then, the associated streamwise velocity defect of $O(1)$ is conveniently measured by the slip velocity U_s and the related quantity λ,

$$U_s(x) = \frac{\partial\Psi}{\partial Y}(x, Y=0), \quad \lambda(x) = U_s\frac{\mathrm{d}U_s}{\mathrm{d}x} - u_e\frac{\mathrm{d}u_e}{\mathrm{d}x} > 0. \tag{9}$$

Note that for $U_s > 0$ and a given adverse pressure gradient, i.e., for $\mathrm{d}u_e/\mathrm{d}x < 0$, the numerical solutions of the boundary layer problem equation (7), presented in SK07A, show that the flow is retarded even at the base of the main layer. That is, in general also $\mathrm{d}U_s/\mathrm{d}x < 0$ hold, whereas λ is found to be positive throughout. Furthermore, from equation (7), one obtains the following asymptotes for $Y \to 0$,

$$\Psi \sim U_s Y + \frac{4}{15}\frac{\lambda^{1/2}}{L_0}Y^{5/2} + \cdots, \quad T = \lambda Y + O(Y^4). \tag{10}$$

2.3 Inner wake layer

As a consequence of equations (6), (8) and (10), the inner wake region has a thickness of $O(\alpha^{3/2})$ and is described by the inner expansions

$$\begin{aligned} &\psi \sim \alpha^{3/2}U_s(x)\overline{Y} + \alpha^{9/4}\overline{\Psi}(x,\overline{Y}) + \cdots, \quad -\left\langle u'v'\right\rangle \sim \alpha^{3/2}\overline{T}(x,\overline{Y}) + \cdots, \\ &\ell \sim \alpha^{3/2}\overline{L}(x,\overline{Y}) + \cdots, \quad p = p_e(x) + O(\alpha), \end{aligned} \tag{11}$$

where $\overline{Y} = Y/\alpha^{1/2} = y/\alpha^{3/2}$. That is, the inner layer exhibits a streamwise velocity defect of $O(\alpha^{3/4})$ with respect to the slip velocity U_s, such that U_t is of $O(\alpha^{3/4})$. To leading order, there the equations of motion, equation (3), reduce to

$$\lambda\overline{Y} = \overline{T} = \overline{L}^2 \frac{\partial^2\overline{\Psi}}{\partial\overline{Y}^2}\left|\frac{\partial^2\overline{\Psi}}{\partial\overline{Y}^2}\right|. \tag{12a}$$

Here, the first of the, respectively, boundary and matching conditions

$$\overline{T}(x,0) = \overline{\Psi}(x,0) = 0, \tag{12b}$$

$$\partial\overline{\Psi}/\partial\overline{Y} - (2/3)(\lambda^{1/2}/L_0)\overline{Y}^{3/2} \to 0, \quad \overline{Y} \to \infty, \tag{12c}$$

has been taken into account. The relationship equation (12b) avoids the occurrence of an additional term of $O(\alpha^{3/4})$ in the expansion for ψ in equation (6).

If one assumes that $\overline{L} = L_0 + o(\overline{Y}^{-3/2})$ as $\overline{Y} \to \infty$ (which is the case for any known mixing length closure, see Scheichl and Kluwick (2007A), Schlichting and Gersten (2000) and Schneider (1991), for example), the solution of equation (12) for the streamwise velocity may conveniently be written as

$$\frac{\partial\overline{\Psi}}{\partial\overline{Y}} = \frac{2}{3}\frac{\lambda^{1/2}}{L_0}\overline{Y}^{3/2} - \int_Y^\infty (\overline{L}^{-1} - L_0^{-1})(\lambda\overline{Y})^{1/2}\,\mathrm{d}\,\overline{Y}. \tag{13}$$

By considering the Hypothesis (A) in connection with the *Re*-dependent scaling of the intermediate layer, introduced in Section 1, one readily infers from the linear behaviour of $\overline{T}$ given in equation (12a) that the $\overline{Y}$- dependent part of the streamwise velocity component varies with $\overline{Y}^{1/2}$ as $\overline{Y} \to 0$. This so-called 'half-power law', known to hold on top of the viscous wall layer for a TBL on the verge of separation (for a further discussion, see Schlichting and Gersten (2000), for instance) can be expressed as

$$\frac{\partial\overline{\Psi}}{\partial\overline{Y}} \sim \overline{U}_s(x) + 2\frac{(\lambda\overline{Y})^{1/2}}{\chi(x)}, \quad \overline{L} \sim \chi(x)\overline{Y}, \quad \overline{Y} \to 0. \tag{14}$$

The quantity $\chi(x)$ is regarded as part of a specific mixing length closure, and, therefore, has to be determined experimentally. As a result of equations (14) and (13), the aforementioned overall slip velocity u_s then takes on the form

$$u_s \sim U_s(x) + \alpha^{3/4}\overline{U}_s(x) + \cdots, \quad \overline{U}_s = -\int_0^\infty (\overline{L}^{-1} - L_0^{-1})(\lambda\overline{Y})^{1/2}\,\mathrm{d}\,\overline{Y} < 0. \tag{15}$$

It is anticipated in equation (15) that the integral exists. As will be shown in Section 3, this is ensured by the behaviour of $\overline{L}$ for $\overline{Y} \to 0$, which is obtained from a match with the intermediate layer for high but finite values of *Re*. Then there is strong evidence that $0 \le \overline{L} < L_0$ for $0 \le \overline{Y} < \infty$, such that $\overline{U}_s < 0$.

2.4 Marginal separation in the triple-deck limit

Considering laminar high-Reynolds-number flows, the so-called triple-deck theory provides a well-established asymptotic framework for describing the locally strong interaction of the boundary layer with the external potential flow, a situation that in many cases is associated with the occurrence of separation. Generally speaking, the local interaction mechanism accounts for the pressure feedback caused by the displacement action of the boundary layer, which becomes significant close to separation.

For an overview, we refer to, e.g., Sychev et al. (1998). As a noteworthy cornerstone of the new asymptotic formulation of a TBL having a large streamwise velocity deficit, it is shown by SK07A how a novel application of that triple-deck formalism allows for a self-consistent asymptotic description of small closed backflow eddies, located at the base of the outer wake layer: the locally strong interaction due to the displacement effect exerted by the flow in that outermost layer, here denoted as the main deck, with the thereby induced potential flow in the so-called upper deck on top of the former is associated with the occurrence of asymptotically small reverse-flow regions at its base, in the so-called lower deck. As the main ingredient of the interaction mechanism, here the induced pressure gradient comes into play in leading order, causing a shift of the unperturbed streamwise velocity at its outer edge. The role of the main deck then is a passive one, namely, to transfer that shift unchanged to the upper deck. Therefore, this velocity shift acts as the aforementioned locally relevant additional boundary layer displacement.

The analysis presented by SK07A can be subsumed as follows: if the pressure gradient $\mathrm{d}p_e/\mathrm{d}x$ reaches a critical strength, described by a critical value β_c of the control parameter β introduced before, the solution of equation (7) exhibits the so-called marginal-separation singularity at some position, say, $x - x_c$, such that $U_s(x \neq x_c) > 0$ and $U_s(x_c) = 0$. Then, an asymptotically correct treatment of equation (3) in the double limit expressed by equation (2) and $\beta \to \beta_c$ requires the appropriate generalisation of the boundary layer approximation equation (7) by taking into account turbulent/irrotational boundary layer interaction at a streamwise distance $\epsilon \propto -1/\ln|\beta - \beta_c|$ upstream of $x = x_c$ and over a small streamwise extent measured by $\sigma \propto (\alpha/\Lambda)^{3/5}$. Here the (positive) coupling parameter Λ characterises the triple-deck limit: it is proportional to $\alpha/\epsilon^{10/3}$ and is kept fixed as $\alpha \to 0$, $\epsilon \to 0$, such that $\sigma = O(\epsilon^2)$. That upstream shift of the interaction region is accounted for by introducing rescaled variables in the form

$$X = (x - x_c + \varepsilon)/\sigma, \quad \hat{Y} = Y/(L_0^{2/3}\sigma^{1/2}). \tag{16a}$$

Then, the lower deck is described in terms of the expansions

$$\begin{aligned} \psi/(L_{00}^{2/3}P_0) &\sim \alpha\sigma^{5/6}\hat{\Psi}(X,\hat{Y}) + \cdots, \\ -\langle u'v'\rangle/(L_{00}^{2/3}P_0) &\sim \alpha\sigma^{1/3}(\partial^2\hat{\Psi}/\partial\hat{Y}^2)^2 + \cdots, \\ p &= p_e(x_c) + \sigma P(X;\Lambda) + O(\alpha), \end{aligned} \tag{16b}$$

where

$$L_{00} = L_0(x_c), \quad P_0 = (\mathrm{d}p_e/\mathrm{d}x)(x_c), \quad P(X;\Lambda) = P_0[X + \Lambda\hat{P}(X)]. \tag{16c}$$

The numerical solutions of the resulting elliptic triple-deck problem comprise both the canonical representations $\hat{\Psi}$ and $\hat{P}$ of the stream function and the induced pressure, respectively. Furthermore, the control parameter Λ accounts for the strength of the induced pressure gradient, relative to that of its imposed counterpart, which is locally given by P_0. As seen from equation (16), both externally impressed and the superimposed induced pressure gradient are quantities of $O(1)$ in the triple-deck limit. For a detailed discussion of both the triple-deck problem and the numerical method applied to it, the reader is referred to SK07A. At this stage of the analysis, we only stress that its solution provides the cornerstone of the theory of turbulent marginal separation. The subsequent

investigation deals with the singular perturbation of that basic solution, originating from the sublayers, which represent higher-order contributions to the solution for finite values of both α and *Re* due to the presence of the surface.

By taking into account the inner wake layer at the base of the lower deck, the expansion equation (15) for the slip velocity is locally replaced by

$$u_s = \sigma^{1/2}\hat{U}_s(X) + O(\alpha^{3/4}), \quad \hat{U}_s(X) = \frac{\partial\hat{\Psi}}{\partial\hat{Y}}(X,\hat{Y}=0). \tag{17}$$

Generally speaking, when $u_s = O(\alpha^{3/10})$ or even smaller, the analysis of that flow region expressed by equations (9)–(15) remains valid if therein the formal substitutions

$$\begin{aligned} &U_s \mapsto \alpha^{1/2}\hat{U}_s, \quad \lambda \mapsto \hat{U}_s \mathrm{d}\hat{U}_s / \mathrm{d}X + P_0 > 0, \\ &p_e(x) \mapsto p_e(x_c) + P(X;\Lambda), \quad x \mapsto x_c \end{aligned} \tag{18}$$

are applied. Both the asymptotic structure of the unperturbed TBL and its local splitting due to the interaction process in the limit equation (2) are sketched in Figure 1. As indicated by equations (17), (15) and (14), a further breakdown of the asymptotic structure is encountered in the case of triple-deck solutions, which exhibit closed reverse-flow regions such that $\hat{U}_s(X)$ changes sign at the positions of flow detachment and reattachment. This situation is of primary interest here, and a representative solution showing this behaviour is plotted in Figure 2, see also Figure 1: sufficiently close to the locations $X = X_D$ and $X = X_R$ of flow detachment and reattachment, i.e., for $u_s = O(\alpha^{3/4})$ a new inner wake region having a correspondingly smaller streamwise extent than the original one, and a sublayer closer to the wall where $y = O(u_s^2)$ when $u_s = o(\alpha^{3/4})$, have to be considered. However, as the inner wake layer analysis remains essentially unaltered there, that new layer is disregarded here.

Figure 1 Weakly interacting wake-type flow: separation bubble in lower deck indicated by detaching streamline; for the emergence of the local sub-splitting (for $|X| \to \infty$) see SK07A

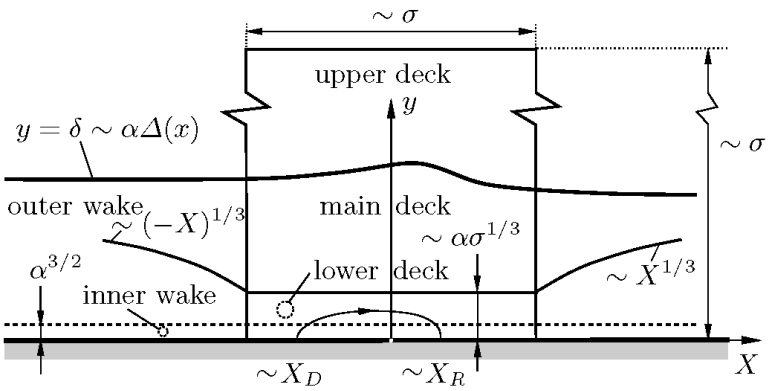

Figure 2 Typical values of the slip velocity $\hat{U}_s(X)$ and the induced pressure $\hat{P}(X)$, being part of a numerical solution of the fundamental interaction problem for Λ = 3 see SK07A

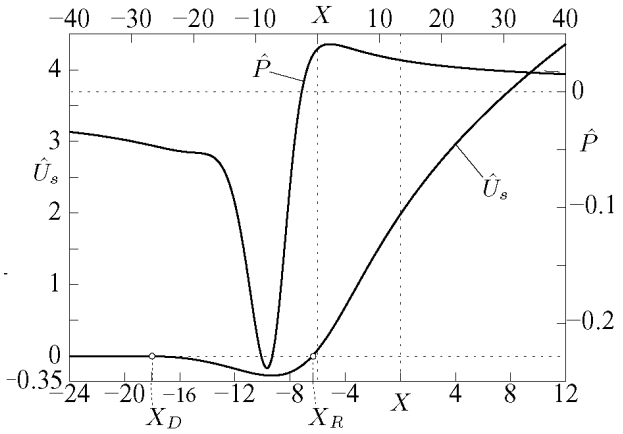

3 The near-wall flow for $1 \gg Re^{-1} > 0$

The analysis of the limit equation (2) outlined above serves as the starting point for the subsequent discussion of both the intermediate layer and the viscous wall region, which completes the flow description for large but finite values of *Re*. For unidirectional flow, i.e., sufficiently far from separation and reattachment (as will be outlined more comprehensively in Sections 3.1 and 3.2), the thereby singularly perturbed solution governing the flow in the wake layers leads to the four-tiered general TBL structure as depicted in Figure 3. As has already been stated in Section 1, and in agreement with Hypothesis (A), in both layers the skin-friction velocity

$$u_\tau = |\tau_w|^{1/2}, \quad \tau_w = Re^{-1}\partial u/\partial y \ \text{ at } \ y = 0, \tag{19}$$

serves as the appropriate velocity scale. We first briefly recall the essential properties of the viscous region close to the wall, which accounts for the no-slip condition expressed by equation (4) and where the Reynolds stresses (and their gradients with respect to y) are of the same magnitude as the viscous shear stress (and its gradient with respect to y). A more comprehensive investigation of this flow region is provided by Mellor (1972) and Scheichl and Kluwick (2007B). Let us also note a remarkable consequence of the Hypothesis (A) revealed by the subsequent analysis, namely, that in the limit equation (1) the time-mean vorticity asymptotically given by $\partial u/\partial y$, is found to be independent of *Re* outside of the viscous wall layer.

We furthermore stress that the analysis presented in Sections 3.1–3.3 also remains valid in the triple-deck limit if the replacements equation (18) are taken into account, apart from the last relationship: the x- dependences of the flow quantities in the viscous sublayer (Section 3.1) then have to be replaced by dependences on *X*.

Figure 3 Four-tiered splitting of the TBL

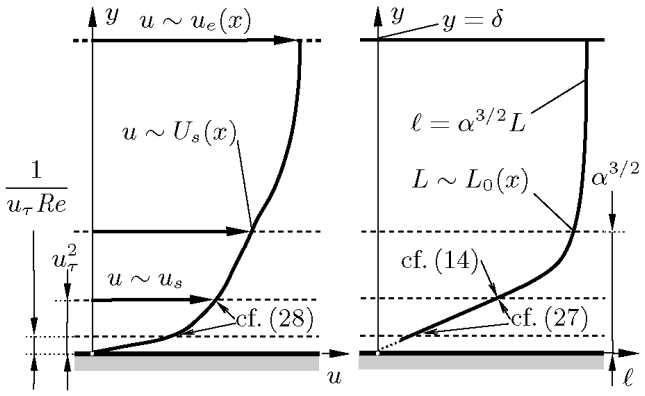

3.1 Viscous wall layer: unidirectional flow

There, we expand in terms of the conventional scalings,

$$\begin{aligned} u / u_\tau &\sim u^+(x, y^+) + \cdots, \\ -\langle u'v' \rangle / u_\tau^2 &\sim \tau^+(x, y^+) + \cdots, \\ p^+ &= (\mathrm{d}p_e / \mathrm{d}x)/(u_\tau^3 Re), \quad y^+ = y u_\tau Re. \end{aligned} \tag{20}$$

In the equations of motion, equation (3), the convective terms then are found to be negligibly small. Hence, they reduce to the balance of viscous and turbulent shear stress and the imposed (and induced) pressure gradient,

$$\partial u^+ / \partial y^+ + \tau^+ \sim \mathrm{sgn}(\tau_w) + p^+ y^+ + \cdots, \quad Re \to \infty. \tag{21}$$

Note that $\partial u^+ / \partial y^+ \to 0$ as $y^+ \to \infty$. Sufficiently far from separation (and also reattachment), the overall slip velocity u_s is a quantity of $O(1)$. Thus, in the intermediate layer, the convective terms are linearised about $u \sim u_s$, and the Reynolds shear stress gradient approximately balances the sum of convection and the pressure gradient as expressed by the definition given in equation (9) of the quantity λ, which enters also equations (10) and (18), such that the intermediate region has a thickness of $O(u_\tau^2)$. Consequently, in the limit $y^+ \to \infty$, the linear rise of τ^+ with respect to y^+ due to the imposed pressure gradient, expressed by p^+, is seen to be cancelled out by the convective terms of higher order, see equation (21). Also, in the case of attached flow considered here, the wall shear stress predominates over the pressure term in equation (21) (otherwise, as discussed in Section 3.3, matching of the streamwise velocity is seen to be incompatible with the assumption of a small velocity defect with respect to $u = U_s(x)$ in the intermediate layer, as anticipated by the expansion given in equation (15)).

As a result, the shear stress in the intermediate layer assumes the value of the wall shear stress τ_w in the overlap region with the wall layer to leading order. This a posteriori justifies the choice of the velocity scale u_τ. Finally, matching of the quantity $y \partial u / \partial y$ then yields the well-established logarithmic law of the wall in its most general form,

$$u^+ \sim [1/A^+(x)] \ln y^+ + B^+(x), \quad y^+ \to \infty. \tag{22}$$

Herein $A^+(x)$ and $B^+(x)$ are empirical functions, and the definition equation (19) of u_τ requires $\mathrm{sgn}(A^+) = \mathrm{sgn}(\tau_w)$. For $\tau_w > 0$, which characterises attached flows, and a perfectly smooth wall A^+ is the celebrated Kármán constant, which is presently taken to be $\kappa \approx 0.384$ and $B^+ \approx 4.1$; these recent values are reported in the experimental study by Österlund et al. (2000). Note that for (mildly) separated flows having $\tau_w < 0$, an asymptotic behaviour akin to equation (22) was already proposed by Simpson (1983) on semi-empirical grounds, together with explicit relationships for the streamwise variations of A^+ and B^+, respectively.

Furthermore, the streamwise velocity components u in the intermediate and the wall layer match provided that the reduced skin-friction velocity defined by $\gamma_s = u_\tau/u_s$ satisfies

$$\gamma_s(x;\varepsilon) \sim A^+(x)/\ln(u_\tau^3 Re)[1 + O(\varepsilon)], \quad \varepsilon = 1/\ln Re, \tag{23}$$

cf. Scheichl (2001). Here, we note that $\mathrm{sgn}(\gamma_s) = \mathrm{sgn}(\tau_w)$. In equation (23), the higher-order terms, abbreviated by the Landau symbol, are seen to be closure-dependent. Inversion of the surface friction law equation (23) yields its explicit representation

$$\gamma_s / A^+(x) \sim \varepsilon[1 - 3\varepsilon \ln \varepsilon + O(\varepsilon)], \quad \mathrm{d}\gamma_s / \mathrm{d}x = O(\varepsilon^2). \tag{24}$$

Then $p^+ = O((\ln Re)^3/Re)$, which suggests one to drop the x-dependence of the leading-order quantities cited in equation (20), at least outside the separated region as indicated by the widely accepted empirical relationships for A^+ and B^+ given above. A more stringent theoretical justification why u^+ and τ^+ may be referred to as 'universal' (as it is commonly the case), i.e., as independent of x, which is even valid for the backflow case $\tau_w < 0$, is provided by the asymptotic model of the unsteady flow in the wall layer put forward by Walker et al. (1989), see also Smith et al. (1991): the presented analysis strongly indicates that the x-dependence (due to pressure disturbances in streamwise direction) of the coherent structure of the time-dependent near-wall flow is asymptotically weak (as it is associated with the random part of the dynamics).

Finally, we remark that by evaluating the vanishing divergence of the fluctuating part of the velocity field, subject to the no-slip condition, given by equation (4), the well-known Taylor expansion for $y^+ \to 0$,

$$u^+ \sim \mathrm{sgn}(\tau_w)\,(y^+ - a^+ y^{+4}), \quad \tau^+ \sim 4\,\mathrm{sgn}(\tau_w)\,a^+ y^{+3}, \tag{25}$$

is extracted from the leading-order balance in equation (20). Note that herein $a^+ \approx 6.1 \times 10^{-4}$ for the case of attached flow, where $\tau_w > 0$, cf. Schlichting and Gersten (2000, p.523).

3.2 Intermediate layer

As pointed out in Section 3.1 and by Scheichl (2001), in the flow region located on top of the viscous wall layer, the governing equations (3) enforce expansions of the form

$$\begin{aligned} u/u_s(x;\alpha) &\sim 1+\gamma_s\hat{u}(x,\zeta)+\cdots, \\ -\langle u'v'\rangle/u_\tau^2 &\sim 1+\lambda(x)\zeta+\cdots, \quad \ell \sim u_\tau^2\hat{l}(x,\zeta)+\cdots, \\ p &= p_e(x)+O(\alpha), \end{aligned} \tag{26}$$

owing to the specific logarithmic match of u provided by equation (22). Herein, the new wall coordinate $\zeta = y/u_\tau^2$ is of $O(1)$. Then

$$\hat{l}\,\partial\hat{u}/\partial\zeta = \sqrt{1+\lambda(x)\zeta}, \quad \zeta\to 0:\ \hat{l}\sim\left|A^+(x)\right|\zeta, \quad \zeta\to\infty:\ \hat{l}\sim\chi(x)\zeta, \tag{27}$$

where the asymptotic behaviour of $\hat{l}$ in equation (27) reflects the relationships presented in equations (22) and (14), respectively. As an important consequence, the match with the ambient layers reveals both the logarithmic as well as the square-root behaviour,

$$\zeta\to 0:\ \hat{u} = \left|A^+(x)\right|^{-1}\ln\zeta + O(1), \quad \zeta\to\infty:\ \hat{u}\sim[2/\chi(x)]\sqrt{\lambda(x)\zeta}. \tag{28}$$

Considering firmly attached flows, it is widely accepted to assume that the empirical function χ, introduced in equation (14), is independent of x and, therefore, equals the v. Kármán constant $\kappa = A^+$. That means the flow is assumed to be 'locally in equilibrium', according to the definition of equilibrium proposed by Townsend (1961). To obtain a closed expression for the velocity variation $\hat{u}(\zeta)$, also for (mildly) separated flows, here we generalise this idea by setting $\hat{l}/\zeta = \chi(x) = \left|A^+(x)\right|$. Then integration of equation (27) gives rise to the so-called extended law of the wall,

$$\chi(x)\hat{u} = \ln\eta - 2\ln\left(\sqrt{1+\eta}+1\right) + 2\sqrt{1+\eta}, \quad \eta = \lambda\zeta, \tag{29a}$$

cf. Townsend (1961), Scheichl (2001) and Scheichl and Kluwick (2007B). Without any loss of generality, the constant of integration in this relationship has been chosen such that a thereby resulting contribution of $O(1)$ to its asymptotic expansion for $\eta\to\infty$ is eliminated, to avoid perturbations of the slip velocity $u_s(x;\alpha)$ arising from finite values of *Re* for the sake of simplicity. In turn,

$$\begin{aligned} &\zeta\to 0:\ \chi(x)\hat{u} = \ln\zeta + \ln(\lambda/4) + 2 + (\lambda\zeta/2) + O(\zeta^2), \\ &\zeta\to\infty:\ \chi(x)\hat{u} = 2(\lambda\zeta)^{1/2} - (\lambda\zeta)^{-1/2} + O(\zeta^{-3/2}). \end{aligned} \tag{29b}$$

Note that the behaviour of u for $\zeta\to\infty$, see equations (28) and (29b), allows for a match with the streamwise velocity component *u* in the inner wake region.

We complete the analysis of the intermediate layer by adding an appealing physical interpretation of the half-power law, see equation (28): since the *y*-dependence of *u* is given by a relationship of the form $u_\tau\hat{u}(y/u_\tau^2)$ in leading order, the function $\hat{u}$ must behave as $\hat{u} = O\left(\sqrt{y/u_\tau^2}\right)$ for $y/u_\tau^2\to\infty$, to account for the Reynolds-number-independent scaling of the inner wake by means of matching the streamwise velocity component. As a result, from a mathematical point of view, the existence of the inner wake layer, characterised by the asymptotic representation of the stream function expressed by equations (11) and (14), turns out to be an immediate consequence of the square-root law, given by equation (28).

3.3 Gradual replacement of the logarithmic law in favour of the half-power law

It is inferred from equations (26) and (24) that the expansion for the skin-friction velocity u_τ given in equation (23) ceases to be valid if $\gamma_s = O(1)$. This situation takes place in the vicinity of the positions where the slip velocity $\hat{U}_s(X)$, which is part of the numerically obtained solution of the triple-deck problem, changes sign, see Figure 2. Stated equivalently, sufficiently close to locations of separation and reattachment, respectively, due to the breakdown of the expansion, see equation (17), mentioned at the end of Section 2.4, both u_s and, as a consequence of equation (24), u_τ are quantities of $O(Re^{-1/3})$. Hence, p^+ entering equation (21) is of $O(1)$, see equation (20). Then the intermediate and the viscous wall layer merge at the base of the inner wake layer, such that the resulting wall region exhibits a thickness of $O(Re^{-2/3})$, see Figure 4. There, the expansions given by equation (20), and the classical wall functions u^+, τ^+ are reformulated by adopting suitably redefined variables in the form

$$\frac{u}{u_p} \sim u^\times(p^\times, y^\times) + \cdots, \quad -\frac{\langle u'v' \rangle}{u_p^2} \sim \tau^\times(p^\times, y^\times) + \cdots,$$
$$p^\times = \mathrm{sgn}(\tau_w)(u_p / u_\tau)^3, \quad u_p = (Re^{-1}\mathrm{d}P/\mathrm{d}X)^{1/3}, \quad y^\times = y u_p Re. \tag{30}$$

Figure 4 Merging of the strongly viscosity-affected near-wall regions as separation or reattachment is approached; here the separating case is shown. The symbols + and × characterise the original wall layer and the merged flow region, respectively, and refer to the superscript in their respective scalings given by equations (20) and (30)

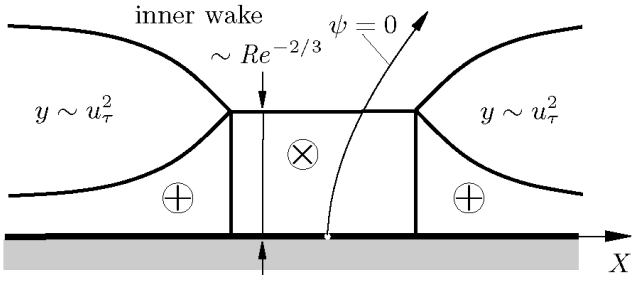

Thus, the merged wall layer is characterised by $y^\times = O(1)$ and the rescaled pressure gradient $p^\times$, which is generally considered to be of $O(1)$. Note that the function $P(X; \Lambda)$ in equation (30) represents the overall pressure variation as defined in equation (16c). According to the leading order, the streamwise momentum balance equation (21) in that region is rewritten as

$$\partial u^\times / \partial y^\times + \tau^\times = \tau_w^\times + y^\times, \quad \tau_w^\times = \mathrm{sgn}(\tau_w)(p^\times)^{-2/3}. \tag{31}$$

Here, the quantity $\tau_w^\times$ denotes the rescaled wall shear stress, which, most important, may change sign (as indicated by the "sgn"-operator). The overall shear stress on the left-hand side of equation (31) varies linearly with respect to $y^\times$ due to the presence of the adverse pressure gradient dP/dX.

Finally, by considering the asymptotic behaviour of the streamwise velocity for large values of $y^{\times}$, which follows from a match with the inner wake layer, one recovers the square-root law, given in equations (14) and (28), such that any logarithmic variation in y is absent now,

$$u^{\times} \sim [2/\chi(x_c)]\sqrt{y^{\times}} + B^{\times}(p^{\times}), \quad y^{\times} \to \infty, \tag{32a}$$

$$B^{\times} \sim u_s / u_p = O(1). \tag{32b}$$

The relationship equation (32a) replaces the logarithmic law, see equation (22), as a consequence of the collapse of the viscous wall and the intermediate layer into the new wall layer. Within the framework of a time-mean flow analysis, the function $B^{\times}(p^{\times})$ has to be determined experimentally. Most important, it represents the asymptotically correct continuation of the skin-friction law, given by equations (23) and (24), into that merged layer, where, as expressed by the possible sign change of $p^{\times}$, flow reversal may take place. Note that expanding equation (23) for $\gamma_s \ln Re \to \infty$ yields the two-term expansion $\gamma_s \ln Re/A^{+} \sim 1 - 3 \ln u_{\tau} / \ln Re$ in the limit $u_{\tau} / \ln Re \to 0$, which expresses the breakdown elucidated at the beginning of Section 3.3. Therefore, by taking into account the scaling given in equation (30), a match of both the skin-friction laws, equations (24) and (32b), which hold for, respectively, $\gamma_s = O(1/\ln Re)$ and $\gamma_s = O(1)$ (including the case $\gamma_s \to \infty$ close to the point of vanishing wall shear stress) requires the one-term asymptote

$$B^{\times} \sim -A^{+} \left|p^{\times}\right|^{-1/3} \ln\left|p^{\times}\right|, \quad \left|p^{\times}\right| \to 0. \tag{33}$$

Also, for $y^{\times} \to 0$, the analogue to equation (25), namely

$$u^{\times} \sim \tau_w^{\times} y^{\times} + y^{\times 2}/2 - a^{\times}(p^{\times})\, y^{\times 4}, \tag{34a}$$

$$\tau^{\times} \sim 4 a^{\times}(p^{\times})\, y^{\times 4}, \tag{34b}$$

is recovered from equation (31). Herein, the function $a^{\times}(p^{\times})$ remains unknown and has to be determined, for example, experimentally. Unfortunately, sufficient experimental data appear not to be available at present. In addition, from equations (34), the position $y = y_s^{\times}$ of the separating streamline $\psi = 0$ close to the surface and near separation and reattachment, respectively, is found to be $y_s^{\times} \sim -3\tau_w^{\times}$ as $\tau_w^{\times} \to 0$_; for a qualitative sketch, see Figure 4.

4 Conclusions and further outlook

In the present paper, a fully self-consistent asymptotic theory of turbulent marginal separation, based on a minimum of physical assumptions regarding the nature of turbulence, is outlined in brief. Herein, the non-dimensional boundary layer slenderness is measured by a small number, denoted by α, which is suggested to remain finite in the limit $Re \to \infty$ and is, therefore, although a fixed figure then, taken as the principal perturbation parameter. As a consequence provided by the shear layer scaling provided by equation (6), α^2 may be regarded as a measure of the turbulent viscosity which,

remarkably, is essentially independent of *Re*. In turn, this finding leads to an asymptotic structure, which is seen to allow for a theoretical explanation of how a TBL is driven towards a marginally separated state by an adverse pressure gradient. Moreover, the resulting two-tiered wake-type TBL flow is perturbed owing to effects of high but finite values of *Re*. The rapid change of the structure of the near-wall flow as the skin-friction changes sign is focussed upon. In particular, it is highlighted how the wall functions u^+ and τ^+ are gradually transformed into their appropriately rescaled counterparts $u^\times$ and $\tau^\times$, respectively, due to a merge of the Reynolds-number-affected near-wall regions close to separation and reattachment. This collapse is due to sufficiently small values of the skin friction τ_w and described in terms of the distinguished limit $\tau_w = O(Re^{-2/3})$. As an important result, the logarithmic variation of u^+ then is superseded by a half-power behaviour of $u^\times$ at the outer edge of the viscous near-wall region.

Open questions concern, amongst others, how to close the skin-friction relationship $B^\times(p^+)$ in equation (32b), subject to the asymptotic behaviour equation (33), where equation (32b) applies to a region of small streamwise extent up- and downstream of the positions of separation and reattachment, respectively, as the slip velocity, u_s, at the base of the wake-type part of the flow is a quantity of $O(Re^{-1/3})$ there. Apart from pure modelling $u^\times(p^\times, y^\times)$, which has to satisfy equations (32a) and (34a), based on a suitably designed experimental investigation of a TBL flow close to zero wall shear stress, a first rational step in this direction is suggested by pursuing the analysis of the time-dependent wall layer dynamics for strictly attached flow by Walker et al. (1989) and Smith et al. (1991). In this connection, we refer to the dependences of A^+ and B^+ on $p^\times$ proposed in Schlichting and Gersten (2000, p.545 ff), which appear to be questionable in the light of the present analysis. We think that the scarceness and the scattering of the data shown there, even for moderate values of $p^\times$, not only reflects inherent difficulties in the measuring procedure but possibly also an incorrect scaling of the anticipated generalised law of the wall, cf. equation (29a), in terms of y^+, which underlies the measurements. On the other hand (and of potential interest for realistic flow simulations employing turbulence closures), once $B^\times(p^+)$ is known, the inversion of this relationship would allow for the calculation of the surface friction τ_w in dependence of the slip velocity u_s, imposed on top of the viscous wall layer, which continues to be asymptotically correct as τ_w changes sign. By considering the rather simple type of algebraic shear stress closures, a first step in this direction is provided by the mixing length model by Granville (1989), which in the present form only applies to attached flow but already takes into account the effect of the pressure term p^+.

Also, the fundamental assumption Hypothesis (A) requires further investigations, both experimentally and theoretically, i.e., on the basis of the unsteady equations of motion.

Acknowledgements

The authors thank the Austrian Science Fund (FWF) for granting this research (FWF Project No. P16555-N12).

References

Granville, P.S. (1989) 'A modified van-driest formula for the mixing length of turbulent boundary layers in pressure gradients', Technical Brief, *J. Fluids Eng. – T. ASME*, Vol. 111, No. 1, March, pp.94–97.

Mellor, G.L. (1972) 'The large Reynolds number, asymptotic theory of turbulent boundary layers', *Int. J. Eng. Sci.*, Vol. 10, No. 10, October, pp.851–873.

Österlund, J.M., Johansson, A.V., Nagib, H.M. and Hites, M. (2000) 'A note on the overlap region in turbulent boundary layers', Letter, *Phys. Fluids*, Vol. 12, No. 1, January, pp.1–4.

Scheichl, B.F. (2001) *Asymptotic Theory of Marginal Turbulent Separation*, Doctoral Thesis, June, Vienna University of Technology, Vienna.

Scheichl, B. and Kluwick, A. (SK07A) (2007A) 'Turbulent marginal separation and the turbulent Goldstein problem', *AIAA J.*, Vol. 45, No. 1, January, pp.20–36.

Scheichl, B. and Kluwick, A. (SK07B) (2007B) 'Non-unique turbulent boundary layer flows having a moderately large velocity defect: a rational extension of the classical asymptotic theory', *Theor. Comput. Fluid Dyn.*, Submitted in revised form (2007)

Schlichting, H. and Gersten, K. (2000) *Boundary-Layer Theory*, 8th ed., Springer-Verlag, Berlin, Heidelberg, New York.

Schneider, W. (1991) 'Boundary-layer theory of free turbulent shear flows', *Z. Flugwiss. Weltraumforsch., J. Flight Sci. Space Res.*, Vol. 15, No. 3, March, pp.143–158.

Simpson, R.L. (1983) 'A model for the backflow mean velocity profile', *AIAA J.*, Technical note, Vol. 21, No. 1, January, pp.142, 143.

Smith, C.R., Walker, J.D.A., Haidari, A.H. and Sobrun, U. (1991) 'On the dynamics of near-wall turbulence', *Phil. Trans. R. Soc. Lond. A*, Turbulent Flow Structure near Walls: Part II, Vol. 336, No. 1641, August, Special Issue, pp.131–175.

Sychev, V.V., Ruban, A.I., Sychev, Vik.V. and Korolev, G.L. (1998) *Asymptotic Theory of Separated Flows*, English ed., Messiter, A.F. and van Dyke, M. (Eds.), Cambridge University Press, Cambridge, UK.

Townsend, A.A. (1961) 'Equilibrium layers and wall turbulence', *J. Fluid Mech.*, Vol. 11, No. 1, pp.97–120.

Walker, J.D.A., Abbott, D.E., Scharnhorst, R.K. and Weigand, G.G. (1989) 'Wall-layer model for the velocity profile in turbulent flows', *AIAA J.*, Vol. 27, No. 2, February, pp.140–149.

Provided for non-commercial research and education use.
Not for reproduction, distribution or commercial use.

4.7 Journal of Fluids and Structures, **24** (2008), 8, 1326–1338

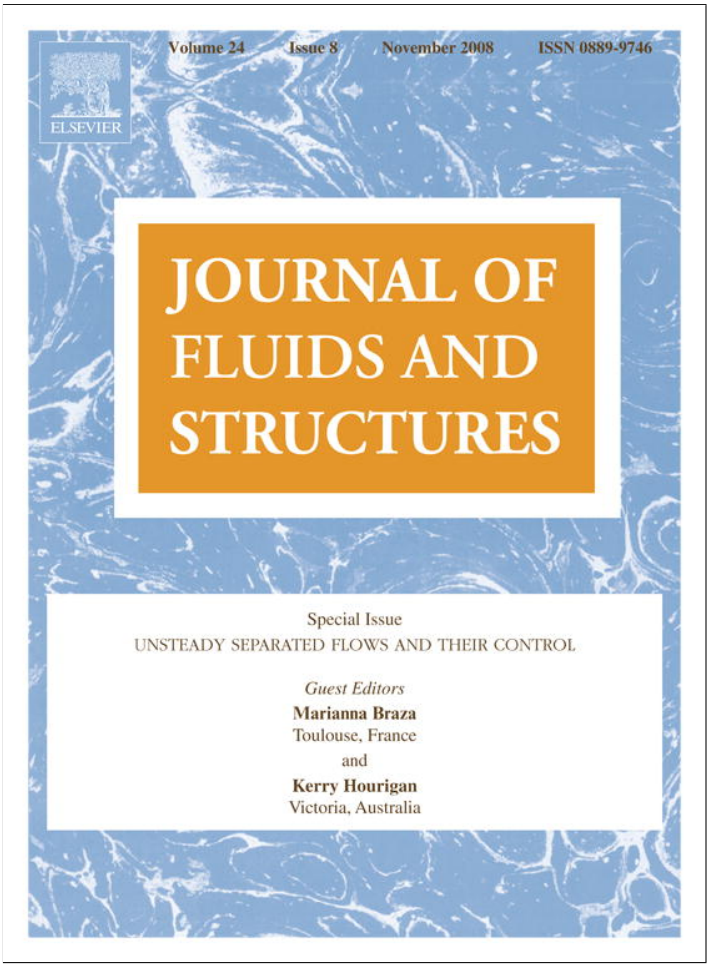

This article appeared in a journal published by Elsevier. The attached copy is furnished to the author for internal non-commercial research and education use, including for instruction at the authors institution and sharing with colleagues.

Other uses, including reproduction and distribution, or selling or licensing copies, or posting to personal, institutional or third party websites are prohibited.

In most cases authors are permitted to post their version of the article (e.g. in Word or Tex form) to their personal website or institutional repository. Authors requiring further information regarding Elsevier's archiving and manuscript policies are encouraged to visit:

http://www.elsevier.com/copyright

Author's personal copy

ELSEVIER

Journal of Fluids and Structures 24 (2008) 1326–1338

JOURNAL OF FLUIDS AND STRUCTURES

www.elsevier.com/locate/jfs

Asymptotic theory of turbulent bluff-body separation: A novel shear layer scaling deduced from an investigation of the unsteady motion

B. Scheichl*, A. Kluwick

Institute of Fluid Mechanics and Heat Transfer, Vienna University of Technology, Resselgasse 3/E322, A-1040 Vienna, Austria

Received 14 January 2008; accepted 15 July 2008
Available online 4 November 2008

Abstract

A rational treatment of time-mean separation of a nominally steady turbulent boundary layer from a smooth surface in the limit $\mathrm{Re} \to \infty$, where Re denotes the globally defined Reynolds number, is presented. As a starting point, it is outlined why the "classical" concept of a small streamwise velocity deficit in the main portion of the oncoming boundary layer does not provide an appropriate basis for constructing an asymptotic theory of separation. Amongst others, the suggestion that the separation points on a two-dimensional blunt body is shifted to the rear stagnation point of the impressed potential bulk flow as $\mathrm{Re} \to \infty$—which is expressed in a previous related study—is found to be incompatible with a self-consistent flow description. In order to achieve such a description, a novel scaling of the flow is introduced, which satisfies the necessary requirements for formulating a self-consistent theory of the separation process that distinctly contrasts former investigations of this problem. As a rather fundamental finding, it is demonstrated how the underlying asymptotic splitting of the time-mean flow can be traced back to a minimum of physical assumptions and, to a remarkably large extent, be derived rigorously from the unsteady equations of motion. Furthermore, first analytical and numerical results displaying some essential properties of the local rotational/irrotational interaction process of the separating shear layer with the external inviscid bulk flow are presented.
© 2008 Elsevier Ltd. All rights reserved.

Keywords: Asymptotics; Coherent motion; Gross separation; Perturbation methods; Turbulent boundary layers; Turbulent shear layers

1. Introduction

The rational description of break-away separation of a statistically steady and two-dimensional incompressible turbulent boundary layer flow past an impermeable rigid and smooth surface in the high-Reynolds-number limit represents a long-standing unsolved hydrodynamical problem. Needless to say that an accurate prediction of the position of separation, in combination with the local behaviour of the skin friction, has great relevance for many

*Corresponding author. Tel.: +43 1 58801 32225; fax: +43 1 58801 32299.
E-mail addresses: bernhard.scheichl@tuwien.ac.at (B. Scheichl), alfred.kluwick@tuwien.ac.at (A. Kluwick).

0889-9746/$ - see front matter © 2008 Elsevier Ltd. All rights reserved.
doi:10.1016/j.jfluidstructs.2008.07.001

Author's personal copy

engineering applications, where e.g. internal flows, like those through diffuser ducts, or flows past airfoils play a crucial role.

1.1. Problem formulation and governing equations

The picture of such flows near separation is sketched in Fig. 1. As a basic assumption, the suitably formed global Reynolds number Re is taken to be asymptotically large:

$$\mathrm{Re} \coloneqq \tilde{U}\tilde{L}/\tilde{\nu} \to \infty, \quad \nu \coloneqq \mathrm{Re}^{-1} \to 0. \tag{1}$$

Herein $\tilde{\nu}$, $\tilde{L}$, and $\tilde{U}$ denote, respectively, the (constant) kinematic viscosity of the fluid, a reference length, typical for the geometry of the portion of the surface under consideration, and a characteristic value of the surface slip velocity impressed by the limiting inviscid stationary and two-dimensional irrotational bulk flow, hereafter formally indicated by $\nu = 0$. All flow quantities are suitably non-dimensionalised with $\tilde{L}$, $\tilde{U}$, and the (uniform) fluid density. Let t, p, $\boldsymbol{x} = (s, n, z)$, and $\boldsymbol{u} = (u, v, w)$ be the time, the fluid pressure, the position, and the velocity vector. Here u, v, and w are the components of $\boldsymbol{u}$ in directions of the natural coordinates s, n, and z, respectively, along, normal to, and projected onto the separating streamline $\mathscr{S}$, given by $n = 0$, of the flow in the limit $\nu = 0$. Furthermore, $u_e(s)$ denotes the surface slip velocity in that limit. The origin $s = n = 0$ is chosen as the location S where $\mathscr{S}$ departs from the surface. Thus, $\mathscr{S}$ coincides with the surface contour for $s \leqslant 0$. Also, note that $\mathscr{S}$ has, in general, a curvature of $\mathcal{O}(1)$ for $|s| = \mathcal{O}(1)$.

In coordinate-free form, the Navier–Stokes equations then are written as

$$\nabla \cdot \boldsymbol{u} = 0, \tag{2}$$

$$\mathrm{D}_t \boldsymbol{u} = -\nabla p + \nu \Delta \boldsymbol{u}, \quad \mathrm{D}_t = \partial_t + \boldsymbol{u} \cdot \nabla, \quad \Delta = \nabla \cdot \nabla, \tag{3}$$

where ∇ is the gradient with respect to $\boldsymbol{x}$. They are subject to the common no-slip condition $\boldsymbol{u} = \boldsymbol{0}$ holding at the surface. As a well-known characteristic, the stationary Reynolds-averaged turbulent flow can be expressed in terms of the time-averaged motion. In the following we employ the conventional Reynolds decomposition of any (in general, tensorial) flow quantity q into its time-mean component $\overline{q}$, see Fig. 1, here regarded as independent of z, and the (in time and space) stochastically fluctuating contribution q',

$$q(\boldsymbol{x}, t, \ldots) = \overline{q}(x, y, \ldots) + q'(\boldsymbol{x}, t, \ldots), \quad \overline{q} \coloneqq \lim_{\Theta \to \infty} \frac{1}{\Theta} \int_{-\Theta/2}^{\Theta/2} q(\boldsymbol{x}, t + \theta, \ldots)\, \mathrm{d}\theta. \tag{4}$$

Herein the dots indicate any further dependences of q apart from on $\boldsymbol{x}$ and t, e.g. on Re. Reynolds-averaging of Eqs. (2) and (3) then yields the well-established Reynolds equations (in the case $\partial_z \equiv 0$ of planar time-mean flow):

$$\nabla \cdot \overline{\boldsymbol{u}} = 0, \tag{5}$$

$$\overline{\mathrm{D}}_t \overline{\boldsymbol{u}} = -\nabla \overline{p} - \nabla \cdot \overline{\boldsymbol{u}'\boldsymbol{u}'} + \nu \Delta \overline{\boldsymbol{u}}, \quad \overline{\mathrm{D}}_t = \overline{\boldsymbol{u}} \cdot \nabla. \tag{6}$$

It is further presumed in the subsequent analysis that all components of the Reynolds stress tensor $-\overline{\boldsymbol{u}'\boldsymbol{u}'}$ are, in general, of asymptotically comparable magnitude (assumption of locally isotropic turbulence). Most important, we disregard any effects due to free-stream turbulence. That is, the turbulent motion originates from the relatively thin fully

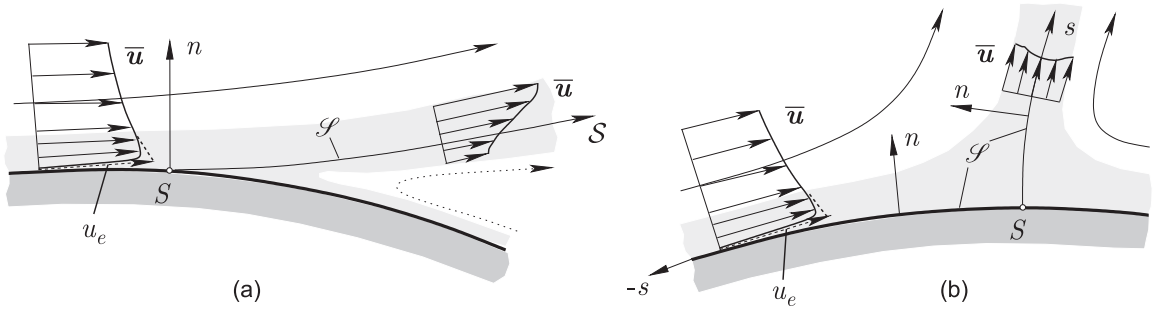

Fig. 1. Time-mean flow near (a) smooth separation (the dotted streamline indicates possible backflow) and (b) separation due to stagnation of the bulk flow, cf. Neish and Smith (1992). The inviscid limit of $\overline{\boldsymbol{u}}$ is shown dashed, and the turbulent shear flow is indicated by a shading.

Author's personal copy

turbulent boundary layer adjacent to the surface, which near S passes into an accordingly slender separated free shear layer along $\mathscr{S}$ for $s>0$.

1.2. Motivation

From an asymptotic point of view, three outstanding contributions to the solution of the problem under consideration have to be mentioned.

Sychev (1983, 1987) was the first who elucidated the question of the asymptotic structure of the oncoming boundary layer by proposing a three-layer splitting of the latter, sufficiently far ahead of S. This scaling, however, is at variance with the classical finding of a two-tiered boundary layer that is found to hold for firmly attached flow only [see, for instance, the pioneering work by Mellor (1972)]. We start the outline of both formulations by noting that each of them adopts the familiar description of the viscous wall layer close to the surface; the same holds for the flow descriptions discussed subsequently. On top of that region the Reynolds shear stress $-\overline{u'v'}$ asymptotically equals the (local) wall shear stress, given by the square of the skin friction velocity u_*, and the streamwise velocity component $\overline{u}$ satisfies the celebrated logarithmic law of the wall. By using the conventional notation, it reads

$$\overline{u}/u_* \sim \kappa^{-1}\ln n^+ + C^+, \quad n^+ = n\,u_*\,\mathrm{Re} \to \infty, \tag{7}$$

where the well-known constants κ and C^+ are quantities of $\mathscr{O}(1)$. The match of the wall region with the adjacent layer then shows that the expansion

$$[\overline{u}, -\overline{u'v'}/u_*^2] \sim [\overline{u}_0, T_0](s,\eta) - \gamma[U_1, T_1](s,\eta) + \mathscr{O}(\gamma^2), \quad \eta = n/\delta \tag{8}$$

holds in the latter. Here, δ is a measure for the thickness of that layer, and, by introducing the so-called slip velocity u_s, the gauge function γ is seen to satisfy the skin-friction law

$$\gamma = u_*/u_s \sim \kappa/\ln \mathrm{Re}, \quad \mathrm{d}\gamma/\mathrm{d}s = \mathscr{O}(\gamma^2), \quad u_s(s) \coloneqq \overline{u}_0(s,0). \tag{9}$$

In the classical two-tiered description of the boundary layer, cf. Mellor (1972), it is assumed that in the fully turbulent main region the (positive) streamwise velocity "defect" with respect to the external potential flow, u_e-u, is asymptotically small. In turn, $\overline{u}_0(s,\eta)\equiv u_s(s)\equiv u_e(s)$, and in the boundary layer limit the momentum balance (6) reduces to a balance between the linearised convective terms and $\partial_n(-\overline{u'v'})$ in leading order, showing that the boundary layer thickness δ is of $\mathscr{O}(\gamma)$. In contrast, according to the approach made by Sychev (1983, 1987), the expansion (8) holds in the additionally introduced middle layer which meets the requirement that the velocity defect u_e-u and, consequently, u_e-u_s are quantities of $\mathscr{O}(1)$. Thus, in the boundary layer approximation to Eq. (6) the convective terms balance both $\partial_n(-\overline{u'v'})$ and the imposed (adverse) pressure gradient $-u_e\,\mathrm{d}u_e/\mathrm{d}s$, such that the thickness δ of the middle layer is of $\mathscr{O}(\gamma^2)$. This wake-type flow structure then allows for a significant decrease in the wall shear stress according to (9) when u_s tends to zero as $s\to 0_-$ and, moreover, for the occurrence of flow reversal further downstream by adopting a local turbulent/irrotational interaction strategy (without the need of a specific turbulence closure).

One readily finds that the gradients $\partial_n\overline{u}$ in the viscous wall layer and the adjacent layer, described by the expansion (8), match on the basis of the logarithmic behaviour (7) provided that $\partial_\eta\overline{u}_0\equiv 0$. Unfortunately, this again gives $\overline{u}_0(s,\eta)\equiv u_s(s)\equiv u_e(s)$ and, thus, contradicts the original assumption of a large velocity defect in the middle layer. That inherent mismatch of the wall layer and the wake region was first noted by Melnik (1989), who used mixing length arguments, in the second work to be highlighted. Therefore, Sychev's approach can hardly be accepted as a self-consistent theory. Let us also note the closely related inconsistency encountered in connection with the two-tiered boundary layer proposed by Afzal (1996), who also suggested a velocity deficit of $\mathscr{O}(1)$ to hold in the outer region. However, Melnik also proposed a non-classical initially three-tiered boundary layer where the outermost part plays the role of the aforementioned middle layer. But most important, and in striking difference to any previous asymptotic treatment of turbulent shear flows, in Melnik's (1989) work the slenderness of the latter is measured by some small non-dimensional parameter, denoted by α, which is regarded to be essentially independent of Re. Melnik's motivation for the resultant two-parameter matched asymptotic expansions of the flow quantities merely relies upon the observation that any commonly employed shear stress closure includes a small number (a most familiar example is the so-called Clauser "constant" $\alpha\approx 0.0168$ in the algebraic Cebeci–Smith model) which is seen to measure the boundary layer thickness if the velocity defect in the fully turbulent flow regime is taken to be of $\mathscr{O}(1)$. This idea has been followed up and substantiated by order-of-magnitude reasoning in the more recent papers by Scheichl and Kluwick (2007a, b), where it is shown to provide a sound basis for developing a self-consistent theory of turbulent marginal separation. On the other hand, it is found that Melnik's theory cannot be extended in order to describe the global separation process due to two serious shortcomings: (i) the proposed flow structure is strongly associated with the adopted coupling

Author's personal copy

$\alpha^{1/2}\ln \mathrm{Re} = \mathcal{O}(1)$, which is apparently inconsistent with the original assumption on α and, hence, does not allow for a correct formulation of the gradual transition from attachment to separation of the flow inside the wall layer; (ii) the impressed potential flow does not exhibit a free streamline departing smoothly from the surface, in order to avoid a Goldstein-type singularity encountered by the boundary layer solution that is evidently unsurmountable by assuming a firmly attached external bulk flow, cf. Scheichl and Kluwick (2007b).

A different viewpoint was taken up in the third contribution to be noticed, by Neish and Smith (1992). They considered the streamwise development of a classical small-defect boundary layer where the irrotational external flow is indeed presumed to be strictly attached; that is, it exhibits a rear stagnation point, see Fig. 1(b). Interestingly, this concept is fully consistent with the following important finding elucidated in the subsequent analysis: in the case of smooth inviscid flow detachment, as depicted in Fig. 1(a), the associated singular behaviour of the surface pressure immediately upstream of the (a priori unknown) position of S does not trigger a significant change in the order of magnitude of the (initially small) velocity defect, which would be necessary to render smooth boundary layer separation possible. Consequently, within the framework of classical turbulent boundary layer theory separation is suggested to occur asymptotically close to the rear stagnation point as $\mathrm{Re}\to\infty$.

Unfortunately, however, it has not been addressed satisfactorily by Neish and Smith (1992) whether and how the small velocity defect may rather abruptly become of $\mathcal{O}(1)$ due to the retardation of the potential flow as the stagnation point S is approached, in order to ensure an uniformly valid flow description. As pointed out in the first part of the present study, the inviscid vortex flow induced in the immediate vicinity of the stagnation point S indeed appears to hamper severely the construction of a self-consistent asymptotic theory. This finding represents the starting point for the subsequent analysis, where it is shown how the closure-independent asymptotic formulation of a turbulent boundary layer having a finite thickness of $\mathcal{O}(\alpha)$, $\alpha\ll 1$, as $\mathrm{Re}\to\infty$ and which may undergo marginal separation, see Scheichl and Kluwick (2007b), can be adapted to that of massive separation. Unlike the theories presented by Melnik (1989) and Neish and Smith (1992), here the formal limit $\alpha = \mathrm{Re}^{-1} = 0$ corresponds to the required class of inviscid flows with free streamlines. Furthermore, we demonstrate how the asymptotic scaling of the (oncoming) flow, which in connection with turbulent marginal separation (Scheichl and Kluwick, 2007b) was based on rather heuristic arguments from a time-averaged point of view, can be deduced by means of a multiple-scales analysis of the equations of motion (2) and (3).

We commence the investigation by considering the evolution of the boundary layer immediately upstream of the surface position S, indicating inviscid separation.

2. Limitations of the small-defect approach

The case where the streamwise velocity defect in the fully turbulent main region of the boundary layer is small, say, $u_e - u = \mathcal{O}(\varepsilon)$, $\varepsilon\ll 1$, is considered first. To be more precise, we assume that $\varepsilon = \gamma$, according to Eqs. (8) and (9) (although the more general assumption $\gamma/\varepsilon = \mathcal{O}(1)$, including $o(1)$, would not alter the following analysis substantially). Therefore, the boundary layer thickness δ is of $\mathcal{O}(\gamma)$ and expanded as

$$\delta/\gamma = \Delta_0(x) + \gamma\Delta_1(x) + \cdots. \tag{10}$$

By setting $U_1/u_e = F_0'(s,\eta)$, $\eta = \mathcal{O}(1)$, the leading-order streamwise momentum equation, supplemented with appropriate boundary and matching conditions, then reads

$$u_e[\mathrm{d}(u_e\Delta_0)/\mathrm{d}s]\eta F_0'' - \Delta_0\partial_s(u_e^2F_0') = u_e^2T_0', \tag{11}$$

$$F_0(s,0) = T_0(s,0) - 1 = 0, \quad F_0'\sim -\kappa^{-1}\ln\eta + \mathcal{O}(1), \quad \eta\to 0, \tag{12}$$

$$F_0'(s,1) = F_0''(s,1) = T_0(s,1) = 0. \tag{13}$$

We mention that in this connection primes denote derivatives with respect to η. Also, it will prove convenient to integrate Eq. (11) with respect to η by using Eq. (12), which gives

$$u_e^2[\mathrm{d}(u_e\Delta_0)/\mathrm{d}s]\eta F_0' - \partial_s(u_e^3\Delta_0F_0) = u_e^3(T_0 - 1). \tag{14}$$

Finally, evaluation of relationship (14) at the boundary layer edge and subsequent integration from some value $s_0<0$ to $s<0$ yields

$$\mathrm{d}[u_e^3\Delta_0F_0'(s,1)]/\mathrm{d}s = u_e^3, \quad u_e^3(\sigma)\Delta_0(\sigma)F_0'(\sigma,1)|_{\sigma=s_0}^{\sigma=s} = \int_{s_0}^{s} u_e^3(\sigma)\,\mathrm{d}\sigma. \tag{15}$$

Author's personal copy

In order to assess the assumption of a small velocity defect holding in the oncoming flow with respect separation, we analyse Eqs. (11)–(13) in the limit $s \to 0_-$ for the two different cases indicated by Fig. 1(a) and (b), respectively. Without adoption of a specific turbulence closure, we begin the analysis by considering the first case.

2.1. Flow slightly upstream of smooth separation

It is well known that, under rather general conditions concerning the flow in the stagnant (i.e.dead-water) or backflow region where $s>0$ and $n<0$,

$$u_e(s)/u_e(0) \sim 1 + 2k(-s)^{1/2} + (10k^2/3)(-s) + \mathcal{O}\left[(-s)^{3/2}\right], \quad s \to 0_-, \tag{16}$$

in the inviscid limit $v = 0$, cf. Imai (1953), Birkhoff and Zarantonello (1957), and Gurevich (1966), for instance. Here the non-negative parameter k parametrises the class of smoothly separating flows as it depends on the position of S on the body contour. It gives rise to a locally adverse and unbounded pressure gradient $-u_e\,\mathrm{d}u_e/\mathrm{d}s \sim k(-s)^{-1/2}$. Therefore, the question arises if the latter provokes a significant increase of the velocity defect in the oncoming boundary layer, which is required for a correct description of flow reversal further downstream. We remark that in the references mentioned above the free streamline is assumed to confine a dead-water zone (Kirchhoff-type potential flow) throughout. However, it can be demonstrated that Eq. (16) holds in the more general case of a (smoothly) separating potential flow that exhibits a relatively weak backflow. We disregard this possibility in the following, since we feel that for a physically realistic flow picture a reverse flow eddy is necessarily associated with viscous effects.

In order to keep the analysis as general as possible, we now only assume that

$$u_e(s)/u_e(0) \sim 1 + \chi(s) + \cdots, \quad |\mathrm{d}\chi/\mathrm{d}s| \to \infty, \quad s \to 0_-. \tag{17}$$

This singular behaviour is expected to provoke a considerable growth of the turbulent velocity scale u_* (and, in turn, of the fluctuations), expressed through a gauge function $\varphi(s)$,

$$F_0 \sim \varphi(s)G(\eta) + \cdots, \quad T_0 \sim \varphi^2(s)R(\eta) + \cdots, \quad \varphi \to \infty, \quad s \to 0_-. \tag{18}$$

From Eqs. (15) and (18), and the fact that u_e in (17) admits a finite limit, there follows a (intuitively rather unexpected) decrease of the boundary layer thickness of the form $\Delta_0 \sim D/\varphi$, where D is a (positive) constant. Also note that the term $\partial_s(u_e^3\Delta_0 F_0)$ in Eq. (14) is bounded for $s \to 0_-$. Since u_e is bounded, too, the first term in Eq. (14) asymptotically equals $-Du_e^3(0)\eta G'(\eta)\,\mathrm{d}(\ln\varphi)/\mathrm{d}s$. As the velocity defect and, in turn, G' are non-negative, that expression tends to $-\infty$ for $s \to 0_-$. Then φ is seen to be proportional to $(-s)^{-1/2}$, as relationship (14) reduces to a balance between that negative term and $u_e^3\varphi^2(s)R(\eta)$. The latter term, however, is non-negative, as is the Reynolds stress T_0 in the oncoming flow. From this contradiction one then infers that F_0, T_0, and Δ_0 are finite for $s \to 0_-$. Consequently, inspection of Eqs. (14) and (17), subject to the condition (13), shows that Eq. (18) is to be replaced by a sub-expansion of the expansion (8),

$$[F_0, T_0, \Delta_0] \sim [F_{00}(\eta), T_{00}(\eta), \Delta_{00}] + \chi(s)[F_{01}(\eta), T_{01}(\eta), \Delta_{01}] + \cdots. \tag{19}$$

Therefore, the velocity defect does not change its order of magnitude. One then concludes that, by specifying $\chi(s)$ in Eq. (17) in accordance with the behaviour given by Eq. (16), the small-defect formulation represents an inadequate description of a turbulent boundary layer approaching smooth separation. Note that the same conclusion can be drawn for turbulent separation at a trailing edge under angle of attack, where the external velocity admits a square-root behaviour akin to that in Eq. (16). More generally spoken, the expansion (19) holds if u_e admits a finite limit, according to Eq. (17). We add that it has been demonstrated numerically by Scheichl (2001) that even in case of a rather sharp step-like decrease of $u_e(s)$ the velocity defect characterised by F_0, T_0, and Δ_0, remains bounded.

Summarising, it is possible to give a rather comprehensive answer to an interesting question raised in the comment on the work of Neish and Smith by Degani (1996), namely, how the small-defect structure responds to different limiting forms of $u_e(s)$ as $s \to 0_-$: apparently, the only scenario that is compatible with a change of magnitude of the velocity defect, as it is required for an asymptotic description of separation, is that of a boundary layer approaching a stagnation point of the (otherwise attached) flow in the inviscid limit $v = 0$. This is exactly the picture of separation originally proposed by Neish and Smith (1992).

2.2. Flow in the vicinity of a rear stagnation point: non-existence of a self-consistent flow picture

Close to a rear stagnation point, see Fig. 1(b), the potential flow is linearly retarded as $u \sim -cs$, $v \sim cn$, where $s, n \to 0$ and c is a positive constant. Then $u_e \sim -cs$, in contrast to Eq. (17). Substitution of that relationship into the

Author's personal copy

expressions in Eqs. (14) and (15) then predicts a growth of both the boundary layer thickness and the velocity defect, as expressed by Eq. (18). Specifically,

$$\Delta_0 \sim D[-\ln(-s)]^{1/2}/(-s), \quad \varphi = D/\left\{2[-\ln(-s)]^{1/2}(-s)^2\right\}, \ s \to 0_-, \tag{20}$$

where D again is a positive constant, cf. Neish and Smith (1992) and Degani (1996). It then follows from Eq. (20) that relationship (14) reduces to the equation $\eta G'(\eta) = R(\eta)$ for $\eta = \mathcal{O}(1)$. Since the scalings represented by Eq. (20) are incompatible with the inhomogeneous boundary conditions (12) required by the match with the viscous wall layer, on top of the latter a sublayer where $\eta = \mathcal{O}(\varphi^{-2})$ has to be introduced. However, as that flow region appears to behave passively with respect to the further analysis, it is disregarded here.

As a consequence of the growth of Δ, see Eq. (20), the boundary layer approximation ceases to be valid close to the stagnation point S when the distance $-s$ and δ become of comparable magnitude. From the expansion (10) then follows that this region is characterised by suitably rescaled coordinates $(X, Y) = (s, n)/\tau$, where $\tau = (D\gamma)^{1/2}[-(\ln\gamma)/2]^{1/4}$. The resulting asymptotic splitting of the flow is depicted in Fig. 2(a). In the new "square" domain II of extent τ the flow quantities are expanded in the form

$$\left[\frac{\overline{u}}{c\tau}, \frac{\overline{v}}{c\tau}, \frac{\overline{p}-\overline{p}_S}{(c\tau)^2}\right] \sim \left[-X, Y, \frac{X^2+Y^2}{2}\right] + \frac{1}{\ln\gamma}[\partial_Y \Psi, -\partial_X \Psi, P] + \mathcal{O}\left[\frac{1}{\ln^2\gamma}\right], \tag{21}$$

where $\overline{p}_S$ is the (time-mean) pressure in S. Here the magnitude of the velocity defect is still asymptotically small and varies only logarithmically with γ. As an important implication, the presence of the logarithmic terms in relationships (20) is seen to prevent the Reynolds stresses, which are of $\mathcal{O}(\tau^2/\ln^2\gamma)$, to affect even the perturbed flow in leading order. Indeed, substitution of the expansion (21) into the momentum equation (6) shows that the perturbation stream function $\Psi(X, Y)$ and the pressure disturbance $P(X, Y)$ satisfy the Euler equations, linearised about the stagnant potential flow:

$$\partial_X(X\partial_Y\Psi) - Y\partial_{YY}\Psi = -\partial_X P, \quad -X\partial_{XX}\Psi + \partial_Y(Y\partial_X\Psi) = -\partial_Y P. \tag{22}$$

By introducing the vorticity $\Omega = (\partial_{XX} + \partial_{YY})\Psi$, elimination of P in Eq. (22) yields the vorticity transport equation, $(X\partial_X - Y\partial_Y)\Omega = 0$. Finally, integration gives

$$(\partial_{XX} + \partial_{YY})\Psi = \Omega(-XY), \tag{23}$$

expressing the well-known property of two-dimensional steady inviscid flows that the vorticity is constant along a streamline. The match with the oncoming boundary layer flow according to Eqs. (18), (20), and (21), and the obvious requirement that the contribution originating from that "square" region to the external potential flow conforms in magnitude to that induced by the incident boundary layer, which is of $\mathcal{O}(\gamma^2)$, then fixes both the vorticity Ω and the boundary conditions supplementing Eq. (23),

$$\Omega = G''(\eta), \quad \eta = -XY, \tag{24}$$

$$\Psi(X, 0) = 0, \tag{25}$$

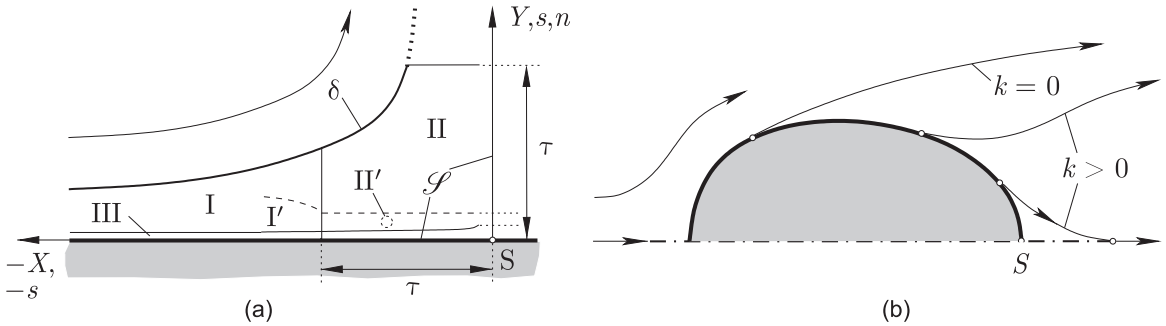

Fig. 2. (a) Asymptotic flow splitting near rear stagnation point S: oncoming boundary layer I with emerging sublayer I′, resulting "square" region II with sublayer II′ (not considered in text), viscous wall layer III (increase of thickness proportional to $1/s$, $s \to 0$, not discussed here), separating streamline $\mathcal{S}$ of the stagnant potential flow; the dotted lines indicate the connection to the regions not considered in the analysis. (b) Smooth inviscid separation from a (here symmetrical) cylindrical body, separating streamlines $\mathcal{S}$ for different values of k in Eq. (16); note the flow showing a cusp-shaped closed cavity which neighbours the attached flow characterised by a rear stagnation point S.

Author's personal copy

$$\Psi \sim G(\eta)/X^2, \quad \eta = \mathcal{O}(1), \quad X \to -\infty, \tag{26}$$

$$\Psi = \mathcal{O}(r^{-2}) \quad \text{or} \quad o(r^{-2}), \quad r := (X^2 + Y^2)^{1/2} \to \infty. \tag{27}$$

Note that $G'(\eta) \sim G'(0) - (2/\kappa)[G'(0)\eta]^{1/2}$, allowing for a match with the aforementioned sublayer, and not $G'(\eta) \sim -\kappa^{-1} \ln \eta + O(1)$, in accordance with the usual near-wall behaviour given by Eq. (12). One then reveals a finite surface slip velocity given by $U_s(X) := (\partial_Y \Psi)(X, 0)$ and a corresponding half-power behaviour $\partial_Y \Psi \sim U_s - (2/\kappa)[G'(0)\, Y/X^{1/2}$ as $Y \to 0$. Also, the reuse of the boundary layer coordinate η introduced before in (24) shows that the edge $n = \delta$ of the turbulent flow region II here is given by $\delta \sim \tau/(-X)$, see Fig. 2(a). Stated equivalently, the curve $-XY = \eta \sim 1$ disjoins the turbulent from the (approximately) irrotational external region as $\Omega = 0$ for $\eta \geqslant 1$.

We seek the solution Ψ of the Poisson problem given by Eqs. (23)–(26) in the range $X < 0$, $Y \geqslant 0$. That is, in the present investigation we do not take into account the "collision" of the oncoming flow with that approaching S for $s \to 0_+$, cf. Figs. 1(b) and 2(a). We conveniently set $\Psi = \Psi_p + \Psi_h$, where $\Psi_p(X, Y)$ is a particular solution of Eqs. (23)–(25) and the homogeneous contribution $\Psi_h(X, Y)$ satisfies Laplace's equation, $(\partial_{XX} + \partial_{YY})\Psi_h = 0$, subject to (25). By defining $G(-\eta) := -G(\eta)$, $\eta \geqslant 0$, and using standard methods, one then obtains

$$\Psi_p = \frac{1}{4\pi} \oint_{-\infty}^{\infty} \oint_{-1/|s|}^{1/|s|} G''(-\sigma\upsilon) \ln[(X - \sigma)^2 + (Y - \upsilon)^2] \, \mathrm{d}\sigma \, \mathrm{d}\upsilon \quad (-\infty < X < \infty, -\infty < Y < \infty), \tag{28}$$

and, after integration by parts and some manipulations

$$\Psi_p = \frac{1}{2\pi} \int_{-1}^{1} G'(\eta) \oint_{-\infty}^{\infty} \frac{|\sigma|\, Y - \eta}{\sigma[\sigma^2 (X - \sigma)^2 + (|\sigma|\, Y - \eta)^2]} \, \mathrm{d}\sigma \, \mathrm{d}\eta \quad (-\infty < X < \infty, -\infty < Y < \infty). \tag{29}$$

The function $\Psi_p(X, Y)$ is skew-symmetric with respect to the origin $X = Y = 0$, where $\Psi_p(0, Y) \equiv \Psi(X, 0) \equiv 0$. Moreover, it is found to vary with R^{-2} for $R^2 = X^2 + Y^2 \to \infty$ and fixed values of $\vartheta := \arctan(Y/X)$ (note that the skew-symmetric distribution of $\Omega(-XY)$ acts like a quadrupole in the far field). On the other hand, $\Psi_p \sim [G(\eta) - H(\eta)]/X^2$ for $X \to -\infty$, with $H \not\equiv 0$ but $H'' \equiv 0$, where η and, in turn, the function $H(\eta)$ (which is not stated explicitly here) are kept fixed. Since $H \not\equiv G$, however $\Psi_h(X, Y)$ must behave as

$$\Psi_h \sim H(\eta)/X^2 (H \not\equiv 0, H'' \equiv 0), \quad \eta = O(1), X \to -\infty, \tag{30}$$

such that Ψ satisfies the upstream condition (26). An asymptotic investigation of Laplace's equation (that takes into account symmetry properties of the solution that are consistent with the aforementioned skew-symmetry of Ψ_p) then shows that $\Psi_h \sim R^{-2}[A \cos(2\vartheta) + B \sin(2\vartheta)]$, where A and B are constants, is the only possible behaviour for $R \to \infty$. Unfortunately, however, and despite its agreement with the far-field conditions (27), this relationship for Ψ_h does not meet the required match with the limiting form (30) as $\vartheta \to \pi_-$ and $X \to -\infty$, Ψ_p is evaluated by exploiting Eq. (29). Thus, the problem posed by Eqs. (23)–(26) has no solution. Therefore, that asymptotic picture of separation taking place close to a rear stagnation point, as originally proposed by Neish and Smith (1992), must be regarded as at least questionable.

A more concise proof of this statement has been found in the course of a private communication with Professor F.T. Smith after submission of the paper (note Acknowledgement): a convenient treatment of the stagnating potential flow considered here is provided by the suitable conformal mapping $\Xi = -Z^2/2$ of the third quarter ($X \leqslant 0$, $Y \geqslant 0$) of the complex plane $Z := X + \mathrm{i}Y$ onto the upper half of the complex plane $\Xi := \zeta + \mathrm{i}\eta$. In turn, Eqs. (23)–(27) subject to the according transformations $\zeta = (Y^2 - X^2)/2$, $\eta = -XY$, and $\hat{\Psi}(\zeta, \eta) := \Psi(X, Y)$ read

$$(\partial_{\zeta\zeta} + \partial_{\eta\eta})\hat{\Psi} = G''(\eta)/[2(\zeta^2 + \eta^2)^{1/2}], \tag{31}$$

$$\hat{\Psi}(\zeta, 0) = 0, \tag{32}$$

$$\hat{\Psi} \sim -G(\eta)/(2\zeta), \quad \eta = \mathcal{O}(1), \ \zeta \to -\infty, \tag{33}$$

$$\hat{\Psi} = \mathcal{O}(1/\rho) \quad \text{or} \quad o(1/\rho), \quad \rho := (\zeta^2 + \eta^2)^{1/2} \to \infty. \tag{34}$$

In that case a particular solution $\hat{\Psi} = \hat{\Psi}_p(\zeta, \eta)$ of Eqs. (31)–(33) found by exploiting standard methods and the aforementioned anti-symmetry of $\Omega(\eta)$ with respect to $\eta = 0$ is given by

$$\hat{\Psi}_p = \frac{1}{8\pi} \oint_{-1}^{1} G''(\upsilon) \, \mathrm{PV} \int_{-\infty}^{\infty} \frac{\ln[(\xi - \sigma)^2 + (\eta - \upsilon)^2]}{(\sigma^2 + \upsilon^2)^{1/2}} \, \mathrm{d}\sigma \, \mathrm{d}\upsilon \quad (-\infty < \zeta < \infty, -\infty \leqslant \eta < \infty). \tag{35}$$

Author's personal copy

Herein, the principal value of the second integral refers to the infinitely remote point, $|\zeta| = \infty$, due to the logarithmic singularity of the integrand there. On the one hand, non-existence of the solution of Eqs. (31)–(34) is indicated by considering the far-field behaviour of an appropriate homogeneous solution $\hat{\Psi} = \hat{\Psi}_h(\zeta, \eta)$ of Eq. (31), in a manner analogous to that adopted in case of the original problem, Eqs. (23)–(27). More simply, however, multiplying of Eq. (31) with η and subsequent integration in the range $-\infty < \zeta < \infty$, $0 \leqslant \eta < \infty$ gives the contradiction $0 \sim (\ln A) \int_0^1 \eta G''(\eta)\, \mathrm{d}\eta \equiv -G(1) \ln A$ as $A \to \infty$. Here this limit is considered as integration of the right-hand side of Eq. (31) is initially carried out from $\zeta = -A$ to $\zeta = A$ and $\eta = 0$ to $\eta \to \infty$.

The formal inconsistency outlined before has not been addressed by Neish and Smith (1992). Apparently, this is due to the neglect of the logarithmic terms in expressions (20) in their discussion of the match with the "square" region II. In turn, they propose a vortex flow there which exhibits a velocity defect relative to the stagnating external flow of $\mathcal{O}(1)$, in striking contrast to the expansion (21). Consequently, in the papers by Neish and Smith (1992) and Degani (1996) both the magnitude of the velocities and the extent of the emerging region II are of $\gamma^{1/2}$. Thus, the flow there is governed by the full Reynolds equations (1), rather than their linearised form (22). It is that fully nonlinear stage which prompted Neish and Smith (1992) and Degani (1996) to conclude that separation would occur a distance of $\mathcal{O}(\gamma^{1/2})$ upstream of S. Also, it is not explained in these papers how the flow region II is transformed into a turbulent shear layer along the separated streamline $\mathscr{S}$, which then coincides with the Y-axis, see Fig. 2(a).

A further uncertainty is raised by another issue that has been put forward by Neish and Smith (1992): it is argued that the position of smooth flow detachment approaches the rear stagnation point if one considers the limit $k \to \infty$ in relationship (16). The flow situation for different values of k is sketched in Fig. 2(b), cf. Birkhoff and Zarantonello (1957): from a topological point of view, the only candidate for a flow exhibiting free streamlines around a cylindrical body that neighbours the completely attached potential flow with a rear stagnation point S is the one which embeds a vanishingly small interior (cusp-shaped) cavity/eddy in the vicinity of S. However, it has not been demonstrated convincingly so far that such a solution is associated with correspondingly large values of k. We note that the class of inviscid flows having free streamlines is currently under investigation. [To this end, the methods of potential flow theory presented by Gurevich (1966) are adopted.]

3. The large-defect boundary layer and smooth separation

The picture of separation considered by Neish and Smith (1992) and Degani (1996) is apparently not in accordance with experimental findings. In fact, separation from a cylindrical body takes place a relatively short distance downstream of the location of its maximum cross-section, even for very large values of Re. This finding, together with the serious difficulties discussed in the previous section, then strongly suggests to abandon the assumption of a small-defect boundary layer in favour of a flow description where a streamwise velocity deficit of $\mathcal{O}(1)$ is stipulated. As outlined in the Introduction, such an asymptotic concept that (i) surmounts the difficulties in the matching procedure due to the logarithmic velocity distribution (7) encountered in Sychev's (1983, 1987) theory, and (ii) is corroborated by any commonly used turbulence closure, has already been proven successful in the description of turbulent marginal separation, see Scheichl and Kluwick (2007a, b).

In this novel flow description the boundary layer thickness δ is measured by a small parameter α which is independent of Re as $\mathrm{Re} \to \infty$. This most remarkable characteristic anticipates the existence of a turbulent shear layer of finite width with a wake-type flow, even in the formal limit $\alpha \to 0$, $\nu = 0$, included in the fundamental assumption (1). In that limit the unsteady flow in the wake region is presumably not affected significantly by the periodically occurring well-known wall layer bursts. As will turn out, this characteristic allows for an investigation of some properties associated with the unsteady motion on the basis of Eqs. (2) and (3).

3.1. The slender-wake limit

In the wake region the Reynolds stresses are quantities of $\mathcal{O}(\alpha)$. Then the nonlinearities in the momentum equation (3) suggest to expand the flow quantities according to

$$[u, v, w, p] \sim [\overline{u}_0, 0, 0, \overline{p}_0](s, N) + \alpha^{1/2}[u_1', v_1', w_1', p_1'](t, s, N, \ldots) + \alpha\{[\overline{u}_2, \overline{v}_2, 0, \overline{p}_2](s, N) + [u_2', v_2', w_2', p_2'](t, s, N, \ldots)r\} + \mathcal{O}(\alpha^{3/2}), \quad \delta/\alpha = \delta_0(s) + \mathcal{O}(\alpha^2). \tag{36}$$

Herein a suitable shear layer coordinate $N = n/\alpha$ is introduced, and the dots indicate dependences on inner spatial and time scales, which are specified later. Note that the omission of the time-averaged terms of $\mathcal{O}(\alpha^{1/2})$ in Eq. (36) is a consequence of the expansion $[\overline{u}, \overline{v}, \overline{p}] \sim [\overline{u}_0, \overline{p}_0, 0] + \alpha[\overline{u}_2, \overline{p}_2, \overline{v}_2] + \mathcal{O}(\alpha^2)$ of the time-mean flow quantities, as suggested by the governing

Author's personal copy

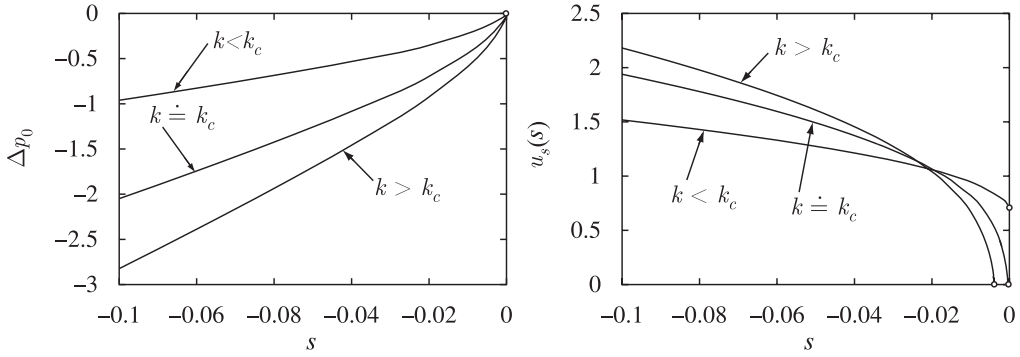

Fig. 3. Local distributions of $\Delta p_0 = p_0(s) - p_0(0)$ and $u_s(s)$ for $k = 1.5$, $k = 2.7 \doteq k_c$, and $k = 3.4$; the circles indicate the occurrence of singular points.

equations (5) and (6). Inserting Eq. (36) into Eqs. (5) and (6) then gives rise to the shear layer approximation

$$\overline{p}_0(s,N) = p_0(s), \quad -\mathrm{d}p_0/\mathrm{d}s = u_e\,\mathrm{d}u_e/\mathrm{d}s, \tag{37}$$

$$\partial_s\overline{u}_0 + \partial_N\overline{v}_2 = 0, \quad \overline{u}_0\partial_s\overline{u}_0 + \overline{v}_2\partial_N\overline{u}_0 = -\mathrm{d}p_0/\mathrm{d}s - \partial_N(\overline{u_1'v_1'}). \tag{38}$$

Eqs. (37) and (38) are seen to govern the turbulent motion along the separating streamline $\mathscr{S}$ to leading order sufficiently far from S, i.e. for $|s| = \mathcal{O}(1)$, see Fig. 1(a). They are subject to the wake-type boundary conditions

$$\overline{v}_2(s,0) = \overline{u_1'v_1'}(s,0) = 0, \quad \overline{u}_0(s,\delta_0(s)) - u_e(s) = \overline{u_1'v_1'}(s,\delta_0(s)) = 0. \tag{39}$$

By excluding the apparent trivial solution $\overline{u}_0 \equiv u_e(s)$, $\overline{v}_2 \equiv \overline{u_1'v_1'} \equiv 0$, which implies a velocity defect of $o(1)$, we seek non-trivial solutions $\overline{u}_0, \overline{v}_2, \delta_0$ of Eqs. (37)–(39) with respect to separation. To this end, it is useful to consider Eqs. (38) and (37) evaluated for $N = 0$,

$$\mathrm{d}(u_s^2 - u_e^2)/\mathrm{d}s = -2[\partial_N(\overline{u_1'v_1'})](s,0). \tag{40}$$

Herein $u_s(s) = \overline{u}_0(s,0)$ again denotes the slip velocity. Note that separation is associated with flow reversal further downstream, which, in turn, requires $u_s(0) = 0$. To gain first insight how the boundary layer behaves as $s \to 0_-$, the problem posed by Eqs. (37)–(39) has been solved numerically, by adopting the same algebraic shear stress closure that was employed successfully for the boundary layer calculations carried out by Scheichl and Kluwick (2007b).

We again discard the possibility that the impressed potential flow exhibits a rear stagnation point S, since inspection of Eq. (40), confirmed by the numerical study, shows that then u_s not necessarily approaches zero in the vicinity of S. Therefore, the picture of a "collision" of two boundary layers is apparently not appropriate for describing turbulent separation. Consequently, separation is seen to be associated with a smoothly separating inviscid flow, according to the situation sketched in Fig. 2(b). As was outlined by Birkhoff and Zarantonello (1957) and Gurevich (1966), only flows having $k \geqslant 0$ are topologically possible. A suitable model for the surface velocity $u_e(s)$ that exhibits the then required local behaviour expressed in Eq. (16) is given by $u_e(s) = (3/2+s)^m[1 + k(-2s)^{1/2}]/(1+k)$, $-1/2 \leqslant s < 0$, such that $u_e(-1/2) = 1$. Here the exponent m represents an eigenvalue of the self-preserving solution for a given value of $u_s(-1/2)$, which serves as the initial condition for the downstream integration of Eqs. (37)–(39) cf. Scheichl and Kluwick (2007b). Specifically, the value $u_s(0) = 0.95$ has been imposed, yielding $m \doteq -0.3292$. The distributions for the impressed adverse difference pressure $p_0(s) - p_0(0)$ and the resulting slip velocity $u_s(s)$ are plotted in Fig. 3 for different values of the control parameter k. It is found that for sufficiently small values of k the integration terminates in a singular manner at $s = 0$ where u_s assumes a finite limit, i.e. $u_s(0) > 0$. For increasing values of k this threshold decreases, such that it finally vanishes for a critical value of k, say, $k = k_c$. We note that near $k = k_c$ the numerical calculations are very sensitive to slight variations in the value of k; for the specific choice of $u_e(s)$ adopted here one finds that $k_c \doteq 2.7$. For $k > k_c$, however, the solution admits a Goldstein-type singularity at a position upstream of $s = 0$ which has been discussed in more detail by Scheichl and Kluwick (2007b). Here we add that a thorough analytical study of the numerically observed singular behaviour of the boundary layer solutions, also expressed through Eq. (40), is a task of the current research.

As a first, rather remarkable, result, the location of turbulent break-away separation in the double limit $\alpha = v = 0$ is seen to be associated with a positive, presumably single-valued, value k_c of k, which has to be found by means of iterative boundary layer calculations. This strikingly contrasts its laminar counterpart, where the so-called Brillouin–Villat condition fixes the position of inviscid flow detachment by the requirement $k = 0$, see Sychev (1972)

Author's personal copy

and Smith (1977). On the other hand, the experimental findings of Tsahalis and Telionis (1975) strongly support the singular behaviour of the turbulent flow in the boundary layer limit there due to a positive value $k = k^*$ as outlined above. Furthermore, the downstream shift of that point for increasing values of k, sketched in Fig. 2(b), explains why, in general, turbulent separation from a cylindrical body takes place further downstream as it is the case when the flow is still laminar. Moreover, first investigations performed by the authors indicate that in the turbulent case the more precise determination of the location of separation for small but finite values of both α and ν is determined by a locally strong rotational/irrotational interaction mechanism, analogous to that proposed by Sychev (1983, 1987).

3.2. Internal structure "derived" from first principles

As a starting point, we consider the well-known transport equation for the time-averaged specific turbulent kinetic energy $\varkappa = \boldsymbol{u}' \cdot \boldsymbol{u}'/2 = (u'^2 + v'^2 + w'^2)/2$, which results from Reynolds-averaging the inner product of $\boldsymbol{u}'$ with the momentum equation (3) by substituting the continuity equation (2),

$$\overline{\mathrm{D}}_t \overline{\varkappa} + \nabla \cdot \overline{(k + p')\boldsymbol{u}'} - \nu \Delta \overline{\varkappa} + \varepsilon_p = -\overline{\boldsymbol{u}'\boldsymbol{u}'} : \nabla \overline{\boldsymbol{u}}, \quad \varepsilon_p := \nu \overline{\nabla \boldsymbol{u}' : \nabla \boldsymbol{u}'}. \tag{41}$$

Herein ε_p is commonly referred to as turbulent (pseudo-)dissipation. By taking into account Eq. (36), the least-degenerate shear layer approximation of Eq. (41) in the double limit given by $\alpha \to 0$ and $\nu \to 0$ is found to be

$$\partial_N(\overline{p_1' v_1'}) + \varepsilon_p \sim -\overline{u_1' v_1'} \partial_N \overline{u}_0. \tag{42}$$

We integrate this relationship across the shear layer thickness, i.e. from $N = 0$ to $N = \delta_0$. Then the net contribution of the diffusive term on the left-hand side of Eq. (42) is seen to vanish, whereas the resulting net turbulent "production" on the right-hand side is positive and of $\mathcal{O}(1)$ since both the Reynolds shear stress $-\overline{u_1' v_1'}$ and the shear rate $\overline{u}_{0,N}$ are apparently non-negative. Remarkably, then ε_p is a quantity of $\mathcal{O}(1)$ in the formal limit $\nu = 0$.

The quantity ε_p is obtained by Reynolds-, or equivalently, time-averaging according to Eq. (4), the stochastically varying quadratic form $\nabla \boldsymbol{u}' : \nabla \boldsymbol{u}'$. By adopting the rather weak assumption that the averaging process leaves its order of magnitude unchanged, we find, with some reservation (due to the at present apparent lack of experimental evidence), that

$$\nabla \boldsymbol{u}' = \mathcal{O}(\nu^{-1/2}) \tag{43}$$

holds for the predominant fraction of intervals of the time t. As the most simple description of the fluctuating motion, we next assume that the turbulent fluctuations are governed by a single spatial "micro-scale", denoted by λ (together with a correspondingly small time scale) apart from the "macro-scales", represented by a streamwise length of $\mathcal{O}(1)$ and the shear layer thickness of $\mathcal{O}(\alpha)$. It then follows from the estimate (43) in combination with Eq. (36) that appropriate "micro-variables" are given by $(t', \boldsymbol{x}') = (t, \boldsymbol{x})/\lambda$ where $\boldsymbol{x}' = (s', n', z')$ and $\lambda = (\nu\alpha)^{1/2}$. That is, the smallest spatial scales are measured by λ. Interestingly, they are asymptotically larger than the (non-dimensional) celebrated Kolmogorov length scale, which is commonly associated with the dissipative small-scale structure of turbulence and given by $(\nu^3/\varepsilon_p)^{1/4}$. It should be mentioned that this novel "micro-scale" is inherently linked to the asymptotic investigation of the equations of motion (2) and (3) as well as the "first moment" of the latter, given by (41). In contrast, the definition of the Kolmogorov scale merely results from dimensional reasoning and, thus, has no profound rational basis.

Hence, the equations of motion (2) and (3) are expanded in the sequence of "inviscid" linear equations

$$\nabla' \cdot \boldsymbol{u}_i' = 0, \tag{44}$$

$$\mathrm{D}_t' \boldsymbol{u}_i' + \boldsymbol{N}_{i-1}' = -\nabla' p_i', \quad \boldsymbol{N}_0' = \boldsymbol{0}, \quad \mathrm{D}_t' = \partial_{t'} + \overline{u}_0(s, N)\partial_{s'}. \tag{45}$$

Here and in the following $i = 1, 2, \ldots$, $\boldsymbol{u}_i' = (u_i', v_i', w_i')$, and ∇' denotes the gradient with respect to $\boldsymbol{x}'$. The inhomogeneous terms $\boldsymbol{N}_i'$ in Eq. (45) are defined by expanding the nonlinear convective operator in Eq. (3), according to Eq. (36),

$$(\boldsymbol{u} \cdot \nabla' - \overline{u}_0 \partial_{s'})\boldsymbol{u}' \sim \alpha^{1/2} \boldsymbol{N}_1' + \alpha \boldsymbol{N}_2' + \cdots. \tag{46}$$

Then the vector $\boldsymbol{N}_i'$ depends on the velocity fluctuations $\boldsymbol{u}_j'$ where $j = 1, 2, \ldots, i$. By eliminating the pressure fluctuations p_i' in Eq. (45), the vorticity fluctuations $\boldsymbol{\omega}_i'$ are seen to satisfy the equations

$$\mathrm{D}_t' \boldsymbol{\omega}_i' = -\nabla' \times \boldsymbol{N}_{i-1}', \quad \boldsymbol{\omega}_i' = \nabla' \times \boldsymbol{u}_i'. \tag{47}$$

Thus, $\mathrm{D}_t' \boldsymbol{\omega}_1' = \boldsymbol{0}$, so that $\boldsymbol{\omega}_1'$ depends on the "micro-variables" $\xi' = s' - \overline{u}_0 t'$, n', and z', but not explicitly on t'. In principle, $\boldsymbol{u}_1'$ then can be calculated from its Helmholtz decomposition, given by the distribution of $\boldsymbol{\omega}_1'$ together with the vanishing divergence as expressed by Eq. (44). Therefore, $\boldsymbol{u}_1'$ and, in turn, $\boldsymbol{N}_1'$ also show no explicit dependence on t', giving $\boldsymbol{\omega}_2' = \boldsymbol{C}' - (\nabla' \times \boldsymbol{N}_1')t'$, where $\boldsymbol{C}'$ is a "constant" of integration. The requirement that the first of the expansions (36) must

Author's personal copy

be uniformly valid with respect to the "micro-time" t' then gives rise to the solvability condition $\nabla' \times \boldsymbol{N}_1' = \boldsymbol{0}$. As a result, one recursively finds that $\mathrm{D}_t' \boldsymbol{\omega}_i' = \boldsymbol{0}$ in general, such that the velocity and pressure fluctuations $\boldsymbol{u}_i'$ and p_i', respectively, depend on ξ', s', n', and z', but, most important, not explicitly on t', and are determined by

$$\nabla' \times \boldsymbol{N}_i' = \boldsymbol{0}, \quad \nabla' p_i' = -\boldsymbol{N}_{i-1}'. \tag{48}$$

Eqs. (48) describe a stationary motion with respect to ξ', i.e. in a frame of reference which moves with the time-mean streamwise velocity $\overline{u}_0(s, N)$ along the separating streamline $\mathscr{S}$ of the flow in the formal limit $v = 0$, see Fig. 1(a). Note that they comprise the full nonlinear steady Euler equations, satisfied by $\boldsymbol{u}_1'$ and p_2'.

This wave-type transport of the stochastic fluctuations along with the time-averaged flow found from the "micro-scales" analysis is commonly termed as "coherent motion": this contribution to the overall turbulent motion is usually associated with spatio-temporal regularity, whereas the dynamics of the stochastic fluctuations acting on the smaller scales involves its random part. As a further consequence of these considerations, the process of time-averaging according to Eq. (4) is seen to provide a filtering of the fluctuating motion with respect to ξ' and, in turn, rather not only with respect to the "micro-time" t' but also to the streamwise "micro-variable" s'. The view that the statistically stationary turbulent flow depends on the spatial "macro-variables" s and N only is, therefore, supported by an asymptotic investigation of the Navier–Stokes equations (2) and (3) and, subsequently, usual time-averaging.

The relationships (44)–(47) are valid for $i < I$ where the index I signifies contributions to Eq. (36) of $\mathscr{O}(v^{1/2})$. For $i = I$ it follows from Eqs. (2) and (3) that the dynamics of these contributions are affected by the viscous term on the right-hand side of Eq. (3). Also, the normal gradient $\partial_N \overline{u}_0$ then enters the momentum balance as a consequence of the "macro-scale" α which describes the time-mean shear layer approximation. This in turn suggests the introduction of a further set $(t^\alpha, \boldsymbol{x}^\alpha) = (t, \boldsymbol{x})/\alpha$ of "micro-variables". Let ∇^α denote the gradient with respect to $\boldsymbol{x}^\alpha$ and $\boldsymbol{e}_s$, $\boldsymbol{e}_n$, and $\boldsymbol{e}_z$ the unit vectors in the respective directions indicated by the subscripts. We then find

$$\nabla' \cdot \boldsymbol{u}_I' = -\nabla^\alpha \cdot \boldsymbol{u}_1', \tag{49}$$

$$\mathrm{D}_t' \boldsymbol{u}_I' + \boldsymbol{N}_{I-1}' + \mathrm{D}_t^\alpha \boldsymbol{u}_1' + \boldsymbol{e}_s v_1' \partial_N \overline{u}_0 = -\nabla' p_I' - \nabla^\alpha p_1' + \Delta' \boldsymbol{u}_1',$$

$$\mathrm{D}_t^\alpha = \partial_{t^\alpha} + \overline{u}_0(s, N)\partial_{s^\alpha}, \quad \Delta' = \nabla' \cdot \nabla'. \tag{50}$$

From Eq. (48) it follows that p_1' is independent of $\boldsymbol{x}'$ since $\boldsymbol{N}_0'$ vanishes, according to Eq. (45). By taking the curl with respect to $\boldsymbol{x}'$ one then obtains from Eq. (50)

$$\mathrm{D}_t' \boldsymbol{\omega}_I' = -\nabla' \times \boldsymbol{N}_{I-1}' - \mathrm{D}_t^\alpha \boldsymbol{\omega}_1' - (\partial_N \overline{u}_0)(\boldsymbol{e}_n \partial_{z'} - \boldsymbol{e}_z \partial_{n'}) v_1' + \Delta' \boldsymbol{\omega}_1'. \tag{51}$$

The right-hand sides of both Eqs. (51) and (49) do not explicitly depend on t'. With the same arguments leading to Eq. (48), then the Helmholtz decomposition of $\boldsymbol{\omega}_I'$ suggests that $\boldsymbol{u}_I'$ and, as a consequence of Eq. (50), p_I' exhibit no explicit t'-dependence too. In turn, the right-hand side of Eq. (51) must vanish. Therefore, Eq. (51) not only determines the quantity $\boldsymbol{u}_{I-1}'$, but can also be interpreted as a linear transport equation for the leading-order contribution $\boldsymbol{\omega}_1'$ to the vorticity with respect to the newly introduced time t^α and $\boldsymbol{x}'$. However, the motion which is affected by the viscous term in Eq. (3) is presumably also governed by convective terms which are nonlinear in the leading-order contribution $\boldsymbol{u}_1'$ to the velocity fluctuations. But, in view of Eq. (50), this is only possible by introducing a set of "intermediate micro-variables" $(\hat{t}, \hat{\boldsymbol{x}}) = (t, \boldsymbol{x})/\alpha^{3/2}$. Thus, the associated new length scale of $\mathscr{O}(\alpha^{3/2})$ is much larger than the viscosity-affected one, λ, but still smaller than the shear layer thickness of $\mathscr{O}(\alpha)$. We close the analysis by noting that this new length scale serves as a measure for the size of the large eddies in the wake region, and, in turn, of the mixing length. This fully agrees with the scaling of the latter found from the time-mean analysis, cf. Scheichl and Kluwick (2007b).

4. Conclusions and further outlook

We have demonstrated that turbulent bluff-body separation requires a streamwise velocity defect of $\mathscr{O}(1)$ as $\mathrm{Re} \to \infty$ in the fully turbulent main region of the oncoming boundary layer, as the classical assumption of a small velocity deficit is intrinsically tied to the idea of a firmly attached external potential flow, and, in turn, leads to a serious inconsistency in the asymptotic hierarchy of the flow, which originates from an asymptotically small vicinity of the rear stagnation point. On the other hand, for the large-defect boundary layer the limiting inviscid solution must be sought in the class of flows exhibiting a free streamline which departs smoothly from the surface. As one remarkable result strikingly contrasting a well-known finding in the theory of laminar separation, here the Brillouin–Villat condition is not met at the separation point. The formulation of the locally strong rotational/irrotational interaction of the separating flow with the external bulk flow is a topic of the current research. Future research activities include, amongst others, the asymptotic investigation of the unsteady motion, where particular emphasis should be placed on the rationally based

Author's personal copy

modelling of turbulent boundary layers undergoing separation. Most important, as a first step in this direction, it has been shown here how the underlying boundary layer concept is strongly supported by such an analysis. Here we note that, to the authors' knowledge, the only attempt currently available in literature to treat turbulent boundary layers by tackling the full Navier–Stokes equations in the limit (1) from a rigorous asymptotic point of view must be attributed to Deriat and Guiraud (1986). As one physically appealing result of the present study, an inner length of $\mathcal{O}(\alpha^{3/2})$ reflecting the size of the large-scale eddies in the wake flow regime is found, which interestingly equals that of the mixing length, given by Scheichl and Kluwick (2007b). Although the analysis also predicts even larger eddies having a diameter of $\mathcal{O}(\alpha)$, those comparable to the mixing length scale determine the distance at which the flow starts to feel the presence of a confining wall. Remarkably, this interpretation of the mixing length not only fully agrees with the mathematical need to introduce a so-called inner wake layer having a thickness of $\mathcal{O}(\alpha^{3/2})$, see Scheichl and Kluwick (2007b). Moreover, it also conforms to the mixing length hypothesis (originally developed by Prandtl), where mid-size eddies are responsible for the turbulence transport from one fluid layer to the adjacent one, as proposed by Hinze (1975).

Finally, we stress that, notwithstanding the strongly encouraging progress made so far, the asymptotic analysis of the unsteady flow is still in a rather early stage. Therefore, its implications on turbulence modelling (of both attached and separating flow) can hardly be reliably projected for the time being. Also, comparison of the theory with both experimental and numerical data obtained for bluff-body flows—see e.g. the recent database provided by Braza et al. (2006)—is clearly a required task of future research efforts.

Acknowledgements

This research was granted by the Austrian Science Fund (Project no. P16555-N12), which is gratefully acknowledged. Also, the authors would like to thank Professor F.T. Smith (Department of Mathematics, University College London, London, UK) for stimulating discussions and the referees for their interesting and helpful comments.

References

Afzal, N., 1996. Wake layer in a turbulent boundary layer with pressure gradient: a new approach. In: Gersten, K. (Ed.), Asymptotic Methods for Turbulent Shear Flows at High Reynolds Numbers. Proceedings of the IUTAM Symposium, Bochum, Germany, June 28–30, 1995. Fluid Mechanics and its Applications, vol. 37. Kluwer Academic Publishers, Dordrecht, Boston, London, pp. 119–132.

Birkhoff, G., Zarantonello, E.H., 1957. Jets, Wakes, and Cavities. Applied Mathematics and Mechanics, vol. 2. Academic Press, New York.

Braza, M., Perrin, R., Hoarau, Y., 2006. Turbulence properties in the cylinder wake at high Reynolds numbers. Journal of Fluids and Structures 22 (6/7), 757–771.

Degani, A.T., 1996. Recent advances in wall-bounded shear flows. Survey of contributions from the USA (invited lecture). In: Gersten, K. (Ed.), Asymptotic Methods for Turbulent Shear Flows at High Reynolds Numbers. Proceedings of the IUTAM Symposium, Bochum, Germany, June 28–30, 1995. Fluid Mechanics and its Applications, vol. 37. Kluwer Academic Publishers, Dordrecht, Boston, London, pp. 119–132.

Deriat, E., Guiraud, J.-P., 1986. On the asymptotic description of turbulent boundary layers. Journal of Theoretical and Applied Mechanics 109–140 (Special issue on Asymptotic Modelling of Fluid Flows, English translation of: Journal de Mécanique Théorique et Appliquée).

Gurevich, M.I., 1966. The Theory of Jets in an Ideal Fluid. International Series of Monographs in Pure and Applied Mathematics, vol. 93. Pergamon Press, Oxford (original Russian book: 1961, Fizmatlit, Moscow).

Hinze, J.O., 1975. Turbulence, second ed. McGraw-Hill, New York.

Imai, I., 1953. Discontinuous potential flow as the limiting form of the viscous flow for vanishing viscosity. Journal of the Physical Society of Japan 8 (3), 399–402.

Mellor, G.L., 1972. The large Reynolds number, asymptotic theory of turbulent boundary layers. International Journal of Engineering Science 10 (10), 851–873.

Melnik, R.E., 1989. An asymptotic theory of turbulent separation. Computers and Fluids 17 (1), 165–184.

Neish, A., Smith, F.T., 1992. On turbulent separation in the flow past a bluff body. Journal of Fluid Mechanics 241, 443–467.

Scheichl, B., Kluwick, A., 2007a. On turbulent marginal boundary layer separation: how the half-power law supersedes the logarithmic law of the wall. International Journal of Computing Science and Mathematics 1 (2/3/4), 343–359 (Special Issue on Problems Exhibiting Boundary and Interior Layers).

Scheichl, B., Kluwick, A., 2007b. Turbulent marginal separation and the turbulent Goldstein problem. AIAA Journal 45 (1), 20–36 (see also: AIAA Technical Paper 2005-4936).

Scheichl, B.F., 2001. Asymptotic theory of marginal turbulent separation. Ph.D. Thesis, Vienna University of Technology, Vienna, Austria.

Smith, F.T., 1977. The laminar separation of an incompressible fluid streaming past a smooth surface. Proceedings of the Royal Society of London, Series A 356 (1687), 443–463.

Author's personal copy

Sychev, V.V., 1972. Laminar separation. Fluid Dynamics 7 (3), 407–417 (English translation of: Izvestiya Akademii Nauk SSSR—Mekhanika Zhidkosti i Gaza 3, 1972, 47–59).

Sychev, Vik.V., 1983. Asymptotic theory of turbulent separation. Fluid Dynamics 18 (4), 532–538 (English translation of: Izvestiya Akademii Nauk SSSR—Mekhanika Zhidkosti i Gaza 18 (4), 1983, 47–54).

Sychev, Vik.V., 1987. Theory of self-induced separation of a turbulent boundary layer. Fluid Dynamics 22 (3), 371–379 (English translation of: Izvestiya Akademii Nauk SSSR—Mekhanika Zhidkosti i Gaza 22 (3), 1987, 51–60).

Tsahalis, D.T., Telionis, D.P., 1975. On the behavior of turbulent boundary layers near separation. AIAA Journal 13 (10), 1261–1262 (Synoptics).

Acta Mech
DOI 10.1007/s00707-008-0078-7

B. Scheichl · A. Kluwick · M. Alletto

"How turbulent" is the boundary layer separating from a bluff body for arbitrarily large Reynolds numbers?

Dedicated to Professor Wilhelm Schneider on the occasion of his 70th birthday

Received: 7 March 2008 / Revised: 15 May 2008
© Springer-Verlag 2008

Abstract The paper deals with separation of a nominally steady and two-dimensional incompressible boundary layer from the smooth surface of a rigid blunt body in the presence of a front stagnation point, here denoted by P_F. In agreement with earlier studies on the flow past a bluff body, it is argued that in the limit of vanishing viscosity, i.e. in the limit where the globally defined Reynolds number Re takes on arbitrarily large values, the solution of this problem is to be sought in the class of steady potential flows with free streamlines. Hence, it is first assumed that for sufficiently large values of Re the boundary layer upstream of separation is a fully developed turbulent one. Accordingly, it is demonstrated numerically and analytically, by adopting asymptotic techniques, how the well-known laminar flow taking place close to P_F is gradually transformed into a fully developed turbulent boundary layer further downstream, which exhibits the well-established typical asymptotic two-layer splitting. However, as has been shown in a preceding study, this type of flow does not allow for a self-consistent rational description of separation, based on the nominally steady form of the equations of motion. From this result, supported by numerical and experimental evidence, the tentative but rather remarkable conclusion is drawn that the boundary layer along the smooth surface of a bluff body never attains a fully developed turbulent state, even in the limit $Re \to \infty$. Most important, these findings are seen to be independent of the choice of a specific turbulence closure.

1 Introduction and motivation

Flow separation from a more-or-less bluff body, i.e. one with diameters of comparable magnitude in and normal to the direction of the oncoming unperturbed stream sufficiently far ahead of the body, in the limit of large values of the globally formed Reynolds number Re not only represents an extremely challenging and long-standing unsolved problem in theoretical hydrodynamics but, needless to say, is also of great engineering relevance. For example, a profound understanding of the very basic physical mechanism underlying flow separation is important in order to allow for further substantial progress in the prediction of undesired separation from airfoils with moderate aspect ratios.

B. Scheichl ( ) · A. Kluwick · M. Alletto
Institute of Fluid Mechanics and Heat Transfer, Vienna University of Technology,
Resselgasse 3/E322, Vienna, Austria
E-mail: bernhard.scheichl@tuwien.ac.at

A. Kluwick
E-mail: alfred.kluwick@tuwien.ac.at

M. Alletto
E-mail: e0127243@student.tuwien.ac.at

In the present study we shall be concerned with a solid plane body of a typical half-diameter $\tilde{L}$, having an impermeable and perfectly smooth surface, and immersed in an otherwise perfectly uniform stream with velocity $\tilde{U}$ of an incompressible fluid of constant density $\tilde{\rho}$ and constant kinematic viscosity $\tilde{\nu}$, respectively. We then assume that

$$Re := \tilde{U}\tilde{L}/\tilde{\nu} \to \infty. \tag{1}$$

Note that, under the above assumptions, the real flow physics is uniquely determined by the value of the single parameter Re. With regard to the subsequent discussion of this flow configuration and the associated notations of characteristic points on the body surface, we refer to the sketch in Fig. 1a referring to the canonical case of the problem, namely, a circular cylinder with radius $\tilde{L}$ in uniform transverse flow.

If in the limit given by Eq. (1) the flow is taken to be strictly laminar and steady, the seminal local asymptotic theory developed by Sychev [14] and Smith [12], see also Sychev et al. [15], applies to the close vicinity of the position of separation. In these studies the flow in the limit of vanishing viscosity has to be sought in the class of irrotational flows with free streamlines which depart smoothly from the surface at the point denoted by P_D. In general, this Helmholtz–Kirchhoff-type flow is associated with a streamwise pressure gradient that tends to infinity immediately upstream of P_D, see e.g. Gurevich [2]. That singular behavior, commonly referred to as Brillouin–Villat (hereafter abbreviated as BV) singularity, then prevents an asymptotic description of separation of the boundary layer (BL) evolving from the front stagnation point, as the solution of the BL problem terminates further upstream in form of a well-known Goldstein singularity, which cannot be surmounted in a rational manner. Therefore, the position of P_D has to be moved sufficiently far upstream such that the BV singularity becomes asymptotically weak (with respect to the value of Re), which in turn allows for a successful treatment of the separation process on the basis of the local viscous/inviscid interaction process.

Unfortunately, however, one has to face the fact that both the flow pattern and the drag coefficient predicted by the above rigorous description of separation are apparently not in satisfactory agreement with the experimental findings: an extensive discussion of the flow field based on measurements of the steady flow past a circular cylinder for various values of Re is presented in [17]. The observed disagreement leads to two major concerns: first of all, the question whether the flow should indeed be regarded as steady and irrotational in the limit $Re \to \infty$, which is crucial, is still unsettled. Surprisingly, it has not attracted many researchers so far. Thus, this assumption still requires a sound confirmation; a first systematic attempt in this direction, adopting both the Navier–Stokes equations and scaling arguments that are based on intuitive physical reasoning, is made in Sect. 3.

The second and most serious objection, however, is raised against the widely believed issue that not only the separated shear flow but even the entire BL upstream of separation becomes fully turbulent for sufficiently large values of Re; for a survey on this topic see [17] and the references therein. Interestingly, detailed measurements of the attached BL flow are rare. As a result, also this hypothesis still lacks a convincing experimental evidence. Moreover, from the oil film flow visualizations of the streamline pattern close to the surface performed by Schewe [10] one can draw the—tentative—conclusion that the BL slightly upstream of separation still exhibits typical laminar-like characteristics, even for values of Re up to approximately 7.7×10^6, whereas separation triggers its rather rapid transition towards a fully developed turbulent free shear layer. In the present study we account for this observation by adopting the approach taken up by Neish and Smith [6]: the level of turbulence intensities in the BL shall not be fixed in advance but governed by a suitably introduced control parameter, say, T. The assumption of a fully turbulent initially attached BL then is captured by considering a suitable distinguished double limit: $T \to \infty$, $Re \to \infty$. However, as far as this latter case is concerned, it has been outlined quite recently, [7], that the typical asymptotic structure of a fully turbulent BL is incompatible with separation provoked by the BV singularity at P_D of the limiting potential flow. This conclusion holds for largely arbitrary positions of P_D when the BV singularity assumes a finite strength. Neish and Smith [6] circumvent that severe shortcoming by exploring the possibility of a strictly attached potential flow, granted that the entire BL is a fully turbulent one (we note that their rationale for these assumptions is neither in agreement with the arguments put forward here nor the present results). In their analysis, separation is expected to take place a (non-dimensional) distance of $O\left[(\ln Re)^{-1/2}\right]$ upstream of the rear stagnation point of the body. However, it has been demonstrated that the proposed local asymptotic splitting of the flow then is incompatible with that deduced from an asymptotic investigation of the full set of the Reynolds-averaged equations of motion [7]. Furthermore, the collapse of P_D with the rear stagnation point can be interpreted as the occurrence of a BV singularity having infinite strength [2,7]. The aforementioned inconsistency encountered when a fully turbulent BL is driven by a potential flow that yields a BV singularity of finite strength, see [7], is presumably met again if

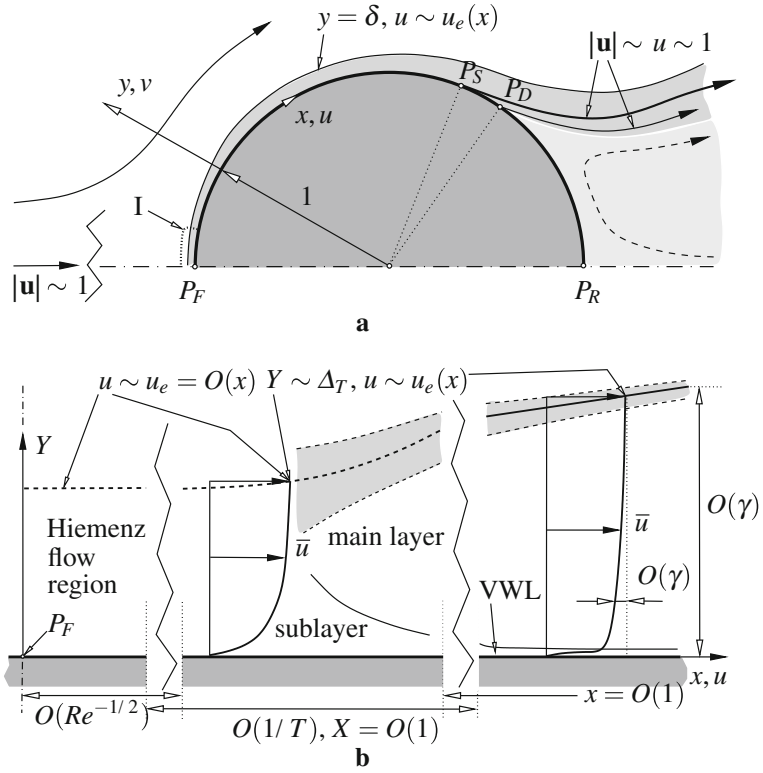

Fig. 1 **a** Flow configuration and natural coordinate system, shown for the case of a circular cylinder with non-dimensional radius 1, representing a bluff body with positive surface curvature $\varkappa(x)$: time-mean streamlines (*arrows* indicate flow direction), BL and separated shear layer (*dark-shaded*), streamlines of irrotational and viscous flow departing in P_D (*normal line*) and P_S (*bold line*), dividing the external flow from the zone with (almost stagnant) reverse flow (*light-shaded*). Separation is assumed to take place in the point P_S, i.e. slightly upstream of P_D, according to the flow picture in [6]. Transitional BL region I near P_F and BL splitting emerging for $T \to \infty$ is zoomed out in **b**, including the viscous wall layer VWL, and the viscous superlayer (*shaded*)

one considers the local flow structure resulting from a slight upstream shift of P_D. As a consequence, relaxing the assumption made in [6] that P_D takes on the form of a rear stagnation point only in the limit $Re \to \infty$ will also unlikely prove successful in establishing a self-consistent description of turbulent separation. In turn, we anticipate the remarkable preliminary result that the attached BL flow approaching separation has to be sought in the class of flows that prevail in a so-called transitional state, as they are neither laminar nor fully turbulent.

Hence, we draw the important conclusion that both a value of T and the position of P_D in the limit $Re \to \infty$ have to be chosen such that the solution of the BL equations meets the necessary requirements of matching with the flow quantities in the region in the immediate vicinity of separation, where the classical BL approximation of the governing equations ceases to be valid. That is, the asymptotic flow structure near separation presumably fixes the value of T, which provides the answer to the question, raised in the paper title, of "how turbulent" is the BL that stretches from the front stagnation point P_F to the position of separation. That flow picture in the limit (1) then strikingly contrasts that proposed by the theory of laminar separation epitomised above. Nevertheless, it agrees fairly well with that inferred from the experiments carried out by Tsahalis and Telionis [16]. These indicate that the observed distinctive deceleration of a turbulent BL closely upstream of separation points to a finite strength of the BV singularity of the limiting potential flow. Moreover, they relate the associated local behavior of the advective terms in the streamwise momentum equation to the occurrence of a pronounced Goldstein singularity if a BL approximation is adopted. Most important, the experimental data indicate that both singularities are characterized by a variation of the streamwise velocity with the square-root of the (upstream) distance along the surface. In fact, the present analysis strongly suggests that the position of P_D adjusts in a subtle manner, such that the solution of the BL equations terminates in form of a Goldstein singularity that (i) takes place at P_D and, simultaneously, (ii) is vanishingly weak, even though the BV singularity is found to be of finite strength.

2 Problem formulation

2.1 Governing equations

Let $\mathbf{x} = \mathbf{e}_x x + \mathbf{e}_y y + \mathbf{e}_z z$, $\mathbf{u} = \mathbf{e}_x u + \mathbf{e}_y v + \mathbf{e}_z w$, t, and p denote, respectively, the position and the velocity vector, the time, and the pressure, non-dimensional with the reference quantities, respectively, $\tilde{L}$, $\tilde{U}$, $\tilde{L}/\tilde{U}$, and $\tilde{\rho}\tilde{U}^2$, introduced in Sect. 1. Here, $\mathbf{x}$ and $\mathbf{u}$ are expressed using natural coordinates, where the unit vectors $\mathbf{e}_x$, $\mathbf{e}_y$, and $\mathbf{e}_z$ point in the directions along and normal to the body contour, which is given by $y = 0$, and perpendicular to the (x, y)-plane, respectively. The origin $\mathbf{x} = \mathbf{0}$ is taken to coincide with the front stagnation point P_F, see Fig. 1a. The Navier–Stokes equations for incompressible flow, subject to the usual no-slip condition holding at the body surface, then read

$$\nabla \cdot \mathbf{u} = 0, \tag{2.1}$$

$$\partial \mathbf{u}/\partial t + \mathbf{u} \cdot \nabla \mathbf{u} = -\nabla p + Re^{-1} \nabla^2 \mathbf{u}, \tag{2.2}$$

$$\mathbf{u}|_{y=0} = \mathbf{0}. \tag{2.3}$$

Equations (2) are supplemented with the requirement $|\mathbf{u}| \to 1$ as $y \to \infty$ for unperturbed parallel incident flow, see Fig. 1a. By adopting the curvilinear coordinate system introduced above, the gradient and the Laplacian are represented by $\nabla = \mathbf{e}_x\, h^{-1}\partial/\partial x + \mathbf{e}_y\, \partial/\partial y + \mathbf{e}_z\, \partial/\partial z$ and $\nabla^2 = h^{-1}[(\partial/\partial x)\,(h^{-1}\,\partial/\partial x) + (\partial/\partial y)\,(h\,\partial/\partial y)] + \partial^2/\partial z^2$, respectively. Herein $h := 1 + \varkappa(x)\, y$, where $\varkappa(x)$ denotes the surface curvature, which is assumed to be a quantity of $O(1)$ in general (and positive for a convex surface contour, as shown in Fig. 1a).

According to a well-known result of ergod theory, for a nominally stationary flow usual Reynolds-averaging of any (tensorial) flow quantity, in the following symbolized by $\mathbf{Q}$, is equivalent to time-averaging. Hence, we introduce the common Reynolds decomposition of $\mathbf{Q}$ into its time-mean value $\overline{\mathbf{Q}}$ and the statistically fluctuating contribution $\mathbf{Q}'$, by virtue of

$$\mathbf{Q}(\mathbf{x}, t; Re) = \overline{\mathbf{Q}}(x, y; Re) + \mathbf{Q}'(\mathbf{x}, t; Re), \tag{3.1}$$

$$\overline{\mathbf{Q}} := \lim_{\tau \to \infty} \frac{1}{\tau} \int_{-\tau/2}^{\tau/2} \mathbf{Q}(\mathbf{x}, t + \theta; Re)\, \mathrm{d}\theta. \tag{3.2}$$

Note that in the process of Reynolds-averaging, Eq. (3.2), the limit $\tau \to \infty$ is evaluated for *finite* values of Re. The accordingly averaged continuity equation (2.1) then is conveniently satisfied by introducing a stream function ψ such that $\partial\psi/\partial y = \overline{u}$, $\partial\psi/\partial x = -h\overline{v}$. In turn, averaging of the momentum equation (2.2) yields the well-known Reynolds equations for a nominally two-dimensional flow, [11] (p. 81),

$$h\left[\frac{\partial\psi}{\partial y}\frac{\partial}{\partial x} - \frac{\partial\psi}{\partial x}\frac{\partial}{\partial y}\right]\frac{\partial\psi}{\partial y} - \varkappa\frac{\partial\psi}{\partial x}\frac{\partial\psi}{\partial y} = -h\frac{\partial p}{\partial x} - h\frac{\partial\overline{u'^2}}{\partial x} - \frac{\partial\, h^2\,\overline{u'v'}}{\partial y} + \frac{h^2}{Re}\frac{\partial\,\nabla^2\psi}{\partial y}, \tag{4.1}$$

$$\left[\frac{\partial\psi}{\partial x}\frac{\partial}{\partial y} - \frac{\partial\psi}{\partial y}\frac{\partial}{\partial x}\right]\left[\frac{1}{h}\frac{\partial\psi}{\partial x}\right] - \varkappa\left[\frac{\partial\psi}{\partial y}\right]^2 = -h\frac{\partial p}{\partial y} - \frac{\partial\, h\overline{v'^2}}{\partial y} - \frac{\partial\overline{u'v'}}{\partial x} + \varkappa\,\overline{u'^2} - \frac{1}{Re}\frac{\partial\,\nabla^2\psi}{\partial x}. \tag{4.2}$$

It is of advantage to consider also the scalar transport equation for the time-mean value of the specific turbulent kinetic energy given by $q^2 := \mathbf{u}'\cdot\mathbf{u}'/2 \equiv (u'^2 + v'^2 + w'^2)/2$. In combination with the equations of motion (2) and (4), this equation conveniently serves to deduce the basic asymptotic scaling properties of the turbulent flow. Written in coordinate-free form,

$$\overline{\mathbf{u}} \cdot \nabla\,\overline{q^2} + \nabla \cdot \overline{(q^2 + p')\,\mathbf{u}'} - Re^{-1}\,\nabla^2\,\overline{q^2} + \varepsilon_p = P, \quad \varepsilon_p := Re^{-1}\,\overline{\nabla\mathbf{u}' : \nabla\mathbf{u}'}, \quad P := -\overline{\mathbf{u}'\mathbf{u}'} : \nabla\,\overline{\mathbf{u}}, \tag{5}$$

it results from Reynolds-averaging the inner product of $\mathbf{u}'$ with Eq. (2.2) by substituting Eq. (2.1). The positive definite quadratic form ε_p and the quantity P are usually referred to as turbulent (pseudo-)dissipation and turbulent production, respectively, [11] (p. 503 ff.).

2.2 Turbulent fluctuating motion

For what follows, we tacitly assume that in the limit (1) the turbulent velocity fluctuations u' and v' at a given point (x, y) are of the same order of magnitude, in general. Accordingly, their correlations $\overline{u'^2}$, $\overline{u'v'}$, $\overline{v'^2}$ are equally scaled (common hypothesis of locally isotropic turbulence). Also, let λ, Λ, and λ^+ denote characteristic values for the shortest spatial scales associated with the limit (1), non-dimensional with $\tilde{L}$, apparent in the fluctuating motion in, respectively, the external flow, the BL, and in the viscous wall layer located at the base of the latter. As a basic property of the fluctuating motion, here we only note that $\lambda \ll 1$.

3 Global asymptotic picture of the flow

We first focus on the intensity of the turbulent fluctuations by adopting a length scale comparable with the body dimensions, i.e. where x, y are quantities of $O(1)$. Then the quadratic form ε_p is asymptotically of $O(1)$ or smaller, as are the remaining contributions to Eq. (5). Following the arguments outlined in [7], it is very likely that λ is not asymptotically smaller than of $O(Re^{-1/2})$. In turn, the viscous term in the equations of motion (2) is seen to be negligibly small in the limit (1). In the region of the external or bulk flow, namely, outside the attached BL, the separated shear layer and the recirculating or wake flow region behind the body, respectively, see Fig. 1a, both $\mathbf{u}$ and p are of $O(1)$. Initially, let us also regard $|\mathbf{u}'|$ and p' as quantities of $O(1)$ there. By introducing appropriate small scales $(\mathbf{x}', t') = (\mathbf{x}, t)/\lambda$ and expanding $(\mathbf{u}, p) \sim (\mathbf{u}_0, p_0) + \cdots$, in this situation the Navier–Stokes equations (2.1) and (2.2) reduce to the Euler equations,

$$\nabla' \cdot \mathbf{u}_0 = 0, \quad \partial \mathbf{u}_0/\partial t' + \mathbf{u}_0 \cdot \nabla' \mathbf{u}_0 = -\nabla' p_0. \tag{6}$$

Herein, ∇' denotes the gradient with respect to $\mathbf{x}'$.

Let $\boldsymbol{\omega}$ denote the vorticity, $\boldsymbol{\omega} := \nabla \times \mathbf{u}$. Using standard algebra yields the scalar identity

$$\overline{\boldsymbol{\omega} : \boldsymbol{\omega}} \equiv \overline{\nabla \mathbf{u} : \nabla \mathbf{u}} - \nabla \cdot [\nabla \cdot (\overline{\mathbf{u} \cdot\cdot \mathbf{u}})]. \tag{7}$$

The specific form of the last term in Eq. (7) follows from substitution of the continuity equation (2.1). That term must be considered to be of $O(1)$ in general, according to Eqs. (3), whereas the above considerations here indicate that $\overline{\nabla \mathbf{u} : \nabla \mathbf{u}} \sim \overline{\nabla' \mathbf{u}_0' : \nabla' \mathbf{u}_0'} = O(\lambda^{-2})$. Therefore, this term provides the predominant contribution to the identity given in Eq. (7). On the other hand, as the oncoming bulk flow is assumed to be uniform, the property $\nabla \times \mathbf{u}_0 \equiv \mathbf{0}$ can be derived from Eqs. (6), indicating an irrotational flow. From Eq. (7) then follows that $\nabla' \mathbf{u}_0$ and, in turn, $\nabla' \mathbf{u}_0'$ vanishes, too. However, the latter result apparently contradicts the initial assumption that $|\mathbf{u}'| = O(1)$. Hence, we infer that in the external-flow region both the turbulent fluctuations and their correlations are small, rather than of $O(1)$. Since any effects of free-stream turbulence are disregarded there, the relatively weak fluctuations in the bulk flow are primarily caused by the much higher turbulence intensities in the attached BL and the separated shear layer, associated with highly concentrated vorticity there. Since these regions are relatively slender, the turbulence intensities there are still small compared to $O(1)$, which suggests that in the wake flow region, which exhibits relatively slow motion, they are of the same magnitude at the most. Let the small parameter α formally measure the magnitude of the components of the Reynolds stress tensor given by $-\overline{\mathbf{u}'\mathbf{u}'}$, without specifying any dependence of α on Re. We then arrive at the conclusion that, in the double limit $\alpha \to 0$ and $Re \to \infty$, the quantities $\mathbf{u}$ and p are (i) given by their time-mean values of $O(1)$ to leading order in the external-flow region, and (ii) are asymptotically small in the wake flow region.

The above considerations give rise to the following important result: in the region where x, y are of $O(1)$ Eqs. (4) reduce to the Euler equations to leading order, so that the bulk flow is to be sought in the class of steady irrotational flows with free streamlines. These detach from the body surface at the point P_D, indicated by $x = x_D$, and confine an (open, as in the case sketched in Fig. 1a, or closed) stagnant-flow region. Therefore, we anticipate the outer expansion

$$[p, \psi] \sim [p_0, \psi_0](x, y; k) + \cdots, \quad \nabla^2 \psi_0 = 0. \tag{8}$$

Here, the leading-order potential-flow solution is uniquely determined by the non-negative so-called BV parameter k, [2,14]. Accordingly, the streamwise gradient of the surface pressure is given by

$$(\partial p_0/\partial x)(x, 0; k) = -u_e \, \mathrm{d}u_e/\mathrm{d}x, \quad u_e(x; k) = (\partial \psi_0/\partial y)(x, 0; k). \tag{9}$$

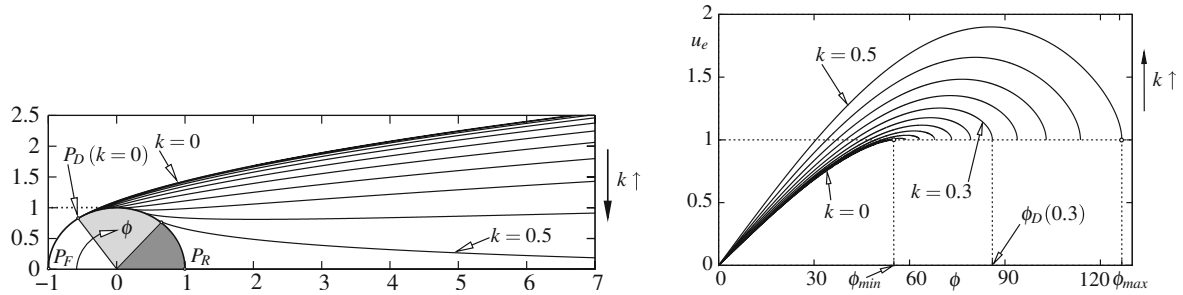

Fig. 2 Kirchhoff flow around a circular cylinder for discrete values $k = i \times 0.05$, $i = 0, 1, \ldots, 10$; **a** separating streamlines (figures on axes measure horizontal and vertical distance from centre in multiples of unit radius), **b** distribution $u_e(x; k)$ over arc angle ϕ [°], terminating in the singular manner given by Eq. (10.2) at $x = x_D(k)$, $\phi = \phi_D(k)$ (for example, $\phi_D(0.3) \doteq 86° 1' 54''$)

It is important for the subsequent analysis (see Subsect 5.3) that near the front stagnation point P_F the surface slip velocity $u_e(x)$ varies as

$$u_e(x; k) \sim b(k)\, x + O(x^2), \quad b(k) > 0, \quad x \to 0_+. \tag{10.1}$$

Moreover, it is well-known that $u_e(x; k)$ exhibits a square-root singularity immediately upstream of P_D, namely, the BV singularity already mentioned in Sect. 1, [2,15],

$$u_e(x; k)/u_e(x_D(k); k) \sim 1 + 2k(-s)^{1/2} + 10\,k^2(-s)/3 + O[(-s)^{3/2}], \quad s = x - x_D \to 0_-. \tag{10.2}$$

In the case $k = 0$, relevant for laminar separation, see Sect. 1, the second-order term in this expansion cancels out, such that $\partial p_0/\partial x$ is bounded at $x = 0$.

Without going into the technical details, we note that the Kirchhoff-type potential-flow problem for the canonical case of a circular cylinder in uniform cross stream, as referred to in Fig. 1a, has been solved numerically by employing the particular methods of conformal mapping elucidated in [2]. The solutions are displayed in Fig. 2. Let $\phi = 180\, x/\pi$ denote the arc angle measured from P_F. One then obtains $\phi = \phi_{\min} \doteq 55° 02' 30''$ for $k = 0$, cf. [2]. In general, for a convex surface contour the BV parameter k increases for increasing values $x = x_D(k)$, $\phi = \phi_D(k)$, characterizing the position of the point P_D. Also, in the case of a body shape which is symmetric with respect to the free-stream flow direction, the free streamlines have the form of a parabola sufficiently far downstream of the body under consideration and, therefore, confine an infinitely large dead-water zone. Specifically, in the canonical case depicted here, the inflection point of the free streamlines is shifted to infinity as $k \to k_{\max} \doteq 0.49079$, so that they meet asymptotically at infinity for $k = k_{\max}$ and $\phi = \phi_{\max} \doteq 126° 43' 32''$.

For geometrical reasons, $k \geq 0$. Also, $k \leq k_{\max}$ if the value of p_0 in P_D, equal to that and in the dead-water region, say, $p_{0,D}$, is that at infinity, say, $p_{0,\infty}$. For $k > k_{\max}$ the quantity of $p_{0,D}$ enters the problem as a further parameter, and the cusp-shaped stagnant-flow region has finite extent, cf. [13]. Here we only note that the strictly attached potential flow considered in [6] then is seen as the limit of a class of flows showing an increase of $p_{0,D}$ from $p_{0,\infty}$ up to the value of the pressure at the front and rear stagnation points P_F and P_R, respectively. Using Bernoulli's law, one finds that the latter is given by $p_{0,\infty} + 1/2$. Therefore, we expect that P_D approaches P_R when $k \to \infty$. In the following, we tacitly restrict the analysis to flows exhibiting an open cavity. Both regions are indicated by the light- and dark-shaded sectors in Fig. 2a.

4 Boundary layer exhibiting partially developed turbulence

4.1 Boundary layer approximation

We now assume "moderate" levels of turbulence intensities, so that the flow close to the surface is correctly described within the well-known framework of laminar BL theory. This is expressed by means of the appropriate inner expansion

$$\left[\psi,\ -\overline{u'v'}\right] \sim Re^{-1/2}\,\{[\Psi,\ T\mathscr{R}](x, Y; k, T) + \cdots\}, \quad Y = Re^{1/2}\, y. \tag{11}$$

The "strength" of the turbulent motion within the BL is accounted for by the (non-negative) turbulence intensity gauge factor T, mentioned in Sect. 1. In the most general case, this quantity is assumed to be of $O(1)$; thus, dots in Eqs. (8) and (11) stand for $O(Re^{-1/2})$. Stated equivalently, the root-mean-square values $(\overline{u'^2})^{1/2}$, $(\overline{v'^2})^{1/2}$ are taken to be of $O(\alpha^{1/2})$, where again a parameter,

$$\alpha := TRe^{-1/2}, \tag{12}$$

is adopted as a measure for the magnitude of the Reynolds stresses.

In combination with Eq. (9), the expansions (8) and (11) give rise to the laminar-type BL approximation of the streamwise momentum equation (4.1), having the form

$$\frac{\partial\Psi}{\partial Y}\frac{\partial^2\Psi}{\partial Y\partial x} - \frac{\partial\Psi}{\partial x}\frac{\partial^2\Psi}{\partial Y^2} = u_e\frac{\mathrm{d}u_e}{\mathrm{d}x} + T\frac{\partial\mathscr{R}}{\partial Y} + \frac{\partial^3\Psi}{\partial Y^3}. \tag{13.1}$$

Equation (13.1) is subject to the no-slip condition (2.3),

$$Y = 0: \quad \mathscr{R} = \Psi = \partial\Psi/\partial Y = 0. \tag{13.2}$$

In addition, matching with the external potential bulk flow requires the asymptotic behavior

$$Y \to \infty: \quad \mathscr{R} \to 0, \quad \partial\Psi/\partial Y \to u_e(x;k). \tag{13.3}$$

The purely laminar flow description is recovered in the case of a trivial solution for the Reynolds stress of the mixed laminar-turbulent BL problem posed by Eqs. (13), i.e. for $T\mathscr{R} \equiv 0$. However, in the subsequent analysis we seek solutions for non-trivial values of $T\mathscr{R}$, in general.

Equations (13) have to be be supplemented with initial conditions that adequately reflect the flow close to the (front) stagnation point $x = y = 0$, where u_e grows linearly with x according to Eq. (10.1). Furthermore, one infers from the hypothesis of local isotropy, stated in Subsect. 2.2, that $\mathscr{R}$ varies proportional to u_e^2. Both these issues are conveniently accommodated by applying the following transformation:

$$[\Psi,\ \mathscr{R}] = [u_e\,\Delta f,\ u_e^2\,r](x,\eta;k,T), \quad \Delta(x;k) = \frac{1}{u_e}\left(2\int_0^x u_e(\xi;k)\,\mathrm{d}\xi\right)^{1/2}, \quad \eta = \frac{Y}{\Delta}. \tag{14.1}$$

Then the BL problem (13) is rewritten as

$$\Delta^2\frac{\mathrm{d}u_e}{\mathrm{d}x}(f'^2-1) - ff'' + u_e\,\Delta^2\left(f'\frac{\partial f'}{\partial x} - \frac{\partial f}{\partial x}f''\right) = u_e\,\Delta\,Tr' + f''', \tag{14.2}$$

$$\eta = 0: \quad r = f = f' = 0, \quad \eta \to \infty: \quad r \to 0, \quad f' \to 1. \tag{14.3}$$

Herein the primes denote derivatives with respect to η. For a given distribution $u_e(x;k)$ satisfying the relationship (10.1), the specific choice of the scaling function $\Delta(x;k,T)$ in Eq. (14.1) results in a smooth approach for $x \to 0_+$ of Δ, r, and f towards the limits $\Delta(0;k) = b^{-1/2}$, $r(0,\eta;k,T) = r_0(\eta) \not\equiv 0$ and the initial condition for f, respectively:

$$f(0,\eta;k,T) = f_0(\eta), \quad f_0'^2 - f_0\,f_0'' = 1 + f_0''', \quad f_0(0) = f_0'(0) = 0, \quad f_0'(\infty) = 1. \tag{14.4}$$

That is, as $x \to 0$ the well-known laminar stagnation point solution, also referred to as Hiemenz flow, of the steady form of the Navier–Stokes equations (2) is recovered, cf. [11].

We finally stress that the solution of the initial-boundary value problem (14), where the imposed external streamwise velocity $u_e(x;k)$ satisfies Eqs. (10.1) and (10.2), is uniquely determined by the values of the two parameters k and T, respectively: the first one reflects the choice of the specific member of the class of Kirchhoff flows, while the second characterizes the magnitude of the Reynolds stress term entering Eq. (14.2). Amongst others (and as already mentioned in the Sect. 1), we will demonstrate numerically in Sect. 6.2 that both k and T can be chosen such that the behavior of the stream function f near $x = x_D$ accounts for the BV singularity, expressed in Eq. (10.2), in a way that allows to establish a local theory of separation.

4.2 Sublayer due to turbulence intensities

According to the definition of Λ given in Subsect. 2.2, its magnitude asymptotically does not exceed that of the BL thickness, which is of $O(Re^{-1/2})$. Inspection of the governing equations (2) then shows that $\mathbf{u}'$ and p' satisfy the Euler equations to leading order. Furthermore, it is demonstrated in [7] that $p' = O(q^2)$, where $q^2 \equiv |\mathbf{u}'|^2 = O(\alpha)$, by virtue of Eq. (12). In turn, for $Y = O(1)$ the least-degenerate BL approximation of Eq. (5) is readily found to be given by the balance between turbulent (pseudo-)dissipation and production,

$$\varepsilon_p \sim P, \quad P \sim T\mathscr{R}\,\partial^2\Psi/\partial Y^2 = O(T). \tag{15}$$

Equation (15) states that $\varepsilon_p = O(T)$ (remember that T is taken as a quantity of $O(1)$, in general). On the other hand, one infers from the definition of ε_p given in Eq. (5) that ε_p is asymptotically not larger than of $O\big(Re^{-1}\,\overline{q^2}/\Lambda^2\big)$. From these order-of-magnitude estimates we deduce that the reference length Λ typical for the most rapid spatial variation of the turbulent motion is presumably of $O(Re^{-3/4})$. Remarkably, its magnitude is comparable to the well-known (non-dimensional) Kolmogorov length that is of $O\big({\varepsilon_p}^{-1/4}\,Re^{-3/4}\big)$ by definition.

Due to the fact that Λ is asymptotically smaller than the BL thickness, in principal (but for $T > 0$ only) a further layer adjacent to the surface—not revealed by the Reynolds equations (4)—having a thickness of $O(\Lambda)$ has to be considered. Let this sublayer be described in terms of a coordinate $\hat{y}$ by setting

$$\hat{y} = y/\Lambda, \quad \Lambda = Re^{-3/4}. \tag{16}$$

For $\hat{y} = O(1)$ the leading-order form of Eq. (5) is seen to include the balance

$$\varepsilon_p \sim Re^{-1}\,\partial^2\overline{q^2}/\partial y^2 \tag{17}$$

in general, as a consequence of the no-slip condition Eq. (2.3). One also infers from Eq. (5) that $P \sim -\,\overline{u'v'}\,\partial\overline{u}/\partial y$ there, which asymptotically cannot be larger than ε_p. Hence, it follows from substituting Eq. (16) into Eq. (5) that the magnitude of $\overline{u}$ then does not exceed $O(Re^{-1/4})$. Moreover, we assume that $\overline{u'v'} = o(\overline{u})$ for $\hat{y} = O(1)$, as the remaining possibility $\overline{u'v'} = O(\overline{u})$ refers to the case of a fully developed turbulent BL, associated with the limit $T \to \infty$, which is addressed separately in Subsect. 5.1. The convective terms in Eqs. (4.2) appear to be negligibly small in the sublayer; the least-degenerate approximation of Eq. (4.1) then reads

$$\partial^2\overline{u}/\partial y^2 - \partial\overline{u'v'}/\partial y \sim \partial p_0/\partial x, \quad \partial p_0/\partial x \sim -u_e\,\mathrm{d}u_e/\mathrm{d}x = O(1). \tag{18}$$

By considering the BL equation (13.1), matching of $\overline{u}$ in the main layer where $Y = O(1)$ and in the sublayer then shows that in the latter $\overline{u} \sim Re^{-1/4}\,\hat{y}\,(\partial^2\Psi/\partial Y^2)_{Y=0}$. Herein the strictly positive coefficient $(\partial^2\Psi/\partial Y^2)_{Y=0}$ varies with x as part of the solution of Eq. (13.1).

In order to estimate the magnitude of the turbulent fluctuations, we also consider the most general least-degenerate form of the momentum equation (2.2) for $\hat{y} = O(1)$,

$$\partial\mathbf{u}'/\partial t + \overline{u}\,\partial\mathbf{u}'/\partial x \sim -\nabla p' + Re^{-1}\,\nabla^2\mathbf{u}'. \tag{19}$$

In this relationship, it is assumed that all components of ∇ are of $O(1/\Lambda)$, and the predominating time-mean quantities have been eliminated by using Eq. (18) and taking into account the aforementioned order-of-magnitude estimates. In Eq. (19) the second term on the left side and the viscous term are seen to be of $O(|\mathbf{u}'|\,Re^{1/2})$. Matching of $\mathbf{u}'$ and p' in the main and the sublayer shows that there is no asymptotically larger term present; otherwise, in the dominant balance $\partial\mathbf{u}'/\partial t \sim -\nabla p'$ the growth of, respectively, p' and the components of $\mathbf{u}'$ for $\hat{y} \to \infty$ would exhibit the identical dependence on $\hat{y}$, which in turn leads to the contradiction $p' = O(\overline{u}\,|\mathbf{u}'|)$ for $\hat{y} = O(1)$. In contrast, the second term in Eq. (19) shows the fastest growth for $\hat{y} \to \infty$ due to the aforementioned linear variation of $\overline{u}$ with $\hat{y}$. Thus, it has to be considered as negligibly small, which is only possible if our original assumption regarding the spatial gradients is relaxed by requiring that $\partial/\partial x = o(1/\Lambda)$. On this condition the leading-order approximation of the continuity equation (2.1) reads $\partial v'/\partial y \sim \partial w'/\partial z$. However, this most likely (albeit it is not demonstrated rigorously here) contradicts the requirement of identical growth rates of both v' and w' for $\hat{y} \to \infty$ due to the basic assumption of local isotropy, see Subsect. 2.2. The only possibility to surmount that disagreement in a self-consistent manner is to abandon that original assumption here by postulating a "degenerate" sublayer where $\partial/\partial z = o(1/\Lambda)$ also and, in turn, $|v'| \ll |u'|$, $|v'| \ll |w'|$. Then the x-component of Eq. (2.2) reduces to $\partial u'/\partial t \sim Re^{-1}\,\partial^2 u'/\partial y^2$. By

adopting the argument used in connection with the continuity equation, one finds that u' exhibits an unbounded growth for $\hat{y} \to \infty$, required by matching, only if the time-derivative can be neglected in this relationship. Finally, the no-slip condition (2.3) implies the expansions

$$[u', w'] \sim (T/Re)^{1/2}\, \hat{y}\, [U_0', W_0'](x, z; Re) + \cdots, \quad v' = T^{1/2} Re^{-3/4}\, \hat{y}^2\, V_0'(x, z; Re) + \cdots, \tag{20}$$

holding for $\hat{y} = O(1)$, where U_0', V_0' and W_0' are quantities of $O(1)$. To leading order, the continuity equation here reduces to the compatibility condition $\partial U_0'/\partial x + \partial W_0'/\partial z \sim -2\, V_0'$, whereas in Eq. (5) all terms are present apart from the first (convective) contribution. In fact, the originally assumed balance given by Eq. (17) is satisfied identically as both terms therein asymptotically equal $\alpha(U_0'^2 + W_0'^2)$. Accordingly, the two-term expansion for $\overline{u}$ simply follows from expanding the solution of Eqs. (13.1) and (13.2) for $Y \to 0$,

$$\overline{u} \sim Re^{-1/4}\, \hat{y}\, (\partial^2 \Psi/\partial Y^2)_{Y=0} - Re^{-1/2}\, \hat{y}^2\, (u_e\, \mathrm{d}u_e/\mathrm{d}x)/2 + \cdots. \tag{21}$$

We conclude from the above analysis that the sublayer behaves purely passive as the boundary conditions given by Eqs. (13.2) and (14.3) remain valid, even though they have to be interpreted correctly as matching conditions for $Y \to 0$ and $\eta \to 0$, respectively. However, in view of Eq. (20) they have to be restated more accurately in the form

$$Y \to 0: \quad \mathscr{R} = O(Y^3), \quad \eta \to 0: \quad r = O(\eta^3). \tag{22}$$

This result provides an important restriction on the formulation of an asymptotically correct Reynolds stress closure.

5 Fully developed turbulent boundary layer

The description of a fully developed turbulent (attached) BL is contained in the present approach by considering an (a priori unknown) appropriate double limit process $T \to \infty, Re \to \infty$, such that in Eq. (13.1) the molecular shear stress term, $\partial^2 \Psi/\partial Y^2$, becomes negligibly small compared to its turbulent counterpart, $T\mathscr{R}$, across the main portion of the BL. As a consequence of the no-slip condition (2.3), then in the so-called (viscous) wall layer located at the base of the main region of the fully turbulent BL the respective shear stress contributions $Re^{-1}\, \partial \overline{u}/\partial y$ and $-\overline{u'v'}$ in the momentum equation (4.1) are of the same order of magnitude.

In the light of the further analysis, we restrict the subsequent derivation of the essential properties of a turbulent BL to the so-called classical case of a two-tiered BL, describing firmly attached flow only. Formally, this is conveniently defined by two independent assumptions:

(A) In the viscous wall layer the (imposed) pressure gradient (which is of $O(1)$, in general) does not enter the leading-order balance of the momentum equation (4.1) in the limit (1);
(B) the outer fully turbulent main region can be directly matched with the viscous wall layer.

5.1 Viscous wall layer

Referring to Subsect. 2.2, that wall layer emerges where $y = O(\lambda^+)$. According to the rationale proposing the sublayer considered in Subsect. 4.2, here $\lambda^+ \ll 1$ measures the spatial scale typical for the turbulent dynamics in the region on its top in the limit (1). Then the balance expressed by Eq. (17) is met again. Herein ε_p is seen to predominate in the limit $y/\lambda^+ \to \infty$, so that further terms in Eq. (5) contribute in leading order to its least-degenerate form for $y = O(\lambda^+)$, hence given by

$$\partial\, \overline{(q^2 + p')v'}/\partial y - Re^{-1}\, \partial^2 \overline{q^2}/\partial y^2 + \varepsilon_p \sim P, \quad P \sim -\overline{u'v'}\, \partial \overline{u}/\partial y. \tag{23}$$

From the expression for P here it follows that $P = O(\overline{u}\, \overline{u'v'}/\lambda^+)$. We eliminate the Reynolds stress from this relationship by considering the presumed balance between the shear stress components, predicting that $\overline{u'v'} = O[\overline{u}/(\lambda^+ Re)]$, which yields $P = O(Re^{-1}\, \overline{u}^2/\lambda^{+2})$. Again, by adopting the assumption of locally isotropic turbulence, see Subsect. 2.2, we follow the arguments put forward in Subsect. 4.2: since P cannot be asymptotically larger than the quantity ε_p, the fundamental estimate $\varepsilon_p = O\left(Re^{-1}\, |\mathbf{u}'|^2/\lambda^{+2}\right)$ then immediately suggests that the magnitude of $\partial \overline{u}/\partial y$ does not exceed that of $\partial |\mathbf{u}'|/\partial y$.

At this point, these basic considerations, solely based on order-of-magnitude estimates of the time-mean quantities, strongly support a widely believed characteristic of the wall layer already proposed in Subsect. 4.2: namely, that $\overline{u}$ and all components of $\mathbf{u}'$ there are asymptotically of comparable magnitude. Stated equivalently, both the Navier–Stokes equations (2) and Eq. (23) are fully recovered to leading order. As the shear stress contributions are of $O(\overline{u}^2)$, the so-called skin-friction velocity u_*, where u_*^2 equals the (local) wall shear stress, provides a proper choice for the reference velocity. We then conveniently set $\lambda^+ = 1/(u_* Re)$ (which is of $O[1/(\lambda^+ Re^{3/2}\varepsilon_p^{1/2})]$ and, therefore, also asymptotically comparable to the Kolmogorov length, cf. Subsect. 4.2). In turn, the conventional wall layer expansion is revealed,

$$\left[\overline{u}/u_*, -\overline{u'v'}/u_*^2\right] \sim [u_0^+, s_0^+](x, y^+) + \cdots, \quad u_* = [Re^{-1}(\partial u/\partial y)_{y=0}]^{1/2}, \quad y^+ = y\, u_* Re. \tag{24}$$

In the momentum equation (4.1) the convective terms are of $O(u_*^2)$. Hence, they are negligibly small compared to the shear stress gradients, which are both of $O(u_*^2/\lambda^+)$. Integration of this balance with respect to y^+ subject to the assumption (A) above gives

$$\partial u_0^+/\partial y^+ + s_0^+ = 1, \tag{25}$$

note that $P/(u_*^5 Re) \sim s_0^+ \partial u_0^+/\partial y^+$, balancing $\varepsilon_p/(u_*^5 Re) = O(1)$. Most important, due to the no-slip condition (2.3) the behavior of the Reynolds stress close to the wall discussed in Subsect. 4.2 and subsumed in Eq. (22) is met again in the form $s_0^+ = O(y^{+3})$ as $y^+ \to 0$. This behavior relies on the reasonable assumption that in this limit both u'/u_* and w'/u_* vary regularly, i.e. linearly, with y^+, giving $v'/u_* = O(y^{+2})$, by virtue of the continuity equation (2.1).

Considering the behavior far from the surface, the obvious requirement that the viscous term in Eq. (25) vanishes is accomplished by the celebrated logarithmic law of the wall,

$$s_0^+ \sim 1 - (\kappa\, y^+)^{-1} + \cdots, \quad y^+ \to \infty, \tag{26.1}$$

$$u_0^+ \sim \kappa^{-1} \ln y^+ + C^+ + \cdots, \quad \kappa \approx 0.384, \quad C^+ \approx 4.1, \quad y^+ \to \infty. \tag{26.2}$$

In Eq. (26.2) the values for the v. Kármán constant κ and the quantity C^+ refer to a perfectly smooth surface [9]. Most important, in recent studies it is pointed out how this commonly assumed behavior can remarkably be deduced from a rigorous investigation of the unsteady motion the viscous wall layer, see [9] and the references therein. Also, there it is found that u_0^+, s_0^+ are presumably representing "universal" functions, i.e. independent of x, even for $y^+ = O(1)$.

5.2 Outer small-defect layer

We now briefly recall the basic characteristics of the main portion of the BL, cf. [11]. At first we note the well-known property that, in striking contrast to the case presented in Sect. 4, a fully turbulent BL typically exhibits a relatively pronounced outer edge. Considering the time-averaged BL having a (local) thickness denoted by δ, here approximated by the curve $y = \delta$, separates the external from the strongly turbulent flow.

The aforementioned assumption (B) of a common overlap conjoining the main layer and the viscous wall layer allows for a match of these flow regions. The matching process based on the wall layer scalings and the behavior for $y^+ \to \infty$ expressed by Eqs. (24) and (26), respectively, then confirms the well-known observation that the streamwise velocity defect defined by $u_e - \overline{u}$ is of $O(u_*)$ across the outer main layer. The associated outer-layer expansions are given by

$$\left[\frac{u_e - \overline{u}}{u_*}, \frac{-\overline{u'v'}}{u_*^2}\right] \sim [h_1', s_1](x, \zeta) + O(\gamma), \quad \delta(x; Re) \sim \gamma\, \delta_1(x) + O(\gamma^2), \quad \zeta = \frac{y}{\delta}, \tag{27.1}$$

provided that the so-called skin-friction law determining the quantity γ in the limit $Re \to \infty$,

$$\gamma := u_*/u_e \sim \kappa\sigma\, [1 + 2\sigma \ln\sigma + O(\sigma)], \quad \sigma := 1/\ln Re, \tag{27.2}$$

holds. In Eq. (27.1) any further dependences, e.g. on the BV parameter k, are not indicated for the sake of simplicity. Furthermore, here and in the following derivatives with respect to ζ are denoted by primes also. Note that the imposed pressure gradient is cancelled by the leading-order convective term, cf. [8], and from

Eq. (27.2) the assumption (B) is found to be consistent with the assumption (A). In turn, the sublayer thickness λ^+ is seen to be of $O[1/(Re\ \ln Re)]$.

Substituting Eqs. (27) into the Reynolds equations (4) results in a leading-order equation exhibiting linearized convective terms. Integrating it with respect to ζ yields

$$u_e^2[\partial(u_e\,\delta_1)/\partial x]\,\zeta h_1' - \partial(u_e^3\delta_1\,h_1)/\partial x = u_e^3(s_1 - 1), \tag{28.1}$$

by taking into account Eqs. (26). That is, h_1, s_1 satisfy the matching and boundary conditions

$$\zeta \to 0: \quad h_1 \to 0, \quad h_1' \sim -\kappa^{-1}\ln\zeta + c_1(x), \quad s_1 \to 1, \quad \zeta = 1: \quad h_1' = s_1 = 0. \tag{28.2}$$

Here, the function $c_1(x)$ is part of the solution for $h_1(x,\zeta)$, and the conditions for $\zeta = 1$ reflect the behavior near the BL edge.

5.3 Gradual departure from Hiemenz flow

The analysis of Subsect. 4.1 indicates that, as a consequence of the behavior of u_e close to the front stagnation point, expressed through Eqs. (10.1) and (14.4), the convective terms still balance both the shear stress contributions in Eq. (14.2) in a small region where $x = O(1/T)$. In the following we focus on that flow regime, which accounts for the laminar-turbulent transition process as $T \to \infty$. Inspection of the momentum equations (4.2) shows that the BL approximation $\partial/\partial y \gg \partial/\partial x$ remains valid there if the parameter α introduced in Eq. (12) is considered to be small in the aforementioned double limit. In turn, the stagnating-flow limit, see Eq. (14.4), is assumed in a narrower region, where both x and y are of $O(Re^{-1/2})$. Furthermore, the BL approximation is assumed to hold also further downstream where $x = O(1)$. Therefore, we treat the flow within the framework of BL theory where $x = O(1/T)$ and then show by matching with the fully developed turbulent flow further downstream that indeed $\alpha \to 0$.

To this end, we introduce suitably rescaled variables, taken to be of $O(1)$, and expand f, r in terms of

$$[f, r] \sim [F, R](X, \eta) + \cdots, \quad \Delta \sim b^{-1/2} + \cdots, \quad X = b^{1/2}\,Tx, \tag{29.1}$$

in accordance with the behavior of u_e given in Eq. (10.1). To leading order, the BL equation (14.2) then is transformed into

$$F'^2 - FF'' + X(F'\,\partial F'/\partial X - F''\,\partial F/\partial X) = 1 + XR' + F'''. \tag{29.2}$$

This equation is subject to the boundary and initial conditions (14.3) and (14.4) where formally f and r have to be replaced by F and R, respectively.

5.3.1 Asymptotic form of the flow far downstream

A treatment of the problem of separation that is consistent with the global flow structure requires the knowledge of the asymptotic splitting of the oncoming BL sufficiently far upstream of P_D, where $x = O(1)$, see Fig. 1. In the case considered here, the attached BL originates from the region of laminar-turbulent transition where $X = O(1)$. Therefore, the picture of the fully turbulent flow has to be deduced from an investigation of the BL equation (29.2), by taking into account Eq. (29.1) and the boundary conditions given by Eq. (14.3), in the limit $X \to \infty$. We emphasize that the scalings expressed by Eqs. (24) and (29.1) are the only assumptions concerning the behavior of the Reynolds shear stress r adopted in the subsequent investigation, which provides the description of the downstream evolution of the BL flow in the region $X = O(1)$. Therefore, the analysis not only turns out to be largely independent of any turbulence closure but, most important, imposes a restriction on any asymptotically correct model for r that is consistent with the generation of the fully turbulent BL for $X \to \infty$.

Specifically, any correct closure has to predict the associated well-known focussing of the BL edge to a pronounced, i.e. for $X \to \infty$ asymptotically narrow zone, namely, the so-called viscous superlayer. As already mentioned in Subsect. 5.2, however, this flow region is disregarded in the following and the position of the "turbulent" BL edge emerging for $X \to \infty$ here is expressed in form of the line $Y \sim \Delta_T(X) \sim Re^{1/2}\delta$. Therefore, the quantity Δ_T characterizes the formation of the "turbulent" BL thickness and is determined in the course of the subsequent analysis. We now discuss the resulting asymptotic flow structure, sketched in Fig. 1.

In the expansions describing the flow in the main layer,

$$[F, R](X, \eta) \sim [H/\rho, S](X, \zeta) + \cdots, \quad \Delta/\Delta_T \sim \rho(X) + \cdots, \quad \zeta = \rho(X)\,\eta, \ \ X \to \infty, \tag{30.1}$$

the "turbulent" BL coordinate ζ is assumed to be of $O(1)$ and the gauge function $\rho(X)$ is not known in advance. In turn, the accordingly transformed Eq. (29.2) gives

$$H'^2 - \rho[\mathrm{d}(X/\rho)/\mathrm{d}X]\,HH'' + X(H'\,\partial H'/\partial X - H''\,\partial H/\partial X) \sim 1 + X\rho S' + \rho^2 H'''. \tag{30.2}$$

The requirement that the viscosity-induced shear rate $\rho^2 H''$ is insignificantly small compared to the Reynolds stress term $X\rho S$ in the limit $X \to \infty$ yields $X/\rho \to \infty$. Furthermore, the boundary conditions to be satisfied at the outer edge of the turbulent BL, here characterized by $\zeta = 1$, give $H'(X, 1) \to 1$ and $S(X, 1) \to 0$ as $X \to \infty$. The first of these relationships then indicates that the expansion

$$[H, S] \sim [H_0, S_0](\zeta) + [\gamma_H(X)\,H_1(\zeta),\ \gamma_S(X)\,S_1(\zeta)] + \cdots, \quad (\gamma_H, \gamma_S) \to (0, 0), \quad X \to \infty, \tag{31}$$

holds in the main layer where $\zeta = O(1)$ with the a priory unknown gauge functions $\gamma_H(X)$, $\gamma_S(X)$.

5.3.2 Case: large-defect flow

We first assume that $S_0 \not\equiv 0$ in Eq. (31). Then the streamwise velocity defect with respect to the external flow is given by $1 - H_0'$ and seen to be of $O(1)$. By substituting Eq. (31) into Eq. (30.2) one readily finds that

$$H_0'^2 - 2\,H_0\,H_0'' = 1 + S_0'/a, \quad H_0(0) = 0, \ \ H_0'(1) = 1, \ \ S_0(1) = 0. \tag{32}$$

Herein a is a (positive) constant of $O(1)$ such that $\rho \sim 1/(aX)$ or, by noticing Eq. (30.1),

$$\Delta_T \sim a\,b^{-1/2}\,X, \quad X \to \infty. \tag{33}$$

Then, as indicated by matching subject to Eqs. (11), (12), and (29.1), the thickness of the fully turbulent BL where $x = O(1)$ is of $O(\alpha)$. In the subsequent two paragraphs we outline in brief that Eq. (32) does not allow for any physically admissible solution H_0, S_0 that is consistent with the asymptotic splitting of the BL flow.

The obvious restrictions $0 \le H_0' \le 1$ and, in turn, $H_0'' \ge 0$ for $0 \le \zeta \le 1$ yield $H_0\,H_0'' \to 0$ as $\zeta \to 0$ and, as a result, $S_0'(0) \le 0$. From the last boundary condition in Eq. (32) then inevitably follows that $S_0(0) > 0$ (and, consequently, $H_0'(0) < 1$). Furthermore, inspection of Eq. (30.2) shows that for small values of ζ the convective and the pressure gradient terms are negligibly small compared to the Reynolds stress gradient. Thus, for $X \to \infty$ close to the surface a sublayer of a relative thickness, say, $\Delta^+(X)$ with $\Delta^+ \to 0$, emerges. That flow region is governed by the limiting forms

$$H \sim \gamma_H^+ \Delta^+ H^+(\zeta^+), \quad S \sim S_0(0)\,S^+(\zeta^+), \quad \zeta^+ = \zeta/\Delta^+ = O(1), \tag{34.1}$$

where an asymptotically correct choice for the gauge function γ_h^+ is provided by

$$\gamma_H^+ \sim a\,S_0(0)\,X^2\Delta^+. \tag{34.2}$$

Equations (30.2) and (34.1) then give rise to the leading-order balance

$$H^{+\prime\prime} + S^+ \sim 1, \tag{34.3}$$

here the primes denote derivatives with respect to the sublayer coordinate ζ^+. Equation (34.3) states that this sublayer is gradually transformed into the viscous wall layer, described in Subsect. 5.1, which takes place where $x = O(1)$, such that ζ^+ is replaced by y^+. Therefore, we expect a behavior of the form

$$H^{+\prime} \sim \kappa^{-1} \ln \zeta^+ + \cdots, \quad S^+ \sim 1 + \cdots, \quad \zeta^+ \to \infty. \tag{34.4}$$

That is, in an additional asymptotic flow region to be considered, located between that sublayer and the main region, Eq. (30.2) reduces to $S \sim S_0(0)$ in leading order. Matching with the adjacent layers then requires that any possibly admissible solution of Eq. (32) is characterized by $H_0'(0) > 0$, which expresses a finite slip velocity at the base of the outermost layer. In turn, it follows from Eq. (34.4) that $\gamma_H^+ \sim -\kappa\,H_0'(0)/\ln\Delta^+$, where $\Delta^+ \sim \kappa\,H_0'(0)/[2\,a\,S_0(0)\,X^2 \ln X]$, according to Eq. (34.2). On the other hand, by virtue of the scalings

provided by Eqs. (24) and (27.2), the thickness of the viscous wall layer asymptotically varies inversely proportional to $x\,\gamma\,Re$ as $x \to 0$. By using Eq. (12), from matching this expression with that for the sublayer thickness, given by $Re^{-1/2}\Delta_T\,\Delta^+$, one then finds that $T \ln T = O(\gamma\,Re^{1/2})$. This is included in the more precise relationship $T \ln^2 T = O(Re^{1/2})$ that follows from matching of both $\overline{u}$ and the shear stress $-\overline{u'v'}$ in the sublayer and the wall layer, which yields $\gamma \sim \gamma_H^+ = O(1/\ln T)$ and, see Eq. (12), $\alpha = \gamma^2\,[= O[1/(\ln Re)^2]]$, respectively. Finally, a "skin-friction law" of the form

$$\gamma \sim \kappa\, H_0'(0)\,\sigma[1 - \sigma \ln\sigma + O(\sigma \ln\sigma)], \tag{35}$$

akin to Eq. (27.2), but for $H_0'(0) < 1$, can be obtained. By considering the BL where $x = O(1)$, one derives an analogous result by matching the viscous wall layer and the middle layer that emanates from the aforementioned intermediate layer and exhibits a small streamwise velocity deficit of $O(\gamma)$ with respect to the slip velocity imposed by the outer layer (having itself a large velocity defect). We note that the here resulting three-tiered BL structure essentially corresponds to that proposed by Melnik [4].

According to the logarithmic variation of u with respect to y^+ in the overlap of the viscous wall layer and the region located on its top, epitomized in [9], the smallest spatial scales in y-direction apparent in these flow layers are given by the thicknesses of the latter, whereas those in x- and z-direction are regarded to be of $O(\lambda^+)$ in both layers, cf. Subsect. 5.1. Specifically, here $-\overline{u'v'} = O(\alpha)$ and, cf. Subsect. 2.2, $\mathbf{u}' = O(\alpha^{1/2})$ throughout the BL, but the smallest spatial scales (in all three directions) are of $O(Re^{-3/4})$ in the outer main layer, see the analysis of Sect. 3, but of $O(\lambda^+)$ in the middle layer. However, this behavior is apparently inconsistent with the existence of a common overlap of these flow regions with respect to matching of $\mathbf{u}'$.

5.3.3 Case: small-defect flow

As a consequence of this inconsistency, it is strongly supposed that the accelerating BL in a transitional state assumes a degenerate form, here expressed through $S_0 \equiv 0$, in the limit $X \to \infty$. From differentiating Eq. (32) one then readily verifies that it is correctly replaced by $H_0' = 1$, giving $H_0 = \zeta$, as the appropriate lowest-order reduction of Eq. (30.2). In this case, evidence for the choice $\gamma_S \to 0$ [tacitly adopted in Eq. (31)], in addition to the, for $S_0 \equiv 0$, also acceptable possibility $\gamma_S = O(1)$, is provided by the subsequent analysis. First, with respect to the expansion (31), we note that the expression $-\gamma_H H_1'$ is recognized as the asymptotic representation for $X \to \infty$ of the strictly positive relative streamwise velocity defect in the main layer, given by $1 - \overline{u}/u_e$. Hence, we stipulate $H_1' > 0$, $H_1 > 0$ there and $\gamma_H < 0$.

Considering the first-order perturbation of the thereby recovered inviscid (Euler flow) limit, see Eq. (31), the least-degenerate form of Eq. (30.2) in the limit $X \to \infty$ reads

$$\Omega_1 H_1' - \Omega_2\,\zeta\,H_1'' \sim X^2 \rho\gamma_S\,S_1', \quad \Omega_1 := \mathrm{d}(X^2\gamma_H)/\mathrm{d}X, \quad \Omega_2 := X\rho\gamma_H[\mathrm{d}(X/\rho)/\mathrm{d}X]. \tag{36}$$

Again, herein the viscous shear stress term is discarded, by assuming

$$X\gamma_S/(\rho\gamma_H) \to -\infty, \quad X \to \infty. \tag{37}$$

Integrating Eq. (36) by parts with respect to ζ and subject to the apparent boundary conditions $H_1(0) = H_1'(1) = S_1(1) = 0$ then yields

$$(\Omega_1 + \Omega_2)\,H_1 - \Omega_2\,\zeta\,H_1' \sim X^2\rho\gamma_S[S_1 - S_1(0)], \quad \Omega_1 + \Omega_2 = (\rho/X)\,\mathrm{d}(X^3\gamma_H/\rho)/\mathrm{d}X. \tag{38}$$

By noting that $H_1(1) > 0$, evaluation of this relationship for $\zeta = 1$ shows that the term on the right-hand side enters its leading-order approximation. Then the main portion of the BL in the flow region where $x = O(1)$ is seen to be of small-defect type, analogous to that considered in Subsect. 5.2. Moreover, it is readily verified that the momentum equations (4.1) and (4.2) give rise to Eq. (28.1) in leading order as the expansions expressed by Eq. (27.1) are retained, where the three gauge functions u_*, u_*^2, and γ for $\overline{u}$, $-\overline{u'v'}$, and δ, respectively, are, in general, replaced by appropriate counterparts. Also, the boundary conditions in Eq. (28.2) hold necessarily, apart from the matching conditions for h_1' and s_1 for $\zeta \to 0$. Specifically, in the case of a more complex (i.e. three-tiered) turbulent BL structure, the latter is to be replaced by $s_1(x, 0) = 0$. Moreover, from Eqs. (10.1) and (28) and the repeated use of ζ in Eqs. (27.1) and (30.1) we infer that

$$[h_1, s_1](x, \zeta) \sim [H_1, S_1](\zeta) + O(x), \quad \delta_1 \sim \Delta_1 x + O(x^2), \quad x \to 0, \tag{39}$$

where Δ_1 is a positive constant. However, then also $s_1(0,0) > 0$, since all terms in Eq. (28.1) are seen to be of $O(x^3)$ as $x \to 0$ and $H_1(1) > 0$. In turn, $s_1 > 0$ for all $x \geq 0$. From the matching conditions provided by the analysis of the wall layer, see Eqs. (26), we then draw the important conclusion that there exists a common overlap with the small-defect (main) layer: that is, the BL at distances of $x = O(1)$ is of the classical small-defect type considered in Subsect 5.2. Finally, we conveniently set $S_1(0) = s_1(x,0) \equiv 1$, and the leading-order form of Eq. (38) reads

$$\zeta H_1' - 2H_1 = 2H_1(1)[S_1 - 1], \quad H_1(1) = 1/(4\Delta_1), \tag{40.1}$$

subject to the boundary conditions

$$\zeta = 0: \quad H_1(0) = 0, \quad H_1 \sim -\kappa^{-1}\ln\zeta + C_1, \quad S_1(0) = 1, \quad \zeta = 1: \quad H_1'(1) = S_1(1) = 0. \tag{40.2}$$

Note that the constant C_1 in Eq. (40.2) is to be determined from the solution for $H_1(\zeta)$.

We now envisage the gauge functions. Matching the thickness δ of the fully turbulent BL involves the gauge function $\rho(X)$, introduced in Eq. (30.1), in the form

$$\delta \sim Re^{-1/2}\Delta_T \sim (b\,Re)^{-1/2}/\rho. \tag{41}$$

Furthermore, since all terms in Eq. (38) are of equal magnitude, comparison with Eq. (40.1) yields

$$X^2\rho\gamma_S \sim -2H_1(1)\,\Omega_1, \quad \Omega_1 = \Omega_2 < 0 \tag{42}$$

(note that $\gamma_H < 0$). The first relationship in Eq. (42) is confirmed by considering Eq. (28.1) as the balance between the Reynolds stress gradient and the convective terms in the form $-\overline{u'v'}/\delta = O[\mathrm{d}(u_e^2\gamma_H)/\mathrm{d}x]$. In agreement with the matching principle, this balance can be expanded when expressed in terms of X and evaluated for $T \to \infty$ with X kept fixed. In fact, by taking into account Eqs. (10.1), (11), (12), (41), the scalings given by Eqs. (14.1), (29.1), (30.1), and noting that $\partial/\partial x \sim T^{-1}\partial/\partial X$, it is rewritten as $X^2\rho\gamma_S \propto -\Omega_1$ to leading order. Furthermore, integration of the latter equality in Eq. (42) can be carried out easily to give

$$X\rho = -\Gamma(X)/\gamma_H, \quad \ln\Gamma = o(\ln X), \quad X \to \infty, \tag{43}$$

by introducing a further (rather slowly varying positive) gauge function $\Gamma(X)$. The behavior of $\ln\Gamma$ in Eq. (43) follows from the estimate $1/\gamma_H = o(X^2)$, deduced from the expression for Ω_1 in Eq. (36). Then Eq. (43) gives $\rho \to 0$. Thus, the variation of δ_1 with x in Eq. (39) complies with the matching condition Eq. (41).

As the main layer analysis outlined so far is not rich enough to determine the gauge functions γ_H, γ_S, ρ, and, hence, the variation of T with Re, we next consider the sublayer close to the surface, where the viscous shear stress comes into play to leading order. That sublayer is gradually transformed into the viscous wall layer taking place where $x = O(1)$; see the above analysis for the (hypothetical) case of a large velocity defect. We introduce further gauge functions $\gamma_H^+(X)$, $\gamma_S^+(X)$ and conveniently describe that sublayer by adopting Eqs. (34). Therein we formally replace $S_0(0)$ by γ_S^+ and, hence, Eq. (34.2) in the now appropriate form

$$\gamma_H^+/\gamma_S^+ = X\Delta^+/\rho. \tag{44.1}$$

From $S_1(0) > 0$ and Eq. (34.4) one then infers

$$\gamma_H = -\gamma_H^+ \sim \kappa/\ln\Delta^+, \quad \gamma_S = \gamma_S^+. \tag{44.2}$$

As a first result, the aforementioned requirements $\Delta^+ \to 0$ and $\gamma_H < 0$ are seen to interdepend mutually, and the assumption stated by Eq. (37) is validated by inserting Eq. (44.1). We then advantageously eliminate γ_S and ρ by substituting Eqs. (44) and (43) into Eq. (42), giving $\Gamma^2 = 2H_1(1)\,X\Delta^+\gamma_H\Omega_1$. By logarithmizing this relationship, one suitably eliminates Δ^+ by means of Eq. (44.2). Taking into account Eqs. (36) and (43) and that $\ln(-\gamma_H) = o(1/\gamma_H)$, eliminating Δ^+ by means of Eq. (44.2) then leads to the least-degenerate form of the dependence of γ_H on X,

$$\kappa/\gamma_H + 2\ln X \sim -\ln(1+\chi), \quad \chi := X(\mathrm{d}\gamma_H/\mathrm{d}X)/(2\gamma_H), \quad X \to \infty. \tag{45}$$

Herein χ is seen to be bounded, since $\gamma_H \to 0_-$ requires $\chi < 0$; otherwise, γ_H would exhibit super-exponential growth, which does not allow for a match. In turn, we arrive at the important results

$$\gamma_H = -\kappa/(2\ln X), \quad \gamma_S = \gamma_H^2/(\Delta_1\Gamma), \quad \rho = 2[\Gamma(X)\ln X]/(\kappa X), \quad \Delta^+ = \Delta_1\rho^2, \quad X \to \infty. \tag{46}$$

The relationships for γ_S, ρ, Δ^+ in Eq. (46) are determined from evaluating Ω_1 in Eq. (36) and by adopting Eqs. (42), (43) and (44.1), where $H_1(1)$ is expressed in terms of Δ_1 by using Eq. (40).

Finally, matching the BL thickness according to Eq. (41) and the Reynolds stress provides two asymptotic relationships that can be cast into the single one

$$\Gamma(X)\,(\ln T)^2/[\alpha\, H_1(1)] \sim 2\ln Re\ \ln T \sim (\ln Re)^2, \quad X = O(T) \quad \Leftrightarrow \quad x = O(1). \tag{47.1}$$

By recalling that the turbulence intensity gauge factor $T = \alpha\, Re^{1/2}$, see Eq. (12), one then finds

$$\Gamma/\alpha \sim 4\, H_1(1) = 1/\Delta_1, \quad \ln\alpha = o(\ln Re). \tag{47.2}$$

Remarkably, the dependence of α on Re is governed by the specific form of the still unknown gauge function $\Gamma(X)$, introduced in Eq. (43). However, it is assumed to assure that $\alpha \to 0$ in the limit (1), in order to justify the BL approximation for $X = O(1)$, and, in turn, that $\gamma_H \sim -\gamma$ for $x = O(1)$. Simultaneously, Eq. (47.2) requires that $\Gamma \to 0$ as $X \to \infty$. For example, if $\Gamma = 4\, H_1(1)/(\ln X)^2$ then $\alpha \sim 1/(\ln T)^2 \sim 4/(\ln Re)^2$, such that $\gamma_S = \kappa^2/4$, see Eq. (46). However, it is very likely that an estimate for $\Gamma(X)$, which is more precise than that given in Eq. (43) and largely independent of a specific Reynolds stress closure, is found in the course of the analysis of the higher-order terms indicated by dots in Eq. (31) (and an investigation of the viscous superlayer), not considered here. Specifically, the expansions given in Eq. (27.1) are unaffected by eigensolutions, such that the remainder terms are correctly anticipated to be of $O(\gamma)$ and $O(\gamma^2)$, respectively, if

$$\Gamma(X) = -\gamma_H/\Delta_1 = \kappa/(2\,\Delta_1 \ln X), \quad \gamma_S = -\gamma_H \quad \Leftrightarrow \quad \alpha \sim \kappa/\ln Re \sim \gamma. \tag{47.3}$$

We note that the question whether there exists an uniquely determined distinguished limit $T \to \infty$ as $Re \to \infty$ is a topic of the current research.

5.4 Fully turbulent flow along body surface

Unfortunately, however, these considerations are apparently inconsistent with the here presumed scaling of the Reynolds shear stress, given by Eqs. (11) and (12), that underlies the specific form of the BL problem (13) obtained for $T \to \infty$: for $\alpha \ll 1$, the wall layer analysis presented in Subsect. 5.1 is expected to hold in slightly modified form, [6], as a novel velocity scale, say, u_T with $u_T = u_*/\alpha^{1/2}$ ($\gg u_*$), replaces u_* and, equivalently, $-\overline{u'v'} \sim \alpha u_T^2 s_0^+$. Accordingly, the stress balance then yields a wall layer thickness $\lambda^+ = 1/(u_T \alpha Re)$.

Most important, the main results of the theory, namely the from of the matching conditions (26), are still valid, such that the outer layer expansion (27.1) is replaced by

$$\left[\frac{u_e - \overline{u}}{u_T},\ \frac{-\overline{u'v'}}{\alpha u_T^2}\right] \sim [h_1', s_1](x,\zeta) + O(\gamma_T), \quad \frac{\delta(x;T,Re)}{\alpha} \sim \gamma_T \delta_1(x) + O(\gamma_T^2), \quad \zeta = \frac{y}{\delta}. \tag{48.1}$$

Herein, the quantity γ_T measuring the velocity defect is determined by the corresponding analogon to the skin-friction law (27.2). By making use of Eq. (12), one now obtains

$$\gamma_T := u_T/u_e \sim \kappa\sigma_T\,[1 - 2\sigma_T \ln\sigma_T + O(\sigma_T)], \quad \sigma_T := 1/(2\,\ln T). \tag{48.2}$$

In turn, Eqs. (28) are recovered. Also, these leading-order results for the outer layer can be readily derived from the BL equations (13), see [6], or, equivalently, (14.1)–(14.3).

For instance, the above description of the turbulent main layer is obtained by expanding Eqs. (13.1) and (13.3) for $\zeta = O(1)$, after inserting

$$Y = Re^{1/2}\gamma_T\,\delta_1\zeta, \quad \Psi \sim Re^{1/2}\gamma_T\,\delta_1 u_e(\zeta - \gamma\, h_1), \quad \mathscr{R} \sim Re^{1/2}\gamma_T^2\, u_e^2 s_1. \tag{49}$$

Accordingly, here the BL edge $y = \delta$ is represented in the form $Y \sim Re^{1/2}\gamma_T\delta_1$, cf. Eq. (41).

Matching the solutions for $X = O(1)$ and $x = O(1)$ then immediately gives $r = O(\gamma_T^2)$, see Eq. (14.1), and $\gamma_H \sim -\gamma_T$ for $x = O(1)$. The latter relationship again yields the in (48.2) anticipated result $\gamma_T \sim \kappa/(2\ln T)$, cf. [6], whereas the former removes the aforementioned uncertainty in the choice of $\Gamma(X)$ (quite naturally) as it requires

$$\Gamma = 1/\Delta_1, \quad \gamma_S = \gamma_H^2 \quad \Leftrightarrow \quad \alpha = o(1). \tag{50}$$

Finally, matching of the BL thickness δ, see Eqs. (48), with its expression given by Eqs. (41) and (43) is easily verified. Equation (50) provides the counterpart to the relationships (47) that fully complies with the large-T limit of, respectively, Eqs. (13) and (14).

As a result, we arrive at the remarkable – preliminary – conclusion that in the limit $T \to \infty$ a generalized form of the classical theory, subsumed in Subsects. 5.1 and 5.2, applies for $x = O(1)$. Then the magnitude of the velocity defect in the outer region is found to be of $O(1/\ln T)$ and reaches its theoretically possible minimum in the case of the classical flow description that refers to a fully developed turbulent BL. As already pointed out in [6], this limit is simply included by setting $\alpha = 1$, i.e. $T = Re^{1/2}$, giving $\gamma_T = \gamma$ (as $\sigma_T = \sigma$). However, since we require $\alpha \to 0$ as $Re \to \infty$, here the existence of this limiting solution is prohibited as a consequence of the specific the asymptotic properties of the flow near the front stagnation point. Therefore, we feel it is important to distinguish between the here used term "fully turbulent" and "fully developed turbulent", which originally refers to the classically scaled turbulent BL.

6 Numerical treatment of the boundary layer flow

6.1 Asymptotically correct Reynolds stress closure

In order to obtain numerical solutions of the BL problem posed by Eqs. (14) for various values of k and T, the Reynolds shear stress is conveniently modelled on the basis of the mixing length formulation, which is associated with the concept of a sharp BL edge $y = \delta$, cf. [11].

In the case $T \to \infty$ the solutions shall assume a behavior that is compatible with the asymptotic structure derived in Sect. 5. This is achieved if the mixing length, here denoted by ℓ, is taken as the product of the two "lengths" l, l^+ that account for the BL flow in the main and the sublayer, respectively,

$$r = [\ell/\hat{\rho}]^2 f''(x,\eta;k,T)^2, \quad \ell = l(\zeta)\, l^+(y^+), \tag{51.1}$$

$$\zeta = \hat{\rho}(x;k,T)\eta, \quad y^+ = T u_T \Delta\eta = [T u_e \Delta f''(x,0)]^{1/2}, \tag{51.2}$$

$$l = c_\ell\, I(\zeta)^{1/2} \tanh[\kappa\,\zeta/c_\ell], \quad I(\zeta) = 1/(1+5.5\,\zeta^6), \quad c_\ell = 0.085, \tag{51.3}$$

$$l^+ = 1 - \exp(-y^+/A^+), \quad A^+ = A_0^+[1-\exp(-y^+/B^+)]^{1/2}, \quad A_0^+ = 27.8, \quad B^+ = 4.8. \tag{51.4}$$

The expression for l in Eq. (51.3) is a modification of the well-known model by Michel et al. [5], [11] (p. 557), where the usual intermittency factor I by Klebanoff [3] has been included. In turn, the associated pronounced decrease of ℓ eliminates the deficiency of the original model to overestimate the turbulence intensities near the BL edge. The sublayer closure, [1], provided by Eq. (51.4) predicts the correct near-wall behavior given by Eqs. (22).

Formally, Eqs. (51.1)–(51.4) represent an appropriate mixing length closure for r in the fully turbulent case in the double limit $T \to \infty$, $X \to \infty$ if the function $\hat{\rho}(x;k,T)$, introduced in Eq. (51.1), is modelled in a way that $\hat{\rho} \sim \rho$. This behavior then also enforces the transition towards the classical small-defect BL for $T \to \infty$ and $x = O(1)$, where Eqs. (51.3) and (51.4) provide a common overlap of the main and the sublayer, according to Eqs. (26) and (28.2), as $\ell \sim \kappa\zeta$ there. In other words, the model provides the widely believed linear variation of ℓ with distance from the wall in the overlap domain, which is usually argued for by bringing forward dimensional reasoning [11]. Specifically, applying the above model to the "universal" sublayer functions $u_0^+(y^+)$ and $s_0^+(y^+)$ yields $s_0^+ = (\kappa\, y^+ l^+ \mathrm{d}u_0^+/\mathrm{d}y^+)^2$, so that u_0^+ then follows from (numerical) integration of Eq. (25), subject to the no-slip condition $u_0^+(0) = 0$; setting $\kappa = 0.384$ here gives $C^+ \doteq 4.8831$, cf. Eq. (26.2), and $s_0^+ \sim a^+ y^{+3} + O(y^{+7/2})$ with $a^+ \doteq 9.16 \times 10^{-4}$.

Nevertheless, Eqs. (51.1)–(51.4) are aimed to predict the Reynolds stress for all positive values of x, Y, T (and k) with satisfactory accuracy, when the quantities ζ, y^+, κ are identified with those defined in Eqs. (27.1), (30.1), (24) and (26.2). This is accomplished efficiently by fixing the "turbulent" BL edge $\eta = \eta_\infty$ as the minimum value of η where f'' is numerically insignificantly small. Then $\eta_\infty \sim T\delta_1/\Delta$ as $T \to \infty$, and the definition

$$\hat{\rho} := 1/\eta_\infty(x;k,T) \tag{51.5}$$

completes the mixing length closure.

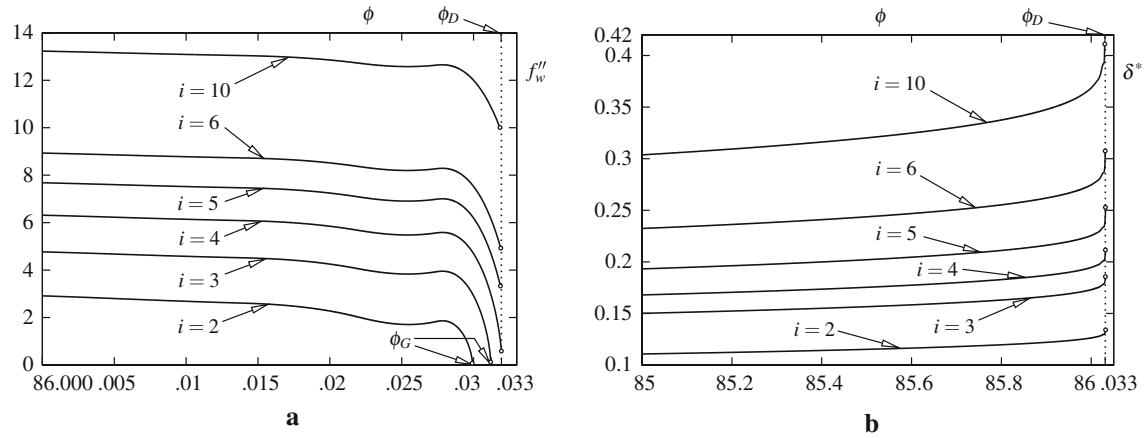

Fig. 3 Numerical solutions of Eqs. (14) and (51), for $k = 0.3$ and $T = i \times 10^4$ over arc angle $\phi\,[^\circ]$ as $\phi - \phi_D(k) \to 0_-$, terminating at $\phi = \phi_G(k, T)$ (positions indicated by *circles*); **a** reduced wall shear stress f''_w, **b** displacement thickness δ^*

6.2 Partially developed turbulent boundary layer near separation

Solutions of the initial-boundary value problem (14), supplemented with Eqs. (51), have been obtained numerically by adopting the method of lines and employing a Keller–Box-type discretization, supplemented with automated adaptive step control in the x-direction. They corroborate the conjecture that the position $x = x_G$ of the Goldstein singularity triggered by the BV singularity, see Eq. (10.2), is shifted downstream for increasing values of k, thereby increasing in strength. Increasing values of T, i.e. increasing turbulence intensities, are expected to foster that downstream shift but, on the other hand, to weaken the strength of the singularity, as turbulent BLs are empirically known to be less prone to separate than the corresponding laminar ones for identical external-flow configurations (i.e. for identical values of k).

This behavior can also be reproduced by calculating solutions for the flow past a circular cylinder with unit radius, as sketched in Fig. 1a, for different values of k and T in a systematic manner, where the potential flow is computed as mentioned briefly in Sect. 3. In order to highlight the consequence of this mechanism, we subsequently discuss solutions of Eqs. (14) for a specific external flow determined by a particular value of k, say, $k = 0.3$. The condition of matching with the external flow in Eq. (14.3) has been satisfied numerically at $\eta = \eta_{\max}$ with $10 \le \eta_{\max} \le 50$, where $\eta_{\max}$ is increased for increasing values of the parameter T. The latter is varied from $T = 0$ up to $T = 10^5$ (higher values result in numerical difficulties which could only be overcome by employing a considerably higher grid resolution). Let $\phi = 180\,x/\pi$ denote the arc angle measured from P_F, see Fig. 2a, hence, the BV singularity is seen to take place at $\phi = \phi_D \doteq 86^\circ\,1'\,54''$, as indicated in Figs. 2b and 3 by vertical dotted lines. The resulting distributions for the reduced wall shear stress and the displacement thickness, given by, respectively, $f''_w := f''(x, 0; k, T)$ and $\delta^*(x; k, T) = \Delta \int_0^\infty (1 - f')\,\mathrm{d}\eta$, are plotted in Fig. 3.

For sufficiently small value of T the BL behaves still laminar-like as the corresponding solutions are found to terminate in form of a Goldstein-type singularity at the location, say, $\phi = \phi_G(k, T)$, i.e. at $x = x_G(k, T)$. That is, f''_w and $\delta^*(x; k, T) - \delta^*(x_G; k, T)$, respectively, vary with $\Delta\phi^{1/2}$, here $\Delta\phi = \phi_G - \phi$, to leading order as $\Delta\phi \to 0_+$. Furthermore, $\phi = \phi_G$ approaches $\phi = \phi_D$ for increasing values of T. Eventually, when T assumes a certain value, say $T = T_D(k)$ (here $T_D \times 10^{-4}$ is slightly below 4), $\phi_G(T_D, k) = \phi_D(k)$. In turn, for $T \ge T_D$ the boundary-layer calculations break down at $\phi = \phi_D(k)$, where f''_w exhibits a finite limit. In fact, the numerical results obtained for relatively large values of T strongly suggest a regular local behavior of the solutions. Consequently, the fully turbulent BL obtained in the limit $T \to \infty$ having a velocity defect of $O(1/\ln T)$, would not separate at all. This result is entirely in line with the analytical investigation given in [9], which applies to a turbulent BL with an asymptotically small velocity deficit as $\phi - \phi_D \to 0_-$, i.e. for $x - x_D \to 0_-$.

From this scenario one then infers that for a certain range of values of k (within the interval $0 < k < 0.5$ in case of the circular cylinder, cf. Subsect. 3) the Goldstein singularity vanishes for critical values of T, denoted by $T_c \ge T_D(k)$. On the other hand, a rational flow description of the local separation process requires that (i) $\Delta\phi = 0$ and, simultaneously, (ii) the Goldstein singularity is vanishingly weak, in order to allow for a viscous/inviscid interaction strategy as in the laminar case, cf. [15]. These conditions suggest that the

streamwise extent of the interaction region is asymptotically small in the limit (1). Therefore, we draw (needless to say, with some caution) the remarkable conclusion that in the BL limit, expressed by the problem posed by Eqs. (14), bluff-body separation is (uniquely) described by critical values $k = k_c$ and $T = T_c = T_D(k_c)$, so that both the above requirements (i) and (ii) are satisfied.

6.3 Transition to fully developed turbulent flow

Considering the case $T \to \infty$ discussed in Subsect. 5.3, reliable solutions of Eqs. (29), (30), subject to Eqs. (14.3), (14.4), are difficult to find due to the extreme thinning of the viscous wall layer as $X \to \infty$ and, therefore, presently available only with limited accuracy. As a first step, however, in Fig. 4a we display the satisfactorily accurate solution of the boundary value problem (40), describing the limiting form of the outer layer as $X \to \infty$. Here l^+, see Eq. (51.4), is correctly replaced by 1, such that $S_1 = (l\, H_1'')^2$, and the sufficiently small cut-off value of the computational domain $10^{-5} \le \zeta \le 1$ accounts for the logarithmic singularity, see Eq. (40.2).

The mixing length closure given by Eqs. (51) enforces the logarithmic law of the wall in the form of Eq. (40.2) and, in turn, transition to a small-defect BL in the limit $X \to \infty$. Nevertheless, the possibility of a large-defect flow, although discarded in Subsect. 5.3 on grounds of considerations regarding the turbulent dynamics, can be taken into account within the framework of the time-mean analysis if the mixing length constant c_ℓ, see Eq. (51.3), is treated as an asymptotically small parameter of $O(\alpha^{1/2})$. The mixing length closure then yields $S_0 = [(\ell/c_l)H_0'']^2$, where Eqs. (51.1) and (51.3) state that $\ell/c_\ell \sim I^{1/2}$, in the following referred to as case (I), in the outermost region of the BL. Although not rigorously justified asymptotically, it is instructive and physically appealing to ascertain the approach of a small velocity defect in the limit (1) by considering numerical solutions $[H_0, S_0](\zeta; \hat\gamma)$ of Eq. (32) that are parametrized by the appropriate coupling parameter

$$\hat\gamma := \gamma_1/c_\ell = O(1), \quad \gamma_1 := \kappa\sigma, \tag{52}$$

see Eq. (35) and the definition of σ in (27.2). Moreover, the match of these self-similar solutions with the then emerging intermediate layer, located between the viscous wall and the main layer and having a thickness of $O(c_\ell^3)$, i.e. of $O(\alpha^{3/2})$, reveals the missing boundary condition $S_0(0; \hat\gamma) = 1$. The latter also holds if a direct match with the viscous wall layer is anticipated, such that the outer and the intermediate layer are treated as a single flow region and, therefore, ℓ is identified with l. Subsequently, this procedure corresponds to case (II).

In addition, since $\alpha = \gamma^2$, Eq. (12) states that $T \sim \gamma_1^2 Re^{1/2}$. From Eqs. (33) and (41) and the definition of δ_1 given by Eq. (27.1) then follows that $\delta_1/x \sim \delta/(\gamma\, x) \sim \gamma\, a(\hat\gamma)$ as $x \to 0$. The results for the thereby (i.e. by the asymptotic theory) expected slope of the BL thickness, $\gamma_1 a(\hat\gamma)$, the suitably defined velocity defect $[1 - H_0'(\zeta; \hat\gamma)]/\gamma$, and the Reynolds shear stress $S_0(\zeta; \hat\gamma)$ are presented in Fig. 4b and Table 1 for different values of $\hat\gamma$, given by Eq. (52), or, equivalently, Re, γ_1, and the aforementioned approximation of T,

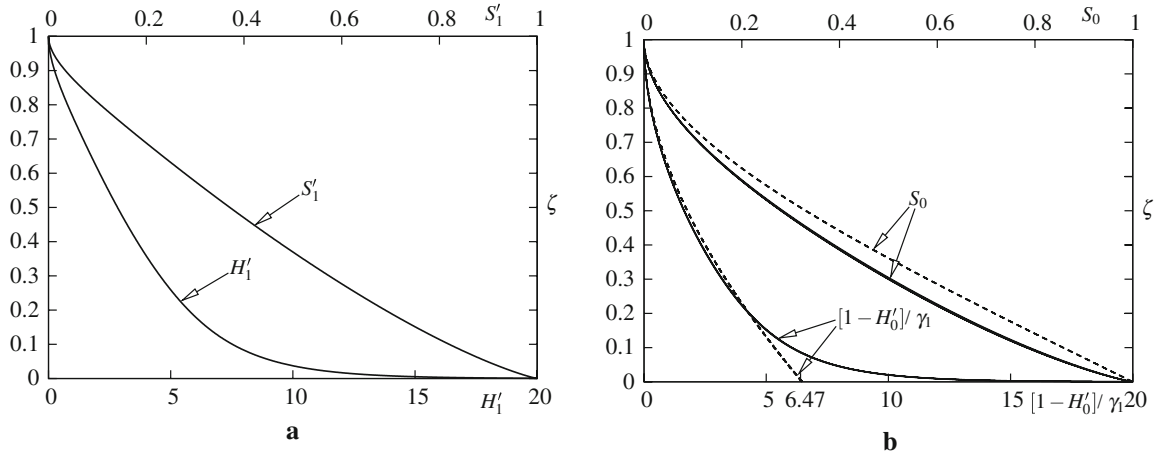

Fig. 4 Numerical solutions of **a** Eqs. (40), giving $\Delta_1 \doteq 0.071658$, $H_1(1) \doteq 3.4888$, and **b** Eq. (32), supplemented with the boundary condition $S_0(0; \hat\gamma) = 1$, for the values of Re given in Table 1

Table 1 Key quantities (rounded values) of the family of solutions of Eq. (32), parametrized by *Re*

lg *Re*	8	10	12	14	16	18	20
$10 \times \gamma_1$	0.20846	0.16677	0.13897	0.11912	0.10423	0.09265	0.08338
$T \sim \gamma_1^2 Re^{1/2}$	4.3	27.8	193.1	1419	10864	85839	695298
$\hat{\gamma}$	0.24525	0.19620	0.16350	0.14014	0.12262	0.10900	0.09810
case (I):							
$\gamma_1 a$	0.11775	0.11633	0.11541	0.11476	0.11427	0.11390	0.11360
$H_0'(0;\hat{\gamma})$	0.86491	0.89200	0.91003	0.92291	0.93256	0.94006	0.94607
$[1 - H_0'(0;\hat{\gamma})]/\gamma_1$	6.48057	6.47632	6.47358	6.47165	6.47022	6.46912	6.46824
case (II):							
$\gamma_1 a$	0.10926	0.10757	0.10647	0.10571	0.10514	0.10471	0.10436

respectively: in both the cases (A) and (B), the data exhibit a remarkable collapse, even for moderate values of lg *Re*. The congruence with the asymptotic limits $[H_1, S_1](\zeta)$, shown in Fig. 4a, becomes more pronounced for increasing values of *Re* (i.e. decreasing values of $\hat{\gamma}$, as one might expect). In fact, the results clearly indicate that $[H_0'(0;\hat{\gamma}),\ a(\hat{\gamma})] \to [1, \infty]$ as $Re \to \infty$, whereas the latter limit is associated with a rather slow convergence $\gamma a \to \Delta_1$, as indicated by the decreasing values of $\gamma_1 a$. Note the arithmetic mean value of the defect of the slip velocity, $[1 - H_0'(0;\hat{\gamma})]/\hat{\gamma} \approx 6.4728$; accordingly, it is found that $\gamma_1 a \approx 0.11515$ in case (I) and $\gamma_1 a \approx 0.10618$ in case (II), respectively. We mention that good agreement of the corresponding results for the class of self-preserving BLs subject to an adverse pressure gradient and having a velocity defect of $O(1)$ with their strictly asymptotically predicted counterparts, showing a velocity defect of $O(\gamma)$, has already been observed by Melnik [4].

The aforementioned transitional flow taking place where $X = O(1)$ is conveniently described in terms of $[H, S](X, \zeta)$ rather than $[F, R](X, \eta)$, see Eqs. (29.1) and (30.1). This choice of the variables advantageously captures the expected pronounced increase of the BL thickness for large values of X. In order to allow for a comparison of the numerical results with the fully turbulent limiting solution $[H_1, S_1](\zeta)$ that is assumed for $X \to \infty$, we introduce a "defect scaling" by redefining the quantities $\gamma_H(X)$, $\rho(X)$, and $\Delta^+(X)$, originally introduced as gauge functions in Eq. (46) where X is considered to be large, in a suitable form valid for $X \geq 0$,

$$\hat{H}(X,\zeta) := (H-1)/\gamma_H, \quad \hat{S}(X,\zeta) := S/\gamma_H^2, \tag{53.1}$$

$$\gamma_H(X) := -\left[\frac{2}{\kappa}\ln\left(\mathrm{e}^{\kappa/2}X + 1\right) + 1\right]^{-1}, \quad \rho(X) := \frac{1}{1 - \Delta_1 X \hat{\gamma}_H}, \quad \Delta^+(X) := \frac{1+X}{\Delta_1 + X}\Delta_1\rho^2. \tag{53.2}$$

The scaling provided by Eq. (53.2) not only properly accounts for the limit $X \to \infty$, expressed in Eq. (46) in the case $\Gamma = 1/\Delta_1$ that conforms to a match with the flow downstream. It also allows for a smooth transition of the solution $[H, S](X, \zeta)$] of Eq. (30.2) for $X \to 0$ towards the Hiemenz flow solution.

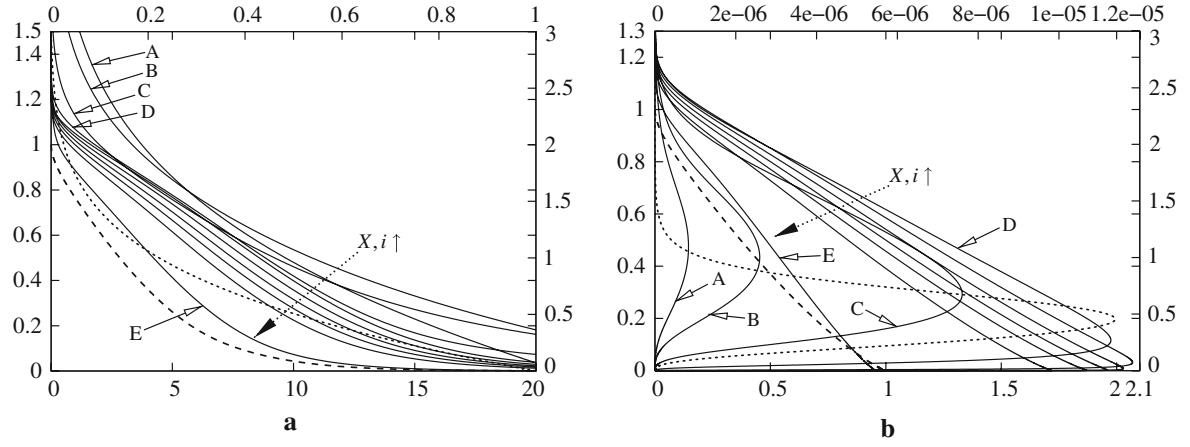

Fig. 5 Distributions for **a** $\hat{H}(X_i, \zeta)$ and **b** $\hat{S}(X_i, \zeta)$, ζ-values indicated by abscissae, values of $\hat{H}$, $\hat{S}$ by ordinates; top abscissae, right ordinates: $X = i = 0$ (Hiemenz solution, *dotted*); bottom abscissae, left ordinates: curves A–D corresponding to i = 1–4, curves in order of direction of *dotted arrows* to i = 5–9, curves E to $i = 10$, *dashed curves* to $H_1(\zeta)$, $S_1(\zeta)$

Hence, we have solved Eq. (30.2) numerically, subject to the boundary and initial conditions (14.3) and (14.4), where in the latter relationships η, $f(\eta)$, and $f_0(\eta)$ are considered to be formally replaced by ζ and $H(0,\zeta)$. Furthermore, here $S=(\ell H'')^2$, where ℓ is given by Eqs. (51.1)–(51.4). Again, the method already explained briefly at the beginning of Subsect. 6.2 has been adopted. The values of ζ vary from 0 to 3. A very accurate solution of the Hiemenz flow problem (14.4), yielding $[H,S](0,\zeta)$, has been obtained by using 1,500 grid points; the subsequent downstream integration of Eq. (30.2) has been carried out by employing further adaptive grid refinement, specifically close to $\zeta=0$, in order to resolve the thin viscous wall layer that emerges as X becomes large. The resulting profiles $[\hat{H},\hat{S}](X_i,\zeta)$, $i=0,1,\ldots,10$, where $X_0=0$ and $X_i=X_1\exp[(i/10)\ln(X_{10}/X_1)]$ for $i=1,2,\ldots,10$, $X_1=100$, $X_{10}=4\times10^6$, are shown in Fig. 5, together with the limiting solution $[H_1,S_1](\zeta)$. The here chosen exponential increase of the specified values of X accounts for the rather slow rate of convergence of the limit process $[\hat{H},\hat{S}](X,\zeta)\to[H_1,S_1](\zeta)$ as $X\to\infty$, due to the logarithmic dependence of the scaling function $\gamma(X)$ on X, cf. Eqs. (53.2) and (46). However, culminating round-off errors result in the above indicated numerical difficulties for X being large and, thus, make the in Fig. 5 indicated near-collapse of the solution for $i=10$ with the profiles $[H_1,S_1](\zeta)$ only conditionally reliable. Also, progressing further downstream by using the current implementation of the numerical method provokes a breakdown of the computations, even for considerably higher grid resolutions.

7 Conclusions and further outlook

The analysis presented so far indicates that neither the assumption of a purely laminar nor a fully turbulent description of a BL evolving from the front stagnation point provide a concept which is feasible to develop a rational description of break-away separation in the limit (1). Therefore, the global complex asymptotic structure of the flow past a bluff body is characterized by a certain level of the turbulence intensities in its attached part. Most interesting, as a consequence of the occurrence of the front stagnation point P_F, cf. Fig. 1, that level, measured by T, is essentially independent of Re: in the limit $T\to\infty$ close to P_F a small region of streamwise extent of $O(1/T)$ accounts for the transition process of the well-known laminar stagnating flow (Hiemenz flow) towards a fully developed turbulent BL flow of the classical two-layer type. However, as strongly substantiated by the numerical results presented in Subsect. 6.2, a rational description of the flow close to separation is severely hampered by the existence of the small streamwise velocity deficit characterizing the outer main part of that BL. As a result, within the framework of BL theory, the (unique) solution to the global flow problem is presumably provided by the solution of Eqs. (14) for a specific choice of the values of both k and T. It is the objective of a currently performed analytical investigation, tied in with that outlined in [7], to rigorously confirm that the classical turbulent BL structure provides no appropriate basis for establishing a local theory of separation. Also, the local qualitative dependence of the solutions on k and T deduced from the numerical results presented in Subsect. 6.2 should be confirmed by a more extensive careful numerical study of Eqs. (14) and (29.2).

A first answer to the question raised in the paper title can now be given as follows: As a consequence of the scaling of the Reynolds shear stress introduced by Eqs. (11) and (12), the BL never attains a fully developed turbulent state, even for $T\to\infty$. That is, the distinguished limit expressed by Eqs. (47.1) and (47.2), originally believed to accompany short-scale transition near P_F towards a fully developed turbulent BL, should be revised in the form given by Eq. (50) in ensuing studies on this topic. Most important, in this presently undetermined form it is still associated with a BL having a velocity defect of $O(1/\ln T)$ along the surface of a bluff body. The associated asymptotic scaling of that BL is described by Eqs. (48.1), rather than by Eqs. (27.1), which govern fully developed turbulent flow. However, the above outlined current status of our knowledge of the asymptotic flow structure near separation suggests that this slightly "underdeveloped" turbulent BL flow is expected to apply only (i) to relatively slender bodies where the BV singularity encountered in the potential flow is correspondingly weak, cf. [15], leading to a laminar-type separation mechanism of the wall-layer flow, or (ii) presumably to an accordingly revised model of bluff-body separation taking place close to the trailing-edge point P_R, cf. Fig. 1, as proposed originally by Neish and Smith [6], cf. [7]. Noteworthy, from matching of the expansions given by Eqs. (27.1) and (31) it is found that the downstream evolution of the transitional BL, emerging for $x=O(1/T)$, as formulated by Eqs. (29), is associated with a specific member of the class of fully turbulent self-preserving BLs, cf. [11]. Hence, the flow governed by Eqs. (30.1) and (40) is considered as the asymptotically correctly described turbulent counterpart to the purely laminar stagnating flow, here expressed by Eq. (14.4); both this limiting turbulent and the possible transitional solution are presented in Figs. 4 and 5, respectively.

Finally, we note that the analysis of the case $T \to \infty$ carried out here can likely be adopted to allow for a rational description of transition of a BL along a flat plate. In analogy to the case of stagnating flow considered here, transition of the Blasius BL is expected to take place close to the leading edge in the limit (1).

Acknowledgements Special thanks are due to Professor Frank T. Smith (Department of Mathematics, University College London) for frank and stimulating discussions.

References

1. Grifoll, J., Giralt, F.: The near wall mixing length revisited. Int. J. Heat Mass Tran. **43**(19), Technical Note, 3743–3746 (2000)
2. Gurevich, M.I.: The theory of jets in an ideal Fluid. Int. Series of monographs in pure and applied mathematics, vol. 93. Pergamon Press, Oxford (1966). Original Russian book: Fizmatlit, Moscow (1961)
3. Klebanoff, P.S.: Characteristics of turbulence in a boundary layer with zero pressure gradient. NACA Report 1247 (1955) [See also: NACA Technical Note 3178, (1954)]
4. Melnik, R.E.: An asymptotic theory of turbulent separation. Comput. Fluids. **17**(1), 165–184 (1989)
5. Michel, R., Quémard, C., Durant, R.: Hypothesis on the mixing length and application to the calculation of the turbulent boundary layers. In: Kline, S.J., Morkovin, M.V., Sovran, G., Cockrell, D.J. (eds.) Proceedings of Computation of Turbulent Boundary Layers—1968 AFOSR-IFP-Stanford Conference, vol. I: Methods, Predictions, Evaluation and Flow Structure, pp. 195–207. Stanford University, Stanford (1969)
6. Neish, A., Smith, F.T.: On turbulent separation in the flow past a bluff body. J. Fluid Mech. **241**, 443–467 (1992)
7. Scheichl, B., Kluwick, A.: Asymptotic theory of bluff-body separation: a novel shear-layer scaling deduced from an investigation of the unsteady motion. J. Fluids Struct. (2008, in print) [See also in: Unsteady Separated Flows and their Control. In: Braza, M., et al. (eds.) Proceedings of the IUTAM Symposium held in Dassia, Corfu Island, Greece, June 18–22, 2007. Springer-Verlag, Dordrecht (2008, in print)]
8. Scheichl, B., Kluwick, A.: On turbulent marginal boundary layer separation: how the half-power law supersedes the logarithmic law of the wall. Int. J. Comp. Sci. Math. (IJCSM) **1**(2/3/4), 343–359 (2007)
9. Scheichl, B., Kluwick, A.: Turbulent shear-layer scaling in the limit of infinite Reynolds number derived from the unsteady equations of motion. Proc. Appl. Math. Mech. (PAMM) **7**(1) (2007, in press), doi:10.1002/pamm.200700526
10. Schewe, G.: Reynolds-number effects in flows around more-or-less bluff bodies. J. Wind Eng. Ind. Aerod. **89**(14), 1267–1289 (2001)
11. Schlichting, H., Gersten, K.: Boundary-Layer Theory, 8th edn. Springer-Verlag, Berlin (2000)
12. Smith, F.T.: The laminar separation of an incompressible fluid streaming past a smooth surface. Proc. R. Soc. Lond. A **356**(1687), 443–463 (1977)
13. Southwell, R.V., F.R.S., Vaisey, G.: Relaxation methods applied to engineering problems. XII. Fluid motions characterised by 'free' streamlines. Phil. Trans. R. Soc. Lond. A **240**(815), 117–161 (1946)
14. Sychev, V.V.: Laminar Separation. Fluid Dyn. **7**(3), 407–417 (1972). Original Russian article In: Izv. Akad. Nauk SSSR, Mekh. Zhidk. i Gaza (3), 47–59 (1972)
15. Sychev, V.V., Ruban, A.I., Sychev, Vic. V., Korolev, G.L.: Asymptotic Theory of Separated Flows. In: Messiter, A.F., Van Dyke, M., (eds.) Cambridge University Press, Cambridge (1998)
16. Tsahalis, D.T., Telionis, D.P.: On the behavior of turbulent boundary layers near separation. AIAA J. **13**(10), Synoptics, 1261–1262 (1975)
17. Zdravkovich, M.M.: Flow Around Circular cylinders. A Comprehensive Guide Through Flow Phenomena, Experiments, Applications, Mathematical Models, and Computer Simulations, vol. 1: Fundamentals. Oxford University Press, Oxford (1997)

5th AIAA Theoretical Fluid Mechanics Conference
23 - 26 June 2008, Seattle, Washington

AIAA 2008-4348

4.9 AIAA Meeting Paper 2008–4348 (2008)

Level of Turbulence Intensity Associated with Bluff-Body Separation for Large Values of the Reynolds Number

Bernhard Scheichl* and Alfred Kluwick†

Vienna University of Technology, A-1040 Vienna, Austria

The paper concerns a rational and physically feasible description of gross separation from the surface of a plane and more-or-less bluff obstacle in an incompressible and otherwise perfectly uniform stream for arbitrarily large values of the globally formed Reynolds number. The analysis is initialized by a remarkable conclusion drawn from recent theoretical results that is corroborated by experimental findings but apparently contrasts common reasoning: the attached boundary layer extending from the front stagnation point to the position of separation at the body surface never attains a fully developed turbulent state, even in the limit of infinite Reynolds number. As a consequence, the boundary layer exhibits a certain level of turbulence intensity that is determined by the separation process governed by locally strong viscous/inviscid flow interaction. This mechanism is expected to be associated with rapid transition of the separating shear layer towards an almost fully developed turbulent state. Here a rigorous asymptotic analysis, essentially carried out without resorting to a specific turbulent closure and supported by a numerical investigation, of the topology of the boundary layer flow close to separation is presented.

Nomenclature

ℓ	Mixing length shape function, see Eq. (85)
$\mathcal{C}$	Curve of free streamline of potential flow
$\mathcal{F}$	Front stagnation point
$\mathcal{G}$	Point of the Goldstein singularity
$\mathcal{R}$	Rear stagnation point
$\mathcal{S}$	Separation point of potential flow
$\mathbf{q}$	Pseudo-vector, used to abbreviate the expansions (21), (31), (40)
$\mathbf{u}$	Velocity vector, see figure 1 (a)
A	Displacement function, see Eqs. (72), (80)
a	Coefficients in expansions (49), (66)
B	Intercept of $\mathcal{O}(1)$ in logarithmic law of the wall, see Eqs. (28), (34), (87)
b	"Bias" $\partial u_e/\partial x$ as $x \to 0_+$
C	Chord length
c	Coefficient (drag/lift)
D	Intercept of $\mathcal{O}(1)$ in logarithmic law of the wall for stagnating flow, see Eq. (37)
E	Quantity of $\mathcal{O}(1)$, entering skin-friction law (38)
F	Defect function, see Eq. (29)
f	Local similarity solution, see Eqs. (63)–(66)
G	Defect function for stagnating flow as $x \to 0_+$, see Eq. (33)
H	Hiemenz flow function, see Eq. (14)

*Postdoctoral Research Fellow, Vienna University of Technology, Institute of Fluid Mechanics and Heat Transfer, Resselgasse 3/E322, A-1040 Vienna, Austria, e-mail: b.scheichl@tuwien.ac.at.

†Full Professor, Vienna University of Technology, Institute of Fluid Mechanics and Heat Transfer, Resselgasse 3/E322, A-1040 Vienna, Austria, e-mail: a.kluwick@tuwien.ac.at, Senior member of AIAA.

Copyright © 2008 by Bernhard Scheichl and Alfred Kluwick. Published by the American Institute of Aeronautics and Astronautics, Inc., with permission.

Level of Turbulence Intensity Associated with Bluff-Body Separation for Large Values of the Reynolds Number

Bernhard Scheichl* and Alfred Kluwick†
Vienna University of Technology, A-1040 Vienna, Austria

The paper concerns a rational and physically feasible description of gross separation from the surface of a plane and more-or-less bluff obstacle in an incompressible and otherwise perfectly uniform stream for arbitrarily large values of the globally formed Reynolds number. The analysis is initialized by a remarkable conclusion drawn from recent theoretical results that is corroborated by experimental findings but apparently contrasts common reasoning: the attached boundary layer extending from the front stagnation point to the position of separation at the body surface never attains a fully developed turbulent state, even in the limit of infinite Reynolds number. As a consequence, the boundary layer exhibits a certain level of turbulence intensity that is determined by the separation process governed by locally strong viscous/inviscid flow interaction. This mechanism is expected to be associated with rapid transition of the separating shear layer towards an almost fully developed turbulent state. Here a rigorous asymptotic analysis, essentially carried out without resorting to a specific turbulent closure and supported by a numerical investigation, of the topology of the boundary layer flow close to separation is presented.

Nomenclature

ℓ	Mixing length shape function, see Eq. (85)
$\mathcal{C}$	Curve of free streamline of potential flow
$\mathcal{F}$	Front stagnation point
$\mathcal{G}$	Point of the Goldstein singularity
$\mathcal{R}$	Rear stagnation point
$\mathcal{S}$	Separation point of potential flow
$\mathbf{q}$	Pseudo-vector, used to abbreviate the expansions (21), (31), (40)
$\mathbf{u}$	Velocity vector, see figure 1 (a)
A	Displacement function, see Eqs. (72), (80)
a	Coefficients in expansions (49), (66)
B	Intercept of $\mathcal{O}(1)$ in logarithmic law of the wall, see Eqs. (28), (34), (87)
b	"Bias" $\partial u_e/\partial x$ as $x \to 0_+$
C	Chord length
c	Coefficient (drag/lift)
D	Intercept of $\mathcal{O}(1)$ in logarithmic law of the wall for stagnating flow, see Eq. (37)
E	Quantity of $\mathcal{O}(1)$, entering skin-friction law (38)
F	Defect function, see Eq. (29)
f	Local similarity solution, see Eqs. (63)–(66)
G	Defect function for stagnating flow as $x \to 0_+$, see Eq. (33)
H	Hiemenz flow function, see Eq. (14)

*Postdoctoral Research Fellow, Vienna University of Technology, Institute of Fluid Mechanics and Heat Transfer, Resselgasse 3/E322, A-1040 Vienna, Austria, e-mail: bernhard.scheichl@tuwien.ac.at.
†Full Professor, Vienna University of Technology, Institute of Fluid Mechanics and Heat Transfer, Resselgasse 3/E322, A-1040 Vienna, Austria, e-mail: alfred.kluwick@tuwien.ac.at, Senior member of AIAA.

h	Surface metric coefficient
i	Counter
J	Reynolds shear stress function as $x \to 0_+$, see Eq. (33)
K	Coefficient in expansions of F_1^* and B_1, see Eqs. (52), (53)
k	BV parameter
l	Mixing length shape function, see Eqs. (85)–(87)
M	Kummer's confluent hypergeometric function
P	Gauge function, rescaled pressure gradient, see Eq. (20)
p	Time-mean pressure
R	Global reference length, given by radius of cylinder
r	Radius, see Eq. (8)
Re	Reynolds number, see Eq. (1)
S	Reynolds shear stress function, see Eq. (29)
s	Local streamwise coordinate, see Eq. (7)
T	Turbulence-level gauge parameter
U	Global reference velocity, i.e. velocity of oncoming parallel flow
u	Time-mean velocity component in x-direction
v	Time-mean velocity component in y-direction
W	Wingspan length
X	Stagnation-flow coordinate in x-direction
x	Distance along body surface measured from $\mathcal{F}$
Y	BL coordinate, see Eq. (11)
y	Distance perpendicular to body surface

Subscripts

$\mathcal{C}$	Value along $\mathcal{C}$
$\mathcal{F}$	Value at $\mathcal{F}$
$\mathcal{G}$	Value at $\mathcal{G}$
$\mathcal{R}$	Value at $\mathcal{R}$
$\mathcal{S}$	Value at $\mathcal{S}$
b	Base of outer defect layer
C	Chord Reynolds number, here $\tilde{C}$ replaces $\tilde{R}$ in Eq. (1)
D	Drag
e	Velocity of external flow evaluated at surface, acting on the BL edge
i	i-th term of asymptotic expansion, i standing for $0, 1, 2, \ldots$
ij	j-th term in i-th term of asymptotic expansion, i and j standing for $0, 1, 2, \ldots$
L	Lift
max	Maximum value
min	Minimum value
p	Particular solution
q	Derivative with respect to q, here standing for x, y, Y, η
t	Total shear stress, see Eq. (19)

Conventions

BL	Boundary layer
BV	Brillouin–Villat
ODL	Outer defect layer, see figure 3
VWL	Viscous wall layer, see figure 3
q^*	q meaning any quantity of $\mathcal{O}(1)$, representative for sublayer of outer defect region, see § III.B.1
$\bar{q}$	q meaning any quantity of $\mathcal{O}(1)$ satisfying linearized BL problem as $s \to 0_-$, see Eqs. (57), (59)–(61)
$\hat{q}$	q meaning any quantity of $\mathcal{O}(1)$, representative for nonlinear flow region, see § III.B.3
I_i	Modified Bessel function of order i, $i = 0, 1$, see Eq. (54)
K_i	Modified Bessel function of order i, $i = 0, 1$, see Eq. (54)
u', v'	Turbulent fluctuations of u, v
u_T	Turbulent reference velocity, see Eq. (17)
$\langle \cdots \rangle$	Reynolds-averaged quantity, latter indicated by dots

Symbols

α Gauge function, see Eq. (62)
β Constant in closure for $l+$, see Eq. (87)
χ Perturbation parameter, see Eq. (29)
Δ Scaled thickness of turbulent BL, see Eq. (30)
δ Relative thickness of turbulent BL, see Eq. (30), figure 1 (b)
ϵ Gauge function, see Eq. (22)
ε Constants of $\mathcal{O}(1)$ in near-wall behavior of Σ^+ and Ψ^+, see Eq. (25), (26)
η Turbulent BL coordinate, see Eq. (30)
Γ Quantity in closure for $l+$, see Eq. (87)
γ Gauge function measuring velocity defect, see Eq. (22), figure 1 (b)
ι Similarity variable of Goldstein region, see Eq. (84), figure 3
κ V. Kármán constant, see Eq. (28)
$\varkappa$ Surface curvature
Λ Coefficient determining wall shear perturbation, see Eq. (65)
λ Gauge function, see Eq. (40)
ν Kinematic viscosity
Ω Reduced wall shear, see Eq. (88), figure 5
ω Constant governing Goldstein singularity, see Eqs. (81)–(83), (89)
Φ Total head in Bernoulli's equation (79)
ϕ Arc angle, measuring position on cylinder surface from $\mathcal{F}$
φ Constant in closure for $l+$, see Eq. (87)
π Gauge function, measuring pressure gradient, see Eq. (58)
Ψ Stream function for BL, see Eq. (11)
ψ Stream function
Σ Reynolds shear stress function, see Eq. (11)
σ Perturbation parameter, see Eq. (29)
τ Perturbation parameter, see Eq. (38)
θ Local polar angle, see Eq. (8)
ϑ Variable of integration
Υ Displacement thickness, see Eq. (88), figure 5
ϱ Density
Ξ "Bias" $\mathrm{d}\Delta_1/\mathrm{d}x$ of thickness of turbulent BL as $x \to 0_+$, see Eq. (33)
ξ Goldstein coordinate in x-direction, see Eq. (81)
ζ Local similarity variable, see Eq. (63)

Superscripts

$'$ Derivative
$+$ Quantity expressed in wall layer scaling, see Eq. (16)
$\sim$ Dimensionful quantity
$\breve{\eta}$ Reduced η, see Eq. (54)

I. Introduction

NOTWITHSTANDING its principal importance for providing a sound basis to predict the extremes of safe flight conditions (i.e. of drag and lift), as well as effective methods of flow control, the rational time-mean description of massive BL separation from a relatively thick airfoil must, unfortunately, still be regarded as one of the most challenging unsolved basic problems in theoretical fluid mechanics. We shall be concerned with this issue in the present paper, where, for the sake of simplicity and clearness, the analysis is restricted to incompressible nominally steady and two-dimensional flow of a fluid with uniform density and viscosity.

I.A. Motivation

The answer to the question, what really has hampered so far a rigorous treatment of this fundamental problem, is probably provided by the fact that it essentially comprises five particular issues, each of them undoubtedly posing a challenge, and their rather complex interplay:

(i) the asymptotically correct picture of the flow past a curved obstacle (having a smooth impermeable rigid surface) on a spatial scale comparable with the body dimensions as the governing parameter, namely the globally formed Reynolds number, Re, takes on arbitrarily large values;

(ii) the presumably locally concentrated mechanism of transition of the originally laminar flow near the leading-edge or front stagnation point $\mathcal{F}$ towards a more-or-less pronounced turbulent BL further downstream as $Re \to \infty$;

(iii) the asymptotic structure of the attached portion of the BL downstream of the location of transition;

(iv) the development of a local asymptotic theory of self-induced separation, which (presumably) in essence requires the description of strong BL interaction, allowing for a gradual transformation of the BL into a separated shear layer;

(v) finally, the description of the separated-flow regions (i.e. separated shear layer, weakly recirculating separated flow region in the lee side of the obstacle, downstream-evolving wake flow).

An attempt to rigorously tackle the questions (i)–(iii) has been made by the authors in a recent preceding study, see Ref. 1. First, there they have (convincingly) outlined that in the limit $Re \to \infty$ the time-averaged global flow is to be sought in the class of the well-known Helmholtz–Kirchhoff-type flows that exhibit free streamlines which depart smoothly from the surface in $\mathcal{S}$.[2,3] Secondly, the authors have seized a physically appealing suggestion to cope with the ab initio unknown level of turbulence intensity – or, equivalently, the order of magnitude of the Reynolds stresses – in the part of the BL that stretches from $\mathcal{F}$ to the position of separation, which must be attributed to Neish and Smith, see Ref. 4: in that previous work on the BL flow past a bluff body flow a classical, i.e. Prandtl-type, BL-formulation is adopted, where the included Reynolds shear stress is assumed to be proportional to a so-called turbulence intensity gauge factor, T, that may assume arbitrarily large values also as $Re \to \infty$.

Amongst others, it has been demonstrated in those preceding studies that in the limit $T \to \infty$ the BL structure is closely related to that of a fully developed turbulent BL which is characterized by the commonly accepted two-tiered asymptotic splitting.[5] As has been pointed out in Refs. 4, 6, this type of a turbulent BL refers to firmly attached flows only, as the interplay between the small relative streamwise velocity deficit of $\mathcal{O}(1/\ln Re)$ in the outer main layer and the comparatively transcendentally thin viscous wall layer is found to preclude a rational description of separation on the basis of first principles (a brief rationale is presented in § V). On the other hand, by considering the aforementioned "mixed" laminar–turbulent BL[1,4] in the limit $T \to \infty$, the velocity deficit is seen to be of $\mathcal{O}(1/\ln T)$, whereas the ratio of the thicknesses of the outer and the wall layer is of $\mathcal{O}[(\ln T/T)^2]$. Most important, as already indicated in Ref. 4, it is very likely that the in item (iv) above raised demand to devise a local interaction theory then can be accomplished on condition that T essentially shows a specific algebraic dependence on Re as $Re \to \infty$. Furthermore, in striking contrast to the well-established local asymptotic theory of purely laminar separation,[7,8] in the turbulent case the well-known so-called BV condition (namely, of an asymptotically weak BV singularity of the potential flow in $\mathcal{S}$) does not hold, despite some close formal resemblances the formulation of the underlying triple-deck problem is expected to bear.

Instead of directly focussing on this particular distinguished limit and the associated local description of separation (and, in turn, heading to the above point (v) then), we feel it much more instructive to initially elucidate the further differences and analogies between the behavior of purely laminar BL flow and that assumed in the large-T limit as separation is approached. Thus, this paper deals with the BL equations in the limit $T \to \infty$, where the driving external Kirchhoff-type flow is parametrized by the so-called BV parameter k that measures the strength the BV singularity and its position on the obstacle surface, indicated by $\mathcal{S}$. The solutions of the BL equations are found to terminate in form of a Goldstein-type singularity[9,10] taking place at $\mathcal{G}$, upstream of $\mathcal{S}$, for $T \geq 0$. Hence, particular emphasis is placed on highlighting the local structure of this singular behavior in dependence of k as $T \to \infty$, when $\mathcal{G}$ approaches $\mathcal{S}$. Since the flow description presented here solely relies on the BL approximation, it is, therefore, inevitably accompanied by the occurrence of those singularities. That is, it is rendered uniformly valid (and physically realistic) except within an asymptotically small region encompassing both singularities in the limit $T \to \infty$. We note that an asymptotically correct global formulation of the separation process then will be completed in a subsequent separate treatment of the above quoted topics (iv) and (v).

I.B. Status Quo of Research

Before we commence the analysis as suggested above, it is useful to first itemize the most important preliminary results it is based on.

- It is well-known that the potential flow past a more-or-less blunt body (with a, respectively, smooth, wedge-, or cusp-shaped trailing edge) that exhibits free streamlines (confining an open or closed cavity) can be mapped onto that about a circular cylinder by means of conformal mapping. Also, the structure of the attached BL flow that stretches from $\mathcal{F}$ to $\mathcal{G}$ is found to be qualitatively independent of the specific distribution of the imposed pressure gradient for all positive values of T.[1] Most important, in the limit $T \to \infty$ the local behavior of the solutions of the BL equations immediately upstream of $\mathcal{G}$ depends essentially only on the structure of the BV singularity.[2,3] As a consequence, any local and global theories that cope with the issues (iv) and (v) above are expected to predict all the properties which are important for a comprehensive understanding of break-away separation independently of the specific choice of the imposed Kirchhoff-type flow. Therefore, the case of a circular cylinder, exposed to strictly uniform cross flow, is supposed to provide the "canonical" situation, sketched in figure 1 (a). In turn, the Reynolds number is introduced in the form

$$Re := \tilde{U}\tilde{R}/\tilde{\nu} \to \infty. \tag{1}$$

  Note that is assumed in figure 1 (a) that the Goldstein singularity takes place upstream of $\mathcal{S}$ and (coincides asymptotically with the separation point.

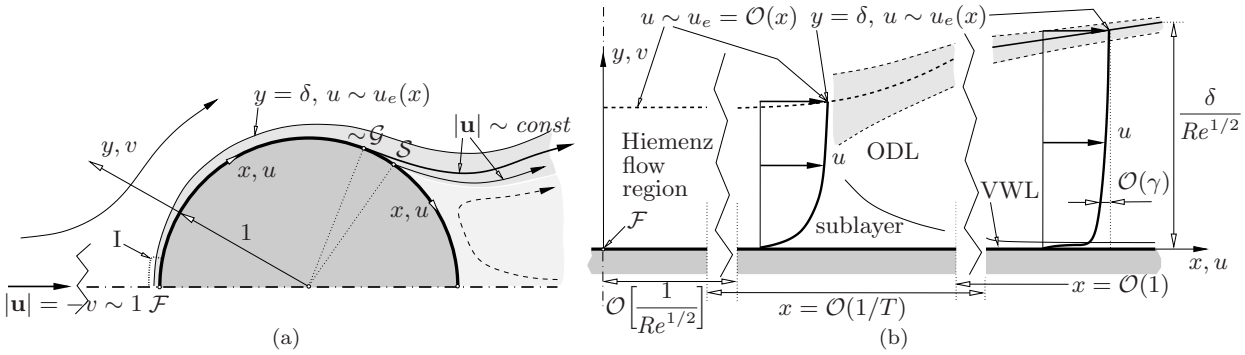

Figure 1. Flow configuration (non-dimensional representation, curvilinear coordinates x, y): (a) global (canonical case, dark-shaded region: BL and separated shear layer, light-shaded region, broken streamline: weakly recirculating flow), (b) region I, asymptotic splitting in the limit $T \to \infty$ near $\mathcal{F}$ (shaded: viscous superlayer, not considered here).

- In the following, we consider an attached BL that behaves "as turbulent as possible", such that T is "as large as possible" as $Re \to \infty$. However, it is interesting to note that the numerical analysis of the BL equations put forward in Ref. 1 points to a second, different picture of massive separation in the limit (1), not pursued further here (cf. § IV.B): in that case, both k and T assume specific (positive) values, such that the Goldstein singularity is vanishingly weak and, simultaneously, $\mathcal{G}$ coincides with $\mathcal{S}$. We note that, for the time being, it is fully unclear whether this limiting solution of the BL equations allows for a self-consistent flow description.

- The analysis of the contrasting case $T \to \infty$ presented in Ref. 1 strongly suggests a rather remarkable property of BL flow issuing from a stagnation point, namely, that T is bounded from above by $\mathcal{O}(Re^{1/2})$. Most important, the (hypothetical) limit $T = Re^{1/2}$ refers to a fully developed turbulent BL that exhibits the well-known two-layer structure,[5] which is essentially governed by perfect equilibrium between the wall shear stress and the sum of the molecular and the turbulent stresses. In that case, however, the Reynolds-averaged Navier–Stokes equations, non-dimensional with $\tilde{U}$, $\tilde{R}$, $\tilde{\nu}$, and the density $\tilde{\varrho}$, would be fully retained (except for curvature effects) in the limit (1) in a square region showing an extent of $\mathcal{O}(Re^{-1/2})$ close to $\mathcal{F}$. The thereby reduced Reynolds number, relevant for the flow in this small region, then has the value 1. Therefore, it is rather unlikely that transition towards fully developed turbulence can develop there. Consequently, we expect a BL type flow in a

region which stretches of $\mathcal{O}(1/T)$ from $\mathcal{F}$, i.e. of asymptotically larger extent than that normal to the wall of $\mathcal{O}(Re^{-1/2})$. We will revert to this consideration in connection with the analysis given in § II.

- Hence, it has been demonstrated in Ref. 1 that this flow, associated with a slightly "underdeveloped" turbulence intensity level ($T \ll Re^{1/2}$), gives rise to a BL that still exhibits the conventional two-tiered asymptotic splitting, known from a fully developed turbulent BL ($T = Rey^{1/2}$),[5] as it evolves along the obstacle surface. The resulting flow splitting is shown in figure 1 (b), where the scalings are derived in § III.A. It is found, amongst others, that the (non-dimensional) BL thickness is of $Re^{-1/2}T/\ln T$. However, the order of magnitude of T in terms of Re as $T \to \infty$ is not known in advance but is expected to be fixed by the answer to the issue (iv) given in § I.A. Here, two strategies are possible to follow, in principle: first, the case $k > 0$ but independent of T, considered in the following. The second possibility assumes $k \to \infty$ as $T \to \infty$ and is tied in with the analysis of trailing-edge flow presented in Refs. 4,6. That is, in the latter case the imposed potential flow is considered as the slightly perturbed well-known strictly attached inviscid-flow solution, having a rear stagnation point $\mathcal{R}$. This will be pursued further in a different study.

- Indeed, the wind tunnel experiments carried out by Schewe[11] strongly suggest that the BL indeed never attains a fully developed turbulent state, even for arbitrarily large values of Re_C. This remarkable (although still tentative) conclusion is drawn from the visualization of oil flow film measurements of the separating flow past the suction side of a more-or-less plane and thick airfoil (aspect ratio $\tilde{W}:\tilde{C} = 6:1$, angle of attack of 12°). Let us first consider the distributions of the drag and lift coefficients c_D and c_L, respectively, shown in figure 2 on the following page (b): here the typical jump-like changes for $Re_C \approx 3.5 \times 10^5$ (associated with hysteresis effects, as indicated by arrows), $Re_C \approx 2.5 \times 10^6$, and $Re_C \approx 7.5 \times 10^6$ reflect the transitions from so-called sub- to trans-, trans- to super-, and, finally, super- to postcritical BL flow, cf. Ref. 12; the extents of these particular flow regimes are indicated by vertical dotted lines. The first three of these notations are commonly adopted to categorize bluff-body flow by attempting to isolate the location of transition to a developed turbulent shear layer, namely – in order of their appearance – downstream, in the immediate vicinity of, and upstream of the position of time-mean separation. In the supercritical regime the location of transition is apparently shifted towards $\mathcal{F}$ as Re_C increases. The postcritical flow is usually believed to be topologically equivalent to its asymptotic state, assumed in the limit $Re_C \to \infty$, as transition then already takes place close to $\mathcal{F}$.[12] Consequently, one is tempted to argue that the upper and lower snapshots of the instantaneous flows displayed in figure 2 (a) refer to, respectively, trans- and fully turbulent supercritical, i.e. postcritical, BL flows. In the first case transition of the separating laminar BL towards a separated turbulent shear layer is associated with the formation of highly three-dimensional vortex structures. However, even in the latter case the streamline pattern of the attached part of the shear layer still shows laminar-like characteristics, where the typical turbulent spots, originating from wall layer bursts, are obviously absent. Most remarkable, in figure 2 (a) the line of separation is clearly visible, and three-dimensionality and unsteadiness are found to be much weaker than in the former case. Therefore, this image can hardly be associated with what is commonly referred to as "fully developed turbulent" flow. We note that to our knowledge corresponding measurements for $Re_C > 7.7 \times 10^6$ are currently not available.

Needless to say, the above interpretation of Schewe's data bears some undeniable uncertainties. The present paper, tied in a series of preceding studies on this topic, attempts to shed light on this remarkable finding from a theoretical point of view.

II. Problem Formulation

Here and in the following all lengths, velocities, and the pressure are non-dimensional with, respectively, $\tilde{R}$, $\tilde{U}$, and $\tilde{\varrho}\tilde{U}^2$. Furthermore, let us adopt natural coordinates x, y, according to figure 1 (a). Then the continuity equation is satisfied identically as $u = \partial\psi/\partial y$, $hv = -\partial\psi/\partial x$. Herein $h = 1 + \varkappa(x)\, y$, where the surface curvature $\varkappa(x) = \mathcal{O}(1)$ in general and taken to be positive for a convex body contour; note that $\varkappa \equiv 1$ for the canonical case of a circular cylinder of radius $\tilde{R}$. The time- or, (due to a well-known result of ergod theory) equivalently, Reynolds-averaged Navier–Stokes equations then read (cf. Ref. 13, p. 81)

$$h(\psi_y\partial_x - \psi_x\partial_y)\psi_y - \varkappa\,\psi_x\psi_y = -hp_x - h\langle u'^2\rangle_x - (h^2\langle u'v'\rangle)_y + Re^{-1}h^2(\nabla^2\psi)_y, \tag{2}$$

$$(\psi_x\partial_y - \psi_y\partial_x)(h^{-1}\psi_x) - \varkappa(\psi_y)^2 = -hp_y - (h\langle v'^2\rangle)_y - \langle u'v'\rangle_x + \varkappa\langle u'^2\rangle - Re^{-1}(\nabla^2\psi)_x, \tag{3}$$

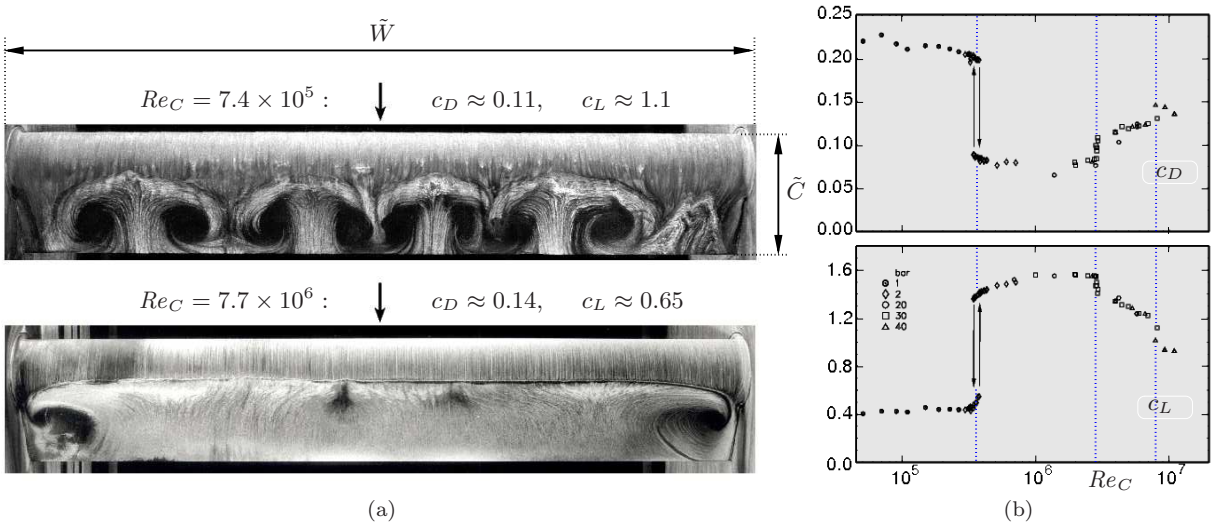

(a) (b)

Figure 2. Measurements on gross separation on the suction side of an airfoil (images by courtesy of and made available by G. Schewe): (a) oil flow film visualizations (vertical arrays indicate main flow direction), (b) c_D and c_L versus Re_C, increasing values (in bar) of the suction pressure of the measuring section of the wind tunnel give increasing values of Re_C (logarithmic scale).

where $\nabla^2 = h^{-1}[\partial_x(h^{-1}\partial_x) + \partial_y(h\partial_y)]$ is the Laplacian. The equations of motion (2), (3) are subject to the usual no-slip condition,

$$y = 0: \quad u = v = u' = v' = 0, \tag{4}$$

and the requirement for unperturbed parallel incident flow, having a velocity of magnitude 1, for $y \to \infty$, see figure 1 on page 5. With respect to the subsequent analysis, we tacitly assume that all components $\langle u'^2\rangle$, $\langle u'v'\rangle$, $\langle v'^2\rangle$ of the Reynolds stress tensor are of equal magnitude for given positive values of x and y (common hypothesis of locally isotropic turbulence).

For moderate levels of the turbulence intensity in the BL that emerges in the limit (1) adjacent to the body surface, the latter is seen to be structurally of traditional laminar (i.e. Prandtl-) type.[1] Let us first consider the external flow.

We anticipate the outer expansion[1]

$$[\psi, p] \sim [\psi_0, p_0](x, y; k) + \mathcal{O}(Re^{-1/2}), \quad y = \mathcal{O}(1), \tag{5}$$

such that the impressed external flow described by ψ_0, p_0 is sought in the one-parameter family of Kirchhoff flows, exhibiting free streamlines that confine an (open or closed) cavity and depart at $x = x_{\mathcal{S}}(k)$ from the surface, see figure 1 on page 5. That potential-flow solution is uniquely determined by the non-negative BV parameter k. Specifically, the surface slip velocity $u_e(x; k)$, given by $\partial_y\psi_0$ evaluated for $y = 0$, then exhibits the asymptotic behavior

$$u_e \sim b(k)\, x + \mathcal{O}(x^2) \quad (b > 0), \qquad x \to 0_+, \tag{6}$$

$$u_e/u_{e,\mathcal{S}} \sim 1 + 2k(-s)^{1/2} + 10k^2(-s)/3 + \mathcal{O}\big[(-s)^{3/2}\big], \qquad s = x - x_{\mathcal{S}} \to 0_- \,. \tag{7}$$

Equation (6) reflects the well-known behavior of the potential flow near a (front) stagnation point, and Eq. (7) states that k measures the strength of the so-called BV singularity taking place at $x = x_{\mathcal{S}}$. Equation (7) stays formally intact even for arbitrarily small values of k if considered as an expansion in the independent double limit $s \to 0_-$, $k \to 0_+$. Note that in the inviscid limit $|\mathbf{u}| \equiv u_{e,\mathcal{S}}(k)$ along $\mathcal{C}$, where $u_{e,\mathcal{S}} = 1$ in case of an open cavity, (according to the definition of $\tilde{U}$), and $u_{e,\mathcal{S}} < 1$ otherwise. Both the derivation of Eq. (7) and the method[3] adopted to obtain global potential-flow solutions, including $u_{e,\mathcal{S}}$ as a function of k, will be presented in a subsequent related study. A brief discussion of the potential flow, based on the numerically obtained solutions, is presented in § IV.A. For the sake of completeness, however, here we mention that the expansion (7) can be calculated from the local behavior of the stream function as $s \to 0_-$, suitably expressed

in polar coordinates,

$$[s, y] = [r\cos\theta, r\sin\theta], \quad r \geq 0, \quad 0 < \theta \leq \pi/2, \tag{8}$$

$$\psi_0/u_{e,\mathcal{S}} \sim r\sin\theta - (4k/3)\, r^{3/2}\cos(3\theta/2) - (5k^2/3)\, r^2 \sin(2\theta) + \mathcal{O}(r^{5/2}), \quad k \geq 0, \quad r \to 0. \tag{9}$$

Also, we briefly mention a procedure how the shape $y = y_{\mathcal{C}}$ of the free streamline that departs from the surface in $\mathcal{S}$ can be determined locally from Eq. (9): this expansion formally ceases to be valid near $\theta \sim (4k/3)r^{1/2}$, which gives the leading-order term in the form

$$y_{\mathcal{C}} \sim (4k/3)s^{3/2} + \mathcal{O}\big(s^{5/2}\big), \quad s \to 0_+ \tag{10}$$

by exploiting the property $\psi_0 = 0$ for $y = y_{\mathcal{C}}$. Note that higher-order terms in Eq. (10) can be calculated recursively in this manner, where those in Eqs. (7) and (9), respectively, are due to the requirement of constant velocity along $\mathcal{C}$.

Concerning the description of the attached BL for $0 \leq x < x_{\mathcal{S}}$, we closely follow Refs. 1, 4. In the inner expansion,

$$[\psi, -\langle u'v'\rangle] \sim Re^{-1/2}[\Psi(x, Y; k, T),\, T\Sigma(x, Y; k, T)] + \mathcal{O}(Re^{-1}), \quad Y = Re^{1/2}\, y, \tag{11}$$

the so-called turbulence-level gauge factor T that accounts for the magnitude of the Reynolds stresses (i.e. the turbulence intensity) in the BL is assumed to be a constant of $\mathcal{O}(1)$, in general. Substitution of Eq. (11) into the governing equations (2)–(4) and taking into account Eq. (6) then gives rise to the leading-order BL problem, describing a generic BL that prevails in a transitional (i.e. neither laminar, nor fully turbulent) state,

$$\Psi_Y\Psi_{Yx} - \Psi_x\Psi_{YY} = -p_{0x}(x, 0; k) + T\Sigma_Y + \Psi_{YYY}, \quad p_{0x}(x, 0; k) = -u_e u_{ex} \tag{12}$$

$$Y \to 0: \quad \Psi \to 0, \quad \Psi_Y \to 0, \quad \Sigma = \mathcal{O}(Y^3), \qquad Y \to \infty: \quad \Psi_Y - u_e \to 0, \quad \Sigma \to 0, \tag{13}$$

$$x \to 0_+: \quad \Psi/(b^{1/2}x) \to H(b^{1/2}Y), \quad \Sigma = \mathcal{O}(x^2). \tag{14}$$

From the last relationships one infers that Ψ matches with the (from the analysis of laminar flows) well-known Hiemenz solution[13] of the full equations (2)–(4) of motion in the limit (1), which holds near $\mathcal{F}$ where x, y are both of $\mathcal{O}(Re^{-1/2})$: $\psi \sim b^{1/2}x\, H(b^{1/2}Y) + \mathcal{O}(Re^{-1})$, with

$$H'^2 - HH'' = 1 + H''', \quad H(0) = H'(0) = H'(\infty) - 1 = 0. \tag{15}$$

Equations (12)–(15), supplemented with an distribution $u_e(s; k)$, characteristic of the impressed inviscid flow, represent a well-posed initial-boundary value problem for Ψ, provided that Σ is modelled such that it exhibits the required asymptotic properties, expressed in Eqs. (13), (14). Note that the behavior of Σ for $x \to 0_+$ reflects the quite obvious (and by any commonly adopted closure provided) proportionality between the Reynolds stress components and u_e^2, in respect of Eq. (6). In turn, the purely laminar case is simply obtained for $T = 0$. In order to take into account the effect of turbulence, we seek "non-trivial" solutions of Eqs. (12)–(14), i.e. such having $\Sigma \not\equiv 0$ for $T > 0$.

In particular, we subsequently focus on the pronounced turbulent case, associated with the limit $T \to \infty$. To be more precise, it is the primary goal of the present study to elucidate the behavior of these limiting solutions immediately upstream of the BV singularity, expressed by the expansion (7).

Most important, in a flow region close to $\mathcal{F}$ that is characterized by $x = \mathcal{O}(1/T$ and $Y = \mathcal{O}(1)$ in the limit $T \to \infty$, the original problem is seen to be formally fully retained in leading order when u_e is represented by bx, see Eq. (6). However, there the full equations of motion (2), (3) allow for a BL approximation of their streamwise component, Eq. (2), only if $T = o(Re^{1/2})$. This is true as long as $T \ll Re^{1/2}$, which is assumed in the following in agreement with the considerations already outlined in § I.B.

III. Large-T Boundary Layer

In the following, the notation "turbulent BL" is adopted for the flow described by Eqs. (12) and (13) in the limit $T \to \infty$. We now focus on the resulting asymptotic structure of that BL, specifically on its behavior near $\mathcal{S}$. It is well-known that in the purely laminar case (for $T = 0$) solutions of the BL problem Eq. (12)–(14) terminate in form of Goldstein singularity for $k > 0$, i.e. if the BV singularity exhibits a finite strength;[2,7] a similar situation has been found for $T > 0$.[1] We now investigate this behavior, by assuming that T takes on arbitrarily large values.

III.A. Initially Attached Flow

In Eq. (12) the Reynolds stress term predominates its viscous counterpart for large values of T if $x = \mathcal{O}(1)$ and Y is sufficiently large, i.e. in the main portion or, equivalently, the fully turbulent region of the BL. Consequently, the problem given by Eqs. (12)–(15) then is singularly perturbed in an (at least) twofold manner,[1] since both shear stress contributions are found to be of the same order of magnitude in two different flow regimes: first, in the so-called transitional-flow region close to $\mathcal{F}$ and sketched in figure 1 on page 5 (b), where rapid laminar–turbulent transition takes place, so that both the suitable streamwise coordinate $X = b^{1/2}\,Tx$ and Y are quantities of $\mathcal{O}(1)$ there; secondly, in the so-called viscous wall layer that is located adjacent to the surface as it evolves from the transitional-flow region, i.e. in the limit $X \to \infty$.

We note that there exists, in addition, a relatively slender so-called superlayer on top of the main region, which is expected to develop from the transitional-flow region also as it accounts for the relatively pronounced outer edge of the turbulent BL and, hence, separates the turbulent motion from the ambient mainly irrotational flow, cf. Ref. 13. However, this overlayer is disregarded here as its existence is rather of minor importance for the understanding of the basic properties the turbulent BL flow which are of interest subsequently. Therefore, by considering Eqs. (12) and the far-field boundary conditions in Eq. (13)), in the following a sharp line $Y = \delta(x; k, T)$, with δ to be determined, will be taken to represent the BL edge with asymptotically sufficient accuracy.

As the process of matching the asymptotic expansions of the flow quantities in those two domains of non-uniformity and with the main layer, respectively, turns out to be essentially governed by the properties of the viscous wall layer, we consider the latter region first. Moreover, a rational description of the turbulent BL, based on minimum of physically motivated assumptions, is advantageously build up from the analysis of that wall region, as the source of the turbulent motion: the turbulent motion originates from its more-or-less universal dynamics that takes place close to the surface;[1] for a more elaborate overview on this topic we refer to Refs. 14–16.

III.A.1. Viscous Wall Layer

The two following basic properties of that region found in the (hypothetical) limiting case $T = Re^{1/2}$ of a fully developed turbulent BL apply unchanged here, cf. Ref. 1:

(A) the time-mean and fluctuating velocity components are of the same order of magnitude, such that $u'v'$ is (at least for most fractions of time) of $\mathcal{O}(u^2)$, and the correlation $\langle u'v'\rangle$ is of $\mathcal{O}(TRe^{-1/2}u^2)$;

(B) for initially firmly attached flow, the imposed pressure gradient, given by $-u_e u_{e_x}$, does not enter the leading-order approximation of Eq. (12).

Due to the scaling anticipated in item (A), convective terms in Eq. (12) are negligibly small. As a consequence of the assumption made in item (B), the BL equation then reduces to the well-accepted balance between the wall shear stress and the sum of the Reynolds and the molecular shear to leading order. The latter is commonly believed to be universal, or in perfect "equilibrium", for all types of turbulent wall-bounded shear flows, as it is considered to be independent of x.[1,14–16] The corresponding wall layer scaling fully agrees with that deduced from usually adopted closure schemes for Σ.[4] In turn, we appropriately set

$$\Psi = \Psi^+(x, Y^+; k, T)/T, \quad \Sigma = u_T^2\Sigma^+(x, Y^+; k, T), \quad Y = Y^+/(Tu_T). \tag{16}$$

Herein, the quantities denoted by the superscript "+" are assumed to be of $\mathcal{O}(1)$. Also, since $-\langle u'v'\rangle$ is seen to be of $\mathcal{O}(TRe^{-1/2}u_T^2)$, the term $Re^{-1/4}T^{1/2}u_T$ is appropriately interpreted as the skin-friction velocity, i.e. the square-root of the wall-shear stress $Re^{-1}\partial u/\partial y$ evaluated at $y = 0$, in agreement with item (A) above. Here we conveniently express it by making use of the BL scaling in the form

$$u_T := [\Psi_{YY}(x, 0; k, T)/T]^{1/2}. \tag{17}$$

Then the BL equations (12) are transformed into the single one

$$\partial_{Y^+}\Sigma_t^+ = P^+ + (Tu_T)^{-2}\big[(\partial_x u_T)(\partial_{Y^+}\Psi^+)^2 + u_T(\partial_{Y^+}\Psi^+\,\partial_{xY^+}\Psi^+ - \partial_x\Psi^+\,\partial^2_{Y^+}\Psi^+)\big]. \tag{18}$$

Herein, the sum of the Reynolds and the viscous shear stress, the so-called total shear stress, is written as

$$\Sigma_t^+ := \Sigma^+ + \partial^2_{Y^+}\Psi^+, \tag{19}$$

and P^+ denotes the rescaled imposed pressure gradient,

$$P^+ := -u_e u_{ex}/(T^2 u_T^3) \to 0, \quad T \to \infty. \tag{20}$$

Then the aforementioned stress balance suggests the expansions

$$\mathbf{q}^+ \sim \mathbf{q}^+_{00}(Y^+) + P^+[\mathbf{q}^+_{11}(Y^+) - \gamma^2 \mathbf{q}^+_{12}(Y^+) + \mathcal{O}(\gamma^3)] - \epsilon\,[\mathbf{q}^+_{21}(x, Y^+; k) + \mathcal{O}(\gamma)], \quad \mathbf{q}^+_{ij} := [\Psi^+_{ij}, \Sigma^+_{ij}], \tag{21}$$

provided that the gauge functions are given by

$$\gamma := u_T/u_e \to 0, \quad \epsilon := 1/(T u_T)^4 \to 0, \quad T \to \infty. \tag{22}$$

Note the following three restrictions that lead to the specific form of the expansion (21), where consistency will be shown later: (i) eigensolutions that are due to matching with the flow quantities in the transitional-flow region have been omitted as they do not affect the main results of the subsequent analysis; (ii) it anticipates the relationship

$$\gamma_x = \mathcal{O}(\gamma^2), \tag{23}$$

implied by the dependence of γ on T (derived in § III.A.2 below), as it is assumed that $u_{Tx} = u_{ex}\gamma + \mathcal{O}(\gamma^2)$, such that the remainder terms, indicated by the Landau symbols, turn out to be proportional to γ_x to leading order; (iii) it is based on the aforementioned equilibrium of universal type, associated with the stress balance, which is expected to hold also for $\mathbf{q}_{11}$ and $\mathbf{q}_{12}$, as the x-dependence of terms of $\mathcal{O}(P^+)$ and $\mathcal{O}(P^+\gamma^2)$, respectively, is absorbed into the gauge functions P^+ and γ solely. The idea behind the last assumption becomes clear immediately by inspection of the accordingly expanded BL equation (18), subject to the boundary conditions (12).

Substituting the expansion (21) into Eqs. (18) and (12) then yields, after integration with respect to Y^+ by taking into account the scalings given by Eqs. (16) and (17) and some manipulations,

$$\Sigma^+_{t\,00} = 1, \quad \Sigma^+_{t\,11} = Y^+, \quad \{\Sigma^+_{t\,12},\ \Sigma^+_{t\,21}\} = \int_0^{Y^+} \left\{ {\Psi^+_{00}}'^2,\ \frac{u_{exx}}{u_e^3}\left[\Psi^+_{00}{}'\Psi^+_{11}{}' - \Psi^+_{00}{}''\Psi^+_{11}\right] + 2\frac{u_{ex}^2}{u_e^4}\,\Psi^+_{00}{}''\Psi^+_{11} \right\} \mathrm{d}\vartheta. \tag{24}$$

Herein, in the integrands Ψ^+_{00} and Ψ^+_{11} are taken to be functions of ϑ. The first two of the relationships (24) represent, respectively, the already mentioned leading-order equilibrium between the total shear and the wall shear stress and the dominant effect of the imposed pressure gradient on the wall layer flow. These relationships initiate the infinite sequence of equations that determine $\Sigma^+_{t\,ij}$. That is, they can be solved hierarchically to predict Ψ^+_{ij} as functions of x, Y^+, and k, subject to the no-slip conditions $\Psi^+_{ij} = \partial_{Y^+}\Psi^+_{ij} = 0$ for $Y^+ = 0$, cf. Eq. (4), once the conditions of matching with the fully turbulent flow for $Y^+ \to \infty$ are known and a suitable closure for Σ^+ is provided. In addition, the near-wall behavior can be elucidated by assuming that

$$\Sigma^+_{ij} \sim \varepsilon_{ij} Y^{+3} + \cdots \quad (\varepsilon_{00} > 0), \quad Y^+ \to 0, \tag{25}$$

in agreement with Eq. (13). Hence, this relation indicates that

$$[\Psi^+_{00}, \Psi^+_{11}, \Psi^+_{ij}] \sim [Y^{+2}/2 - \varepsilon_{00} Y^{+5}/20,\ Y^{+3}/6 - \varepsilon_{11} Y^{+5}/20,\ -\varepsilon_{ij} Y^{+5}/20] + \cdots \quad (i+j > 2), \quad Y^+ \to 0, \tag{26}$$

since the effects of wall shear stress and the pressure gradient in the expansion (21) are subsumed into the dominant "equilibrium" terms $\mathbf{q}^+_{00}$ and $\mathbf{q}^+_{11}$, respectively.

The behavior of the leading-order quantities Σ^+_{00}, Ψ^+_{00} on top of the viscous wall layer is crucial for the subsequent analysis. First, since the viscous contribution, ${\Psi^+_{00}}''$, to $\Sigma^+_{t\,00}$ is presumed to vanish there,

$$\Sigma^+_{00} \to 1, \quad Y^+ \to \infty. \tag{27}$$

Secondly, we conclude the wall layer analysis by introducing the celebrated logarithmic law of the wall, which is commonly believed to hold for fully developed turbulent wall-bounded flow flow and has been introduced by adopting asymptotic reasoning in the seminal paper by Mellor:[5] there are convincing reasons to believe that the behavior

$${\Psi^+_{00}}' \sim \kappa^{-1} \ln Y^+ + B^+, \quad Y^+ \to \infty, \tag{28}$$

is typical for the universal character of the time-averaged flow in the near-wall region.[1,4,14–17] Most important, integration of the first of the relationships (24) by employing any realistic closure model for the turbulent stress function Σ^+ then is assumed to reproduce the presently accepted empirical values[18] $\kappa \approx 0.384$ and $B^+ \approx 4.1$, which refer to a perfectly smooth surface.

We will see in the following that the adoption of the logarithmic law (28) indeed implies the initial assumption (B) or, equivalently, the limits expressed in Eqs. (20) and (22).

III.A.2. Outer Defect Layer

As has already been outlined in Ref. 1, see also § I, § II, and figure 1 on page 5 (b), the downstream evolution of the transitional BL for $X \to \infty$ exhibits a small streamwise velocity defect with respect to the external flow in the outer main portion of the BL. Accordingly, the Reynolds stress function Σ there becomes small, too.

Let the velocity defect and Σ be measured by the two gauge functions $\chi(T)$ and $\sigma(T)$ in the form

$$[\eta - \Psi/(u_e\delta),\ \Sigma/(u_e^2\sigma)] = \chi\,[F, S], \quad (\chi, \sigma) \to (0, 0), \quad T \to \infty. \tag{29}$$

From inspection of Eq. (12) one then readily infers that $\delta = \mathcal{O}(T\sigma)$. In turn, a suitable outer-layer coordinate η is introduced by setting

$$Y = \delta\eta, \quad \delta := T\sigma\Delta(x; k, T). \tag{30}$$

Then the flow quantities are expected to have expansions of the form

$$\big\{[F, S],\ \Delta\big\} \sim \chi\mathbf{q}_1 + \chi^2\mathbf{q}_2 + \mathcal{O}(\chi^3), \quad \mathbf{q}_i := \big\{[F_i, S_i](x, \eta; k),\ \Delta_i(x; k)\big\}. \tag{31}$$

Again, here we have disregarded the occurrence of eigensolutions that result from matching the main layer with the transitional-flow region, without loss of generality.

With respect to the subsequent investigation, it is sufficient to inspect the (homogeneous) leading-order equation only, which exhibits linearized convective terms. It is obtained by inserting Eq. (31) into Eq. (12), subsequent integration with respect to η, and imposing the proper boundary condition $F_1(x, 0) = 0$,

$$u_e^2(u_e\Delta_1)_x\eta F_{1_\eta} - (u_e^3\Delta_1 F_1)_x = u_e^3(S_1 - S_{1,b}), \quad S_{1,b} := S_1(x, 0; k). \tag{32}$$

We first consider the specific role of matching the representations of the flow in the main layer with those in the transitional region,[1] which requires that $[F_1, S_1](0, \eta; k)$ exists, where $F_1(0, \eta; k) > 0$ for $0 < \eta \leq 1$, $S_1(0, \eta; k) > 0$ for $0 < \eta < 1$, and $\Delta_1 \to 0$ as $x \to 0_+$. Since patching the flow at the BL edge is only possible if $F_{1_\eta}(x, 1; k) = S_1(x, 1; k) = 0$, the shear stress term S_1 in Eq. (32) then is seen to enter the least-degenerate form that equation takes on in this limit; otherwise, the resulting problem for $[F_1, S_1](0, \eta; k)$ would have no solution. By taking into account Eq. (6), one consequently finds that all terms of Eq. (32) are retained in the limit $x \to 0_+$ and, interestingly, the dependence on k disappears. As a remarkable finding, the solution of Eq. (32) that holds for $x = 0$ admits an universal form,

$$[F_1, S_1] \sim [G, J](\eta) + \mathcal{O}(x), \quad \Delta_1 \sim \Xi x + \mathcal{O}(x^2) \quad (\Xi > 0), \quad x \to 0_+. \tag{33}$$

These considerations also show why the case $S_{1,b} = 0$ is to be excluded: it would imply that (the for $x > 0$ strictly positive) quantity $u_e^3\Delta_1 F_1(x, 1; k)$ is independent of x and, thus, yield the contradiction $\Delta_1 F_1(x, 1; k) = \mathcal{O}(x^{-3})$ as $x \to 0_+$. Most important, then the matching conditions (27) and (28) allow for a direct match of the wall layer with the outer main layer. In turn, both the parameters χ and σ are conveniently identified formally with γ, cf. figure 1 on page 5 (b), leaving Eq. (32) unchanged, when we again anticipate the estimate (23). As a result, $S_{1,b} = 1$, and Eq. (32) is supplemented with the boundary and matching conditions[1]

$$\eta \to 0: \quad F_1 \to 0, \quad F_{1_\eta} \sim -\kappa^{-1}\ln\eta + B_1(x; k), \quad S_1 \to 1, \quad \eta = 1: \quad F_{1_\eta} = F_{1_{\eta\eta}} = S_1 = 0. \tag{34}$$

Herein, the (positive) function $B_1(x; k)$ is considered as part of the solution for $F_1(x, \eta; k)$, and the requirement $S_1 = 0$ for $\eta = 1$ is associated with vanishing vorticity, expressed through $u_T F_{1_{\eta\eta}}/\delta$, at the BL edge. Also, it is useful to state the aforementioned relationship that follows from evaluation of Eq. (32) for $\eta = 1$,

$$\big[(u_e^3\Delta_1)(x; k)\,F_1(x, 1; k)\big]_x = u_e^3(x; k), \quad (u_e^3\Delta_1)(x; k)\,F_1(x, 1; k) = \int_0^x u_e^{-3}(\vartheta; k)\,\mathrm{d}\vartheta. \tag{35}$$

The latter of these relationships represents the integral momentum balance for the small-defect description of turbulent BL flow,[13] which is obtained by making use of Eq. (33).

The knowledge of the universal functions G, J then completes Eqs. (32) and (34) to an initial-boundary value problem for F_1, S_1 for $x \geq 0$. In principle, this can be solved by means of downstream integration if an asymptotically correct closure for S is provided that accounts for the logarithmic singularity of F_{1_η}, see

Eq. (34). Evaluation of Eqs. (32) and (34) for $x \to 0_+$ shows that G, J are self-similar solutions of these equations,[1]

$$2\Xi[\eta G' - 2G] = J - 1, \quad \Xi = 1/[4\,G(1)], \tag{36}$$

$$\eta \to 0: \quad G \to 0, \quad G' \sim -\kappa^{-1} \ln \eta + D, \quad G(1) = J(1) = 0. \tag{37}$$

By considering Eq. (37), one finds that $D = \lim_{x\to 0} B_1(x;k)$ and, thus, not known in advance. Interestingly, the universal boundary value problem posed by Eqs. (36) and (37) can be interpreted as the turbulent counterpart to the Hiemenz or laminar stagnating-flow problem (15). Note that the transitional flow "connects" the Hiemenz flow, serving as an initial condition for $X = 0$, and its limiting downstream form, given by Eqs. (36) and (37) and obtained for $X \to \infty$.[1]

Finally, matching of the streamwise velocity, Ψ_Y, completes the leading-order analysis as it reveals the yet missing dependence of γ on T and the relationship (23) in terms of the "skin-friction law"

$$\gamma \sim \kappa\tau\,[1-\tau(2\ln\tau+E)+4\tau^2\ln\tau\,(\ln\tau+E+1)+\mathcal{O}(\tau^2)], \quad E := \kappa(B^+ + B_1) + \ln(\kappa^2 u_e \Delta_1), \quad \tau := \frac{1}{2\,\ln T}. \tag{38}$$

This relationship is consistent with the assumption (B) made at the beginning of § III.A.1 as it justifies the limits expressed in Eq. (20) and, in turn, Eq. (22), and the estimate (23). We remark that the remainder terms in the expansion (38), indicated by the Landau symbol, are already affected by terms of $\mathcal{O}(\gamma^2)$ in the expansion (31). Also, note that the viscous stress term Ψ_{YY}, entering Eq. (12), is asymptotically given by $-u_e F_{1\eta\eta}/(T\Delta_1)$.

The analysis carried out so far confirms that the investigation of the large-T BL can essentially be traced back to that of a conventional fully developed turbulent BL[1] when T is formally replaced by its theoretical upper bound $Re^{1/2}$, which can never be reached here, however.

III.B. Boundary Layer Structure near Separation

First, let us refer to the sketch in figure 3 that depicts the asymptotic splitting of the BL deduced in the subsequent investigation.

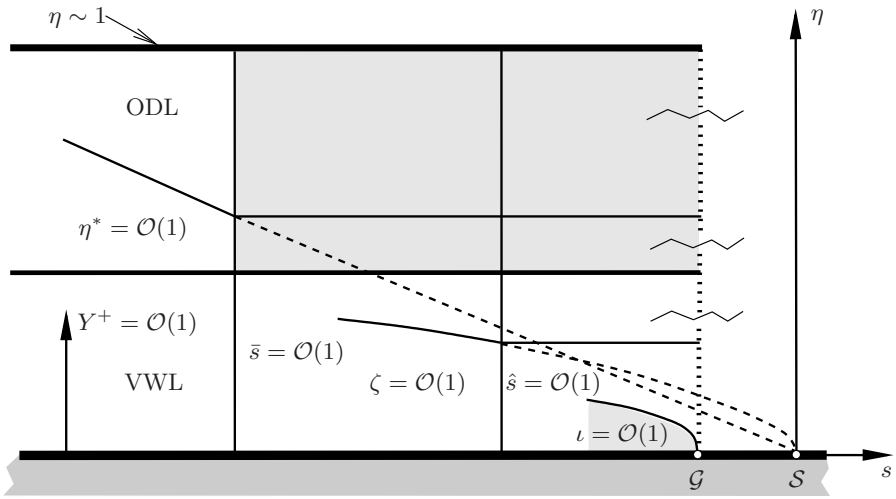

Figure 3. Asymptotic splitting of BL flow near $x = x_S$ (schematic), light-shaded regions not discussed explicitly in the text (Goldstein region and passive small-defect regions near $\mathcal{G}$), broken lines confine fictitious extension of respective regions, dotted vertical line indicates abrupt breakdown of flow description at $\mathcal{G}$.

The matching principle states that an asymptotically correct description of the BL flow in the limit $T \to \infty$ is initiated by seeking a solution of Eqs. (36), (37) and, in the following, of Eq. (32) by means of downstream integration. Therefore, we first envisage the behavior of its solution F_1, S_1 as $s \to 0_-$.

III.B.1. Outer Defect Layer

The local behavior of the small-defect flow near separation has already been accounted for briefly in Ref. 6. Here we present the analysis in a more precise manner, which, amongst others, accounts for the impact of

higher-order terms in the resulting expansion, in close connection with the logarithmic behavior required by Eq. (34).

Inspection of Eqs. (7) and (the second relationship in Eq.) (35) shows that the product $\Delta_1 F_1(x,1;k)$ is bounded in the limit $s \to 0_-$. Since $F_1 > 0$ for $\eta > 0$, the second term in Eq. (32) then is a quantity of $\mathcal{O}(1)$. Furthermore, physically motivated reasoning, substantiated by inspection of any commonly employed (outer-layer) turbulence closure,[1,6] strongly suggests that

$$S = \mathcal{O}\big(F_{1_{\eta\eta}}^2\big). \tag{39}$$

In turn, if one assumes (the rather unexpected case) $S_1 \to 0$ as $s \to 0_-$ it is readily found that all terms apart from $u_e^3 S_1$ will enter the leading-order balance of Eq. (32). However, for the same reason explained for the case $x \to 0_+$ treated above, the resulting equation determining F_1 for $S_1 \to 0$ is inconsistent with the boundary conditions (34). Therefore, we are left with the two remaining possibilities $S_1 \to \infty$ or $S_1 = \mathcal{O}(1)$. In the first case Eq. (32) would reduce to a balance between the left-most term and $u_e^3 S_1$ in leading order (accompanied by the emergence of a sublayer, located between the viscous wall and the main layer, due to the apparent inconsistency of the boundary conditions (34) with that balance). However, Eq. (39) then implies $F_1 \to \infty$ and, consequently, $\Delta_1 \to 0_+$ as $s \to 0_-$. The last finding not only is felt to misinterpret the physical mechanism of separation, but, more drastically, causes the first term in Eq. (32) to have negative sign and, therefore, a contradiction.

As a preliminary (and rather startling) result, the flow quantities assume finite limits when the external flow encounters the BV singularity. We then appropriately expand

$$\big\{[F_1, S_1], \Delta_1\big\} \sim \mathbf{q}_{10} + \lambda'(s)\,\mathbf{q}_{11} + (-s)^{1/2}\mathbf{q}_{12} + (-s)\mathbf{q}_{13} + \mathcal{O}(\lambda), \quad \mathbf{q}_{1j} = \big\{[F_{1j}, S_{1j}](\eta;k), \Delta_{1j}(k)\big\}. \tag{40}$$

where $\lambda(s) \to 0$, $\lambda'(s) \to 0$, and $s \to 0_-$. Note that $F_{10} > 0$ and that S_{10} is non-negative; both these quantities are part of the global solution of Eqs. (32) and (34). In the expansion (40) the term $\mathbf{q}_{11}$ refers to an eigensolution of, for the time being, unknown strength λ, and the contributions $\mathbf{q}_{1j}$, $j > 1$, primarily account for the local behavior (7) of u_e and the coupling between F_1 and Δ_1 in Eq. (32); the flow is seen to be inviscid for terms of lower order than of $\mathcal{O}(-s)$. Inserting the expansion (40) into Eq. (32) yields the equations determining $\mathbf{q}_{11}$ and $\mathbf{q}_{12}$ as

$$F_{11} = (\Delta_{11}/\Delta_{10})(\eta F_{10_\eta} - F_{10}), \quad F_{12} = (2k + \Delta_{12}/\Delta_{10})\,\eta F_{10_\eta} - (6k + \Delta_{12}/\Delta_{10})\,F_{10} + \cdots. \tag{41}$$

Herein, the dots indicate possible inhomogeneities due to a coupling between F_{11} and Δ_{11}, enforced by Eq. (32). However, the solution for F_{11} does not satisfy the condition of vanishing vorticity, given by $F_{11_{\eta\eta}}$, for $\eta = 1$ according to Eq. (34) (except for unlikely circumstances where $(\partial_\eta^3 F_{10})(1;k) = 0$). Consequently, we assume $\lambda = 0$, so that Eq. (40) reduces to an expansion in terms of integer powers of $(-s)^{1/2}$. Note that $(F_{12_\eta})(1;k) = 0$, and adopting the aforementioned condition for F_{12} in Eq. (41) then yields the solvability conditions

$$F_{12} = -4kF_{10}, \quad \Delta_{12} = -2k\Delta_{10}. \tag{42}$$

In principle, proceeding in this fashion gives $\mathbf{q}_{1j}$, $j > 1$, where the boundary conditions for $\eta = 1$ can be fulfilled solely by exploiting the convective operator in Eq. (32).

Next, we stipulate that

$$F_{10} \sim F_{10,b}(\eta;k) := [-\kappa^{-1}(\ln\eta - 1) + B_{1,\mathcal{S}}]\eta, \quad B_{1,\mathcal{S}} := B_1(x_\mathcal{S};k), \quad S_{10} \to 1, \quad \eta \to 0, \tag{43}$$

in accordance with the requirements of matching with the near-wall flow given in Eq. (34). Unfortunately, F_{12_η} then will also exhibit a logarithmic singularity, cf. Eq. (42), which clearly violates the original near-wall condition for F_{1_η} (and, in turn, for S_1). This inconsistency can only be resolved by the introduction of a sublayer of (the initially unknown) relative thickness $\Delta^*(s)$. The therewith suggested stretching transformation

$$[F_1/\Delta^*(s),\, S_1] = [F^*,\, S^*](s, \eta^*; k) = \mathcal{O}(1), \quad \eta = \Delta^*(s)\,\eta^*, \quad \Delta^* \to 0_-, \quad s \to 0_-, \tag{44}$$

casts Eq. (32) into the form

$$u_e^2(u_e\Delta_1\Delta^*)_s\,\eta^* F^*{}_{\eta^*} - (u_e^3\Delta_1\Delta^* F^*)_s = u_e^3(S^* - 1). \tag{45}$$

Substitution of the appropriate expansions

$$[F^*,\, S^*] \sim [-\eta^*\kappa^{-1}\ln\Delta^* + F_{10,b}(\eta^*;k),\, 1] + (-s)^{1/2}\left[4k\,\eta^*\kappa^{-1}\ln\Delta^* + F_1^*(\eta^*;k),\, S_1^*(\eta^*;k)\right] + \cdots, \quad (46)$$

into Eq. (45) and taking into account Eqs. (7) and the second of the relationships (42) then shows that the least-degenerate form of Eq. (45) reduces to a balance that is aimed at to determine F_1^* and S_1^*,

$$2k(-s)^{-1}\Delta^* F_{10,b}(\eta^*;k) - 4k\,\eta^*\kappa^{-1}\Delta_s^* + \Delta_s^*\,\eta^* F_{1\eta^*}^* - [\Delta_s^* - (-2s)^{-1}\Delta^*]F_1^* + \mathcal{O}\left[(-s)^{-1/2}\Delta^*\ln\Delta^*\right] \sim S_1^*. \quad (47)$$

This suitably reduced equation not only proves consistency with the assumed behavior (43). Most important, it fixes that

$$2k\eta^*[B_{1,\mathcal{S}} + \kappa^{-1}(3 - \ln\eta^*)] - \eta^* F_{1\eta^*}^* + (3/2)F_1^* = S_1^*, \quad \Delta^* = -s, \quad (48)$$

in order to allow for a solution $[F_1^*, S_1^*](\eta^*;k)$ that satisfies the required matching and boundary conditions

$$\eta^* \to \infty: \quad F_{1\eta^*}^* \sim a_0^*\eta^{*1/2} + 4k(\kappa^{-1}\ln\eta^* - B_{1,\mathcal{S}}) + \mathcal{O}\left(\eta^{*-1/2}\right), \quad \eta^* = 0: \quad F_1^* = S_1^* = 0 \quad [F_1^{*\prime} = \mathcal{O}(1)]. \quad (49)$$

Herein, the condition for $\eta^* \to \infty$ follows from the asymptotic behavior of Eq. (48) and the first of the relationships (42). According to Eq. (43), matching with the main region where $\eta = \mathcal{O}(1)$ yields

$$F_{10\eta} \sim F_{10,b}{}'(\eta;k) + a_0^*\eta^{1/2} + \cdots \quad (a_0^* > 0), \quad \eta \to 0. \quad (50)$$

Herein, a_0^* is determined by the global solution of Eqs. (32) and (34). Interestingly, an analogous square-root behavior of the leading-order velocity profile is well-known to hold (albeit in the context of a quite different asymptotic framework) for a turbulent BL on the verge of marginal separation.[17,19]

If a particular Reynolds stress closure in agreement with Eq. (39) is chosen, like the mixing-length-based formulation

$$S^* := (\kappa\eta^*\partial_{\eta^*}^2 F^*)^2, \quad S_1^* = 2\kappa\eta^*\partial_{\eta^*}^2 F_1^*, \quad (51)$$

which is commonly believed to hold on top of the viscous wall layer,[13] Eq. (48) provides a third-order equation in $F_1^*(\eta^*)$. Specifically, the second relationship in the model for S^* given by Eq. (51) then follows from linearization about the terminal velocity profile, F_{10}', by using Eq. (43) and Eq. (46). In turn, one recognizes that only the conditions for $\eta^* = 0$ in Eq. (49) represent true boundary conditions. Those for $\eta^* \to \infty$ are seen to be satisfied identically. By adopting the simple model given by Eq. (51), evaluation of Eqs. (48) subject to the boundary conditions (49) for $\eta^* \to 0$ yields

$$F_1^* \sim K\eta^* - k/(2\kappa^2)\,\eta^{*2}\ln\eta^* + [K/(8\kappa) + k(9 + 2\kappa B_{1,\mathcal{S}})/(4\kappa^2)]\,\eta^{*2} + \mathcal{O}\left(\eta^{*3}\ln\eta^*\right), \quad K := F_{1\eta^*}^*(0;k). \quad (52)$$

The absence of a logarithmic behavior of $F_{1\eta^*}^*$ for $\eta^* \to 0$ a posteriori justifies the introduction of the sublayer. In fact, the velocity defect at the base of the defect layer is increased by an amount of $\mathcal{O}[(-s)^{1/2}\ln(-s)]$ as it follows from Eqs. (34) and (46) that

$$B_1 \sim B_{1,\mathcal{S}} + (-s)^{1/2}[(4k/\kappa)\ln(-s) + K] + \mathcal{O}[(-s)\ln(-s)]. \quad (53)$$

In passing we mention that a closed solution of Eqs. (48) and (49), based on the rather simple but asymptotically correct closure (51), is given by[20]

$$F_1^* = \check{\eta}\,\mathrm{e}^{-\check{\eta}/4}\left[\frac{a_0^*\,\pi^{1/2}}{(2\kappa^{-1})^{3/2}}\left[(\check{\eta}+1)I_1\Big(\frac{\check{\eta}}{4}\Big) + (\check{\eta}+3)I_0\Big(\frac{\check{\eta}}{4}\Big)\right] - \frac{4k}{3}\left[(\check{\eta}+1)K_1\Big(\frac{\check{\eta}}{4}\Big) - (\check{\eta}+3)K_0\Big(\frac{\check{\eta}}{4}\Big)\right]\right] + F_{1,p}^*,$$
$$F_{1,p}^* = (16k/3) - 4k\eta^*[B_{1,\mathcal{S}} + \kappa^{-1}(1 - \ln\eta^*)], \quad \check{\eta} := \kappa^{-1}\eta^*. \quad (54)$$

Inspection of the scalings (16) and (30) indicates a collapse of the sublayer where $\eta^* = \mathcal{O}(1)$ with the viscous wall layer when $-s = \mathcal{O}[(T\gamma)^{-2}]$. However, we will see subsequently that this scenario is prevented by the asymptotic structure of the wall layer as $s \to 0_-$, which assigns the outer layer an essentially passive role. Hence, we conclude the analysis of the analysis of the outer defect layer by emphasizing the basic result that the primary expansion (31) is seen to be uniformly valid in the (independent) double limit $s \to 0_-$, $\chi = \gamma \to 0$.

III.B.2. Viscous Wall Layer

The more demanding part of the analysis concerns the near-wall flow. Here both the pressure gradient and convective term are found to be initially negligibly small in Eq. (18), cf. Eqs. (20)–(22), but inevitably provide a leading-order effect near separation where the gradients with respect to x become arbitrarily large, as a consequence of the behavior (7). Let us first demonstrate how they come into play in a rather subtle manner as $s \to 0_-$.

In the latter limit expansion (21) remains valid and, simultaneously, accounts for the sequence (24) as long as $\mathbf{q}_{11}$ enters the equation determining $\mathbf{q}_{21}$ as a quantity that is regarded as known already. In other words, as long as this condition holds, each term in Eqs. (21) and (24) can be expanded into integer powers of $(-s)^{1/2}$, according to Eq. (7). This is accomplished by expanding the quantity E in Eq. (38) according to Eq. (53) and keeping T fixed, giving

$$\gamma \sim \gamma_0 + \mathcal{O}[\tau^2(-s)^{1/2}\ln(-s)], \quad s \to 0_-, \quad \gamma_0 := \lim_{s\to 0_-}\gamma \sim \kappa\tau\,[1 - 2\tau\ln\tau + \mathcal{O}(\tau)], \tag{55}$$

so that $\gamma_x = \mathcal{O}[\gamma_0^2/(-s)^{1/2}]$ now suitably replaces the relationship (23). Substituting these expressions into the expansion (21) then results in an uniformly valid expansion holding in the (independent) double limit $s \to 0_-$, $T \to \infty$, which ceases to be valid when $\epsilon\,\mathbf{q}_{21}^+ = \mathcal{O}(P^+)$. In the expression for $\Sigma_{t\,21}^+$ in Eq. (24) the first term then predominates the second as $s \to 0_-$; hence, the breakdown occurs when $u_{exx}/u_{ex} \sim 1/(-2s) = \mathcal{O}(T^2\gamma)$, i.e. where $-s = \mathcal{O}[1/(T^2\gamma)]$. Note that Eqs. (38) and (55) then yield

$$\gamma \sim \gamma_0 + \mathcal{O}(\tau^{3/2}\ln T/T), \quad \gamma_x = \mathcal{O}\big(\gamma_0^{5/2} T\ln T\big). \tag{56}$$

We now concentrate on this distinguished limit by introducing a suitable streamwise coordinate $\bar{s} = \mathcal{O}(1)$,

$$s = \bar{s}/(T^2 u_{T0}), \quad u_{T0} := \gamma_0\, u_{e,\mathcal{S}}. \tag{57}$$

We then obtain from Eqs. (20) and (55)–(57)

$$P^+ \sim \pi^+(-\bar{s})^{-1/2}\,[1 + \mathcal{O}(\tau^{1/2}/T)], \quad \pi^+ := k/[T\gamma_0^{5/2}u_{e,\mathcal{S}}]. \tag{58}$$

In the expansion of Ψ^+, Σ^+, resulting from inspection of Eq. (18), then only the first two terms are of interest for the subsequent analysis,

$$[\Psi^+, \Sigma^+] \sim [\Psi_{00}^+, \Sigma_{00}^+](Y^+) + \pi^+\big\{[\bar{\Psi}^+, \bar{\Sigma}^+](\bar{s}, Y^+) + \mathcal{O}(\gamma_0^2)\big\}, \quad T \to \infty. \tag{59}$$

Herein, $\bar{\Psi}^+$, $\bar{\Sigma}^+$ are quantities of $\mathcal{O}(1)$. Inserting Eq. (59) into the BL equation (18) and expanding gives rise to a linear initial-boundary value problem for these quantities,

$$\partial_{Y^+}\bar{\Sigma}^+ + \partial_{Y^+}^3\bar{\Psi}^+ = (-\bar{s})^{-1/2} + \Psi_{00}^{+\prime}\partial_{\bar{s}Y^+}\bar{\Psi}^+ - \Psi_{00}^{+\prime\prime}\partial_x\bar{\Psi}^+, \quad \Psi_{00}^+ = \Psi_{00}^+(Y^+), \tag{60}$$

$$Y^+ = 0: \quad \bar{\Psi}^+ = \partial_{Y^+}\bar{\Psi}^+ (= \bar{\Sigma}^+) = 0, \quad \bar{s} \to -\infty: \quad [\bar{\Psi}^+, \bar{\Sigma}^+] \sim (-\bar{s})^{-1/2}\,[\Psi_{11}^+, \Sigma_{11}^+]\,\big(+\mathcal{O}\big[|\bar{s}|^{-3/2}\big]\big). \tag{61}$$

Equations (60) and (61) have to be supplemented with appropriate matching conditions for $Y^+ \to \infty$. These provide a match with the outer defect layer as they follow from the matching conditions to be imposed on the equations for $\Sigma_{t\,11}^+$ and $\Sigma_{t\,21}^+$ for $-s = \mathcal{O}(1)$, see Eq. (24). Note that they depend on the higher-order properties of any specific closure for Σ^+ that accounts for the leading-order overlap behavior given by (27) and (28). For the present investigation, however, it is only relevant to consider the behavior of the solution to the problem posed by Eqs. (60) and (61) in the limit $\bar{s} \to 0_-$. We stress that the understanding of the BL flow near separation is essentially provided by the local interplay between the two terms quoted in the expansion (59) in the double limit $\bar{s} \to 0_-$, $Y^+ \to 0$. Hence, the following analysis shows close resemblance with that of the purely laminar case, where we refer to the study by Messiter and Enlow[21] and the synopsis presented in Ref. 2: the only striking difference is that here $k = \mathcal{O}(1)$ and the problem for perturbation stream function $\bar{\Psi}^+$ accounts for the relatively weak convective terms in the strongly viscosity-affected near-wall flow region, whereas in the laminar case the corresponding perturbation is due to an asymptotically weak BV singularity, giving $k = \mathcal{O}(Re^{-1/16})$, but convection predominates throughout.

It is obvious that the shear stress terms do not enter the leading-order balance Eqs. (60) reduces to in the limit $\bar{s} \to 0_-$. Then the behavior of $\bar{\Psi}^+$ for $\bar{s} \to 0_-$ and $Y^+ = \mathcal{O}(1)$ in its most general form is found in the form

$$\bar{\Psi}^+ \sim \bar{\Psi}_0^+(Y^+) + \alpha(\bar{s})\,\Psi_{00}^{+\prime}(Y^+) - 2(-\bar{s})^{1/2}\,\Psi_{00}^{+\prime}(Y^+)\left[\frac{1}{Y^+} + \int_0^{Y^+}\left(\frac{1}{\vartheta^2} - \frac{1}{[\Psi_{00}^{+\prime}(\vartheta)]^2}\right)\mathrm{d}\vartheta\right] + \mathcal{O}(-\bar{s}), \tag{62}$$

where both the contribution of $\mathcal{O}(1)$, $\bar{\Psi}_0^+$, and the gauge function $\alpha(\bar{s})$ that accounts for the occurrence of eigensolutions are a priori unknown. However, the local solution given in Eq. (62) does not satisfy the no-slip condition (61). Therefore, a sublayer has to be introduced where the viscous stress term plays a dominant role. By inspection of Eqs. (60) and (26), this region emerges for $Y^+ = \mathcal{O}[(-\bar{s})^{1/3}]$. Moreover, since the pressure gradient dominates over the stress gradients in Eq. (60) as $\bar{s} \to 0_-$, it must also balance their viscous contribution in that sublayer. We finally arrive at the appropriate near-wall behavior

$$\Psi_{00}^+ \sim (-\bar{s})^{2/3}\zeta^2/2 + \mathcal{O}[(-\bar{s})^{5/3}], \quad \bar{\Psi}_0^+ \sim (-\bar{s})^{1/2} f(\zeta) + \mathcal{O}\big[(-\bar{s})^{3/2}\big], \quad Y^+ = (-\bar{s})^{1/3}\zeta, \quad \zeta = \mathcal{O}(1). \tag{63}$$

Substituting these expansions into Eqs. (60) and (61) yields

$$\zeta^2 f''/3 - \zeta f'/2 + f/2 = -1 + f''', \quad f(0) = f'(0) = 0. \tag{64}$$

The solution to this problem that exhibits sub-exponential growth for $\zeta \to \infty$ can be expressed through confluent hypergeometric functions by adopting standard techniques:[20]

$$f(\zeta) = -2\zeta \int_0^\zeta \big[\Lambda\, M(\tfrac{1}{6}, \tfrac{5}{3}, \vartheta^3/9) + [M(-\tfrac{1}{2}, \tfrac{1}{3}, \vartheta^3/9) - 1]/\vartheta^2\big]\, \mathrm{d}\vartheta, \quad \Lambda := \frac{\Gamma(\frac{1}{3})\,\Gamma(\frac{7}{6})}{3^{1/3}\,\pi^{1/2}\,\Gamma(\frac{5}{3})} \doteq 1.0770, \tag{65}$$

$$f \sim -a_0\zeta^{3/2} + a_1\zeta - 2 + \mathcal{O}\big(\zeta^{-3/2}\big), \quad \zeta \to \infty, \quad [a_0, a_1] := \left[\frac{4\,\Gamma(\frac{1}{6})}{3\,\Gamma(\frac{2}{3})},\, 48^{1/3}\,\Gamma(\tfrac{2}{3})\right] \doteq [5.4809, 4.9212]. \tag{66}$$

Note the pronounced increase of the resulting negative perturbation in the resulting expansion of the wall shear:

$$Y^+ = 0: \quad \partial_{Y^+}^2 \Psi^+ \sim 1 - 4\Lambda\,\pi^+(-\bar{s})^{-1/6} + \cdots, \quad \bar{s} \to 0_-, \quad T \to \infty. \tag{67}$$

Finally, matching the region where $\zeta = \mathcal{O}(1)$ and the main portion of the viscous wall layer, where $Y^+ = \mathcal{O}(1)$, then gives

$$\bar{\Psi}_0^+ \sim -a_0 Y^{+3/2}, \quad Y^+ \to 0; \quad \alpha \sim a_1(-\bar{s})^{1/6}, \quad \bar{s} \to 0_-. \tag{68}$$

That is, $\bar{\Psi}^+$ is bounded for $\bar{s} \to 0_-$, and, accordingly, the contribution to the Reynolds stress, $\bar{\Sigma}^+$, assumes a finite limit,

$$\bar{\Sigma}^+ \sim \bar{\Sigma}_0^+(Y^+) + (-\bar{s})^{1/6}\bar{\Sigma}_1^+(Y^+) + \cdots, \quad \bar{s} \to 0_-. \tag{69}$$

Remarkably, the terminal structure of the problem (60), (61) in the limit $\bar{s} \to 0_-$ is found to be universal, i.e. independent of the specific form of the (exponentially decreasing) eigensolutions for $\bar{s} \to -\infty$, which trigger a non-zero wall shear contribution, $(\partial_{Y^+}^2 \bar{\Psi}^+)(\bar{s}, Y^+ = 0) \not\equiv 0$, that results in the perturbation given in the expansion (67). That is, the existence of these eigensolutions, not considered here, is crucial for the asymptotic structure of the flow as $\bar{s} \to 0_-$.

We also note that the expansion (40) remains essentially intact, as a consequence of the logarithmic behavior (28), in the narrow region where $\bar{s} = \mathcal{O}(1)$, if γ is replaced by γ_0. Moreover, it will turn out in § III.B.3 below that the flow in the outer main layer is virtually unaffected by the wall layer flow for $1/T \ll x < x_{\mathcal{G}}$ throughout, i.e. even for the terminal distinguished limit $\bar{s} \to 0_-$ as $T \to \infty$.

III.B.3. Nonlinear Breakdown

Most important, a further breakdown of the hitherto existing asymptotic structure is encountered when $\pi^+\bar{\Psi}_0^+ = \mathcal{O}(\Psi_{00}^+)$ or, by inspection of Eqs. (59), (63), or (67), for $(-\bar{s})^{1/6} = \mathcal{O}(\pi^+)$, thus, giving rise to a new sublayer. Therefore, this flow regime is conveniently described by assuming that the streamwise coordinate $\hat{s}$, defined by

$$\bar{s} = \pi^{+6}\hat{s}, \tag{70}$$

is a quantity of $\mathcal{O}(1)$. Let us first consider the main portion of the wall layer, namely the so-called core region, where both Y^+ and $\hat{s}$ are quantities of $\mathcal{O}(1)$.

Note that the pressure gradient term P^+ then has increased in magnitude from $\mathcal{O}(\pi^+)$, see Eq. (58), to $\mathcal{O}(1/\pi^{+2})$ here. Now its contribution to Eq. (60) is seen to be of $\mathcal{O}(1/\pi^{+3})$, whereas the predominating convective terms appear to be of $\mathcal{O}(1/\pi^{+6})$ therein. From inspection of the original wall layer equation (18), subject to the requirements (26) and (25), and matching with the flow upstream that is represented by the

expansions (59), (62), and (69), the flow quantities in the core region then are easily found to be expanded in the form

$$[\Psi^+, \Sigma^+] \sim [\Psi_{00}^+, \Sigma_{00}^+](Y^+) + \pi^+[\bar\Psi_0^+, \bar\Sigma_0^+](Y^+) + \pi^+\sum\nolimits_{i=1}^{\infty}(\pi^+)^i[\hat\Psi_i^+, \hat\Sigma_i^+](\hat s, Y^+) + \cdots . \tag{71}$$

Herein, the sum in Eq. (71) accounts for the nonlinear convective terms in Eq. (18), where the dominant ones of $\mathcal{O}(\gamma_0/\pi^{+6})$ are those proportional to u_T within the brackets. The details of the general analysis of a mainly inviscid core region of a fluid layer with relatively small streamwise extent can be found in Ref. 2. The most important results are that the leading-order terms depend on Y^+ only and that the expressions for $\hat\Psi_i^+$, $i > 0$, contain eigensolutions that are proportional to $\Psi_{00}^{+\prime}$:

$$\hat\Psi_1^+/\Psi_{00}^{+\prime}(Y^+) = \hat A_1(\hat s) \quad (\sim a_1(-\hat s)^{1/6} + \cdots , \quad \hat s \to -\infty), \tag{72}$$

$$\hat\Psi_2^+/\Psi_{00}^{+\prime}(Y^+) = \hat A_2(\hat s) - \hat A_1(\hat s)\int_{Y_b^+}^{Y^+}\frac{(\bar\Psi_0^{+\prime}\Psi_{00}^{+\prime\prime} - \bar\Psi_0^{+\prime\prime}\Psi_{00}^{+\prime})(\vartheta)}{[\Psi_{00}^{+\prime}(\vartheta)]^2}\,\mathrm{d}\vartheta, \tag{73}$$

$$\begin{aligned}\hat\Psi_3^+/\Psi_{00}^{+\prime}(Y^+) = \hat A_3(\hat s) &- \int_{Y_b^+}^{Y^+}\frac{(\bar\Psi_0^{+\prime}\hat\Psi_{2\,Y^+}^+ - \bar\Psi_0^{+\prime\prime}\hat\Psi_2^+)(\vartheta) + [\hat A^2(\hat s)/2](\Psi_{00}^{+\prime\prime 2} - \Psi_{00}^{+\prime}\Psi_{00}^{+\prime\prime\prime})(\vartheta)}{[\Psi_{00}^{+\prime}(\vartheta)]^2}\,\mathrm{d}\vartheta \\ &- 2(-\hat s)^{1/2}\Psi_{00}^{+\prime}(Y^+)\left[\frac{1}{Y^+} + \int_0^{Y^+}\left(\frac{1}{\vartheta^2} - \frac{1}{[\Psi_{00}^{+\prime}(\vartheta)]^2}\right)\mathrm{d}\vartheta\right].\end{aligned} \tag{74}$$

The behavior of $\hat A$ in the limit $\hat s \to \infty$ given in Eq. (72) follows from Eq. (68). The lower bound Y_b^+ of the integrals in Eqs. (73) and (74) must be positive, in order to account for the singular behavior of the integrands due to the near-wall behavior given by (26) and (25), but otherwise can be chosen arbitrarily. The relationship (74) for $\hat\Psi_3^+$ is affected by the pressure gradient, cf. Eq. (62). The functions $\hat A_i$ are determined in the course of matching the flow quantities in the core region with that in the aforementioned sublayer, considered next.

Hence, we introduce sublayer quantities $\hat\Psi$, $\hat Y$ of $\mathcal{O}(1)$ as

$$\Psi^+ \sim \pi^{+4}\,\hat\Psi(\hat s, \hat Y) + \mathcal{O}(\pi^{+10}), \quad Y^+ = \pi^{+2}\,\hat Y. \tag{75}$$

Note that Σ^+ is seen to be of $\mathcal{O}(\pi^{+6})$ and, in turn, negligibly small in this sublayer. As a result, here the BL equations of classical, i.e. laminar, type are fully retained to leading order:

$$\hat\Psi_{\hat Y}\hat\Psi_{\hat Y\hat s} - \hat\Psi_{\hat s}\,\hat\Psi_{\hat Y\hat Y} = -(-\hat s)^{-1/2} + \hat\Psi_{\hat Y\hat Y\hat Y}, \tag{76}$$

$$\hat Y = 0: \quad \hat\Psi = \hat\Psi_{\hat Y} = 0, \quad \hat Y \to \infty: \quad \hat\Psi_{\hat Y}\hat\Psi_{\hat Y\hat s} - \hat\Psi_{\hat s}\,\hat\Psi_{\hat Y\hat Y} \sim -(-\hat s)^{-1/2}, \tag{77}$$

$$\hat s \to -\infty: \quad \hat\Psi \sim (-\hat s)^{2/3}\zeta^2/2 + (-\hat s)^{1/2}f(\zeta), \quad \zeta = \hat Y/(-\hat s)^{1/3}\ [= \mathcal{O}(1)]. \tag{78}$$

Herein, the initial conditions for $\hat s \to -\infty$ provide a match with the flow in the region where $\bar s = \mathcal{O}(1)$ and imply $\hat\Psi \sim \hat Y^2/2 + \mathcal{O}[(-\hat s)^{-1/6}]$ for $\hat Y = \mathcal{O}(1)$, in agreement with the expansion (67). The matching condition for $\hat Y \to \infty$, see Eq. (77), reflects the inviscid nature of the flow on top the sublayer, i.e. within the core region.

It is instructive to outline how the behavior of $\hat\Psi$ for $\hat Y \to \infty$ then can be derived solely from the conditions (78) of matching with the flow upstream. Integration of the inviscid part of Eq. (76) reveals that Bernoulli's law holds in the limit $Y^+ \to \infty$, here expressed through

$$\hat\Psi_{\hat Y}^2/2 - 2(-\hat s)^{1/2} \sim \Phi(\hat\Psi), \quad \Phi'(\hat\Psi) = \hat\Psi_{\hat Y\hat Y}, \quad \hat Y \to \infty. \tag{79}$$

Herein, $-2(-\hat s)^{1/2}$ and $\Phi(\hat\Psi)$ represent, respectively, the pressure term and an at first unknown total head. By taking into account Eq. (66), one infers from matching the sublayer with the region where $\zeta = \mathcal{O}(1)$ that $\hat\Psi \sim \hat Y^2/2 - a_0\hat Y^{3/2} + \mathcal{O}[(-\hat s)^{1/6}\hat Y]$ in the double limit $\hat s \to -\infty$, $\zeta \to \infty$. The first two terms of this expansion allow to determine $\Phi(\hat\Psi)$ in the limit $\hat\Psi \to \infty$: since higher-order terms are inherently s-dependent and, correspondingly, lead to an additional s-dependence of Φ, they cannot contribute to the "inviscid" part of Φ. By disregarding them, integration of the second of the relationships (79) then yields $\Phi = \hat\Psi - 2^{-1/4}a_0\,\hat\Psi^{3/4}$; from subsequent integration of the first of those relationships one obtains

$$\hat\Psi \sim \hat Z^2/2 - a_0\hat Z^{3/2} - 2(-\hat s)^{1/2} + \mathcal{O}\big(\hat Z^{-3/2}\big), \quad \hat Z := \hat Y + \hat A_1(\hat s), \quad \hat Y \to \infty. \tag{80}$$

In this expansion the pressure term is found as a particular solution of Eq. (79) and terms of $\mathcal{O}(\hat{Z}^{-3/2})$ are affected by the shear stress term in Eq. (76). Furthermore, the "constant" $\hat{A}_1$ of integration with respect to $\hat{Y}$ follows from a match with the core region, according to Eq. (72).

The initial-boundary value problem posed by Eqs. (76)–(78) describes a BL under the action of an adverse pressure gradient. Most important, its solution is well-known to terminate at an (a priori unknown) position $\hat{s} = \hat{s}_{\mathcal{G}} < 0$ in form of a Goldstein singularity; here we refer to Refs. 2,9,10, and the remarks stated by Neish and Smith[4] in connection with an akin situation that arises in their treatment of trailing-edge flow. (A thorough numerical treatment of Eqs. (76)–(78) that rigorously clarifies this property and determines the value of $\hat{s}_{\mathcal{G}}$ will be provided in a subsequent related paper.) Here we only present the most relevant results from the local analysis of these equations by considering the representative limit

$$\xi := [\omega(\hat{s}_{\mathcal{G}} - \hat{s})]^{1/4} \to 0, \tag{81}$$

where the (positive) constant ω and the (negative) value of $\hat{s}_{\mathcal{G}}$ are fixed by the solution of Eqs. (76)–(78):[9,10]

$$\hat{Y} = \mathcal{O}(1): \quad \hat{\Psi} - \hat{\Psi}_0(\hat{Y}) \sim \hat{\Psi}_0'(\hat{Y})\,\xi^2[1 + \mathcal{O}(\xi)], \qquad \hat{Y} = 0: \quad \hat{\Psi}_{\hat{Y}\hat{Y}} \sim (-\hat{s}_{\mathcal{G}})^{-1/2}\,\xi^2[1 + \mathcal{O}(\xi)], \tag{82}$$

$$\hat{Y} \to 0: \quad \hat{\Psi}_0 \sim (-\hat{s}_{\mathcal{G}})^{-1/2}[\hat{Y}^3/6 - (-\hat{s}_{\mathcal{G}})^{-1/2}\omega\hat{Y}^5/240 + \mathcal{O}(\hat{Y}^6)]. \tag{83}$$

Strictly speaking, the asymptotically correct description of that singular behavior requires the introduction of a further region where $\hat{Y} = \mathcal{O}(\xi)$ or, equivalently, $\hat{\Psi} = \mathcal{O}(\xi^3)$. In turn, this Goldstein region is characterized by the distinguished limit

$$\iota := \hat{Y}/\xi = \mathcal{O}(1). \tag{84}$$

The crucial result is provided by the square–root singularity exhibited by the shear rate $\hat{\Psi}_{\hat{Y}\hat{Y}}$ evaluated at the surface in terms of $\hat{s}_G - \hat{s}$, cf. Eq. (82).

IV. Comparison with Numerical Results

IV.A. Kirchhoff-type Flow

Without going into the technical details, we note that the Kirchhoff-type potential-flow problem for the canonical case of a circular cylinder in uniform cross stream, as referred to in figure 1 on page 5 (a), has been solved numerically by employing the particular methods of conformal mapping elucidated in.[3] We now discuss the solutions displayed in figure 4. Let $\phi := 180\,x/\pi$, such that the position of $\mathcal{S}$ is characterized by the angle $\phi_{\mathcal{S}}$, which is a function of k: $\phi_{\mathcal{S}}(k)$. One then obtains $\phi_{min} := \phi_{\mathcal{S}}(0) \doteq 55^\circ\,02'\,30''$, cf. Ref. 3. In general, for a convex surface contour the BV parameter k increases for increasing values $x = x_{\mathcal{S}}(k)$, $\phi = \phi_{\mathcal{S}}(k)$. Also, the case of a body shape which is symmetric with respect to the free-stream flow direction serves as a sufficient condition that the free streamlines have the form of a parabola sufficiently far downstream of the body under consideration. Therefore, then they confine an infinitely large dead-water zone. Specifically, in the canonical case depicted here, the inflection point of the free streamlines is shifted to infinity as $k \to k_{max} \doteq 0.49079$, so that they meet asymptotically at infinity for $k = k_{max}$ and $\phi_{max} := \phi(k_{max}) \doteq 126^\circ\,43'\,32''$.

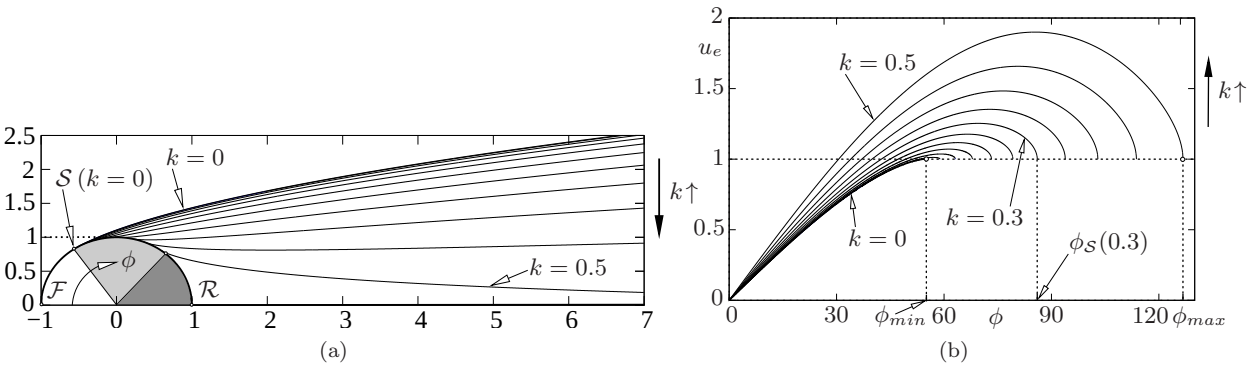

Figure 4. Kirchhoff flow around a circular cylinder for discrete values $k = i \times 0.05$, $i = 0, 1, \ldots, 10$: (a) separating streamlines (figures on axes measure horizontal and vertical distance from centre in multiples of unit radius), (b) distribution $u_e(x;k)$ over $\phi\,[^\circ]$, terminating at $x = x_D(k)$, $\phi = \phi_D(k)$ in form of the BV singularity, see Eq. (7) (e.g. $\phi_{\mathcal{S}}(0.3) \doteq 86^\circ\,1'\,54''$).

Note that $k \geq 0$ for geometrical reasons. Also, for $k \leq k_{max}$ the dead-water region is semi-infinitely open, so that there the value of the pressure equals $p_{0,\mathcal{S}}$ or, equivalently, $p_{0,\mathcal{C}}$ and that of the pressure at infinity, denoted by $p_{0,\infty}$. For $k > k_{max}$, however, the dead-water pressure $p_{0,\mathcal{S}}$ enters the problem as a further parameter. In that case the stagnant-flow region is cusp-shaped and of finite extent, cf. Ref. 22. This type of potential flow is currently under investigation. Here we only note that the strictly attached potential flow, exhibiting a rear-stagnation point $\mathcal{R}$, considered by Neish and Smith[4] then is seen as the limit of a class of flows that show an increase of $p_{0,\mathcal{S}}$ from $p_{0,\infty}$ up to the limiting value $p_{0,\mathcal{R}}$. According to Bernoulli's law, one readily finds that $p_{0,\mathcal{S}} + u_{e,\mathcal{S}}^2/2$, with $p_{0,\mathcal{S}} = p_{0,\mathcal{C}}$ and $u_{e,\mathcal{S}} = u_{e,\mathcal{C}}$, equals the value $p_{0,\infty} + 1/2\,(= p_{0,\mathcal{F}})$ of the total head, characteristic of the free streamline $\mathcal{C}$. Furthermore, due to the strong inflection of the $\mathcal{C}$ near $\mathcal{S}$ as expressed by Eq. (10), $u_e \to 0$ in the limit $k \to \infty$. Therefore, we expect that $\mathcal{S}$ approaches $\mathcal{R}$ then. Also, in this limiting case the need of a further potential-flow region in the vicinity of $\mathcal{S}$ is indicated as the expansions (7), (9), and (10) are only valid for $|s| \ll k^{-2}$.

In the present study, however, we tacitly restrict the analysis to flows exhibiting an open cavity. This assumption agrees with the original finding of a class of potential flows that are only parametrized by k, as already mentioned in § II. Both the regimes of the values of k that refer to an open and closed stagnant-flow region, respectively, are indicated by the light- and dark-shaded sectors in figure 4 (a).

IV.B. Boundary Layer Flow

IV.B.1. Asymptotically Correct Reynolds Stress Closure

In order to obtain numerical solutions of the BL problem posed by Eqs. (12)–(15) for various values of k and T, the Reynolds shear stress function Σ is conveniently modelled on the basis of the mixing length formulation, which is associated with the concept of a rather sharp BL edge $Y = \delta$, cf. Ref. 13. In addition, in the case $T \to \infty$ the solutions shall assume a behavior that is compatible with the asymptotic structure of the BL derived in § III. This is achieved if the mixing length is modelled as proportional to the "turbulent" BL thickness δ times a shape function, here denoted by ℓ, which is taken as the product of the two "lengths", l and l^+. These account for the BL flow in the outer main region and the viscous sublayer, respectively,

$$\Sigma = [\delta\,\ell\,\Psi_{YY}(x, Y; k, T)]^2, \quad \ell = l(\eta)\,l^+(Y^+), \tag{85}$$

$$l := \mu\,I(\zeta)^{1/2}\tanh[\kappa\,\eta/c_\ell], \quad I := 1/(1 + 5.5\,\eta^6), \quad \mu := 0.085, \tag{86}$$

$$l^+ := 1 - \exp(-Y^+/\Gamma), \quad \Gamma := \beta\,[1 - \exp(-Y^+/\varphi)]^{1/2}, \quad \beta := 27.8, \quad \varphi := 4.8\,. \tag{87}$$

In these relationships η is defined according to Eq. (30), where δ is appropriately determined as the minimum value of Y where Σ is found to be numerically insignificantly small. The expression for l in Eq. (86) is a modification of the well-known model by Michel, Quémard, and R. Durant[23] (see also Ref. 13, p. 557), where the usual intermittency factor I by Klebanoff[24] has been included. In turn, the associated pronounced decrease of ℓ eliminates the deficiency of the original model to overestimate the turbulence intensities near the BL edge. The sublayer closure[25] provided by Eq. (87) predicts the correct near-wall behavior given by Eqs. (13), (25), and (26). In Eqs. (85)–(87) the turbulent reference velocity u_T enters the definition of the wall layer coordinate Y^+, given by Eq. (16), in the form $u_T := \kappa\tau u_e$, according to Eqs. (22) and Eq. (38), rather than by adopting the original definition Eq. (17). This advantageously agrees with the asymptotic structure near separation discussed in § III.B without encountering an unbounded increase of the wall layer thickness as $u_T \to 0$ for $s \to 0_-$.

Formally, Eqs. (85)–(87) represent an appropriate mixing length closure for in the fully turbulent case, expressed by the limit $T \to \infty$. In this limit it enforces the transition towards the small-defect BL, considered in § III.A, as Eqs. (86) and (87) provide a common overlap of the main and the sublayer as it predicts the widely believed linear variation of ℓ with distance from the wall in the overlap domain, $\ell \sim \kappa\eta$, which is usually argued for by bringing forward dimensional reasoning.[13] This fully agrees with the form of the closure already addressed in § III.B.1 and expressed through Eqs. (39) and (51). In turn, the overlap behavior given by Eqs. (27), (28), and (34), is revealed. Specifically, applying the above model to the "universal" sublayer functions $\Psi_{00}^+(Y^+)$ and $\Sigma_0^+(Y^+)$ yields $vSi_0^+ = [\kappa\,Y^+ l^+ \Psi_{00}^{+\prime\prime}(Y^+)]^2$, so that Ψ_0^+ then follows from (numerical) integration of the first of the Eqs. (24), subject to the no-slip condition, see Eq. (13). Setting $\kappa = 0.384$[18] here gives $B^+ \doteq 4.8831$ and $\Sigma_0^+ \sim \varepsilon_{00} Y^{+3} + O(Y^{+\,7/2})$ with $\varepsilon_{00} \doteq 9.16 \times 10^{-4}$. That is, the near-wall behavior given by Eqs. (25) and (26) is satisfied, in numerically good agreement with experimental findings.[25,26]

IV.B.2. Partially Developed Turbulent Boundary Layer near Separation

For a numerical treatment of Eqs. (12)–(15), these equations have been suitable transformed in order to capture the smooth transition towards the Hiemenz flow as $x \to 0_+$. This procedure is presented in Ref. 1. Solutions of the transformed equations have been achieved by adopting the method of lines and employing a Keller–Box-type discretisation, supplemented with automated adaptive step control in the x-direction and an automated remeshing strategy regarding the grid in Y-direction. The latter was resolved by using approximately 10^4 grid points.

Solutions have been found by prescribing Kirchhoff-type potential flows with an open cavity, i.e. for $0 \leq k \geq k_{max}$ and for a wide range of values of T. The solutions corroborate the conjecture that the position $x = x_{\mathcal{G}}$ of the Goldstein singularity triggered by the BV singularity, see Eq. (7), is shifted downstream for increasing values of k, thereby increasing in strength. Increasing values of T, i.e. increasing turbulence intensities, are expected to foster that downstream shift as turbulent BLs are empirically known to be less prone to separate than laminar ones for identical external-flow configurations (i.e. for identical values of k). In the following, we solely discuss the solutions obtained for the specific value $k = 0.3$, which exhibit the rather surprising property that the strength of the Goldstein-singularity weakens for increasing values of T: from this scenario one then infers (needless to say, with some caution) that for a certain range of values of k (within the interval $0 < k < k_{max}$ in case of the circular cylinder) the Goldstein singularity vanishes for critical values of T.

The condition of matching with the external flow has been satisfied numerically at $Y = \delta$ within the range $10 \leq \delta \leq 100$, where δ has been increased properly for increasing values of the parameter T. The latter is varied from $T = 0$ up to $T = 10^5$; higher values result in numerical difficulties which could only be overcome by employing a considerably higher grid resolution. Hence, the BV singularity is seen to take place at $\phi = \phi_{\mathcal{S}} \doteq 86^\circ\, 1'\, 54''$, as indicated in figure 4 on page 18 (b) and figure 5 by vertical dotted lines. The resulting distributions for the reduced wall shear stress, Ω, together with that for the displacement thickness, Υ, defined by

$$\Omega(x;k,T) := \Psi_{YY}(x, Y=0;k,T)/u_e(x;k), \quad \Upsilon(x;k,T) := \int_0^\infty (1 - \Psi_Y/u_e)\,\mathrm{d}Y, \tag{88}$$

are plotted in the last figure.

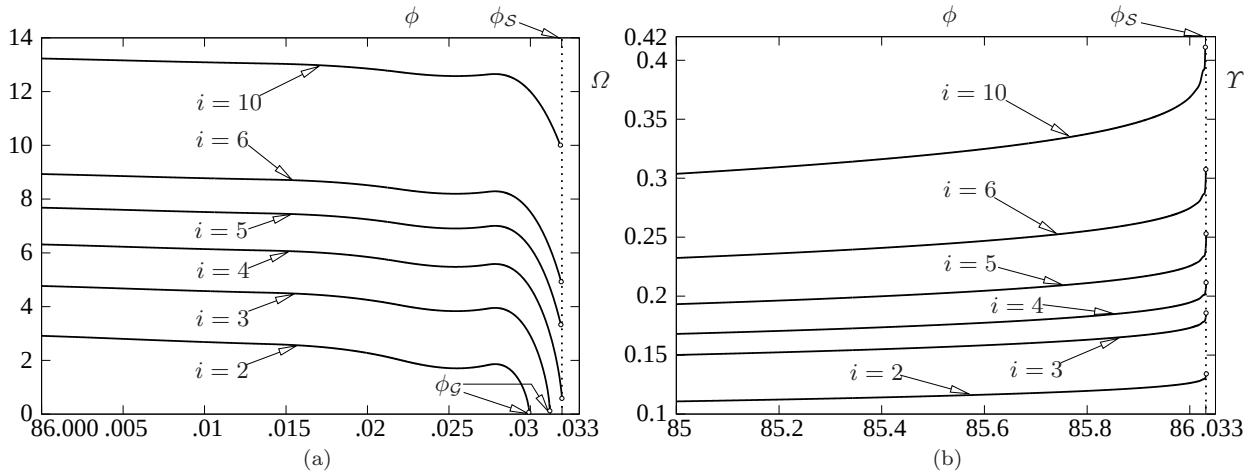

Figure 5. Key quantities of solutions of BL equations (12)–(15), for $k = 0.3$ and $T = i \times 10^4$ over arc angle $\phi\,[^\circ]$ as $\phi - \phi_{\mathcal{S}}(k) \to 0_-$, terminating at $\phi = \phi_{\mathcal{G}}(k,T)$ (positions indicated by circles): (a) reduced wall shear stress Ω, (b) displacement thickness Υ.

For sufficiently small value of T the BL behaves still laminar-like as the corresponding solutions are found to terminate in form of a Goldstein-type singularity at the location $\phi = \phi_{\mathcal{G}}(k,T)$, i.e. for $x = x_{\mathcal{G}}(k,T)$. That is, $\Omega(x;k,T) - (x_{\mathcal{G}};k,T)$ and $\Upsilon(x;k,T) - \Upsilon(x_{\mathcal{G}};k,T)$, respectively, vary with $(\phi_{\mathcal{G}} - \phi)^{1/2}$ to leading order as $\phi - \phi_{\mathcal{G}} \to 0_-$, in agreement with the analytical results of § III.B.3. Furthermore, $\phi = \phi_{\mathcal{G}}$ approaches $\phi = \phi_{\mathcal{S}}$ for increasing values of T. Eventually, when T assumes a certain value, say $T = T_{\mathcal{S}}(k)$ (here $T_{\mathcal{S}} \times 10^{-4}$ is slightly below 4), $\phi_{\mathcal{G}}(T_{\mathcal{S}}, k) = \phi_{\mathcal{S}}(k)$. In turn, for $T \geq T_{\mathcal{S}}$ the boundary-layer calculations break down at $\phi = \phi_{\mathcal{S}}(k)$, where Ω exhibits a finite limit. In fact, for $k = 0.3$ the numerical results obtained for relatively

large values of T strongly suggest a regular local behaviour of the solutions. Consequently, the fully turbulent BL obtained in the limit $T \to \infty$ having a velocity defect of $O(1/\ln T)$, would not separate at all. This result is entirely in line with the analytical investigation given in Ref. 6, which applies to the outer defect layer of a generic turbulent BL with an asymptotically small velocity deficit as $\phi - \phi_{\mathcal{S}} \to 0_-$, i.e. for $x - x_{\mathcal{S}} \to 0_-$. However, it apparently contradicts the analytically obtained results of § III.B.

V. Conclusions and Further Outlook

The present analysis is initiated by the assumption that, in the limit Eq. (1), the BL that stretches from $\mathcal{F}$ towards the point $\mathcal{S}$ of detachment of the free streamline is highly turbulent. Within the framework of BL theory this flow is governed by the Eqs. (12)–(15) for large values of T and under the action of a pressure gradient $-u_e u_{ex}$ that is impressed by the external Kirchhoff-type flow, parametrized by the BV parameter k. It has been shown in Ref. 1 that, in the limit $T \to \infty$, such a BL assumes the well-accepted two-tiered splitting. Furthermore, the existence of a front-stagnation point of the external potential flow ensures that $T \ll Re^{1/2}$. The hypothetical limit $T = Re^{1/2}$ pertains to a fully developed turbulent BL, where the viscous wall layer is characterized by a perfect equilibrium between the total and the wall shear stress to leading order. Moreover, we have demonstrated here that in this limit the strength of the Goldstein singularity that is induced by the rather abrupt pressure rise, expressed by Eq. (7), increases whereas the distance between its position and that of the BV singularity decreases asymptotically. This behavior is conveniently expressed by recasting the behavior of $\hat{\Psi}_{\hat{Y}\hat{Y}}$ for $\hat{Y} = 0$ given in Eq. (82) with the aid of Eqs. (16), (57), (58), (70), (75), and (81),

$$\Psi_{YY}(x, Y = 0; k, T) \sim T\gamma_0^6 (u_{e,\mathcal{S}}^{3/2}/k^3)[(\omega/\hat{s}_{\mathcal{G}})(x - x_{\mathcal{G}})]^{1/2} \quad (x \to x_{\mathcal{G}\_}), \quad x_{\mathcal{S}} - x_{\mathcal{G}} = \mathcal{O}[k^6/(T^8\gamma_0^{16}u_{e\mathcal{S}}^4)]. \tag{89}$$

It is also seen from these relationships that for sufficiently large but fixed values of T the strength of the Goldstein singularity decreases further, accompanied by a corresponding shift of $\mathcal{G}$ towards $\mathcal{S}$, in the limit $k \to 0_+$ that refers to laminar massive separation.[2,7,8] Contrarily, in the limit $k \to \infty$, i.e. for $u_{e,\mathcal{S}} \to 0$ as $\mathcal{S}$ is shifted towards $\mathcal{R}$, which is associated with the problem of trailing-edge flow considered in Refs. 4 and Ref. 6, the singularity decreases in strength whereas the breakdown of the BL equations is correspondingly delayed. Most important, as a consequence of the streamwise velocity defect of $\mathcal{O}(1/\ln T)$ that characterizes the outer main portion of the BL, this region is found to be largely unaffected by the singular behavior expressed in Eq. (89): it exhibits a perturbation about the terminal velocity profile, expressed by $F_{0\eta}(\eta; k)$, which is essentially of $\mathcal{O}[(-s)^{1/2}]$, see Eq. (40).

It is quite interesting that this theoretically predicted behavior of a turbulent BL slightly upstream of separation is strongly supported by the interpretation of experimental findings as well as numerical solutions of the BL equations based on commonly employed turbulence closure schemes, see Tsahalis and Telionis.[27] One should concede, however, albeit with some reservation, that the numerical results presented in § IV.B do not exclude the possibility that the Goldstein singularity is avoided for certain values of k. To the authors' present opinion, this situation is closely related to the suppression of eigensolutions that trigger the asymptotic splitting of the wall layer flow elucidated in § III.B.2. Of course, further research is required to shed light on the possibility of a second, different type of separation associated with this behavior.

Needless to say, however, an asymptotically correct description of the separation process requires an investigation of the full Reynolds-averaged equations of motion (2)–(4). Such a theory is presumably devised by exploiting the triple-deck formalism,[2] in order to take into account locally strong viscous/inviscid interaction in the vicinity of $\mathcal{S}$. The consequences of such a strategy include, amongst others, a distinguished limit $T = T(Re)$ as $T \to \infty$ and $Re \to \infty$ and were already alluded to by Neish and Smith,[4] who propose $T = \mathcal{O}(Re^{-1/18})$ for the case $0 < k < \infty$ of interest here. They arrive at this conclusion by exploiting scaling arguments and the assumption that the canonical triple-deck problem describing laminar break-away separation, established by Sychev[7] and originally solved numerically by Smith[8] (see also Ref. 2), can even be applied to the developed turbulent case. The latter property apparently has a profound basis as the region of nonlinear breakdown discussed in § III.B.3 then plays the role of the lower deck. In our point of view, however, their conclusion seems tentative for three reasons: first, their finding does not properly take into account the logarithmic law of the wall (28) and the inherently associated asymptotically small velocity deficit in the upper deck that is located at the base of the outer main region of the BL. Secondly, as has been demonstrated by Melnik and Chow,[28] the BL approximation ceases to be valid already in a region of streamwise extent of $\mathcal{O}(Re^{-1/2}T\gamma)$ that compares with the BL thickness, according to Eqs. (11) and (30),

and where the effect of the pressure gradient acting normal to the surface becomes important. Third, it is not clear for the time being how turbulence alters the downstream conditions that supplement the original triple-deck problem and account for the development of a separated shear layer and the region of weak reverse flow. These issues are topics of the ongoing research. Here we only give a rather coarse estimate for an upper bound of T: since the governing equations (2), (3) are required to reduce to a BL approximation in the lower deck, its streamwise extent must be asymptotically larger than that perpendicular to the surface in the limit (1). One deduces from Eqs. (11), (30), (38), (57), (58), and (70) that the former is of $\mathcal{O}[Re^{-1/2}(T\gamma_0)^{-1}]$ and the latter of $\mathcal{O}(T^{-4}\gamma_0^{-14})$, giving $T \ll Re^{1/6}(\ln Re)^{13/3}$. The most interesting feature, however, of the interaction problem to be derived concerns uniqueness of its solution. As in the laminar case,[8,29,30] it is very likely that a solution only exists for a single value of k with $0 < k < \infty$, which remains the only parameter entering that problem. Hence, in contrast to the laminar case where the solution approximately fixes the value of $kRe^{1/16}$ as $Re \to \infty$, for a developed turbulent BL the position of $\mathcal{S}$ on the body surface and hence the global potential flow is presumably selected by the solution of the local interaction problem.

A BL description akin to that presented here likely applies also to a further related topic of interest from the point of view of aerodynamics, namely, turbulent trailing edge-flow past a plate under angle of attack, then measured by k. Here we refer the preliminary asymptotic results given by Melnik and Chow.[28] Most important, it is very likely that a rational description of separation then also predicts a maximum level of turbulence intensity in the oncoming attached BL. As a remarkable – although tentative – conclusion drawn from these considerations is that the Reynolds stresses in a turbulent BL along a body of finite dimensions that undergoes break-away separation never exhibit their theoretically maximum possible magnitude, associated with the well-established two-tiered fully developed turbulent BL that was described in a self-consistent manner by Mellor[5] and is recovered in the case $T = Re^{1/2}$. A discussion of the consequences of this finding are certainly beyond the scope of the present analysis. However, it is corroborated by the fact that for fully developed turbulent flow the viscous wall layer is exponentially thin compared to the outer defect layer as these regions have thicknesses of $\mathcal{O}(\ln Re/Re)$ and $\mathcal{O}(1/\ln Re)$, respectively, cf. Eqs. (16), (30), by noting that $\sigma = \gamma$, and (38): that is, the triple-deck structure then does not apply here as the displacement exerted by the lower deck located in the wall layer is too weak to generate a sufficiently large pressure feedback in the same region which originates from the upper deck in the small defect-region. It seems that such a BL withstands a pressure rise that is associated with a value of k of $\mathcal{O}(1)$, cf. Eq. (7), which, however, contradicts the basic assumption of a free streamline originating in $\mathcal{S}$. In turn, it is felt that a proper coupling between k, T, and Re in the aforementioned case $k \to \infty$ implies larger values of T than those allowed in the case $k = \mathcal{O}(1)$, which is also indicated by Eq. (89). A treatment of this type of trailing-edge flow, based on the preceding analysis given in Refs. 4, 6, will be presented in a subsequent study.

Acknowledgments

Special thanks are due to Professor Frank T. Smith (Department of Mathematics, University College London, London, UK) for frank and stimulating discussions.

References

[1]Scheichl, B., Kluwick, A., and Alletto, M., ""How Turbulent" is the Boundary Layer Separating from a Bluff Body for Arbitrarily Large Reynolds Numbers?" *Acta Mechanica*, 2008, Special issue on the occasion of the 70th birthday of Professor Wilhelm Schneider, accepted for publication.

[2]Sychev, V. V., Ruban, A. I., Sychev, Vic. V., and Korolev, G. L., *Asymptotic Theory of Separated Flows*, edited by A. F. Messiter and M. Van Dyke, Cambridge University Press, Cambridge, UK, 1998.

[3]Gurevich, M. I., *The Theory of Jets in an Ideal Fluid*, Vol. 93 of Int. Series of Monographs in Pure and Applied Mathematics, Pergamon Press, Oxford, 1966, original Russian book: 1961, Moscow: Fizmatlit.

[4]Neish, A. and Smith, F. T., "On Turbulent Separation in the Flow past a Bluff Body," *Journal of Fluid Mechanics*, Vol. 241, Aug. 1992, pp. 443–467.

[5]Mellor, G. L., "The Large Reynolds Number, Asymptotic Theory of Turbulent Boundary Layers," *International Journal of Engineering Science*, Vol. 10, No. 10, 1972, pp. 851–873.

[6]Scheichl, B. and Kluwick, A., "Asymptotic Theory of Bluff-Body Separation: A Novel Shear-Layer Scaling Deduced from an Investigation of the Unsteady Motion," *Journal of Fluids and Structures*, Vol. 24, No. 8, Dec. 2008, Special issue on the IUTAM Symposium on Separated Flows and their Control, accepted for publication.

[7]Sychev, V. V., "Laminar Separation," *Fluid Dynamics*, Vol. 7, No. 3, 1972, pp. 407–417, original Russian article in *Izv. Akad. Nauk SSSR, Mekh. Zhidk. i Gaza* (3), 1972, 47–59.

[8]Smith, F. T., "The Laminar Separation of an Incompressible Fluid Streaming past a Smooth Surface," *Proceedings of the Royal Society of London* A, Vol. 356, No. 1687, 1977, pp. 443–463.

[9]Goldstein, S., "On Laminar Boundary Layer Flow near a Position of Separation," *The Quarterly Journal of Mechanics and Applied Mathematics*, Vol. 1, No. 1, 1948, pp. 43–69.

[10]Stewartson, K., "Is the singularity at separation removable?" *Journal of Fluid Mechanics*, Vol. 44, No. 2, Nov. 1970, pp. 347–364.

[11]Schewe, G., "Reynolds-number Effects in Flows Around More-or-less Bluff Bodies," *Journal of Wind Engineering & Industrial Aerodynamics*, Vol. 89, No. 14, 2001, pp. 1267–1289.

[12]Zdravkovich, M. M., *Flow Around Circular Cylinders. A Comprehensive Guide Through Flow Phenomena, Experiments, Applications, Mathematical Models, and Computer Simulations. Vol. 1: Fundamentals*, Oxford University Press, Oxford, New York, Tokyo, 1997.

[13]Schlichting, H. and Gersten, K., *Boundary-Layer Theory*, Springer-Verlag, Berlin, Heidelberg, Germany, 8th ed., 2000.

[14]Walker, J. D. A., Abbott, D. E., Scharnhorst, R. K., and Weigand, G. G., "Wall-Layer Model for the Velocity Profile in Turbulent Flows," *AIAA Journal*, Vol. 27, No. 2, Feb. 1989, pp. 140–149.

[15]Walker, J. D. A., "Turbulent Boundary Layers II: Further Developments," *Recent Advances in Boundary Layer Theory*, edited by A. Kluwick, Vol. 390 of *CISM Courses and Lectures*, Springer-Verlag, Vienna, New York, 1998, pp. 145–230.

[16]Scheichl, B. and Kluwick, A., "Turbulent shear-layer scaling in the limit of infinite Reynolds number derived from the unsteady equations of motion," *Proceedings of Applied Mathematics and Mechanics (PAMM)*, Vol. 7, No. 1, Dec. 2007, Special Issue: Sixth International Congress on Industrial Applied Mathematics (ICIAM07) and GAMM Annual Meeting – Zrich 2007, Paper ID 526 / DOI: 10.1002/pamm.200700526, accepted for publication.

[17]Scheichl, B. and Kluwick, A., "On turbulent marginal boundary layer separation: how the half-power law supersedes the logarithmic law of the wall," *International Journal of Computing Science and Mathematics (IJCSM)*, Vol. 1, No. 2/3/4, 2007, pp. 343–359, Special Issue on Problems Exhibiting Boundary and Interior Layers.

[18]Österlund, J. M., Johansson, A. V., Nagib, H. M., and Hites, M., "A Note on the Overlap Region in Turbulent Boundary Layers," *Physics of Fluids*, Vol. 12, No. 1, 2000, pp. 1–4, Letter.

[19]Scheichl, B. and Kluwick, A., "Turbulent Marginal Separation and the Turbulent Goldstein Problem," *AIAA Journal*, Vol. 45, No. 1, Jan. 2007, pp. 20–36, see also *AIAA paper 2005-4936*.

[20]Abramowitz, M. and Stegun, I. A., *Handbook of Mathematical Functions*, Dover Publications, New York, 9th ed., 1972.

[21]Messiter, A. F. and Enlow, R. L., "A Model for Laminar Boundary-Layer Flow near a Separation Point," *SIAM Journal on Applied Mathematics*, Vol. 25, No. 4, Dec. 1973, pp. 655–670.

[22]Southwell, R. V., F.R.S. and Vaisey, G., "Relaxation Methods Applied to Engineering Problems. XII. Fluid Motions Characterised by 'Free' Streamlines," *Phil. Trans. R. Soc. Lond.* A, Vol. 240, No. 815, Nov. 1946, pp. 117–161.

[23]Michel, R., Quémard, C., and Durant, R., "Hypothesis on the Mixing Length and Application to the Calculation of the Turbulent Boundary Layers," *Proceedings of Computations of Turbulent Boundary Layers – 1968 AFOSR-IFP-Stanford Conference. Methods, Predictions, Evaluation and Flow Structure*, edited by S. J. Kline, M. V. Morkovin, G. Sovran, and D. J. Cockrell, Vol. 1, Stanford University, Stanford, CA, 1969, pp. 195–207.

[24]Klebanoff, P. S., "Characteristics of Turbulence in a Boundary Layer with Zero Pressure Gradient," NACA Rept. 1247, NASA – Langley Research Center, Hampton, VA, 1955, see also NACA TN 3178, 1954.

[25]Grifoll, J. and Giralt, F., "The Near Wall Mixing Length Revisited," *International Journal of Heat and Mass Transfer*, Vol. 43, No. 19, 2000, pp. 3743–3746, Technical Note.

[26]Kays, W. M., "Turbulent Prandtl Number – Where Are We?" *ASME Journal of Heat Transfer*, Vol. 116, No. 2, May 1994, pp. 284–295.

[27]Tsahalis, D. T. and Telionis, D. P., "On the Behavior of Turbulent Boundary Layers near Separation," *AIAA Journal*, Vol. 13, No. 10, Oct. 1975, pp. 1261–1262, Synoptics.

[28]Melnik, R. E. and Chow, R., "Asymptotic Theory of Two-Dimensional Trailing-Edge Flow," NAS-1-12426, Grumman Aerospace Corporation, NASA – Langley Research Center, Hampton, VA, 1975.

[29]Korolev, G. L., "Numerical Solution of the Asymptotic Problem of Laminar Boundary-Layer Separation from a Smooth Surface," *Uch. zap. TsAGI*, Vol. 11, No. 2, Feb. 1980, pp. 27–36.

[30]van Dommelen, L. L. and Shen, S. F., "Interactive Separation from a Fixed Wall," *Numerical and Physical Aspects of Aerodynamic Flows II, Proceedings of the 2nd Symposium held at California State University, Long Beach, CA, 17–20 January, 1983*, edited by T. Cebeci, Springer-Verlag, New York, Berlin, Heidelberg, Tokyo, 1984, pp. 393–402.

Under consideration for publication in J. Fluid Mech.

Break-away separation for high turbulence intensity and large Reynolds number

B. SCHEICHL[1,2], A. KLUWICK[1] AND F. T. SMITH[3]

[1]Institute of Fluid Mechanics and Heat Transfer, Vienna University of Technology, Resselgasse 3/E322, A-1040 Vienna, Austria

[2]AC[2]T research GmbH, Austrian Center of Competence for Tribology, Viktor Kaplan-Straße 2, A-2700 Wiener Neustadt, Austria

[3]Department of Mathematics, UCL, Gower Street, London, WC1E 6BT, UK

(Received 3 March 2010; revised 10 August 2010; accepted 16 September 2010)

Massive flow separation from the surface of a plane bluff obstacle in an incompressible uniform stream is addressed theoretically for large values of the global Reynolds number Re. The analysis is motivated by a conclusion drawn from recent theoretical results which is corroborated by experimental findings but apparently contrasts with common reasoning: the attached boundary layer extending from the front stagnation point to the position of separation never attains a fully developed turbulent state, even for arbitrarily large Re. Consequently the boundary layer exhibits a certain level of turbulence intensity that is linked with the separation process, governed by local viscous–inviscid interaction. Eventually, the latter mechanism is expected to be associated with rapid change of the separating shear layer towards a fully developed turbulent one. A self-consistent flow description in the vicinity of separation is derived, where the present study includes the predominantly turbulent region. We establish a criterion that acts to select the position of separation. The basic analysis here which appears physically feasible and rational is carried out without needing to resort to a specific turbulence closure.

Key Words: Boundary Layers, Separation, Turbulent Flows

1. Introduction

Incompressible flow separation past a blunt cylinder with an impervious inflexible smooth surface is of vital interest from an engineering point of view where a reliable method is sought to predict the position of time-mean gross separation of the turbulent boundary layer. As Sandborn & Liu (1968) state at the very beginning of their experimental study, "Turbulent boundary-layer separation is normally listed as one of the most important unsolved problems in fluid mechanics . . . ", which represents quite a challenge. Considerable theoretical efforts however have not yet led to a fully self-consistent picture of the separation process even within the framework of a time-mean description of the flow. Also, despite the rapid progress made in recent years in Direct Numerical Simulation (DNS) and semi-direct numerical methods such as Large-Eddy and Detached-Eddy Simulation, existing computational techniques do not master fully this great challenge by producing sufficiently accurate solutions of the unsteady Navier–Stokes equations in particular. This is largely because in practical applications for instance in aerodynamics the relevant Reynolds numbers must be large enough for the boundary and separated shear

layer to exhibit rather high levels of turbulence intensity, and these Reynolds numbers are often too large to be dealt with adequately by numerical methods currently available.

The present study aims to shed some light on the intricate flow structure near separation with the goal of fostering future progress in modelling turbulent separating flows. It is desirable to gain deeper insight into two fundamental aspects which constitute the core problem: (i) the behaviour of the nominally two-dimensional steady flow in the vicinity of separation, and (ii) how the local theory describing (i) fits into the global picture of the flow past the obstacle under consideration. In the following all flow quantities are non-dimensional with respect to the speed $\tilde{U}$ of the unperturbed oncoming uniform flow, a typical body dimension $\tilde{L}$ (see figure 1a), and the (constant) fluid density. Furthermore, the global Reynolds number Re takes on arbitrarily large values,

$$Re = \tilde{U}\tilde{L}/\tilde{\nu} \gg 1. \tag{1.1}$$

where the constant $\tilde{\nu}$ is the kinematic viscosity of the fluid. Analytical methods such as matched asymptotic expansions then provide an appropriate means to establish a rational theory on the basis of the time- or, equivalently, Reynolds-averaged Navier–Stokes (RANS) equations, i.e. the Reynolds equations.

In laminar flow (however inadequate that presumption may be on physical grounds) the triple-deck structure provides a rational description of break-away separation for (1.1), at least locally: Sychev (1972), Smith (1977). For an overview of the laminar bluff-body problem, including the controversy concerning the validity and preference of a particular model of the large-scale separated flow, see Smith (1979, 1985, 1986), Chernyshenko (1988), Sychev *et al.* (1998) for instance; the currently accepted solution was put forward by Chernyshenko (1988), and an overview of the whole subject is in Sychev *et al.* (1998). In turbulent flow the current state of asymptotic theory for the fully developed turbulent case is described by Kluwick & Scheichl (2009). A local description of the separation process was attempted systematically in interesting original works by Sychev & Sychev (1980), Sychev (1983), Sychev (1987), Melnik (1989); for further references and a discussion of these enthralling and illuminating attempts see Neish & Smith (1992), Scheichl & Kluwick (2008a). In a recent development (Scheichl, Kluwick & Alletto 2008; Scheichl & Kluwick 2008b) a self-consistent flow structure matching the boundary layer region with the small region of pronounced laminar–turbulent transition near the leading edge of the obstacle is found to agree with the classical picture of a two-tiered turbulent boundary layer. It consists of (first) the fully turbulent outer main region comprising most of the boundary layer, which exhibits a small defect of the streamwise velocity component with respect to its value imposed by the external potential flow and has Reynolds stresses dominating over the viscous shear stress, and (second) the viscous wall layer, where the turbulent shear stress and its molecular counterpart are of comparable magnitude. In the present study that classical structure is adjusted in order to also account for *underdeveloped* turbulence (following the measurements of Schewe 2001 and suggestions of Scheichl *et al.* 2008, Scheichl & Kluwick 2008b below), i.e. for a boundary layer characterised by a level of turbulence intensity below that of a fully developed turbulent boundary layer flow. In the present investigation this concept is restricted to sufficiently high turbulence intensities, so that the turbulent boundary layer already exhibits the aforementioned typical two-tiered structure. More specifically, here the notion of *slightly underdeveloped* turbulence turns out to be crucial.

This type of 'transitional' boundary layer flow was originally proposed by Neish & Smith (1992). In its form adopted here two asymptotically small perturbation parameters are employed: a measure for the velocity defect, ϵ, and a further one, σ, for the boundary

layer thickness, denoted by δ. Hence, the quantity

$$I_t = \alpha\epsilon^2, \quad \text{with} \quad \alpha = \sigma/\epsilon, \tag{1.2}$$

measures the magnitude of the correlation of the turbulent velocity fluctuations, i.e. of the Reynolds stresses or the turbulence intensity, in the shear layer. We deal with slightly underdeveloped turbulent flow if both of the following relationships hold:

$$\epsilon \ln Re = O(1), \tag{1.3a}$$

$$\alpha \ll 1. \tag{1.3b}$$

This eventually assumes its fully developed form if both σ and ϵ are of $O(1/\ln Re)$, i.e. then $\alpha = O(1)$. The ranges (1.3) control the turbulence intensity levels, where (1.3*b*) alone emerges to characterise underdeveloped turbulence. The process of laminar–turbulent transition provides a source (Scheichl *et al.* 2008; Scheichl & Kluwick 2008*b*) of delaying the boundary layer flow from becoming a fully developed turbulent one, so that we speak of a laminar-turbulent boundary layer in the following. Self-consistency of the slightly-underdeveloped-flow scaling is confirmed by considering the local asymptotic structure of the boundary layer close to separation: free-stream convection penetrates through the outer layer to the top of the wall layer, which is exponentially thin compared to the former in the classical (fully developed) case. Then the pressure feedback exerted by the induced inviscid region that feels the local displacement of the flow adjacent to the surface is too weak to alter this near-wall flow to leading order and avoid the formation of a Goldstein singularity (cf. Rothmayer & Smith 1998; Sychev *et al.* 1998). Thus a sound formulation of this locally strong viscous–inviscid interaction process requires the von Kármán number δ^+ (namely the ratio of the inner- and the outer-layer thicknesses) to vary essentially algebraically with $1/\delta$ rather than exponentially as in the classical case. In other words, δ is found to depend predominantly algebraically on Re rather than logarithmically, associated with the classical scaling. Moreover a detailed analysis of a turbulent boundary layer evolving from the leading edge towards the location of separation (Scheichl & Kluwick 2008*b*) indicates that the first situation leads to a specific (distinguished) double limit $\epsilon \to 0$, $\alpha \to 0$, such that the associated dependence of α on Re determines the ultimate value of the turbulence-intensity level I_t possible.

Altogether, turbulent separation is found to be associated with a quite complex interplay of a so-called inner and an outer mechanism of local viscous–inviscid interaction. In this paper we concentrate on both mechanisms; however, particular details of the latter and its interplay with the inner interaction will be addressed more elaborately in a later study. The outer interaction is of paramount importance for the understanding of the drastic change of the flow in the wall layer as it undergoes separation, itself governed by the inner interaction process. The inner interaction process gives rise to a novel internal triple-deck structure which is located at the base of the boundary layer and which eventually fixes the value of I_t.

The concept of slightly underdeveloped turbulence adopted in the present analysis is novel and somewhat unconventional but is supported by the oil-flow measurements carried out by Schewe (2001) as discussed by Scheichl *et al.* (2008), Scheichl & Kluwick (2008*b*). Also Sandberg & Sandham (2008) conclude, albeit with some reservation, from the results of their DNS study that the turbulent flow close to the trailing edge of a flat plate aligned in a uniform stream exhibits characteristics which point to the well-known triple-deck structure as in laminar flow: see Rothmayer & Smith (1998), Sychev *et al.* (1998). Although not directly concerned with separation from a smooth surface, this finding is of particular interest: it is demonstrated below how the asymptotic representation

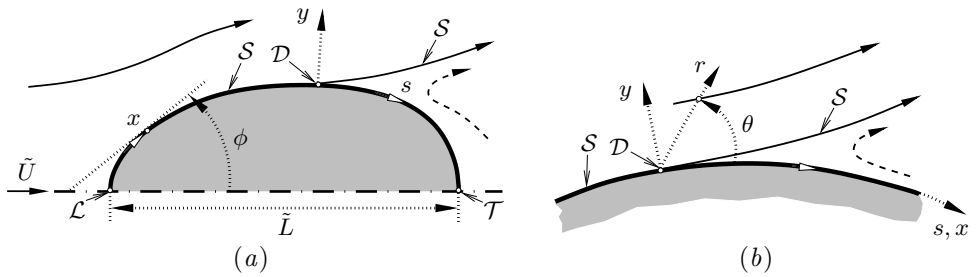

FIGURE 1. Sketch of flow situation, including streamlines of inviscid flow (arrows indicate flow direction, for caption see text): —— free-stream region, - - - - slipstream;
(a) global (here shown for a symmetric body), (b) local (near the position $\mathcal{D}$ of flow detachment).

of the flow near separation in the regime of the outer interaction is closely related to that occurring in the turbulent flow past the trailing edge of a flat plate at angle of attack as considered first by Melnik & Chow (1975). The differences are mainly due to different near-wall boundary conditions downstream of separation.

The paper is organised as follows. After the problem description on the basis of the Reynolds equations in § 2 an outline for the external and boundary layer flows is given in § 3, concluded by the rationale supporting the existence of underdeveloped turbulent boundary layer flow and the definition of the slightly underdeveloped case. The results presented lead to a complete flow picture and a thorough investigation of the inner and (less elaborately) the outer interaction process as in § 5. The solutions of the impressed potential flow as well as the boundary layer equations that govern the outer small-defect portion of the oncoming turbulent flow enter the interactive-flow description in the form of certain parameters and require both an analytical and numerical treatment: they are discussed separately in § 4. Finally, the implications of the description of separation here are highlighted in § 6. Also, those assumptions made in the course of the analysis with the most important repercussions on its progress are summarised there.

2. Problem formulation

As a starting point, we formulate the basic equations governing the time-mean flow past the cylindrical body under consideration. In this section and in § 3 we tacitly refer to figure 1 whenever necessary.

Let x, y, u, v, ψ, p denote natural coordinates along and perpendicular to the upper part of the perfectly smooth body surface, respectively, having the origin in the point $\mathcal{L}$ defining the leading edge of the cylinder, the velocity components in x- and y-directions, the stream function, and the pressure. Furthermore, $\phi(x)$ denotes the angle of inclination of the surface contour at a distance x measured counter-clockwise from the direction of the oncoming parallel flow. Then the value of the surface curvature

$$\varkappa(x) = -\mathrm{d}\phi/\mathrm{d}x \tag{2.1}$$

is positive/negative for a convex/concave part of the contour. In turn, the continuity equation is satisfied identically with $u = \partial_y\psi$, $hv = -\partial_x\psi$, where $h = 1 + \varkappa y$. Hence, the Reynolds equations consist of the momentum equations for the x- and y-directions (see e.g. Schlichting & Gersten 2003, p. 81),

$$h^2 D_t\partial_y\psi - \varkappa(\partial_x\psi)(\partial_y\psi) = -h\partial_x p - h\partial_x\langle u'^2\rangle - \partial_y(h^2\langle u'v'\rangle) + \nu h^2\partial_y\nabla^2\psi, \tag{2.2a}$$

$$-hD_t(h^{-1}\partial_x\psi) - \varkappa(\partial_y\psi)^2 = -h\partial_y p - \partial_y(h\langle v'^2\rangle) - \partial_x\langle u'v'\rangle + \varkappa\langle u'^2\rangle - \nu\partial_x\nabla^2\psi, \tag{2.2b}$$

where $\nu = Re^{-1}$ (for the sake of brevity) and the total derivative and the Laplacian are written as

$$D_t = h^{-1}[\partial_y\psi\,\partial_x - \partial_x\psi\,\partial_y], \quad \nabla^2 = h^{-1}[\partial_x(h^{-1}\partial_x) + \partial_y(h\partial_y)]. \tag{2.2c}$$

Also, u', v' denote the turbulent fluctuations of the x- and y-velocity components respectively. Thus, the components of the Reynolds stress tensor are identified by $\langle\cdot\rangle$. Equations (2.2) are supplemented with the usual no-slip and no-penetration boundary conditions at the solid cylinder surface and the requirement for uniform parallel flow infinitely remote from the body, such that for

$$y = 0\colon \quad u = v = u' = v' = 0, \tag{2.3}$$

$$y \to \infty\colon \quad [u, v, u', v', p] \to [\cos\phi, -\sin\phi, 0, 0, 0]. \tag{2.4}$$

Here ϕ is the slope angle introduced before.

Furthermore, in the following we tacitly assume that all components of the Reynolds stress tensor have the same order of magnitude under the assumption (1.1) (hypothesis of locally isotropic turbulence, cf. Kolmogorov 1961 and references therein).

We subsequently aim at investigating the flow in the vicinity of separation in the regime (1.1) on the basis of (2.2)–(2.4). To this end, we start with considerations regarding the overall asymptotic picture of the (non-interactive) flow as put forward by Scheichl *et al.* (2008) and Scheichl & Kluwick (2008*b*). This is the subject of § 3.

3. Overall background and preliminary results

The structure of the flow on the scale of body dimensions under the assumption (1.1) represents a decisive but delicate issue still under debate. Nonetheless, its rather few salient properties underlying the present analysis seem plausible.

3.1. *Does Euler flow provide a feasible asymptotic state for large values of Re?*

As will be argued in § 3.4.1, the attached boundary layer emanating from $\mathcal{L}$ exhibits underdeveloped turbulence and thus typically shrinks towards the line $y = 0$ as Re increases. On the other hand, it is a widely accepted fact that a free turbulent shear layer is a fully developed and 'thick' one insofar as its thickness is essentially independent of Re and measures the turbulence intensity concentrated in it. However, from an empirical point of view such a shear layer can still be regarded as relatively slender though, as was put in a formal asymptotic concept first successfully by Schneider (1991); for boundary layers see Melnik (1989), Scheichl & Kluwick (2007*b*). Hence, the existence of separated flow here does not restrain us from regarding the Reynolds stresses as negligibly small entirely within an extent of a typical body dimension from the body surface, so that (2.2*a*), (2.2*b*) reduce to the Euler equations in the present regime. Therefore the question posed at the beginning of this section is answered in the affirmative, even if tentatively.

We concede of course that the real behaviour of the flow may be different due to the effect of the free shear layers, but, hopefully, not too different from the model proposed here, so that it can be adapted in a self-consistent manner. We are also aware that the picture of the global flow remains incomplete as long as transition of the just separated shear layer to a fully developed one is accepted without being understood in detail. An interesting step in this direction was made recently by Sychev (2010).

This flow behaviour considered here then is accounted for by the leading-order term of the expansion

$$[\psi, u, v, p] \sim [\psi_0, u_0, v_0, p_0](x, y; k) + O(\epsilon\sigma), \quad y = O(1), \tag{3.1}$$

which is suggested by the form of the small-defect structure of the boundary layer as already addressed in § 1. The non-negative parameter k shall account for the initially unknown location $x = x_{\mathcal{D}}(k)$ of the point $\mathcal{D}$ where the free streamline, on which $\psi_0 = 0$ by definition and here denoted by $\mathcal{S}$, detaches tangentially from the body surface. A precise definition of k that involves the structure of the flow near $\mathcal{D}$ is given in the course of its further discussion (see § 3.3). Next, we subsume the essential topological properties of that Euler flow which, in view of (1.1), is formally assumed in the limit of arbitrarily large values of Re.

3.2. *Global picture of inviscid flow*

The inviscid free-stream flow, characterised by $y \geqslant y_{\mathcal{S}}$, is irrotational. The potential flows past a cylinder that are parametrised by k and leave a (semi-infinitely) open cavity, i.e. a dead-water zone where $p_0 \equiv 0$ according to the far-field conditions (2.4), downstream of the body are usually referred to as Helmholtz–Kirchhoff (HK) flows; for an extensive treatment see e.g. the textbook by Gurevich (1979). It is self-evident that in this case (2.4) only holds outside the cavity. In contrast to the more general approach proposed subsequently but according to what is conventionally suggested in previous related studies, it should be mentioned that Sychev *et al.* (1998) (also cf. the references therein) and Schlichting & Gersten (2003) consider this type of a potential flow as the only physically realistic one that is representative in the case (1.1), in agreement with the prerequisites of the original analysis of laminar separation by Sychev (1972), at least as far as steady flows are concerned.

In the following we relax the assumption that in the inviscid-flow limit, formally expressed as $Re^{-1} = 0$, the slipstream of the body degenerates into an open cavity: it is equivalently reasonable from the viewpoint of first principles that the terminal asymptotic picture of the flow about the cylinder exhibits a closed region that either forms a dead-water cavity (cf. Eppler 1954; Gurevich 1979) or even an inviscid recirculating flow with (negative) vorticity, hereafter denoted by ω_0, behind the body. This region then is assumed to have an extent comparable to a characteristic dimension of the body and thus to lie within a distance $y = O(1)$ from the trailing edge, denoted by $\mathcal{T}$. Under the assumption of a dead-water region confined by $\mathcal{S}$ the first possibility applies when $\mathcal{D}$ is sufficiently close to $\mathcal{T}$. Then the uniform k-dependent value of p_0 typical for the (cusp-shaped) dead-water zone is positive. One should mention, however, that this patently contrasts with experimental findings as these support the existence of a sub-pressure cavity (cf. Zdravkovich 1997), even for $Re \doteq 1.782 \times 10^7$ for a circular cylinder and Re formed with its diameter (Jones, Cincotta & Walker 1969). The second possibility is associated with a rich variety of complex flow pictures and comprises the first situation by including the trivial case $\omega_0 \equiv 0$ ($y \geqslant 0$). Due to the inherent impact of turbulent unsteadiness on the flow even for arbitrarily large values of Re, for $\omega_0 \not\equiv 0$ the (two) counter-rotating eddies are not necessarily of the celebrated Prandtl–Batchelor type, where each eddy is identified by a uniform value of ω_0 (Batchelor 1956*a*,*b*): the latter situation only applies if the unsteady terms in the Navier–Stokes equations tend to zero faster than the viscous ones for increasing values of Re. In passing we note that critical overviews on such categories of inviscid flows, exhibiting different forms of closed wakes, are put forward by Wu (1972), Zdravkovich (1997), and Sychev *et al.* (1998). Both scenarios discussed so far are displayed in figure 2, where $\mathcal{C}$ denotes the point confining either the cavity or the wake flow on the centreline. In the first the free streamlines $\mathcal{S}$ indicated by I, II, III refer to the cases $k < k_c$ (HK flow), $k = k_c$ ($\mathcal{C}$ infinitely remote), and $k > k_c$ ($\mathcal{C}$ finitely remote), respectively, for some critical value k_c depending on the body geometry.

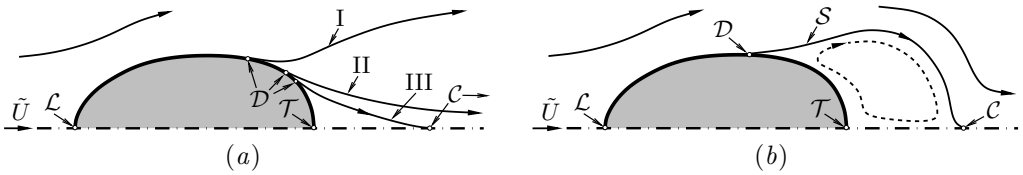

FIGURE 2. Sketch of inviscid (here symmetric) bluff-body flows (for caption see text and figure 1): $\mathcal{S}$ separating (a) a cavity, (b) a vortex flow (here assumed to form a cusp near $\mathcal{C}$).

We now focus briefly on the specific asymptotic structure of the external Euler flow and the initially attached boundary layer, by both taking up a global point of view and scrutinising the vicinity of the point of separation $\mathcal{D}$.

3.3. *Inviscid free-streamline theory reappraised*

The reasoning outlined so far in § 3 implies that the Euler flow around the cylinder is sought in the class of flows that are irrotational far upstream (and downstream), exhibit free streamlines and, as a consequence, are essentially parametrised by the parameter k. A careful investigation of the inviscid flow near $\mathcal{D}$ provides a first step towards the understanding of the separation process.

By introducing a local coordinate

$$s = x - x_{\mathcal{D}}(k), \tag{3.2}$$

let $y = y_{\mathcal{S}}(s;k)$ describe the position of $\mathcal{S}$, so that $y_{\mathcal{S}} = 0$ for $s \leqslant 0$ (upstream of $\mathcal{D}$) and $y_{\mathcal{S}} > 0$ for $s > 0$ (downstream of $\mathcal{D}$). That is, $\mathcal{S}$ separates the irrotational free-stream flow ($y \geqslant y_{\mathcal{S}}$) from the slipstream ($s > 0$, $0 \leqslant y < y_{\mathcal{S}}$). Also, we introduce the speed $U_{\mathcal{S}}(x;k)$ of the inviscid flow on $\mathcal{S}$. The flow in $\mathcal{D}$ then is characterised by the as yet unknown values $u_{0\mathcal{D}} = U_{\mathcal{S}}(x_{\mathcal{D}};k) = u_0(x_{\mathcal{D}},0;k)$, $p_{0\mathcal{D}} = p_0(x_{\mathcal{D}},0;k)$, and the local surface curvature $\varkappa_{\mathcal{D}} = \varkappa(x_{\mathcal{D}})$ according to (2.1). For $s > 0$, in the following the subscripts $+$ and $-$ distinguish the different values of $U_{\mathcal{S}}$ for $y - y_{\mathcal{S}} = 0_+$ and $y - y_{\mathcal{S}} = 0_-$ respectively. In light of the central investigation it seems expedient to demonstrate concisely how one can determine the asymptotic representations of ψ_0, p_0 (see (3.1)), $U_{\mathcal{S}}$, and $y_{\mathcal{S}}$ in the vicinity of $\mathcal{D}$ term by term iteratively (in principle with arbitrary accuracy) by prescribing $\omega_0(\psi_0;k)$. As a matter of fact, the specific form of $\omega_0(\psi_0;k)$ is expected to be known once the self-consistent asymptotic structure of the large-scale separated flow under the assumption (1.1) is understood satisfactorily well.

Here we list the results of that local analysis possessing ramifications on the remaining study, where the details are left to Appendix A. At first we obtain

$$\psi_0/U_{\mathcal{S}} \sim y - \varkappa y^2/2 + O(y^3), \quad s \leqslant 0, \quad y \to 0. \tag{3.3}$$

By setting $p_{\mathcal{S}}(x;k) = p_0$ on $\mathcal{S}$ we have

$$p_{\mathcal{S}} + U_{\mathcal{S}}^2/2 = 1/2, \quad \psi_0 \geqslant 0, \tag{3.4}$$

and $p_{0\mathcal{D}} = (1 - u_{0\mathcal{D}}^2)/2$ for the pressure at separation. Polar coordinates

$$r = \sqrt{s^2 + y^2}, \quad \theta = \arctan(y/s) \quad (\pi \geqslant \theta \geqslant 0) \tag{3.5}$$

come into operation as they facilitate the resultant expansion of ψ_0 in suitable form,

$$\psi_0/u_{0\mathcal{D}} \sim r\sin\theta + \psi_{0,3/2}(r,\theta;k) + \psi_{02}(r,\theta;k) + O(r^{5/2}), \quad \pi \geqslant \theta > 0, \quad r \to 0, \tag{3.6a}$$

$$\psi_{0,3/2} = -\frac{4k}{3} r^{3/2}\cos(3\theta/2), \quad \psi_{02} = -r^2\left\{\frac{5k^2}{3}\sin(2\theta) + \frac{\varkappa_{\mathcal{D}}}{4}\left[1 - \cos(2\theta)\right]\right\}. \tag{3.6b}$$

Finally, we obtain

$$U_{\mathcal{S}} \sim b(k)x + O(x^2), \quad b(k) > 0, \quad x \to 0_+, \tag{3.7a}$$

$$U_{\mathcal{S}}/u_{0\mathcal{D}} \sim 1 + 2k(-s)^{1/2} + (10k^2/3)(-s) + O\big[(-s)^{3/2}\big], \quad s \to 0_-, \tag{3.7b}$$

and in turn, with the aid of (3.4),

$$p_{\mathcal{S}}/u_{0\mathcal{D}}^2 \sim \big(u_{0\mathcal{D}}^{-2} - 1\big)/2 - 2k(-s)^{1/2} - (16k^2/3)(-s) + O\big[(-s)^{3/2}\big], \quad s \to 0_-, \tag{3.8}$$

and

$$U_{\mathcal{S}+}/u_{0\mathcal{D}} \sim 1 - (\omega_{0\mathcal{D}}/u_{0\mathcal{D}}^2)(2k/3)s^{3/2} + O(s^{5/2}), \quad s \to 0_+, \tag{3.9a}$$

$$y_{\mathcal{S}} \sim (4k/3)s^{3/2} + O(s^{5/2}), \quad s \to 0_+. \tag{3.9b}$$

From (3.9b) it immediately follows that indeed $k \geqslant 0$ for geometrical reasons. The region of non-uniformity along $\mathcal{S}$ mentioned at the end of item (i) in Appendix A emerges for $y = O(s^{3/2})$ and represents the early-stage separated shear layer in the inviscid limit. In the above added form (3.7a) of $U_{\mathcal{S}}$ near $\mathcal{L}$ the coefficient b reflects the local behaviour of the stagnant potential flow. Expansions (3.6)–(3.9) represent a summary of the results that are essential for the further analysis. We remark that they are uniformly valid in the regime $k \geqslant 0$.

The vorticity ω_0 is found to enter the description of the potential flow only in the truncated terms in (3.6a), (3.7b), (3.8), not considered here. The singular behaviour of ψ_0 near $\mathcal{D}$ accounted for by the second contributions to these expansions and in (3.9) reflects the well-known Brillouin–Villat (BV) singularity (cf. Gurevich 1979), which here we have retrieved without restricting to the conventional assumption that the free streamline $\mathcal{S}$ confines a dead-water region ($\omega_0 \equiv 0$). Accordingly, the here important result (3.6) has been derived directly rather than from the global solution of the potential flow, which in the existing literature is usually obtained in a distinctly more cumbersome manner by means of conformal mapping. A short survey on this procedure is presented in Appendix B.

The strength of the BV singularity is measured by the flow parameter k, which virtually controls the magnitude of the unbounded adverse pressure gradient immediately upstream of $\mathcal{D}$, given by (3.8) in the form $\mathrm{d}p_{\mathcal{S}}/\mathrm{d}x \sim k(-s)^{-1/2} + O(1)$ as $s \to 0_-$. In this study we deal with $k = O(1)$, which contrasts with the description of laminar break-away separation where $k = O(Re^{-1/16})$ (cf. Sychev 1972; Smith 1977; Sychev *et al.* 1998). However, it is well-accepted that turbulent boundary layers are less prone to separate than laminar ones, which substantiates the present approach, by Neish & Smith (1992) referred to as 'non-smooth' separation, in allusion to the singular behaviour of the curvature of $\mathcal{S}$ given by (3.9b). That is, we anticipate that one cannot determine the actual value of k and, in turn, the position of $\mathcal{D}$ without having gained a considerably deeper insight in the interplay of the boundary layer and the large-scale separated-flow structure. In case of $\omega_0 \equiv 0$ and for a convex cylinder $x_{\mathcal{D}}$ is shifted towards $\mathcal{T}$ for increasing values of k, accompanied by decreasing values of $u_{0\mathcal{D}}$. It should be mentioned that the assumption $k \gg 1$ refers to separation asymptotically close to $\mathcal{T}$ where $u_{0\mathcal{D}}$ becomes asymptotically small (see figure 2a). This limiting scenario has been addressed first by Neish & Smith (1992) and critically reviewed by Scheichl & Kluwick (2008a), at least for the case of a fully developed turbulent boundary layer immersed in fully attached potential flow, here recovered in the formal limit $k^{-1} = 0$ under the premise (1.1).

3.4. *Incident attached boundary layer*

The attached portion of the boundary layer forming in the regime (1.1) is 'trapped' as it stretches approximately from $\mathcal{L}$ to $\mathcal{D}$ over a finite distance, regardless of the actual value of Re. This characteristic of bluff-body flows is apparently strongly linked to the effective magnitude of the asymptotic parameters ϵ, σ, and α, introduced in § 1, and the associated level of turbulence intensity I_t, defined in (1.2), that prevails in the entire boundary layer. We start with an outline of the generation of the turbulent boundary layer close to $\mathcal{L}$. This specific picture of short-scale transition then is remarkably found to promote the assumption of underdeveloped turbulence. Finally, this state of flow is identified by (1.3*b*), which results from the order-of-magnitude analysis of ϵ and σ performed in § 3.4.3.

3.4.1. *Onset of turbulence*

In the setting of the original formulation of boundary layer turbulence by Neish & Smith (1992) that also covers underdeveloped turbulence the Reynolds shear stress in the boundary layer is written as

$$-\langle u'v'\rangle = TRe^{-1/2}\bar{\Sigma}(x,\bar{y};k,T), \quad \bar{y} = yRe^{1/2}. \tag{3.10}$$

Here T and $\bar{\Sigma}$ denote, respectively, the non-negative constant so-called turbulence-intensity gauge factor that serves to quantify the magnitude of the Reynolds shear stress, and a shape function (that has to be modelled). Owing to this scaling, the term $T\partial_{\bar{y}}\bar{\Sigma}$ adds to the conventional Prandtl-type boundary layer equations (formed with x, $\bar{y}$ used as independent variables). Their solutions then are parametrised by T (aside from k). They describe purely laminar flow for $T = 0$, whereas the subsequently interesting case of highly developed turbulence is indicated by $T \gg 1$. It will become evident in the course of the subsequent investigation that the latter case is preferably described by virtue of the formalism already outlined in § 1: i.e. in terms of the two parameters ϵ and σ, forming I_t, and their asymptotic dependencies both on T and Re, instead of T and Re.

The analysis by Scheichl *et al.* (2008) and Scheichl & Kluwick (2008*b*) suggests that for arbitrarily large values of Re the boundary layer evolves from the well-understood stagnant laminar flow (cf. Schlichting & Gersten 2003) taking place in a small vicinity of $\mathcal{L}$ with an extent of $Re^{-1/2}$ and undergoes rapid laminar–turbulent transition in a relatively small adjacent region where the flow is still of boundary layer type. The idea that $U_{\mathcal{S}}$ provides the only reference velocity of that flow stimulates the scaling relation $\bar{\Sigma} = O(U_{\mathcal{S}}^2)$. Inspection-of-magnitude analysis of (2.2*a*) in connection with (3.7*a*) then yields the estimates $x = O(T^{-1})$, $\bar{y} = O(1)$ for this region of transition, which in turn implicates

$$TRe^{-1/2} \ll 1. \tag{3.11}$$

Furthermore, we recall that in the regime (1.1) the turbulent dynamics is more-or-less constricted to a relatively thin boundary layer present for $x = O(1)$. Under this basic supposition matching this developed turbulent boundary layer flow with that early-stage turbulent flow is found to require a small streamwise velocity deficit with respect to $U_{\mathcal{S}}$ in the bulk of the former, i.e. $1 - u/U_{\mathcal{S}} \ll 1$. However, the scalings of the Reynolds stresses and in turn of the boundary layer thickness δ first remain unknown. A most simple strategy, motivated by physical reasoning and consistent with the considerations above leading to (3.11), to proceed with the scaling of the flow is to assume that both regions have in common that the turbulent motion is governed by a single velocity scale: this is initially represented by $U_{\mathcal{S}}$, which is superseded by a turbulent reference velocity $u_t(x;k,Re)$ when $x = O(1)$, so that there

$$1 - u/U_{\mathcal{S}} = O(\gamma), \quad \bar{\Sigma}/U_{\mathcal{S}}^2 = O(\gamma^2), \quad \text{with} \quad \gamma = u_t/U_{\mathcal{S}} \sim \epsilon. \tag{3.12}$$

The advanced (far-downstream) stage of the transition process characterised by an intermediate limit of the form $T^{-1} \ll x \ll 1$ is associated with a correspondingly pronounced reduction of the streamwise velocity defect in the main region of the boundary layer. Simultaneously, the value of the turbulence-intensity level I_t increases and eventually reaches its maximum for $x = O(1)$. There the velocity defect is of $O(\epsilon)$ finally, which motivates us to stipulate asymptotic proportionality between ϵ and γ in (3.12). Specifically, it will become evident below how the definition of ϵ is traced back to this relation, without any loss of generality.

The turbulent boundary layer is driven by $U_{\mathcal{S}}$, known from the solution for ψ_0, from $\mathcal{L}$ towards $\mathcal{D}$. Its behaviour near these critical points is essentially determined by the local expansions (3.7). We initially reconsider the relevant conclusions inferred from the first-order description of (underdeveloped) turbulent boundary layer flow.

3.4.2. *First-order theory*

As brought out by e.g. Schlichting & Gersten (2003), turbulent shear flows are intrinsically tied to a rather pronounced change from the external almost irrotational to the fully turbulent flow inside the boundary layer. In a rigorous asymptotic framework this is accounted for by the outermost tier of the boundary layer that is extremely thin relative to its main region. It is formed at the aforementioned final stage of the transition process and accompanied by an increase of the boundary layer thickness proportional to x (which reflects the vanishing effect of the viscous shear stress and thus the lack of a typical boundary layer length scale in the regime $T^{-1} \ll x \ll 1$). Since in the present context the specific properties of that overlayer do not play an important role, it can be approximated with sufficient accuracy by the sharp line $y = \delta$, with $\delta = O(\sigma)$. Then the distinct outer edge of the boundary layer and its thickness δ are well-defined. Thereby a patching of the flow quantities is required at $y = \delta$, specifically for u and the boundary layer approximation $-\partial_y u$ of the vorticity, such that u is smooth there. Taking up the more computational point of view, we accomplish this by employing a mixing-length-based closure of the Reynolds shear stress, notwithstanding the alternative (rather more conventional) eddy-viscosity-based approach in favour of claiming a diffusive decay of vorticity. This is aligned with the usual technique of matching as known from laminar shear flows and adopted by e.g. Neish & Smith (1988, 1992).

As an even more important finding, (2.2), (3.3) imply $p \sim p_{\mathcal{S}} + U_{\mathcal{S}}^2 \varkappa y + O(\epsilon^2, \alpha^2\epsilon^2)$ throughout the turbulent boundary layer. In the outer small-defect region (2.2a) then reduces to the differential form of (3.4), $\mathrm{d}p_{\mathcal{S}}/\mathrm{d}x = -U_{\mathcal{S}}\,\mathrm{d}U_{\mathcal{S}}/\mathrm{d}x$ to leading order, and the defect structure is essentially described by the scaling introduced in § 3.4.1. Inspection of (2.2a), (3.3) then shows that for any $\epsilon \ll 1$, $\sigma \ll 1$ the flow in the small-defect region is governed by the expansions

$$\left[\frac{U_{\mathcal{S}}\eta - \psi/\delta}{u_t}, \frac{-\langle u'v'\rangle}{\alpha u_t^2}\right] \sim [F, \Sigma](x, \eta; k) + O(\epsilon, \alpha\epsilon), \quad \frac{\delta}{\sigma} \sim \Delta(x; k) + O(\epsilon), \qquad (3.13a)$$

$$0 < x < x_{\mathcal{D}}, \quad \eta = y/\delta, \quad 0 < \eta \leqslant 1. \qquad (3.13b)$$

Here higher-order contributions of $O(\epsilon)$ are triggered by the nonlinearities of the inertia terms in (2.2a), which, however, appear to be unessential in view of the subsequent investigation.

An investigation of the boundary layer approximation of (2.2a) involving the first-order quantities F, Σ, Δ reveals that these can only be matched with the flow quantities in the aforementioned region of rapid transition if Σ assumes a finite limit at the base of the defect layer (Scheichl *et al.* 2008; Scheichl & Kluwick 2008*b*, 2009; Kluwick &

Scheichl 2009). This is accounted for by choosing u_t such that $\Sigma \to 1$ as $\eta \to 0$. Also, as a start it proves sufficient to only discard the (meaningless) case $\alpha \gg 1$, so that $U_{\mathcal{S}} - u$ predominantly accounts for the velocity defect characteristic of the turbulent boundary layer rather than for absorbing the effect of the surface curvature on the potential flow, as seen from (3.3) and the truncated terms in (3.13*a*). Furthermore, the inertia terms are seen to be negligibly small in the viscous wall layer. This allows for a direct match of the latter with the defect layer, which is crucial for the particular two-layer structure of the boundary layer. By adopting the basic idea behind the classical theory of (fully developed) wall-bounded turbulent flow, we have in consequence that u_t also serves as a suitable reference velocity for both u and the Reynolds stresses in the viscous sublayer. Accordingly, I_t measures the magnitude of the Reynolds stresses in both tiers.

As a result of these considerations, the scalings

$$\left[\frac{u}{u_t}, \frac{-\langle u'v'\rangle}{\alpha u_t^2}\right] = [u^+, \tau_t^+](x, y^+; k, Re), \quad y^+ = \frac{y}{\delta_\nu}, \quad \delta_\nu = \frac{1}{\alpha u_t Re} \sim \frac{1}{\sigma Re U_{\mathcal{S}}}, \tag{3.14}$$

are appropriate in the comparatively thin wall layer; note (3.12), (3.13*a*). The expression for the wall layer thickness δ_ν in (3.14) is underpinned by the form of momentum equation (2.2*a*) for $y^+ = O(1)$ when integrated with respect to y subject to (2.3),

$$\tau^+ \sim 1 + p^+ y^+ + i^+ \left\{ \int_0^{y^+} \frac{\partial_x \left[u_t\, u^+(x,t;k,Re)^2\right]}{u_t}\, \mathrm{d}t - u^+ \int_0^{y^+} \partial_x u^+(x,t;k,Re)\, \mathrm{d}t \right\} + O(\delta_\nu), \quad \tau^+ = \tau_t^+ + \partial_{y^+} u^+, \quad i^+ = \delta_\nu/\alpha, \quad p^+ = (i^+/u_t^2)\, \mathrm{d}p_{\mathcal{S}}(x;k)/\mathrm{d}x. \tag{3.15}$$

Here the dominant contribution to the remainder term is due to the Reynolds normal stress. Most importantly, it is indicated by (3.15) that one conveniently identifies the wall shear stress, given by $\tau_w = Re^{-1}\partial u/\partial y$ for $y = 0$, with αu_t^2; that is

$$\tau_w / U_{\mathcal{S}}^2 = \alpha \gamma^2. \tag{3.16}$$

To leading order, (3.15) reduces to the expected balance of the sum of the viscous and the Reynolds shear stresses with the wall shear stress as the pressure gradient contributes to higher-order effects. This situation is enforced by the match with the fully turbulent small-defect flow in the bulk of the boundary layer. Then both the quantities p^+ and i^+ provide asymptotically small gauge functions that control the effects of the pressure gradient and inertia, respectively, in the resulting (formal) expansions,

$$p^+ \sim -\pi^+ U_{\mathcal{S}}^{-2} \mathrm{d}U_{\mathcal{S}}/\mathrm{d}x + \cdots, \quad \pi^+ = (\epsilon\sigma^2 Re)^{-1} \ll 1, \tag{3.17a}$$

$$[u^+, \tau^+] \sim [u_0^+(y^+), 1] + p^+ [u_p^+(y^+), y^+] + i^+ \big\{ [u_i^+, \tau_i^+](x, y^+; k) + \cdots + \pi^+ [u_{ip}^+, \tau_{ip}^+](x, y^+; k) + \cdots \big\}. \tag{3.17b}$$

For the derivation of (3.17*a*) we refer to (3.15), (3.12), (3.4). In (3.17*b*) the common key assumption is made that the wall layer flow is in equilibrium: the wall functions $u_0^+(y^+)$ and $u_p^+(y^+)$ are taken as 'universal', i.e. they do not exhibit any dependence on streamwise variations of the flow.

Strictly speaking, $u_0^+(y^+)$ and $u_p^+(y^+)$ have to be determined experimentally or via DNS. The only information available in an asymptotic flow description using turbulence-closure-free RANS is the broadly believed behaviour

$$-\langle u'v'\rangle = O(y^{+3}), \quad y^+ \ll 1, \tag{3.18}$$

which is supported by evaluating the continuity equation for the fluctuating motion for $y = 0$ in combination with (2.3) (cf. Monin & Yaglom 1971, pp. 270–272), and the

conditions of matching with the small-defect flow on top of the viscous sublayer. These basic considerations yield for

$$y^+ \to 0\colon \quad [u_0^+, u_p^+] \sim [y^+, y^{+2}/2] + O(y^{+4}), \tag{3.19a}$$

$$y^+ \to \infty\colon \quad u_0^+ \sim \kappa^{-1} \ln y^+ + C^+, \quad \kappa \doteq 0.384, \quad C^+ \doteq 4.173\,. \tag{3.19b}$$

The relationship (3.19b) represents the celebrated logarithmic law of the wall. The (currently accepted) empirical values for the von Kármán constant κ and the intercept C^+ have been reported by Nagib, Chauhan & Monkewitz (2007). Although found for the canonical zero-pressure-gradient boundary layer, they seem admissible in the present context in view of the asymptotic equilibrium expressed through (3.17b).

The considerations above complete the description of the flow in the outer tier. Integrated once with respect to η, the leading-order boundary layer equation then reads

$$U_{\mathcal{S}}^{-1}\partial_x(U_{\mathcal{S}}\Delta)\eta\partial_\eta F - U_{\mathcal{S}}^{-3}\partial_x(U_{\mathcal{S}}^3\Delta F) = \Sigma - 1. \tag{3.20}$$

Equation (3.20) is subject to the conditions of matching and patching with the flow representations in the wall region and the irrotational external flow, respectively, for

$$\eta \to 0\colon \quad F \to 0 \quad (\Sigma \to 1), \quad \partial_\eta F \sim -\kappa^{-1} \ln \eta + C(x;k), \tag{3.21a}$$

$$\eta = 1\colon \quad \partial_\eta F = \partial_\eta^2 F = \Sigma = 0. \tag{3.21b}$$

With respect to the further analysis, it is interesting to note that the scaling velocity u_t prevents higher-order terms in the expansion of F provided by (3.13a) from exhibiting a logarithmic singularity similar to that given in (3.21a). The function $C(x;k)$ depends on the actual turbulence closure adopted to model Σ. The condition for $\partial_\eta^2 F$ imposed at the boundary layer edge is due to vanishing vorticity. Also, (3.20) is supplemented with universal initial conditions, as predicted by (3.20) and (3.7a) and revealed from the limiting form for

$$x \to 0_+\colon \quad [F, \Sigma](x,\eta;k) \sim [F_0, \Sigma_0](\eta) + O(x), \quad [\Delta/x, C](x;k) \sim [\Delta_0, C_0] + O(x). \tag{3.22}$$

Here the subscript 0 indicates the stagnant-flow solution that describes the terminal stage of the laminar–turbulent transition process as treated in § 3.4.1 and in more depth and breath by Scheichl *et al.* (2008). The values of the quantities F_0, Σ_0, and the (positive) constants Δ_0, C_0 are the solutions of the boundary value problem

$$2\Delta_0(\eta F_0' - 2F_0) = \Sigma_0 - 1, \tag{3.23a}$$

$$\eta \to 0\colon \quad F_0 \to 0, \quad F_0' \sim -\kappa^{-1} \ln \eta + C_0, \quad \eta = 1\colon \quad F_0' = F_0'' = \Sigma_0 = 0, \tag{3.23b}$$

representing the limiting forms of (3.20) and (3.21) as $x \to 0_+$; here and in the following primes on F denote ordinary derivatives with respect to the independent variable.

Finally, matching the small-defect and the wall layer according to (3.19b), (3.21a), and (3.12) yields

$$\gamma/\epsilon \sim 1 - \epsilon[\kappa^{-1} \ln(U_{\mathcal{S}}\Delta) + C + C^+] + O(\epsilon^2), \quad \epsilon = \kappa/\ln(\sigma^2 Re) \ll 1, \tag{3.24}$$

which determines u_t (in agreement with the asymptotic errors anticipated in (3.13a)), provides a first relationship between ϵ, σ, and Re, and, in view of (3.16), represents the skin-friction law. It is noted that (3.24) confirms that the pressure gradient affects the wall layer equilibrium only in second order, as anticipated in (3.15) and (3.17).

3.4.3. *Boundary layer scaling: T- versus (ϵ,σ)-formalism*

In the first instance, (3.24) asserts that δ is much larger than $Re^{-1/2}$, measuring the thickness of a strictly laminar or a laminar–turbulent boundary layer (a notion in-

troduced in § 3) having $T = O(1)$. Let us reconsider the match of $\bar{\Sigma}$ for $x = O(T^{-1})$, defined by (3.10), and for $x = O(1)$, where it has the form given by (3.12). Without loss of generality, we assume $\bar{\Sigma}/u_t^2 \sim \Sigma_0 = O(1)$ in the intermediate regime $T^{-1} \ll x \ll 1$ according to (3.13*a*) and (3.22) and thereby readily reveal by using (3.11) the existence of an underdeveloped turbulent boundary layer flow as

$$\alpha = TRe^{-1/2} \ll 1. \tag{3.25a}$$

This relationship, backed by the proposed specific picture of short-scale transition path to turbulence, underlies (1.3*b*). From (1.2) and (3.24) then follows

$$\epsilon \sim \epsilon_T = \kappa/(2\ln T), \quad \sigma \sim \alpha\epsilon_T, \quad I_t \sim \alpha\epsilon_T^2, \tag{3.25b}$$

which completes the scaling of the boundary layer in terms of T and Re as proposed originally by Neish & Smith (1992). Hence, for $T \gg 1$ the boundary layer thickness is augmented in magnitude by the factor $\epsilon_T T$ whereas that of the emerging wall layer is reduced by the same factor when compared to the thickness of a laminar–turbulent boundary layer mentioned above.

Also, first conclusions that prove useful for the subsequently preferred description of the interactive boundary layer flow in terms of the asymptotic parameters ϵ and σ are drawn from (3.24): when the value of I_t is increased for Re kept fixed then σ (i.e. δ) increases and ϵ, the wall layer thickness δ_ν given by (3.14) and in turn the von Kármán number,

$$\delta^+ = \delta_\nu/\delta \sim 1/(\sigma^2 ReU_S\Delta) \tag{3.26}$$

decrease as $\mathrm{d}[\sigma,\epsilon]/\mathrm{d}I_t \sim [1/\epsilon, -2\epsilon/(\kappa\sigma)]$. A possibly appealing aspect of these findings is noted, namely that they allow to 'simulate' the variations of I_t and ϵ by passing through all possible dependences of σ on Re as σ is increased. If $\sigma^2 Re$ is sufficiently large to vary predominantly algebraically with Re, so that δ^+ varies accordingly with some negative power of Re, see (3.14), we already arrive at the traditional asymptotic scaling of the velocity defect as $\epsilon = O(1/\ln Re)$. Then we are concerned with the precise definition of *slightly* underdeveloped turbulent boundary layer flow, so that (1.3) supplemented with (3.24) now is expressed in the more accurate form

$$\sigma = \chi(Re)Re^{\mu-1/2}, \quad \epsilon \sim \kappa/(2\mu\ln Re), \quad \text{with} \quad \ln\chi = o(\ln Re), \quad 0 < \mu < 1/2. \tag{3.27}$$

Here the slowly varying gauge function $\chi(Re)$ and the exact value of the constant μ are determined by the inner mechanism of viscous–inviscid interaction and eventually provide an accurate estimate of the value of I_t in the regime (1.1) as it fixes the dependences of ϵ and α on Re.

We revert to this issue in § 5.1 in more depth. Here we only note that the relationships (3.27) conform to the internal scaling of the associated triple-deck structure, as already anticipated in § 1: any further increase of σ (or, equivalently, of I_t) that is accompanied by a weaker, i.e. not basically algebraic, rate of decay of σ for increasing values of Re is precluded as it implies super-algebraic growth of Re in the dependence on $1/\sigma$ and, in turn, a correspondingly strong unacceptable decay of δ^+ in the dependence on σ, according to (3.26). Eventually, the hypothetical upper and lower limits of σ (i.e. of I_t) and ϵ, respectively, which refer to the classical (i.e. fully developed) turbulent boundary layer, are attained when μ assumes its least upper bound given by 1/2 and for $\sigma = \chi$ chosen proportional to ϵ, i.e. for $\alpha = O(1)$. This entails $\epsilon \sim \kappa/\ln Re$; a situation exactly unmasking the scaling of the classical (i.e. fully developed) turbulent boundary layer. Then u_t serves as the single reference quantity for scaling both the velocity defect and the Reynolds stresses, see (3.13*a*). In that case δ^+ varies with $\exp(-\kappa/\epsilon)/\epsilon^2$ or, equivalently, with $(\ln Re)^2/Re$, in agreement with (3.14), which expresses the well-established

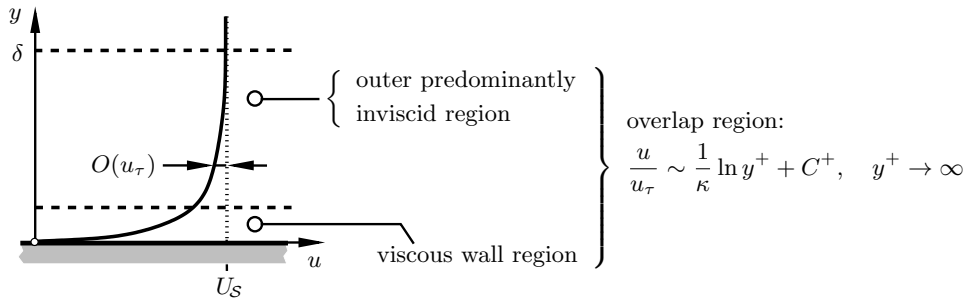

FIGURE 3. Asymptotic substructures of incident boundary layer and overlap behaviour (3.19*b*) (not to scale, for caption see text).

property that the wall layer is transcendentally thin when compared to the outer defect layer.

The sketch in figure 3 depicts the resulting two-tiered structure of the attached turbulent boundary layer. Next, we study its asymptotic subdivision when the boundary layer flow approaches the point $\mathcal{D}$ of inviscid flow detachment, i.e. when exposed to a free-stream speed U_S that locally has the form (3.7*b*).

4. Non-interactive boundary layer near separation

The flow behaviour in the outer main (small-defect) part of the boundary layer as $x \to x_\mathcal{D}$ is important for the local separation process. Particular emphasis is placed below on a further sublayer that emerges as that main part splits, before we address the viscous wall layer.

4.1. *Small-defect layer*

It has been pointed out by Scheichl & Kluwick (2008*a*,*b*) that the velocity defect, scaled Reynolds stresses, and the boundary layer thickness take on finite limits with

$$\begin{aligned}\big\{[F,\Sigma],\Delta\big\} \sim \big\{[F_\mathcal{D},\Sigma_\mathcal{D}](\eta;k),\Delta_\mathcal{D}(k)\big\} + (-s)^{1/2}\big\{[F_{1/2},\Sigma_{1/2}](\eta;k),\Delta_{1/2}(k)\big\} \\ + (-s)\big\{[F_1,\Sigma_1](\eta;k),\Delta_1(k)\big\} + O\big[(-s)^(3/2)\big] \quad \text{as} \quad s \to 0_-,\end{aligned} \tag{4.1}$$

where s is defined by (3.2) and the quantities with subscripts are of $O(1)$, from (3.20) and (3.21). The quantities with subscript 1/2 are unaffected explicitly by the Reynolds shear stress. For the equations determining the quantities with subscript 1/2 and 1 one infers from the requirement $F''_{1/2}(1;k) = F''_1(1;k) = 0$ (by disregarding the rather unlikely case $F'''_\mathcal{D}(1;k) = 0$), see (3.21*b*), the solvability conditions (cf. Scheichl & Kluwick 2008*a*,*b*)

$$\Delta_{1/2} = -2k\Delta_\mathcal{D}, \quad \Delta_1 = \Delta_\mathcal{D}(2k^2/3 - \beta), \quad \beta = \Sigma''_\mathcal{D}(1;k)/[F'''_\mathcal{D}(1;k)\Delta_\mathcal{D}] \ (>0). \tag{4.2}$$

Consequently, one obtains

$$F_{1/2} = -4kF_\mathcal{D}, \quad F_1 = -\beta\eta F'_\mathcal{D} + (60k^2/3 + \beta)F_\mathcal{D} + \Sigma_\mathcal{D}/\Delta_\mathcal{D}. \tag{4.3}$$

The results (4.2), (4.3) involve terms already found for the contributions of $O[(-s)^{1/2}]$. Also they give values of $\Sigma_{1/2}$, Σ_1 according to the chosen Reynolds stress model and the corresponding linearisation of the shear rate F'' about $F''_\mathcal{D}$. Higher-order terms in (4.1) can be determined by proceeding in this manner. Eventually, we find from (3.13*a*), together with (3.7*b*), (1.3*b*), that the velocity defect locally has the form

$$(U_S - u)/u_{0\mathcal{D}} \sim \epsilon F'_\mathcal{D}[1 - 2k(-s)^{1/2} + O(-s)] + O(\epsilon^2). \tag{4.4}$$

Since $F_{\mathcal{D}}$ is subject to (3.21a) for $x = x_{\mathcal{D}}$, each member of the sequence $F_{1/2}, F_1, \ldots$ exhibits a similar logarithmic singularity (as indicated by (4.3)), which violates the original boundary conditions (3.21a) for F. This inconsistency shows that the initial–boundary value problem posed by (3.20)–(3.23) is singularly perturbed as $s \to 0_-$. Thus a small so-called adjustment region arises where $\eta = O(-s)$, so that the balance of linearised convection with the Reynolds stress gradient expressed by (3.20) is retained to leading order. We accordingly define

$$[F/(-s), \Sigma] = [\hat{F}, \hat{\Sigma}](s, \hat{\eta}; k), \quad \hat{\eta} = \eta/(-s) = O(1), \quad s \to 0_-, \tag{4.5}$$

and end up with the appropriate expansions

$$F_{\mathcal{D}} \sim \hat{F}_{\mathcal{D}}(\eta; k) = \big[C_{\mathcal{D}} + \kappa^{-1}(1 - \ln \eta)\big]\eta, \quad C_{\mathcal{D}} = C(x_{\mathcal{D}}; k), \quad \eta \to 0, \tag{4.6a}$$

$$[\hat{F}, \hat{\Sigma}] \sim \big[-\kappa^{-1}\hat{\eta}\ln(-s) + \hat{F}_{\mathcal{D}}(\hat{\eta}; k),\, 1\big] + (-s)^{1/2}\big[4k\kappa^{-1}\hat{\eta}\ln(-s) + \hat{F}_1(\hat{\eta}; k), \hat{\Sigma}_1(\hat{\eta}; k)\big] + \cdots, \quad s \to 0_-. \tag{4.6b}$$

The quantities $\hat{F}_1$, $\hat{\Sigma}_1$ describe the dominant deviations from the behaviour determined by (3.21a) that governs $\hat{F}$, $\hat{\Sigma}$, and they satisfy the correspondingly reduced form of (3.20),

$$-\hat{\eta}\hat{F}_1' + (3/2)\hat{F}_1 = \hat{\Sigma}_1 + 2k\hat{\eta}[\kappa^{-1}(\ln\hat{\eta} - 3) - C_{\mathcal{D}}]. \tag{4.7a}$$

The matching with the quantities in the main region where η is $O(1)$ and the conditions to resolve the mismatch with the wall layer flow give

$$\hat{\eta} \to \infty\colon \quad \hat{F}_1 \sim \hat{a}(k)\big[(2/3)\hat{\eta}^{3/2} + \cdots\big] - 4k\hat{F}_{\mathcal{D}}(\hat{\eta}; k) + \cdots, \tag{4.7b}$$

$$\hat{\eta} \to 0\colon \quad \hat{F}_1 = \hat{\Sigma}_1 = 0, \;\; \hat{F}_{1\hat{\eta}} = O(1). \tag{4.7c}$$

The terms proportional to the unknown function $\hat{a}(k)$ are due to the homogeneous part of (4.7a). The second contribution to (4.7b) arises from the particular solution of (4.7a) and provides consistency with (4.6a). The variation of the streamwise velocity component with the square root of wall distance on top of the logarithmic region here is like that in the immediate vicinity of comparatively 'mild', i.e. marginal, turbulent separation (Scheichl & Kluwick 2007b,a), even though the local flow description there closely resembles that of a turbulent boundary layer in quasi-equilibrium showing global internal separation (cf. Schlichting & Gersten 2003).

It is widely believed that on top of the viscous wall layer the mixing-length model of Prandtl holds,

$$-\langle u'v'\rangle \sim (\kappa y)^2 \partial_y u |\partial_y u|, \tag{4.8}$$

where it predicts the logarithmic velocity distribution as a result of the approximately constant shear stress (cf. Schlichting & Gersten 2003). If (4.8) is chosen as a specific shear stress closure for the adjustment region we then arrive at $\hat{\Sigma} = (\kappa\hat{\eta}\,\partial_{\hat{\eta}}^2\hat{F})^2$ and, by linearisation in view of (4.6),

$$\hat{\Sigma}_1 = 2\kappa\hat{\eta}\,\partial_{\hat{\eta}}^2\hat{F}_1. \tag{4.9}$$

In turn, one recognises that only (4.7c) represents a true boundary condition for (4.7a) and (4.7b) is satisfied identically. In fact, for any value of $\hat{a}$ in (4.7b) the two homogeneous solutions of (4.7a), (4.9) are represented by the dominant algebraic behaviour proportional to $\hat{a}$, so that the dots in parentheses stand for $-\hat{\eta}^{1/2} + O(\hat{\eta}^{-1/2})$ and terms that vary basically with $\exp[-\hat{\eta}/(2\kappa)]$. In consequence, (4.7$b$) is supplemented with $\hat{\Sigma} \sim \hat{a}\hat{\eta}^{1/2} + 8k + O(\hat{\eta}^{-1/2})$ as $\hat{\eta} \to \infty$, which matches $\Sigma_{\mathcal{D}}$ and $\Sigma_{1/2}$ in (4.1), and we obtain a two-term expansion at the base of the defect region close to separation,

$$F_{\mathcal{D}} \sim \hat{F}_{\mathcal{D}} + (2/3)\hat{a}(k)\eta^{3/2} + \cdots, \quad \Sigma_{\mathcal{D}} \sim (\kappa\eta F_{\mathcal{D}}'')^2 \sim 1 + \hat{a}(k)\kappa\eta^{1/2} + \cdots, \quad \eta \to 0. \tag{4.10}$$

So $\hat{a}(k)$ is determined by the overall solution of the boundary layer problem upstream of $x = x_{\mathcal{D}}$. Moreover, we deduce from (4.9) the near-wall behaviour

$$\hat{F}_1 \sim \hat{b}\hat{\eta} - k/(2\kappa^2)\,\hat{\eta}^2 \ln\hat{\eta} + \big[\hat{b}/(8\kappa) + k(9+2\kappa C_{\mathcal{D}})/(4\kappa^2)\big]\hat{\eta}^2 + O\big(\hat{\eta}^3\ln\hat{\eta}\big), \quad \hat{\eta}\to 0, \tag{4.11}$$

where $\hat{b} = \hat{F}_1(0;k)$ depends linearly on $\hat{a}$. The absence of a logarithmic behaviour in $\hat{F}_{1\hat{\eta}}$ for $\hat{\eta}\to 0$ a posteriori justifies the introduction of the sublayer. Furthermore, from (4.6) the velocity defect at the base of the small-defect region is increased by an amount of $O[(-s)^{1/2}\ln(-s)]$ as

$$C \sim C_{\mathcal{D}} + (-s)^{1/2}\big[4k\kappa^{-1}\ln(-s) + \hat{b}\big] + O[(-s)\ln(-s)], \quad s\to 0_-. \tag{4.12}$$

Finally, problem (4.7) supplemented with (4.9) can be solved in closed form for a given $\hat{a}(k)$. To this end, we conveniently decompose $\hat{F}_1(\hat{\eta};k) = \hat{F}_{1h} + \hat{F}_{1p}$, where

$$\hat{F}_{1h}(\hat{\eta};k) = \mathrm{e}^{-\check{\eta}}\check{\eta}\Big\{\hat{a}(k)\sqrt{\kappa^3\pi/2}\big[(4\check{\eta}+3)I_0(\check{\eta}) + (4\check{\eta}+1)I_1(\check{\eta})\big] + (4k/3)\big[(4\check{\eta}+3)K_0(\check{\eta}) - (4\check{\eta}+1)K_1(\check{\eta})\big]\Big\}, \quad \check{\eta} = \hat{\eta}/(4\kappa), \tag{4.13a}$$

represents a homogeneous solution of (4.7a) expressed in terms of the modified Bessel functions I_0, I_1 and K_0, K_1 of the first and the second kind, respectively, and

$$\hat{F}_{1p}(\hat{\eta};k) = 16k/3 - 4k\hat{F}_{\mathcal{D}}(\hat{\eta};k) \tag{4.13b}$$

a particular one.

4.2. *Numerical results*

We now demonstrate that the results of § 4.1 are in fair agreement with numerical solutions of the boundary layer problem posed by (3.20)–(3.23). Here we consider the canonical HK flow around a circular cylinder of radius $\tilde{L}$, equal to 1 in non-dimensional form. In particular, we focus on the behaviour of the key quantities $U_{\mathcal{S}}(x;k)$ and $\Delta(x;k)$. The specific form of $F_{\mathcal{D}}(Y;k)$ is part of the solutions, parametrised by the potential flow parameter k.

Solving this problem represents the only stage in the present analysis where the Reynolds shear stress has to be modelled explicitly in the entire bulk of the boundary layer, but without affecting any of the results of the analysis qualitatively. We close these equations by adopting the traditional formalism based on the mixing length ℓ, which is defined for $0\leqslant y\leqslant\delta$ by setting $-\langle u'v'\rangle = \ell^2\partial_y u|\partial_y u|$, with $\ell = 0$ for $y = 0$, $\ell > 0$ for $y > 0$, and ℓ being finite for $y = \delta$. This approach then is consistent with the conditions (3.21b) of smooth patching with the external flow, and the matching conditions (3.21a) are accounted for when we assume that (4.8) holds in the overlap of the defect and the viscous wall layer, viz. $\ell\sim\kappa y$. The algebraic closure by Michel *et al.* (1969), utilised quite frequently in the literature on turbulent boundary layers, provides a most simple but sufficiently complex example for such an asymptotically correct modelling. Specifically, here we employ a slight modification of the model in the form

$$\Sigma = [(\ell/\delta)\,\partial_\eta^2 F]^2, \quad \ell/\delta = c_\ell I_K^{1/2}\tanh(\eta\kappa/c_\ell), \quad I_K = 1/(1+5.5\,\eta^6), \quad c_\ell = 0.085, \tag{4.14}$$

where the inclusion of the intermittency factor $I_K(\eta)$ proposed by Klebanoff (1955) is expected to cope with the usually observed overestimate of Δ and Σ near the boundary layer edge (when compared with results obtained with eddy-viscosity-based models). We use the value of κ noted in (3.19b).

In order to obtain a highly accurate solution of (3.20)–(3.23), supplemented with (4.14), we adopted an advanced numerical scheme with a Keller–Box discretisation, combined

with the method of lines with respect to the streamwise direction, and an automatic adaptive remeshing strategy. Downstream-integration is performed using a higher-order backward-differentiation-formula technique or alternatively a Theta method, where the tolerance e_m of the (locally estimated) absolute error is given by $m^{1/2}$ with m denoting the relative machine precision ($m \approx 10^{-16}$ in our case). It is initiated by solving (3.23) with the local absolute error bounded by e_m. This is accompanied by the automated generation of a non-uniform initial mesh for the variable η, having typically 550 nodes optimally distributed in the interval $\eta_0 \leqslant \eta \leqslant 1$, where $\eta_0 = 10^{-5}$ (lower values of η_0 result in severe numerical difficulties due to the logarithmic singularity in (3.21)). Therefore the associated methodical error matches the numerical error expected to be encountered in the calculation of the HK flow, as explained in § B.3 (Appendix B): both $U_{\mathcal{S}}(x;k)$ and $\mathrm{d}U_{\mathcal{S}}/\mathrm{d}x$ are imposed by evaluation of two cubic B-splines that interpolate $U_{\mathcal{S}}$ and x between values of these quantities computed for uniformly spaced values of the auxiliary variable ϱ. Consequently, the spacing between consecutive x-values is properly condensed near the BV singularity, according to (B 6). A typical number of 450 spline knots for $0 \leqslant x \leqslant x_{\mathcal{D}}$ ($-\pi/2 \leqslant \varrho \leqslant 0$) renders the additional error due to the spline interpolation sufficiently small. We note that the boundary layer problem is singular not only for $x = x_{\mathcal{D}}$ but also for $x = 0$, as is the convective operator in (3.20) due to the disappearance of both $U_{\mathcal{S}}$ and Δ, see (3.7*a*) and (3.22). Accordingly, the interval of downstream integration is given by $e_m \leqslant x \leqslant x^*$, $x_{\mathcal{D}} - x^* = \Delta x > 0$, with Δx having the magnitude of e_m, which proves satisfactorily accurate. It should be noted that the value $x = x^*$ of termination of the solution is largely affected by the internal stopping criteria implemented in the integrator used (which apparently impedes a higher resolution of the results close to $x = x_{\mathcal{D}}$).

We discuss the results for $k = 0.45$ as an example, which yields $x_{\mathcal{D}}(0.45) \doteq 1.9849 \doteq 113^\circ\, 43'\, 28''$ and represents a physically reliable choice in view of the semi-empirical knowledge of bluff-body separation in the regime (1.1) (cf. Zdravkovich 1997). It is found that $C_0 \doteq 1.3212$, $\Delta_0 \doteq 0.07166$, and (by extrapolation to $x = x_{\mathcal{D}}$) $C_{\mathcal{D}} \doteq 18.1760$, $\Delta_{\mathcal{D}} \doteq 0.4464$.

Figures 4 (*a*,*b*) show the solutions for $\partial_\eta F$ and Σ: the defect profiles become more and more pronounced (i.e. they deviate from the log-law in the overlap as C increases, see 3.21*a*) the more the boundary layer approaches separation. Simultaneously, the position where the Reynolds shear stress assumes its maximum moves from the overlap region outwards into the defect layer. Such shear stress profiles are typically observed in any type of separating turbulent boundary layer. Also, the smooth patching with the external flow as $[F', \Sigma] = O[(1-\eta)^2]$ is clearly visible, and we note that $\Sigma - 1 = O(\eta \ln \eta)$ as $\eta \to 0$ (deduced from (3.20) and (3.21*a*)). It is noted that here $x_{\mathcal{D}}$ is identified with x^*. In figure 4(*c*) the values of the key quantities $U_{\mathcal{S}}$ and Δ including their asymptotes (see (3.22), (4.1), (4.2)) and the coefficient $c_{p\mathcal{S}}$ of the surface pressure, $c_{p\mathcal{S}} = 1 - U_{\mathcal{S}}^2$, are plotted.

Finally, the log-log plots in figure 5 display a comparison of the numerical with the asymptotic results holding at the onset of separation. This exploits the two-term expansion (4.1) with $[g_1, g_2] = [2k(-s)^{1/2}, -s]$ and $[\Delta_1, \Delta_2] = [\Delta g_1/(1-g_1), \Delta_{\mathcal{D}}(1-g_1) - \Delta]$ serving as gauge functions and reference quantities respectively. The behaviours $\Delta_1 \sim \Delta_{\mathcal{D}} g_1 + O(g_1^2)$, $\Delta_2 \sim -\Delta_1 g_2 + O\big(g_2^{3/2}\big)$ are easily verified. Here the asymptote of the first relationship is reproduced excellently, whereas that of the second suffers a more distinct deviation from the numerical data due to the relatively larger effect of higher-order terms. The closure-dependent (negative) value of the coefficient Δ_1 is confirmed by evaluation of (4.2).

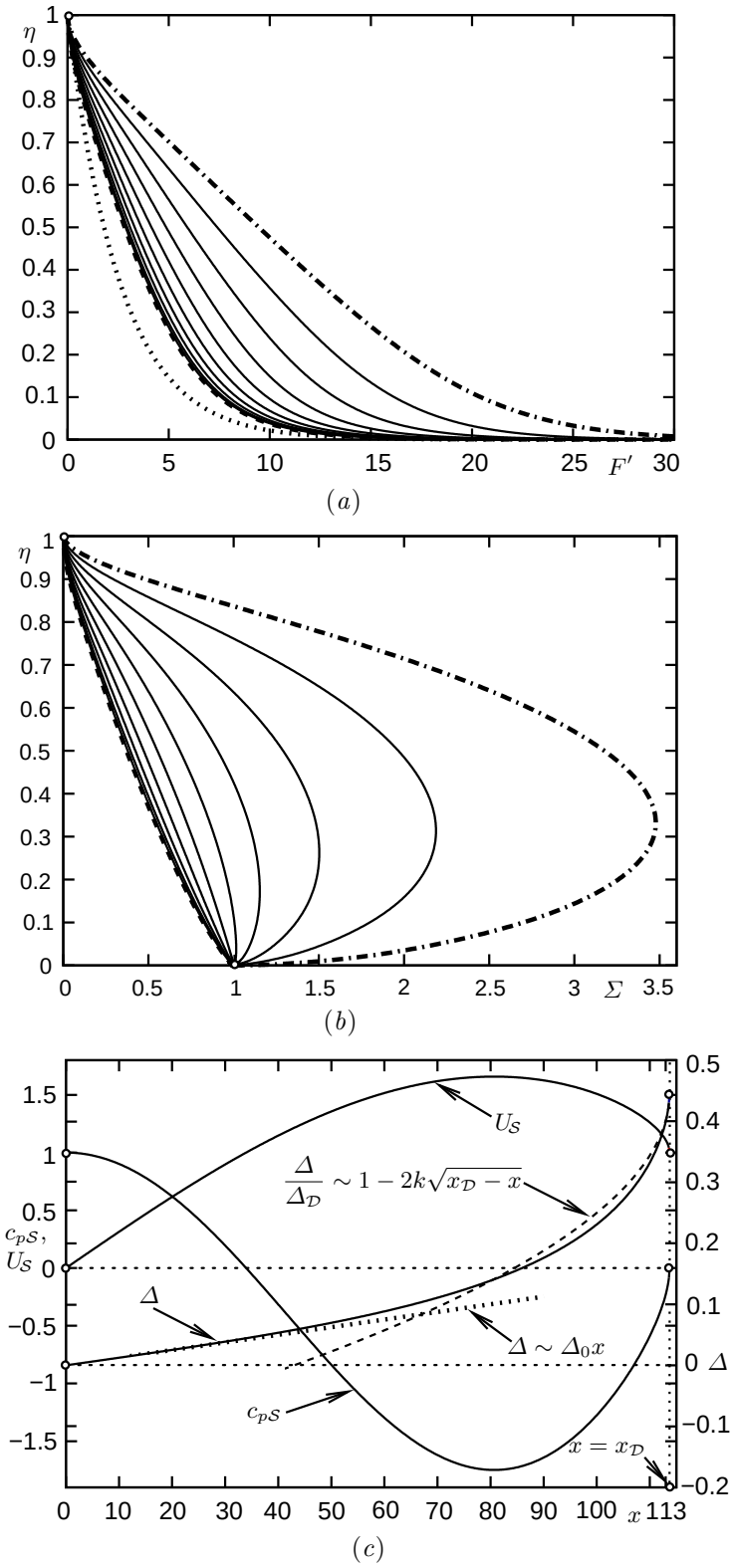

FIGURE 4. Solution of (3.20)–(3.23) for $k = 0.45$ (for caption see text): (*a*), (*b*) - - - - $x \doteq 0$ (stagnation), —— $x = x_D[1 - (i/10 - 1)^2]$, $i = 1, 2, \ldots, 9$ (curves from left to right refer to increasing values of i), - · - · - $x = x^* \doteq x_D$ (incipient separation), ····· asymptote $F' \sim -\kappa^{-1} \ln \eta$, (*c*) key quantities.

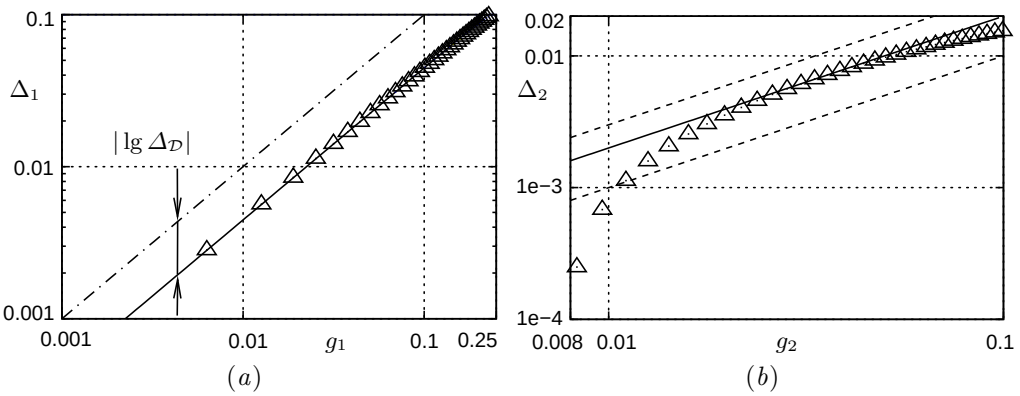

FIGURE 5. Comparison of numerical and asymptotic errors of Δ near $x = x_{\mathcal{D}}$ (for caption see text): $\triangle$ data points, —— asymptotes;
(a) first order, - · - · - median line, (b) second order, - - - - $(-\Delta_1 \pm 0.1)g_2$.

4.3. *Wall layer*

To complete the description of the non-interactive flow, the behaviour of the wall layer flow approaching $\mathcal{D}$ has to be investigated next. One infers from (3.15), (3.17), (3.24) that

$$\tau_i^+ = \frac{U_{\mathcal{S}}'}{U_{\mathcal{S}}} \int_0^{y^+} u_0^{+2}(t)\,\mathrm{d}t, \quad U_{\mathcal{S}}' = \frac{\mathrm{d}U_{\mathcal{S}}(x;k)}{\mathrm{d}x}, \tag{4.15a}$$

$$\tau_{ip}^+ = \frac{\mathrm{d}}{\mathrm{d}x}\left[\frac{U_{\mathcal{S}}'}{U_{\mathcal{S}}^2}\right] u_0^+ \int_0^{y^+} u_p^+(t)\,\mathrm{d}t - \frac{1}{U_{\mathcal{S}}}\frac{\mathrm{d}}{\mathrm{d}x}\left[\frac{U_{\mathcal{S}}'}{U_{\mathcal{S}}}\right] \int_0^{y^+} u_0^+(t)\,u_p^+(t)\,\mathrm{d}t. \tag{4.15b}$$

Expanding p^+, τ_i^+, τ_{ip}^+ for $s \to 0_-$ according to (3.7b) gives rise to corresponding subexpansions in (3.17b).

4.3.1. *First breakdown*

The wall layer has a thickness of $O[1/(\sigma Re)]$, according to (3.14) and is thus expected to merge with the adjustment region discussed in § 4.1 when $\delta_\nu \ll -s = O[1/(\sigma^2 Re)]$ by (3.14). Hence, the flow in this region of the first breakdown of the original wall layer structure is again of boundary layer type. It is characterised by perturbations of the original leading-order stress balance that introduce corresponding variations of the wall shear stress. At present the detailed structure of this collapse is not completely understood but does not affect the essential characteristics of the second breakdown further downstream.

4.3.2. *Second breakdown*

To the order of accuracy considered here the wall layer analysis which neglects the interplay with the small-defect flow, resulting in the first breakdown, agrees with that performed by Scheichl & Kluwick (2008b) in the different context of (3.10) for $T \gg 1$. Thus it is not repeated here but it suffices to recast the central findings in terms of the perturbation parameters ϵ, σ by using the relationships (3.12) and (3.25) as follows.

The original asymptotic hierarchy reflecting the shear stress balance and the effects of pressure gradient and inertia on the oncoming wall layer flow breaks down when the last two terms become of the same order of magnitude. As seen from (3.17b) and (4.15), this structural change of the near-wall flow occurs when $i^+\tau_{ip}^+$, which grows like $(-s)^{-3/2}$, is

of $O[(-s)^{-1/2}]$, i.e. when $\bar{s} = s/\bar{\delta} = O(1)$ with

$$i^+ \sim \bar{\delta} = \epsilon/(u_{0\mathcal{D}}\sigma^2 Re) \gg \delta_\nu, \quad \bar{s} \to 0_-, \tag{4.16}$$

here we refer to (3.15), (3.14), (1.3b). That is, this second breakdown of the wall layer takes place in a region of boundary layer type on a streamwise scale of $O(\epsilon)$ smaller than that characterises the first breakdown.

Let the new perturbation parameter

$$\bar{\pi}^+ = \pi^+ k/(\bar{\delta}^{1/2} u_{0\mathcal{D}}) = k/(u_{0\mathcal{D}}^{1/2}\epsilon^{3/2}\sigma Re^{1/2}) \ll 1, \tag{4.17}$$

as suggested by (3.15) and (3.17a), account for the pressure rise as $p^+ \sim \bar{\pi}^+(-\bar{s})^{-1/2} + \cdots$ for $0 < -\bar{s} = O(1)$. Substitution of the appropriate expansion $[u^+, \tau_t^+] \sim [u_0^+(y^+), 1] + \bar{\pi}^+[\bar{u}^+, \bar{\tau}^+](\bar{s}, y^+) + O(\epsilon^2\bar{\pi}^+)$ into (3.15) finally yields to second order the linear boundary layer problem

$$u_0^+\frac{\partial \bar{u}^+}{\partial \bar{s}} - \frac{\mathrm{d}u_0^+}{\mathrm{d}y^+}\int_0^{y^+}\frac{\partial \bar{u}^+}{\partial \bar{s}}(\bar{s}, t)\,\mathrm{d}t = -\frac{1}{\sqrt{-\bar{s}}} + \frac{\partial \bar{\tau}^+}{\partial y^+}, \quad \bar{\tau}^+ = \bar{\tau}_t^+ + \frac{\partial \bar{u}^+}{\partial y^+}, \tag{4.18a}$$

$$y^+ = 0\colon \ \bar{u}^+ = \bar{\tau}_t^+ = 0, \quad y^+ \to \infty\colon \ \bar{u}^+ \sim \frac{2\kappa\sqrt{-\bar{s}}}{\ln y^+}, \ \frac{\partial \bar{\tau}_t^+}{\partial y^+} \to 0, \tag{4.18b}$$

$$y^+ = O(1), \ \ \bar{s} \to -\infty\colon \ \sqrt{-\bar{s}}\,[\bar{u}^+, \bar{\tau}^+] \to [u_p^+(y^+), y^+]. \tag{4.18c}$$

Here the conditions for y^+ large in (4.18b) are enforced by a balance of the pressure gradient with the inertia terms in (4.18a) on the basis of (3.19b), in order to allow for matching u in the wall layer and in the small-defect region. This behaviour is apparently incompatible with the balance of the pressure and shear stress gradients of the oncoming flow, as expressed by (4.18c). In order to resolve this inconsistency, one then has to consider in addition a limit where both y^+ and $-\bar{s}$ are large and all terms in (4.18a) are of comparable order of magnitude. In this context we mention that $u_p^+ \sim y^+/(2\kappa)$ as $y^+ \to \infty$, by exploitation of (4.8) and taking into account that $\tau_p^+ = y^+$. Then this limit is characterised by $y^+ = (-\bar{s})^{1/2}/\ln(-\bar{s})$ as $-\bar{s} \to \infty$ and its investigation is expected to shed light on the first breakdown and higher-order contributions to the upstream conditions (4.18c).

The problem (4.18) can be solved for $\bar{u}^+$ in the range $-\infty < \bar{s} < 0$ by means of downstream integration provided $\bar{\tau}_t^+$ is modelled properly. However, the behaviour of $[\bar{u}^+, \bar{\tau}^+]$ for $\bar{s} \to 0_-$, discussed extensively by Scheichl & Kluwick (2008b), is crucial for the subsequent analysis rather than is the full solution. One finds that the flow then is essentially governed by inertia terms. Specifically, we obtain for

$$\bar{s} \to 0_-\colon \quad [\bar{u}^+, \bar{\tau}^+] \sim [\bar{u}_0^+, \bar{\tau}_0^+](y^+) + (-\bar{s})^{1/6}\Big[a_-\frac{\mathrm{d}\bar{u}^+}{\mathrm{d}y^+}, \bar{\tau}_1^+(y^+)\Big] + O\big[(-\bar{s})^{1/2}\big], \tag{4.19a}$$

$$y^+ \to 0\colon \quad \bar{u}_0^+ \sim -\bar{b}{y^+}^{3/2} + \cdots, \tag{4.19b}$$

$$a_- = 48^{1/3}\,\Gamma(\tfrac{2}{3}) \doteq 4.9212, \quad \bar{b} = (4/3)\Gamma(\tfrac{1}{6})/\Gamma(\tfrac{2}{3}) \doteq 5.4809. \tag{4.19c}$$

Here $\bar{u}_0^+(y^+)$, $\bar{\tau}_0^+(y^+)$ depend on the particular form of $u_p^+(y^+)$ in the upstream conditions (4.18c) (apart from the modelling of $\bar{\tau}_t^+$). We also note that $\bar{u}_0^+ = o(1/\ln y^+)$ as $y^+ \to \infty$ due to (4.18b). Specifically, (4.19) follows from the investigation of a new adjustment region where $y^+/(-\bar{s})^{1/3} = O(1)$ and the viscous stress term plays a dominant role: there the flow is laminar-like as $u_0^+ \sim {y^+}^2/2$, fitting to (3.19a), and the solution of (4.18) is predominantly unaffected by $\bar{\tau}_t^+$, according to (4.18b), and hence of universal self-similar character.

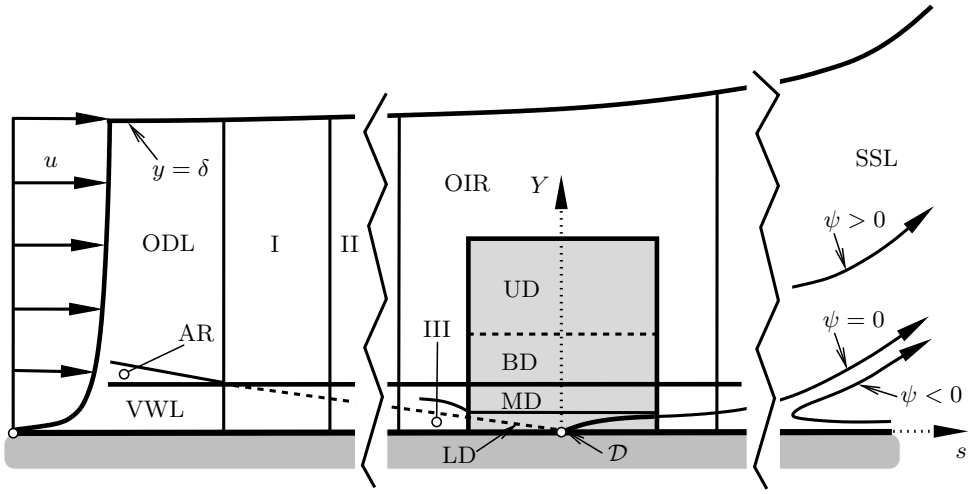

FIGURE 6. Asymptotic substructures of interactive boundary layer near $\mathcal{D}$ (not to scale, for caption see text): outer defect layer (ODL), viscous wall layer (VWL), adjustment region (AR) of § 4.1 (the broken line indicates its virtual continuation towards $\mathcal{D}$), positions of first (I), second (II), and third (III) wall layer breakdown, outer interaction region (OIR), separated shear layer (SSL), triple-deck (shaded), lower deck (LD), main deck (MD), buffer deck (BD), upper deck (UD).

As a further finding of the analysis in that adjustment region, we have for

$$y^+ = 0, \quad \bar{s} \to 0_-: \quad \frac{\partial u^+}{\partial y^+} \sim 1 - \frac{\bar{c}\bar{\pi}^+}{(-\bar{s})^{1/6}} + \cdots, \quad \bar{c} = \frac{\Gamma(\frac{1}{6})\Gamma(\frac{1}{3})}{3^{1/3}\pi^{1/2}\Gamma(\frac{2}{3})} \doteq 4.3078. \tag{4.20}$$

The behaviour (4.20) indicates that the wall shear stress is reduced significantly and no longer determined by (3.16) and (3.24) for $\bar{s} = O(\bar{\pi}^{+6})$. Even more importantly, then a third (nonlinear) breakdown of the wall layer flow takes place in the aforementioned adjustment region as u^+ and $\bar{\pi}^+\bar{u}^+$ become of the same order of magnitude. It is shown below that this scenario has to be considered from the viewpoint of viscous–inviscid interaction.

5. The interaction process

In the small-defect region of the boundary layer the wall-normal pressure gradient $\partial_y p$ becomes of the order of magnitude of the streamwise one, $\partial_x p$, when $-s$ decreases to $O(\delta)$. The conventional boundary layer approximation then ceases to be valid in the region of outer viscous–inviscid interaction in the vicinity of $\mathcal{D}$. However, a thorough investigation of this interaction mechanism has to account also for the flow at distances $y \ll \delta$ and thus requires knowledge of the near-wall flow and the associated scaling of the boundary layer. Therefore its properties, associated with the inner interaction process, are discussed next, while the outer interaction is topic of § 5.2.

The therewith completed local subdivision of the interactive boundary layer flow is anticipated by the sketch in figure 6. Here the actual point of separation coincides with $\mathcal{D}$ for the sake of clarity.

5.1. *Inner interaction: internal triple-deck structure*

We begin by outlining the strategy adopted here to work out the triple-deck structure.

5.1.1. *Basic considerations*

One faces two key points in the analysis of the wall layer flow approaching $\mathcal{D}$: (first) the merging with the adjustment region, as addressed briefly in § 4.3.1 (first breakdown), and (second) the terminal structure of the non-interactive wall layer flow as $\bar{s} \to 0$ presented at the end of § 4.3.2 (second breakdown).

The first breakdown of the wall layer applies only on condition that $\delta \ll Re^{-1/3}$ or $\delta = O(Re^{-1/3})$; if $\delta \gg Re^{-1/3}$ it is displaced by the occurrence of the outer interaction. In that case the adjustment region is continued as a so-called blending or Reynolds stress sublayer located at the base of the interaction region and having a thickness measured by δ^2, where the momentum equation (2.2a) still reduces to a balance between linearised convective terms and the turbulent effect $-\partial_y\langle u'v'\rangle$ to leading order. This situation is described by Melnik & Chow (1975) in their study of the small-defect flow past the trailing edge of an inclined flat plate in a uniform stream. (Unfortunately, from the present point of view their assumption of an incident fully developed turbulent boundary layer renders a self-consistent description of the wall layer flow passing the trailing edge an intractable task.) More generally, such a flow region is also found in other types of interacting fully developed turbulent boundary layers (see e.g. Melnik & Chow 1975; Sykes 1980; Agrawal & Messiter 1984). Therefore determining the order of magnitude of δ in terms of Re not only completes the scaling of the boundary layer but also answers the question of the existence of that blending layer and in turn the asymptotic structure of the flow near $\mathcal{D}$.

This task is intrinsically tied to the second issue, which implies the formation of a further sublayer where the nonlinear inertia terms in (2.2a) are fully retained (cf. Scheichl & Kluwick 2008b). As found from (3.15), there rescaled coordinates

$$\bar{X} = \bar{s}/\bar{\pi}^{+6}, \quad \bar{Y} = y^+/\bar{\pi}^{+2} \tag{5.1a}$$

are quantities of $O(1)$. However, strong viscous–inviscid interaction of a boundary-layer-type flow in a small region encompassing both $\mathcal{D}$ and the actual point of separation, and thus dominated by the full nonlinear convective terms, is the sole possibility to regularise the BV singularity within the limits of the Reynolds equations (2.2). This sublayer must serve as the active or lower deck in the expected triple-deck structure (cf. Neish & Smith 1992; Rothmayer & Smith 1998; Sychev *et al.* 1998). There the pressure gradient $\partial_x p$ is self-induced such that it both surmounts the BV singularity and avoids the formation of a Goldstein singularity. Henceforth let

$$\delta_{TD} = \bar{\delta}\bar{\pi}^{+6}, \quad \delta_{LD} = \delta_\nu \pi^{+2} \tag{5.1b}$$

define the triple-deck length scale and the thickness of the lower deck respectively.

Consequently, for $\bar{X} = O(1)$ the core of the wall layer acts as the main deck where the flow must also be of boundary layer type, i.e. the ratio of its thickness to the length of the sublayer in the x-direction is small. From (4.16), (4.17), (1.2), and the wall layer scaling given by (3.14) and (1.2) this ratio is found to be measured by $\epsilon^8\sigma^7 Re^3$ for $k = O(1)$, which yields the estimate $Re^{-1/2} \ll \sigma \ll Re^{-3/7}(\ln Re)^{8/7}$, in agreement with (3.24). Then $\delta \ll Re^{-1/3}$, which as a first remarkable result here precludes the existence of a blending layer.

5.1.2. *Lower deck and near-wall flow reversal*

Inspection of (3.14), (3.15), (5.1) indicates that appropriate lower-deck expansions read

$$\alpha Re\psi \sim \bar{\pi}^{+4}\bar{\Psi}(\bar{X},\bar{Y}) + \cdots, \quad p - p_{0\mathcal{D}} \sim \bar{\delta}^{1/2}\bar{\pi}^{+3}u_{0\mathcal{D}}^2 kP(\bar{X}) + \cdots, \quad \bar{\pi}^+ \ll 1. \tag{5.2}$$

Furthermore, the velocity gradient $\partial_{y^+}u^+ = O(1)$ but $\tau_t^+ = O(\bar\pi^{+6})$, according to (3.18). Thus (2.2a), (2.3) give rise to the lower-deck problem for quasi-laminar separation in canonical form,

$$\partial_{\bar Y}\bar\Psi\,\partial_{\bar Y\bar X}\bar\Psi - \partial_{\bar X}\bar\Psi\,\partial_{\bar Y}^2\bar\Psi = -\mathrm{d}P/\mathrm{d}\bar X + \partial_{\bar Y}^3\bar\Psi, \tag{5.3a}$$

$$\bar Y = 0\colon\ \bar\Psi = \partial_{\bar Y}\bar\Psi = 0, \quad \bar Y \to \infty\colon\ \bar\Psi/\bar Z^2 \to 1/2,\ \ \bar Z = \bar Y + A(\bar X), \tag{5.3b}$$

$$\bar X \to -\infty\colon\ \bar\Psi \to \bar Y^2/2,\ \ P/(-\bar X)^{1/2} \to -2, \quad \bar X \to \infty\colon\ \ P \to 0. \tag{5.3c}$$

Once these equations are closed by the interaction law between the pressure and displacement functions $P(\bar X)$ and $-A(\bar X)$ (see § 5.1.4), they constitute the core problem governing the separation process. (The corresponding non-interactive problem considered by Scheichl & Kluwick 2008b is obtained formally by setting $P = -2(-\bar X)^{1/2}$).

The behaviour of $\bar\Psi$ for $\bar Y \to \infty$ is again triggered by the predominance of the inertia terms in (5.3a) in combination with the upstream conditions in (5.3c). A thorough examination of the non-interactive flow region far upstream where $\bar Y/(-\bar X)^{1/3} = O(1)$ or, equivalently, $y^+/(-\bar s)^{1/3} = O(1)$ recovers the universal laminar-type near-wall part of the terminal structure of the non-interactive wall layer flow and the associated nonlinear breakdown as outlined in § 4.3.2. We finally obtain for

$$\bar X \to -\infty\colon\quad A \sim a_-(-\bar X)^{1/6} + \cdots, \quad (\partial_{\bar Y}^2\bar\Psi)(\bar X, 0) \sim 1 - \bar c(-\bar X)^{-1/6} + \cdots, \tag{5.4a}$$

$$\bar Z \to \infty\colon\quad \bar\Psi \sim \bar Z^2/2 - \bar b\bar Z^{3/2} + P(\bar X) + O(\bar Z^{-3/2}), \tag{5.4b}$$

in agreement with (4.19), (4.20). In the following we demonstrate that the form of $\bar\Psi$ far downstream is fully determined by (5.3) when supplemented with an interaction law, provided gross separation takes place for some $\bar X = \bar X_S$ (where the rescaled wall shear stress $(\partial_{\bar Y}^2\bar\Psi)(\bar X, 0)$ changes sign). Expansion (5.4b) reflects the predominantly inviscid flow on top of the lower deck.

For $\bar X \gg 1$ the expansion (5.4b) apparently breaks down in the region of a mixing layer which encompasses the location of the separating streamline defined by $\bar Y = \bar Y_S(\bar X)$ with $\bar\Psi(\bar X, \bar Y_S) = 0$. This shear layer has an extent in the wall-normal direction of, say, $B(\bar X)$ with $B = O(1)$ or larger and $-B/A \ll 1$ as $-A \gg 1$, $\bar X \gg 1$, so that $\bar\Psi \sim B(\bar X)^2\bar F(\bar\eta)$, $\bar\eta = \bar Z/B = O(1)$. Inserting these last expressions into (5.3a) shows that the pressure gradient $\mathrm{d}P/\mathrm{d}\bar X$ is negligibly small there, and balancing inertia and viscous terms yields $B \sim \bar X^{1/3}$ and the mixing-layer problem as in the laminar counterpart of the separation problem: $\bar F'^2/3 - (2/3)\bar F\bar F'' = \bar F'''$, together with the two conditions governed by the convective terms and compatible with the ambient flow, $\bar F \sim \bar\eta^2/2$ as $\bar\eta \to \infty$ and $\bar F'(-\infty) = 0$, and $\bar F(\bar\eta_S) = 0$. Here $\bar\eta = \bar\eta_S$ defines the yet unknown position of the separating streamline which itself is regarded as part of the full solution of (5.3): $\bar Y_S \sim -A(\bar X) + \bar\eta_S B(\bar X)$. Therefore, $\bar\eta_S$ is arbitrary for the time being as it is determined by an higher-order analysis. However, the solution $\bar F$ is unique when written in the form $\bar F(\bar\eta - \bar\eta_S)$ with $\bar F(-\infty) = -\bar a \doteq -1.2539$ (Neiland 1971; Stewartson & Williams 1973; Diesperov 1984). Accordingly, for $\bar Y = O(A)$ we expect backflow that is governed by the inviscid form of (5.3a). Eliminating the pressure gives $\partial_{\bar Y}^2\bar\Psi \sim -\bar\omega(\bar\Psi)$, where $\bar\omega$ denotes the vorticity. From matching $\bar\Psi$ with its representation holding in the mixing layer we conclude that $\partial_{\bar Y}^2\bar\Psi = O(B^2/A^2)$, hence $\bar\omega$ is treated as negligibly small. In turn, the slow irrotational reversed flow in the bulk of the lower deck is found to be described by $\bar\Psi \sim \bar a\bar X^{2/3}\bar Y/A(\bar X) < 0$, $P \sim -\bar a^2\bar X^{4/3}/(2A^2)$, $\bar X \gg 1$, where A varies basically algebraically with $\bar X$. Finally, a sublayer emerges for $\bar Y = O[\bar X^{1/6}(-A)^{1/2}]$ where all terms in (5.3a) are retained to leading order, governing viscous self-preserving reversed flow.

Therefore, even without knowing in advance the behaviour of $A(\bar X)$ for $\bar X \to \infty$ in detail we end up with a three-tiered structure of the downstream flow as in the laminar

case, where $A = O(\bar{X}^{3/2})$ as discussed elaborately by Sychev (1972), Sychev *et al.* (1998), in particular.

5.1.3. *Main deck*

Expansion (5.4*b*) allows for a match with the flow in the bulk of the wall layer for $\bar{X}$ of $O(1)$. There the leading-order stress balance stays intact and the corresponding expansions (taken directly from the non-interactive analysis, see Scheichl & Kluwick 2008*b*) are

$$\alpha Re\psi \sim \int_0^{y^+} [u_0^+(t) + \bar{\pi}^{+}\bar{u}_0^+(t)]\,\mathrm{d}t + \bar{\pi}^{+2}A(\bar{X})u_0^+(y^+) + O(\bar{\pi}^{+3}), \tag{5.5a}$$

$$p - p_{0\mathcal{D}} \sim \bar{\delta}^{1/2}\bar{\pi}^{+3}u_{0\mathcal{D}}^2 kP(\bar{X}) + \cdots, \tag{5.5b}$$

supplemented by $-\langle u'v'\rangle \sim \alpha\epsilon^2 u_{0\mathcal{D}}^2\tau_0^+(y^+) + \cdots$. Expansion (5.5*a*) in combination with (5.4*a*) matches (4.19*a*). We remark that the logarithmic law of the wall is still present, according to (3.19*b*).

The separating streamline, originating in the lower deck, penetrates into the core of the wall layer far downstream, where $\bar{Y} \sim A = O(1/\bar{\pi}^{+2})$. There the forms of the wall functions $u_0^+(y^+)$, $\tau_0^+(y^+)$ are finally modified substantially.

5.1.4. *Upper deck and boundary layer scaling*

In an ad-hoc analysis assuming non-interactive flow (i.e. for $P = -2(-\bar{X})^{1/2}$ and $A(\bar{X})$ known from the solution of (5.3)) the expansions (5.5) provide a match with the flow in the small-defect region (cf. Scheichl & Kluwick 2008*b*). In striking contrast, here the flow structure on top of the wall layer is crucial for the determination of the interaction law. Since the flow there is predominantly governed by the equations for inviscid flow, we specifically have to deal with a square region having an extent measured by $O(\delta_{TD})$, so that here $\hat{Y} = y/\delta_{TD} = O(1)$.

The BV singularity can only be avoided by the flow in the upper deck if the first $\bar{X}$-dependent term in the expansion of ψ there accounts for the leading-order variations of both the pressure and the displacement, exerted by the lower deck and transferred unchanged through the main deck. We thus conclude that this expansion starts with terms 'frozen' at $x = x_{\mathcal{D}}$ known from the non-interactive flow analysis of the small-defect region (rewritten in terms of $\hat{Y}$ and accordingly expanded) is followed by the $\bar{X}$-dependent contribution arising from the displacement of the lower deck and accounting for the mechanism of inner interaction: we, therefore, write by inspection of (3.19*b*), (3.14), and (5.2)

$$\psi - \delta_{TD}u_{0\mathcal{D}}\hat{Y} + \cdots \sim (\alpha Re)^{-1}\bar{\pi}^{+2}\ln(\sigma Re/\delta_{TD})\kappa^{-1}\Psi_{TD}(\bar{X},\hat{Y}) + \cdots, \tag{5.6a}$$

$$p - p_{0\mathcal{D}} \sim \bar{\delta}^{1/2}\bar{\pi}^{+3}u_{0\mathcal{D}}^2 kP_{TD}(\bar{X},\hat{Y}) + \cdots. \tag{5.6b}$$

Herein Ψ_{TD} and P_{TD} are governed by the linearised Euler equations the equations of motion (2.2) reduce to in the approximation considered. This requires the ratio of the coefficients of Ψ_{TD} and P_{TD} in (5.6) to be proportional to $\delta_{TD}/(\Gamma u_{0\mathcal{D}})$ with Γ denoting a similarity parameter assumed to be of $O(1)$. Since the terms on the left-hand side of (5.10*a*) due to the incident flow 'frozen' at $x = x_{\mathcal{D}}$ are independent of $\bar{X}$, (2.2) then reduces to

$$[\partial_{\hat{Y}}, -\partial_{\bar{X}}]\partial_{\bar{X}}\Psi_{TD} = -\Gamma[\partial_{\bar{X}}, \partial_{\hat{Y}}]P_{TD}. \tag{5.7}$$

We furthermore obtain with the aid of (1.2), (4.16), (4.17), (5.1*b*), and (3.24) in the

regime (1.1) the relationships

$$\bar{\chi} \sim \bar{K}\left(\frac{\kappa Re}{\epsilon^{10}\ln\bar{\chi}}\right)^{1/9}, \quad \bar{\chi} = \sigma Re^{5/9} \gg 1, \quad \bar{K} = \left(\frac{k^8}{9\Gamma u_{0\mathcal{D}}^4}\right)^{1/9} = O(1). \tag{5.8}$$

From (5.8) the desired scaling of the interactive boundary layer is found in terms of

$$\epsilon \sim 9\kappa/\ln Re, \quad \sigma = \bar{K}Re^{-4/9}/\epsilon, \tag{5.9a}$$

$$\delta_\nu = O(\epsilon Re^{-5/9}), \quad \delta_{TD} = O(Re^{-4/9}), \quad \delta_{LD} = O(Re^{-6/9}), \tag{5.9b}$$

$$\bar{\delta} = O(\epsilon^3 Re^{-1/9}). \tag{5.9c}$$

The relationships (5.9*a*) describe slightly underdeveloped turbulent flow according to (3.27), where we end up with $\chi = \bar{K}/\epsilon$ and $\mu = 1/18$. Also, we find that $I_t = \bar{K}Re^{-4/9}$ and $\alpha = \bar{K}(9\kappa)^{-2}(\ln Re)^2 Re^{-4/9}$ by (1.2), which gives $T = O\big[(\ln Re)^2 Re^{1/18}\big]$ by (3.25*a*) and finally confirms (3.25*b*). The length scales quoted in (5.9*b*) follow accordingly from (3.14) and (5.1*b*), with the help of (4.17), and basically agree with those suggested by Neish & Smith (1992). We note, however, that according to the more detailed analysis carried out here the upper-deck scale δ_{TD} is smaller than the boundary layer scale δ by a factor ϵ. This has two remarkable consequences: (first) it means that the triple-deck scale is slightly smaller than in laminar case where it is of $O(Re^{-3/8})$ (cf. Rothmayer & Smith 1998; Sychev *et al.* 1998), and (second) the triple-deck structure is 'squashed' in the square region with an extent measured by δ, which renders the notions of inner and outer interaction sensible. We finally note that δ^+ defined by (3.26) varies with $\epsilon^2 Re^{-1/9}$ and (5.9*c*) is a consequence of (4.16). Thus the second breakdown of the wall layer flow occurs upstream of the onset of the outer interaction.

As a result of the 'frozen' state of the boundary layer expressed by (4.1) and (3.21*a*), one finds the vorticity in the upper deck to vary as $-\epsilon u_{0\mathcal{D}}\kappa^{-1}/(\delta_{TD}\hat{Y}) + \cdots$, which is of $O(1/\sigma)$. Also, the flow in the upper deck is still of small-defect form and thence matches that in the region of the outer interaction identically. In order to clarify this situation further in view of the scalings (5.9*a*) with $\bar{K}$ given by (5.8), we now re-establish the upper-deck expansions (5.6) by using (5.1*b*) as

$$\psi/u_{0\mathcal{D}} - \delta_{TD}\hat{Y} + \cdots \sim \delta_{TD}^{3/2} k[\Psi_{TD}(\bar{X},\hat{Y})/\Gamma + O(\epsilon)] + \cdots, \tag{5.10a}$$

$$(p - p_{0\mathcal{D}})/u_{0\mathcal{D}}^2 \sim \delta_{TD}^{1/2} k[P_{TD}(\bar{X},\hat{Y}) + O(\epsilon)] + \cdots. \tag{5.10b}$$

Here the terms of $O(\epsilon)$ in brackets arise from (5.5*a*) subject to the logarithmic behaviour (3.19*b*).

It is noted that matching of the gradients with respect to y requires the introduction of a so-called 'buffer' deck, located between the main and the upper deck, as a consequence of (5.5*a*) and (3.19*b*). Comparison of the latter expansion with (5.10*a*) shows that $\ln Re\,\hat{Y}\partial_{\hat{Y}}\Psi_{TD}$ is of the same order of magnitude as $y^+ \mathrm{d}u_0^+/\mathrm{d}y^+$ there. By taking notice of (5.11*b*), one immediately infers that this additional layer is located at $\hat{y} = \hat{Y}/\epsilon = O(1)$. This indicates that the ratio of its thickness to that of the upper deck is again given by ϵ. However, this buffer deck behaves fully passive as the expansions of the flow quantities holding there are essentially found by re-expanding their counterparts in the adjacent layers when rewritten in terms of $\hat{y}$. We therefore refrain from considering this region in more detail.

Elimination of the pressure P_{TD} in (5.7) yields Laplace's equation in Cartesian coordinates,

$$\bar{\nabla}_c^2 \Psi_{TD} = 0, \quad \bar{\nabla}_c^2 = \delta_{TD}^2 \nabla_p^2 = \partial_{\bar{X}}^2 + \partial_{\hat{Y}}^2, \tag{5.11a}$$

in agreement with (3.5), (A 7), (2.2c), as a possible $\bar{X}$-independent 'constant' of integration is conveniently absorbed in the 'frozen'-flow contribution to (5.10a). From matching (5.10) and (5.5) we find that

$$\Psi_{TD}(\bar{X},0)=A(\bar{X}),\quad \partial_{\hat{Y}}\Psi_{TD}(\bar{X},0)=-\Gamma P(\bar{X}),\quad P(\bar{X})=P_{TD}(\bar{X},0) \tag{5.11b}$$

and deduce that $\Psi_{TD}\sim A(\bar{X})-\Gamma P(\bar{X})\hat{Y}$ for $|\bar{X}|\to\infty$, $\hat{Y}=O(1)$. A standard investigation of the Laplacian subject to the conditions for P, A in (5.3c), (5.4a) and the form of the downstream decay of P elucidated at the end of § 5.1.2 then suggests for

$$\bar{R}=\frac{r}{\delta_{TD}}=\sqrt{\bar{X}^2+\hat{Y}^2}\to\infty\colon\ \ \Psi_{TD}\sim\frac{\Gamma}{k}\psi_{0,3/2}(\bar{R},\theta)+\Lambda\bar{R}^{1/2}\cos(\theta/2)$$
$$+\left(2a_-/\sqrt{3}\right)\bar{R}^{1/6}\cos(\theta/6)+O(\ln\bar{R}). \tag{5.11c}$$

Here r, θ, and $\psi_{0,3/2}$ are defined by (3.5) and (3.6b) respectively. Expansion (5.11) was already established by Brown & Stewartson (1970) and Melnik & Chow (1975) in their study of laminar non-symmetric flow past a sharp trailing edge, where the external flow exhibits a BV-like singularity and thus an upper deck having alike properties. They demonstrated that the dominant eigensolution of Laplace's equation proportional to the constant Λ unknown at this stage indeed varies strictly algebraically with $\bar{R}^{1/2}$ in order to match the upstream behaviour of the lower-deck solution governed by (5.3) and (5.4). Expansion (5.11c) closes the upper-deck problem (5.11), based on potential flow theory and being fully equivalent to that in the laminar case (cf. Sychev *et al.* 1998).

The higher-order contributions in the far-field behaviour (5.11c) allow for corresponding estimates of $A(\bar{X})$ and $P(\bar{X})$, more accurate than those given in (5.3c) and (5.4a) as necessary for later considerations. We obtain for

$$\bar{X}\to-\infty\colon\quad A\sim a_-(-\bar{X})^{1/6}+O[\ln(-\bar{X})], \tag{5.12a}$$

$$P\sim-2(-\bar{X})^{1/2}-\frac{\Lambda}{2\Gamma}(-\bar{X})^{-1/2}-\frac{a_-}{6\sqrt{3}\Gamma}(-\bar{X})^{-5/6}+\cdots, \tag{5.12b}$$

$$\bar{X}\to\infty\colon\quad A\sim-a_+\bar{X}^{3/2}+\Lambda\bar{X}^{1/2}+\frac{2a_-}{\sqrt{3}}\bar{X}^{1/6}+O(\ln\bar{X}),\quad a_+=\frac{4\Gamma}{3}, \tag{5.12c}$$

$$P\sim-p_+\bar{X}^{-5/3}+\cdots,\quad p_+=(\bar{a}/a_+)^2/2. \tag{5.12d}$$

The relationship (5.12d) attests to a structure of the early-stage reversed flow, having its origin in the lower deck as outlined in § 5.1.2, known from the laminar counterpart. In the case considered here the free streamline penetrates into the bulk of the viscous wall layer for $\delta\ll s=O(\epsilon^{2/3}Re^{-10/27})$, according to the comments given in § 5.1.3, (5.12c), (5.1a), and (4.17). Therefore the wall function $u_0^+(y^+)$ and the leading-order stress balance in the wall layer, reading $\tau_0^+=1$, remain unaltered even for $s=O(\delta)$, the length scale characteristic of the outer interaction.

Equation (5.7) states that ΓP_{TD}, $-\partial_{\bar{X}}\Psi_{TD}$ represent a harmonic conjugate pair. An analogous conclusion holds for the derivatives of the function $\Psi_{TD}-(\Gamma/k)\psi_{0,3/2}$, harmonic in the upper half-plane $\hat{Y}\geqslant 0$ and subject to (5.11b). Then

$$\bar{P}=\Gamma P+2\Gamma H(-\bar{X})(-\bar{X})^{1/2},\quad -\bar{A}'=-\mathrm{d}A/\mathrm{d}\bar{X}-2\Gamma H(\bar{X})\bar{X}^{1/2} \tag{5.13a}$$

with H denoting the Heaviside unit step function form a Hilbert pair,

$$[\bar{P},-\bar{A}'](\bar{X})=\frac{1}{\pi}\int_{-\infty}^{\infty}\frac{[\bar{A}',\bar{P}](S)}{\bar{X}-S}\,\mathrm{d}S. \tag{5.13b}$$

As an important aspect, (5.13) guarantees the downstream decay of P originally required

by (5.3*c*). Finally, these relationships together with the dominant behaviour of P far upstream fixes that of A far downstream, see (5.12*c*), and thus the structure of the postseparated flow according to the analysis of § 5.1.2. The resulting interaction law (5.13) closes the lower-deck problem (5.3), then forming a triple-deck problem, parametrised by Γ, which is formally identical with that found in the theory of laminar separation as suggested for the turbulent case by Neish & Smith (1992). Smith (1977) demonstrated by a numerical investigation that a (unique) solution to this triple-deck problem only exists for a specific (positive) eigenvalue of Γ; refined solutions were obtained by Korolev (1980) and van Dommelen & Shen (1984). This problem can be cast into standard form (cf. Sychev *et al.* 1998) by means of the affine transformation $\bar{X} \mapsto \bar{X}/\bar{\Gamma}^6$, $\hat{Y} \mapsto \hat{Y}/\bar{\Gamma}^2$, $\bar{\Psi} \mapsto \bar{\Psi}/\bar{\Gamma}^4$ (i.e. $A \mapsto A/\bar{\Gamma}^2$), $P \mapsto P/\bar{\Gamma}^4$, with

$$2\Gamma^{1/8} = 2\bar{\Gamma} \doteq 0.415 \pm 0.005 \tag{5.14}$$

as the currently most accurate figure of this eigenvalue given by the latter authors. This situation renders the scalings (5.9) and, notably, the value of Λ uniquely determined for a given value of the external-flow parameter k. The far-field eigensolution of Laplace's equation proportional to Λ as seen from (5.11*c*), (5.12*b*), (5.12*c*) reflects the invariance of the triple-deck solution with respect to an arbitrary shift of the origin $\bar{X} = 0$ for $|\bar{X}|$ large. In contrast to the laminar case, here Λ proves crucial in connection with matching the 'inner' and the 'outer' interacting flow as shown next.

5.2. *Outer interaction and separation criterion*

We introduce appropriately stretched variables $[R, X, Y, \Psi] = [r, s, y, \psi/u_{0\mathcal{D}}]/\delta_{\mathcal{D}}$, which are assumed to be of $O(1)$ in the square region of the outer interaction, forming the continuation of the main tier of the boundary layer and continued as a separated shear layer further downstream. Here $R = (X^2 + Y^2)^{1/2}$ and $\delta_{\mathcal{D}}$ denotes the value of the boundary layer thickness for $s = 0$, expanded as $\delta_{\mathcal{D}} \sim \sigma[\Delta_{\mathcal{D}} + O(\epsilon)]$ according to (3.13*a*) and (4.1). It is convenient to write

$$\delta_{TD}/\delta_{\mathcal{D}} \sim (\epsilon/K)[1 + O(\epsilon)], \quad K = k^2\Delta_{\mathcal{D}}(k)/(9\Gamma) = O(1), \tag{5.15}$$

which follows after some manipulations from (5.1*b*), (4.17), (5.8), (5.9*a*).

In the asymptotic limit currently under focus separation is seen to take place at the origin $R = 0$, which then forms a singular point in the flow description. Moreover, in the viscous wall layer expansions of the type (5.5*a*) hold,

$$\alpha Re\psi \sim \int_0^{y^+} u_0^+(t)\,\mathrm{d}t + \cdots + \bar{\pi}^{+2}u_0^+(y^+) \begin{cases} a_-(-KX/\epsilon)^{1/6} + \cdots, & X < 0, \\ -a_+(KX/\epsilon)^{3/2} + \cdots, & X > 0, \end{cases} \tag{5.16a}$$

$$p - p_{0\mathcal{D}} \sim -\delta_{\mathcal{D}}^{1/2}u_{0\mathcal{D}}^2 k \begin{cases} 2(-X)^{1/2} + \cdots, & X < 0, \\ p_+(\epsilon/K)^{13/6}X^{-5/3} + \cdots, & X > 0, \end{cases} \tag{5.16b}$$

in agreement with (5.12). In turn, matching the stream function with its representations in the wall layer for $X \neq 0$, the upper deck for $R \to 0$ in the form (5.11*c*), the external flow as given by (3.1), (3.6), and, eventually, the oncoming boundary layer as expressed by (3.13), (4.1), (3.7*b*), and taking note of the dominance of inertia terms in (2.2) in the region of the outer interaction suggests the expansions

$$\begin{aligned} \Psi \sim Y &+ \delta_{\mathcal{D}}^{1/2}\Psi_{OP}(X, Y; k) + O(\delta_{\mathcal{D}}) \\ &- \epsilon[F_{\mathcal{D}}(Y; k) - \delta_{\mathcal{D}}^{1/2}\Psi_{OI}(X, Y; k) + O(\delta_{\mathcal{D}})] + O(\epsilon^2), \end{aligned} \tag{5.17}$$

$$\delta/\delta_{\mathcal{D}} \sim 1 + \delta_{\mathcal{D}}^{1/2}[D_{1/2}(X; k) + O(\epsilon)] + O(\delta_{\mathcal{D}}). \tag{5.18}$$

That is, effects of surface curvature are insignificant for the outer interaction process, and the small-defect structure is preserved as $F_{\mathcal{D}}(Y;k)$ represents the locally 'frozen' state of the oncoming boundary layer: convective terms in (2.2) are linearised about the unperturbed velocity expressed by $[u,v]=[u_{0\mathcal{D}},0]$, and the leading-order boundary layer velocity profile given by $F'_{\mathcal{D}}$ is transferred unchanged into the separated shear layer, forming for large values of X. We remark that the Reynolds shear and normal stress gradients first enter the equations that govern contributions of $O(\epsilon\delta_{\mathcal{D}})$ in (5.18), in the form of inhomogeneities.

The equations governing Ψ_{OP} and Ψ_{OI} are derived from (2.2) by elimination of the pressure in straightforward manner as in § 5.1.4. One then finds in leading order the potential flow problem

$$\nabla_c^2\Psi_{OP}=0,\quad \nabla_c^2=\delta_{\mathcal{D}}^2\nabla_p^2=\partial_X^2+\partial_Y^2, \tag{5.19a}$$

$$X<0\colon\ \Psi_{OP}(X,0;k)=0,\quad X>0\colon\ \partial_Y\Psi_{OP}(X,0;k)=0, \tag{5.19b}$$

$$R\to 0\colon\ |\Psi_{OP}|/R^{3/2}<\infty,\quad R\to\infty\colon\ \Psi_{OP}\sim\psi_{0,3/2}(R,\theta;k), \tag{5.19c}$$

where we refer to (3.5), (A 7), (3.6b). The condition for $R\to 0$ in (5.19c) asserts that a singularity at the separation point $R=0$ stronger than the original BV singularity is unacceptable in a self-consistent interactive-flow description. By exploiting the extremal properties of solutions of Laplace's equation or applying the Mellin transform one can show that

$$\Psi_{OP}\equiv\psi_{0,3/2}(R,\theta;k)=\big(2\sqrt{2}k/3\big)\breve{\Psi},\quad \breve{\Psi}(X,Y)=(R-2X)\sqrt{R+X}, \tag{5.20}$$

is the only conceivable solution of (5.19). This not only confirms (5.16) and agrees with (5.11c) by matching but also a posteriori justifies the strategy followed in § 5.1: namely, that the BV singularity is effectively avoided by means of the inner interaction mechanism.

As a crucial result, the contribution of $O\big(\epsilon\delta_{\mathcal{D}}^{1/2}\big)$ to the expansion (5.18) describes an induced vortex flow that accounts for the interaction of the boundary layer flow with the irrotational leading-order disturbance of $O\big(\delta_{\mathcal{D}}^{1/2}\big)$. Here the vorticity transport equation reduces to Poisson's equation,

$$\nabla_c^2\Psi_{OI}=-F'''_{\mathcal{D}}(Y;k)\,\Psi_{OP}(X,Y;k). \tag{5.21a}$$

Now primes denote derivatives with respect to Y. The right-hand side of (5.21a) represents the negative X-dependent leading-order contribution of the vorticity generated in the boundary layer upstream and convected with the irrotational flow. Here a further X-independent adding term that results from integration in the derivation of (5.21a) has been set to zero as it would imply perturbations of $O(\sigma^{1/2})$ in (3.13a) and, thus, unacceptably alter the original structure of the incident (attached) boundary layer flow. Also, we have for

$$X<0\colon\ \Psi_{OI}(X,0;k)=0,\quad X>0,\ Y\to 0\colon\ \partial_Y\Psi_{OI}+F''_{\mathcal{D}}\Psi_{OP}\to 0, \tag{5.21b}$$

$$X\to-\infty\colon\ \Psi_{OI}\sim 2k\sqrt{-X}\,G_{\mathcal{D}}(Y;k),\ \ G_{\mathcal{D}}=2F_{\mathcal{D}}-YF'_{\mathcal{D}}, \tag{5.21c}$$

$$Y=1\colon\ \partial_Y\Psi_{OI}=0. \tag{5.21d}$$

The conditions (5.21b) arise from matching the stream function and the pressure in the outer and the wall layer, according to (5.16). The requirements of matching with the oncoming boundary layer, see (4.1) and (4.4), lead to (5.21c), where the near-wall form of $F_{\mathcal{D}}(Y;k)$ is given by (4.6a) and (4.10). Here we add that Ψ_{OI} is obviously subject to subexponential growth for $X\to\infty$. Furthermore, (5.21d) is due to patching the solution

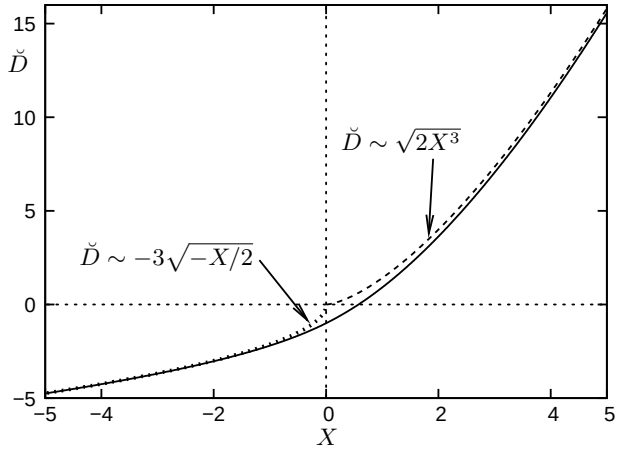

FIGURE 7. Boundary layer thickness near separation in normalised form (for caption see text).

with the disturbance of $O(\epsilon\delta)$ in the ambient external flow as given by (3.1) for $X = O(1)$, $y = O(1)$. Finally, an investigation of (5.21*a*) subject to (5.21*b*) gives for

$$\pi > \theta > 0, \quad R \to 0\colon \quad \Psi_{OI} \sim E(k) R^{1/2} \cos(\theta/2) + \cdots, \quad E = 9\Lambda/[k\Delta_{\mathcal{D}}(k)], \tag{5.22}$$

where the specific form of the coefficient E is required by matching the outer and the inner interacting flow by using (5.10*a*), (5.11*c*), (5.17), with the aid of (5.15).

Apart from the matching conditions (5.21*b*) for $X > 0$ and (5.22), the description of the outer interaction here closely resembles that in fully developed turbulent trailing-edge flow as put forward by Melnik & Chow (1975, pp. 224–225, with 5.21*a* having the wrong sign on its right-hand side). However, the presence of a wall further downstream, as in the problem considered here, leads to a change in detail and makes the treatment more involved. This becomes evident by evaluation of (5.21*a*) subject to (5.21*b*) and supplemented with (5.20), which reveals a contribution adding to the logarithmic portion of the initial velocity profile $F'_{\mathcal{D}}(Y;k)$ upstream of separation, superseded by a stronger singular behaviour immediately downstream as for

$$Y \to 0\colon \quad \Psi_{OI} \sim -\frac{2k}{3\kappa} \begin{cases} 3(-X)^{1/2} Y \ln Y + O(Y), & X < 0, \\ 2X^{3/2} \ln Y + O(1), & X > 0. \end{cases} \tag{5.23}$$

The analysis of the interaction process described so far is unaffected by any turbulence closure. This enables us to also express the local variation of the boundary layer edge represented by $D_{1/2}$ in (5.18) in closed form. It is found by patching the vorticity reading $-\nabla^2\psi \sim -(u_{0\mathcal{D}}/\delta_{\mathcal{D}})\nabla_c^2\Psi$ for $y = \delta$. There it must vanish up to and including the orders quoted explicitly in (5.17), which yields $D_{1/2} = -\Psi_{OP}(X, 1; k)$ by (5.21*a*) (since $F'''_{\mathcal{D}}(1;k) > 0$). This result matches the variation of δ in the oncoming flow as expressed by (3.13*a*), (4.1), (4.2) as $D_{1/2} \sim -2k(-X)^{1/2} + \cdots$, $X \to -\infty$, and gives $D_{1/2} \sim (4k/3)X^{3/2} + \cdots$, $X \to \infty$. The latter expression confirms that the region of outer interaction recovers as a separated shear layer which coincides with the region of breakdown along $\mathcal{S}$ for $s \to 0_+$ addressed briefly in connection with (3.9*b*). We remark that this local variation of the boundary layer thickness is already indicated in figure 6. Its canonical representation $\breve{D}(X) = -\breve{\Psi}(X, 1)$ inferred from (5.20) is displayed in figure 7, together with the asymptotes for $|X|$ being large noted above.

A particular solution of the elliptic problem posed by (5.21) can be constructed through

exploitation of standard methods. Hence we differentiate (5.21a) triply with respect to X, in order to cope with the growth of the inhomogeneity for $|X| \to \infty$ resulting from (5.20), which gives in the limit

$$\varepsilon = \frac{Y}{X} \to 0: \quad \Psi_{OP} \sim 2k|X|^{1/2} \begin{cases} Y[1+\varepsilon^2/24+O(\varepsilon^4)], & X \to -\infty, \\ (2X/3)[-1+3\varepsilon^2/8+O(\varepsilon^4)], & X \to \infty. \end{cases} \tag{5.24}$$

By writing $\Psi_{OI}(X,Y;k) = \Psi_{OIh} + \Psi_{OIp}$, we then find

$$\Psi_{OIp}(X,Y;k) = \int_{-\infty}^{X} \left[\int_{-\infty}^{S_1} \int_{-\infty}^{S_2} \Phi(S_3,Y;k)\,\mathrm{d}S_3\,\mathrm{d}S_2 + k\frac{H(-S_1)}{\sqrt{-S_1}}\,G_{\mathcal{D}}(Y;k) \right] \mathrm{d}S_1 + 2kH(-X)\sqrt{-X}\,G_{\mathcal{D}}(Y;k), \tag{5.25a}$$

$$\Phi(X,Y;k) = -\frac{1}{2\pi} \int_{-1}^{1} \mathrm{sgn}(Z) F_{\mathcal{D}}'''(|Z|;k) \int_{-\infty}^{\infty} \Pi(S,|Z|;k) \ln R^\star \,\mathrm{d}S\,\mathrm{d}Z, \tag{5.25b}$$

$$\Pi(X,Y;k) = \partial_X^3 \Psi_{OP} = -3\,\Psi_{OP}/(8R^3), \quad R^\star = \sqrt{(X-S)^2+(Y-Z)^2}, \tag{5.25c}$$

for a particular solution of (5.21a) which satisfies (5.21b) and (5.21c) rather than (5.21d) and (5.22). The determination of a complementary non-trivial homogeneous solution $\Psi_{OIh}(X,Y;k)$ which supplements (5.25) to yield a (unique) composite solution of (5.21) is critical for an advanced flow description, and efforts to solve (5.21) are under way.

Eventually, the procedure of fixing the value of the external-flow parameter k, i.e. the position $x = x_{\mathcal{D}}(k)$ of inviscid flow detachment, on the basis of a rationally derived separation criterion for turbulent flow is delineated by the following four steps:

(A) extract the (non-vanishing) value of the coefficient Λ in the second-order term of (5.12c) from the unique eigensolution of the triple-deck problem;

(B) seek a formal solution of the well-posed problem (5.21) in dependence of k;

(C) compute the quantity E in (5.22), either (semi-)analytically or numerically;

(D) evaluate the resulting solvability condition for (5.21),

$$9\Lambda = k\,\mathcal{F}_{x=0}^{x=x_{\mathcal{D}}}\{U_{\mathcal{S}}(x;k)\}, \quad \mathcal{F} = \Delta_{\mathcal{D}} E, \tag{5.26}$$

representing the desired separation criterion.

It is insinuated in (5.26) that $\mathcal{F}$ represents a functional of the surface speed $U_{\mathcal{S}}$ that drives the boundary layer from stagnation towards separation. Here we point to the dependences of the flow variables Ψ_{OP}, Ψ_{OI} on k and the 'frozen' state of the boundary layer entering the right-hand side of (5.21a). Thus (5.26) accounts for the global external flow as well as the upstream history of the boundary layer, as one would expect from a separation criterion that deals with the case $k = O(1)$, though deduced from local asymptotic analysis. It is intriguing how this is achieved by matching due to the universal structure of the triple-deck solution.

The separation criterion (5.26) completes the description of the entire process of turbulent separation to the leading approximation.

6. Conclusions and further outlook

The comprehensive description of time-mean bluff-body separation presented here appears to be self-consistent and physically relevant when the global Reynolds number Re is so large that the potential flow parameter k is independent of Re. In this situation separation is provoked at a distance from the leading edge of the body that is comparable to its typical dimension $\tilde{L}$. It is significant that the asymptotic picture of the initially attached boundary layer is founded on a minimum of assumptions merely regarding the

scaling of the turbulent motion. These consequently determine the flow structure in a region centred around the point of separation with an extent comparable to the boundary layer thickness δ. It is interesting that the scaling properties of the boundary layer cannot be determined entirely unless the process of viscous–inviscid interaction that governs separation is taken into account. We further emphasize that the major results of the analysis are qualitatively unaffected by a specific turbulent shear stress closure provided that it satisfies restrictions which reflect the asymptotic properties of the overlap of the predominantly turbulent region of the boundary layer and the viscous wall layer. Effectively, classical mixing-length-based arguments suffice to disclose all the essential features of the separating flow. Altogether, the theory is essentially based upon the following premises:

(I) the body has a perfectly impermeable rigid smooth surface;

(II) the flow is nominally two-dimensional;

(III) the flow on the body scale in the high-Reynolds-number limit is described by the Euler equations;

(IV) free-stream turbulence is of no importance;

(V) all components of the Reynolds stress tensor are of comparable magnitude;

(VI) each subregion of the turbulent boundary layer is characterised by a single velocity scale;

(VII) the wall layer is in equilibrium (initially firmly attached turbulent boundary layer).

We find that a rational description of separation starting with the classical picture of an initially attached fully developed two-tiered turbulent boundary layer is affected by two key aspects, depending on whether the adverse pressure gradient near separation exerted by the external flow is bounded or not. In the first case flow reversal in the predominantly inviscid small-defect region that reaches close to the wall requires a pressure rise of $O(1)$ acting on a relatively short streamwise distance, which contradicts the original assumption; in the second the transcendentally thin viscous sublayer prevents the formation of viscous–inviscid boundary layer interaction that is sufficiently strong to ensure a smooth continuation of the incident boundary layer into a separated shear layer (cf. Sykes 1980). In order to overcome this dilemma, two disparate routes to separation can be established: in the first situation the assumption of a large velocity defect leads to a multi-layered flow structure that distinctly differs from that outlined here and in turn to the theory of turbulent marginal separation (Scheichl & Kluwick 2007*a*,*b*). The massively separating flow considered here pertains to the second case. Then the structure of the stagnant-flow near the leading edge of a bluff body provides the remedy as the turbulence intensity level in the boundary layer further downstream seems inevitably associated with so-called slightly underdeveloped turbulence: the von Kármán number varies essentially algebraically with δ, but the velocity defect is of $O(1/\ln Re)$ as in the classical theory. In contrast to what is known from a marginally separating turbulent boundary layer, here the logarithmic law of the wall is not eradicated as the vast bulk of the small-defect layer is transferred unchanged into a separated shear layer – a probably surprising observation.

As an intriguing interpretation of the present flow description, the boundary layer undergoing separation is always influenced by its laminar origins near the leading edge, irrespective of how large Re is. Above all, this conclusion is interestingly supported by experimental findings (Schewe 2001), although yet not conclusively. The rapid evolution towards a free fully developed turbulent shear layer of finite width is likely to take place at a rather short distance downstream of separation (cf. Sychev 2010). The related mechanism is still to be ascertained, and much more effort both experimentally and in DNS seems required in order to fully corroborate this flow picture.

It is noteworthy that the scenario of an underdeveloped turbulent boundary layer allows for a self-consistent time-averaged picture of quite rapid laminar–turbulent transition and thus a complete description of the boundary layer from transition towards separation. Therefore, it is promising for completing the theory of the turbulent flow past a sharp trailing edge at angle of attack (cf. Melnik & Chow 1975), associated with a Brillouin–Villat-type singularity in the potential flow. Beyond that it might be useful for future self-consistent descriptions of, for example, turbulent boundary layer flows over wall-mounted obstacles (cf. Sykes 1980) or turbulent boundary layer/shock wave interaction (cf. Agrawal & Messiter 1984 and references therein) that include separation.

Apart from the description of the separated shear layer, open points mainly concern the precise position $x = x_{\mathcal{D}}$ of inviscid flow detachment or, equivalently, the value of k. In lieu of attempting to settle this question first, here we have drawn attention to the local structure of the separating flow by having in mind a particular value of k. The latter is predicted for a prescribed body geometry by the separation criterion derived rationally from the interplay of the inner with the outer interaction mechanism, which is encouraging. The exploration of this criterion, based on a thorough investigation of the underlying vortex-flow problem, will prove crucial for further progress. The forecast of $x_{\mathcal{D}}$ is linked to the correct choice of the inviscid-flow model and in turn to solving the long-standing problem of the asymptotic structure of the large-scale turbulent separated flow. This consists of the free shear layer along the free streamline $\mathcal{S}$ having a thickness that grows linearly with the arc length along $\mathcal{S}$, the adjacent near wake that exhibits (two) reversed-flow eddies, and the wake further downstream that results from the merging of the two former flow regions. In view of present knowledge the chances of establishing a complete description of self-induced massive separation are viewed as high. When it comes to the investigation of viscous effects on the separated inviscid flow we might expect an interesting comparison between the asymptotic eddy models of laminar steady flow (finally resolved in all essentials by Chernyshenko 1988, cf. Smith 1986; Sychev *et al.* 1998) and the turbulent case, partly due to the small-defect structure of the separating turbulent boundary layer (cf. Sychev 2010). This, among other things, is a topic of current and future exciting research.

Fruitful discussions with Professor Sergei I. Chernyshenko are gratefully acknowledged. The authors also wish to express their thanks to the referees for helpful comments.

Appendix A. Brillouin–Villat singularity

We adopt the well-known vorticity transport theorem, deduced from (2.2), and cast the problem governing the inviscid flow into the form

$$\nabla^2\psi_0 = -\omega_0(\psi_0;k), \quad y \geqslant y_{\mathcal{S}}(s;k)\colon \ \omega_0 = 0, \tag{A 1a}$$

$$\psi_0(x,0;k) = \psi_0(x,y_{\mathcal{S}}(s;k);k) = 0. \tag{A 1b}$$

The kinematic boundary condition (A 1b) reflects (2.3) for $s \leqslant 0$. The quantity ω_0 may exhibit a discontinuity at $y = y_{\mathcal{S}}$ for $s > 0$. We have

$$U_{\mathcal{S}} = \sqrt{u_0^2 + v_0^2} \quad \text{for} \quad y = y_{\mathcal{S}}, \tag{A 2}$$

so that $U_{\mathcal{S}} = u_0$ for $s \leqslant 0$, according to (A 2) and (A 1b). This gives (3.3), which is in line with (A 1a), (2.2c). Then the requirement for smooth flow detachment reads

$$s \to 0_-\colon \ U_{\mathcal{S}} \to u_{0\mathcal{D}}(k) > 0, \quad s \to 0_+\colon \ U_{\mathcal{S}+} \to u_{0\mathcal{D}}(k), \ U_{\mathcal{S}-} \to 0. \tag{A 3}$$

Moreover, our concern is with separation on the upper part of the cylinder, so that $\psi_0 \geqslant 0$ for $y \geqslant y_{\mathcal{S}}$, whereas the stagnant-flow or backflow region under consideration is characterised by $\psi_0 = \omega_0 = 0$ or both $\psi \leqslant 0$ and $\omega_0 < 0$ for $0 \leqslant y < y_{\mathcal{S}}$ respectively.

The pressure p_0 is required to be continuous on $\mathcal{S}$ since the asymptotically slender separated viscous shear layer along $\mathcal{S}$ emerging in the case (1.1) exhibits a correspondingly weak variation of p in the direction transverse to $\mathcal{S}$ (which mostly compensate centripetal forces proportional to $U_{\mathcal{S}}^2$ times the curvature of $\mathcal{S}$). Employing Bernoulli's theorem together with (2.4) then states that

$$p_0 + \frac{u_0^2 + v_0^2}{2} = B_0(\psi_0; k) = \begin{cases} 1/2, & \psi_0 \geqslant 0, \\ p_{0\mathcal{D}}(k) - \displaystyle\int_0^{\psi_0} \omega_0(t; k)\,\mathrm{d}t, & \psi_0 < 0, \end{cases} \tag{A 4}$$

which yields (3.4) along with the relationship

$$p_{\mathcal{S}} + U_{\mathcal{S}-}^2/2 = (1 - u_{0\mathcal{D}}^2)/2, \quad \psi_0 < 0, \tag{A 5}$$

calculated from (A 3). Finally, (A 1) is supplemented with the resulting dynamic jump condition

$$U_{\mathcal{S}+}^2 - U_{\mathcal{S}-}^2 = u_{0\mathcal{D}}^2, \tag{A 6}$$

according to the jump of B_0 across $\mathcal{S}$, given by $1/2 - p_{0\mathcal{D}}$.

We now derive the final expansions (3.6)–(3.9) in a stepwise fashion by invoking (A 1) and (A 6):

(i) we advantageously introduce polar coordinates, see (3.5), and investigate (A 1) for $y \geqslant y_{\mathcal{S}}$ near $\mathcal{D}$. To this end, we express ∇^2 in terms of r, θ by inspection of (2.2c), (3.5). Since $\psi_0 \sim u_{0\mathcal{D}} y + \cdots$, $y = r\sin\theta$, as $r \to 0$, according to (3.3) and (A 3), in this limit one can write

$$\nabla^2 \psi_0 \sim [\nabla_p^2 + \varkappa_{\mathcal{D}}\,\partial_y + \cdots][1 + O(r)]\psi_0, \tag{A 7a}$$

$$\nabla_p^2 = r^{-1}\partial_r(r\partial_r) + r^{-2}\partial_\theta^2, \quad \partial_y = \sin\theta\,\partial_r + r^{-1}\cos\theta\,\partial_\theta, \tag{A 7b}$$

with ∇_p^2 being the Laplacian in the case of a planar surface ($\varkappa \equiv 0$). In the present context, $\psi_0 = 0$ for $\theta = \pi$. The analysis of the eigensolutions of Laplace's equation $\nabla^2\psi_0 = 0$ then yields the asymptotic expansion

$$\psi_0/u_{0\mathcal{D}} \sim r\sin\theta + \psi_{0\lambda}(r, \theta; k) + \cdots + \psi_{02}(r, \theta; k) + \cdots, \quad \pi \geqslant \theta > 0, \quad r \to 0, \tag{A 8a}$$

$$\psi_{0\lambda} = a_\lambda(k)\, r^\lambda \sin[\lambda(\pi - \theta)], \quad \psi_{02} = r^2\big\{a_2(k)\sin(2\theta) - (\varkappa_{\mathcal{D}}/4)[1 - \cos(2\theta)]\big\}, \tag{A 8b}$$

matching (3.3) as $\theta \to \pi$, with $\nabla_p^2[\psi_{0\lambda}, \psi_{02}] = [0, -\varkappa_{\mathcal{D}}]$ and both the constant $\lambda > 1$ and the dependences of the parameters $a_\lambda \neq 0$ and a_2 on k unknown at this stage. Specifically, we seek the smallest value of λ by utilising the kinematic and dynamic boundary conditions (A 1b) and (A 6), respectively, that hold on $\mathcal{S}$. (We notice the passive nature of the inherent breakdown of the expansion (A 8) in the limit $y - y_{\mathcal{S}} \to 0_+$. Hence, we first can ignore the region of non-uniformity and the expansion of ψ_0 is restated solely by rearranging the terms that result from expanding each term in (A 8a) in this limit.)

(ii) Inserting (A 1b) into (A 8a) provides the one-term estimate $\theta \sim c_\lambda r^{\lambda-1} + \cdots$ and, by using (3.5), $\theta \sim c_\lambda s^{\lambda-1} + \cdots$ for $y_{\mathcal{S}} \sim c_\lambda s^\lambda + \cdots$, $c_\lambda = -a_\lambda \sin(\lambda\pi) > 0$, as $s \to 0_+$. Consequently we infer from (A 2), (A 7) that $U_{\mathcal{S}+}^2 \sim [(\partial_r\psi_0)^2 + r^{-2}(\partial_\theta\psi_0)^2][1 + O(\varkappa_{\mathcal{D}} r^\lambda)]$ for $y = y_{\mathcal{S}}$ in this limit. After some algebra we then derive from the aforementioned one-term approximation and the three-term expansion (A 8) the expression

$$\begin{aligned}(U_{\mathcal{S}+}/u_{0\mathcal{D}})^2 \sim 1 - 2\lambda a_\lambda s^{\lambda-1}\cos(\lambda\pi) + [\lambda + 2(\lambda-1)\sin(\lambda\pi)^2]\lambda a_\lambda^2 s^{2\lambda-2} \\ + 4a_2 s + O(s^\lambda, s^2), \quad s \to 0_+.\end{aligned} \tag{A 9}$$

(*iii*) Next, we envisage the flow in the slipstream zone close to $\mathcal{D}$, near which it is of cusp-type shape, according to the estimate for $y_{\mathcal{S}}$ given in item (*ii*). In turn, for $\omega_0 < 0$ we have $|v_0| \ll |u_0| = O(U_{\mathcal{S}-})$ there. One then finds that ψ_0 assumes the self-similar form $\psi_0/(y_{\mathcal{S}}U_{\mathcal{S}-}) \sim f(\xi) + \cdots$, $\xi = y/y_{\mathcal{S}}$, as $s \to 0_+$. Substituting this expression into (A 1) results in the least-degenerate form of this problem,

$$U_{\mathcal{S}-}f'' - 2\lambda c_\lambda^2 s^{2\lambda-1}U'_{\mathcal{S}-}(\xi f' - f) + c_\lambda^2 s^{2\lambda}U''_{\mathcal{S}-}f \sim -c_\lambda s^\lambda \omega_0, \quad s \to 0_+, \quad \text{(A 10}a\text{)}$$

$$f(0) = f(1) = 0, \quad f'(1) = 1; \quad \text{(A 10}b\text{)}$$

primes on $U_{\mathcal{S}-}$ denote derivatives with respect to s. The relationships (A 10) give rise to a boundary value problem fixing both $f(\xi)$ and $U_{\mathcal{S}-}$ near $\mathcal{D}$. The first term in (A 10a) contains the highest derivative with respect to ξ and must, therefore, be retained to leading order. Since $U_{\mathcal{S}-} \to 0_+$, according to (A 6), the second and thus the third term in (A 10a) are negligibly small. Hence, (A 10a) is seen to reduce to a balance of the first and the term on the right-hand side, where we impose the apparent restriction that ω_0 is bounded as $\psi_0 \to 0_-$ and define $\omega_{0\mathcal{D}} = \omega_0(0_-; k) \leqslant 0$. By using (A 10$b$), we then arrive at the reverse-flow representation $f(\xi) = (\xi^2 - \xi)/2$ as the possibly slowest decay of $U_{\mathcal{S}-}$ reads

$$U_{\mathcal{S}-} \sim -\omega_{0\mathcal{D}}\, c_\lambda s^\lambda + \cdots, \quad s \to 0_+. \quad \text{(A 11)}$$

(*iv*) We now evaluate (A 6) by inserting (A 9), (A 11), in order to fix λ, a_λ, a_2. One then finds that $U_{\mathcal{S}+} = o(s^{\lambda-1})$. From (A 9) we infer that λ is a member of the sequence of eigenvalues $\lambda = 3/2, 5/2, 7/2, \ldots$ as $\psi_{0\lambda}$ is seen to represent a homogeneous eigenfunction of the Laplacian with $\partial_\theta\psi_{02} = 0$ for $\theta = 0$ and $\psi_{02} = 0$ for $\theta = \pi$ and coefficients a_λ that cannot be determined by the local analysis. Next, we conclude that integer powers of s have to be eliminated in (A 9), which demands $a_2 = -15a_\lambda^2/16$ for $\lambda = 3/2$ and $a_2 = 0$ for $\lambda > 3/2$. Also, higher-order terms indicated by dots are seen to be of $O(r^{\lambda+1})$ in (A 8a) and of $O(r^\lambda)$, $O(s^\lambda)$, and $O(s^{\lambda+1})$, respectively, in the three relationships expressing the shape of $\mathcal{S}$ as $s \to 0_+$ in item (*ii*) above. However, only the terms stated explicitly will turn out to significantly affect the further description of separation and are thus under focus here.

(*v*) Let λ take on its minimum value $3/2$, corresponding to the most general application. We then define $a_{3/2} = a_\lambda = c_\lambda$, $\psi_{0,3/2} = \psi_{0\lambda}$, where it proves convenient to introduce the constant k by setting $a_{3/2} = 4k/3$. Eventually, we restate (A 8) in the form (3.6) and obtain the expressions (3.7b) and (3.9a) from (A 6) and (A 11), respectively, where (3.5) and (A 7) are employed. We note that (3.6)–(3.9) capture the general case $\lambda \geqslant 3/2$ as $\lambda = 3/2$ for $k > 0$ and the case $\lambda = 5/2$ in the degenerate limit $k = 0$.

Appendix B. Computation of potential flow

The classical way to solve the problem of potential flow around a finite two-dimensional body that exhibits (two) detaching streamlines confining a dead-water cavity, as formulated by (A 1) with $\omega_0 \equiv 0$, is provided by Levi–Cività's method (with certain additions, cf. Gurevich 1979).

B.1. *Preliminaries*

The associated conformal transformation maps the region of flow in the physical plane (see figure 1), with complex variable z, onto a closed contour lying in the plane of a complex variable ζ and its interior (see figure 8). This contour consists of the upper half-unit circle $\mathcal{H}'$, the points $\zeta = \mp 1$, and the portion $\mathcal{R}'$ of the real axis between these points, which are, respectively, the images of the wetted fraction of the body surface,

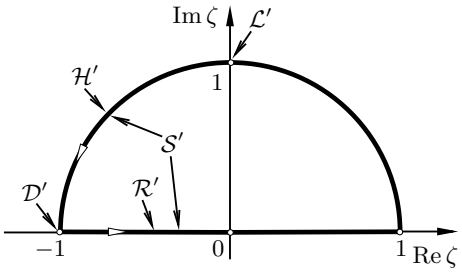

FIGURE 8. Flow situation in the complex ζ-plane (for caption see text in § B.1).

the points of flow detachments, and the detached parts of the free streamlines. Here the bijective function $\zeta(z)$ is regarded as analytic in the whole z-plane except for $z = \infty$, having the image $\zeta = 0$, where it has a pole. For a symmetric problem as considered here, let $\mathcal{D}'$ at $z = -1$ and $\mathcal{L}'$ at $\zeta = \mathrm{i}$ be the images of the detachment and stagnation points $\mathcal{D}$ and $\mathcal{L}$ respectively. Accordingly, the upper detaching streamline $\mathcal{S}$ is mapped onto the curve $\mathcal{S}'$, which consists of the right halves of $\mathcal{H}'$ and $\mathcal{R}'$.

Also, we introduce the complex potential $w_0(z;k) = \varphi_0 + \mathrm{i}\psi_0$ and the function $\Omega(\zeta;k) = \mathrm{i}\ln[(\mathrm{d}w_0/\mathrm{d}z)/u_{0\mathcal{D}}] = \vartheta_0 + \mathrm{i}\ln(V/u_{0\mathcal{D}})$. We stress that w_0 and Ω are analytic inside and on the contour comprising $\mathcal{H}'$ and $\mathcal{R}'$ apart from, respectively, $\zeta = 0$ (where w_0 has a pole) and $\zeta = i$ as

$$\Omega \sim \mathrm{i}\ln(\zeta - \mathrm{i}) + O(1), \quad \zeta - \mathrm{i} \to 0 \tag{B 1}$$

(since $\mathrm{d}w_0/\mathrm{d}z$ vanishes in a regular manner at the point $\mathcal{L}$). Thus V and ϑ_0 denote the (positive) flow speed and the flow angle respectively. On $\mathcal{H}'$ we have $\psi_0 = 0$ and $\vartheta_0 = \phi$ with ϕ satisfying (2.1). The image of $\mathcal{S}$ then is parametrised in terms of a real parameter ϱ that increases in the flow direction (as indicated by the arrows on $\mathcal{S}'$ and $\mathcal{R}'$ in figure 8) by setting, respectively,

$$\zeta = \exp[\mathrm{i}(\pi + \varrho)], \ \ -\pi/2 \leqslant \varrho \leqslant 0\colon \quad \psi_0 = 0, \ \ V = U_{\mathcal{S}}, \ \ \vartheta_0 = \phi, \tag{B 2a}$$

$$\zeta = -1 + \varrho, \ \ 0 < \varrho < 1\colon \quad \psi_0 = 0, \ \ V = U_{\mathcal{S}+} \equiv u_{0\mathcal{D}}\ (> 0). \tag{B 2b}$$

The last identity follows by equating $p_{\mathcal{S}}$ and $U_{\mathcal{S}-}$ (A 5) with the constant cavity pressure $(1 - u_{0\mathcal{D}}^2)/2p_0$ and 0, respectively, according to (A 3), and upon substitution in (A 6). Finally, the corresponding relationships

$$s \leqslant 0, \ \ y = 0\colon \quad \mathrm{d}\varphi_0/\mathrm{d}l = U_{\mathcal{S}}(x;k), \ \ l = s, \ \ x = x_{\mathcal{D}} + s, \tag{B 3a}$$

$$s > 0, \ \ y = y_{\mathcal{S}}(s;k)\colon \quad \mathrm{d}\varphi_0/\mathrm{d}l = u_{0\mathcal{D}} \tag{B 3b}$$

between the real flow potential φ_0 and V holding on $\mathcal{S}$ are imposed, so that l denotes the arc length along $\mathcal{S}$ measured from $\mathcal{D}$. Also, $\varphi_0 > 0$ and $\mathrm{d}\varphi_0/\mathrm{d}\varrho > 0$ for $-\pi/2 \leqslant \varrho < 1$.

B.2. *Flow along $\mathcal{S}$ close to detachment*

The results (3.7*b*), (3.9*b*) evince the behaviour of the potential flow near the BV singularity with sufficient accuracy. We first demonstrate in a nutshell how these are recovered readily by exploiting the real parts of the Taylor series about $\mathcal{D}'$ derived from (B 2),

$$w_0 \sim \varphi_{\mathcal{D}} + W_2[(\zeta + 1)^2 + (\zeta + 1)^3] + O[(\zeta + 1)^4], \tag{B 4a}$$

$$\Omega \sim \phi_{\mathcal{D}} + \Omega_1(\zeta + 1) + \Omega_2(\zeta + 1)^2 + O[(\zeta + 1)^3], \tag{B 4b}$$

with some real coefficients $\varphi_{\mathcal{D}}\,(>0)$, $W_2\,(>0)$, $\phi_{\mathcal{D}}$, Ω_1, Ω_2: by substituting (B 2a) into (B 4) the image of the flow on $\mathcal{S}$ near $\mathcal{D}$ for $s\to 0_-$ is represented in the form

$$\varphi_0 \sim \varphi_{\mathcal{D}} - W_2\varrho^2 + O(\varrho^4), \tag{B 5a}$$

$$U_{\mathcal{S}}/u_{0\mathcal{D}} \sim \exp[\Omega_1\varrho + O(\varrho^3)] \sim 1 + \Omega_1(\varrho + \varrho^2/2) + O(\varrho^3), \tag{B 5b}$$

$$\phi \sim \phi_{\mathcal{D}} + (\Omega_1/2 - \Omega_2)\varrho^2 + O(\varrho^4), \tag{B 5c}$$

as $\varrho\to 0_-$. By rewriting (B 3a) as $(\mathrm{d}\varphi_0/\mathrm{d}\varrho)(\mathrm{d}\varrho/\mathrm{d}s) = U_{\mathcal{S}}$ we now extract from (B 5a) the relationship $\mathrm{d}(\varrho^2)/\mathrm{d}s \sim -(u_{0\mathcal{D}}/W_2)[1+\Omega_1\varrho + O(\varrho^2)]$ as $s\to 0_-$; one then easily obtains

$$\Omega_1\varrho \sim 2k(-s)^{1/2}[1 + 2k(-s)^{1/2}/3 + O(-s)], \quad s\to 0_-, \tag{B 6}$$

$$k = \Omega_1\varsigma^{1/2}/2, \quad \varsigma = u_{0\mathcal{D}}/W_2\ (>0). \tag{B 7}$$

Here we have reintroduced the potential flow parameter k. Inserting (B 6) into (B 5b) finally yields the three-term expansion (3.7b). Furthermore, we infer from (B 5c) that

$$\varsigma(\Omega_1/2 - \Omega_2) = \varkappa_{\mathcal{D}}. \tag{B 8}$$

For the flow along the detached portion of $\mathcal{S}$ governed by (B 2b), (B 3b) the relations (B 4) then give $\varrho \sim (\varsigma l)^{1/2} - (\varsigma l)/2 + O(l^{3/2})$ and, in turn,

$$\vartheta_0 \sim \phi_{\mathcal{D}} + 2kl^{1/2} - \varkappa_{\mathcal{D}} l + O(l^{3/2}), \quad l\to 0_+. \tag{B 9}$$

This last result accounts for the curvature $-\mathrm{d}\vartheta_0/\mathrm{d}l$ of $\mathcal{S}$ (with the sign conforming to the definition (2.1) of $\varkappa$) immediately downstream of $\mathcal{D}$, in agreement with (3.9b) since $l\sim s+\cdots$, $\mathrm{d}\vartheta_0/\mathrm{d}l \sim \mathrm{d}^2y_{\mathcal{S}}/\mathrm{d}s^2 + \cdots$ as $s\to 0_+$. In this context, the BV singularity is commonly described by (3.8) and (B 9), see e.g. Sychev *et al.* (1998, p. 10).

We have shown that the representation of the flow in the ζ-plane together with the choice of the auxiliary parameter ϱ as the independent variable allows for a convenient regularisation of the BV singularity. Nonetheless, calculating the local form (3.6) of ψ_0 by means of the method described in § B.2 is definitely less gratifying when compared to the procedure outlined in § 3.3. On the other hand, Levi–Cività's method provides a powerful tool for constructing a numerical solution of the overall potential flow problem (A 1).

B.3. *Global flow: numerical treatment*

Here we restrict the application of Levi–Cività's method to the case of an open cavity, i.e. by anticipating $u_{0\mathcal{D}} = 1$ in (B 2b) by (A 4) and (2.4). The main focus lies on the determination of the surface flow speed $U_{\mathcal{S}}(x;k)$ for a prescribed (non-negative) value of k.

We consider a specific conformal mapping $\zeta(z)$ that achieves

$$w_0 = [\varpi(k)(\zeta + 1/\zeta)/2]^2, \tag{B 10}$$

with the yet unknown function $\varpi(k)$ being real. The relation (B 10) has all the desired properties of the potential w_0 discussed in § B.1, also see (B 2). In addition, it reflects the symmetry of the problem as ϕ_0 and ψ_0 are respectively symmetric and antisymmetric with respect to both the imaginary and the real axis of the ζ-plane. Corresponding requirements then have to be met by $\Omega = \vartheta_0 + \mathrm{i}\ln V$: in the upper half-plane ϑ_0 (V) are antisymmetric (symmetric) with respect to the imaginary axis, and the converse conditions hold in the lower half-plane; note (B 2b) with $V=1$ and $\vartheta_0 = 0$ for $z=\infty$ or $\zeta = 0$). Moreover, (B 1) gives evidence that

$$\Xi(\zeta;k) = \Omega(\zeta;k) - \pi - \mathrm{i}\ln[(\zeta-\mathrm{i})/(\zeta+\mathrm{i})] \tag{B 11}$$

is analytic inside and on the boundary of the unit circle and exhibits symmetry properties identical with those of Ω. That is, Ξ can be expanded in the Taylor series $\Xi \sim \sum_{n=1}^{\infty} \Xi_{2n-1}\zeta^{2n-1}$, $|\zeta| \leqslant 1$, with $\operatorname{Im}\Xi_n = 0$.

The aforementioned symmetry properties are revealed by expansions of the form $\phi \sim \pi/2 + O(\upsilon)$, $U_{\mathcal{S}}/U_{\mathcal{S}0}(k) \sim \upsilon + U_1(k)\upsilon^3 + O(\upsilon^5)$ as $\upsilon = \pi/2 + \varrho \to 0_+$, with $U_{\mathcal{S}0}(k)$ being a positive quantity. They confirm the stagnating-flow behaviour (see figures 1*a* and 8). By noticing (B 2*a*), we then end up with the Fourier representation of $\Xi\big[\mathrm{e}^{\mathrm{i}(\pi+\varrho)}; k\big]$,

$$\varrho = -\frac{\pi}{2}\colon \quad \phi = \frac{\pi}{2}, \quad \Upsilon = \ln(2U_{\mathcal{S}0}) = -\sum\nolimits_{n=1}^{\infty}(-1)^n \Xi_{2n-1}, \tag{B 12a}$$

$$0 \geqslant \varrho > -\frac{\pi}{2}\colon \quad \phi - \frac{\pi}{2} + \mathrm{i}\ln\frac{U_{\mathcal{S}}(1-\sin\varrho)}{\cos\varrho} = -\sum\nolimits_{n=1}^{\infty}\Xi_{2n-1}\exp[\mathrm{i}(2n-1)\varrho], \tag{B 12b}$$

In turn, the antisymmetry of $U_{\mathcal{S}}$ with respect to $\upsilon = 0$ is confirmed by the limiting form $\operatorname{Im}\Xi\big[\mathrm{e}^{\mathrm{i}(\pi/2+\upsilon)}; k\big] \sim \Upsilon + \upsilon^2(U_1 - 1/12) + O(\upsilon^4)$ as $\upsilon \to 0_+$. Also, evaluation of (B 2*a*), (B 11), (B 12*b*) for $\varrho = 0$ gives

$$\phi_{\mathcal{D}} = \Omega_0 = \pi/2 - \sum\nolimits_{n=1}^{\infty}\Xi_{2n-1}. \tag{B 13}$$

A collocation method can be set up for a prescribed inclination angle (flow angle) $\phi(x)$, $0 \leqslant x \leqslant x_{\mathcal{D}}$, of the body surface to approximately compute ϖ and Ξ_n with $n = 1, 2, \ldots, N$ for some index N. First, we notice that (B 10) yields $\varphi_0 = (\varpi\cos\varrho)^2$ on $|\zeta| = 1$ and find $\varpi = W_2^{1/2}$ by using (B 5*a*). Then we rewrite (B 3*a*) with the help of (2.1),

$$-\pi/2 \leqslant \varrho < 0\colon \quad \varkappa\,\varpi^2\sin(2\varrho) = U_{\mathcal{S}}\,\mathrm{d}\phi/\mathrm{d}\varrho, \tag{B 14a}$$

$$\varrho = 0\colon \quad 2\varkappa_{\mathcal{D}}\,\varpi^2 = \mathrm{d}^2\phi/\mathrm{d}\varrho^2; \tag{B 14b}$$

applying de l'Hôpital's rule to (B 14*a*) gives (B 14*b*), in agreement with (B 5*c*), (B 7), and (B 8). In turn, elimination of Ω_1 from (B 7) with the aid of (B 5*b*) reveals the effect of the control parameter k in terms of a compatibility condition,

$$\varrho = 0\colon \quad 2k\varpi = \mathrm{d}U_{\mathcal{S}}/\mathrm{d}\varrho. \tag{B 15}$$

We now treat the surface curvature $\varkappa$ as a function of ϕ and have the right-hand sides of (B 14), (B 15) expressed through (B 12), where we terminate the sum at some index $n = N$, N being sufficiently large. Then the evaluation of (B 14*a*) at $N-1$ different locations $\varrho = \rho_n$, $-\pi/2 < \varrho_n < 0$, $n = 1, 2, \ldots, N-1$, supplemented with (B 14*b*) and (B 15) establishes a set of $N+1$ nonlinear transcendental equations for N unknown coefficients Ξ_{2n-1}, $n = 1, 2, \ldots, N$, and $\varpi\,(>0)$. Their roots can be found efficiently by using standard numerical methods. Finally, (B 13) gives the flow angle $\phi = \phi_{\mathcal{D}}(k)$ at the detachment point $\mathcal{D}$. As the simplest but most important example, we consider the canonical problem of the flow around the unit cylinder, where $\varkappa \equiv 1$, $x = \pi - \phi$, $x_{\mathcal{D}}(k) = \pi - \phi_{\mathcal{D}}(k)$ (see figure 1*a*). Here we choose equidistantly spaced values of $\varrho_n = (\pi/2)(n/N - 1)$, $n = 1, 2, \ldots, N$, and $N = 350$. It is demonstrated in the theory of Fourier analysis that $\Xi_N = O(N^{-2})$ or smaller for $N \gg 1$. However, here even $\Xi_N = o(N^q)$ for any $q < 0$ due to analyticity of Ξ, which in turn suggests the absolute numerical error then to be reduced to the order of 10^{-5} or smaller.

The physically admissible solutions have been discussed extensively by Scheichl *et al.* (2008), Scheichl & Kluwick (2008*b*) for the particular range $0 \leqslant k \leqslant k_c \doteq 0.4911$ (referring to monotonically increasing values of the separation angle $x_{\mathcal{D}}$). Specifically, the limiting values attract most interest. First, $x_{\mathcal{D}}(0) \doteq 55^\circ\,2'\,30''$ denotes the so-called BV angle that points to laminar separation (Sychev 1972; Sychev *et al.* 1998; Smith 1977). A simplified version of the procedure presented here, successfully applied to this case much

earlier, must be attributed to several authors appreciated by Gurevich (1979). Second, let us refer to figure 2(a) discussed in § 3.2: then $x_{\mathcal{D}}(k_c) \doteq 124^\circ\,12'\,11''$ represents the critical downstream limit of $x_{\mathcal{D}}$ in the sense of case II. Note that values of k larger than k_c imply a contradiction to the original assumption of a semi-infinite cavity as they predict a non-smooth intersection of $\mathcal{S}$ with the real (symmetry) axis of the z-plane at a finitely remote point. A simple criterion for the occurrence of this situation is indicated by the Taylor expansion of (B 11) about $\zeta = 0$. This gives $\vartheta_0 \sim \pi - (2 - \Xi_1)\zeta + (2/3 + \Xi_2)\zeta^3 + O(\zeta^5)$ and thus describes the shape of $\mathcal{S}$ far downstream when $\zeta \to 0_-$. It asymptotes to the well-known Kirchhoff parabola (case I, $0 \leqslant k < k_c$) for $\Xi_1 < 2$, which degenerates to a cusp (case II, $k = k_c$) for $\Xi_1 = \Xi_{1c} = 2$.

Early numerical computations of HK flows around the circular cylinder were carried out by Woods (1955). The integral method he exploited, however, is considerably more complicated and less straightforward to apply compared to that proposed here, based on Levi–Cività's method.

REFERENCES

Agrawal, S. & Messiter, A. F. 1984 Turbulent boundary-layer interaction with a shock wave at a compression corner. *J. Fluid Mech.* **143**, 23–46.

Batchelor, G. K. 1956*a* On steady laminar flow with closed streamlines at large Reynolds number. *J. Fluid Mech.* **1** (2), 177–190.

Batchelor, G. K. 1956*b* A proposal concerning laminar wakes behind bluff bodies at large Reynolds number. *J. Fluid Mech.* **1** (4), 388–398.

Brown, S. N. & Stewartson, K. 1970 Trailing-edge stall. *J. Fluid Mech.* **42** (3), 561–584.

Chernyshenko, S. I. 1988 The Asymptotic Form of the Stationary Separated Circumfluence of a Body at High Reynolds Numbers. *PMM U.S.S.R.* **52** (6), 746–753, original Russian article in *Prikl. Mathem. Mekhan.* **52** (6), 1988, 958–966.

Diesperov, V. N. 1984 On the Existence and Uniqueness of Self-Similar Solutions Describing the Flow in Mixing Layers. *Dokl. Akad. Nauk SSSR* **275** (6), 1341–1346.

van Dommelen, L. L. & Shen, S. F. 1984 Interactive Separation from a Fixed Wall. In *Numerical and Physical Aspects of Aerodynamic Flows II, Proc. 2nd Symp. California State University, Long Beach, CA, 17–20 January, 1983* (ed. T. Cebeci), pp. 393–402. New York, Berlin, Heidelberg, Tokyo: Springer.

Eppler, R. 1954 Beiträge zur Theorie und Anwendung der Unstetigen Strömungen. *Rat. Mech. Anal.* **3**, 591–644, in German.

Gurevich, M. I. 1979 *Theory of Jets in Ideal Fluids*, 2nd edn. New York, London: Academic Press, original Russian edition: 1965, Moscow: Nauka.

Jones, G. W., Cincotta, J. & Walker, W. 1969 Aerodynamic Forces on a Stationary and Oscillating Circular Cylinder at High Reynolds Numbers. *Tech. Rep.* R-300. NASA.

Klebanoff, P. S. 1955 Characteristics of Turbulence in a Boundary Layer with Zero Pressure Gradient. *Tech. Rep.* 1247. NASA, also NACA *Tech. Note* 3178 (1954).

Kluwick, A. & Scheichl, B. 2009 High-Reynolds-Number Asymptotics of Turbulent Boundary Layers: From Fully Attached to Marginally Separated Flows. In *BAIL 2008 – Boundary and Interior Layers. Proceedings of the Int'l Conf. Boundary and Internal Layers – Computational and Asymptotic Methods, Limerick, July 2008* (ed. A. F. Hegarty, N. Kopteva, E. O'Riordan & M. Stynes), *Lecture Notes in Computational Science and Engineering*, vol. 69, pp. 3–22. Berlin, Heidelberg, New York: Springer, invited.

Kolmogorov, A. N. 1961 A refinement of previous hypotheses concerning the local structure of turbulence in a viscous incompressible fluid at high reynolds number. *J. Fluid Mech.* **13** (1), 82–85.

Korolev, G. L. 1980 Numerical Solution of the Asymptotic Problem of Laminar Boundary-Layer Separation from a Smooth Surface. *Uch. zap. TsAGI* **11** (2), 27–36.

Melnik, R. E. 1989 An Asymptotic Theory of Turbulent Separation. *Comput. Fluids* **17** (1), 165–184.

Melnik, R. E. & Chow, R. 1975 Asymptotic Theory of Two-Dimensional Trailing-Edge Flow. *Tech. Rep.* NAS1-12426. NASA.

Michel, R., Quémard, C. & Durant, R. 1969 Hypothesis on the Mixing Length and Application to the Calculation of the Turbulent Boundary Layers. In *Proc. Computation of Turbulent Boundary Layers – 1968 AFOSR-IFP-Stanford Conference. Vol. I: Methods, Predictions, Evaluation and Flow Structure* (ed. S. J. Kline, M. V. Morkovin, G. Sovran & D. J. Cockrell), pp. 195–207. Stanford University.

Monin, A. S. & Yaglom, A. M. 1971 *Statistical Fluid Mechanics: Mechanics of Turbulence, Vol. 1*. Cambridge, London: The MIT Press.

Nagib, H. M., Chauhan, K. A. & Monkewitz, P. A. 2007 Approach to an asymptotic state for zero pressure gradient turbulent boundary layers. *Phil. Trans. R. Soc.* A **365** (1852), 755–770.

Neiland, V. Ya. 1971 Flow Behind the Boundary-Layer Separation Point in a Supersonic Stream. *Fluid Dyn.* **6** (3), 378–384, original Russian article in *Izv. Akad. Nauk SSSR, Mekh. Zhidk. i Gaza* (3), 1971, 19–27.

Neish, A. & Smith, F. T. 1988 The turbulent boundary layer and wake of an aligned flat plate. *J. Eng. Math.* **22** (1), 15–42.

Neish, A. & Smith, F. T. 1992 On turbulent separation in the flow past a bluff body. *J. Fluid Mech.* **241**, 443–467.

Rothmayer, A. P. & Smith, F. T. 1998 Part III. High Reynolds Number Asymptotic Theories. In *The Handbook of Fluid Dynamics* (ed. R. W. Johnson), pp. III.1–25.26. Boca Raton, Heidelberg: CRC, Springer.

Sandberg, R. D. & Sandham, N. D. 2008 Direct numerical simulation of turbulent flow past a trailing edge and the associated noise generation. *J. Fluid Mech.* **596**, 353–385.

Sandborn, V. A. & Liu, C. Y. 1968 On turbulent boundary-layer separation. *J. Fluid Mech.* **32** (2), 293–304.

Scheichl, B. & Kluwick, A. 2007*a* On turbulent marginal boundary layer separation: how the half-power law supersedes the logarithmic law of the wall. *Int. J. Computing Science and Mathematics (IJCSM)* **1** (2/3/4), 343–359, Special Issue on Problems Exhibiting Boundary and Interior Layers.

Scheichl, B. & Kluwick, A. 2007*b* Turbulent Marginal Separation and the Turbulent Goldstein Problem. *AIAA J.* **45** (1), 20–36.

Scheichl, B. & Kluwick, A. 2008*a* Asymptotic theory of bluff-body separation: a novel shear-layer scaling deduced from an investigation of the unsteady motion. *J. Fluids Struct.* **24** (8), 1326–1338, Special Issue on the IUTAM Symposium on Separated Flows and their Control.

Scheichl, B. & Kluwick, A. 2008*b* Level of Turbulence Intensities Associated with Bluff-Body Separation for Large Values of the Reynolds number. *Meeting Paper* 2008-4348. AIAA.

Scheichl, B. & Kluwick, A. 2009 Evolution of a Boundary Layer from Laminar Stagnation-Point Flow Towards Turbulent Separation. In *Progress in Turbulence III. Proc. iTi Conference in Turbulence 2008* (ed. J. Peinke, M. Oberlack & A. Talamelli), *Springer Proceedings in Physics*, vol. 131, pp. 187–190. Berlin, Heidelberg: Springer.

Scheichl, B., Kluwick, A. & Alletto, M. 2008 "How turbulent" is the boundary layer separating from a bluff body for arbitrarily large Reynolds numbers? *Acta Mech.* **201** (1–4), 131–151, Special Issue dedicated to Professor Wilhelm Schneider on the occasion of his 70th birthday.

Schewe, G. 2001 Reynolds-number effects in flows around more-or-less bluff bodies. *J. Wind Eng. Ind. Aerod.* **89** (14), 1267–1289.

Schlichting, H. & Gersten, K. 2003 *Boundary-Layer Theory*, 8th edn. Berlin, Heidelberg, New York: Springer.

Schneider, W. 1991 Boundary-layer theory of free turbulent shear flows. *Z. Flugwiss. Weltraumforsch. (J. Flight Sci. Space Res.)* **15** (3), 143–158.

Smith, F. T. 1977 The laminar separation of an incompressible fluid streaming past a smooth surface. *Proc. R. Soc. Lond.* A **356** (1687), 443–463.

Smith, F. T. 1979 Laminar flow of an incompressible fluid past a bluff body: the separation, reattachment, eddy properties and drag. *J. Fluid Mech.* **92** (1), 171–205.

Smith, F. T. 1985 A structure for laminar flow past a bluff body at high Reynolds number. *J. Fluid Mech.* **155**, 175–191.

Smith, F. T. 1986 Concerning inviscid solutions for large-scale separated flows. *J. Eng. Math.* **20** (3), 271–292.

Stewartson, K. & Williams, P. G. 1973 On Self-Induced Separation II. *Mathematika* **20** (6), 90–108.

Sychev, V. V. 1972 Laminar Separation. *Fluid Dyn.* **7** (3), 407–417, original Russian article in *Izv. Akad. Nauk SSSR, Mekh. Zhidk. i Gaza* (3), 1972, 47–59.

Sychev, Vik. V. 1983 Asymptotic Theory of Turbulent Separation. *Fluid Dyn.* **18** (4), 532–538, original Russian article in *Izv. Akad. Nauk SSSR, Mekh. Zhidk. i Gaza* (4), 1983, 47–54.

Sychev, Vik. V. 1987 Theory of Self-Induced Separation of a Turbulent Boundary Layer. *Fluid Dyn.* **22** (3), 371–379, original Russian article in *Izv. Akad. Nauk SSSR, Mekh. Zhidk. i Gaza* (3), 1987, 51–60.

Sychev, Vik. V. 2010 On Asymptotic Theory of Separated Flows Past Bodies. *Fluid Dyn.* **45** (3), 441–457, original Russian article in *Izv. Ross. Akad. Nauk, Mekh. Zhidk. i Gaza* **45** (3), 2010, 110–128.

Sychev, V. V., Ruban, A. I., Sychev, Vic. V. & Korolev, G. L. 1998 *Asymptotic Theory of Separated Flows*. Cambridge: Cambridge University Press.

Sychev, V. V. & Sychev, Vik. V. 1980 On turbulent separation. *U.S.S.R. Comput. Math. Math. Phys.* **20**, 133–145.

Sykes, R. I. 1980 An asymptotic theory of incompressible turbulent boundary-layer flow over a small hump. *J. Fluid Mech.* **101** (3), 631–646.

Woods, L. C. 1955 Two-dimensional flow of a compressible fluid past given curved obstacles with infinite wakes. *Proc. R. Soc. Lond.* A **227** (1170), 367–386.

Wu, Th. Y. 1972 Cavity and Wake Flows. *Annu. Rev. Fluid Mech.* **4**, 242–284.

Zdravkovich, M. M. 1997 *Flow Around Circular Cylinders. A Comprehensive Guide Through Flow Phenomena, Experiments, Applications, Mathematical Models, and Computer Simulations. Vol. 1: Fundamentals*. Oxford, New York, Tokyo: Oxford University Press.

5 Break-away separation: summary and perspectives

Summary. A first rigorous description of gross separation is highlighted in brief, where an initially firmly attached boundary layer undergoes laminar–turbulent transition asymptotically close to the stagnation point on the surface of a plane bluff obstacle in uniform stream. We deal with nominally two-dimensional steady incompressible flow of constant density and and a smooth impermeable solid body surface. Recent theoretical results concerning the local structure of break-away separation are accompanied by a numerical study.

5.1 Preliminary remarks

Consider a parallel flow just disturbed by the presence of a bluff body and let Re, formed with the unperturbed free-stream velocity and a typical body dimension, take on arbitrarily large values: what is the actual position of flow separation? This question represents a long-standing but nevertheless central challenge in theoretical hydrodynamics. Matched asymptotic expansions prove the adequate means for a rigorous treatment of this problem. Here we present the essential results of this analysis by starting with the overall flow structure and leaving the technical details to Scheichl et al. (2008b) and Scheichl et al. (2010).

In contrast to the description of marginal, i.e. mild or internal, separation studied by Scheichl and Kluwick (2007a,b) here the global Reynolds number Re is found to represent the only parameter entering the description of the Reynolds-averaged flow. It shall be large enough to ensure that laminar–turbulent transition takes place in a correspondingly small region encompassing the stagnation point. Consequently, the concomitant asymptotic hierarchy starts with the external Helmholtz–Kirchhoff potential flow, which detaches at an initially unknown point, say $\mathcal{D}$, from the body, driving the turbulent boundary layer. It is found that the separation mechanism is inherently reminiscent of the transition process. Hence, the local analysis of separation not only fixes the actual scaling of the entire boundary layer but is also expected to eventually predict the position of $\mathcal{D}$ in a rational way.

5.2 Non-interactive global and boundary layer flow

In the following x, y, u denote natural coordinates along and normal to the body surface, with $x = y = 0$ indicating the stagnation point $\mathcal{S}$, and the velocity component in x-

direction, respectively.

Two findings are decisive. Firstly, laminar–turbulent transition near $\mathcal{S}$ generates a boundary layer that is basically characterised by (i) a main layer exhibiting an asymptotically small relative streamwise velocity deficit and (ii) the classical shear stress equilibrium in the viscous wall layer. Together with the required direct match of both flow regions items (i) and (ii) establish the picture of a classical turbulent boundary layer but with an a priori unknown scaling. This reflects the remarkable property that it never attains a fully developed turbulent state, even for arbitrarily large values of Re. Such an "underdeveloped" turbulent boundary layer contrasts with common reasoning but is reliable as viscous–inviscid flow interaction near separation requires the wall layer thickness to vary predominantly algebraically with the boundary layer thickness δ rather than exponentially as in the classical case. The asymptotic structure of the boundary layer in the latter case is sketched in Figure 5.1, together with the logarithmic law of the wall in the common notation (cf. Mellor, 1972; Schlichting and Gersten, 2003; Kluwick and Scheichl, 2009): κ, C^+, u_τ, and y^+ denote the von Kármán constant, the second empirical constant in the law of the wall, the skin friction velocity, and the wall layer coordinate, respectively. Here $u_\tau = Re^{-1/2}(\partial u/\partial y)^{1/2}$ evaluated at $y = 0$ and $y^+ = y u_\tau Re$.

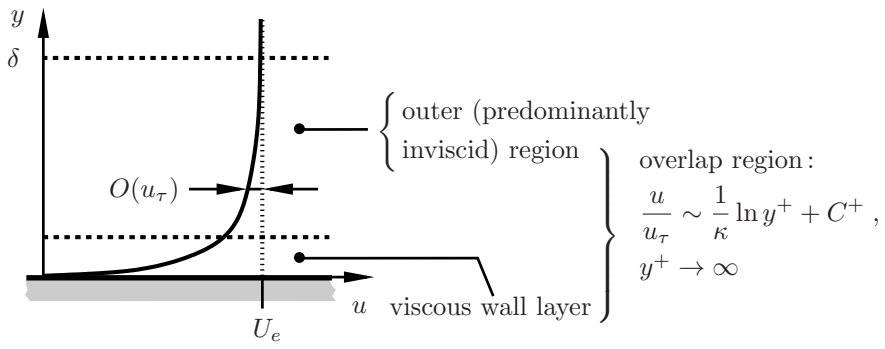

Figure 5.1: Structure of classical two-tiered boundary layer.

Secondly, it has become evident from the data provided by Roshko (1961) and numerous subsequent related experimental studies that for increasing values of Re the point of gross separation approaches a position a finite distance remote from its rear stagnation point observed in case of fully attached potential flow. This contradicts the conclusion drawn in the first theoretical investigation of this problem that accounts for the global flow structure by Neish and Smith (1992). A critical review by Scheichl and Kluwick (2008a) has finally promoted the aforementioned experimental observation as a starting point for further analysis. This in turn suggests that here in the formal limit $Re^{-1} = 0$ the free-stream flow past the body is to be sought in the class of Helmholtz–Kirchhoff flows, parametrised solely by the position of $\mathcal{D}$ where the well-known Brillouin–Villat (BV) singularity is encountered. Then the surface velocity imposed on the attached boundary layer given by U_e and the perturbation stream function F that accounts for the velocity defect satisfy the fundamental asymptotic

relationships

$$U_e(x;k) \sim 1 + 2k\sqrt{-s} + O(-s)\,, \qquad s = x - x_{\mathcal{D}}(k)\,, \qquad s \to 0_-\,, \tag{5.1}$$

$$1 - u/U_e(x;k) \sim \epsilon\,\partial_\eta F(x,\eta;k) + O(\epsilon^2)\,, \qquad \eta = y/\delta(x;Re)\,, \qquad \epsilon \to 0\,. \tag{5.2}$$

Here the positive control parameter k measures the strength of the BV singularity and in turn the position $x_{\mathcal{D}}$ of $\mathcal{D}$. Determining both the correct value of k and the dependencies of δ and the defect measure ϵ on Re represents one crucial goal of this research. Notable previous works (e.g. Melnik, 1989; Sychev, 1983, 1987, to cite the most relevant ones) unfortunately lacked the discussion of the global flow and thus led to different (large-defect) structures of the boundary layer, where the resulting inconsistencies precluded a uniformly valid flow description.

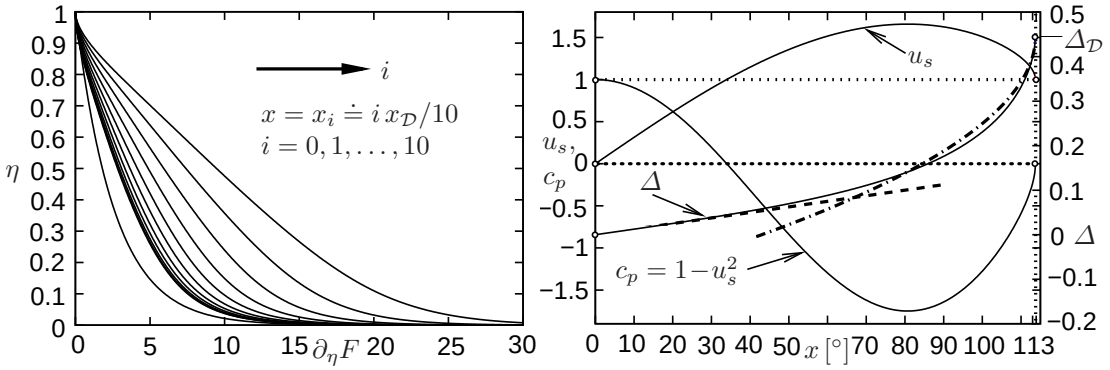

Figure 5.2: Defect function $\partial_\eta F$ and key quantities, including asymptotes of $\Delta(x;k)$ (*dashed*: linear rise in $x = 0$, *dashed-and-dotted*: square-root behaviour near $x = x_{\mathcal{D}}$).

The canonical situation of the flow around the circular unit cylinder (Re formed with the cylinder radius) is tackled numerically. We first approximate the potential flow by choosing $k = 0.45$ or, by exploitation of Levi–Cività's method, $x_{\mathcal{D}} \doteq 113.5°$. This seems reliable in view of the experimentally observed separation angles for the largest values of Re available so far ($Re \approx 10^6 - 10^7$) and the basic assumption concerning the asymptotic flow state. Integration of the leading-order small-defect equations subject to $U_e(x;k)$ and supplemented with an (asymptotically fully consistent) algebraic mixing-length closure based on that by Michel et al. (1969) starts at stagnation. It yields the results displayed in Figure 5.2: an initially favourable and then adverse pressure gradient acts on the boundary layer. In contrast to usual reasoning (cf. Schlichting and Gersten, 2003), it is not in "quasi-equilibrium" (a specific situation addressed by Kluwick and Scheichl, 2009) as the variation of F with x is fully present. The profiles of $\partial_\eta F$ at various x-stations exhibit the logarithmic near-wall behaviour and admit a wake-type shape near $x = x_{\mathcal{D}}$, well-recognised in other adverse-pressure-gradient turbulent boundary layers (but for strictly attached potential flow): see Melnik (1989), Neish and Smith (1992), and Kluwick and Scheichl (2009). Furthermore, let the $O(1)$-quantity $\Delta(x;k)$ denote the appropriately scaled boundary layer thickness. The

expansion $[F, \Delta] \sim [(1 - 4k\sqrt{-s})F_{\mathcal{D}}(\eta), (1 - 2k\sqrt{-s})\Delta_{\mathcal{D}}] + O(-s),\ s \to 0_-$, is derived from (5.1) and (5.2) and revealed by the numerical data by exploiting the values of the function $F_{\mathcal{D}}(\eta)$ and the constant $\Delta_{\mathcal{D}}$. However, due to the associated splitting of $\partial_\eta F$ in an infinite series of logarithmic velocity portions as $\eta \to 0$ a direct match of the small-defect and the wall layer is only accomplished by the introduction of a so-called intermediate layer immediately upstream of $\mathcal{D}$.

A Detached Eddy Simulation (DES) carried out by Paton (2010) underlies the snapshot of instantaneous circular-cylinder flow in Figure 5.3 (a). Here $Re = 10^6$ and an radius/width aspect ratio of $1 : 10$ ensures considerable suppression of three-dimensional effects in the time-averaged flow picture. This yields $x_{\mathcal{D}} \doteq 95°$, which is also promising.

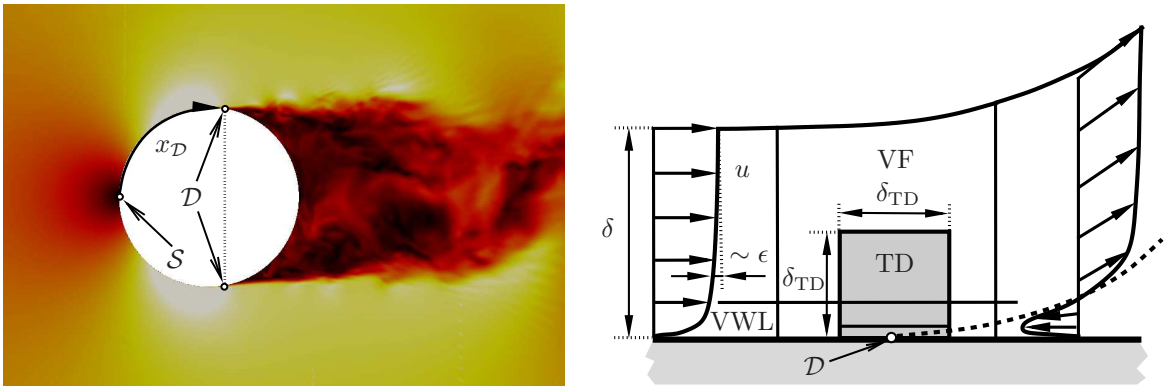

(a) (b)

Figure 5.3: (a) DES: colours distinguish isotachs; (b) sketch of separating flow: viscous wall layer (VWL), triple deck (TD, *shaded*), vortex-flow region (VF), separating streamline (*dashed*).

5.3 "Inner" and "outer" flow interaction

The separation process is vitally governed by the interplay of two locally strong interaction mechanisms, see Figure 5.3 (b): an "inner" (viscous–inviscid) one associated with a novel triple-deck structure, and an "outer" (rotational–irrotational) one expressed by a linear problem describing an inviscid vortex flow. The latter is subject to a solvability condition that arises from matching both interactive flow regimes. This is currently expected to finally fix the actual value of k for a given body shape.

In the classical description of the viscous wall layer the shear stress equilibrium is followed by the influence of the pressure and finally the inertia terms on the momentum equation in x-direction. The BV singularity triggers a rather complex multi-stage breakdown of this asymptotic hierarchy a short distance upstream of $\mathcal{D}$, initiated by the emergence of the intermediate layer mentioned above. This eventually leads to the formation of a so-called lower deck adjacent to the surface of streamwise extent δ_{TD},

say, where all those contributions except for the turbulent shear stress are in operation at leading order. Hence, separation takes place within a distance of $O(\delta_{\mathrm{TD}})$ from $\mathcal{D}$ as a self-consistent flow description in terms of viscous–inviscid interaction aims at avoiding the occurrence of both the well-known Goldstein and the BV singularity. This mechanism intrinsically renders the wall layer locally a passive main deck: it transfers the flow displacement exerted by the lower deck to an upper deck formed on its top (together with a passive buffer layer). Here the induced potential flow accounts for the pressure feedback in the lower deck. Herewith the interaction loop is closed and the triple-deck structure mentioned above completed. As a result, the BV singularity is resolved in a manner formally identical to that found in the asymptotic theory of laminar break-away separation (see Sychev, 1972; Smith, 1977).

This situation is virtually unaffected by the outer small-defect portion of the boundary layer. On the other hand, expansion (5.2), applicable to the oncoming boundary layer sufficiently far upstream of $\mathcal{D}$, subject to (5.1) ceases to be valid in the square region of outer interaction where both s and y are of $O(\delta)$ and which encloses the triple deck. Finally, the triple-deck structure requires that $\delta_{\mathrm{TD}}/\delta = O(\epsilon)$, with $\epsilon \propto 1/\ln Re$ (which agrees with the classical boundary layer scaling) and $\delta_{\mathrm{TD}} = Re^{-4/9}$ (which specifies the notion of underdeveloped flow).

5.4 Conclusions and outlook

A self-consistent asymptotic theory describing gross separation associated with flows past (more-or-less) blunt bodies or, to put it more precisely, flows which start at a stagnation point rather than a sharp leading edge, has been developed. Most importantly, a recent careful numerical investigation of the time-mean flow for the canonical case of a circular cylinder, presented, among others, by Scheichl et al. (2008b), Scheichl and Kluwick (2008c), undoubtedly indicates that the boundary layer approaching separation exhibits a small rather than a large velocity defect. However, the accompanying asymptotic analysis based on the turbulence intensity gauge model introduced by Neish and Smith (1992), however, strongly suggests that a boundary layer forming on a body of finite extent and originating in a front stagnation point does not reach a fully developed turbulent state, even in the limit $Re \to \infty$. Specifically, it is found that the boundary layer thickness δ and the Reynolds shear stress are slightly smaller than predicted by classical small-defect theory, while, most important, the thickness of the wall layer is slightly larger. In fact, δ varies predominantly algebraically with Re, whereas the velocity defect measure ϵ in the outer region is still of $O(1/\ln Re)$, which is decisive for the classical flow description. As a consequence, the outer large-momentum region does not penetrate to distances from the wall which are transcendentally small. In turn, this situation opens the possibility to formulate a local interaction mechanism that describes the detachment of the boundary layer from the solid wall within the framework of free-streamline theory at pressure levels which are compatible with experimental observation. This is a topic of intense current investigations; for the preliminary state of research see Scheichl et al. (2009, 2010). Activities of the planned research include the aforementioned determi-

nation of the singularity parameter k and the description of the associated body- and large-scale separated flow.

Bibliography

A. Kluwick and B. Scheichl. High-Reynolds-Number Asymptotics of Turbulent Boundary Layers: From Fully Attached to Marginally Separated Flows. Invited Paper. In A. F. Hegarty, N. Kopteva, E. O'Riordan, and M. Stynes, editors, *BAIL 2008 – Boundary and Interior Layers. Proceedings of the International Conference on Boundary and Interior Layers – Computational and Asymptotic Methods, Limerick, July 2008*, volume 69 of Lecture Notes in Computational Science and Engineering, pages 3–22. Springer-Verlag, Berlin, Heidelberg, 2009.

G. L. Mellor. The Large Reynolds Number, Asymptotic Theory of Turbulent Boundary Layers. *Int. J. Engng Sci.*, 10(10):851–873, 1972.

R. E. Melnik. An Asymptotic Theory of Turbulent Separation. *Computers & Fluids*, 17(1):165–184, 1989.

R. Michel, C. Quémard, and R. Durant. Hypothesis on the mixing length and application to the calculation of the turbulent boundary layers. In S. J. Kline, M. V. Morkovin, G. Sovran, and D. J. Cockrell, editors, *Proceedings of Computation of Turbulent Boundary Layers – 1968 AFOSR-IFP-Stanford Conference*, volume 1, pages 195–207. Stanford University, CA, 1969.

A. Neish and F. T. Smith. On turbulent separation in the flow past a bluff body. *J. Fluid Mech.*, 241:443–467, August 1992.

J. Paton. Private communication, 2010.

A. Roshko. Experiments on the flow past a circular cylinder at very high Reynolds number. *J. Fluid Mech.*, 10(3):345–356, 1961.

B. Scheichl and A. Kluwick. Turbulent Marginal Separation and the Turbulent Goldstein Problem. *AIAA J.*, 45(1):20–36, 2007a. See also *AIAA Meeting paper 2005-4936*.

B. Scheichl and A. Kluwick. On turbulent marginal boundary layer separation: how the half-power law supersedes the logarithmic law of the wall. *Int. J. Computing Science and Mathematics (IJCSM)*, 1(2/3/4):343–359, 2007b. Special Issue on Problems Exhibiting Boundary and Interior Layers.

B. Scheichl and A. Kluwick. Asymptotic theory of bluff-body separation: a novel shear-layer scaling deduced from an investigation of the unsteady motion. *J. Fluids Struct.*, 24(8):1326–1338, December 2008. Special Issue on the IUTAM Symposium on Separated Flows and their Control.

B. Scheichl, A. Kluwick, and M. Alletto. "How turbulent" is the boundary layer separating from a bluff body for arbitrarily large Reynolds numbers? *Acta Mech.*, 201(1–4):131–151, 2008b. Special Issue dedicated to Professor Wilhelm Schneider on the occasion of his 70th birthday.

B. Scheichl and A. Kluwick. Level of Turbulence Intensities Associated with Bluff-Body Separation for Large Values of the Reynolds number. Meeting paper 2008-4348, AIAA, 2008c.

B. Scheichl, A. Kluwick, and F. T. Smith. Time-mean description of turbulent bluff-body separation in the high-Reynolds-number limit. In B. Eckhardt, editor, *Advances in Turbulence XII. Proceedings of the 12th EUROMECH European Turbulence Conference, September 7-10, 2009, Marburg, Germany*, volume 132 of Springer Proceedings in Physics, pages 577–580. Springer-Verlag, Berlin, Heidelberg, New York, 2009.

B. Scheichl, A. Kluwick, and F. T. Smith. Break-away separation for high turbulence intensity and large Reynolds number. *J. Fluid Mech.*, in press, 2010.

H. Schlichting and K. Gersten. *Boundary-Layer Theory.* Springer-Verlag, Berlin, Heidelberg, New York, 8th edition, 2003.

F. T. Smith. The laminar separation of an incompressible fluid streaming past a smooth surface. *Proc. R. Soc. Lond.* A, 356(1687):443–463, 1977.

V. V. Sychev. Laminar Separation. *Fluid Dyn.*, 7(3): 407–417, 1972. Original Russian article in *Izvestiya Akademii Nauk SSSR, Mekhanika Zhidkosti i Gaza* (3), 47–59, 1972.

Vik. V. Sychev. Asymptotic Theory of Turbulent Separation. *Fluid Dyn.*, 18(4):532–538, 1983. Original Russian article in *Izvestiya Akademii Nauk SSSR, Mekhanika Zhidkosti i Gaza* (4), 47–54, 1983.

Vik. V. Sychev. Theory of Self-Induced Separation of a Turbulent Boundary Layer. *Fluid Dyn.*, 22(3):371–379, 1987. Original Russian article in *Izvestiya Akademii Nauk SSSR, Mekhanika Zhidkosti i Gaza* (3), 51–60, 1987.

6 About the candidate

The information about the candidate taken from the webpage

`http://www.fluid.tuwien.ac.at/BernhardScheichl`

hosted by the Institute of Fluid Mechanics and Heat Transfer at the Vienna University of Technology is displayed at the next page. Both this webpage and the **list of publications** linked at its bottom are updated regularly.

Dipl.-Ing. Dr.techn. Bernhard Scheichl

Resselgasse 3/1/3
A-1040 Vienna, Austria

Tel., Fax, e-mail

Curriculum vitae

15/04/1969	born in Mödling, Austria permanent residence: Mödling, Austria
	Education
1975-1979	Elementary school in Mödling
1979-1987	Grammar school, BGuBRG Mödling
1987-1995	Studies of Mechanical Engineering (specialization in Chemical Engineering), TU Vienna, Austria
10/1995	Master's Degree (Dipl.-Ing.), thesis: *Nonlinear stability analysis of wave propagation phenomena in suspensions* (in German), supervisor: Prof. A. Kluwick
1995-1996	Civilian service, municipality of Mödling
1997-2001	Post-graduate (PhD) studies as research assistant at the Institute of Fluid Mechnics and Heat Transfer (IFMHT), TU Vienna, Austria
6/2001	Doctoral Degree (Dr. techn.), thesis: *Asymptotic theory of marginal turbulent separation*, supervisors: Prof. A. Kluwick, Prof. H. Sockel
	Post-graduate employments in industry
1996	Process and commissioning engineer at Hoerbiger Ventilwerke AG , Vienna
2-3/1997	Real Time Computersoftware GmbH, Vienna
8/2001-10/2002	Process engineer (biotechnology) at Vogelbusch AG, Vienna
	Post-doctoral research positions
11/2002-7/2003	*Kplus* project: *Simulation of Spinning-Process Technologies* granted by the Austrian Research Promotion Agency (FFG), project leader: Prof. A. Kluwick, at IFMHT, joint with *Kplus* Competence Center Carinthian Tech Research (CTR) and SEZ AG (now Lam Research AG), both Villach, Austria
8/2003-8/2007	Austrian Science Fund (FWF) project # P16555-N12: *Interaction theory of turbulent marginal separation*, project leader: Prof. A. Kluwick, at IFMHT
9/2007-	Research fellow at IFMHT, including teaching and industry-related activities

10/2008-	Key Scientist for *Modelling and Simulation* at AC²T research GmbH and Leader of Area *Multi-scale Modelling* at the *Excellence Center of Tribology* granted by the COMET program of the Austrian Research Promotion Agency (FFG), Wiener Neustadt, Austria
10/2010	Habilitation (Fluid Mechanics) submitted at TU Vienna

Teaching

Exercises in Fundamentals of fluid mechanics / Fluid Mechanics (IFMHT, 1998-2001, 2006), Mass transfer (IFMHT, 2006), Basics of fluid mechanics (OMV Well Academy, 2008), co-supervision of Master and PhD theses (IFMHT)

Research interests

- High-Reynolds-number flows (boundary layer theory)
- Wall-bounded and separated turbulent shear layers
- Flow on a rotating disc (hydraulic jump)
- Lubricant flow (cavitation, film rupture, inertia effects, mixed/boundary lubrication)
- Applied mathematics (singular perturbation methods)
- Numerical mathematics

Reviewing

for *AIAA Journal*, *Journal of Engineering Mathematics*, *Tribology International* and others

Publications

For a list of recent publications visit the publication database of the university.

Asymptotische Theorie wandgebundener und abgelöster turbulenter Scherströmungen

Addendum zur Habilitationsschrift

eingereicht an der

Technischen Universität Wien,
Fakultät für Maschinenwesen und Betriebswissenschaften,

zur Erlangung der Lehrbefugnis (Venia Legendi) im Fachgebiet

Strömungsmechanik

Dipl.-Ing. Dr.techn. Bernhard Scheichl

Wien, 29. November 2010

Asymptotic theory of wall-bounded and separated turbulent shear flows

Supplement to the Habilitation thesis

submitted at the

Vienna University of Technology,
Faculty of Mechanical and Industrial Engineering,

to achieve the Venia Legendi in

Fluid mechanics

Dipl.-Ing. Dr.techn. Bernhard Scheichl

Vienna, 29 November 2010

Contents

1 Preface

This supplement to the principal part of the Habilitation thesis contains additional material that shall demonstrate the diversity of the candidate's knowledge in fluid mechanics and heat transfer. The specific scientific approach adopted in the contributions presented here comprises perturbation and corresponding numerical techniques and thus serves as the methodical link to the main topic of the thesis.

The supplement consists of three selected peer-reviewed conference papers and two technical reports. The reports were accomplished in the course of two industrial projects carried out at the Institute of Fluid Mechanics and Heat Transfer, Vienna University of Technology. The individual contributions are enumerated as follows:

[1] B. Scheichl, A. Kluwick: *Annular spread of a thin liquid film over a rotating disk*, in: "Compilation of Abstracts for the Second M.I.T. Conference on Computational Fluid and Solid Mechanics, June 17–20, 2003", K. J. Bathe (ed.), Massachusetts Institute of Technology, Cambridge, MA, USA (2003), p. 187;

[2] V. G. Marian, B. Scheichl, N. Tungkunagorn, G. Vorlaufer, F. Franek: *Evaluation of Mass Conservative Models for the Tribological Analysis of Porous Bearings*, in: "11th International Conference on Tribology – SERBIATRIB '09. PROCEEDINGS", Serbian Tribology Society and Faculty of Mechanical Engineering, Belgrade (2009), ISBN: 978-86-7083-659-4, pp. 220–223;

[3] A. Neacşu, B. Scheichl, S. Eder, G. Vorlaufer: *Cavitation in Porous Journal Bearings Lubricated with Ionic Liquids*, short abstract, accepted for oral presentation/extended abstract/full paper at the "3rd European Conference on Tribology (ECOTRIB 2011)", Vienna, Austria, June 7–9, 2011;

[4] B. Scheichl: *On the Turbulent/Inertial Range in Fully Hydrodynamic Lubrication*, short abstract, accepted for oral presentation/extended abstract/full paper at the "3rd European Conference on Tribology (ECOTRIB 2011)", Vienna, Austria, June 7–9, 2011;

[5] B. Scheichl, A. Kluwick: *Local heat conduction in the sheet membrane of the* iSi *Helium inflator due to the impingement of the combustion gas jetting from the ignition chamber*, Research report (2007);

[6] B. Scheichl: *Feasibility study of a novel hydrodynamically lubricated thrust bearing device operated with water or saturated water vapour*, Technical report (2009).

Paper [1] refers to the preliminary investigation of thin liquid layers on rotating discs. Papers [2]–[4] reflects the recent efforts in the rigorous prediction of lubricant flow including effects as cavitation and the occurrence of turbulence, carried out in the course of the in the course of the candidate's current scientific engagement at the Competence Center for Tribology, located at the Austrian Center of Competence for Tribology in Wiener Neustadt and funded within the *COMET K2* program of the Austrian Research Promotion Agency (FFG). Both the topics dealt with by paper [1] and papers [2]–[4], respectively, are highly relevant not only from the viewpoint of basic research but also for engineering applications. The papers [5] and [6] represent the technical reports.

PLEASE NOTE: The technical reports and the included information have to be considered as strictly confidential by the reader, according to the non-disclosure agreement between the company partners involved and the university.

2 Selected contributions

The contributions are enclosed subsequently in the order of the list given in chapter 1.
Each contribution represents a section of this chapter.

Annular spread of a thin liquid film over a rotating disk

Bernhard Scheichl & Alfred Kluwick
Institute of Fluid Dynamics and Heat Transfer, Vienna University of Technology,
Resselgasse 3/1/3, A-1040 Vienna, Austria
bernhard.scheichl@tuwien.ac.at

Liquid jet impingement on a spinning disk is of vital importance in many engineering applications. Specifically, in semiconductor industries it is adopted for machining and cleaning the surface of silicium wafers. However, although the associated flow physics has been appreciated by many researchers in the special case of a stationary surface (for an overlook see e.g. [1]), radially spreading thin-film flow adjacent to a rotating disk has only been examined numerically for nozzle-like inlet conditions ([2]). In this contribution a thorough analytical/numerical investigation of the flow field generated by an impinging jet is presented, strictly based on first principles.

We consider a non-rotating circular jet carrying a volume flux $\tilde{Q}$ of a liquid with kinematic viscosity $\tilde{\nu}$. It shall impinge perpendicularly with cross-section-averaged velocity $\tilde{U}$ on the center of a disk which rotates with constant angular velocity $\tilde{\Omega}$ in a horizontal plane. The jet flow is assumed to be essentially inviscid. Thus, a boundary layer and, sufficiently far from the center, a thin viscous film forms above the disk. Employing asymptotic methods, the different flow regimes reflecting varying effects of viscous shear and centrifugal body force are elucidated. As a consequence of jet-forcing, the influence of gravity on the flow is seen to be negligibly small, which, most important for numerical reasons, in turn allows for a parabolic shallow-water approximation of the non-dimensionalized equations of motion.

As one crucial result of the analysis, the spread of the film appears to be primarily characterized solely by the Rossby number *Ro* of the problem if an appropriately defined reference radius $\tilde{R}$ is introduced, that is

$$Ro = \tilde{U}/(\tilde{\Omega}\tilde{R})\,, \quad \tilde{R} = \tilde{Q}^{2/3}/(4\pi^2\,\tilde{U}\tilde{\nu})^{1/3}\,.$$

Numerical solutions of the shallow-water equations have been obtained for a wide range of values of *Ro*. To this end, the inviscid inlet conditions were chosen to represent the practically important case of a parabolic velocity profile in the oncoming jet. Interestingly, if *Ro* exceeds a certain threshold, the radial distribution of the film thickness exhibits a maximum at a distinct radius while it tends to zero for large radii.

In addition, emphasis is put on the cases $Ro \to \infty$ and $Ro \to 0$. The latter one appears to be associated with a breakdown of the asymptotic structure of the flow, requiring a separate treatment. The corresponding limits of application of the theory presented are discussed.

References

[1] LIENHARD V, J. H. 1995 Liquid Jet Impingement. In *Ann. Rev. Heat Transfer* (ed. C.-L. Tien), Vol. VI, pp. 199–270. Begell House.

[2] RAHMAN, M. M. & FAGHRI, A. 1992 Numerical simulation of fluid flow and heat transfer in a liquid film over a rotating disk. *Int. J. Heat Mass Transfer* **35**, 1441–1453.

Serbian Tribology Society

SERBIATRIB '09

11th International Conference on Tribology

University of Belgrade Mechanical Engineering Faculty

Belgrade, Serbia, 13 - 15 May 2009

EVALUATION OF MASS-CONSERVATIVE MODELS FOR THE TRIBOLOGICAL ANALYSIS OF POROUS BEARINGS

Victor G. Marian [1,2], Bernhard Scheichl [1,3], Natchana Tungkunagorn [1], Georg Vorlaufer[1], Friedrich Franek[1,4]

[1] Austrian Center of Competence for Tribology, Wiener Neustadt, Austria, marian@ac2t.at
[2] University Politehnica of Bucharest, Chair of Machine Elements and Tribology, Romania
[3] Vienna University of Technology, Institute of Fluid Mechanics and Heat Transfer, Austria
[4] Vienna University of Technology, Institute of Sensor and Actuator Systems, Austria

Abstract: *Two theoretical mass-conservative models for the tribological evaluation of porous journal bearings are investigated rigorously. The first model supposes that the lubricating fluid film is fully contiguous in the range between two angles, i.e. effects due to cavitation are excluded. The fluid pressure distribution is determined numerically by solving a modified Reynolds equation which governs the fluid film and accounts for the porous surface and the well-known Darcy's law that describes the flow through the porous matrix in the usual manner. These equations are supplemented with the integral angular momentum equation applied to the fluid film and the integral mass balance between the flow rates of the lubricant entering into and leaking from the clearance, respectively. Considering the second theoretical model, we again solve the Laplace equation governing the pressure distribution due to Darcy's law that holds in the porous bearing seat, but adopt a modification of the Elrod's model in order to study the flow in the clearance.*

Keywords: *hydrodynamic lubrication, journal porous bearings, cavitation, angular momentum equation, Elrod's model*

1. NOTATIONS

c – bearing clearance
D – shaft diameter
D_b – bearing outer diameter
$\overline{F}$ – load parameter, $\overline{F} = \dfrac{Fc^2}{\eta U r_i^2 L}$
g – switch (unit step) function
h – film thickness
L – bearing seat width
$M_{\theta 1}$ – circumferential momentum flow rate across oil-film surface at inlet end of oil region ($\theta = \theta_1$)
$M_{\theta 2}$ – circumferential momentum flow rate across oil-film surface at trailing end of oil region ($\theta = \theta_2$)
$M_{\theta c}$ – circumferential momentum flow rate across oil-film surface at both axial ends
p – fluid pressure
p_c – cavitation pressure
q_{in} – flow from porous matrix in the fluid film
q_c – axial leakage flow from both ends through the clearance gap
r – radial coordinate
r_i – internal radius of bearing seat
z – axial coordinate
$\overline{h}$ – dimensionless film thickness, h/c
$\overline{p}$ – dimensionless pressure, $\overline{p} = \dfrac{c^2 p}{r_i^2 \eta \omega}$
$\overline{r}$ – dimensionless radial coordinate, r/r_i
$\overline{z}$ – dimensionless axial coordinate, $z/(L/2))$
ε – bearing eccentricity
η – oil viscosity
ϕ – material permeability
θ – angular coordinate
σ – oil film volume fraction

2. INTRODUCTION

Self lubricated porous journal bearings are used in a lot of applications due to several advantages: they are cheaper than rolling bearings and produce less noise. Therefore they can be used in a lot of applications, like household appliances, all sorts of fans, and tool kits. Numerous articles in the literature present experimental tests in order to evaluate the cavitation zone in the fluid film [1] or the film thickness and friction torque of these bearings [2]. Theoretical models are also presented based on different assumptions:

- the lubricating fluid film is fully contiguous in the range between two angles and the integral angular momentum equation is applied to the fluid film [3];
- the cavitation model of Elrod is applied in the clearance region [4], [5], [6].

Recently the flexibility of porous liner was introduced in the numerical computations [7], [8].

Due to the fact that the model proposed by Kaneko [3] was not compared to any experimental data, a more rigorously analysis of the above models is needed.

In the present paper the results obtained by means of the numerical exploitation of two mass-conservative models [3], [5] are compared with experimental data [2] in order to establish which of the two models in more appropriate for the modelling of the tribological performance of self lubricated porous bearings and more suited for further developments.

3. GOVERNING EQUATIONS

2.1 Kaneko's model

The first model supposes that the lubricating fluid film is fully contiguous in the range $\theta_1 < \theta < \theta_2$ (Figure 1), i.e. effects due to cavitation are excluded [3]. The fluid pressure distribution is determined numerically by solving a modified Reynolds equation which governs the fluid film and accounts for the porous surface and Darcy's law that describes the flow through the porous matrix in the usual manner.

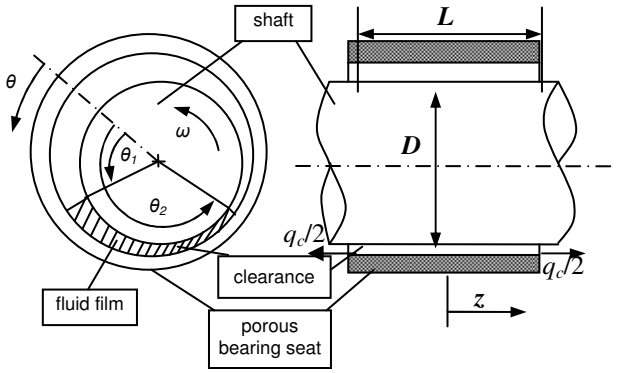

Figure 1. Schematic of the bearing

Modified Reynolds equation in the fluid film

The Reynolds equation in the fluid film was modified in order to account for the permeability of the bearing housing:

$$\frac{\partial}{\partial\theta}\left(\bar{h}^3\frac{\partial\bar{p}}{\partial\theta}\right)+\left(\frac{D}{L}\right)^2\frac{\partial}{\partial\bar{z}}\left(\bar{h}^3\frac{\partial\bar{p}}{\partial\bar{z}}\right)=\frac{\partial\bar{h}}{\partial\theta}-12\phi\left.\frac{\partial\bar{p}}{\partial\bar{r}}\right|_{\bar{r}=1} \quad \textbf{(1)}$$

Equation in porous media

The equation describing the lubricant flow in the porous media is the Darcy's equation which in terms of pressure is the Laplace equation:

$$\frac{1}{\bar{r}}\frac{\partial}{\partial\bar{r}}\left(\bar{r}\frac{\partial\bar{p}_p}{\partial\bar{r}}\right)+\frac{1}{\bar{r}^2}\frac{\partial^2\bar{p}_p}{\partial\theta^2}+\left(\frac{D}{L}\right)^2\frac{\partial^2\bar{p}_p}{\partial\bar{z}^2}=0 \quad \textbf{(2)}$$

Continuity of flow

The flow that enters in the film from the porous matrix is equal to the axial leakage flow through the clearance gap.

$$q_{in}=q_c \quad \textbf{(3)}$$

Momentum equation

Applying the momentum of momentum equation yields (the torque radius being constant and the control volume is the fluid film):

$$M_{\theta 1}-M_{\theta 2}-M_{\theta c}=0 \quad \textbf{(4)}$$

where:

$$M_{\theta 1} = 2\int_0^{L/2}\int_0^{h_{\theta 1}} \rho(u_{\theta|\theta=\theta 1})^2 dydz \quad (5)$$

$$M_{\theta 2} = 2\int_0^{L/2}\int_0^{h_{\theta 2}} \rho(u_{\theta|\theta=\theta 2})^2 dydz \quad (6)$$

$$M_{\theta c} = 2r_i\int_{\theta 1}^{\theta 2}\int_0^{h} \rho\,(u_\theta \cdot u_z)\big|_{z=L/2} dyd\theta \quad (7)$$

2.2 Model by Giudicelli and Elrod

Model describing the fluid film

The Elrod's model was employed in order to solve the Reynolds equation in the fluid film. In the zone with negative pressures, a homogeneous mixture of oil, oil vapour and air is built.

The universal differential equation in the fluid film contains the oil fraction σ as variable. The relation between p and σ is:

$$p = p_c + g\beta(\sigma - 1) \quad (8)$$

where:
$g = 1$ and $\sigma > 1$ when $p > p_c$
$g = 0$ and $\sigma \le 1$ when $p = p_c$

Then the modified Reynolds equation is:

$$g\nabla_{\theta,z}\cdot(h^3 + 6Kh)\nabla_{\theta,z}p = 6\eta\omega\left[g\frac{dh}{d\theta} + (1-g)\frac{\partial(\sigma h)}{\partial\theta}\right] - 12K\frac{\partial\overline{p}}{\partial r}(r_i,\theta,z) \quad (9)$$

Equation in porous media

The equation in the porous media is again the Darcy's equation as in the previous model.

The coupling between the two equations above was realized by considering the continuity of mass flow through the interface between the fluid film and the porous media.

4. METHOD OF SOLUTION

The system of differential equations was solved by using the finite-difference method, where second-order accuracy was achieved. The resulting system of algebraic equations was solved iteratively by adopting the Gauss-Seidel method.

5. RESULTS

The pressure distribution was computed using the two models presented above for the following input parameters: ε = 0.7, D = 19mm, L = 33mm, c = 32μm, D_b = 25mm, ϕ = 15 x 10^{-14}m^2, η = 0.035 Pa s, n = 870 r.p.m., p_c = -0.1bar.

The pressure distribution using the model proposed by Kaneko is presented in Figure 2.

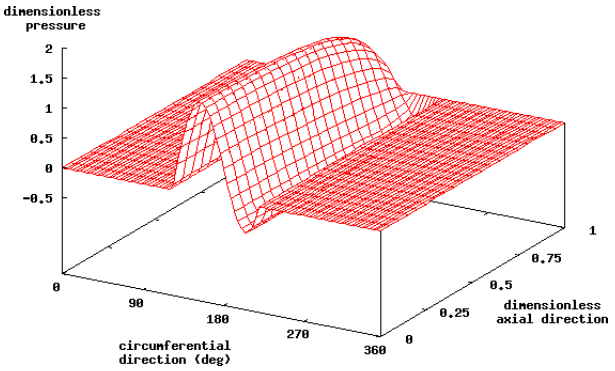

Figure 2. Pressure distribution in the fluid film – Kaneko's model

One clearly observes a small region in the divergent zone where negative pressures occur.

The pressure distribution obtained by using the Elrod's model is presented in Figure 3.

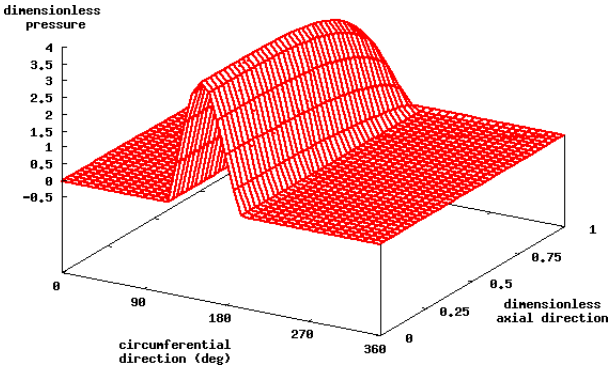

Figure 3. Pressure distribution in the fluid film – Elrod's model

It can be seen that the maximal pressure is double in the case of the Elrod's model. This could be due to the fact that the Kaneko's model allows negative pressures in the computation procedure.

The variation of the eccentricity as a function of the load parameter is presented in Figure 4, where the two theoretical models are compared with the experimental data. All the experimental data are clearly provided and discussed vividly in the literature cited, except for the values of temperatures and, consequently, the viscosities in the fluid film. Hence, rather rough estimates for the latter had to be made.

In passing we note that in case of the Kaneko's model, numerical difficulties were encountered due to the relatively high values of the eccentricities obtained.

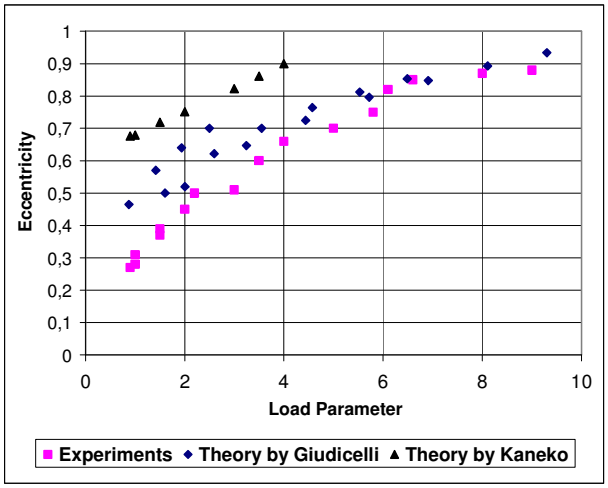

Figure 4. Eccentricity of the shaft versus load parameter

Using the Kaneko's model higher eccentricities are obtained compared to the experimental data. In case of the Elrod's model the obtained eccentricities are slightly higher, but the results better approximate the experimental data.

The variation of the friction coefficient as a function of load parameter is presented in Figure 5.

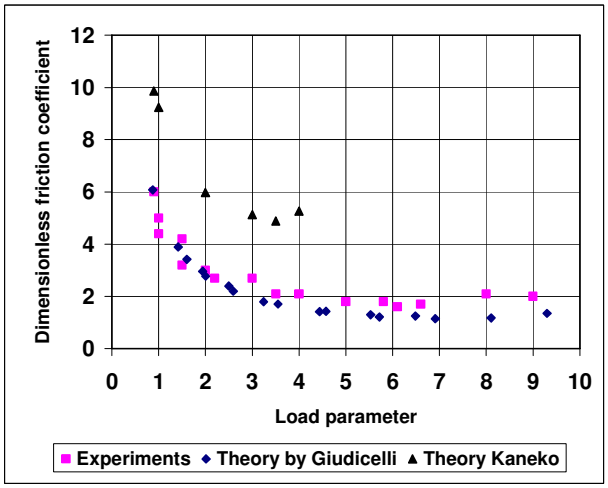

Figure 5. Friction behaviour versus load parameter

We can remark that the friction coefficients obtained by employing the Kaneko's model are much higher than the corresponding experimental data. In the case of the Elrod's model the friction coefficients are slightly higher but the results are qualitatively quite similar.

6. CONCLUSION

Two theoretical models concerning the evaluation of frictional properties of unsupplied porous bearings have been evaluated in this paper.

It is found that the results based on the cavitation algorithm proposed by Giudicelli and Elrod agree considerably better with the experimental findings.

ACKNOWLEDGMENTS

The authors want to thankfully acknowledge the support of the European Commission through the project MRTN-CT-2006-035589 WEMESURF. Partial support of this work was provided by the Austrian K*plus* funding program for centers of competence.

REFERENCES

[1] A. L. Braun, *Porous Bearings*, Tribology International, Vol. 15, No.5, pp. 235-242, 1982

[2] M. O. A. Mokhtar, M. Rafaat and G.S.A. Shawki, 1984, *Experimental Investigations Into the Performance of Porous Journal Bearings*, S.A.E. Paper No. 840097, 1984

[3] S. Kaneko, H. Takabatake, K. Ito, *Numerical Analysis of Static Characteristics at Start of Operation in Porous Journal Bearings with Sealed Ends*, Journal of Tribology, Vol. 121, pp.62-68, 1999

[4] Elrod, H.G., *A cavitation alghoritm*, ASME Journal of Lubrication Technology, Vol. 103, No.2, pp.350-354, 1981

[5] Giudicelli, B., *Modeles hydrodynamiques conservatifs pour des paliers autolubrifiants poreux en regime permanent*, These de Doctorat, Institut National des Sciences Appliquees de Lyon, France, 1993

[6] M. Meurisse, B. Giudicelli, *A 3D Conservative Model for Self-Lubricated Porous Journal Bearings in a Hydrodynamic Steady State*, Journal of Tribology, Vol. 121, pp. 529-537, 1999

[7] A. A. Elsharkawy, L. H. Guedouar, *Hydrodynamic lubrication of porous journal bearings using a modified Brinkman-extended Darcy model*, Tribology International, Vol. 34, pp.767-777, 2001

[8] A. Marinkovic, F. Franek, A. Pauschitz, *Simulation and optimum design of porous journal metal bearing under elastohydrohynamic lubrication*, World Tribology Conference, Washington, 2005

CAVITATION IN POROUS JOURNAL BEARINGS LUBRICATED WITH IONIC LIQUIDS

Adina Neacşu[1], Bernhard Scheichl[1,2], Stefan Eder[1], Georg Vorlaufer[1]

Keywords: *cavitation, hydrodynamic lubrication, ionic liquids, porous journal bearings, Reynolds equation.*

1 PRELIMINARIES

Ionic liquids are organic salts with very low vapour pressures. This property renders them potential candidates for lubricants. Specifically, our concern here is with the phenomena of film cavitation in porous journal bearings lubricated with ionic liquids. The associated rather steep pressure gradients near the bearing edges require specific attention in the computational schemes.

2 APPROACH

Regarding the theoretical considerations, we solve the well-known Reynolds equation by adopting an improvement of the original Elrod's model [1] and its application [2] to the flow situation considered here: the pressure-density relationship is kept, but the solution is obtained by using a simulated-annealing strategy in order to account for the nonlinearity introduced by the expected occurrence of cavitation regions. This not only proves advantageous from a numerical point of view but also captures the fact that the fluid density varies inside the cavitation region but is constant in the fully contiguous liquid regime. Furthermore, the solution of the Reynolds equation is coupled in terms of pressure with the widely-used Darcy's law, which describes the flow through the porous seat of the bearing with satisfactory accuracy. The numerical results aim at a most reliable prediction of the pressure and density distributions of the coupled problem, where a major goal is to determine the boundaries of applicability of classical cavitation theory, i.e. to extend the flow description towards the mixed-lubrication regime. In this sense we vary several parameters, in first instance the eccentricity ε and the permeability Φ. Two particular situations are considered in detail: (i) the onset of cavitation, i.e. the first appearance of a small cavitation region, and (ii) the limit $\varepsilon \rightarrow 1$, associated with a locally large pressure rise and finally the need to properly include effects of surface roughness in the flow description.

Also, spatial variations of Φ can be included conveniently in the numerical scheme. An improved description of the surface porosity by means of homogenisation techniques is currently under way, which we expect to provide a more rationally founded expression for Φ. First results are presented.

3 REFERENCES

[1] Elrod, H. G.: A cavitation algorithm. ASME Journal of lubrication technology (1981), 103, 350-354.

[2] Giudicelli, B.: A 3D conservative model for self-lubricated porous journal bearings in a hydrodynamic state. ASME Journal of lubrication technology (1999), 121, 529-537.

[1] *Austrian Center of Competence in Tribology, Austria, neacsu@ac2t.at*

[2] *Institute of Fluid Mechanics and Heat Transfer, Vienna Technical University, Austria, b.scheichl@tuwien.ac.at*

ON THE INERTIAL/TURBULENT RANGE IN FULLY HYDRODYNAMIC LUBRICATION

Bernhard Scheichl[1, 2]

Keywords: *high-speed lubrication, internal flows, matched asymptotic expansions, wall-bounded turbulence.*

1 PRELIMINARIES

The classical long-standing theory of lubrication in the fully hydrodynamic regime is essentially traced back on the assumptions of (i) a relatively slender gap between the counter-sliding rigid surfaces, (ii) a Newtonian lubricant, (iii) the neglect of inertia terms in the Navier-Stokes equations, and (iv) strictly laminar flow. Issues (i)-(iv) prove sufficient for a rigorous derivation of the well-known Reynolds equation (in the most general form) governing the pressure distribution in the gap. In engineering applications as e.g. thrust bearings for oil- or steam-lubricated high-speed rotors, however, the Reynolds number *Re* formed with a typical gap height may take on rather large values, thus rendering prerequisite (iii) questionable. It is pointed out on the basis of quantitative results relevant for the global stability bounds of internal flows that relaxing assumption (iii) also involves a critical review of supposition (iv), which finally suggests the inclusion of turbulence. Here we restrict the investigation to incompressible fully developed turbulent flow between smooth surfaces.

2 RATIONAL EXTENSION OF THE CLASSICAL FLOW DESCRIPTION

As a consequence of the above findings, the present analysis contrasts with associated previous extensions of the usual lubrication approximation towards the regime of boundary-layer flow, both laminar (cf. [1]) and superlaminar or turbulent (cf. [2]). In the latter case the few studies available rely on the rather ad-hoc inclusion of the turbulent shear stress in the Prandtl-type boundary layer equations exhibiting nonlinear convective terms. However, studying high-*Re* turbulent lubricant flow by rigorous asymptotic analysis of the ensemble-averaged equations of motion has patently not attracted many researchers. Although desirable, the establishment of such a theory is severely hampered by the correct scaling of the a priori unknown pressure rise induced by the interplay of the sliding motion and the wedge effect. Also, the yet limited understanding of laminar-turbulent transition in internal flows currently does not provide a pathway, but the well-accepted theory of turbulent channel flow does: the lubricant flow differs mainly due to crucial effects of inertia. First numerical results supplement the new theory, which does not rely on a specific turbulence closure.

3 REFERENCES

[1] Tuck, E. O.; Bentwich, M.: Sliding sheets: lubrication with comparable viscous and inertia forces. Journal of Fluid Mechanics (1983), 135, 51-69.

[2] Frêne, J.; Arghir, M.; Constantinescu, V.: Combined thin-film and Navier-Stokes analysis in high Reynolds number lubrication. Tribology International (2006), 39, 734-747.

[1] *AC²T research GmbH, Wiener Neustadt, Austria, scheichl@ac2t.at*

[2] *Institute of Fluid Mechanics and Heat Transfer, Vienna University of Technology, Austria, b.scheichl@tuwien.ac.at*

Local heat conduction in the sheet membrane of the *iSi* Helium inflator due to the impingement of the combustion gas jetting from the ignition chamber

Research report – final version, 02/19/2007

B. Scheichl* and A. Kluwick
*Principal investigator and corresponding author
E-mail: bernhard.scheichl@tuwien.ac.at

Abstract: The spatial and temporal temperature distribution across the the sheet membrane, which serves as a closing of the inflator filled with pressurized Helium, due to the heat flux impressed by the hot combustion gas jet impinging on its surface is calculated. As the main objective, this calculation shall provide an input for a subsequent conservative estimate of the mechanical fatigue of the sheet and, consequently, its burst, intended to be carried out by the customer. As the highest temperature (which are critical for the mechanical behavior of the material) are expected on the surface of the membrane near the stagnation point of the impinging jet (apex of the membrane), it proves sufficient to restrict the analysis to the vicinity of the axis of the jet. Most important, in order to obtain a conservative estimate of the temperature distribution, it is assumed that the temperature at the surface of the membrane is below its melting temperature. In connection with some further simplifications justified by the purpose of this study, this supposition allows for a most simple analytical approximate solution of the problem.

INSTITUTION CARRYING OUT THE STUDY

INSTITUTE OF FLUID MECHANICS AND HEAT TRANSFER
RESSELGASSE 3/E322
A-1040 VIENNA
AUSTRIA
www.fluid.tuwien.ac.at

TECHNISCHE UNIVERSITÄT WIEN
VIENNA UNIVERSITY OF TECHNOLOGY

CUSTOMER

***iSi* Automotive GmbH & Co KG**
Scheydgasse 30–32,
A-1210 Vienna, Austria

BASIC CONVENTIONS

- Symbols for physical quantities:

  a ... Thermal diffusivity
  c ... Specific heat capacity (at constant pressure)
  g ... Weighting function
  h ... Step response function
  H ... Heaviside unit step function
  j ... Heat flux
  k ... Wave number
  M ... Molecular weight
  n ... Counter
  p ... Pressure
  R ... Ideal-gas constant
  S ... Stagnation point of gas jet
  t ... Time
  T ... Temperature
  y ... Spatial coordinate
  Z ... Real-gas factor
  δ ... Thickness of thermal boundary layer

Δ ... Difference symbol
θ ... Relative temperature
λ ... Heat conductivity
ρ ... Density
$\mathcal{R}$ ... Molar ideal-gas constant, $\mathcal{R} \doteq 8.341\,\mathrm{J/mol\,K}$

- Subscripts ...
  - ... referring to medium:
    g ... (hot) gas
    He ... Helium
    s ... solid (sheet membrane)
  - ... referring to point of time:
    c ... critical
    e ... endpoint
    ig ... ignition

  av ... averaged across membrane thickness

- Dimensional quantities are denoted by symbols with a tilde (apart from constants denoted by calligraphic symbols), non-dimensionalized quantities without a tilde.

- Results, comments, and the referring section headings which are considered to be of immediate interest for the customer are displayed in red.

1 PURPOSE OF STUDY

The temperature distribution inside the sheet membrane shall be predicted near its apex, with the aim to adopt it for a subsequent calculation of the deformation of the membrane, leading to its rupture. The latter analysis is intended to be carried out by the customer.

2 BASIC ASSUMPTIONS

- Close to the stagnation point of the impinging jet (apex of the membrane) the variations of the temperature at the upper side of the membrane with distance from the centerline may be neglected.

- Natural convection inside the Helium chamber due to the heat flux input from the adjacent membrane may be disregarded (as a consequence of the geometric dimensions of the inflator).

- As a presumption usually adopted for rigid materials, the temperature in the sheet membrane shall not depend on the deformations. It is rather regarded to be prescribed independently in case of determining the stresses with deformation of the membrane.

- The ambient temperature $\tilde{T}_0$ is set to 20 °C throughout.

Physikalische Eigenschaften

Dichte	$\tilde{\rho}$	8,5 g/cm³
Schmelzbereich	$\tilde{T}_m$	1290–1350 °C
Permeabilität bei 20°C		1,005

Temperatur T °C	Spezifische Wärme $\tilde{c}_s$ J/kg K	Wärme-leitfähigkeit $\tilde{\lambda}_s$ W/mK	Elektrischer Widerstand μ Ω cm	Elastizitäts-modul kN/mm²	Ausdehnungs-beiwert $\tilde{\alpha}$ von 20 °C bis T 10^{-6}/K
20	415	9,8	128	209	
100	435	11,2	130	202	12,8
200	460	12,8	132	195	13,1
300	480	14,4	133	190	13,4
400	505	16,3	135	185	13,7
500	525	17,3	136	178	14,1
600	550	19,3	136	170	14,6
700	575	21,0	136	162	15,2
800	600	22,6	136	153	15,8
900	625	24,6	135	142	16,4
1000	650	26,7	132	128	17,0

Figure 1: Relevant physical properties of the membrane material (original notations in German).

- The temperature $\tilde{T}_g$ on the surface of the membrane due to the hot gas jet is assumed to be 1000 °C. That is, with respect to the data given in the table provided by the customer and displayed in Figure 1, $\tilde{T}_g$ is below its melting temperature $\tilde{T}_m$. In turn, the deformations of the material are locally regarded as negligibly small, which agrees with the the magnitude of the thermal expansion coefficient denoted by $\tilde{\alpha}$ in that table (note: in the author's opinion the correct scaling factor must be $10^{-6}\,\mathrm{K}^{-1}$, in order to obtain values of $\tilde{\alpha}$ which are comparable to those usually attributed to steel).

Important consequence: If the calculation of the fatigue of the membrane exhibits local yielding of the membrane material, the latter two assumptions provide a conservative estimate, following from an underestimate of the temperature distribution (due to the neglect of latent heat).

3 FURTHER IDEALIZATION OF THE PROBLEM

The situation considered is sketched in Figure 2. Under the assumptions given in Section 2, the local temperature distribution in both the membrane and the (pressurized) Helium is governed by the well-known one-dimensional heat conduction equation

$$\tilde{c}_i\tilde{\rho}_i\frac{\partial\tilde{T}}{\partial\tilde{t}} = -\frac{\partial\tilde{j}_i}{\partial\tilde{y}} = \tilde{\lambda}_i\frac{\partial^2\tilde{T}}{\partial\tilde{y}^2} + \frac{\mathrm{d}\tilde{\lambda}_i}{\mathrm{d}\tilde{T}}\left(\frac{\partial\tilde{T}}{\partial\tilde{y}}\right)^2, \qquad (1)$$

according to Fourier's law,

$$\tilde{j}_i = -\tilde{\lambda}_i\,\partial\tilde{T}/\partial\tilde{y}. \qquad (2)$$

In these relationships the index i means either He or s.

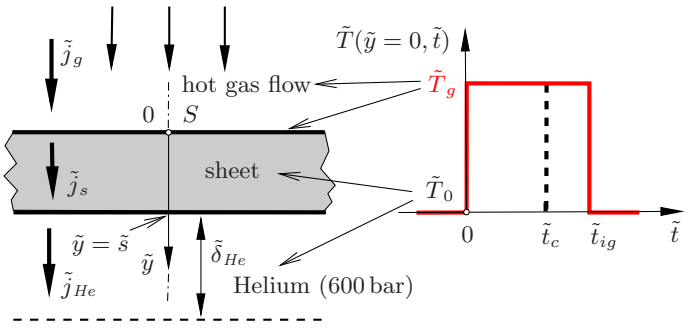

Figure 2: Configuration of the problem. For $\tilde{t} < 0$ both the sheet and the Helium "pad" assume the temperature $\tilde{T}_0$ of the environment.

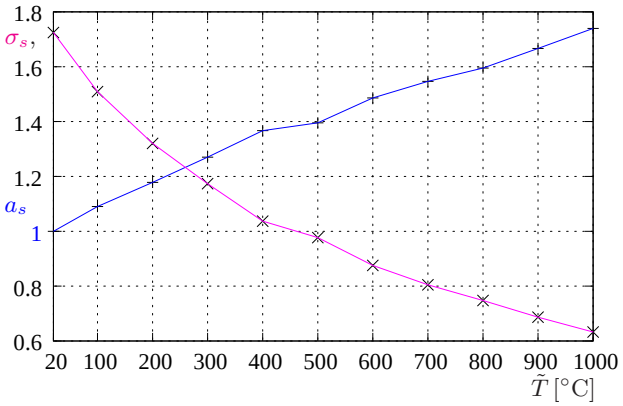

Figure 3: Evaluation of the data shown in Figure 1.

3.1 Local thermal conduction in the sheet

From the balance (1) the reference time

$$\tilde{t}_s = \tilde{s}^2 \tilde{\rho}_s \tilde{c}_s(\tilde{T}_0)/\tilde{\lambda}_s(\tilde{T}_0) \doteq 11,7 \times 10^{-3}\,\mathrm{s}, \qquad (3)$$

characteristic of the heat conduction inside the membrane (which is initially of temperature $\tilde{T}_0$) is formed; for the material data see Figure 1. Considering the sheet, we furthermore introduce the following non-dimensional quantities

$$\theta = \frac{\tilde{T}-\tilde{T}_0}{\tilde{T}_g-\tilde{T}_0}, \quad a_s = \frac{(\tilde{\lambda}_s/\tilde{c}_s)(\tilde{T})}{(\tilde{\lambda}_s/\tilde{c}_s)(\tilde{T}_0)}, \quad \sigma_s = \frac{1}{\tilde{\lambda}_s}\frac{\mathrm{d}\tilde{\lambda}_s}{\mathrm{d}\theta},$$
$$y = \tilde{y}/\tilde{s}, \quad t = \tilde{t}/\tilde{t}_s. \qquad (4)$$

For the sheet (1) then takes on the form

$$\frac{\partial\theta}{\partial t} = a_s\left[\frac{\partial^2\theta}{\partial y^2} + \sigma_s\left(\frac{\partial\theta}{\partial y}\right)^2\right], \quad 0 \le y \le 1. \qquad (5)$$

Evaluation of the data in Figure 1 indicates that the slope $\mathrm{d}\tilde{\lambda}/\mathrm{d}\tilde{T}$ can hardly be approximated better than by an average value formed by the limit values $\tilde{\lambda}_s(\tilde{T}_g) = 26.7\,\mathrm{W/(Km)}$ and $\tilde{\lambda}_s(\tilde{T}_0) = 9.8\,\mathrm{W/(Km)}$. This gives

$$\frac{\mathrm{d}\tilde{\lambda}_s}{\mathrm{d}\theta} = (\tilde{T}_g-\tilde{T}_0)\frac{\mathrm{d}\tilde{\lambda}_s}{\mathrm{d}\tilde{T}} \approx \tilde{\lambda}_s(\tilde{T}_g) - \tilde{\lambda}_s(\tilde{T}_0) \doteq 16.9\,\frac{\mathrm{W}}{\mathrm{mK}}. \qquad (6)$$

From the data in Figure 1 then the values for both σ_s and a_s are formed according to (4); see Figure 3. By focusing on the aim of calculating a conservative estimate of $\tilde{T}$, a lower bound for the temporal variation of $\tilde{T}$ and, in turn, $\tilde{T}$ itself, will be obtained by adopting the following simplifications:

- We omit the non-negative term proportional to σ in (5).
- In the whole range $\tilde{T}_0 \le \tilde{T} \le \tilde{T}_g$ of interest we set the thermal diffusivity a_s to the value of 1 it assumes for $\tilde{T} = \tilde{T}_0 \approx 20\,^\circ\mathrm{C}$.

Most important, and as will be shown in Section 4, this *ad hoc*-linearization of (5) allows for an analytical treatment of this equation. It is expected (but has to be shown *a posteriori*) that the anticipated error is of a few percent with respect to the analytical solution of the thereby idealized problem. We note that a numerical solution of the full heat conduction problem governed by (5), which takes into account the temperature-dependence of the thermal properties of the sheet, is beyond the scope of the present study.

3.2 Boundary condition at the sheet/jet interface

Near the stagnation point S the complexity of the hot gas flow can be reduced considerably by applying the first law of thermodynamics along the streamline which collapses with the jet axis, cf. Figure 2: Since the pressure inside the jet is approximately equal to ambient value (by neglecting shock wave interactions), the energy theorem states that the specific total enthalpy (the sum of enthalpy and kinetic energy) is constant along a gas particle path from the ignition chamber orifice to the membrane surface. Moreover, the radially spreading film, embedding (thermal) boundary layer, near S is expected to be not fully developed within the time period $\tilde{t}_{ig}$ characteristic of the duration of the combustion; for further details of the boundary layer flow see cf. Schlichting and Gersten (2000). As a first approximation, then the term $\partial\tilde{p}_g/\partial\tilde{t}$ may be neglected in that energy balance even close to the surface. In turn, these consideration allow for the simplest model possible of the temperature $\tilde{T}_g$ on the membrane surface adjacent to the hot gas close to S and for $0 < \tilde{t} < \tilde{t}_{ig}$:

- $\tilde{T}_g$ is almost equal to the temperature $\tilde{T}_{ig} \approx 3800\,\mathrm{K}$ in the ignition chamber issuing the jet (at speed of sound). The value of $\tilde{T}_{ig}$ is provided by the customer.
- $\tilde{T}_g$ is approximately constant, giving rise to the pulse-type surface temperature distribution sketched in Figure 2.

By evaluating the pressure measurements in the ignition chamber provides by the customer, for what follows we

assume

$$\tilde{t}_{ig} \approx 2 \times 10^{-3}\,\mathrm{s}, \quad \tilde{T}_g = 1000\,^{\circ}\mathrm{C}. \tag{7}$$

Not that the purpose of this underestimate of $\tilde{T}_g$ has already been discussed Section 2.

Comment on modelling $\tilde{T}_g$: We add that a more precise prediction of $\tilde{T}_g$ would be based on a much more elaborate investigation of the hot gas flow, based on its thermodynamic properties which, in turn, are highly sensitive to the rather complex chemical composition of the gas. Due to the rather high temperature, deviations from the state of an ideal gas would have to be taken into account. However, we stress that we do not expect that such an analysis would improve the estimate of the temperature distribution in the sheet essentially.

3.3 Boundary condition at the sheet/Helium interface

Let $\tilde{T}_{He}$ and $\tilde{j}_{s,He}$ denote the temperature and the heat flux at the interface $\tilde{y} = \tilde{s}$; see Figure 2. By taking into account (2), an order-of magnitude estimate yields

$$-\tilde{j}_{s,He} \sim \tilde{\lambda}_s(\tilde{T}_g - \tilde{T}_{He})/\tilde{s} \;\sim\; \tilde{\lambda}_{He}(\tilde{T}_{He} - \tilde{T}_0)/\tilde{\delta}_{He}. \tag{8}$$

Herein $\tilde{j}_{s,He}$ is expressed in terms of both the sheet material and the Helium properties. From elimination of $\tilde{j}_s$ evaluated at the interface by using (2) again then follows the non-dimensional expression for the temperature gradient at the interface

$$\left.\frac{\partial\theta}{\partial y}\right|_{y=1} \sim \frac{\tilde{T}_{He} - \tilde{T}_0}{\tilde{T}_g - \tilde{T}_{He}} \frac{\tilde{\lambda}_s}{\tilde{\lambda}_{He}} \frac{\tilde{s}}{\tilde{\delta}_{He}}. \tag{9}$$

In analogy to (3), the heat conduction equation (1) allows for estimating a time constant

$$\tilde{t}_{He} = \tilde{\delta}_{He}^2\, \tilde{\rho}_{He}\, \tilde{c}_{He}(\tilde{T}_0)/\tilde{\lambda}_{He}(\tilde{T}_0), \tag{10}$$

characteristic of the heat transfer across the boundary layer thickness $\tilde{\delta}_{He}$. Since both $\tilde{t}_s$ and $\tilde{t}_{He}$ are typical for the heat transfer at the interface, they may be equated. In turn, the boundary layer thickness $\tilde{\delta}_{He}$ can be eliminated in (9). Then the latter relation is written as

$$\left.\frac{\partial\theta}{\partial y}\right|_{y=1} \sim \frac{\tilde{T}_{He} - \tilde{T}_0}{\tilde{T}_g - \tilde{T}_{He}} \sqrt{\frac{\tilde{\lambda}_{He}\,\tilde{\rho}_{He}\,\tilde{c}_{He}}{\tilde{\lambda}_s\,\tilde{\rho}_s\,\tilde{c}_s}}. \tag{11}$$

The first factor on the right-hand side of (11) is clearly smaller than 1. For a numerical estimate of this relationship we use the values of Figure 1 by assuming that $\tilde{T}_{He} = 400\,^{\circ}\mathrm{C}$. We note that the results discussed in Section 4.3 *a posteriori* confirm that this value is a realistic estimate. For the following properties of the Helium we refer to VDI Wärmeatlas (2002). By assuming that the Helium behaves as an ideal gas, the density is approximately calculated by means of the equation of state, i.e.

$$\tilde{\rho}_{He} \approx \tilde{p}/(\tilde{Z}_{He}\,\tilde{R}_{He}\,\tilde{T}_0) \doteq 100\,\mathrm{kg/m^3}. \tag{12}$$

Here the real-gas factor $\tilde{Z}_{He} \approx 1$, and $\tilde{R}_{He} = \mathcal{R}/\tilde{M}_{He}$ where $\tilde{M}_{He} \doteq 4 \times 10^{-3}\,\mathrm{kg/mol}$. Then substitution of (12) and the values

$$\tilde{\lambda}_{He} \doteq 0.152\,\mathrm{W/(Km)}, \quad \tilde{c}_{He} \doteq 5193\,\mathrm{J/(kgK)} \tag{13}$$

into (11) gives an estimate for the non-dimensional temperature gradient $(\partial\theta/\partial y)(y = 1, t)$ of the magnitude of 10^{-2}. With respect to the simplifications made so far, this value may be considered as negligibly small in the following. That is, the pressurized Helium is seen to serve as an insulator.

4 IDEALIZED HEAT CONDUCTION PROBLEM

Customer's requirement: The membrane shall burst within a critical time $\tilde{t}_c \doteq 1.3 \times 10^{-3}\,\mathrm{s}$. The values given in (3) and (7) then yield

$$t_{ig} = \tilde{t}_{ig}/\tilde{t}_s \doteq 0.17, \quad t_c = \tilde{t}_c/\tilde{t}_s \doteq 0.11. \tag{14}$$

These values are critical for the non-dimensional distribution θ of the temperature.

4.1 The standard problem

Making use of the simplifications discussed in Section 3, one has to solve the linear heat conduction equation for $\theta(y, t; t_{ig})$,

$$\partial\theta/\partial t = \partial^2\theta/\partial y^2, \quad 0 \le y \le 1, \;\; t \ge 0, \tag{15a}$$

subject to the, respectively, initial and boundary conditions

$$\theta(y, 0; t_{ig}) = 0, \tag{15b}$$

$$(\partial\theta/\partial y)(1, t; t_{ig}) = 0, \tag{15c}$$

$$\theta(0, t; t_{ig}) = \theta_0(t; t_{ig}), \quad \theta_0(t > t_s; t_{ig}) = 0. \tag{15d}$$

The dependence of θ on the parameter t_{ig} results from the very simple model we use in the present study for describing the hot gas flow impinging on the membrane surface. Thus, θ_0 is approximated by the aforementioned (unit) pulse of duration time t_{ig},

$$\theta_0(t; t_{ig}) = H(t) - H(t - t_{ig}). \tag{16}$$

Herein $H(t < 0) = 0$ and $H(t \ge 0) = 1$.

4.2 Analytical solution

A formal solution of the initial/boundary value problem (15) is commonly found by using the Laplace transform with respect to t. Under rather weak conditions, for an arbitrarily prescribed surface temperature $\theta_0(t; t_{ig})$ the solution is found in terms of the convolution integral

$$\theta(y, t; t_{ig}) = \int_0^t \theta_0(t - \tau; t_{ig})\, g(y, \tau)\, \mathrm{d}\tau. \tag{17}$$

Note that the so-called weighting function $g(y,t)$ is a (here fictitious) solution of (15) if $\theta_0(t;t_{ig})$ in the boundary condition (15d) equals the Dirac delta function $\delta(t)$. By skipping further (rather subtle) mathematical details, we note that the Laplace transform of $g(y,t)$ and, in turn, its inverse can be expanded in a series. The resulting Fourier representation for $g(y,t)$ can conveniently be cast in the form

$$g(y,t) = 2\sum_{n=0}^{\infty}(-1)^n k_n\, g_n(t)\cos[k_n(1-y)],$$
$$k_n = \pi(n+1/2), \quad g_n(t) = \exp(-k_n^2 t), \quad t>0. \quad (18)$$

The structural dependence on y and t of that specific solution can be checked by adopting the standard method of separation of variables; then it is readily seen that $\theta = g(y,t)$ satisfies (15a) as well as the boundary condition (15c). However, the coefficients k_n have to be determined by inverting the Laplace transform of $g(y,t)$.

In the particular case (16) considered in the present study, it follows from (17) and (18) that the solution of (15) reads

$$\theta(y,t;t_{ig}) = 2\sum_{n=0}^{\infty}(-1)^n\, h_n(t;t_{ig})\cos[k_n(1-y)]/k_n,$$
$$h_n(t;t_{ig}) = 1 - g_n(t) - H(t-t_{ig})\,[1-g_n(t-t_{ig})],$$
$$0<y\le 1, \quad t\ge 0. \quad (19)$$

In the following this temperature distribution is evaluated numerically and discussed from the physical point of view.

4.3 Numerical evaluation via FFT

The Fourier series (18) and (19), respectively, define functions which are periodic in y with a periodicity of 4, i.e. the interval $0\le y\le 1$ represents a quarter period. In addition, the function defined by the series (19) is discontinuous at $y=0$ as its value is zero there but its one-side limit for $y\to 0_+$ indeed equals $\theta_0(t;t_{ig})$, which in the case considered here is given by (16). Moreover, that series is seen to converge uniformly on $0<y\le 1$.

These considerations then suggest to compute the temperature distribution $\theta(y,t;t_{ig})$ by means of an approximate computation of the Fourier series (19) for $0<y\le 1$ and by setting it equal to its one-side limit $\theta_0(t;t_{ig})$ at $y=0$. The numerical evaluation of the series is accomplished most efficiently by applying a Fast Fourier Transform (FFT) by assuming a quarter-period of 1 to a certain number n of the Fourier coefficients in (19) for all specific values of the time t where the temperature is considered to be of interest. The choice of $n=2000$ Fourier modes proves satisfactory to obtain a sufficiently smooth discrete approximation of the solution (note that due to the well-known Gibbs' phenomenon the Fourier representation behaves highly oscillatory as $y\to 0_+$, even for an arbitrarily large number of n).

In Figure 4 (see next page) the solution $\theta(y,t;t_{ig})$ is plotted for the values of t_{ig} and t_c given in (14).

5 CONCLUSIONS

Since the sheet temperature assumes its minimum value at the surface adjacent to the Helium given by $\tilde{y}=\tilde{s}$, its value at this location and for the critical time $t=t_c$ provides a critical lower bound $\tilde{T}_c$ for a sufficiently intense heating of the sheet, such that the resulting stresses immediately initiates the bursting process (by disregarding melting, see Section 2).

Employing the values given in (14), one infers from the solution for $\theta(y,t;t_{ig})$ that $\theta_c = \theta(y=1, t=t_c; t_{ig}) \approx 0.07$, see Figure 4 (next page). Equivalently, by using (4), that means that an estimate for $\tilde{T}_c$ is given by

$$\tilde{T}_c = \tilde{T}_0 + \theta_c(\tilde{T}_g - \tilde{T}_0) \approx 159\,^{\circ}\mathrm{C}. \quad (20)$$

As expected from a conservative estimate, this value is below the experimental finding $\tilde{T}_c \approx 240\,^{\circ}\mathrm{C}$ reported by the customer.

Finally, the values $\tilde{T}_{av}$ of the temperatures averaged across the membrane thickness for different times, up to $\tilde{t}\approx\tilde{t}_c$, are presented in the table below. They are calculated by means of

$$\tilde{T}_{av} = \tilde{T}_0 + \theta_{av}(\tilde{T}_g - \tilde{T}_0). \quad (21)$$

Here the original value of $\tilde{T}_{av}\approx 3800\,\mathrm{K}$ is used; see Section 3.2.

$\tilde{t}\ [10^{-3}\,\mathrm{s}]$	0	0.16	0.32	0.47	0.63	0.79
$\tilde{T}_{av}\ [^{\circ}\mathrm{C}]$	37.6	486	676	821	944	1052
$\tilde{t}\ [10^{-3}\,\mathrm{s}]$	0.95	1.11	1.26	1.42	1.58	1.74
$\tilde{T}_{av}\ [^{\circ}\mathrm{C}]$	1149	1239	1323	1402	1476	1.547

Important consequence: It is readily seen that after approximately 0.4×10^{-3}s and 1.3×10^{-3}s, respectively, the temperature $\approx 700\,^{\circ}\mathrm{C}$ that characterises the upper limit of linear-elastic behavior (customer information), and the melting temperature $\tilde{T}_m$, see Figure 1, are exceeded.

REFERENCES

Schlichting, H. and Gersten, K. (2000) *Boundary-Layer Theory*, 8th edn. Berlin, Heidelberg: Springer-Verlag.

Verein Deutscher Ingenieure (VDI), VDI-Gesellschft Verfahrenstechnik und Chemieingenieurwesen (GVC), ed. (2002) *VDI Wärmeatlas. Berechnungsblätter für den Wärmeübergang*, 9th edn (in German). Berlin, Heidelberg: Springer-Verlag.

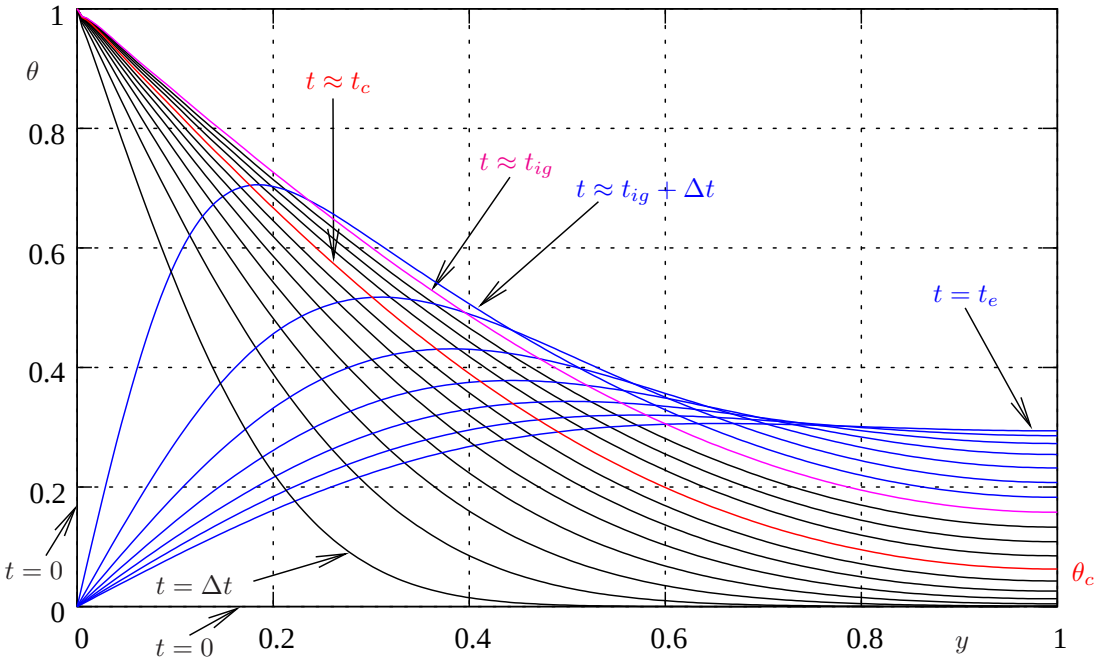

Figure 4: $\theta(y,t;t_{ig})$ for discrete times t, differing by $\Delta t \doteq 1.35 \times 10^{-2}$ in the range $0 \le t \le t_e = 1.5\,t_c \doteq 2.56$. The blue curves are the values for $t_{ig} < t \le t_e$, showing the tendency of the temperature to adjust with its ambient value for larger values of t.

TECHNICAL REPORT

Feasibility study of a novel hydrodynamically lubricated thrust bearing device operated with water or saturated water vapour

Dr. Bernhard Scheichl

e-mail: bernhard.scheichl@tuwien.ac.at

Institute of Fluid Mechanics and Heat Transfer, Vienna University of Technology,
Resselgasse 3/E322, A-1040 Vienna, Austria

Client

ANDRITZ AG, Mechanical Pulping Systems,
Eibesbrunnergasse 20, A-1120 Vienna, Austria

Final version

27/02/2009

Summary

A feasibility study concerning the stationary operation mode of a novel thrust bearing device, to be used in pulping systems, is presented. In essence, it consists of a circular stator, centrically parallel to the axisymmetric rotor, such that the tilting of the clearance between these two discs controls the hydromechanical operation of the bearing. Unlike the commonly adopted tilted-pads bearings, here the specific gap geometry is achieved by milling an annulus consisting of adjacent identical sectors from the surface of the stator, such that the tilting of the clearance in circumferential direction accounts for the hydrodynamical bearing behaviour. The maximum load-bearing capacity is found by optimising the azimuthal pitch. The lubricant is supplied radially at the inner edge of the annulus. As a consequence of the imposed supply pressure, the bearing operates in both hydrostatic and hydrodynamic mode, i.e. in hybrid mode, associated with the flow in radial and azimuthal direction, respectively. Both the cases water and saturated water vapour used as lubricants are investigated. In order to predict the hydromechanical performance, the basic equations of lubrication theory are solved by adopting both analytical and numerical methods.

Nomenclature

Br	Brinkmann number
Re	Reynolds number
$\tilde{B}$	Width of bearing in radial direction [mm]
$\tilde{F}$	Thrust force, load-bearing capacity [kN]
$\tilde{g}$	Gravitational acceleration, $\tilde{g} \approx 9.81\,\mathrm{m/s^2}$
$\tilde{H}$	Minimum clearance height [mm]
$\tilde{M}$	Overall mass flow rate [kg/s]
$\tilde{P}$	Friction power [kW]
$\tilde{p}$	Pressure of lubricant [bar]
$\tilde{Q}$	Overall volume flow rate [l/s]
$\tilde{R}_\mathrm{i}$	Inner radius [mm]
$\tilde{T}$	Operating temperature [°C]
B	Width of bearing in radial direction [-]
F	Thrust force, load-bearing capacity [-]
h	Local value of clearance height [-]
j	Exponent, $j = 0$ or 1
K	Parameter measuring strength of tilting of clearance
m	Mass flux integrated across height of clearance [-]
n	Circumferential pitch, number of tilted sectors
p	Pressure of lubricant [-]
r	Radius [-]
S	State of saturated vapour
s	Variable of integration
t	Tilting of clearance either in x- or y-direction
u	Radial velocity component [-]
v	Azimuthal velocity component [-]
w	Axial velocity component [-]
x	Radial coordinate [-]
y	Azimuthal coordinate [-]
z	Axial (vertical) coordinate, measured from rotor surface [-]

Subscripts

0	$\varphi = 0$ ($y = 0$)
1	$\varphi = \varphi_\mathrm{max}$ ($y = 1$)
r	r-direction
φ	φ-direction
x	x-direction
y	y-direction
g	Gaseous (saturated water vapour)
i	Supply value, holding at inner edge of bearing ring, $\tilde{r} = \tilde{R}_\mathrm{i}$
l	Liquid (water)
max	Maximum value
min	Minimum value
o	Ambient value, holding at at outer edge of bearing ring, $\tilde{r} = \tilde{R}_\mathrm{i} + \tilde{B}$
r	Reference quantity
s	Value at surface of rotor and stator

Symbols

$\tilde{\beta}$	Volumetric thermal expansion coefficient at constant pressure of lubricant[1/K]
$\tilde{\lambda}$	Thermal conductivity of lubricant [W/(m K)]
$\tilde{\mu}$	Dynamic viscosity of lubricant [Pa s]
$\tilde{\Omega}$	Angular velocity of the rotor [r.p.m.]
$\tilde{\varrho}$	Density of lubricant [kg/m^3]
Δ	Difference value

ϵ	Thin-film parameter
γ	Control parameter for studying stability
λ	Thermal conductivity of lubricant [-]
μ	Dynamic viscosity of lubricant [-]
τ	Wall shear stress [-]
θ	Difference between actual and temperature at inner edge of bearing ring [-]
φ	Azimuthal angle
ϱ	Density of lubricant [-]

Superscripts

$\sim$	Dimensionful quantity

I. Introduction

It is the primary goal of the present study to estimate the behaviour of an axial thrust bearing with respect to the maximum load-bearing capacity gained. Hydrodynamically operating (i.e. self-acting) thrust bearings are normally engineered as tilted- or, equivalently, sector pad slider bearings. However, in striking contrast to the conventional designs of such bearings, here the disc where usually tilted pads are mounted in circumferential direction in order to form a more-or-less contiguous annulus, only penetrated by narrow grooves that separate adjacent pads, is replaced by a rigid one where correspondingly adjacent sectors are milled from, which account for the hydrodynamic bearing operation. As an important consequence, the pressure in the grooves here not necessarily equals the ambient pressure but has to be calculated. It seems expedient to first provide a concise description of the bearing design, the lubricant to be considered, and the techniques used to investigate the lubricant flow in this report.

In essence, the bearing device consists of a circular stationary disc, i.e. the stator, centrically parallel to an axisymmetric rotating disc, i.e. the rotor, where both plates are taken to have the same radius. Furthermore, they are considered as flexurally rigid solids, both having a for the lubricant impervious surface. The (constant) tilting in azimuthal (and radial) direction of the thickness of the relatively small bearing gap between these two discs controls the hydromechanical operation of the bearing. The specific gap geometry is achieved by milling identical adjacent, i.e. aligned, sectors of an annulus (i.e. the bearing ring), having an outer radius which equals that of the discs, into the surface of the stationary disc. The maximum load-bearing capacity is found by optimising the circumferential pitch. The lubricant, entirely filling the clearance separating the discs, is supplied radially at the inner edge of the annulus by imposing a positive differential pressure with respect to the ambient pressure that holds at its outer edge. Therefore, the bearing operates in both hydrostatic and hydrodynamic mode, i.e. in hybrid mode, associated with the flow in radial and azimuthal direction, respectively. Both the cases water and (at feed-in) saturated water vapour used as lubricants are investigated. In order to predict the hydromechanical performance of the bearing, the basic equations of lubrication theory are solved by adopting both analytical and advanced numerical methods.

II. Operating conditions

The essential geometrical properties of the bearing gap, i.e. of the clearance, for a single sector pad are sketched in figure 1 (not to scale). The specific data that refer to the principal quantities defining steady operation of the bearing and are used as reference values in the subsequent analysis are displayed in table 1.

Table 1. Reference values and minimum (required) thrust force $\tilde{F}_{\min}$.

$\tilde{R}_\mathrm{i}$	$\tilde{B}$	$\tilde{H}$	$\tilde{\Omega}$	$\tilde{p}_\mathrm{i}$	$\tilde{p}_\mathrm{o}$	$\tilde{T}_\mathrm{l}$	$\tilde{T}_\mathrm{g}$	$\tilde{\varrho}_\mathrm{l}$	$\tilde{\varrho}_{\mathrm{g,i}}$	$\tilde{\varrho}_{\mathrm{g,o}}$	$\tilde{\mu}_\mathrm{l}$	$\tilde{\mu}_\mathrm{g}$	$\tilde{\boldsymbol{F}}_{\mathbf{min}}$
500	300	0.1	1800	20	5	150	220	917.45	9.787	2.247	1.825×10^{-4}	1.650×10^{-5}	**1850**

The value of $\tilde{H}$ is characteristic of the minimum clearance height that is possible from the viewpoint of manufacturing. Note that the effect of hydrodynamic bearing requires $\tilde{H} \leq \tilde{H}_1 < \tilde{H}_0$, since, with respect to figure 1, the rotor is assumed to turn counter-clockwise. The values of $\tilde{R}_\mathrm{i}$ and $\tilde{B}$ conform to the actual geometry of the pulping machine. Here we anticipate that the value of $\tilde{H}$ represents an upper bound for the effective (nominal) minimum clearance height and the values of $\tilde{R}_\mathrm{i}$, $\tilde{B}$, and $\tilde{p}_\mathrm{i}$ are found to provide lower bounds, required to achieve the value of $\tilde{F}_{\min}$.

The values of $\tilde{T}_\mathrm{l}$ and $\tilde{T}_\mathrm{g}$ approximately refer to the saturation temperature of water vapour for, respectively, the lower and the upper bound for the pressure, given by $\tilde{p} = \tilde{p}_\mathrm{o}$ and $\tilde{p} = \tilde{p}_\mathrm{i}$, and are taken from Ref. 1. This specific choice of the operation temperatures are not only associated with realistic operating conditions but, most important, is consistent with the assumption of discarding the possibility of phase transition, i.e. partial condensation, of the lubricant. Also, the analysis and the calculations show that the relative temperature changes are small, justifying a posteriori the here made assumption of isothermal flow. The values of $\tilde{\mu}_\mathrm{l}$ and $\tilde{\mu}_\mathrm{g}$ refer to the lower (case: liquid) and the upper (case: vapour) pressure bound, $p = \tilde{p}_\mathrm{o}$ and $p = \tilde{p}_\mathrm{i}$, respectively, cf. Ref. 1: the relative increase of the viscosities with, respectively, increasing (liquid) and decreasing (vapour) pressure (for a given temperature) are approximately 0.2% (liquid) and 2.3% (vapour) for $\tilde{p}_\mathrm{o} \leq \tilde{p} \leq \tilde{p}_\mathrm{i}$ and, in turn, here neglected.

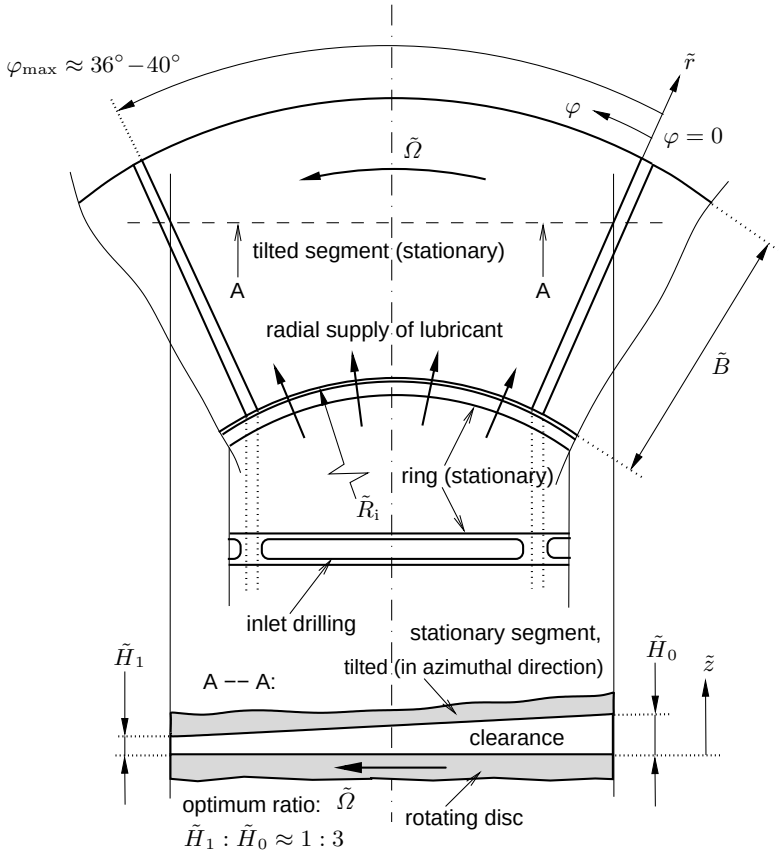

Figure 1. Geometry of a single tilted bearing sector (for caption see text).

As a consequence of the specific choice of the values of $\tilde{\mu}_\mathrm{l}$ and $\tilde{\mu}_\mathrm{g}$, the predicted value of thrust force $\tilde{F}$ is regarded as a lower bound for its actual value.

III. Problem formulation

We now provide an overview how the pressure distribution in the bearing, determining $\tilde{F}$, is calculated. To this end, we provide the basic equations governing the transport of mass, momentum, and energy of the flow through the bearing and the assumptions under which the approximations made within the framework of lubrication theory are valid, for the latter cf. Refs. 2,3. Most important, we demonstrate that regarding the flow as isothermal allows for a rationally simplified and self-consistent description of the flow that captures all its essential properties. For the full set of governing equations see e.g. Ref. 4.

III.A. Governing equations

We introduce appropriate non-dimensional quantities

$$r = \tilde{r}/\tilde{R}_\mathrm{i}\,, \quad B = \tilde{B}/\tilde{R}_\mathrm{i}\,, \quad x = (\tilde{r} - \tilde{R}_\mathrm{i})/\tilde{B}\,, \quad y = \varphi\, n/(2\pi) \quad (n = 1, 2, 3 \ldots)\,, \quad z = \tilde{z}/\tilde{H}\,, \tag{1}$$

$$h = \tilde{h}/\tilde{H}\,, \quad u = \tilde{u}/(\tilde{\Omega}\tilde{R}_\mathrm{i})\,, \quad v = \tilde{v}/(\tilde{R}_\mathrm{i}\tilde{\Omega})\,, \quad w = \tilde{w}/(\tilde{\Omega}\tilde{H})\,, \quad p = \tilde{p}/\tilde{p}_\mathrm{r}\,, \quad \varrho = \tilde{\varrho}/\tilde{\varrho}_\mathrm{r}\,, \quad \mu = \tilde{\mu}/\tilde{\mu}_\mathrm{r}\,, \tag{2}$$

$$\theta = (\tilde{T} - \tilde{T}_\mathrm{i})/\Delta\tilde{T}_\mathrm{r}\,, \quad \lambda = \tilde{\lambda}/\tilde{\lambda}_\mathrm{r}\,. \tag{3}$$

For what follows, note that $\varphi_{\max} = 2\pi/n$, cf. figure 1, and the relationship $r = 1 + Bx$. The dependent quantities, given in (2) and (3), are regarded as functions of the variables r, φ, z, apart from $h = h(x, y)$, which will prove convenient further below. The specific choice of the reference state is a topic of the subsequent analysis.

III.A.1. Geometry of clearance

In order to allow for milling the clearance geometry in each of n sectors, the clearance height is assumed to take on a bilinear form in each of the sectors:

$$h(x,y) = t_x\, t_y\ , \quad [t_x,\, t_y] = \begin{cases} [1 + K_x(1 - x/x_{\max}),\, 1 + K_y(1 - y/y_{\max})] & \dots \quad [x \le x_{\max},\, y \le y_{\max}]\ , \\ 1 & \dots \quad [x > x_{\max},\, y > y_{\max}]\ . \end{cases} \tag{4}$$

Since $p_\mathrm{i} > p_\mathrm{o}$ and the rotor turns counter-clockwise (see figure 1), the effect of hydrostatic bearing (due to radial flow) and hydrodynamic bearing (due to azimuthal flow) increases for increasing tilting of the bearing gap height in radial and azimuthal direction, measured by K_x and K_y, respectively. Furthermore, by taking into account operation after lubrication-system failure, it proves advantageous to slightly blunt the milled contour where the clearance height takes on rather small values ('tapered land' bearing, $t_x \approx 1,\ t_y \approx 1$). Considering the specific form of h proposed in (4), this is accomplished by requiring $0 \le 1 - x_{\max} \ll 1$ and $0 \le 1 - y_{\max} \ll 1$. Therefore, in the following we assume

$$K_x \ge 0 \quad K_y \ge 0\,, \quad x_{\max} = y_{\max} = 0.95\,. \tag{5}$$

Here we anticipate that varying the values of $x_{\max}$ and $y_{\max}$ within the range $0.92 \dots 0.98$ do not alter the results, shown in § IV.B and § IV.C, significantly.

Furthermore, we note that the case $K_y = 0$ refers to a perfectly axisymmetric bearing ring, which then behaves hydrodynamically as a (tapered) sealing ring (i.e. no pitch at all, purely hydrostatic bearing). In that case the clearance geometry and, thus, the flow through the bearing is independent of the specific choice of n.

III.A.2. Conservation of linear momentum, energy, and mass

We conveniently introduce the (non-dimensional) groups

$$\epsilon := \tilde{H}/\tilde{R}_\mathrm{i}\ , \quad \mathrm{Re} := \tilde{H}\tilde{R}_\mathrm{i}\tilde{\Omega}\tilde{\varrho}_\mathrm{r}/\tilde{\mu}_\mathrm{r}\ , \quad \mathrm{Br} := \tilde{\mu}_\mathrm{r}(\tilde{R}_\mathrm{i}\tilde{\Omega})^2/(\tilde{\lambda}_\mathrm{r}\Delta\tilde{T}_\mathrm{r})\ , \tag{6}$$

representative of the flow through the bearing.

The flow is investigated within the framework of lubrication theory. That is,

(A) the pressure is approximately constant across the clearance, i.e. the bearing gap (thin-film approximation);

(B) effects due to convection, here by centrifugal forces, are negligibly small.

Inserting (1) and (2) into the basic equations of motion, namely the Navier–Stokes equations for strictly steady flow, which consist of the continuity equation and the momentum equations in r-, φ-, and z-direction, respectively, shows that these two independent conditions are expressed equivalently in the form

(A) $\epsilon \ll 1$,

(B) $\epsilon\,\mathrm{Re} \ll 1$.

Here all non-dimensional flow quantities given in (2) and (3) are considered to be of $\mathcal{O}(1)$. Also, effects of gravity on the pressure distribution can be neglected: a conservative estimate of this effect can be expressed as the ratio $\tilde{\varrho}_\mathrm{l}\tilde{g}(\tilde{R}_\mathrm{i} + \tilde{B})/\tilde{p}_\mathrm{o} \approx 1.57\%$ (where the lubricant is assumed to be water as the density takes on its largest value).

In view of these approximations, we advantageously define

$$\tilde{p}_\mathrm{r} := \tilde{\mu}_\mathrm{r}\tilde{\Omega}\tilde{R}_\mathrm{i}^2/\tilde{H}^2 = \tilde{\mu}_\mathrm{r}\tilde{\Omega}/\epsilon^2\ . \tag{7}$$

Then the accordingly reduced equations for the linear momentum in the r- and φ-direction, respectively, read

$$\frac{\partial p}{\partial r} = \frac{\partial}{\partial z}\left[\mu\frac{\partial u}{\partial z}\right]\ , \quad \frac{1}{r}\frac{\partial p}{\partial \varphi} = \frac{\partial}{\partial z}\left[\mu\frac{\partial v}{\partial z}\right]\ , \quad \frac{\partial p}{\partial z} = 0\ , \tag{8}$$

and the correspondingly simplified thermal energy equation is written as

$$-\frac{1}{\mathrm{Br}}\frac{\partial}{\partial z}\left[\lambda\frac{\partial\theta}{\partial z}\right] = \tilde{\beta}\tilde{T}\left[u\frac{\partial p}{\partial x}+\frac{v}{r}\frac{\partial p}{\partial\varphi}\right]+\mu\left[\left(\frac{\partial u}{\partial z}\right)^2+\left(\frac{\partial v}{\partial z}\right)^2\right] . \tag{9}$$

In (9) the left-hand side and the last contribution represent, respectively, the gradient of the heat flux density across the bearing gap, expressed in terms of Fourier's law, and the dissipation function. The latter equals the negative internal power of viscous forces per volume unit. Note that θ and λ enter the energy equation (9) solely. The equations (8), (9) are supplemented with the exact form of the continuity equation,

$$\frac{\partial(r\varrho u)}{\partial r}+\frac{\partial(\varrho v)}{\partial\varphi}+r\frac{\partial(\varrho w)}{\partial z}=0 . \tag{10}$$

The resulting set of equations (8)–(10) governs the flow quantities u, v, w, p, and θ. It is subject to the boundary conditions

$$z=0: \qquad u=w=0 , \quad v=r , \quad \theta=\theta_s , \tag{11}$$

$$z=h(x,y): \qquad u=v=w=0 , \quad \theta=\theta_s , \tag{12}$$

$$x=0: \qquad p=p_\mathrm{i} , \tag{13}$$

$$x=1: \qquad p=p_\mathrm{o}\ (<p_\mathrm{i}) , \tag{14}$$

and the obvious requirement for periodicity,

$$q(r,\varphi,z)\equiv q(r,\varphi+\varphi_\mathrm{max},z) , \quad 0<\varphi<\varphi_\mathrm{max} , \quad q=u,v,w,p,\theta . \tag{15}$$

The relationships (11) and (12) account for the no-slip and no-penetration conditions in combination with the thermal boundary conditions, and (13) and (14) represent the inlet and outlet conditions, respectively. Note that the thermal conductivity of the steel is much larger than that of water of saturated vapour: then the lubricant acts as an isolator, and the heat conduction equation for the solid discs is supplemented with isolating boundary conditions, i.e. vanishing temperature gradient normal to the surfaces of both the rotor and the stator. In turn, it is reliable to assume that both surfaces take on the universal temperature θ_s of the (otherwise also isolated) neighbouring parts of the machine (which is mainly due to mechanical dissipation during operation), as expressed in (11) and (12).

III.B. Effects of compressibility and inertia

For lack of reliable estimates for $\tilde{T}_\mathrm{s}$, here the reduced transport equation (9) for the temperature shall not be invoked furthermore. However, setting $\mathrm{Br}=1$ in (9) gives rise to suitable values of $\Delta\tilde{T}_\mathrm{r,l}$ and $\Delta\tilde{T}_\mathrm{r,g}$, according to the definition of Br in (6). The corresponding values, resulting from the specific properties of water found in Ref. 1 and shown table 2, are found to be rather small compared with the values $\tilde{T}_\mathrm{l}$ and $\tilde{T}_\mathrm{g}$, respectively, that characterise the operation conditions of the bearing. As a result and in agreement with the statement made in § II, one follows that the flow may regarded as isothermal with sufficient accuracy. Hence, $\tilde{T}_\mathrm{i}$ is identified with $\tilde{T}_\mathrm{l}$ and $\tilde{T}_\mathrm{g}$, respectively, quoted in table 1. In addition, the following important conclusion is inferred from the data given in Ref. 1: in the here interesting effective temperature range $\tilde{T}=220^\circ\mathrm{C}-300^\circ\mathrm{C}$ expected in the clearance (see table 1) in the case of saturated and (slightly) superheated vapour as lubricant (cf. § II) the equation of state is fairly accurately approximated by the observation that p/ϱ merely depends on θ, rather than on p. Furthermore, for both liquid and gaseous water the relative changes of $\tilde{\mu}$ for the temperatures considered here are found to depend insignificantly on $\tilde{p}$. As a consequence,

$$\mu\equiv 1 , \quad \varrho=\varrho(p): \begin{cases} \varrho\equiv 1 & \ldots \text{ liquid (water)} , \\ \varrho/p\equiv 1 & \ldots \text{ gas (saturated vapour)} . \end{cases} \tag{16}$$

Then $\tilde{\varrho}_\mathrm{r}:=\tilde{\varrho}_\mathrm{l}$, $\tilde{\mu}_\mathrm{r}:=\tilde{\mu}_\mathrm{l}$ for liquid water and $\tilde{\varrho}_\mathrm{r}:=\tilde{\varrho}_\mathrm{g,i}$, $\tilde{\mu}_\mathrm{r}:=\tilde{\mu}_\mathrm{g}$ for vapour, respectively, as lubricants. If the vapour is assumed to be saturated at the inlet, its change of state when pushed through the bearing in merely radial direction due to a difference pressure $\tilde{p}_\mathrm{i}-\tilde{p}_\mathrm{o}$ is sketched in figure 2: the real behaviour is

Table 2. Reference values of temperature (note the values of $\tilde{T}_\mathrm{l}$, $\tilde{T}_\mathrm{g}$ adopted in [K], found by adding 273.16 to those in [°C] given in table 1).

$\Delta\tilde{T}_{\mathrm{r,l}}$	$\Delta\tilde{T}_{\mathrm{r,l}}/\tilde{T}_\mathrm{l}$	$\Delta\tilde{T}_{\mathrm{r,g}}$	$\Delta\tilde{T}_{\mathrm{r,g}}/\tilde{T}_\mathrm{g}$
2.38	0.0056	3.70	0.0075

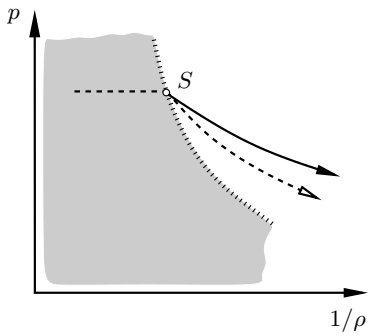

Figure 2. Change of state of vapour, saturated at S, flow through bearing indicated by arrows: region of wet steam (shaded), saturated-vapour line (dotted), ideally isothermal (dashed) and real (solid) behaviour.

associated with a relatively moderate temperature rise, and for fully saturated vapour any here disregarded pressure rise by the effect of lubrication is inevitably associated with condensation.

The resulting approximate values of ϵ, Re (together with that of Br, for the sake of completeness), introduced in (6), for both modifications of water are shown in table 3. Unfortunately, it is seen that the condition (B) is only satisfied for the case of vapour (and even then with some reservation). However, the lubrication approximation implied by both the requirements (A) and (B) stated in § III.A.2 is adopted in both cases. For further comments see § V.

Table 3. Values of non-dimensional flow parameters.

ϵ	Re_l	Re_g	Br
2×10^{-4}	4.74×10^{4}	0.129×10^{4}	1

III.C. Reynolds equation

Integration of (8) with respect to z, subject to (16) and the no-slip and and no-penetration conditions given by (11), (12) yields the parabolic velocity distributions

$$u = (z-h)\frac{z}{2}\frac{\partial p}{\partial r}\,, \quad v = (z-h)\left[\frac{z}{2r}\frac{\partial p}{\partial \varphi} - \frac{r}{h}\right]. \tag{17}$$

Both the u- and the v-component represent so-called Couette–Poiseuille flow, cf. Ref. 4, where the Hagen–Poiseuille part denotes the first contribution to their representations in (17). Its contribution to the u-component gives rise to the hydrostatic bearing performance as it is induced by the imposed pressure difference $p_\mathrm{i} - p_\mathrm{o}$, apart from its origin in the radial tilting of the clearance in case of finite values of K_x. Most important, the boundary condition (11) accounts for the additional Couette flow contribution to the v-component and, hence, the capability of hydrodynamic bearing due to the angular speed of the rotor. Accordingly, integration of (10) across the bearing gap subject to (11), (12) gives

$$\frac{\partial(rq_r)}{\partial r} + \frac{\partial q_\varphi}{\partial \varphi} = 0; \quad [m_r, m_\varphi](r,\varphi) := \int_0^{h(x,y)} [\varrho u, \varrho v](r,\varphi,z)\,\mathrm{d}z\,, \tag{18}$$

where, by substitution of (17),

$$m_r = -\varrho\frac{h^3}{12}\frac{\partial p}{\partial r}\,, \quad m_\varphi = \frac{\varrho}{2}\left[rh - \frac{h^3}{6r}\frac{\partial p}{\partial \varphi}\right]. \tag{19}$$

Finally, with the aid of (16) we arrive at the well-known Reynolds equation, here specified for a thrust bearing in stationary operation and for isothermal flow conditions,

$$\frac{\partial}{\partial r}\left[rh^3p^j\frac{\partial p}{\partial r}\right]+\frac{1}{r}\frac{\partial}{\partial\varphi}\left[h^3p^j\frac{\partial p}{\partial\varphi}\right]=6r\frac{\partial(p^jh)}{\partial\varphi}\quad\begin{cases}j=0 & \ldots\ \text{liquid (water)}\ ,\\ j=1 & \ldots\ \text{gas (saturated vapour)}\ .\end{cases}\tag{20}$$

The elliptic second-order equation (20) governing the pressure distribution $p(r,\varphi)$ is subject to the inlet and outlet boundary conditions (13), (14). In addition, boundary conditions at the edges of the sectors stretching in radial direction, given by $y=0$ and $y=1$, i.e. near the grooves between adjacent tilted sectors, see figure 1, have to be supplied: without going into details, it can be shown that (15) also holds for $\varphi=0$ and $\varphi=\varphi_{\max}$. However, here the pressure distribution contrasts that provoked by tilted pads that commonly assemble thrust bearings so that p assumes the value of the ambient pressure near the grooves insofar as the value of p for $\varphi=0$ is a priori unknown. In essence, this weaker form of the condition of periodicity only expresses the fact that the grooves are rather narrow compared to the circumferential extent of a specific tilted sector. In turn, from combining this strict periodicity of the flow with respect to the φ-direction with the global conservation of mass one then infers that the mass flow rates entering the clearance at $\varphi=0$ and $\varphi=\varphi_{\max}$, respectively, are equal for identical values of r,

$$\int_1^r m_\varphi(r,0)\,\mathrm{d}s=\int_1^r m_\varphi(r,2\pi/n)\,\mathrm{d}s\ ,\quad 1<r\le 1+B\ .\tag{21}$$

Since this equation must be valid for any value of r in the given range, one infers that

$$m_\varphi(r,0)=m_\varphi(r,2\pi/n)\ ,\quad 1<r\le 1+B\ .\tag{22}$$

Finally, by making use of (16) and (19), we arrive at the conditions of periodicity

$$p(r,0)=p(r,2\pi/n)\ ,\quad \left[6r^2p^jh-h^3p^j\frac{\partial p}{\partial\varphi}\right]_{\varphi=0}=\left[6r^2p^jh-h^3p^j\frac{\partial p}{\partial\varphi}\right]_{\varphi=2\pi/n}\ ,\quad 1<r\le 1+B\ .\tag{23}$$

Hence, the problem posed by (20), (13), (14), (23), (4) in connection with (5), and the number of sectors n determines $p(r,\varphi)$. This problem is linear in case of liquid water and nonlinear (quasi-linear) in case of vapour as lubricant, respectively. As a consequence of (7) and (16), the value of $\tilde{p}$ is independent of the actual value of the reference quantity $\tilde{\varrho}$. Moreover, the analysis presented so far demonstrates that the various parameters characteristic of the problem enter p in the form

$$p=p(r,\varphi;p_\mathrm{i},p_\mathrm{o},n,B,K_x,K_y,x_{\max},y_{\max})\ .\tag{24}$$

Once the pressure distribution has been obtained, other relevant (global) data are evaluated easily.

IV. Load-bearing capacity

The sought load-bearing capacity $\tilde{F}$, the supplied mechanical power (due to friction) $\tilde{P}$, $\tilde{Q}$, and $\tilde{M}$ then are readily calculated by integrating p, the negative value of the wall shear stress in circumferential direction, and u across the overall area of the bearing ring and the inlet gap at $\tilde{r}=\tilde{R}_\mathrm{i}$, respectively,

$$\tilde{F}=\tilde{p}_\mathrm{r}\tilde{R}_\mathrm{i}^2F\ ,\quad F:=\int_1^{1+B}r\int_0^{2\pi}p(r,\varphi)\,\mathrm{d}\varphi\,\mathrm{d}r\ ,\tag{25}$$

$$\tilde{P}=\tilde{P}_\mathrm{r}\int_1^{1+B}r\int_0^{2\pi}[-\tau_\varphi(r,\varphi)]\,\mathrm{d}\varphi\,\mathrm{d}r\ ,\quad -\tau_\varphi:=\left.\frac{\partial v}{\partial z}\right|_{z=0}=\frac{h}{2r}\frac{\partial p}{\partial\varphi}+\frac{r}{h}\ ,\tag{26}$$

$$\tilde{Q}=\tilde{Q}_\mathrm{r}\int_0^{2\pi}m_r r\,\mathrm{d}\varphi=-\tilde{Q}_\mathrm{r}\int_0^{2\pi}r\frac{h^3}{12}\left[\frac{p}{p_\mathrm{i}}\right]^j\frac{\partial p}{\partial r}\,\mathrm{d}\varphi\ ,\quad 1\le r\le 1+B\ ,\tag{27}$$

$$\tilde{M}=\tilde{\varrho}_\mathrm{i}\tilde{Q}\ .\tag{28}$$

Herein, $\tilde{\varrho}_\mathrm{i}=\tilde{\varrho}_\mathrm{l}$ for liquid water and $\tilde{\varrho}_\mathrm{i}=\tilde{\varrho}_{\mathrm{g,i}}$ for water vapour, respectively (see table 1), and

$$\tilde{Q}_\mathrm{r}:=\tilde{R}_\mathrm{i}^2\tilde{H}\tilde{\Omega}\ ,\quad \tilde{P}_\mathrm{r}:=\tilde{p}_\mathrm{r}\tilde{Q}_\mathrm{r}\ .\tag{29}$$

The approximate values of $\tilde{p}_\mathrm{r}$, see (7), $\tilde{Q}_\mathrm{r}$, and $\tilde{P}_\mathrm{r}$ are shown in table 4. Note that the expression for the volume flow rate $\tilde{Q}$ that enters the clearance at its inner edge within the range $1 < r \leq 1 + B$ follows from the requirement (23) for identical mass flow rates through the circumferential borders of the clearance with the aid of (16). In order to avoid numerical difficulties arising from a possibly weak singular behaviour of p near $\varphi = 0$ and $\varphi = 2\pi/n$ for $r = 1$ and $r = 1 + B$, detected by inspection of (20), (13), (14), and (23), but not discussed here in detail, the numerical evaluation of the integral in (27) is carried out for $r \approx 1 + B/2$.

Table 4. Scaling values.

$\tilde{p}_{\mathrm{r,l}}$	$\tilde{p}_{\mathrm{r,g}}$	$\tilde{Q}_\mathrm{r}$	$\tilde{P}_{\mathrm{r,l}}$	$\tilde{P}_{\mathrm{r,g}}$
8.600	0.7775	4.71	4.05	0.366

Before evaluating (25)–(27), one has to solve the aforementioned problem determining p by prescribing a specific distribution $h(x, y)$, i.e. K_x and K_y, numerically, in general. We note that an analytical solution can be obtained if $\partial h/\partial y \equiv 0$, i.e. in case of a perfectly axisymmetric bearing, which then behaves hydrodynamically as a (tapered) sealing ring. However, it proves convenient to include this special case into a sensitivity analysis with respect to different values of K_y that is performed by solving the problem numerically throughout. Notwithstanding the result (presented in § IV.B) that the maximum value of $\tilde{F}$ is found for $n = 8$ to 10, it is seemingly worthwhile to also consider the advantages that are due to perfect axial symmetry ($\partial/\partial\varphi \equiv 0$):

- simple geometry, bearing ring relatively feasible to design and manufacture;
- pressure distribution and, hence, resulting load independent of rotational speed and medium (i.e. of $\tilde{\Omega}$, $\tilde{\varrho}$, $\tilde{\mu}$) – the load depends solely on geometry of the clearance, $\tilde{p}_\mathrm{i}$, $\tilde{p}_\mathrm{o}$;
- pressure distribution is exact solution of (20) and its prediction, therefore, more reliable than for a more complex geometry.

In case of liquid water, the linearity of the problem can be exploited with the aim to superpose the load that results from the constant pressure $p \equiv p_\mathrm{o}$ (and, thus, can be determined very easily) and the differential load that is determined numerically by solving the problem subject to a prescribed pressure difference $p_\mathrm{i} - p_\mathrm{o}$, such that this value replaces p_i. However, also in the incompressible case it is convenient to numerically solve the composite problem.

IV.A. Numerical method

The Reynolds equation (20) and the boundary conditions (23) are discretised with second-order accuracy, cf. Ref. 5. To this end, an equidistantly spaced mesh in x- and y-direction is adopted. In order to use the classical three-point stencils throughout except from the discretised borders given by $x \equiv 0$, $x \equiv 0$, $x \equiv 1$, $y \equiv 0$, $y \equiv 1$, the second order derivatives are treated explicitly, such that both the first and second derivatives are approximated with central finite differences. Specifically, 200×200 grid points are used in the square range $0 \leq x \leq 1$, $0 \leq y \leq 1$. The resulting algebraic system of equations, supplemented with the remaining boundary conditions (13) and (14), is solved numerically by employing the software *SPARSOL* that has been designed by the author for generally solving very large systems of (both nonlinear and linear) equations in a highly user-friendly way. In essence, *SPARSOL* adopts a Newton-Raphson method, accompanied by a global strategy to achieve robustness with respect to the choice of the initial guess of the solution. Most important, *SPARSOL* effectively accounts for the sparsity pattern of the Jacobian: it is detected automatically, the non-zero entries of the Jacobian are computed numerically, and a direct sparse solver for the solution of the underlying linear system is invoked. For more details the reader is referred to Ref. 6.

IV.B. Numerical results for nominal conditions

The optimum load-bearing capacity is found iteratively for $K_y \approx 3$, as already indicated in figure 1, and $K_x \approx 1$, see (5). The results for the cases of liquid water and saturated water vapour as lubricant are shown in tables 5 and 6, respectively. Interestingly, the slightly higher loads achieved in latter case suggest a positive effect of compressibility on the load-bearing capacity that overcompensates the, compared to the

former case, about a factor of 10 reduced viscosity (cf. table 1). The data for the load are also displayed as solid curves in figure 3.

Table 5. Results for liquid water and $K_y = 3$, $K_x = 1$.

	$\tilde{p}_\mathrm{i} = 20\,\mathrm{bar}$, $\tilde{p}_\mathrm{o} = 5\,\mathrm{bar}$				$\tilde{p}_\mathrm{i} = \tilde{p}_\mathrm{o} = 5\,\mathrm{bar}$			
n	$\tilde{F}$	$\tilde{P}$	$\tilde{Q}$	$\tilde{M}$	$\tilde{F}$	$\tilde{P}$	$\tilde{Q}$	$\tilde{M}$
2	1840.5	12.58	651.66	597.86	620.3	12.58	0.086	0.079
3	1843.1	12.85	651.63	597.84	622.9	12.85	0.057	0.053
4	1844.9	13.14	651.61	597.82	624.7	13.14	0.042	0.038
5	1846.2	13.42	651.60	597.81	626.0	13.42	0.032	0.029
6	1847.1	13.69	651.60	597.81	626.9	13.69	0.025	0.023
7	1847.6	13.95	651.59	597.80	627.4	13.95	0.020	0.019
8	1847.8	14.18	651.59	597.80	627.6	14.18	0.016	0.015
9	**1847.8**	**14.39**	**651.58**	597.79	627.6	14.39	0.013	0.012
10	1847.7	14.58	651.58	597.79	627.5	14.58	0.010	0.009
11	1847.5	14.75	651.58	597.79	627.3	14.57	0.008	0.007
12	1847.3	14.91	651.58	597.79	627.1	14.91	0.006	0.005
13	1847.0	15.04	651.57	597.79	626.8	15.04	0.004	0.003
14	1846.7	15.17	651.57	597.78	626.5	15.17	0.002	0.002

Table 6. Results for saturated water vapour and $K_y = 3$, $K_x = 1$.

	$\tilde{p}_\mathrm{i} = 20\,\mathrm{bar}$, $\tilde{p}_\mathrm{o} = 5\,\mathrm{bar}$				$\tilde{p}_\mathrm{i} = \tilde{p}_\mathrm{o} = 5\,\mathrm{bar}$			
n	$\tilde{F}$	$\tilde{P}$	$\tilde{Q}$	$\tilde{M}$	$\tilde{F}$	$\tilde{P}$	$\tilde{Q}$	$\tilde{M}$
2	1980.5	1.14	4504	44.09	613.3	1.14	0.086	8.5e-4
3	1980.7	1.16	4504	44.09	613.5	1.16	0.058	5.6e-4
4	1980.9	1.19	4504	44.09	613.7	1.19	0.042	4.1e-4
5	1981.0	1.22	4504	44.09	613.8	1.21	0.032	3.2e-4
6	1981.1	1.24	4504	44.09	613.9	1.24	0.025	2.5e-4
7	1981.1	1.26	4504	44.09	614.0	1.26	0.020	2.0e-4
8	1981.2	1.28	4504	44.09	614.0	1.28	0.016	1.6e-4
9	**1981.2**	**1.30**	**4504**	**44.09**	614.0	1.30	0.013	1.3e-4
10	1981.2	1.32	4504	44.09	614.0	1.32	0.010	1.0e-4
11	1981.1	1.34	4504	44.09	613.9	1.33	0.008	7e-5
12	1981.1	1.35	4504	44.09	613.9	1.35	0.006	5e-5
13	1981.1	1.36	4504	44.09	613.9	1.36	0.004	4e-5
14	1981.1	1.38	4504	44.09	613.9	1.37	0.002	2e-5

Most important, it appears that in the here considered case $\tilde{p}_\mathrm{i} = 20\,\mathrm{bar}$ the maximum load is obtained for $n = 8$ to 9 (indicated by bold fonts in tables 5 and 6). The data for the (here fictitious) case $\tilde{p}_\mathrm{i} = 5\,\mathrm{bar}$, i.e. for purely hydrodynamic bearing mode, reveal that the effect of hydrostatic bearing due to the flow in radial direction provoked by the imposed difference pressure $\tilde{p}_\mathrm{i} - \tilde{p}_\mathrm{o}$ contribute to approximately 2/3 of the overall load. This effect is even more pronounced for the case of vapour, as inferred from the relatively small value of $\tilde{p}_\mathrm{r}$ compared to $\tilde{p}_\mathrm{i}$ and $\tilde{p}_\mathrm{o}$, see table 4. Also, this observation agrees with the finding that the radial pressure drop has only insignificant effect on the friction power, which is a consequence of the flow in circumferential direction: the latter is triggered by (i) the angular speed of the rotor and (ii) the azimuthal tilting of the clearance, represented by the non-zero value of K_y. Accordingly, the azimuthal component v of the fluid velocity and, in turn, the associated shear stress component τ_φ are composed of a

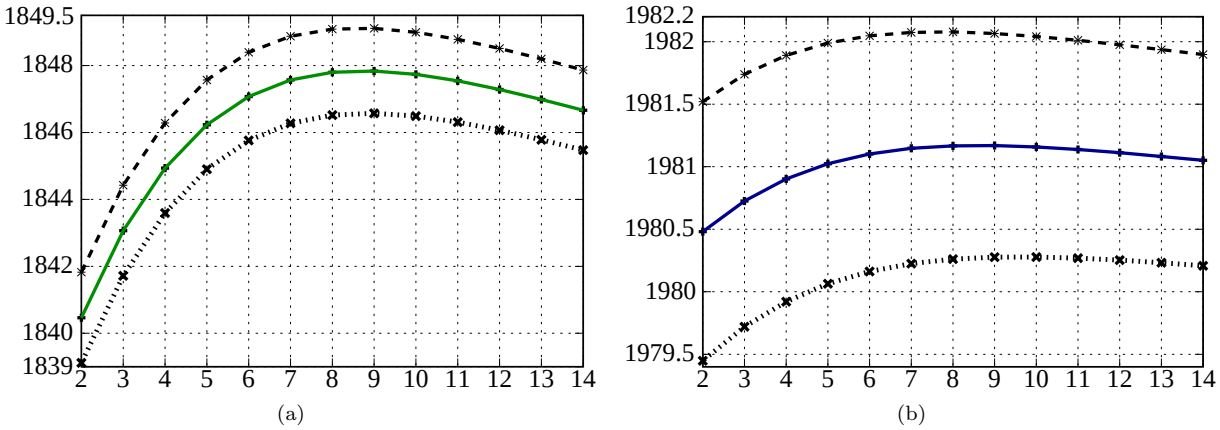

Figure 3. Load-bearing capacity $\tilde{F}$ (ordinates) vs. n (abscissae) for (a) liquid water, (b) saturated water vapour: discrete points connected by straight lines, $\gamma = 0$ (solid), $\gamma = -0.01$ (dashed), $\gamma = 0.01$ (dotted).

Couette and Hagen–Poiseuille flow contribution, cf. (17) and (26), that account for the effects (i) and (ii), respectively. However, one then infers from (20), (13), (14), and (26) that for relatively large values of the radial pressure drop $p_i - p_o$ and, correspondingly, of the gradient $\partial p/\partial r$ the shear stress τ_φ merely originates from the Couette flow contribution to v in a first approximation, which is independent of the actual pressure difference $p_\mathrm{i} - p_\mathrm{o}$. This behaviour is due to the specific product composition of the clearance geometry described by (4): as the flow triggered by the radial pressure loss is approximately governed by the left-hand side of (20) solely, it is almost independent of φ. As a most relevant implication, the predominance of the radial flow is also recognised through the rather tremendous difference of $\tilde{Q}$ and $\tilde{M}$ compared to the values referring to purely hydrodynamic operation.

IV.C. Stability of steady-state operation

Following the usual considerations on stability of the stationary operation of a hydrodynamic bearing, the response times typical for the dynamics describing deviations of steady-state conditions are taken to be sufficiently large in order to allow for a quasi-static treatment of the problem. Then an operating point $(\tilde{H}, \tilde{F})$ is regarded as stable if $\tilde{F}$ increases/decreases for decreasing/increasing values of $\tilde{H}$; conversely, it is unstable, cf. Refs. 2, 3.

To be more precise, stability is investigated by calculating $\tilde{F}$ for varying values of a control parameter γ that accounts for a relative change of $\tilde{H}$ as the minimum clearance height is given by $\tilde{H}(1+\gamma)$, $\gamma > -1$, and all other parameters are kept fixed. That is, the minimum value of h is kept equal to 1, such that the expression for h in (4) is replaced by $(h+\gamma)/(1+\gamma)$. In view of (24) and (25), stability then is encountered for

$$\partial[(1+\gamma)^{-2}F]/\partial\gamma < 0\,, \tag{30}$$

where the dependence of F on γ has to be determined numerically. Consequently, stability is investigated by carrying out a corresponding sensitivity analysis for F. To this end, the computations discussed in § IV.B and referring to the case $\gamma = 0$ are repeated by having γ take on slightly negative and slightly positive values. Therefore, the specific results displayed in figure 3 point to stable operating conditions, according to (30).

V. Concluding remarks

The analysis carried out so far allows for drawing the following conclusions and proposing adequate further measures:

- it has been demonstrated that the required load-bearing capacity is achieved by using both liquid water and, with some reservation concerning the possibility of phase transition, saturated water vapour as lubricants (the latter case giving rise to slightly enhanced loads);
- in both cases stable operation with respect to small deviations of the load $\tilde{F}$ and the minimum clearance height $\tilde{H}$ from their nominal values is expected;

- in view of the unsatisfactorily large values of Re due to the relatively large value of $\tilde{\Omega}$, in particular in the case of liquid water as lubricant, the validity of the results can be improved significantly by rendering the application of the lubrication approximation more reliable as $\tilde{H}$ is reduced about a factor of 10 or even more;
- otherwise, condition (B) given in § III.A.2 is violated, such that a more realistic prediction of the pressure distribution requires to retain the convective terms in the equations of motion (then the thin-film approximation $\partial p/\partial z = 0$ gives rise to a boundary-layer problem, cf. Ref. 4), where in the case of vapour corresponding additional effects due to compressibility play an important role;
- the inclusion of elasto-hydrodynamical effects would probably improve the accuracy of the predicted loads $\tilde{F}$ considerably, in view of the impact of the resulting deflections of both the stator and the rotor on the clearance geometry;
- as a further improvement of the bearing design, it is suggested to supply the lubricant through one relatively small borehole in each sector, parallel to the axis of the stationary disc; for a sketch made by the customer see figure 4. Note that solving the full Navier–Stokes equation, i.e. by employing commercial software in the field of Computational Fluid Dynamics, then might be required in order to investigate more elaborately the associated supposed enhancement of the load-bearing capacity.

With respect to the last three issues, the execution of a subsequent research project is strongly recommended. In order to account properly for the rather high values of Re, this should include the possible occurrence of turbulence, associated with drastically enlarged friction. Also, in view of the probably unsatisfactorily large values of the flow rates $\tilde{Q}$ and $\tilde{M}$, see tables 5 and (6), the idea of a (sintered) porous bearing, to the author's knowledge not addressed so far in the present context, seems noteworthy. In that case the stator would act as the porous segment-bearing shell, which then serves as the storage of the specific lubricant. As a major advantage of such a (without a doubt, rather unconventional) design, the power losses associated with the relatively high flow rates, as predicted in the present investigation, are avoided due to the presence of the lubricant reservoir. As a different suggestion, the machining of functional surfaces is potentially a further means adding to a substantial reduction of the overall lubricant transfer rate.

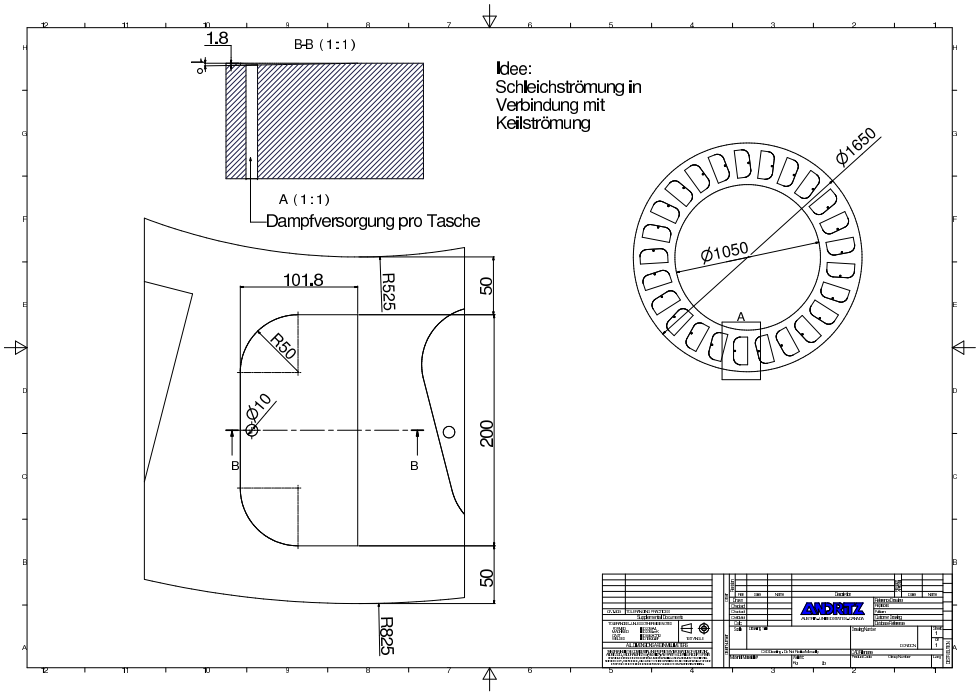

Figure 4. Proposition: milled clearance with borehole (drawing by Andritz AG)

Finally, it is remarked that a more detailed study of effects of both compressibility and phase transition of the lubricant is not only of great engineering relevance but also of interest from the viewpoint of fundamental

research in fluid mechanics.

References

[1]Lemmon, E. W., McLinden, M. O., and Friend, D. G., "Thermophysical Properties of Fluid Systems," *NIST Chemistry WebBook, NIST Standard Reference Database*, edited by P. J. Linstrom and W. G. Mallard, No. 69, National Institute of Standards and Technology, Gaithersburg, MD, Standard Reference Data Program, `http://webbook.nist.gov/chemistry/fluid/` (retrieved February 11, 2009).

[2]Cameron, A., *Basic Lubrication Theory*, Series in Engineering Science, Ellis Horwood Limited, Chichester, UK, 2nd ed., 1976.

[3]Szeri, A. Z., *Fluid Film Lubrication: Theory and Design*, Cambridge University Press, Cambridge, UK, 1st ed., 1998.

[4]Schlichting, H. and Gersten, K., *Boundary-Layer Theory*, Springer-Verlag, Berlin, Heidelberg, Germany, 8th ed., 2000.

[5]Venner, C. H. and Lubrecht, A. A., *Multilevel Methods in Lubrication*, Vol. 37 of *Tribology Series*, Elsevier, Amsterdam, 1st ed., 2000.

[6]Dennis, Jr., J. E. and Schnabel, R. B., *Numerical Methods for Unconstrained Optimization and Nonlinear Equations*, Vol. 16 of *Classics in Applied Mathematics*, Society for Industrial and Applied Mathematics (SIAM), Philadelphia, PA, 1996.